



International
Building
Performance
Simulation
Association
Australasia

AUSTRALASIAN BUILDING SIMULATION

JULY 20-21, 2022 • BRISBANE

CONFERENCE
PROCEEDINGS



MAJOR SPONSOR



TRADE DISPLAY
SPONSOR



INDUSTRY
PARTNER



DISCLAIMER

The information or advice contained in these technical papers is intended for use only by professionals who have had adequate technical training in the field to which the paper relates. At the time of publication, these technical papers have undergone a formal peer-review process.

These documents have been compiled as an aid only, and the information or advice should be verified before it is put to use. The user should also establish the applicability of the information or advice in relation to any specific circumstances. While the information or advice is believed to be correct, no responsibility is taken by AIRAH or IBPSA Australasia for any statements made within.

AIRAH and IBPSA Australasia, its officers, employees and agents, disclaim responsibility for any inaccuracies contained within the documents, including those due to any negligence in the preparation and publication of the said technical papers.

COPYRIGHT

This work is copyright. Apart from any use as permitted under the Copyright Act 1986, no part may be reproduced by any process without prior written permission from either the Australian Institute of Refrigeration, Air Conditioning and Heating (AIRAH) or the International Building Performance Simulation Association (IBPSA) Australasia.

ISBN

978-0-949436-54-2

TABLE OF CONTENTS

	Page
Foreword	4
Message from the organisers	4
Keynote speakers	5
Committees	7
Program	8
Technical papers	
Improved real-time year weather data services with Bureau of Meteorology data presented by Trevor Lee, Affil.AIRAH, Exemplary Energy	10
Extreme climate data files for design resilience presented by Trevor Lee, Affil.AIRAH, Exemplary Energy	18
Development of a whole-of-home energy rating tool for new housing presented by Zhenggen Ren, CSIRO	27
Future changes to building code energy efficiency provisions for commercial buildings presented by Grace Foo, M.AIRAH, DeltaQ	39
Disaggregation of precipitation data applicable for climate-aware planning in built environments presented by Trevor Lee, Affil.AIRAH, Exemplary Energy	59
Heating electrification impacts on commercial HVAC performance today and in the future: A case study presented by Yunlong Ma, Affil.AIRAH, Queensland University of Technology	71
Study of using a simplified transient heat transfer model for borehole heat exchangers using artificial neural network to predict various output parameters presented by Michael Kostevski, Toronto Metropolitan University	83
Gap analysis: Pushing NABERS ratings through energy simulation presented by Manasa Marasani, Atelier Ten	93
The incorporation of precipitation into climate data and its impacts on hygrothermal simulations presented by Freya Su, University of Tasmania	105
The effect of cellular blinds on aged care, now and in the future presented by Sherif Zedan, M.AIRAH, Queensland University of Technology	121
Double skin façade's energy performance in a mixed-mode office building presented by Soha Matour, Stud.AIRAH, Queensland University of Technology	136
Adaptation to present-day and future thermal stress in a Bangladesh ready-made garment factory presented by Aaron Bach, Griffith University	150
Optimisation of a building integrated photovoltaic façade for conceptual design support presented by Tharushi Samarasinghalage, RMIT University	163
Heat and power flow: Modelling, simulation, and experimental investigations of BIPV presented by Dominika Knera, Lodz University of Technology	175
Building retrofits with En-ActivETICS – design in practice using simulation techniques presented by Michal Krempski-Smejda, Lodz University of Technology	185
Feasibility study of wastewater energy transfer for an existing campus building cluster presented by Monica Brands, Toronto Metropolitan University	194
Comfort data for Brisbane: Using data collected by low-cost monitoring devices to improve prediction accuracy presented by Tobias Kramer, Queensland University of Technology	207

Sensitivity analysis of passive design strategies for office buildings in the tropics presented by Arinda Rachman, Institut Teknologi Bandung	220
Prediction of occupants' perception of natural ventilation effectiveness presented by Le Li, Victoria University	231
Optimisation of economy-cycle operation and supply air temperature control for VAV systems presented by Paul Bannister, L.AIRAH, DeltaQ	242
Insights from changes to stringency in the National Construction Code presented by PC Thomas, Team Catalyst	259
The ripple effect of smart engineering presented by Rob Lord, M.AIRAH, SEED Engineers	271
A real-world application of machine learning and optimal control simulation for chilled water plants presented by Michael Berger, Conserve It	284
Enhancing of building sustainability via disarticulating of sensible and dehumidifying coils in HVAC systems presented by Esmail Lavasani, University of Bucharest	297
Pushing the boundaries of net zero in the Australian outback presented by Manasa Marasani and Priya Gandhi, M.AIRAH, Atelier Ten	314
Challenges in computational fluid dynamics (CFD) simulation presented by Ken Thomson, M.AIRAH, Fusion HVAC	321

FOREWORD

The Building Simulation Conference 2022 was organized jointly by AIRAH and IBPSA Australasia and held in Brisbane from July 20–21, 2022, as both a live and online event.

In order to address the main Conference theme “Carbon and climate responsive – Getting it done” authors share their research and projects in a number of areas: weather and climate modelling, new simulation modelling, simulation for renewable and regenerative design, and adaptive design. All submissions have been double-blind reviewed – from the abstract to the full paper stage – and each submission was reviewed by at least 2 reviewers from any of these countries: Australia, Austria, Argentina, Czechia, New Zealand, Norway, and Singapore.

Initially, 44 abstract submissions were received. After the first stage of review, 43 abstracts were accepted, and their authors were invited to submit the full papers. A total of 30 full papers were subsequently submitted and reviewed, resulting in 26 full papers being accepted then presented at the Conference and included in these Proceedings. It is important to note that, in addition to Australia, the countries of origin of these authors include the USA, Canada, Poland, and Indonesia.

While most papers are based on research that was conducted by academia or researchers, quite a number of contributions are from the building industry. The diversity in the type of contributions provides a balance between theory, research, and practice to the Conference. There are also a number of papers based on the authors’ PhD research and such contributions really add a value to the conference and this proceedings as they demonstrate a promise to the future of building performance simulation.

We hope these proceedings will be useful to government bodies, industry and practitioners including building regulators and code officials to develop or revise building codes and standards. We expect the papers will also be useful to engineers, building architects and designers in improving the design of the built environment, and to researchers in understanding the complex issues surrounding carbon and climate responsive solutions and the role building performance simulation can play to achieve these goals.

On behalf of the Organising and Scientific Committee I would like to express our gratitude to all the authors for submitting their work and presenting it at the Conference, and to all reviewers who contributed their time significantly in the review process of the papers.

Veronica Soebarto
Scientific Chair, Organising Committee

MESSAGE FROM THE ORGANISERS

On behalf of AIRAH, I would like to thank the IBPSA Australasian technical organising committee for all their hard work in shaping the Australasian Building Simulation 2022 conference which was held in Brisbane, Australia on July 20-21.

With close to 100 delegates attending either in person or online, it was pleasing to see the support from industry for this year’s conference, after the past few years of COVID-19 lockdowns.

The conference also was fortunate to have four fantastic keynote speakers each bringing something for the audience to take away and we thank them for their time and effort in sharing their thoughts with us over the two days.

Brendan PejkoVIC
Organising Committee

KEYNOTE SPEAKERS

Victor Olgay (USA)

Rocky Mountain Institute Carbon Free Buildings Practice

Designing for the climate we want

We can design the world we want to live in – or we can stumble along and see where we end up! Designing for the climate we want is critically important, and it can be profitable as well as an opportunity for creative, exciting work. Building from 20 years of projects with Rocky Mountain Institute (RMI), this presentation describes a recipe for carbon free buildings, as well as the constituent ingredients. Deep energy retrofits of existing buildings, portfolio approaches, roadmaps for carbon neutrality, grid integrated building developments and embodied carbon concerns will be illustrated with successful and compelling built examples. While the future is unwritten, we can all pick up a pencil and help design the climate we want.

Professor Joe Clarke (Scotland)

University of Strathclyde

Building performance simulation: The final push

This keynote presentation will focus on how building performance simulation (BPS) can be applied to address the issues underpinning the six conference themes: energy transitions, adaptive design, attaining resilience, health and wellbeing, retrofitting, and future cities. After characterising the state-of-the-art and differentiating the real simulation approach from what is often pursued in practice, Joe will identify the developments that are needed in the near-to-medium term and conclude with three essentials: the formal connection of user requirements with new developments; the evolution of harmonised application standards; and the connection of the virtual world of modelling and simulation with the real world of component manufacture. The presentation is intended to be somewhat critical of the present approach to BPS development and use, and thought-provoking in relation to how it could be done so much better.

Professor Susan Ubbelohde (USA)

Loisos + Ubbelohde

Simulation in practice: Collaboration, iteration, visualisation and validation

Using simulation in practice often feels like the biathlon event in the winter Olympics. There's a pull between accuracy and timeliness, between the intricacy of the simulation and the many competing voices of the design team and owner.

Over many years, Loisos + Ubbelohde has developed expertise in the design of high-performance buildings, providing thermal and lighting simulations that include energy use, thermal comfort, resilience, renewable sources, daylighting, shading, glazing, electric lighting, visual comfort and solar reflections. Our methods and tools have been sharpened in practice and advanced through research over three decades, and we have discovered ways to thread the needle between accuracy and speed.

This presentation will discuss the complexities of simulation and collaboration through recent projects that illustrate what Loisos + Ubbelohde has learned about the fusion of simulation, collaboration, iteration, visualisation and validation in practice.

Associate Professor Jen Martin (Australia)

School of Biosciences | Faculty of Science, University of Melbourne

How to be a more effective communicator – and why it matters

The COVID-19 pandemic, on top of the climate and biodiversity crises, highlights that we live at a time in which it has never been more critical for people working in technical fields to be able to communicate the findings, relevance, and implications of their work to wide and diverse audiences. But research has established that over time, the way we communicate science has become more and more difficult for non-scientists, or even scientists in other fields, to understand.

Way back in 1975, Michael Crichton lamented obfuscation in medical writing, but despite his call to action to make technical ideas more accessible, the opposite has occurred. In this talk, Jen will consider why this is the case and what can be done about it. In particular, she'll share advice and tips on how to work more effectively in inter-disciplinary teams by writing and speaking in effective and inclusive ways.

COMMITTEES

Technical organising committee

Nicki Parker, M.AIRAH, Norman Disney & Young
Quentin Jackson, M.AIRAH, Aurecon
Priya Gandhi, M.AIRAH, Atelier Ten

Organising committee

Emily McLaughlin, AIRAH
Brendan PejkoVIC, AIRAH

Scientific committee

Veronica Soebarto, University of Adelaide – Chair
Adam Greaves, M.AIRAH, Lucid Consulting
Adrian Chong, National University Singapore
Ashfaque Chowdhury, Affil.AIRAH, CQ University Australia
Brendon McNiven, University of Melbourne
Hossein Omrany, University of Adelaide
James Wong, RMIT University
Karel Kabele, Czech Technical University
Mark Dewsbury, M.AIRAH, University of Tasmania
Mary Myla Andamon, RMIT University
Matt Webb, M.AIRAH, Griffith University
Matthias Haase, President of IBPSA Nordic
Mike Donn, Victoria University (NZ)
Paul Bannister, L.AIRAH, DeltaQ
Paul Davy, M.AIRAH, dsquared Consulting
PC Thomas, Team Catalyst
Priya Gandhi, M.AIRAH, Atelier Ten
Priyadarsini Rajagopalan, RMIT University
Quentin Jackson, M.AIRAH, Aurecon
Raul Ajmat, Universidad Nacional de Tucumán
Robert McLeod, TU Graz
Terry Williamson, The University of Adelaide
Wendy Miller, Affil.AIRAH, Queensland University of Technology
Zhenjun Ma, F.AIRAH, Sustainable Buildings Research Centre, University of Wollongong

DAY ONE – WEDNESDAY, JULY 20		
Time	Presentation	Speaker
8.20–8.50	Registration, arrival tea and coffee	
8.50–9.00	Day one welcome address	Quentin Jackson, M.AIRAH IBPSA Australasia President
9.00–9.45	Conference keynote address: Designing for the climate we want*	Victor Olgay (USA) Rocky Mountain Institute Carbon Free Building Practice
9.45–10.05	Improved real-time year weather data services with Bureau of Meteorology data	Trevor Lee, Affil.AIRAH Exemplary Energy
10.05–10.25	Extreme climate data files for design resilience	Trevor Lee, Affil.AIRAH Exemplary Energy
10.25–10.45	Sponsor address	PC Thomas Design Builder Software Australia
10.45–11.15	Morning tea	
	SIMULATION FOR RENEWABLE AND REGEN DESIGN	
11.15–11.35	Development of a whole-of-home energy rating tool for new housing	Zhengen Ren CSIRO
11.35–11.55	Future changes to building code energy efficiency provisions for commercial buildings	Grace Foo, M.AIRAH DeltaQ
11.55–12.15	Disaggregation of precipitation data applicable for climate-aware planning in built environments	Trevor Lee, Affil.AIRAH Exemplary Energy
12.15–12.35	Heating electrification impacts on commercial HVAC performance today and in the future: A case study	Dr Yunlong Ma, Affil.AIRAH Queensland University of Technology
12.35–1.35	Lunch	
	NEW SIMULATION MODELLING	
1.35–1.55	Study of using a simplified transient heat transfer model for borehole heat exchangers using artificial neural network to predict various output parameters*	Michael Kostevski Toronto Metropolitan University
1.55–2.15	Gap analysis: Pushing NABERS ratings through energy simulation	Manasa Marasani Atelier Ten
2.15–2.35	The incorporation of precipitation into climate data and its impacts on hygrothermal simulations*	Freya Su University of Tasmania
2.35–3.05	Afternoon tea	
	ADAPTIVE DESIGN	
3.05–3.25	The effect of cellular blinds on aged care, now and in the future	Dr Sherif Zedan, M.AIRAH Queensland University of Technology
3.25–3.45	Double skin façade's energy performance in a mixed-mode office building	Soha Matour, Stud.AIRAH Queensland University of Technology
3.45–4.05	Adaptation to present-day and future thermal stress in a Bangladesh ready-made garment factory	Aaron Bach Griffith University
4.05–4.50	Conference keynote address: Building performance simulation: The final push (<i>recorded video presentation with live Q&A</i>)	Professor Joe Clarke (Scotland) University of Strathclyde
4.50–5.00	Closing address	
5.00–7.00	Cocktail function	

* Livestreamed presentation

DAY TWO – THURSDAY, JULY 21

Time	Presentation	Speaker
8.20–8.50	Registration, arrival tea and coffee	
8.50–9.00	Day two welcome address	IBPSA/AIRAH
9.00–9.45	Conference keynote address: Simulation in practice: Collaboration, iteration, visualisation and validation*	Professor Susan Ubbelohde (USA) Loisos + Ubbelohde
9.45–10.30	Conference keynote address: How to be a more effective communicator – and why it matters	Associate Professor Jen Martin (Australia) School of Biosciences Faculty of Science, University of Melbourne
10.30–11.00	Morning tea	
	EXISTING BUILDINGS	
11.00–11.20	Optimisation of a building integrated photovoltaic façade for conceptual design support*	Tharushi Samarasinghalage RMIT University
11.20–11.40	Heat and power flow: Modelling, simulation, and experimental investigations of BIPV	Dominika Knera Lodz University of Technology
11.40–12.00	Building retrofits with En-ActivETICS – design in practice using simulation techniques	Michal Krempski-Smejda Lodz University of Technology
12.00–12.20	Feasibility study of wastewater energy transfer for an existing campus building cluster	Monica Brands Toronto Metropolitan University
12.20–1.10	Lunch	
	CLIMATE CHANGE AND ADAPTIVE DESIGN	
1.10–1.30	Comfort data for Brisbane: Using data collected by low-cost monitoring devices to improve prediction accuracy	Tobias Kramer Queensland University of Technology
1.30–1.50	Sensitivity analysis of passive design strategies for office buildings in the tropics*	Arinda Rachman Institut Teknologi Bandung
1.50–2.10	Prediction of occupants' perception of natural ventilation effectiveness*	Le Li Victoria University
2.10–2.30	Optimisation of economy-cycle operation and supply air temperature control for VAV systems	Paul Bannister, L.AIRAH DeltaQ
2.30–3.00	Afternoon tea	
	PAVING THE WAY TO TRANSITION	
3.00–3.20	Insights from changes to stringency in the National Construction Code	PC Thomas Team Catalyst
3.20–3.40	The ripple effect of smart engineering	Rob Lord, M.AIRAH SEED Engineers
3.40–4.00	A real-world application of machine learning and optimal control simulation for chilled water plants	Michael Berger Conserve It
4.00–4.20	Enhancing of building sustainability via disarticulating of sensible and dehumidifying coils in HVAC systems*	Esmaeil Lavasani University of Bucharest
4.20–4.40	Pushing the boundaries of net zero in the Australian outback	Manasa Marasani Atelier Ten
4.40–5.00	Challenges in computational fluid dynamics (CFD) simulation	Ken Thomson, M.AIRAH Fusion HVAC
5.00–5.05	Closing address	
5.05–6.05	Cocktail function	

* Denotes livestreamed presentation

IMPROVED REAL-TIME YEAR WEATHER DATA SERVICES WITH BUREAU OF METEOROLOGY DATA

TREVOR LEE, DAVID FERRARI, NAMAN JAIN AND DARIO TARQUINI

Exemplary Energy
32 Fihelly Street, Fadden, Canberra, Australia
trevor.lee@exemplary.com.au

ABOUT THE AUTHOR

Trevor Lee is a Canberra-based architect and consultant on energy conservation in the built environment through the multi-disciplinary firm Exemplary Energy. He is lead author of the Australian Solar Radiation Data Handbook and team leader developing the expanded Australian Climate Data Bank – 1990–2021 for around 250 locations.

Researching the impact of climate change on the built environment, this work flowed into the Ersatz Future Meteorological Years (EFMYs) data sets for two scenarios to 2030 and four scenarios to 2050.

From 1990 to 2004 Trevor served as executive director of the funds manager Australian Ethical Investment Ltd (ASX code AEF), now managing over \$6.5 billion.

ABSTRACT

Real-Time Year (RTY) weather data services are a valuable tool to produce benchmarking simulations for various applications, particularly when comparing them to the long-term average climate conditions. This paper examines how our Exemplary Weather and Energy (EWE) Index analysis offers a comparison of the performance of different archetypical buildings and a domestic Photovoltaic (PV) system under RTY weather conditions, with the long-term average and future climate conditions.

The results are offered in the form of deviation of the monthly means of minimum, average and maximum recorded data, as well as a comparison of the energy performance of the buildings and the PV system. Both RTYs and the EWE index can be useful to current PV owners, by monitoring their system performance with our benchmark, and to Green Star, Smart, NatHERS and NABERS-rated building owners and facility managers. Users employ the tools to trigger investigations into underperforming buildings, evaluate potential corrective actions, or determine the likelihood that lower performance is be driven by climate anomalies.

INTRODUCTION

A Real-Time Year (RTY) data set is a collection of historical real-time weather data acquired from the Bureau of Meteorology (BOM) which can be provided to clients for their various needs. This data set includes elements like Global Horizontal Irradiation (GHI), Direct Normal Irradiation (DNI), Diffuse Horizontal Irradiation (DIF), Relative Humidity, Wind Speed, Wind Direction, Cloud Cover, Temperature, and Pressure. Exemplary Energy is able to provide these

data sets in three different formats – Typical Metrological Year (TMY), Energy Plus Weather (EPW), and Australian Climate Data Bank (ACDB).

Historically, RTYs have been available for 200 Australian locations since 1990, albeit with considerable delays caused by BOM’s QA processes. However, following the death in November 2019 of their key staff member, Dr. Ian Grant—whose last publication on the subject (Grant, 2019) informs this work on an ongoing basis—the Bureau of Meteorology suspended its dissemination of satellite solar data after July 2019.

Nonetheless, timely RTY data is available to Exemplary Energy for the cities of Brisbane, Canberra, Perth and Sydney – by courtesy of arrangements with, respectively, Queensland University of Technology (QUT), The Commonwealth Scientific and Industrial Research Organisation (CSIRO), Murdoch University, and the Department of Planning, Industry and Environment (formerly Macquarie University).

1. EXEMPLARY WEATHER AND ENERGY INDEX

To help understand how the RTY weather compares to the long-term average and the medium-term future climates, we offer a monthly free public service by publishing the Exemplary Weather and Energy (EWE) Index through our e-newsletter “Exemplary Advances” since November 2014, which has recently been converted into a blog where we publish our analysis of the EWE index, highlighting interesting results for any of the 4 cities for which we receive the RTY data.

The EWE index aims to compare the performance of three archetypical buildings and a domestic solar PV system under these RTY weather conditions with the Reference Meteorological Year (RMY) data weather condition in a particular location – including elements such as dry-bulb temperature, solar insolation, wind speed and relative humidity.

Thanks to Exemplary’s in-house software, ClimateCypher, we are able to produce the RMY data that are then used every month to obtain the long-term average climate condition for Canberra, Brisbane, Perth and Sydney. RMYs (classified as RMY-A, B, or C according to the weighting give to the weather elements, with A having the greatest weighting given to solar irradiation) represent the entire time duration of the weather data in a single synthesized year and provides a convenient way to model building and energy systems (Lee, 2011).

For some of those locations that we include in the EWE index analysis, we also introduced a normalisation of the RTY surface weather data. In fact, the data for Canberra and Sydney, sourced via Automated Weather Stations (AWS) located, respectively, in CSIRO’s Black Mountain campus and at Macquarie University (Exemplary Energy, 2013a; 2013b) contain specific factors in the temperature and wind speed readings – thus, we normalise the RTY surface weather data based on correlations we have found with respect to readings from BOM’s official site at Canberra Airport via empirically derived formulas (Exemplary Energy, 2013a) and with respect to readings from BOM’s official CBD site at Sydney RO (Regional Office) (Exemplary Energy, 2013b).

1.1 Archetypical buildings and systems

The building performance is compared for a 3-storey office building, a 10-storey office building, and a ground-level supermarket. The 3-storey and 10-storey buildings take their geometry and characteristics from models developed for the Australian Building Codes Board during the development of requirements for the Building Code (now the National Construction

Codem NCC) in 2006 and updated to the current NCC requirements. Together the three models are broadly representative of commercial buildings under contemporary development. We also compare a 5kW PV System under the RTY weather conditions with the long-term average and future climate conditions.

1.1.1 Building archetypes

The building services energy consumptions—primary cooling and heating—are compared as part of this building performance comparison by simulating the archetypical building models in EnergyPlus™, a software developed by the US Department of Energy (DOE) and the National Renewable Energy Laboratories (NREL). The various archetypes differ from each other, based on the city they are referred to, following the National Construction Code – graphical models of the archetypes used in the simulations are shown in Figure 1. Thanks to these simulations, our technique is able to offer comments on peak loads, sensible and latent load and consumption distinctions, and N-E-S-W perimeter and central zone distinctions.

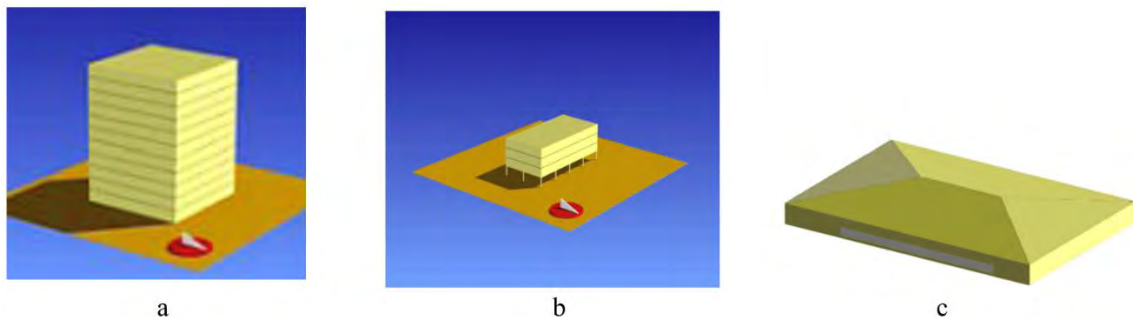


Figure 1. Graphical models of the archetypical buildings used in EWE simulations – a: 10-storey office building, b: 3-storey office building, c: Supermarket.

1.1.2 PV System

Historically, we included a 3kW_{peak} domestic PV system for the EWE index analysis. This was recently upgraded to a 5kW_{peak} system to account for the increased capacity of ‘typical’ Australian rooftop PV deployment and trends that better reflect the market.

In fact, Giles Parkinson (2021) reported that the average size of rooftop PV systems installed in Australia had reached a record high of 8.7kW in June 2021. However, according to our partner Global Sustainable Energy Solutions (GSES), this figure is skewed by a relatively small number of high powered 3 phase systems – in fact, many residential systems are now connected to a single-phase power supply and a more representative system would be a 6.6kW_{DC} array paired with a 5kW_{AC} inverter. Thus, while the EWE index analysis is focused on non-residential buildings, the focus of our analysis is on residential PV installations which currently dominate the market.

Additionally, we note that efficiencies of scale for PV system are relatively trivial, therefore the results obtained in the analysis can be indicative for all fixed-array systems, whether they are residential or commercial rooftop systems.

1.1.3 Results

In the following tables, it is shown an example of the results obtained for three months, characteristic of last three recent seasons: winter (July 2021), spring (October 2021), and summer (January 2022) – the results were published in our blog issues of Exemplary Advances, respectively in August 2021, November 2021, and February 2022.

2021 July	Weather Index (monthly means) ¹						Weather and Energy Index (%)						
	Temperature (°C)			Rel. Humidity (%)			10-Storey		3-Storey		Supermarket		Solar PV
	Min	Avg	Max	Min	Avg	Max	Heat	Cool	Heat	Cool	Heat	Cool	
Brisbane	-3.1	-3.3	-3.5	+48.0	+18.8	+1.0	+141	-21.0	+169	-25.7	+29.6	-100	-11.4
Canberra	+0.9	+0.1	-0.7	-4.0	+1.5	0.0	-6.7	+54.7	-14.2	+46.8	-16.6	-	-0.1
Perth	+4.0	+2.0	+0.4	+17.0	+4.2	-2.0	-56.5	-9.9	-56.9	-3.5	-45.8	-95.8	-11.2
Sydney	+1.8	+1.8	+0.2	-6.0	-19.4	-16.0	-43.1	+13.3	-43.7	+15.5	-37.1	-46.6	+3.9

Table 1. Results for a month during winter season – July 2021

2021 October	Weather Index (monthly means)						Weather and Energy Index (%)						
	Temperature (°C)			Rel. Humidity (%)			10-Storey		3-Storey		Supermarket		Solar PV
	Min	Avg	Max	Min	Avg	Max	Heat	Cool	Heat	Cool	Heat	Cool	
Brisbane	-3.3	-0.9	+1.2	+56.0	+19.8	+2.0	-	-14.5	-	-18.8	-	-87.1	-14.6
Canberra	-0.2	-0.8	-0.5	0.0	-3.3	-2.2	+2.2	+0.5	-23.2	+0.7	+6.6	-36.9	+0.4
Perth	-0.1	-0.6	-0.6	-3.0	+3.6	-6.0	-	-6.3	-	-10.4	-	-43.4	-35.7
Sydney	+0.4	+0.2	+0.1	+3.0	-6.1	-6.0	-	+0.6	-	+0.7	-	-4.9	+8.2

Table 2. Results for a month during spring season – October 2021

2022 January	Weather Index (monthly means) ¹						Weather and Energy Index (%)						
	Temperature (°C)			Rel. Humidity (%)			10-Storey		3-Storey		Supermarket		Solar PV
	Min	Avg	Max	Min	Avg	Max	Heat	Cool	Heat	Cool	Heat	Cool	
Brisbane	+3.5	+2.9	+2.5	+3	-1.7	1.8	-	+3	-	+2	-	-	-13
Canberra	+1.5	-0.3	-1.2	+9.0	+9.5	-1.0	-	+6		+10		+11	+5.4
Perth	+1.6	+1.6	+1.8	+2.0	-2.3	-7.0	*N.A.	*N.A.	*N.A.	*N.A.	*N.A.	*N.A.	*N.A.
Sydney	-0.6	-1.1	-1.9	+34	+12	+2.0	-	-4	-	-4	-	-5	+8.3

*An instrument malfunction has resulted in an inability to obtain solar radiation measurements for this site, subsequently the Energy Index was unavailable in the analysis.

Table 3. Results for a month during summer season – January 2022

As can be seen in Table 1, 2, and 3, the Weather analysis of the EWE index reports the deviation of the monthly means of minimum, average and maximum recorded data for RTY weather elements with the long-term average data. Also, the Energy analysis based on the building archetypes, and the domestic solar PV system previously discussed, shows the difference in heating and cooling energy consumptions in the three different buildings and the energy outputs from the solar PV system simulated with the RTY and the RMY data.

In our analysis, we also report a comparison of the building performance under the RTY condition with the RMY and the Ersatz Future Meteorological Year (EFMY) energy

performance, showing its trend over the last three months – an example of the October 2021 analysis is shown in Figure 2.

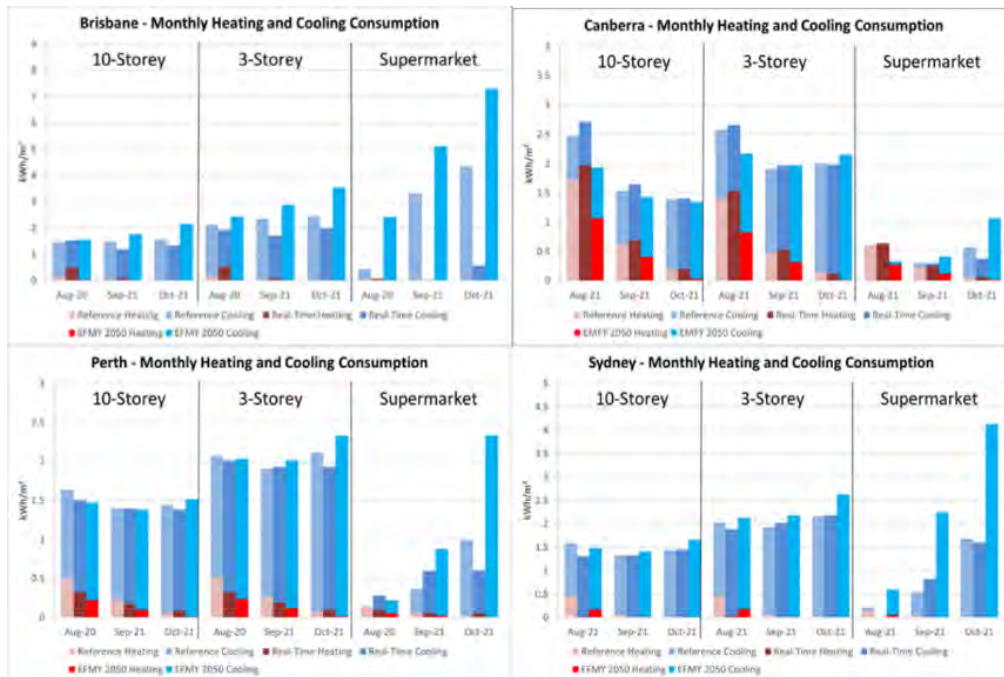


Figure 2. An example of Energy consumption comparison and trends for the three archetypal buildings in different locations – October 2021

Similarly, after simulating the 5kW domestic PV system under the RTY weather data, using System Advisor Model (SAM)—a software developed by the US DOE and the NREL—we compare the results with the simulations using the RMY and EFMF data and we analyse the trend of the 4 different capital cities over the last three months – the October 2021 results are showed in Figure 3.

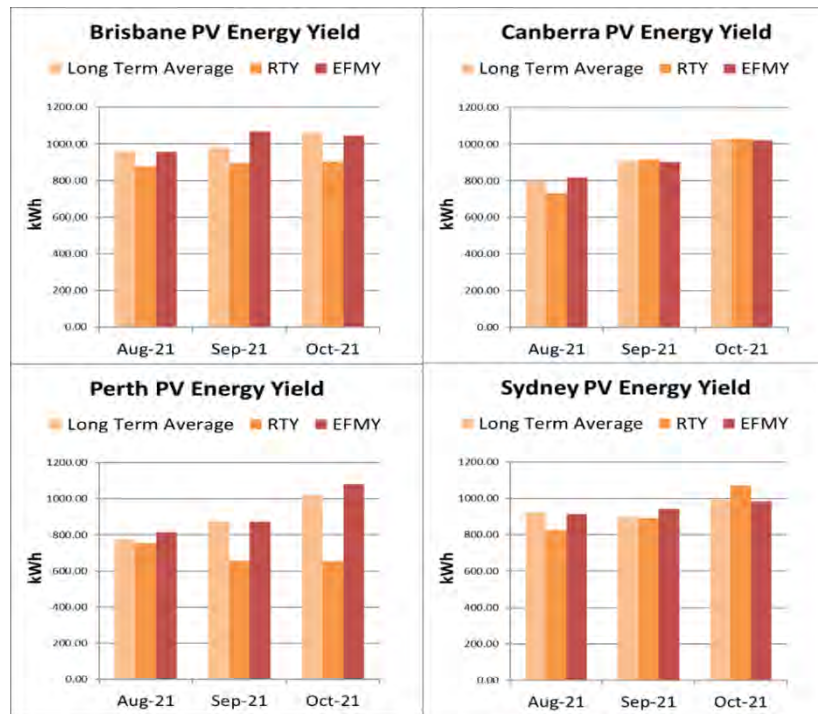


Figure 3. An example of Solar PV results for different locations – October 2021

2.1 Further developments

We are currently looking to geographically expand our RTY data set, to further extend the EWE index analysis to all Australian state/territory capitals. In fact, in August 2021 BOM had inaugurated its new source of real-time solar data, derived via the Heliosat-4 radiation model, which uses imager observations from the Himawari-8 satellite – this is expected to be active until later this year when the Himawari-9 satellite will become operational.

For the surface weather data such as dry-bulb temperature, wind speed, wind direction, and relative humidity, we are planning to subscribe to one of the many real-time products (Bureau of Meteorology, 2021) provided by BOM to complement accessing its monthly subscription service for ground-based measurements.

Despite the hard work of our helpful sources in providing us timely RTY data for 4 capital cities, a series of problems have already happened in the past with more than one weather station, resulting in the temporary disruption of our analyses (as it can be seen in Table 3 for Perth). The improved RTY weather data will provide more consistent and reliable results compared to the existent data. While we are always actively working towards a solution when these disruptions happen, and we at all times aim to include coverage of full historic data to compensate for these issues, it is clear how these developments will greatly improve our services.

CONCLUSION

Both the RTYs and the EWE Index have many applications (Lee, 2009; Lee and Edwards, 2015) and can be used for:

- Simulation Model Calibration
- Building or energy system monitoring which helps to identify underperformance and take early restorative actions.
- Renewable energy generator monitoring.
- Measuring actual output or consumption in the previous 12 months or month relative to RMYs.

Furthermore, current PV owners can monitor their system performance against our simulated benchmark to identify underperformance and take early corrective actions, while prospective PV owners can get an idea of how much energy production they can expect. Similarly, Green, Smart, NatHERS and NABERS rated building owners can also compare their heating and cooling energy utilisations against our simulated benchmarks and conduct corrective actions if their building is underperforming.

ACKNOWLEDGEMENTS

The authors acknowledge the Australian Bureau of Meteorology as the intended source of all the raw data products and other members of the Exemplary team who have made this work possible: Zhongran Deng, Yoke Fung, Miao (Chris) Wang, and Chun Yin Wu. For support in our early work with real-time data, we thank the hard-working and helpful sources: QUT Brisbane (especially Dr Aaron Liu), CSIRO Canberra (especially Mark Kitchen and Chris Russell), Murdoch University Perth (especially Philip Good), and Macquarie University Sydney (especially the late Dr Grant Edwards).

REFERENCES

Bureau Of Meteorology, 2021, 'Real-time Data Service'
<http://reg.bom.gov.au/reguser/reguser.shtml>

Bureau Of Meteorology, n.d., 'Satellite derived, bias-corrected Solar Radiation and Exposure User Guide' http://reg.bom.gov.au/catalogue/satellite_solar_data.pdf

Exemplary Energy, 'Exemplary Advances', monthly since November 2014, Canberra
<http://www.exemplary.com.au/information/exemplary-advances.php>

Exemplary Energy, 2013a, 'QA and Normalisation of CSIRO Canberra Data to the BOM Canberra Standard'
<http://www.exemplary.com.au/download/ExE%20RTY%20QA%20Report%20-%20Canberra%202013-07-01.pdf>

Exemplary Energy, 2013b, 'QA and Normalisation of Macquarie University Data to the BOM Sydney RO (Regional Office) Standard'
<http://www.exemplary.com.au/download/ExE%20RTY%20QA%20Report%20-%20Sydney%202013-07-01.pdf>

Grant, I, 2019, A Comprehensive Quality Assessment of the Bureau of Meteorology's Satellite Gridded Solar Data, Proceedings APSRC, Canberra

Lee, T, 2009, 'Climate data for building optimisation in design and operation in Australia' <http://www.exemplary.com.au/download/Lee%20-%20Paper%201298%20-%20Climate%20Data%20For%20Building%20Optimisation%20for%20IBPSA%202011.pdf>

Lee, T, 2011, 'Climate data for building optimisation in design and operation in Australia', *Proceedings of Building Simulation 2011: 12th Conference of International Building Performance Simulation Association*, 14-16 November, Sydney

Lee, T and Edwards, G, 2015, 'Weather Affects Building and PV Performance Simulation v Monitoring', *Asia-Pacific Solar Research Conference 2015*, 8 – 10 December, Brisbane <http://www.exemplary.com.au/download/Lee%20-%20AVPV3%20Weather%20Affects%20Building%20and%20PV%20Performance%20-%20Simulation%20v%20Monitoring%20V3%20POSTER.pdf>

DISCLAIMER

The information or advice contained in these technical papers is intended for use only by professionals who have had adequate technical training in the field to which the paper relates. At the time of publication, these technical papers have undergone a formal peer-review process.

These documents have been compiled as an aid only, and the information or advice should be verified before it is put to use. The user should also establish the applicability of the information or advice in relation to any specific circumstances. While the information or advice is believed to be correct, no responsibility is taken by AIRAH or IBPSA Australasia for any statements made within.

AIRAH and IBPSA Australasia, its officers, employees and agents, disclaim responsibility for any inaccuracies contained within the documents, including those due to any negligence in the preparation and publication of the said technical papers.

COPYRIGHT

This work is copyright. Apart from any use as permitted under the Copyright Act 1986, no part may be reproduced by any process without prior written permission from either the Australian Institute of Refrigeration, Air Conditioning and Heating (AIRAH) or the International Building Performance Simulation Association (IBPSA) Australasia.

EXTREME CLIMATE DATA FILES FOR DESIGN RESILIENCE

DAVID FERRARI, NIHAL ABDUL HAMEED, NAMAN JAIN, TREVOR LEE

Managing Director

Exemplary Energy

32 Fihelly Street, Fadden ACT 2904, Australia

david.ferrari@exemplary.com.au

ABOUT THE AUTHOR

Dr David Ferrari is an engineer with a long-held interest in the energy transition, having spent two decades in government, industry and academia working to address the challenges and support the urgently needed change. He has worked in energy policy and programs with the United Nations regional secretariat, Victorian Government, RMIT and the Australian Bureau of Meteorology.

He holds a PhD in Engineering from the ANU along with Bachelors of Engineering (Sustainable Energy Systems) and is a Certified Measurement and Verification Professional.

ABSTRACT

There is an ever increasing need to improve energy efficiency in buildings and their resilience while maintaining the required indoor comfort and environmental quality standards. This has led to an increasing reliance on building energy simulations which require inputs including extreme weather data to understand how the building performs even in the most adverse situations. The majorly available extreme weather data are derived primarily from historic temperature and solar irradiation data. This study analyses the validity of such extreme weather data for use in these building energy simulation applications. The result of this analysis shows that the extreme weather data defined in this way proves to be incapable of correctly representing the actual extreme conditions that the building is subjected to and that a more sophisticated approach will be required.

INTRODUCTION

Rapid urbanization and increase in buildings, which contributes to 30-70 per cent of total primary energy consumption in cities (Chen et al., 2017), calls for a reduction in building energy use and associated greenhouse gas emissions. At the same time, maintaining human comfort inside these buildings is of paramount importance, the lack of which can even affect the productivity of the occupants (Graham et al., 2021). To achieve both, the importance of building energy performance modelling to understand the optimum sizing of Heating, Ventilation and Air Conditioning (HVAC) systems is increasing. HVAC systems are the largest contributor to the building energy consumption, which amount to 40-60 per cent of the total building energy consumption and 15 per cent of the world's total energy consumption. Due to its high impact on the thermal comfort of the occupants and its responsiveness to external

weather conditions, it is a major part of these modelling exercises (Pérez-Lombard et al., 2008; Rafique et al., 2018; Stopps & Touchie, 2020).

The operation of these HVAC systems strongly responds to the outside environment of the building, especially in the context of operational efficiency (Homaei & Hamdy, 2021). For example, if the interior spaces inside the building require cooling while the outdoor air is at low temperature, then the HVAC system can use extra outside air in addition to or instead of mechanical cooling to achieve the desired conditions. If on the contrary, the outside air is too warm, then it would be more efficient to just use mechanical cooling at that time. Therefore, the use of outside weather conditions is necessary for the simulations of the HVAC systems as well as for the building envelope.

Modellers apply extreme weather conditions to simulations (Katal et al., 2019) in order to verify the performance of proposed HVAC systems and verify their capacity under all feasible weather. Through this, attention is being paid to the resilience of the building to infrequent but high impact conditions, which according to the Intergovernmental Panel on Climate Change (IPCC) are predicted to increase in frequency and intensity (Graham et al., 2021). Experts have even suggested that these kinds of adverse events may require impact analysis for an urban region to ensure stability of the grid network due to higher energy demand from buildings at that time (Homaei & Hamdy, 2021).

Analyses of historic extreme climate data is therefore required to understand the nature and likelihood of extreme events to inform such resilience analysis of buildings and urban areas.

This paper focuses on evaluating the applicability of currently available extreme climate data sets for such analysis and the validity of these files for applications related to building energy modelling and resilience studies.

1. EXTREME CLIMATE DATA

A synthesised or selected year of data representing typical local weather conditions provides a practical approach to characterising climate for simulation purposes. This idea was the motivation for developing Reference Meteorological Year (RMY) weather data (Freeman, 1979; Aguiar et al. 1999; Hui & Cheung, 1997). A similar hypothetical eXtreme Meteorological year (XMY) data set representing past extreme weather conditions would provide similar advantages when it comes to simulations and modelling. A review of the existing literature is needed to understand the existing techniques used to define and generate such reference extreme climate data.

1.1 Literature survey

Frank (2005) developed a Warm Reference Year for Zurich and Switzerland considering the months with the highest mean dry bulb temperature in the period 1984-2004. Analysing the dry bulb temperature statistics and looking for the hottest summer months and the coldest winter months in Australian locations, was the basis of defining XMY weather data according to Ferrari & Lee (2008). Crawley and Lawrie (2015) defined XMY which was based on the daily and hourly maximum and minimums of weather elements like dry bulb and dew point temperatures, solar irradiation, precipitation, relative humidity, and wind speeds for a 15-year period from 1999-2013 and developed an XMY for each weather element. Narowski et al. (2013) proposed an Untypical Meteorological Year (UMY) by giving weights to different weather elements and developed three types of UMY by adjusting the weights in each of the three. The weather elements given high importance in this study were dry bulb temperature,

solar radiation, and wind speeds. Nik (2016, 2017) developed an Extreme Cold Year and an Extreme Warm Year by expanding the selection algorithm proposed by Hall et al. (1978) which considered dry bulb temperature.

From the literature survey, it was seen that most of the XMY data was defined based on the dry bulb temperature. The other primary weather element considered was solar irradiation, as seen in the works of Crawley & Lawrie (2015) and Narowski et al. (2013). Crawley & Lawrie (2015) also reported that relative humidity and wind speeds XMYs have relatively minor impact on the heating or cooling energy demand of the buildings. Therefore, this study initially develops XMY data based on the dry bulb temperature and solar irradiation to replicate the existing XMY generation models.

1.2 Probabilistic approach to Extreme Meteorological Year generation

The P01, P10, P90, and P99 data in statistics refer to a value that is expected to exceed 1%, 10%, 90%, and 99% of the cases in a given temporal sample respectively and may be done through the process of Monte Carlo simulation (Dobos, Kasberg and Gilman, 2012). This probabilistic approach is used in this study as it has various advantages in the actual world. The energy consumption corresponding to P99 and P90 weather data is expected to be exceeded 99% and 90% of the time, therefore the building should be designed to accommodate these conditions with acceptably brief excursions of internal conditions.

The energy consumption corresponding to P01 data is the annual energy demand that would be expected to be exceeded during 1% of the years of operation, and catering to these conditions may require high-cost design improvements such as increasing the capacity of the HVAC system. A lower-cost option would be designing to the P10 conditions while accepting diminished performance – in the form of divergence from comfortable internal conditions – during more extreme weather in about 10% of the years of operation.

2. APPLICATION OF EXISTING EXTREME CLIMATE DATA MODELS TO BUILDING MODELS

Existing methods (described below) are available to generate XMY data sets which result in ‘extreme’ performance of a solar PV system. The authors applied these data to a set of building models to evaluate their applicability by comparing the results to those from using historic weather data – if these “PV XMY” data are valid for buildings, the results should correspond to approximately the same level of extremity as when historic yearly weather data are applied.

The following resources and methodology were adopted in this study to generate XMY data that is similar to those already defined by various researchers and to test their validity in the building energy simulation applications.

2.1 Resources used

System Advisor Model (SAM) is a simple, free and readily available software developed by National Renewable Energy Laboratories, USA, that simulates the energy output of a user defined renewable energy generator such as a Photovoltaic (PV) power system. The output is based on the solar irradiation that falls on the PV panels and the cell temperature of the PV panel (Gilman P et al., 2018). The cell temperature is a function of the dry bulb temperature (and, to a lesser extent, wind speed). Therefore, SAM was a suitable software candidate to validate extreme climate data sets based on solar irradiation and dry bulb temperature. The

P50/P90 simulation feature of SAM performed the P10, P50, and P90 analysis and gives the 10th, 50th and 90th percentiles along with maximum and minimum energy outputs from the PV system for a minimum of 10 years of single-year weather data (National Renewable Energy Laboratories, 2020).

ClimateCypher is an in-house software of Exemplary Energy and is capable of reading files containing satellite-derived solar data and surface-measured weather data including any ground-measured solar data. It then produces the weather data for the user's required period of years in the TMY2 (Typical Meteorological Year) and ACDB (Australian Climate Data Bank) weather file formats. ClimateCypher is also capable of generating RMY and XMY data in the TMY2 and ACDB formats. The XMY data is selected based on the results obtained from SAM and this process is detailed in the Methodology section below.

EnergyPlus is an open-source building energy performance simulation software developed by the US Department of Energy. This software was used in this study to simulate the yearly energy consumption of the 3-storey office building archetype used in simulations behind the Exemplary Weather and Energy Index published monthly (Exemplary Energy, 2014; Lee et al., 2022). The input required for the simulation in EnergyPlus is the weather file in EPW (Energy Plus Weather) file format and IDF (Input Data File) file containing the building data. EnergyPlus provides the option to convert TMY2 weather file format to EPW file format and this provision was used to convert the ClimateCypher generated weather files.

2.2 Methodology

2.2.1 Generating the XMY data

ClimateCypher was recently enhanced to generate the P01, P10, P90 and P99 weather files by selecting the most appropriate 12 historic calendar months and concatenating them such that the resultant synthesised year closely matches the 1st, 10th, 90th and 99th percentile criteria respectively for a PV system output. The percentile criteria were adapted from the results of the SAM P50/P90 simulate functionality and the maximum and minimum energy outputs were considered to be the P01 and P99 percentile energy outputs respectively, while the P10 and P90 energy outputs were considered to be the single year energy output closest to the P10 and P90 energy outputs generated by SAM (the maximum and minimum energy outputs that SAM generates are already single calendar year energy outputs while P10 and P90 energies that SAM generates are formula based and does not correspond exactly to a single year energy). This iterative process was conducted for all eight Australian Climate Zones in the National Construction Code and was presented at the Asia Pacific Solar Research Conference 2020 and 2021 (Hameed et al., 2020 & 2021).

The P01, P10, P90 and P99 weather files generated by ClimateCypher, for the period from 1990-2017, based on the percentile criteria obtained from SAM comprise the XMY data used in this study. Since SAM was used to refine the criteria, the XMY data is strongly dependent on the solar irradiation and dry bulb temperature values and hence can be used to study the validity of applying such climate years for building energy modelling purposes.

This study was conducted for two Australian building regulatory climate zones: Climate zones 2 and 7 for the cities of Brisbane and Canberra respectively.

2.2.2 Simulating the total building energy consumption with EnergyPlus

EnergyPlus was used to input the single year weather files and with the typical 3 storey office building archetype, the total building energy consumption for each year from 1990 to 2017 was computed. Also, the total and end use component energy consumptions corresponding to the hypothetical P01, P10, P90 and P99 weather data from ClimateCypher were also computed.

From the yearly total building energy consumption, the percentile values corresponding to the 1st percentile, 10th percentile, 90th percentile and 99th percentile were calculated as explained in Section 2.2.3.

2.2.3 Calculating the kth percentile of a dataset

The kth percentile of a dataset can be calculated by first sorting the dataset in increasing order and then using the following formula (Mann P S, 2010):

$$P_k = \text{Value of the } \left(\frac{k n}{100} \right) \text{ term in the data set} \quad (1)$$

where:

P_k = approximate value of the kth percentile

k = percentile value

n = number of terms in the dataset

Using equations (1) the 1st, 10th, 90th and 99th percentile of the total building energy consumption of each year from 1990-2017 was calculated and compared with the building energy consumption corresponding to P01, P10, P90 and P99 climate file generated from ClimateCypher.

3. RESULTS

P01, P10, P90 and P99 hypothetical year XMYs were generated via ClimateCypher and are thus known to reflect the conditions under which a solar PV system generates P01, P10, P90 and P99 levels of output.

Each XMY and each historic year for both Brisbane and Canberra were applied to the 3-storey building model in EnergyPlus and the total energy consumption was computed. The results are shown in Figure 1 and Figure 2, with the yearly total consumption plotted in ascending order. The hypothetical XMYs are highlighted with coloured bars in the charts to clearly show their placements with respect to the yearly historical data. The theoretical 1st, 10th, 90th and 99th percentile building energy consumptions calculated based on Equation (1) are also shown in the two figures.

It can be seen from Figure 1 that the energy consumption of the XMY P01, P10 and P90 results correlate poorly with the Theoretical 1st, 10th and 90th percentiles for Brisbane. Only the XMY P99 consumption closely matches with the respective Theoretical 99th percentile result.

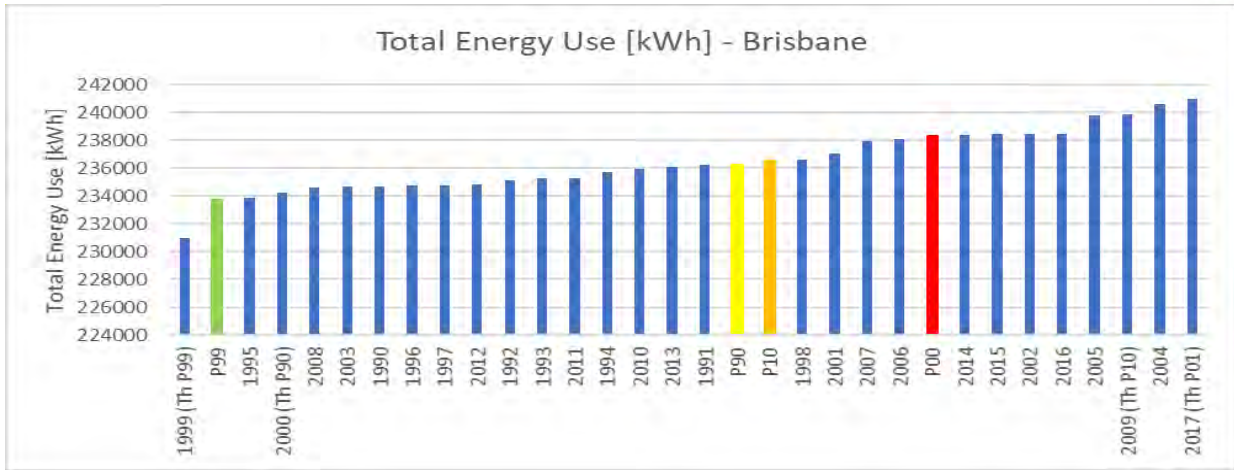


Figure 1. Total Building Energy Consumption of Single Years during 1990-2017 and the energy corresponding to the percentile XMY weather data for Brisbane.

The results for Canberra (Figure 2) indicate that the Theoretical 90th and 10th percentile energy consumption closely matches the XMY P90 and P10 (respectively), while the P01 and P99 energy consumption values are far from coincident with the Theoretical 1st and 99th percentiles.

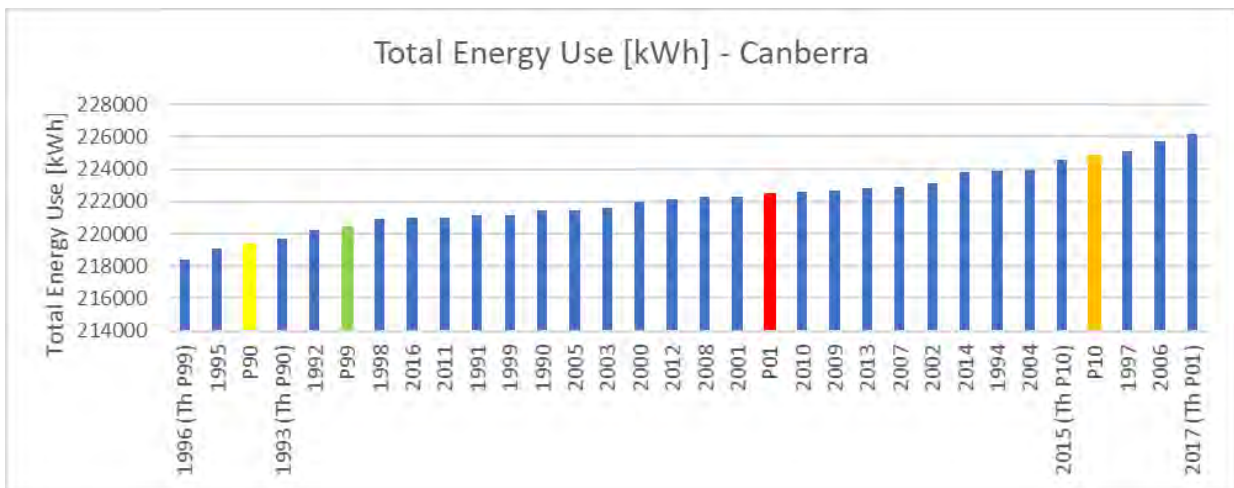


Figure 2. Total Building Energy Consumption of Single Years during 1990-2017 and the energy corresponding to the percentile XMY weather data for Canberra.

Overall, it is apparent that the correlation between XMY and theoretical extremity is both poor and inconsistent.

CONCLUSION

This work focused on investigating the validity of existing methods of defining Extreme Climate Data which is largely based on Solar Irradiation and Dry Bulb Temperature for PV system evaluation. The software SAM was utilised as a part of this study to generate probabilistic XMYs. EnergyPlus was used to compute the total building energy consumption corresponding to these probabilistic XMY weather data.

The results of this analysis for Canberra and Brisbane show that the total building energy consumption corresponding to the probabilistic XMY data does not closely match with the percentile total energy consumption observed during the 28-year period of 1990-2017.

This indicates the inadequacy of using just the two elements of solar irradiation and temperature to determine extremity when applying to building energy models. HVAC loads are highly dependent on other weather elements including Humidity and Wind Speeds as they affect the latent heat load of the building in summer and infiltration of outside air. Since HVAC loads themselves constitute 40-60 per cent of building energy consumption, this explains the inaccuracy seen in the results of this study.

Accordingly, further analysis into XMY generation is needed for building energy performance simulation applications, with closer attention to the key end use components of heating and cooling. Research into new algorithms for this purpose is continuing. Furthermore, this research only studied two sample climates, and further research is required on more climate locations.

ACKNOWLEDGEMENTS

The authors acknowledge the Australian Bureau of Meteorology as the source of all the raw data and the other members of the Exemplary team, especially Chithral Kodagoda and ZhongRan (Dan) Deng.

REFERENCES

- Aguiar, R., Camelo, S., & Gonçalves, H. (1999). Assessing the value of typical meteorological years built from observed and from synthetic data for building thermal simulation. *Proceedings from 6th International IBPSA Conference Building Simulation '99*. Kyoto (Japan), 13-15 September 1999.
- Chen, Y., Hong, T., & Piette, M. A. (2017). Automatic generation and simulation of urban building energy models based on city datasets for city-scale building retrofit analysis. *Applied Energy*, 205, 323-335.
- Crawley, D. B., & Lawrie, L. K. (2015). Rethinking the TMY: is the 'typical' meteorological year best for building performance simulation?. *Proceeding from Building Simulation*. Hyderabad (India), 7-9 December.
- Dobos, A. P., Gilman, P., & Kasberg, M. (2012). *P50/P90 analysis for solar energy systems using the system advisor model*. National Renewable Energy Lab. (NREL), Golden, CO (United States).
- Exemplary Energy (2014), *Exemplary Advances* (monthly e-newsletter since November 2014); <http://www.exemplary.com.au/information/exemplary-advances.php>

- Ferrari, D., & Lee, T. (2008). Beyond TMY: climate data for specific applications. *Proceedings from 3rd International Solar Energy Society conference—Asia Pacific region*. Sydney (Australia), 25-28 November.
- Frank, T. (2005). Climate change impacts on building heating and cooling energy demand in Switzerland. *Energy and buildings*, 37(11), 1175-1185.
- Freeman, T. L. (1979). *Evaluation of the typical meteorological years for solar heating and cooling system studies*. Final report (No. SERI/TR-8150-1). Altas Corp., Santa Cruz, CA (USA).
- Gilman, P., DiOrio, N. A., Freeman, J. M., Janzou, S., Dobos, A., & Ryberg, D. (2018). *SAM photovoltaic model technical reference 2016 update*. National Renewable Energy Lab. (NREL), Golden, CO (United States).
- Gilman, P., DiOrio, N. A., Freeman, J. M., Janzou, S., Dobos, A., & Ryberg, D. (2018). *SAM photovoltaic model technical reference 2016 update* (No. NREL/TP-6A20-67399). National Renewable Energy Lab. (NREL), Golden, CO (United States).
- Graham, L. T., Parkinson, T., & Schiavon, S. (2021). Lessons learned from 20 years of CBE's occupant surveys. *Buildings and Cities*, 2(1).
- Hall, I. J., RR, P., HE, A., & EC, B. (1979). *Generation of typical meteorological years for 26 SOLMET stations*. Sandia National Laboratories, Albuquerque (United States)
- Hameed, N. A. Jain, N., Lee, T. & Deng, Z. (2020). Verification of ClimateCypher Climate Data Outputs with System Advisor Model (SAM), *Proceeding from Asia Pacific Solar Research Conference*. Sydney (Australia), 16-17 December.
- Hameed, N. A., Lee, T., Anderson, G. & Deng, Z. (2020). Verification of ClimateCypher Climate Data Outputs with System Advisor Model (SAM), *Proceeding from Asia Pacific Solar Research Conference*. Melbourne (Australia), 30 November-2 December.
- Hensen, J.L.M. & Lamberts R. (Eds). (2011). *Building Performance Simulation for Design and Operation*. Routledge. London (UK).
- Homaei, S., & Hamdy, M. (2021). Thermal resilient buildings: How to be quantified? A novel benchmarking framework and labelling metric. *Building and Environment*, 201, 108022.
- Hui, S. C., & Cheung, K. P. (1997, September). Multi-year (MY) building simulation: is it useful and practical. *Proceedings from 5th International IBPSA Conference Building Simulation '97*. Prague (Czech Republic), 8-10 September.
- Katal, A., Mortezaadeh, M., & Wang, L. L. (2019). Modeling building resilience against extreme weather by integrated CityFFD and CityBEM simulations. *Applied Energy*, 250, 1402-1417.
- Lee T., Ferrari D., Jain N. & Tarquini D. (2022) Improved Real-Time Year weather data services with Bureau of Meteorology data. *Proceedings AIRAH-IBPSA Australasian Building Simulation Conference 2022*, Brisbane, Australia, July.
- Mann, P. S., (2010). *Introductory Statistics*, John Wiley & Sons, New Jersey (United States)
- Narowski, P., Janicki, M., & Heim, D. (2013). Comparison of Untypical Meteorological Years (UMY) and their influence on building energy performance simulations. *Proceeding from Building Simulation*. Chambery (France), 26-28 August.
- National Renewable Energy Laboratories (2020). SAM Help, NREL, (United States)

Nik, V. M. (2016). Making energy simulation easier for future climate–Synthesizing typical and extreme weather data sets out of regional climate models (RCMs). *Applied Energy*, 177, 204-226.

Nik, V. M. (2017). Application of typical and extreme weather data sets in the hygrothermal simulation of building components for future climate–A case study for a wooden frame wall. *Energy and Buildings*, 154, 30-45.

Pérez-Lombard, L., Ortiz, J., & Pout, C. (2008). A review on buildings energy consumption information. *Energy and buildings*, 40(3), 394-398.

Rafique, M. M., & Rehman, S. (2018). *Renewable and Sustainable Air Conditioning. Sustainable Air Conditioning Systems*. IntechOpen.

Stopps, H., & Touchie, M. F. (2020). Managing thermal comfort in contemporary high-rise residential buildings: Using smart thermostats and surveys to identify energy efficiency and comfort opportunities. *Building and Environment*, 173, 106748.

DISCLAIMER

The information or advice contained in these technical papers is intended for use only by professionals who have had adequate technical training in the field to which the paper relates. At the time of publication, these technical papers have undergone a formal peer-review process.

These documents have been compiled as an aid only, and the information or advice should be verified before it is put to use. The user should also establish the applicability of the information or advice in relation to any specific circumstances. While the information or advice is believed to be correct, no responsibility is taken by AIRAH or IBPSA Australasia for any statements made within.

AIRAH and IBPSA Australasia, its officers, employees and agents, disclaim responsibility for any inaccuracies contained within the documents, including those due to any negligence in the preparation and publication of the said technical papers.

COPYRIGHT

This work is copyright. Apart from any use as permitted under the Copyright Act 1986, no part may be reproduced by any process without prior written permission from either the Australian Institute of Refrigeration, Air Conditioning and Heating (AIRAH) or the International Building Performance Simulation Association (IBPSA) Australasia.

DEVELOPMENT OF A WHOLE HOUSE ENERGY RATING TOOL FOR NEW HOUSING

ZHENGGEN REN PHD
Principal Research Scientist
CSIRO Energy
Research Way Clayton VIC 3168
Zhengen.ren@csiro.au

AI JIAN
Software Engineer
CSIRO Energy
Research Way Clayton VIC 3168
Ai.jian@csiro.au

DONG CHEN PHD
Senior Principal Research Scientist
CSIRO Energy
Research Way Clayton VIC 3168
Dong.chen@csiro.au

ABOUT THE AUTHOR

Dr Zhengen Ren is a principal research scientist at the CSIRO Energy Division, where he manages the development of decision support tools (such as the AusZEH design tool and WoH software tools for new and existing houses) to simulate energy consumption for residential buildings. He is also a key member for further development of the Chenath engine and AccuRate for the Nationwide House Energy Rating Scheme.

Zhengen has extensive experience and expertise relating to building energy performance simulation, ventilation and indoor environment, zero-energy housing, and off-grid houses in Australia. He has published more than 100 peer-reviewed papers and technical reports on the related work.

In 2002, Zhengen completed his PhD at Queen's University Belfast, where his work focused on indoor environment.

ABSTRACT

In 2019, Energy Ministers agreed the Trajectory for Low Energy Buildings (the Trajectory). One of the key aspects in the Trajectory for residential buildings is to expand Nationwide House Energy Rating Scheme (NatHERS) to offer nationally accredited whole-of-home (WoH) tools to enable compliance requirements in the National Construction Code (NCC). CSIRO was commissioned by the NatHERS Administrator to develop a benchmark WoH tool in the required timeframe. For this purpose, the WoH tool was developed by implementing new modules for space heating and cooling, water heating, lighting, swimming pool, other appliances, solar PV and battery into the modified version of AusZEH design tool. The initial version of the tool was released in December 2019 for evaluation. After receiving feedbacks

of stakeholders, the WoH tool was recently updated with the extensive input from the NatHERS Technical Advisory Committee (TAC) and other industry experts.

INTRODUCTION

In February 2019 the Council of Australian Governments (COAG) Energy Council agreed on the Trajectory, which identified cost effective opportunities for energy efficiency improvements through the building system, from building envelope thermal performance to appliance energy usage and renewable energy generation. In summary, the Trajectory aims to:

- Set a trajectory towards zero energy (and carbon) ready buildings;
- Implement cost-effective increases to the energy efficiency provisions in NCC 2022; and
- Expand NatHERS to offer nationally accredited WoH tools to enable verification requirements in the NCC.

The consultation draft of NCC 2022 was released in August 2021 by the Australian Building Codes Board (ABCB). A WoH annual energy use budgets for Class 1 and Class 2 dwellings were proposed in the amendments of the consultation draft. The annual energy use includes space heating and cooling, water heating, lighting and pool and spa pumps. The annual energy use budget is based on ‘societal cost of energy’, which is related to infrastructure (e.g. grid stress, requirements of energy storage etc.) and environmental impacts (e.g. global warming caused by carbon emissions). Societal cost includes the cost of energy used by the building and the broader ‘cost’ to society for the use of that energy. Societal energy costs associated with energy use are dependent on time of use and the energy supply mix. Please refer to the ABCB Scoping Study [1] for details of how the societal cost of energy is defined. If the residential building is installed with on-site renewable energy systems (e.g., rooftop PV), this can provide an offset to the societal cost of the energy used in the building.

To support the objectives of the Trajectory, including the proposed energy efficiency provisions for NCC 2022, the NatHERS is being expanded to provide WoH energy assessments and ratings. Since February 2019 the NatHERS Administrator has held discussions with NSW Planning and Environment, the Victorian Department of Environment, Water, Land and Planning, Sustainability Victoria and CSIRO regarding tool harmonisation opportunities. After these discussions, the consensus was that a WoH benchmark tool under the NatHERS framework should be developed. CSIRO was commissioned to deliver a benchmark WoH tool in the required timeframe.

A Technical Expert Panel (TEP) and workshops were organised by NatHERS Administrator to seek recommendations from the TEP to inform the policy agreement on assumptions/settings behind whole of house modules for tools. Following these assumptions/settings, CSIRO developed a WoH tool by implementing new modules for water heating, lighting, swimming pool, other appliances, and solar PV battery into the modified version of the AusZEH design tool [2, 3]. The energy requirement for space heating and cooling was estimated by the Chenath engine. The energy efficiency of HVAC and other appliances refers to the Equipment Energy Efficiency [4] program, one of the programs implemented by the COAG Energy Council. The initial version of the tool was released in December 2019 for evaluation. After receiving feedbacks of stakeholders, the WoH tool was recently updated with the extensive input from the TEP and other industry experts. This report details the modules implemented in the WoH tool.

1. IMPLEMENTING MODULES INTO THE AUSZEH DESIGN TOOL

The Whole of Home framework builds on the existing NatHERS framework and technology. The CSIRO Chenath engine is applied to calculate energy requirements for space heating and cooling with hourly data over a period of one year. In collaboration with the NatHERS TAC and other industry experts, methods were developed for calculating the energy demand of a home [5], including space heating and cooling appliances, hot water system, lighting, pool and spa pumps, on-site solar PV system, on-site battery and plug in appliances.

1.1 Space heating and cooling

Hourly energy use for a zone is calculated using Equation 1:

$$E_{z,hr} = \frac{L_{z,hr}}{(1-LS) \times COP_A} \quad (1)$$

where

$E_{z,hr}$ = hourly energy use for the zone (MJ)

$L_{z,hr}$ = hourly energy load for the zone (MJ) calculated using the Chenath engine

COP_A = coefficient of performance for the specified appliance, detailed in [5]

LS = the system loss specified for the system type (e.g., ductwork), default losses for specified equipment losses are set out in Table 1.

Note that a constant COP_A value is applied in the energy consumption calculation for a specified HVAC system as the system is not modelled actively by the Chenath engine.

Equipment type	Default system loss LS
Ducted systems (less than 10 years old)	15%
Ducted systems (more than 10 years old)	25%
Hydronic heaters (panel type)	10%
Concrete slab heating (any type)	15%
Other non-ducted systems	15%

Table 1. *Default system losses for specified equipment types*

Note that for window or wall mount heating and cooling equipment, the system loss is assumed to be ignored.

Currently, for the NatHERS thermal performance calculation the home is assumed to be fully occupied all the time (24 hours per day, 365 days per year), and the Chenath Engine therefore ensures that the temperature remains within the comfort band at all times. Feedback of stakeholders suggests this fully occupied profile may be representative of some household types, but may not be appropriate for other household structures where absence during the day will impact on how and when energy is used in the home. The Whole of Home Occupancy Working Group recommended that for Whole of Home calculations a dual occupancy profile approach shall be applied to estimate thermal loads for calculating heating and cooling

equipment energy use. For the development of this WoH tool, two different occupancy profiles in NCC2022 of ‘All-Day’ and ‘Work-Day’ in combination are used to calculate whole home energy consumption. Consequently, the WoH tool will undertake two separate calculations using two different occupancy profile assumptions. These two separate calculations are:

- The single profile of ‘Fully Occupied’ is applied for the dwelling’s thermal performance assessment (i.e., the existing NatHERS star rating).
- The dual profiles of ‘All-Day’ and ‘Work-Day’ is used for the dwelling’s Whole of Home assessment (energy consumption and productions from appliances).

To obtain a single combined WoH assessment result for a parameter of interest (e.g., energy consumption for space heating/cooling), the values obtained for each of the separate performance assessments (All-Day and Work-Day) must be weighted using Equation 2:

$$P_{WoH} = 0.6 \times P_{All-Day} + 0.4 \times P_{Work-Day} \quad (2)$$

where

P_{WoH} = the weighted value of the subject parameter

$P_{All-Day}$ = the value of the subject parameter as assessed using the All-Day occupancy profile

$P_{Work-Day}$ = the value of the subject parameter as assessed using the Work-Day occupancy profile

1.2 Water heating

Research carried out by Energy Efficient Strategies in 2019 [6] identified a recommended daily hot water allowance per occupant, and equations to determine the annual energy use of different hot water systems was developed. This approach was confirmed by the NatHERS Whole of Home Water Heater Working Group in 2021. The energy used by the hot water system is mainly determined by three components:

- Hot water demand (by households)
- Location (Solar climate zones 1-4 plus Heat Pump HP5-AU)
- Hot water system type

It is assumed that 40 L hot water is required per person per day winter peak demand. Using the same approach as used for the NatHERS thermal performance assessment [5], the number of occupants is calculated using Equation 3:

$$N_{Occ} = 1.525 \ln(A_D) - 4.533 \quad (3)$$

Where

N_{Occ} = number of the occupants in the dwelling, the valid range between 1 and 6, and rounded to be the nearest 2nd decimal place – i.e.#.xx

A_D = area of the dwelling (m²), defined as the total floor area of all zones, excluding the garage

The winter peak hot water demand can be estimated as:

$$K_{wp} = \frac{40 \times N_{Occ}}{y} \quad (4)$$

where

K_{wp} = the winter peak hot water demand (MJ/day)

N_{Occ} = the number of occupants in the dwelling

y = the average Litres of hot water per MJ for a 1MJ peak load in Winter by climate zone, shown in Table 2.

Climate	Zone 1 and HP1-AU	Zone 2 and HP2-AU	Zone 3 and HP3-AU	Zone 4 and HP4-AU	HP5-AU
L/MJ (y)	6.144	5.482	5.107	4.746	4.514

Table 2. Average water volume per MJ winter peak hot water demand by climate zone

Note that for the purposes of simulation under AS/NZS 4234, the assumed conditions for heat pumps in zones HP1-AU to HP4-AU are the same as Zones 1 to 4 for other types of water heaters.

The annual energy demand is defined in Equation 5:

$$E_{wd} = \frac{365 \times 0.904521 \times K_{wp}}{1000} \quad (5)$$

where

E_{wd} = the annual hot water energy demand (GJ/year)

K_{wp} = the winter peak hot water demand (MJ/day)

365 is days in a standard year, 1000 is a factor to convert MJ to GJ, and 0.904521 is a factor to convert a winter peak demand MJ/day into an average annual daily demand, taking into account days per month and the seasonal hot water demand profile in AS/NZS 4234.

Based on a third order polynomial with coefficients for each specific water heater type in each climate zone, the annual energy input E_{wi} can be estimated from the annual energy demand E_{wd} in Equation 6:

$$E_{wi} = a \times E_{wd}^3 + b \times E_{wd}^2 + c \times E_{wd} + d \quad (6)$$

where

E_{wi} = the annual hot water energy purchased (energy input) in MJ/year

E_{wd} = the annual hot water energy demand in GJ/year from Equation 5

All coefficients a , b , c , and d for each specific water heater type in each climate zone are detailed in Appendix B of [5].

The water heaters that are currently covered are:

- Solid fuel
- Off-peak electric (assumes ‘large’ MEPS compliant storage unit)
- Continuous electric (assumes ‘small’ MEPS compliant storage unit)
- Instantaneous electric
- Electric boosted solar thermal – a range of sizes and performance levels
- Gas boosted solar thermal – a range of sizes and performance levels
- Heat pump – a range of sizes and performance levels
- Gas storage (4.0, 4.5 or 5.0 stars)
- Gas instantaneous (4.0 to 7.0 stars in 0.5star increments)

Taking into account the monthly energy profile and the days per month in a standard year, the share of hot water demand from the water heater by month is set out in Table 3, which is also used to allocate annual energy into month for instantaneous water heaters. For other type of heaters, the share of purchased energy by month is detailed in [5].

Month	Hot water demand	Month	Hot water demand
Jan	6.5728%	Jul	9.3897%
Feb	6.7848%	Aug	9.3897%
Mar	7.9812%	Sep	9.0868%
Apr	8.1781%	Act	8.9202%
May	8.9202%	Nov	8.1781%
Jun	9.0868%	Dec	7.5117%

Table 3. Share of hot water demand by month for all climate zones

Daily energy use can be calculated using Equation 7:

$$E_{d,m} = \frac{F_{m,z} \times E_{wi}}{Days_m} \quad (7)$$

where

$E_{d,m}$ = daily energy consumption for relevant month water heating (MJ/day)

$F_{m,z}$ = factor for relevant month and climate zone as specified in Table 3 or detailed in [5].

E_{wi} = the annual hot water energy purchased (MJ/year)

$Days_m$ = number of days in the specified month in a standard year (365days for a year)

Hourly loads will depend on the type of water heater and the energisation profile. Some initial assumptions regarding time of energy input into the water heater are defined in [5].

The hourly breakdown of energy is defined using Equation 8:

$$E_{hourly} = F_{hourly} \times E_{d,m} \quad (8)$$

where

E_{hourly} = hourly energy use for hot water (MJ/hour)

F_{hourly} = factor of relevant hour defined in [5]

$E_{d,m}$ = daily energy consumption for relevant month water heating (MJ/day), defined in Equation 7

1.3 Lighting module

The annual energy consumption for lighting is calculated using Equation 9:

$$E_{tot} = \frac{365 \times P_L \times H_{avg} \times A_{tot} \times 3.6}{1000} \quad (9)$$

where

E_{tot} = total annual energy consumption for lighting (MJ)

P_L = light power density (W/m^2), 5 W/m^2 is used as default in this development

H_{avg} = average hours for lighting use per day (hours), 1.6 hours are used for this development

A_{tot} = the total floor area (m^2), excluding garage zone, subfloor, roofspace, glazed common area and basement car park zones

365 is days per year, 3.6 converts kWh to MJ, and 1000 converts Wh to kWh.

Not all lights are on at the same time, and therefore the lighting load should be distributed across the day. An average hourly use is therefore calculated, based on the number of hours per day that any lights are assumed to be on. All outputs are to be broken down by hour, which is defined in Table 37 of [5].

Hourly energy consumption for lighting is calculated using Equation 10:

$$E_{m,hr} = E_{tot} \times F_{L,hr} \quad (10)$$

where

$E_{m,hr}$ = hourly energy consumption for lighting (MJ/hour)

E_{tot} = total annual energy consumption for lighting (MJ), calculated by Equation 9

$F_{L,hr}$ = lighting hourly factor, defined by Table 37 of [5].

Note that although heat from lighting is considered in the internal heat gains for thermal performance simulation by Chenath engine, but it is not integrated with the outputs calculated by Equation 10.

1.4 Pool and spa equipment module

Pool pump energy consumption is assumed to be primarily driven by the size of the pool and the type of pump used. If pool volume is known, pool volume is directly entered by the user. If pool volume is not known, the user should estimate pool volume based on pool surface area using Equation 11:

$$V_p = 1.5A_p \times 1000 \quad (11)$$

where

V_p = pool volume (L)

A_p = pool area (m^2)

Base pump sizes are assumed to correlate with pool size, which is defined in Equation 12:

$$Base\ Size\ (kW) = \frac{0.0598V_p^{0.9377}}{1000} \quad (12)$$

Pump energy is based on the pump size and the efficiency of the system. Three types of pump speed are included in this study: single speed, dual speed and multi speed.

Pump operating power reflects the average power of the pool pump across its operating cycle, which is calculated using Equation 13:

$$Operating\ Power = Base\ Size \times Power\ Adjustment\ Factor \quad (13)$$

Power adjustment factor is defined in Table 4.

Type	Power adjustment factor
Single Speed	1
Dual Speed	0.336
Multi Speed	0.113

Table 4. Power adjustment factor for pool pumps

If the star rating under the 2019 GEMS determination is known, this can be entered by the user.

If the star rating is not known, it is estimated based on pump technology. This is defined in Table 5.

Pump type	Star Rating
Single Speed	2
Dual Speed	5
Multi-Speed	8

Table 5. Assumed pump star rating

With the pump star rating, a weighed energy factor is required to calibrate star rating against the pump size using Equations 14 and 15:

$$WEF = e^{((SR-1) \times \ln(1.25) + \ln(Baseline))} \quad (14)$$

$$Baseline = -4.5 \ln(Base Size) + 13.5 \quad (15)$$

where

WEF = weighed energy factor (L/wh)

SR = star rating

Base Size = base pump size defined in Equation 12

Average flow rate is calculated using Equation 16:

$$Flow Rate = WEF \times Operating Power \times 1000 \quad (16)$$

where

Flow Rate = average flow rate (L/hr)

The Run Time, in hours, required to cycle the pool once is calculated using Equation 17:

$$T_{Cyc} = \frac{V_p}{Flow Rate} \quad (17)$$

where

T_{Cyc} = Run Time, rounded up to the nearest whole integer (i.e., 5.99 = 6, 6.01 = 7)

Pool pumps are assumed to run longer during swimming seasons than non-swimming seasons. Pumps are assumed to be turned on a set time, and run until the required number of cycles is achieved. Pump off time is defined by Equation 18:

$$Off\ Time = [On\ Time] + T_{Cyc} \times [Cycles\ per\ Days] \quad (18)$$

The pump schedule is defined in Table 6.

Cycles per day	On Time
1	8:00 am

Table 6. Pool pump operating schedule

Cleaning energy is different depending upon filter and pump type, which is detailed in [5].

1.5 Plug loads

Apart from equipment already covered in the previous sections of this report, this section will address energy consumption for other equipment, such as whitegoods, audio visual, small appliances, computers and peripherals, other electronic and standby power.

In this development, the assumed annual plug loads have been based on work undertaken previously for Sustainability Victoria and the Australian Building Codes Board (ABCB). From this work annual average total plug loads per number of occupants were derived, which are calculated using Equation 19:

$$E_{Plug} = 7022.4 + N_{Occ} \times 441.65 \quad (19)$$

where

E_{Plug} = total annual plug energy load (MJ/year)

N_{Occ} = number of occupants in the home, defined in Equation 3

Plug loads are not evenly distributed across the day or cross the seasons. The annual plug load value is broken down into hourly loads across the year based on the expected distribution of those loads across the year. Hourly loads of plug loads are calculated using Equation 20:

$$E_{Plug.hr} = E_{Plug} \times F_{Plug.hr} \quad (20)$$

where

$E_{Plug.hr}$ = hourly energy load for hour of day in each month (MJ)

E_{Plug} = total annual plug energy load (MJ/year)

$F_{Plug.hr}$ = hourly plug load factor for hour of day in month, defined in [5] (Tables 44 and 45 of [5] for All-day profile and for Work-day profile, respectively)

1.6 On-site energy generation and battery storage

The power output from a PV array can be calculated using Equation 21:

$$E_{sol} = f \times Y \times \frac{I_T}{1000 \times I_S} \quad (21)$$

where

E_{sol} = the power output from a PV array (kW)

Y = the rated capacity of the PV array (kW), sometimes called the peak capacity of the PV array, the amount of power it would produce under standard test conditions of a panel with 25°C and 1kW/m² irradiance

I_S = the standard amount of radiation used to rate the capacity of the PV array (1kW/m²)

I_T = the global solar radiation incident on the surface of the PV array (W/m²), which is detailed in [5,7]

f = the PV derating factor, considering system losses, impacts of shading, etc.

1000 converts W to 1kW.

1.6.1 PV system losses

The total system losses include ambient temperature related losses, soiling relating losses, DC wiring relating losses, and conversion losses. The total system losses are calculated using Equation 22:

$$L_{TOT} = (1 - L_A) \times (1 - L_S) \times (1 - L_W) \times (1 - L_C) \quad (22)$$

where

L_{TOT} = total PV system loss factor

L_S = soiling related losses, varying depending on the site and washing practices, a default value of 5% is used for this development

L_W = DC wiring losses, varying based on circuit length and conductor thickness, a default value of 3% is used for this study

L_C = conversion losses, varying slightly based on the inverter and its loading, a default value of 3% is used for this study

L_A = the ambient temperature related losses (%), which is calculated for each hour using Equation 23:

$$L_A = [(T_{amb} + 0.03125 \times G_{inc}) - 25] \times 0.4 \quad (23)$$

where

T_{amb} = the ambient air temperature (°C)- the dry bulb temperature in the climate file for that hour

G_{inc} = the incident radiation (W), derived from the climate file for that hour

Considering the system losses, the hourly PV generation is calculated by Equation 24:

$$E_{solD} = E_{sol} \times L_{TOT} \quad (24)$$

where

E_{solD} = electricity generated by the solar PV system for 1 hour (kWh)

E_{sol} = electricity generated by the solar PV panel before system losses for 1 hour (kWh), see Equation 21

L_{TOT} = total PV system loss factor, see Equation 22

The output of PV generation with de-rating factor must be limited according to the capacity (C_i) of the associated inverter (i.e., $E_{solD} \leq C_i$).

1.6.2 Battery storage

A battery may be used to store the excess generation from solar PV that exceeds hourly demand for electricity of the household in any given hour for use at a later time (e.g., at night time). The complexity of modelling the performance of batteries depends significantly on the technology. In this study, batteries are modelled as simple energy storage tanks (as applicable to Lithium-ion batteries) and the battery control system is assumed to be a basic system that is not responsive to either the expected future load profile or current or future network price signals. Whenever excess generation is available, it is stored and whenever on-site demand exceeds available supply from a PV system, then the battery is used to make up any shortfall in any particular hour (all subject to the charge, discharge and capacity limitations of the battery) [5].

CONCLUSION

With the extensive input from the NatHERS TAC and other industry experts, the WoH tool for new houses was significantly updated, including module updating of space heating and cooling, water heating, lighting and solar PV, and additional modules of battery and other plug-in loads. With requirement of NCC 2022, the 2005 RMY weather files were upgraded to 2016 RMY weather files and related space heating and cooling load limits were implemented. For whole house energy consumption calculation, the Chenath engine was modified to simulate two occupancy profiles of ‘All-day’ and ‘Work-day’.

REFERENCES

- [1] Australian Building Codes Board (2019). Energy efficiency – NCC 2022 and beyond scoping study (Available from <https://consultation.abcb.gov.au/engagement/energy-efficiency-scoping-study-2019/>, accessed on 21 December 2021).
- [2] Ren, Z., Foliente, G., Chan, W., Chen, D., Ambrose, M. and Paevere, P. (2013). A model for predicting household end-use energy consumption and greenhouse gas emissions in Australia. *International Journal of Suitable Building Technology and Urban Development* 4, 210-228.
- [3] Ren, Z., Chen, D. and James, M. (2018). Evaluation of a whole-house energy simulation tool against measured data. *Energy and Buildings* 171, 116-130.
- [4] Energy Rating: The Equipment Energy Efficiency (E3) Program (Available from <https://energyrating.gov.au/about>, accessed on 22 December 2021).
- [5] Nationwide House Energy Rating Scheme (2021). Draft NatHERS whole of home national calculation methods. Draft Version 3.0, November 2021, Personal communication (not available to public yet at this stage).
- [6] Energy Efficient Strategies (2019). Review of hot water energy consumption data as input to the whole of house rating proposal under NatHERS.
- [7] Ren, Z., Jian, A. and Chen, D. (2019) Development of Whole-of-Home (WoH) energy rating tool. CSIRO report ETB R-212783-01 submitted to Australian Government Department of Industry, Science, Energy and Resources.

DISCLAIMER

The information or advice contained in these technical papers is intended for use only by professionals who have had adequate technical training in the field to which the paper relates. At the time of publication, these technical papers have undergone a formal peer-review process.

These documents have been compiled as an aid only, and the information or advice should be verified before it is put to use. The user should also establish the applicability of the information or advice in relation to any specific circumstances. While the information or advice is believed to be correct, no responsibility is taken by AIRAH or IBPSA Australasia for any statements made within.

AIRAH and IBPSA Australasia, its officers, employees and agents, disclaim responsibility for any inaccuracies contained within the documents, including those due to any negligence in the preparation and publication of the said technical papers.

COPYRIGHT

This work is copyright. Apart from any use as permitted under the Copyright Act 1986, no part may be reproduced by any process without prior written permission from either the Australian Institute of Refrigeration, Air Conditioning and Heating (AIRAH) or the International Building Performance Simulation Association (IBPSA) Australasia.

FUTURE CHANGES TO BUILDING CODE ENERGY EFFICIENCY PROVISIONS FOR COMMERCIAL BUILDINGS

GRACE FOO, B.ENG (HONS)

Principal Consultant

DeltaQ Pty Ltd

sg.foo@dqcs.com.au

DR PAUL BANNISTER

Director of Innovation

DeltaQ Pty Ltd

Paul.bannister@dqcs.com.au

HONGSEN ZHANG

Director

Enerefficiency Pty Ltd

Hongsen.zhang@enerefficiency.com

ABOUT THE AUTHOR

Grace Foo is Principal Consultant at DeltaQ, coordinating the team to deliver the technical analysis assessing the future trajectory of the energy efficiency provisions for commercial buildings in the National Construction Code. Grace is also a Climate Active registered consultant, advising clients on pathways towards Carbon Neutral and Net-Zero. To keep her grounded on the practicalities of achieving net-zero buildings, she continues to be involved in deep retrofit projects, conducting due diligence on pre-loved building performance potential and project managing implementation of identified opportunities. She is an Energy Efficiency Council (EEC) Certified Energy Efficiency Leader (CEEL).

ABSTRACT

The National Construction Code (NCC) provisions for energy efficiency in commercial buildings were extensively updated in 2019 with an effective increase in stringency of over 30% relative to 2016 (Bannister and Zhang, 2017). This paper reports on preliminary work to consider how these provisions can be further enhanced for NCC 2025.

The results indicate that cost-beneficial energy improvements of the order of 29% of NCC2019 baseline regulated energy consumption is feasible, whilst maintaining occupant thermal comfort, even with buildings operating in future climate. Recommendations are derived for the onward process of Code development, learning from the experience of this preliminary study.

INTRODUCTION

The National Construction Code (NCC) provisions for energy efficiency in commercial buildings were extensively updated in 2019 with an effective increase in stringency of over 30% relative to 2016.

DeltaQ was contracted to provide an assessment of cost-effective energy performance potential of commercial buildings, intended to inform the Australian Building Codes Board (ABCB) work program. The foundational basis of this work was the 2018 low energy commercial buildings trajectory report (SPR and Energy Action, 2018), which was prepared using interim NCC2019 provisions before formal implementation of the NCC2019 code. DeltaQ updated the 2018 report, by using more realistic base case building archetypes compliant with the final NCC2019 DTS. The proposed changes extend the thermal comfort criterion currently in the NCC2019 Verification Methods to Deemed-to-Satisfy (DTS) provisions and account for the average future climate that the building is expected to operate in.

This paper reports on preliminary work to consider how these provisions can be further enhanced for NCC 2025. IES<VE> dynamic thermal simulations were used qualitatively to assess the energy performance for buildings compliant to NCC2019 and changes in energy efficiency measures in 2025, 2028 and 2034 building codes.

1. METHODOLOGY

The starting point for this process was a reconsideration of the building archetypes used for the assessment of efficiency measures. These should be as representative of new buildings as is possible, within the constraint that an archetype cannot represent the myriad of different building designs constructed. All archetypes were then configured to achieve NCC2019 compliance.

To assess potential efficiency improvements, packages of energy efficiency measures, including building fabric and HVAC improvements, were adapted from previous work and applied to the archetypes. Simulation models in IES<VE> 2021.1.1.0 and its detailed modelling packages ApacheHVAC and Radiance were used to predict the improvement in performance using future climate files, ensuring that the proposed measures result in a building that meets thermal comfort requirements (Predicted Mean Vote, PMV of ± 1). Thermal comfort requirements and modelling parameters are provided in Appendix 3. The future climate files used were RCP8.5 2050 climate files developed by the CSIRO (2021). The energy results were then fed into a cost-benefit analysis to achieve a minimum benefit-cost ratio of greater than 1.0.

As in most cases, the original package of measures achieved a benefit-cost ratio of greater than 1.0, so additional measures were tested to achieve greater energy savings while maintaining a whole-of-package benefit-cost ratio greater than 1.0. Note that the study concentrated on the development of the cost-effective package of measures rather than the assessment of each measure. As such, the incremental impact of each measure was not reinvestigated and would be expected to be firmed up for each building class as part of the detailed technical development for NCC2025 to be completed by the ABCB in 2022-23.

2.1 Simulated Building Archetypes

The process to redefine Australian building archetypes first identified representative building archetypes in industry using data from development approval applications for each building class in each climate zone capital city (ABS SA4)¹. This data was provided by Strategy Policy Research, as part of their work in updating the Australian Commercial Buildings Baseline Study. Strategy Policy Research used a bottom-up approach utilising CSIRO and Geoscape satellite data to estimate the average floor plate size and the number of building floors for each building class and climate zone. This information from Strategy Policy Research informed the starting points for the building size and number of floors; however, the data sources used did not indicate the building shapes.

To determine the building shape, a sample of satellite photos were used to identify general building shapes for each building class in the various climate zone capital cities. The combination of data sources and methods that informed the representative building sizes in Australia were audited by experts at the request of this project’s Advisory Group members – including two roundtable discussions organised by the Property Council of Australia.

Building shape only indirectly impacts a building’s energy consumption. The direct correlation to energy consumption is the surface-to-volume ratio, which is influenced by building shape. As such, the various building shapes identified were mapped to standardised aspect ratios published by Winiarski *et al.* (2008)’s work for the US Department of Energy (DOE), as shown in Table 1. This defines the aspect ratio of rectangular buildings as the ratio of the longest to the shortest wall, irrespective of building height. For all other building shapes, the ratio is an effective ratio of building footprint to the perimeter. These aspect ratios were used in the final building archetypes shown in Appendix 1 of this paper.

Building shape	Aspect Ratio
Square	1.0
Rectangle	2.0
Other shapes (L-shape, H-shape etc)	4.0

Table 1: Building shape and aspect ratios (Winiarski et al. 2008).

Further details on the modelled building archetypes are presented in Appendix 1.

2.1 Opaque construction

The baseline of opaque constructions critically affects economic final provisions due to the cost of the wall framing. Frameless wall construction, such as single-skin masonry walls, potentially cost more to insulate than framed construction because of the framing and lining costs necessitated by the addition of insulation. Informal industry interviews and roundtable discussions with industry informed base case opaque constructions that best represent the range of structures used in the market and the process by which these are typically insulated. Common construction techniques for the Northern Territory were informed by discussions with local builders and HVAC contractors in Darwin and Alice Spring, recognising the significant

¹ Statistical Areas Level 4 (SA4) are geographical areas built from whole Statistical Areas Level 3 (SA3s). The SA4 regions are the largest sub-State regions in the main structure of the Australian Statistical Geography Standard (ASGS), and have been designed for the output of a variety of regional data, including data from the 2016 Census of Population and Housing. These are defined by the Australian Bureau of Statistics (ABS).

differences in practice occurring in the Territory relative to the rest of the country. Further details on the modelled opaque construction are presented in Appendix 2.

2.1 Glazing

In the NCC2019 revision work, the glazing baseline was determined as the cheapest and smallest window that delivers a 3% to 5% daylight factor. For this study, the window-to-wall ratio (WWR) was taken from a study by Foo and Shen (2018) in which an empirical survey of the WWR of Australian commercial buildings was conducted for office, aged care, retail hospitals, education and hotel buildings. More detail regarding the specific WWR modelled in this study is provided in Appendix 1. The final glazing solution selected for the base case was the cheapest window² that could realistically be built to meet NCC2019 DTS requirements for the given window-to-wall ratio.

2.1 HVAC technology

The finalised building archetypes were assessed to establish appropriate plant types for each building class. Industry interviews were undertaken to inform this component of the work. Industry consultation also informed the chiller technology types that were mapped to building thermal load. HVAC technology customised for small offices (Class 5), small hotels (motels) (Class 3), retail shops (Class 6) and schools (Class 9b) building archetypes are all-electric. Only large building archetypes and the hospital ward still use gas boilers for space heating.

2. PROPOSED CHANGES

A range of measure packages was tested using the archetypes, and an iterative process was used to optimise the packages to achieve a national benefit-to-cost ratio (BCR) of 1 to 1.5, from a societal perspective. The resultant measures are described in this section. The national BCR calculations were conducted by economists Strategy Policy Research Pty Ltd.

2.2 Chillers and unitary AC efficiencies

Chiller efficiencies are set to current best practice levels for the technology type. The best practice chiller performance currently available in the market is used for the 2025 chiller performance. This is about a 35% improvement in full load efficiency and a sizeable 57% improvement in part-load efficiency relative to current NCC2019 Deemed-to-Satisfy (DTS) requirements. This is expected to be significant due to the tendency for chillers, particularly those in temperate and cooler climates, to operate at less than design full load.

Equipment	2025	
	COP	IPLV
Air-Cooled Chiller	4.02	6.43
Water-Cooled Chiller	6.29	11.18

Table 2. Summary of coefficient of performance (COP) and integrated part-load value (IPLV) changes for chillers.

² The capital costs for glazing were based on various industrial experts' estimation and supplier's retail prices provided upon inquiry. The values used are consistent with those used in the ASBEC *Built to Perform: An Industry Led Pathway to a Zero Carbon Ready Building Code* and 2018 Energy Action/SPR report *Achieving Low Energy Commercial Buildings in Australia*.

For unitary AC units such as split and package units, the improvement was calculated based on an increase in COP by 0.1 per annum from the current MEPS level in 2021. This modest ~10% improvement in 2025 reflects the historical increases in MEPS stringencies and the average efficiency of available units.

Unit Capacity	Current MEPS Level	2025
< 4kW	3.66	4.06
≥ 4kW and < 10kW	3.22	3.62
≥ 10kW and < 39kW	3.10	3.50
≥ 39kW	2.90	3.30

Table 3. Summary of coefficient of performance (COP) for unitary AC units.

2.3 Outside air treatment

Depending on the building type and climate, several measures for minimum outside air treatment were applied.

The use of dew point coolers³ on the dedicated outside air supply to temper minimum outside air when the occupied space requires cooling provides an additional 1 to 18% energy savings for a DTS-compliant building.

For heat recovery purposes, a plate heat exchanger or rotary wheel heat recovery system installed on the outside air duct allows heat and coolth to be recovered from the building relief air when conditions are beneficial. Otherwise, outside air heat recovery is bypassed.

Building type	Measure applicable to Climate Zone 2	Measure applicable to Climate Zone 5	Measure applicable to Climate Zone 6	Measure applicable to Climate Zone 7
Hotel	Dew point cooler	Dew point cooler	Plate heat exchanger + Dew point cooler	n/a
Hospital Ward	Thermal wheel	Thermal wheel	Thermal wheel	Thermal wheel
Office	Thermal wheel + dew point cooler	Thermal wheel + dew point cooler	Thermal wheel + dew point cooler	Plate heat exchanger + CO ₂ demand-controlled ventilation + dew point cooler
Retail shop	Dew point cooler	Dew point cooler	Plate heat exchanger + dew point cooler	Plate heat exchanger + dew point cooler
Schools	Dew point cooler	Plate heat exchanger + dew point cooler	Thermal wheel + dew point cooler	Thermal wheel + dew point cooler

Table 4. Summary of outside air treatment using dew point coolers and enhanced heat recovery measures for various buildings and climate zones.

2.4 Ductwork pressure reduction

For centralised air distribution systems, the pressure drop in the ductwork system was decreased by 25% from current NCC2019 DtS levels.

³ A dew point cooler utilises a network of air-to-air heat exchangers with alternating dry and wet channels to cool outside air to a temperature close to the dew point temperature, without added humidity to the supply air into the building. Due to size and cost practicalities, this study examined the use of dew point coolers on the dedicated outside air supply only.

2.5 Economy cycle

An economy cycle is applied to AHUs, regardless of supply airflow rates. Current DTS levels (NCC2019 Table J5.2) apply various climate-zone dependent minimum flow thresholds before an economy cycle is required.

2.6 Lighting control improvements

Lighting controls are occupancy controlled. In general, this was represented by a 20% reduction in the base case peak lighting load, which was set at the current NCC2019 modelling profiles for the verification method using a reference building (JV3).

Building type	Base case peak lighting load	2025 peak lighting load
Hotel	80%	60%
Office	100%	80%
School	95%	75%
Retail shop	100%	80%
Hospital ward	80%	60%

Table 5. Comparison of modelled lighting operating profile peak load in the base case (NCC2019) versus proposed NCC2025 changes.

2.7 Solar admittance control

The impact of reduced solar admittance was tested by reducing the window-to-wall ratio on modelled building archetypes found to have higher glazing ratios based on development application (DA) approvals in the past decade.

The window-to-wall ratio of the modelled buildings was set to achieve the natural daylight metric, spatial daylight autonomy (sDA) in the perimeter zone. The SDA levels were set to current LEED / Green Star requirements, i.e. at least 55% of occupied area achieves 300 lux for 50% of the occupied period. The use of SDA reflects the industry's feedback that daylight factor is not appropriate for Australian climates as it is based on a uniformly grey sky, which is more appropriate for climates such as the UK.

This measure was tested for the office and retail shop building archetypes, particularly those where the base case window-to-wall ratio exceed 50%. The resultant building archetypes have a window-to-wall ratio ranging between 30% and 40%.

2.8 External wall fabric colour

The external wall absorptance was set at 0.4, with the lighter colour decreasing solar radiation absorbed by the walls.

2.9 External wall insulation

External wall insulation was set at a level that avoids the need to increase standard stud frame depth (90mm) by double framing. This generally corresponds to the introduction of insulation to achieve total external wall R-values of 2 to 2.5. The current NCC2019 DTS minimum R-value requirement is 1.0.

2.10 Airtightness

Tightened building sealing was modelled by reducing the infiltration rate from 0.7 ACH to 0.15 ACH when the HVAC system is not operational. While the current NCC2019 DTS is

silent on performance requirements for building sealing, the new airtightness level is commensurate with airtightness in the newly introduced JV4 verification method for airtightness ($5\text{m}^3/\text{hr.m}^2$). The base case airtightness level of 0.7 ACH is taken from the current modelling guidelines in the NCC2019 when using the verification method using a reference building (JV3). Generally, this measure was only found to be cost-beneficial in cooler climate zones (6 and 7).

2.11 Glazing upgrade

Glazing selections are set to be tinted low-E double glazed units. This differs slightly depending on the orientation, but in general, window U-values of 2.4 and SHGC 0.21 were modelled.

2.12 External shading

To represent the potential for active and passive shading to be included in the NCC, external shutters controlled to maintain perimeter temperatures was modelled.

Building type	External Shading Applied?			
	Climate Zone 2	Climate Zone 5	Climate Zone 6	Climate Zone 7
Hotel	Yes	Yes	No	Yes
Hospital Ward	Yes	Yes	Yes	No
Office/School/ Retail shop	No	No	No	No

Table 6. Summary of external shading applications for building types and climate zone.

3. MODELLING RESULTS

Modelling of the combination of measure packages described above indicates that 29% unweighted building-level energy savings are available when calculated using the regulated energy intensity (NCC regulated energy divided by conditioned floor area). All modelled buildings meet the current Section J Verification Method thermal comfort requirement of Predict Mean Vote +/-1 in future climate. When the energy savings are weighted based on the projected gross floor area by building type across Australia, the weighted building-level energy savings is 26%.

Building type	Average Regulated Energy Intensity Reduction (%)
Hotel	16%
Office	26%
Retail Shop	22%
Hospital Ward	44%
School	36%
Unweighted Average Building-level Energy Savings	29%
Weighted average building-level energy saving (based on expected building stock area growth projection)	26%

Table 7. Summary of cost-effective building-level regulated energy savings, relative to NCC2019 DtS levels.

Table 8 shows the energy consumption intensity for each modelled building. The simple average energy consumption intensity is still a fair distance from net-zero energy, at 217MJ/m^2 .

Building type	Climate Zone	Energy Consumption Intensity (MJ/m ²)
3 Hotel	2	262
	5	245
	6	239
	7	213
5 Office	2	160
	5	129
	6	115
	7	113
6 Retail	2	450
	5	392
	6	321
	7	316
9a Hospital Ward	2	200
	5	138
	6	100
	7	147
9b School	2	279
	5	212
	6	145
	7	157

Table 8. Regulated energy intensity with energy efficiency measures package implemented in 2025

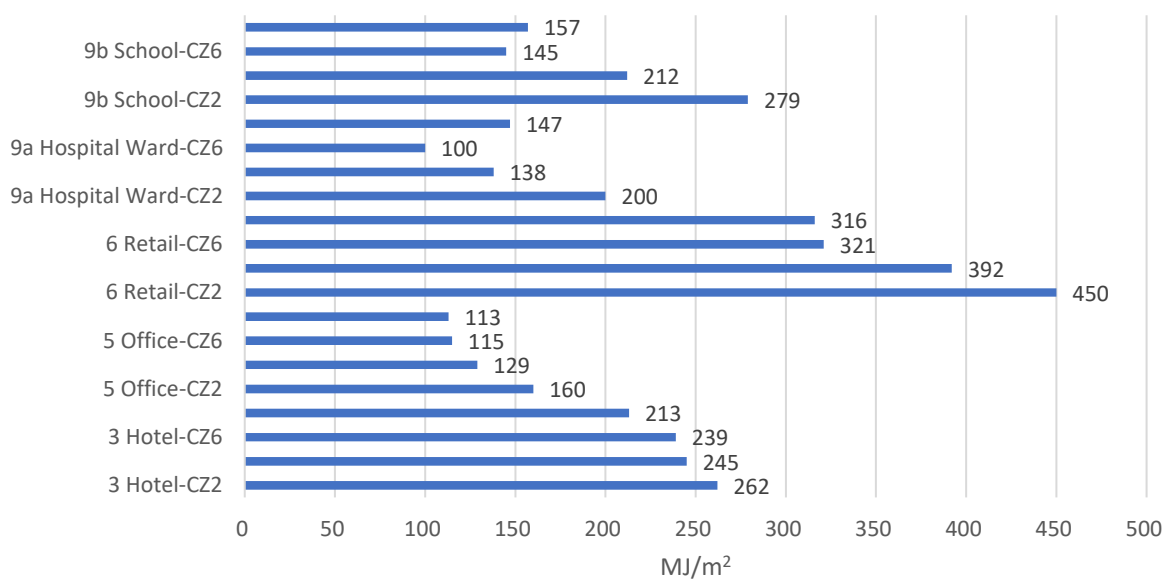


Figure 1. Regulated energy intensity with energy efficiency measures package implemented in 2025.

4. DISCUSSION

This study has found that there is still substantial energy savings potential by pursuing further energy efficiency improvements within the built environment. While building fabric changes such as higher wall-glazing thermal performance and natural efficiency improvements in air-conditioning equipment still form part of the measure packages, new opportunities for integration within the 2025 building code include:

- Prescription of air permeability or airtightness requirements
- Introduction of active or passive external shading on overnight buildings
- Outside air treatment, using a dew point cooler or enhanced heat recovery methods.
- Expansion of air-side economy cycle requirements to all air handling systems, regardless of size.
- Improving unitary air conditioning equipment efficiency performance, either by lifting the current GEMS (Greenhouse and Energy Minimum Standards) levels or by decoupling building code minimum standards from the GEMS levels.

However, it is not possible to achieve net-zero energy at the building level purely based on the above energy efficiency measures in 2025. In particular, on-site and off-site renewables are a critical addition to the zero-energy commercial building narrative. This topic has been explored further by the authors but is not reported here.

The study also revealed opportunities for further study:

- HVAC services could potentially be quantified via a whole-of-system coefficient of performance, making the Code truly technology-neutral.⁴ Similar concepts have been implemented in the US using the Total System Performance Ratio (TSPR) (Goel, S, Rosenberg, M, Gozalez, J and Lerond, J, 2021) and in Singapore via the Air Conditioning and Mechanical Ventilation (ACMV) Total System Efficiency (TSE). This approach would streamline Code provisions since those relevant to specific technologies would no longer be required, and they would keep pace with cost-efficient technology improvements in fans, chillers, and packaged AC.
- At the equipment level, the NCC could adopt a similar technology-neutral performance-based approach. Currently, the NCC specifies minimum efficiency levels for different fan and chiller technology types. Design decisions can result in inappropriate technologies for fans or chillers being selected, which could result in a substantial energy penalty even while meeting Code. This type of measure would promote better equipment selection and, to some extent, decouple the NCC from Greenhouse and Energy Minimum Standards (GEMS) standards for individual equipment. Efficiency improvements from this approach are likely to be substantial, given that fans and chillers dominate total energy consumption in commercial buildings.
- The Code technical development work for NCC2025 should consider the integration of fixed shading within DTS requirements for glazing, starting by redefining the functional parameters of a window based on spatial daylight autonomy (sDA), useful daylight illuminance (UDI) and/or glare. A revised basis for the treatment of the window-to-wall ratio will require the use of sDA or UDI to define the smallest and least cost window. In this study, we applied sDA to the current DTS measures and found that this led to significant excess daylighting and therefore solar heat gain and visual discomfort (glare)⁵. Furthermore, we found that simply decreasing window sizes was not always a practical solution to the issue.
- Future code development work should account that gas heating systems would not be practical in cooling-dominated climate zones or buildings with low residual gas

⁴ We note that the authors have been engaged to further research and quantify this opportunity, including how such a concept could be implemented within the NCC. It is acknowledged that careful specification will be required to avoid issues of gaming, such as detailed specification of parameters that should be used to calculate the whole-of-HVAC performance or via the use of dedicated software such as the US-developed Asset Score Tool.

⁵ SDA was used as the metric for this analysis following stakeholder feedback. Future work could re-examine this issue using the alternative metric, UDI.

consumption intensity. The technical development work for NCC2025 should consider the electrification of building heating systems particularly for buildings with very low residual gas consumption intensity and for buildings in cooling-dominated climate zones. Once cost-effective energy efficiency was modelled, the residual gas consumption intensity in all archetypes, except for two (hospital wards in climate zone 6 and 7), were lower than 10 MJ/m², a thermal capacity that could easily be serviced by a small electric heat pump available off-the-shelf. This applies to the majority of new buildings by area (>90%). There is therefore no commercial viability for continuing to model low gas intensity archetypes in the NCC or to design these in real buildings.

- Future work should consider the impact of tightened thermal comfort requirements. The PMV criterion of +/-1 was determined based on existing NCC requirements. At these values, 80% of occupants are satisfied and 20% of occupants are dissatisfied based on the design metabolic rate, clothing insulation, air temperature, radiant temperature, airspeed and humidity values modelled. However, the thermal comfort level set by the current NCC is less stringent compared to the ASHRAE Standard 55 definition of *comfort zone*, which is based on PMV +/-0.5. Furthermore, earlier work by the authors found existing work on the economic benefits of tightening of PMV⁶ in various buildings used for different economic activities was scarce, which makes it difficult to quantify the benefits of introducing such changes in the NCC in a regulatory impact statement (RIS). As such, technical research and development on more appropriate thermal comfort requirements should also be accompanied by corresponding research into economic benefits of such introductions.

5. CONCLUSIONS

This paper has found that there is still substantial potential for energy efficiency stringency improvements in the NCC2025 Section J DTS, relative to the current code. These measure packages were found to achieve a national benefit-to-cost ratio (BCR) above 1, indicating that the overall suite of measures is viable on a whole-of-economy basis.

Promising measures include both HVAC and building fabric. Specifically, more stringent requirements for air-conditioning equipment, a greater focus on outside air treatment via heat recovery and the use of dew point coolers, broader application of air-side economy cycle, greater focus on reduced solar admittance through a reduction in glazing ratios, upgraded glazing performance and introduction of external shading, control of heat transmitted through external walls using insulation and reduced solar absorptance, as well as improved airtightness.

Modelling of five case study buildings (office, school, retail shops, hotel and hospital ward) in four climate zones (2, 5, 6 and 7) under NCC2019 and proposed NCC2025 compliance scenarios show regulated energy intensity reductions in the region of 16% to 44%, with a weighted average regulated energy saving of 26%.

⁶ For example, the relationship between reduced comfort (in terms of PMV) and productivity could quantify the benefits of tightened comfort parameters in a Regulatory Impact Assessment for a building used for office workers but may not be appropriate for buildings such as retail, healthcare or schools. The definition of thermal comfort input parameters is also fraught with complexity and subject to gaming if not specified correctly. For example, comfort parameters for awake and sleeping conditions in a hotel are different; spaces which have different occupant attributes (e.g., shoppers versus workers in a retail environment, or healthcare workers versus patients in a hospital ward) also require different modelling parameters to be specified.

ACKNOWLEDGEMENTS

This work was funded by the Department of Industry, Science, Energy and Resources (DISER) on behalf of all States and Territories under the Trajectory for Low Energy Buildings, a national plan that sets a trajectory towards zero energy (and carbon) ready buildings for Australia.

The contributions and support of the consulting team at DeltaQ Pty Ltd, Strategy Policy Research (Philip Harrington) and Sam Moffitt in the research and analysis for this work are gratefully acknowledged.

REFERENCES

1. Bannister and Zhang (2017). Building Performance Improvements from NCC2019, AIRAH/IBPSA Australasian Building Simulation Conference Melbourne, November 2017
2. CSIRO (2021). Predictive weather files for building energy modelling. Accessed: <https://agdatashop.csiro.au/future-climate-predictive-wea20ther>
3. SPR and Energy Action (2018). Achieving Low Energy Commercial Buildings in Australia. Accessed: https://web.archive.org/awa/20210603110856mp_/https://energyministers.gov.au/sites/prod.energycouncil/files/publications/documents/Achieving%20Low%20Energy%20Commercial%20Buildings%20in%20Australia_0.pdf
4. Winiarski, D.W.; Halverson, M.A. and Jiang, W., (2008). “DOE’s Commercial Building Benchmarks - Development of Typical Construction Practices for Building Envelope and Mechanical Systems from the 2003 CBECS.” In Proceedings of 2008 Summer Study on Energy Efficiency in Buildings, American Council for an Energy-Efficient Economy
5. Foo, G. and Shen, D. (2018). “Australian Commercial Buildings Window to Wall Ratios.” In International Conference of the Architectural Science Association (pp. 231-240)
6. Goel, Supriya, Rosenberg, Michael I., Gonzalez, Juan, and Lerond, Jérémy. Total System Performance Ratio—A Systems Based Approach for Evaluating HVAC System Efficiency. United States: N. p., 2021. Web. doi:10.3390/en14165108.
7. Lan, L, Zhai, Z. and Lian, Z (2018). A two-part model for evaluation of thermal neutrality for sleeping people. Building and Environment Volume 132, 15 March 2018, (Pages 319-326)

APPENDIX 1

The archetypes used in this study were presented in Table 9 to Table 13.

Hotel (Class 3)	CZ2	CZ5	CZ6	CZ7
Building Shape	Rectangle	Square	Square	Rectangle
Total Area (m²)	9,680	10,240	11,748	2,904
Conditioned Area (m²)	9,280	8,800	8,800	2,520
Levels	10	10	10	3
Floor Plate (m²)	968	1,024	1,175	968
Aspect Ratio	2:1	1:1	1:1	2:1
WWR (glazing % of façade)	32%	32%	32%	16%
Floor to Ceiling Height (m)	2.7	2.7	2.7	2.7
Ceiling Space Height (m)	0.9	0.9	0.9	0.9
Underground Carpark	Y	Y	Y	N
Roof plant	Y	Y	Y	N
HVAC	DOAS, FCU, Central plant	DOAS, FCU, Central plant	DOAS, FCU, Central plant	Non-ducted reverse cycle split units
Chiller Air-cooled / Water-cooled?	Air-cooled screw chiller	Air-cooled screw chiller	Air-cooled screw chiller	n/a

Table 9: Overview of the building archetype for hotels (building class 3).

Office (Class 5)	CZ2	CZ5	CZ6	CZ7
Building Shape	Square	Square	Square	Rectangle
Total Area (m²)	12,250	12,250	7,350	3,456
Conditioned Area (m²)	11,040	11,040	6,624	3,120
Levels	10	10	6	3
Floor Plate (m²)	1,225	1,225	1,225	1,152
Aspect Ratio	1:1	1:1	1:1	2:1
WWR (glazing % of façade)	60%	60%	60%	35%
Floor to Ceiling Height (m)	2.7	2.7	2.7	2.7
Ceiling Space Height (m)	0.9	0.9	0.9	0.9
Underground Carpark	Y	Y	Y	N
Roof plant	Y	Y	Y	N
HVAC	VAV, AHU, Central plant	VAV, AHU, Central plant	VAV, AHU, Central plant	Heat pump – air-cooled reverse cycle PAC
Chiller Air-cooled / Water-cooled?	Air-cooled screw chiller	Air-cooled screw chiller	Air-cooled screw chiller	n/a

Table 10 Overview of the building archetype for offices (building class 5).

Retail (Class 6)	CZ2	CZ5	CZ6	CZ7
Building Shape	Rectangle	Rectangle	Rectangle	Rectangle e
Total Area (m²)	1,000	1,000	1,000	1,000
Conditioned Area (m²)	1,000	1,000	1,000	1,000
Levels	1	1	1	1
Floor Plate (m²)	1,000	1,000	1,000	1,000
Aspect Ratio	5:2	5:2	5:2	5:2
WWR (glazing % of façade) - North	57%	57%	57%	57%
WWR (glazing % of façade) – East and West	33.75%	33.75%	33.75%	33.75%
WWR (glazing % of façade) - South	0	0	0	0
Average WWR (glazing % of façade)	30%	30%	30%	30%
Floor to Ceiling Height (m)	6	6	6	6
Ceiling Space Height (m)	0.9	0.9	0.9	0.9
Underground Carpark	N	N	N	N
Roof plant	N	N	N	N
HVAC	Air-cooled heat pump	Air-cooled heat pump	Air-cooled heat pump	Air-cooled heat pump

Table 11: Overview of the building archetype, fabric and services for retail (building class 6).

Hospital Ward (Class 9aD)	CZ2	CZ5	CZ6	CZ7
Building Shape	Rectangle	Square	Rectangle	Rectangle
Total Area (m²)	8,900	9,697	2,890	2,880
Conditioned Area (m²)	7,200	7,392	2,746	2,736
Levels	9	6	2	1
Floor Plate (m²)	989	1,616	1,445	2,880
Aspect Ratio	5:1	1:1	5:1	5:1
WWR (glazing % of façade)	30%	30%	30%	30%
Floor to Ceiling Height (m)	3.3	3.3	3.3	3.3
Ceiling Space Height (m)	0.9	0.9	0.9	0.9
Underground Carpark	Y	Y	N	N
Roof plant	Y	Y	N	N
HVAC	VAV, AHU, Central plant	VAV, AHU, Central plant	VAV, AHU, Central plant	VAV, AHU, Central plant
Chiller Air-cooled / Water-cooled?	Water-cooled Centrif	Water-cooled Centrif	Water-cooled Centrif	Water-cooled Centrif

Table 12: Overview of the building archetype for hospital wards (building class 9a)

School (Class 9bE)	CZ2	CZ5	CZ6	CZ7
Building Shape	Rectangle	Rectangle	Rectangle	Rectangle
Total Area (m²)	2,304	3,456	3,456	2,304
Conditioned Area (m²)	2,048	3,072	3,072	2,048
Levels	4	3	3	2
Floor Plate (m²)	576	1,152	1,152	1,152
Aspect Ratio	2:1	2:1	2:1	2:1
WWR (glazing % of façade)	32%	32%	32%	32%
Floor to Ceiling Height (m)	3.3	3.3	3.3	3.3
Ceiling Space Height (m)	0.9	0.9	0.9	0.9
Underground Carpark	N	N	N	N
Roof plant	N	N	N	N
HVAC	Non-ducted reverse cycle split units	Non-ducted reverse cycle split units	Non-ducted reverse cycle split units	Non-ducted reverse cycle split units

Table 13: Overview of the building archetype, fabric and services for schools (building class 9b).

APPENDIX 2

Hotel (Class 3)	CZ2	CZ5	CZ6	CZ7
External wall	<ul style="list-style-type: none"> • 5mm metal cladding • 50mm air cavity • 0.8mm vapour barrier • Insulation • 13mm plasterboard 	<ul style="list-style-type: none"> • 5mm metal cladding • 50mm air cavity • Insulation • 13mm plasterboard 	<ul style="list-style-type: none"> • 5mm metal cladding • 50mm air cavity • Insulation • 13mm plasterboard 	<ul style="list-style-type: none"> • 5mm metal cladding • 50mm air cavity • Insulation • 13mm plasterboard
Roof	<ul style="list-style-type: none"> • 200mm concrete • 50mm air cavity • 0.8mm vapour barrier • Insulation 	<ul style="list-style-type: none"> • 200mm concrete • 50mm air cavity • Insulation 	<ul style="list-style-type: none"> • 200mm concrete • 50mm air cavity • Insulation 	<ul style="list-style-type: none"> • 0.48mm colorbond • Insulation
Ground contact floor	200mm concrete (carpark)	200mm concrete (carpark)	200mm concrete (carpark)	<ul style="list-style-type: none"> • 8mm carpet • 200mm concrete
Floor above underground carpark	<ul style="list-style-type: none"> • 8mm carpet • 200mm concrete • Insulation 	<ul style="list-style-type: none"> • 8mm carpet • 200mm concrete • Insulation 	<ul style="list-style-type: none"> • 8mm carpet • 200mm concrete • Insulation 	N/A
Internal floor	<ul style="list-style-type: none"> • 8mm carpet • 200mm concrete 	<ul style="list-style-type: none"> • 8mm carpet • 200mm concrete 	<ul style="list-style-type: none"> • 8mm carpet • 200mm concrete 	<ul style="list-style-type: none"> • 8mm carpet • 200mm concrete
Ceiling	13mm plasterboard	13mm plasterboard	13mm plasterboard	13mm plasterboard
Internal wall	<ul style="list-style-type: none"> • 13mm plasterboard • 70mm air cavity • 13mm plasterboard 	<ul style="list-style-type: none"> • 13mm plasterboard • 70mm air cavity • 13mm plasterboard 	<ul style="list-style-type: none"> • 13mm plasterboard • 70mm air cavity • 13mm plasterboard 	<ul style="list-style-type: none"> • 13mm plasterboard • 70mm air cavity • 13mm plasterboard
Core area wall	<ul style="list-style-type: none"> • 110mm brick • 70mm cavity • 13mm plasterboard 	<ul style="list-style-type: none"> • 110mm brick • 70mm cavity • 13mm plasterboard 	<ul style="list-style-type: none"> • 110mm brick • 70mm cavity • 13mm plasterboard 	<ul style="list-style-type: none"> • 110mm brick • 70mm cavity • 13mm plasterboard

Table 14: Details of the opaque construction (walls, floors, roofs) used to model hotels (building class 3)

Office (Class 5)	CZ2	CZ5	CZ6	CZ7
External wall	<ul style="list-style-type: none"> • 5mm metal cladding • 50mm air cavity • 0.8mm vapour barrier • Insulation • 13mm plasterboard 	<ul style="list-style-type: none"> • 5mm metal cladding • 50mm air cavity • Insulation • 13mm plasterboard 	<ul style="list-style-type: none"> • 5mm metal cladding • 50mm air cavity • Insulation • 13mm plasterboard 	<ul style="list-style-type: none"> • 5mm metal cladding • 50mm air cavity • Insulation • 13mm plasterboard
Roof	<ul style="list-style-type: none"> • 200mm concrete • 50mm air cavity • 8mm vapour barrier • Insulation 	<ul style="list-style-type: none"> • 200mm concrete • 50mm air cavity • Insulation 	<ul style="list-style-type: none"> • 200mm concrete • 50mm air cavity • Insulation 	<ul style="list-style-type: none"> • 0.48mm colorbond • Insulation
Ground contact floor	<ul style="list-style-type: none"> • 200mm concrete (carpark) 	<ul style="list-style-type: none"> • 200mm concrete (carpark) 	<ul style="list-style-type: none"> • 200mm concrete (carpark) 	<ul style="list-style-type: none"> • 8mm carpet • 200mm concrete
Floor above underground carpark	<ul style="list-style-type: none"> • 8mm carpet • 200mm concrete • Insulation 	<ul style="list-style-type: none"> • 8mm carpet • 200mm concrete • Insulation 	<ul style="list-style-type: none"> • 8mm carpet • 200mm concrete • Insulation 	N/A
Internal floor	<ul style="list-style-type: none"> • 8mm carpet • 200mm concrete 	<ul style="list-style-type: none"> • 8mm carpet • 200mm concrete 	<ul style="list-style-type: none"> • 8mm carpet • 200mm concrete 	<ul style="list-style-type: none"> • 8mm carpet • 200mm concrete
Ceiling	13mm plasterboard	13mm plasterboard	13mm plasterboard	13mm plasterboard
Internal wall	<ul style="list-style-type: none"> • 13mm plasterboard • 70mm air cavity • 13mm plasterboard 	<ul style="list-style-type: none"> • 13mm plasterboard • 70mm air cavity • 13mm plasterboard 	<ul style="list-style-type: none"> • 13mm plasterboard • 70mm air cavity • 13mm plasterboard 	<ul style="list-style-type: none"> • 13mm plasterboard • 70mm air cavity • 13mm plasterboard
Core area wall	<ul style="list-style-type: none"> • 110mm brick • 70mm cavity • 13mm plasterboard 	<ul style="list-style-type: none"> • 110mm brick • 70mm cavity • 13mm plasterboard 	<ul style="list-style-type: none"> • 110mm brick • 70mm cavity • 13mm plasterboard 	<ul style="list-style-type: none"> • 110mm brick • 70mm cavity • 13mm plasterboard

Table 15: Details of the opaque construction (walls, floors, roofs) used to model offices (building class 5)

Shop	CZ2	CZ5	CZ6	CZ7
External wall	<ul style="list-style-type: none"> • 5mm metal cladding • 50mm air cavity • 0.8mm vapour barrier • Insulation • 13mm plasterboard 	<ul style="list-style-type: none"> • 5mm metal cladding • 50mm air cavity • Insulation • 13mm plasterboard 	<ul style="list-style-type: none"> • 5mm metal cladding • 50mm air cavity • Insulation • 13mm plasterboard 	<ul style="list-style-type: none"> • 5mm metal cladding • 50mm air cavity • Insulation • 13mm plasterboard
Roof	<ul style="list-style-type: none"> • 0.48mm colorbond • 0.8mm vapour barrier • Insulation 	<ul style="list-style-type: none"> • 0.48mm colorbond • Insulation 	<ul style="list-style-type: none"> • 0.48mm colorbond • Insulation 	<ul style="list-style-type: none"> • 0.48mm colorbond • Insulation
Ground contact floor	<ul style="list-style-type: none"> • 8mm Vinyl tile • 200mm concrete 	<ul style="list-style-type: none"> • 8mm Vinyl tile • 200mm concrete 	<ul style="list-style-type: none"> • 8mm Vinyl tile • 200mm concrete 	<ul style="list-style-type: none"> • 8mm Vinyl tile • 200mm concrete

Shop	CZ2	CZ5	CZ6	CZ7
Floor above underground carpark	N/A	N/A	N/A	N/A
Internal floor	N/A	N/A	N/A	N/A
Ceiling	13mm plasterboard	13mm plasterboard	13mm plasterboard	13mm plasterboard
Internal wall	<ul style="list-style-type: none"> • 13mm plasterboard • 70mm air cavity • 13mm plasterboard 	<ul style="list-style-type: none"> • 13mm plasterboard • 70mm air cavity • 13mm plasterboard 	<ul style="list-style-type: none"> • 13mm plasterboard • 70mm air cavity • 13mm plasterboard 	<ul style="list-style-type: none"> • 13mm plasterboard • 70mm air cavity • 13mm plasterboard
Core area wall	N/A	N/A	N/A	N/A

Table 16: Details of the opaque construction (walls, floors, roofs) used to model retail (building class 6)

Ward	CZ2	CZ5	CZ6	CZ7
External wall	<ul style="list-style-type: none"> • 5mm metal cladding • 50mm air cavity • 0.8mm vapour barrier • Insulation • 13mm plasterboard 	<ul style="list-style-type: none"> • 5mm metal cladding • 50mm air cavity • Insulation • 13mm plasterboard 	<ul style="list-style-type: none"> • 5mm metal cladding • 50mm air cavity • Insulation • 13mm plasterboard 	<ul style="list-style-type: none"> • 5mm metal cladding • 50mm air cavity • Insulation • 13mm plasterboard
Roof	<ul style="list-style-type: none"> • 200mm concrete • 50mm air cavity • 8mm vapour barrier • Insulation 	<ul style="list-style-type: none"> • 200mm concrete • 50mm air cavity • Insulation 	0.48mm colorbond Insulation	0.48mm colorbond Insulation
Ground contact floor	<ul style="list-style-type: none"> • 200mm concrete (carpark) 	<ul style="list-style-type: none"> • 200mm concrete (carpark) 	<ul style="list-style-type: none"> • 8mm carpet • 200mm concrete 	<ul style="list-style-type: none"> • 8mm carpet • 200mm concrete
Floor above underground carpark	<ul style="list-style-type: none"> • 8mm carpet • 200mm concrete • Insulation 	<ul style="list-style-type: none"> • 8mm carpet • 200mm concrete • Insulation 	N/A	N/A
Internal floor	<ul style="list-style-type: none"> • 8mm carpet • 200mm concrete 	<ul style="list-style-type: none"> • 8mm carpet • 200mm concrete 	<ul style="list-style-type: none"> • 8mm carpet • 200mm concrete 	<ul style="list-style-type: none"> • 8mm carpet • 200mm concrete
Ceiling	13mm plasterboard	13mm plasterboard	13mm plasterboard	13mm plasterboard
Internal wall	<ul style="list-style-type: none"> • 13mm plasterboard • 70mm air cavity • 13mm plasterboard 	<ul style="list-style-type: none"> • 13mm plasterboard • 70mm air cavity • 13mm plasterboard 	<ul style="list-style-type: none"> • 13mm plasterboard • 70mm air cavity • 13mm plasterboard 	<ul style="list-style-type: none"> • 13mm plasterboard • 70mm air cavity • 13mm plasterboard
Core area wall	<ul style="list-style-type: none"> • 110mm brick • 70mm cavity • 13mm plasterboard 	<ul style="list-style-type: none"> • 110mm brick • 70mm cavity • 13mm plasterboard 	<ul style="list-style-type: none"> • 110mm brick • 70mm cavity • 13mm plasterboard 	<ul style="list-style-type: none"> • 110mm brick • 70mm cavity • 13mm plasterboard

Table 17: Details of the opaque construction (walls, floors, roofs) used to model hospital wards (building class 9a)

School	CZ2	CZ5	CZ6	CZ7
External wall	<ul style="list-style-type: none"> • 5mm metal cladding • 50mm air cavity • 0.8mm vapour barrier • Insulation • 13mm plasterboard 	<ul style="list-style-type: none"> • 5mm metal cladding • 50mm air cavity • Insulation • 13mm plasterboard 	<ul style="list-style-type: none"> • 5mm metal cladding • 50mm air cavity • Insulation • 13mm plasterboard 	<ul style="list-style-type: none"> • 5mm metal cladding • 50mm air cavity • Insulation • 13mm plasterboard
Roof	<ul style="list-style-type: none"> • 0.48mm colorbond • 0.8mm vapour barrier • Insulation 	<ul style="list-style-type: none"> • 0.48mm colorbond • Insulation 	<ul style="list-style-type: none"> • 0.48mm colorbond • Insulation 	<ul style="list-style-type: none"> • 0.48mm colorbond • Insulation

School	CZ2	CZ5	CZ6	CZ7
Ground contact floor	<ul style="list-style-type: none"> • 8mm carpet • 200mm concrete 	<ul style="list-style-type: none"> • 8mm carpet • 200mm concrete 	<ul style="list-style-type: none"> • 8mm carpet • 200mm concrete 	<ul style="list-style-type: none"> • 8mm carpet • 200mm concrete
Floor above underground carpark	N/A	N/A	N/A	N/A
Internal floor	<ul style="list-style-type: none"> • 8mm carpet • 200mm concrete 	<ul style="list-style-type: none"> • 8mm carpet • 200mm concrete 	<ul style="list-style-type: none"> • 8mm carpet • 200mm concrete 	<ul style="list-style-type: none"> • 8mm carpet • 200mm concrete
Ceiling	13mm plasterboard	13mm plasterboard	13mm plasterboard	13mm plasterboard
Internal wall	<ul style="list-style-type: none"> • 13mm plasterboard • 70mm air cavity • 13mm plasterboard 	<ul style="list-style-type: none"> • 13mm plasterboard • 70mm air cavity • 13mm plasterboard 	<ul style="list-style-type: none"> • 13mm plasterboard • 70mm air cavity • 13mm plasterboard 	<ul style="list-style-type: none"> • 13mm plasterboard • 70mm air cavity • 13mm plasterboard
Core area wall	<ul style="list-style-type: none"> • 110mm brick • 70mm cavity • 13mm plasterboard 	<ul style="list-style-type: none"> • 110mm brick • 70mm cavity • 13mm plasterboard 	<ul style="list-style-type: none"> • 110mm brick • 70mm cavity • 13mm plasterboard 	<ul style="list-style-type: none"> • 110mm brick • 70mm cavity • 13mm plasterboard

Table 18: Details of the opaque construction (walls, floors, roofs) used to model schools (building class 9b)

APPENDIX 3

Thermal comfort parameters modelled in the study are presented in Table 14 and 15.

Building Archetype	Thermal Comfort Condition
Hotel (3)	<ul style="list-style-type: none"> • PMV+/-1, and • Awake Conditions (Lan, L, Zhai, Z. and Lian, Z, 2018): Operative temperature (winter 18°C, summer 27°C), and • Asleep Condition (Lan, L, Zhai, Z. and Lian, Z, 2018): Operative temperature (winter 16.5°C, summer 27°C)
Others	<ul style="list-style-type: none"> • PMV+/-1

Table 19: Thermal comfort parameters used.

Clothing insulation (clo) and metabolic rate (met) values modelled for each building class is shown in Table 20.

Building Archetype	Minimum clo	Maximum clo	Metabolic Rate (met)
Hotel (3)	0.4	1.12	1
Office (5)	0.5	1.09	1.1
Retail (6)	0.345	0.99	1.7
Hospital Ward (9a)	1.07	1.83	0.86
School (9b)	0.365	1.145	1

Table 20: Modelled clothing insulation (clo) and metabolic rates (met).

DISCLAIMER

The information or advice contained in these technical papers is intended for use only by professionals who have had adequate technical training in the field to which the paper relates. At the time of publication, these technical papers have undergone a formal peer-review process.

These documents have been compiled as an aid only, and the information or advice should be verified before it is put to use. The user should also establish the applicability of the information or advice about any specific circumstances. While the information or advice is believed to be correct, no responsibility is taken by AIRAH or IBPSA Australasia for any statements made within.

AIRAH and IBPSA Australasia, its officers, employees and agents, disclaim responsibility for any inaccuracies contained within the documents, including those due to any negligence in the preparation and publication of the said technical papers.

COPYRIGHT

This work is copyright. Apart from any use as permitted under the Copyright Act 1986, no part may be reproduced by any process without prior written permission from either the Australian Institute of Refrigeration, Air Conditioning and Heating (AIRAH) or the International Building Performance Simulation Association (IBPSA) Australasia.

DISAGGREGATION OF PRECIPITATION DATA APPLICABLE FOR CLIMATE-AWARE PLANNING IN BUILT ENVIRONMENTS

DAVID FERRARI¹, MASOUME MAHMOODI², CHITHRAL KODAGODA¹,
NIHAL ABDUL HAMEED¹, TREVOR LEE¹, GRAHAM ANDERSON¹

¹ Exemplary Energy, 32 Fihelly Street, Fadden, Canberra, Australia; trevor.lee@exemplary.com.au

² College of Engineering and Computer Science, Australian National University, Canberra, Australia; masoume.mahmoodi@anu.edu.au

ABOUT THE AUTHOR

Dr Dave Ferrari is an engineer with a long-held interest in the energy transition, having spent two decades in government, industry and academia working to address the challenges and support urgently needed change across the energy sector. He first worked with Exemplary as an Intern in 2003 and recently returned as Managing Director. In the interim he has worked in energy policy and programs with the United Nations regional secretariat (UN ESCAP), Victorian Government, RMIT and the Australian Bureau of Meteorology. He holds a PhD in Engineering from the ANU along with Bachelors of Engineering (Sustainable Energy Systems) and Science (Mathematics), and is a Certified Measurement and Verification Professional (CMVP).

ABSTRACT

High temporal resolution precipitation data of the past along with other data of weather elements are required for applications in the design and simulation of built environments. However, the available data of precipitation is either low-resolution, e.g., daily, or not long enough to produce reliable and climate-responsive results for built environment applications. In this paper, we develop a stochastic algorithm based on Markov chain Monte Carlo (MCMC) methods to generate hourly temporal resolution precipitation data given daily precipitation data. To improve the accuracy of the generated disaggregated precipitation series, a combination of data recorded for several weather elements such as temperature, relative humidity, wind speed and cloud cover are incorporated along with the precipitation data. The algorithm uses simulated annealing based on the Metropolis-Hastings algorithm. In this model, desired properties, such as the correlation between the generated precipitation series with other weather elements, are formulated in an objective function through which the algorithm generates the desired precipitation series. Finally, we conduct a comparison between these two algorithms. The outputs produced by this disaggregation algorithm will find use in including hourly precipitation data from 1990 to present, to the weather and climate data produced for various Australian cities, an exercise carried out by Exemplary Energy.

INTRODUCTION

Modelling and simulation of scenarios relating to built environments have become common for various applications, including finding the optimal design parameters in a cost-effective manner, estimating the performance of the system in various operating conditions and to create a better understanding of risk factors [1]. These scenarios are commonly modelled for their efficacy and energy efficiency of a building as a whole – the envelope, the lighting and the HVAC in an operating building. They also model key parts of the building like the façade for those same criteria but also for their hygrothermal performance. An integral part of these models is the input of the historical weather data or a climate file distilled from that longer record that can be used to understand the different physical conditions the built environment is likely to face and its performance under these varying conditions.

To estimate the role of precipitation in the local climate, analyses based on historical data dedicated to each region will be necessary. According to the World Meteorological Organization, 30 years of historical data is recommended to define a climate normal, and especially in the case of precipitation, the data of a period less than 30 years may not produce reliable statistics due to the variation in the annual precipitation over the years [2].

In the Australian scenario, weather stations recording precipitation that were operated by the Australian Bureau of Meteorology (BoM) were upgraded to have an automatic Tipping Bucket Rain Gauge from the early 2000s, allowing recording of hourly precipitation data. However, prior to this, a manual method of recording daily precipitation was employed in many locations, where volunteers read the rain gauge at 9AM each day [3]. The precipitation disaggregation algorithms developed in this study will provide estimates of the hourly historical precipitation data in Australian locations based on daily precipitation measurements.

Hourly precipitation data, with coincident wind speed and direction data, is essential for reliable hygrothermal modelling of external components of the building envelope of built environments [4] as is evident from the various applications seen in the existing literature. It is essential for understanding the moisture-induced damages in buildings, including houses, and has gained relevance in recent times due to the emphasis on building healthy and energy-efficient living environments. In Australia, the National Construction Code (NCC) emphasises the need to consider the impact of moisture on the building, and reliable precipitation data is key to evaluating condensation, mould formation and other moisture-related risks.

DISAGGREGATION ALGORITHM

Disaggregation is the process of mapping information from a coarse scale to a finer scale in a manner that is statistically consistent with the original data [5]. In this study, the daily precipitation data recorded by the BoM is transferred to hourly resolution data. Since a disaggregated series is a “realisation” from the original coarse time series, stochastic approaches are preferred to reproduce the suitable statistical characteristics of the data at the required finer time scale [6]. Stochastic precipitation modelling historically has followed two approaches: 1) one type of the model is to incorporate the physical factors such as terrains, local temperature and pressure, while the other type 2) utilises statistical means and purely relies on the precipitation data available [7].

Along the lines of the physical factors approach, the point process models which treat each precipitation event as a cluster of many small rainy cells with a random period of rain based on Poisson distribution was developed [8]. Such cluster-based models include the Neymann Scott

and Bartlett-Lewis processes. However, these processes were recorded to be unrealistic in continuous time and have shown some disagreements along with the need for a large number of parameters for modelling [9]. Due to the recorded drawbacks of the physical approach and since the statistical approaches like the Markov chain model has been widely used for Australian locations to stochastically generate daily precipitation data for impact assessment of agricultural and hydrological applications which utilised high resolution data [10], this study will focus on the statistical approach for the development of the disaggregated precipitation data. The Markov chain is a system that stays in one of the finite states and progresses from one state to another at each time step based on a transition probability matrix (TPM) [11]. Although Markov chain models can generate series that preserve certain properties of the observed precipitation series, they often fail to reproduce other important features like correlation with cloud cover and changes in temperature, humidity and pressure. To overcome this issue, other stochastic models, namely the Markov Chain Monte Carlo (MCMC) methods, which utilise the bootstrap techniques for resampling, are introduced [12]. In MCMC-based models, the states of the Markov chain are defined on the set of possible time series of precipitation, not as a sample from a probabilistic model. In these models, the desired properties are incorporated in an objective function, and a series with the desired properties is generated through optimising this objective function.

In this paper, to improve the accuracy of the disaggregated precipitation data, a combination of the physical approach and statistical approach is conducted where a combination of data recorded for other weather elements – temperature, relative humidity, wind speed, cloud cover and solar irradiation – is incorporated into the algorithm alongside precipitation. For comparison, this combination is applied on both the commonly used Markov chain model and the MCMC-based model. In the MCMC-based model, the simulated annealing technique based on the Hastings algorithm is utilised.

1.1 Data and correlation analysis

For our study, we use the historic data for Canberra in South-eastern Australia, where the hourly weather data including precipitation is available from 2010 to 2019. In addition to the precipitation data, the BoM provided other weather elements such as global horizontal irradiance (GHI), direct normal irradiance (DNI), diffuse horizontal irradiance (DIF), total sky cover (TSC), dry-bulb temperature (DBT), dew point temperature (DPT), relative humidity (RH), atmospheric pressure (AP) and wind speed (WS), with an hourly resolution from 1990-2019. However, prior to 2010, precipitation was recorded manually at 9AM each day, and therefore from 1990 to 2009, only daily precipitation values are available. Our models aim to disaggregate these daily values to hourly resolution data.

To obtain a statistical relationship between precipitation and other weather elements, we perform a correlation analysis which is explained in detail in a previous study [13] and all significant correlations are summarised in Table 1.

Analysis based on		Correlation Between	Value
Rain Days	Onsets		
	✓	P(t) and variance(DBT(t-1:t))	0.5
	✓	P(t) and variance(DBT(t-2:t))	0.48
	✓	P(t) and variance(RH(t-1:t))	0.45
	✓	P(t) and variance(RH(t-2:t))	0.43
✓		P(t) and P(t-1)	0.41
		⋮	
		⋮	
		⋮	
✓		P(t) and P(t-2)	0.23

Table 1: A summary of significant correlations in %

MONTE CARLO MARKOV CHAIN MODEL USING SIMULATED ANNEALING

In this section, we present a Monte Carlo Markov chain (MCMC) model to exploit the high correlations between precipitation onsets and other weather elements. MCMC-based models do not utilise the probabilistic information but rather they directly use the observed properties of the precipitation series, such as the correlation between precipitation onsets and other weather elements [12]. The states of the MCMC model in this case are defined on the set of possible precipitation time series, not as a sample from a probabilistic model. To generate the synthesised precipitation series, an optimisation technique called simulated annealing introduced by Kirkpatrick et al. in 1983 [14] is utilised. The simulated annealing optimisation works on the Metropolis-Hastings algorithm, where the objective function aims to minimise the differences between the properties of the generated series and the corresponding observed dataset.

In the MCMC model, hourly precipitation series is modelled as a random vector $P = [P(1), P(2), \dots, P(T)] \in \mathbb{R}^T$ where T is the length of the series (or total number of under-study hours). All possible values for each element of this vector can be obtained using the observed historical data. For instance, all the possible hourly precipitation values for Canberra, using the training dataset (a dataset of several years with both half-hourly and daily precipitation used to facilitate machine learning of their statistical association), include $\{0, 0.2, \dots, 36.8\}$ millimeter (mm). Therefore, the precipitation of each timestamp has 194 possible values and thus the total possible precipitation series for T timestamps is 194^T . Note that assessing all possible series when T is a large number (e.g., hourly for one year or more as is typical for building simulations) is practically impossible. Instead, we can only consider two possible series namely P_1 and P_2 and assign the conditional probabilities to them:

$$\pi_1 = P(P_1|P = P_1 \text{ or } P_2) \quad (1)$$

$$\pi_2 = P(P_2|P = P_1 \text{ or } P_2) \quad (2)$$

where $P(\cdot|\cdot)$ denotes the conditional probability. We then utilise the Metropolis-Hastings algorithm, which is an MCMC method for obtaining a sequence of random samples from a probability distribution from which direct sampling is difficult [14]. Based on this algorithm, an acceptance ratio is defined for the two considered series P_1 and P_2 , as follows:

$$\alpha_{12} = \frac{\pi_1}{\pi_2} \quad (3)$$

If the acceptance ratio α_{21} is great than 1, which means the probability π_2 is greater than π_1 , we choose series P2 over the other candidate, i.e., P1. This is because $\pi_2 > \pi_1$ shows that the series P2 is more probable to be the desired precipitation series compared to the series P1. However, if $\alpha_{21} \leq 1$ then a uniform random number $u \in [0, 1]$ is generated and by comparing the acceptance ratio α_{21} with u , the algorithm decides to either accept or reject each candidate. In summary:

$$\begin{cases} \text{Accept the candidate P2 if } \alpha_{21} \geq 1 \\ \text{Accept the candidate P2 if } u \leq \alpha_{21} < 1 \\ \text{Reject the candidate P2 otherwise} \end{cases} \quad (4)$$

To assign the probabilities π_1 and π_2 , we need to define the desired properties of the precipitation series. For this purpose, we use the simulated annealing approach where these probabilities are defined using an objective function (f) which depends on the corresponding series. Therefore, the probability of a given precipitation series P is defined as follows:

$$\pi(P) = e^{-f(P)} \quad (5)$$

where the desired properties of the precipitation series are included in the objective function $f(P)$ as follows:

$$f(P) = \sum_{l=1}^L (\delta_l - \delta_l^*) \quad (6)$$

where δ_l represents the l th property of the generated series and δ_l^* shows the corresponding desired property which is obtained using the training data. Also, L denotes the total number of properties. The advantage of this objective function is that any desired properties of the series such as correlations between precipitation onsets with other weather elements can be directly incorporated in the model. Note that based the above two equations, smaller $f(P)$ fulfils the desired properties better or in other words, it leads to higher probability value, i.e., higher π which in turn results in higher chance of being accepted. Ideally, we like to achieve $f(P) = 0$, however, in this paper we accept all series with $f(P) \leq \epsilon$, where ϵ denotes a constant tolerance specified by the modeller. The algorithm continues until the stopping criterion, i.e., $f(P) \leq \epsilon$ is achieved.

2.1 Simulated Annealing Technique Based on Hastings-Metropolis Algorithm

To obtain the disaggregated precipitation series using the simulated annealing technique based on the Hastings-Metropolis algorithm, we take three steps: 1) data preparation process, 2) generating an initial random precipitation vector and 3) resampling to generate a new candidate series and Hastings-Metropolis algorithm. These steps and their details are summarised in the flowchart Figure 7 shown in the Appendix.

In the data preparation process we use the training data to obtain the correlations between precipitation and other weather elements. Based on the analysis carried out in a previous study [13], the weather elements with the highest correlations are summarised below and are considered as the desired properties of the precipitation series.

In the second step, we utilise the observed historical hourly precipitations to generate an initial random precipitation series. To this end, we require to determine the number of rainy hours and the amount of rain for each hour such that their sum for a specific day is equal to the available daily rain. To obtain the number of rainy hours for each day, we use the training data and for each daily rain value we obtain the histogram of the number of rainy hours in the corresponding day. A histogram of hourly rain values is obtained using the training data. This histogram is shown in Figure 1. Therefore, for each day we first determine the total number of rainy hours and then using the histogram in Figure 1 we generate hourly rain values for the specified rainy hours such that the sum of these hourly rains is equal to the given daily rain value. We repeat this process for all test days and thus generate an initial random precipitation series for the whole considered time period (in our case, for two years 2018 and 2019).

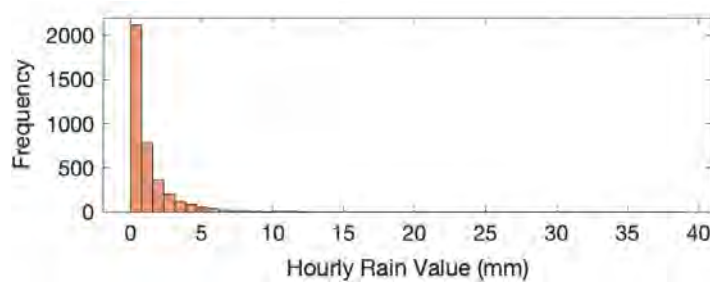


Figure 1. Histogram of hourly rain values obtained from training data

The next step is to generate another candidate for the precipitation series using resampling. For this purpose, we randomly choose d days and for each day, two times $t_1 \neq t_2$ are selected to swap their hourly rain values. Note that swapping is done with the condition that the amount of hourly rain values is different for the selected times. This process is called resampling and generates a new time series. To accept or reject the new candidate the probability of the two series is calculated using (5) and (6). Then, the acceptance ratio (3) is calculated and based on the criterion (5), the algorithm decides either accept or reject the new candidate. This procedure is demonstrated Figure 2. The resampling process is repeated for M times. The algorithm will stop when the stopping criterion $f(P) \leq \epsilon$ is reached.

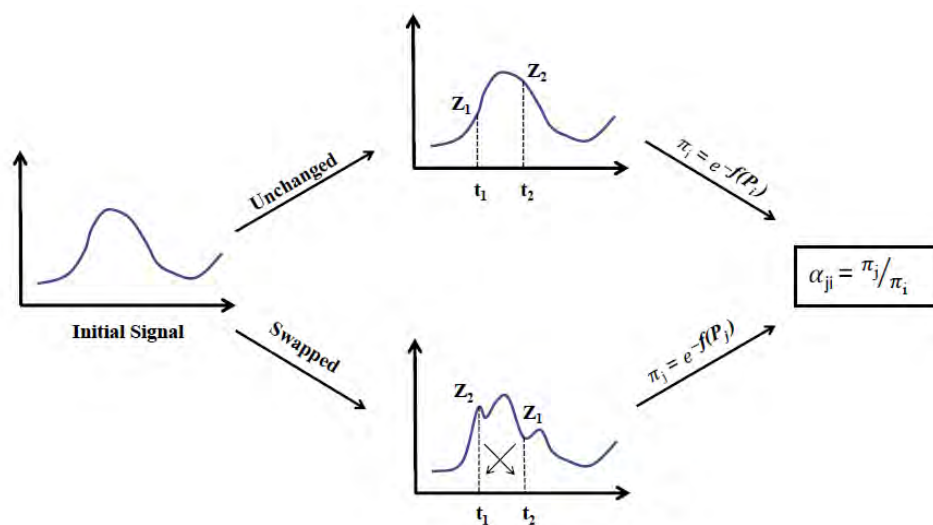


Figure 2. Resampling procedure

RESULTS

In this section, we perform six different experiments taking the significant correlations in Table 1 into account and using the MCMC model. The experiments include:

- 1) P (Lag1): considering only Lag 1 of the precipitation and
- 2) P (Lags 1, 2): considering Lag 1 and Lag 2 of the precipitation,
- 3) Var (RH1): considering variance of relative humidity during the past hour,
- 4) Var (RH2): considering variance of relative humidity during the past two hours,
- 5) Var (DBT1): considering variance of dew point temperature during the past hour, and
- 6) Var (DBT2): considering variance of dew point temperature during the past two hours.

We repeat the MCMC algorithm 100 times to account for the uncertain nature of this algorithm. We calculate the RMSE between the generated and the actual precipitation series. The boxplot is shown in Figure 4 (a) demonstrates this RMSE for all the experiments. Also, the relative error between the total number of rainfall hours in the generated series with the corresponding number in the observed series is shown in Figure 4 (b). We observe that the RMSEs obtained using MCMC algorithm are two times less than the error of the series obtained using the simple Markov chain algorithm (errors ~ 0.7 compared to error ~ 1.4). In comparison, if we equally distribute the daily precipitation across the 24 hours as shown in Figure 3, the resulting RMSE obtained is around 0.9, implying a higher deviation from the observed readings.

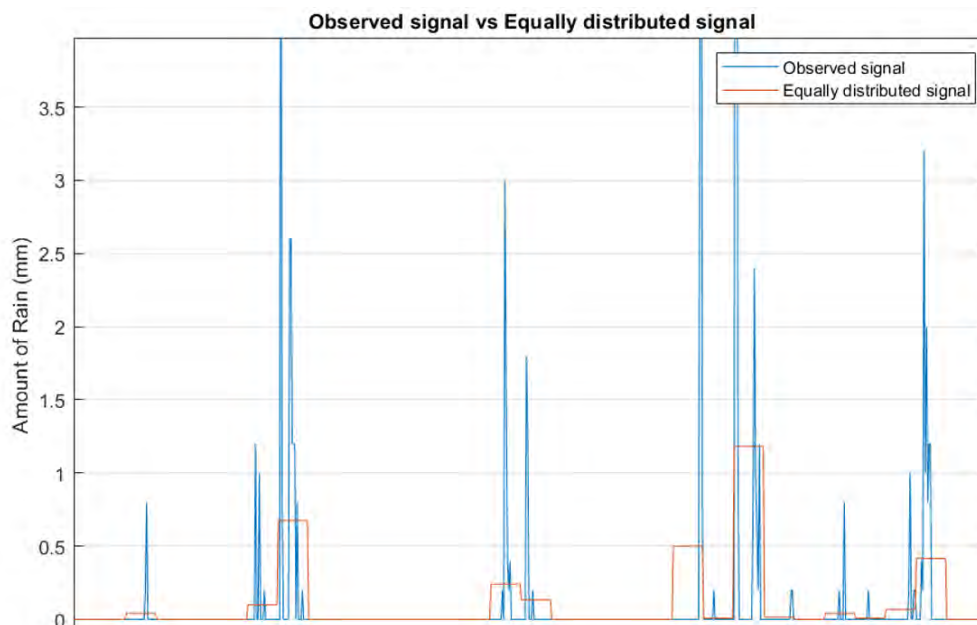


Figure 3. Comparing an equally distributed precipitation signal to the observed signal

In addition to these metrics, the number of correctly detected rainfall hours and correctly detected precipitation onset hours are obtained as shown in Figure 5 and Figure 6, respectively. We observe that the MCMC algorithm detects at least 60 per cent of the rainfall hours with less than two hours error. It also detects at least 50 per cent per cent of the precipitation onset hours with the same error.

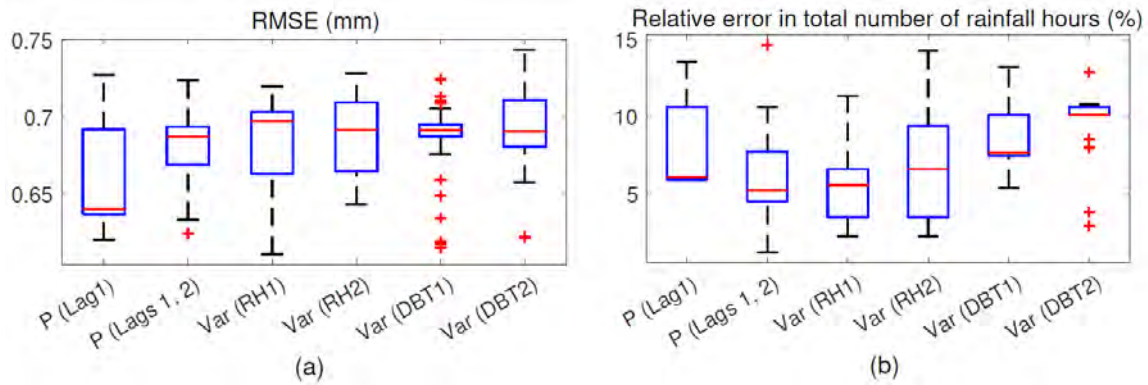


Figure 4. Comparison of the generated precipitation series for different experiments using MCMC algorithm where two metrics are considered: (a) root mean square error between the generated and observed series, (b) relative error between total number of rainfall hours for generated and observed series

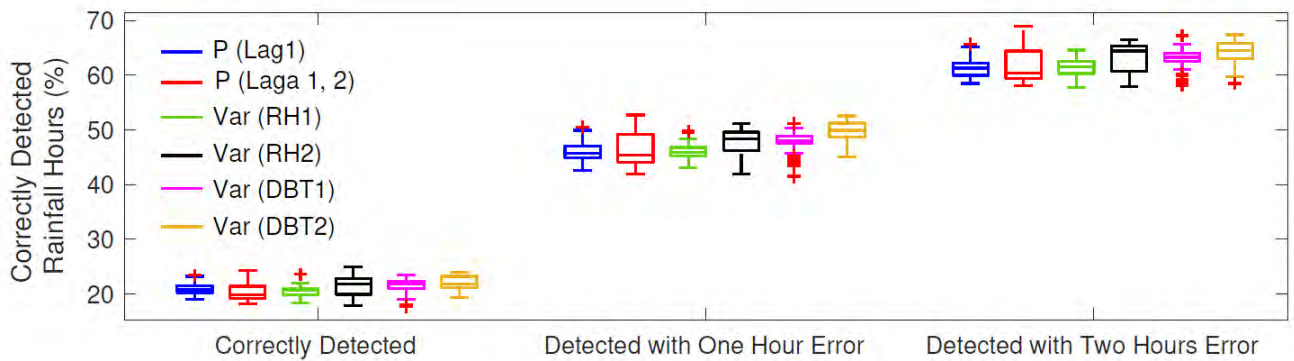


Figure 5. Percentage of correctly detected rainfall hours with no error, one hour error and two hours error, respectively, for all experiments when MCMC algorithm is used

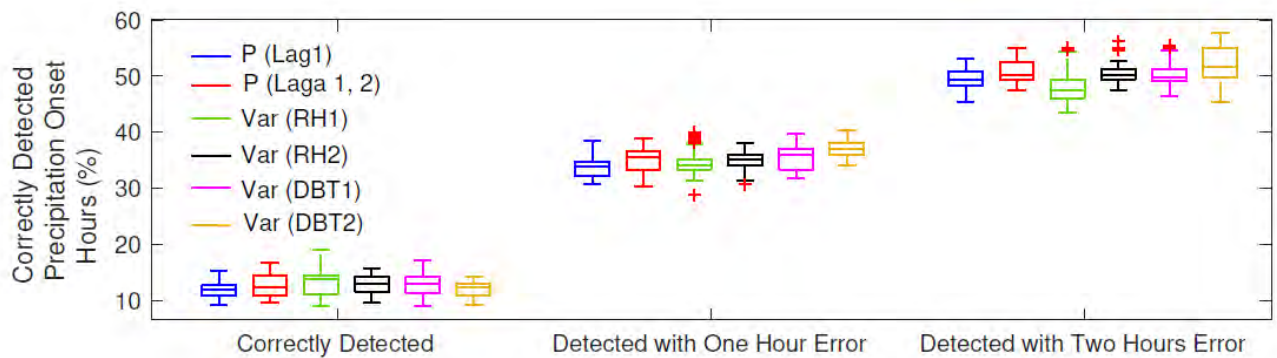


Figure 6. Percentage of correctly detected precipitation onset hours with no error, one hour error and two hours error, respectively, for all experiments when MCMC algorithm is used

CONCLUSION

This paper develops a stochastic algorithm based on Markov chain Monte Carlo (MCMC) methods to generate hourly temporal resolution precipitation data in Australian locations based on the daily precipitation data recorded by the Bureau of Meteorology (BoM) before 2000. The proposed algorithms use a combination of data recorded for weather elements like temperature, relative humidity and cloud cover, along with the precipitation data. The generated synthesised hourly precipitation series are compared with the observed series using three metrics including 1) least-square residuals, 2) the total number of rain hours, and 3) the total number of matching onset hours between the generated and observed precipitation series. We observe improvements in the considered metrics when the other weather elements are integrated in the developed algorithms.

Based on the results obtained for the MCMC algorithm, when considering only precipitation with an hour lag, the least deviation from the actual series was obtained. When considering other weather elements, the addition of relative humidity with an hour lag shows promising results. This model is intended to be expanded to include different climate zones of Australia and, if successful, will be used to include precipitation data from 1990 to the present, to the weather and climate data of over 250 Australian locations which Exemplary Energy produces. Thus, the precipitation data in these weather data, being present for over 30 years, will fulfill the condition of a climate normal as per WMO and can be reliably used for modelling and simulations of varied nature in the Built Environment domain.

To improve the accuracy of the generated synthetic signals, some of the avenues that will be investigated in the future include: 1) effects of implementing raw data with half hourly resolution, and 2) the impact of segregating the training and testing data by seasonality.

ACKNOWLEDGEMENTS

The authors acknowledge the Australian Bureau of Meteorology as the source of all the raw data, the College of Engineering and Computer Science, Australian National University, and the other members of the Exemplary team.

REFERENCES

- [1] T. Asim, R. Mishra, S. Rodrigues and B. Nsom, “Applications of Numerical Simulations in Built,” *International Journal of COMADEM*, vol. 22, p. 9–14, 2019.
- [2] Y. Lai and D. Dzombak, “Use of Historical Data to Assess Regional Climate Change,” *Journal of Climate*, vol. 32, p. 4299–4320, 2019.
- [3] Australian Government, “B.O.M. Observation of Rainfall,” 2010. [Online]. Available: <http://www.bom.gov.au/climate/how/measure.shtml>.
- [4] G. Brigandì and G. Aronica, “Generation of Sub-Hourly Rainfall Events through a Point Stochastic Rainfall Model,” *Geosciences*, vol. 9, 2019.

- [5] F. Lombardo, E. Volpi, D. Koutsoyiannis and F. Serinaldi, “A theoretically consistent stochastic cascade for temporal disaggregation of intermittent rainfall.,” *Water Resources Research*, vol. 53, p. 4586–4605, 2017.
- [6] L. Guenni and A. Bárdossy, “A two steps disaggregation method for highly seasonal monthly rainfall,” *Stochastic Environmental Research and Risk Assessment (SERRA)*, vol. 16, p. 88–206, 2002.
- [7] C. Miao, J. Chen, J. Liu and H. Su, “An improved Markov chain model for hour-ahead wind speed prediction.,” *2015 34th Chinese Control Conference (CCC)*, p. 8252–8257, 2015.
- [8] C. Onof, R. Chandler, A. Kakou, P. Northrop, H. Wheeler and V. Isham, “Rainfall modelling using Poisson-cluster processes: a review of developments.,” *Stochastic Environmental Research and Risk Assessment*, vol. 14, p. 0384–0411, 2000.
- [9] P. Cowpertwait, V. Isham and C. Onof, “Point process models of rainfall: developments for fine-scale structure.,” *Proceedings of the Royal Society A: Mathematical, Physical and Engineering Sciences*, vol. 463, p. 2569–2587, 2007.
- [10] R. Srikanthan, T. Harrold, A. Sharma and T. McMahon, “Comparison of two approaches for generation of daily rainfall data.,” *Stochastic Environmental Research and Risk Assessment*, vol. 19, p. 215–226, 2005.
- [11] Y. Zou, Z. Kong, T. Liu and D. Liu, “A Real-Time Markov Chain Driver Model for Tracked Vehicles and Its Validation: Its Adaptability via Stochastic Dynamic Programming.,” *IEEE Transactions on Vehicular Technology*, vol. 66, p. 3571–3582, 2017.
- [12] A. Bárdossy, “Generating precipitation time series using simulated annealing,” *Water Resources Research*, vol. 34, p. 1737–1744, 1998.
- [13] D. Ferrari, M. Mahmoodi, C. Kodagoda, N. Abdul Hameed, T. Lee and G. Anderson, “Temporal Disaggregation of Precipitation Data Applicable for Climate-aware Planning in Built Environments,” in *Asia Solar Pacific Conference*, Sydney, 2021.
- [14] S. Kirkpatrick, C. Gelatt and M. Vecchi, “Optimization by simulated annealing,” *science*, vol. 220, p. 671–680, 1983.

APPENDIX

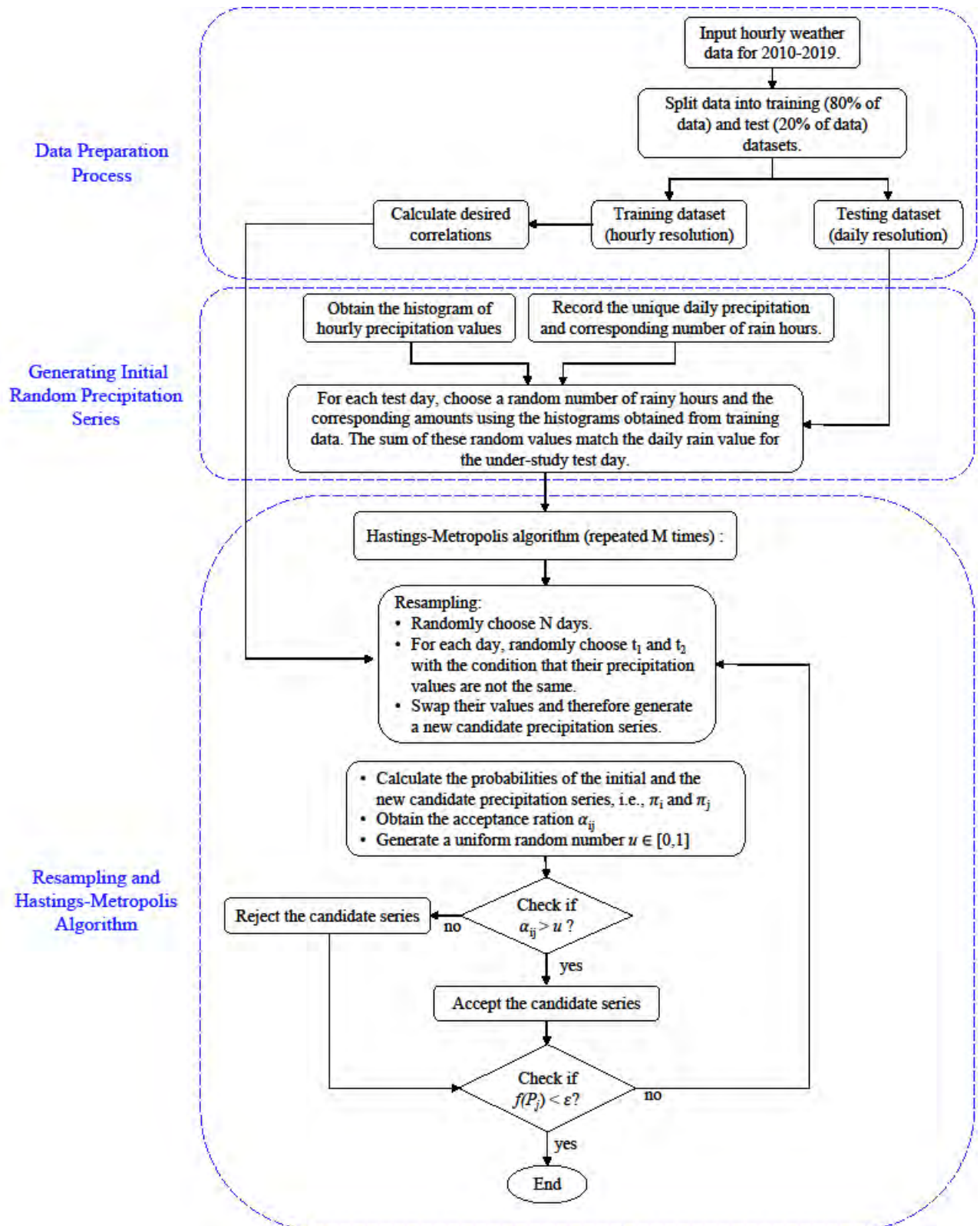


Figure 7. The flowchart of MCMC model using simulated annealing based on Hastings-Metropolis algorithm

DISCLAIMER

The information or advice contained in these technical papers is intended for use only by professionals who have had adequate technical training in the field to which the paper relates. At the time of publication, these technical papers have undergone a formal peer-review process.

These documents have been compiled as an aid only, and the information or advice should be verified before it is put to use. The user should also establish the applicability of the information or advice in relation to any specific circumstances. While the information or advice is believed to be correct, no responsibility is taken by AIRAH or IBPSA Australasia for any statements made within.

AIRAH and IBPSA Australasia, its officers, employees and agents, disclaim responsibility for any inaccuracies contained within the documents, including those due to any negligence in the preparation and publication of the said technical papers.

COPYRIGHT

This work is copyright. Apart from any use as permitted under the Copyright Act 1986, no part may be reproduced by any process without prior written permission from either the Australian Institute of Refrigeration, Air Conditioning and Heating (AIRAH) or the International Building Performance Simulation Association (IBPSA) Australasia.

HEATING ELECTRIFICATION IMPACTS ON COMMERCIAL HVAC PERFORMANCE TODAY AND FUTURE: A CASE STUDY

YUNLONG MA (PhD)

Queensland University of Technology (QUT)
2 George St, Brisbane, QLD 4000
yunlong.ma@connect.qut.edu.au

AARON LIU (PhD)

Queensland University of Technology (QUT)
2 George St, Brisbane, QLD 4000

SHERIF ZEDAN (PhD)

Queensland University of Technology (QUT)
2 George St, Brisbane, QLD 4000

WENDY MILLER (PhD)

Queensland University of Technology (QUT)
2 George St, Brisbane, QLD 4000

BRUCE BONNEY

Children's Health Queensland (CHQ)
501 Stanley St, South Brisbane, QLD 4101

JASON SANDERS

Children's Health Queensland (CHQ)
501 Stanley St, South Brisbane, QLD 4101

MICHAEL CAMPBELL

Children's Health Queensland (CHQ)
501 Stanley St, South Brisbane, QLD 4101

ABOUT THE AUTHOR

Dr Ma is a research fellow in School of Architecture and Built Environment, QUT. He is a specialist in building and HVAC energy simulation. His research interests include: building energy simulation, HVAC, solar cooling, renewable energy, building energy code, and life cycle assessment.

Dr Liu is a research fellow at QUT's Faculty of Engineering, an Australian Representative on International Energy Agency Annex 82 Energy Flexible Buildings and a registered professional engineer with a PhD in energy investment decisions. He is a Fellow of Higher Education Academy. Currently, Dr Liu is the project manager for one of the ARENA iHub living labs, testing innovative technologies at a major Australian public hospital.

Dr Zedan is a certified energy efficiency assessor, with a PhD in stakeholder management of energy efficient housing. He has a degree in Architectural Engineering, and over 10 years' experience in the construction industry. He is currently the project manager for one of the iHub living labs, where innovative technologies are implemented, tested, and evaluated.

Dr. Wendy Miller is an Associate Professor in School of Architecture and Built Environment, QUT. Dr Miller has a long history of engagement with industry and government on issues relating to energy and the built environment, and research on socio-technical challenges. She is the Living Laboratory Activity Leader for the Innovation Hub for Affordable Heating and Cooling (iHub). She engages with the international community through IEA Annex 80 – resilient cooling, and with industry through AIRAH’s Resilience Taskforce.

ABSTRACT

Heating, Ventilation, and Air Conditioning (HVAC) systems in commercial buildings represent about 43% of the total commercial building energy consumption in Australia. In order to reduce energy use and greenhouse gas (GHG) emissions from commercial HVAC systems, this paper investigates the feasibility of heating electrification coupled with renewable energy investment for commercial HVAC renovation. A case study building, the Centre for Children’s Health Research (CCHR), and its HVAC systems are simulated in DesignBuilder under current and future climate conditions in a subtropical climate. Our case study results showed that heating electrification for the CCHR building HVAC plant with solar PV integration has significant potential to reduce energy consumption and CO₂ emissions under both current and future climate conditions. It is a promising alternative for building decarbonisation from energy, environmental and economic perspectives.

INTRODUCTION

Urbanisation and climate change are significantly increasing building energy demand and building carbon emissions. In Australia, commercial buildings account for about 25% of the total national electricity energy use (Ernst & Young, 2019), 61 per cent of the total building energy use, and contribute to 10 per cent of the total national carbon emissions (Harrington et al., 2018). Heating, Ventilation, and Air Conditioning (HVAC) systems, as the largest energy use contributor in commercial buildings, have significant potential to reduce building energy consumption and CO₂ emissions. A recent report indicated that up to 50 per cent of the total HVAC energy use could be saved through efficient HVAC strategies (AIRAH, 2015). Building electrification, as an effective technology to building decarbonisation, has recently come to wide attention due to the significant effect on site-level greenhouse gas (GHG) emission reductions, especially when combined with renewable and zero-carbon electricity resources (U.S. Department of Energy, 2021). Electrification involves the switch of a building system that would traditionally use fossil fuels (such as, natural gas, fuel oil, or propane) to the use of electrical power. Currently there are many studies about the heating electrification performance on building energy efficiency and decarbonisation. Pease et al. (Pease et al., 2021) investigated the impacts of different HVAC intervention strategies for an office building in different U.S. climates. They found that heating electrification by replacing a natural gas boiler with an electric boiler could achieve 0 per cent to 5 per cent annual energy savings. However, energy cost savings and carbon savings were negative.

Tarroja et al. (Tarroja et al., 2018) quantified the heating electrification impacts on building energy use to future GHG emissions and electric grid capacity requirements in California using EnergyPlus simulation. They concluded that heating electrification prompted a 30 per cent to 40 per cent reduction in GHG emissions but required significant grid resource capacity increases.

Padovani et al. (Padovani et al., 2021) conducted a techno-economic analysis of heating electrification for rural residential buildings in cold climates in the U.S. Upper Midwest and Northeast. It was found that heating electrification is economically viable through a life cycle cost analysis, and combining PV with heat pumps can reduce residential building GHG emissions by up to 50 per cent immediately.

Walker et al. (Walker et al., 2022) investigated the carbon and energy cost impacts of electrification of space heating with heat pumps in the U.S. They concluded that the variability in CO₂-e content of electricity and the differences between electricity and natural gas prices are very important when making decisions about home heating decarbonisation efforts.

Eguiarte et al. (Eguiarte et al., 2020) studied the heating electrification effects of using air-to-air heat pumps for a residential building from energy, environment, and economic aspects in different European climates. They found that despite the more energy efficient performance of heat pumps, the higher cost of electricity over fossil fuel prevents the use of heat pumps in certain cases. Therefore, the promotion of initiatives for energy efficiency and development of renewable sources should be necessary to incentivise heating electrification.

The above literature shows that heating electrification has the potential to achieve building energy efficiency and decarbonisation with suitable technical and economic conditions. Heating electrification integrated with renewable energy investment is a promising solution to decarbonisation from both energy and environmental aspects. This study aims to investigate the heating electrification effect with renewable energy integration on Australian commercial HVAC performance under both current and future climates.

1. METHODOLOGY

The effect of heating electrification combined with renewable energy resources for Australian building decarbonisation were analysed by dynamic building energy simulation using DesignBuilder (DesignBuilder, 2019). A case study building, the Centre for Children's Health Research (CCHR) which is located in South Brisbane, and its HVAC systems were simulated under both Brisbane current and future climates. Roof-mounted solar PV systems were considered as the renewable energy investment combining with heating electrification, which is achieved by replacing the natural gas powered hot water boiler with the electricity powered hot water boiler in the CCHR's HVAC plant.

1.1 Case study building description

The CCHR building is a 9-storey complex building built in 2015 with a total floor area of 14,108m² and roof area of 1,740m². It combines children's health research and services with the Queensland Children's Hospital (QCH). Five levels of the CCHR are dedicated to research laboratories and the remaining levels accommodate the QCH Pathology service, office areas, reception, car parking and a COVID19 testing area (Liu et al., 2020). It has five different types of HVAC systems, including CAV systems, VAV systems and chilled water fan coil units (FCUs) serving 41 different zones. Cooling and heating are supplied by a central chilled water plant and a central natural gas fuelled hot water plant, respectively. The building 3D model and its HVAC system diagram in DesignBuilder are shown in Figure 1.

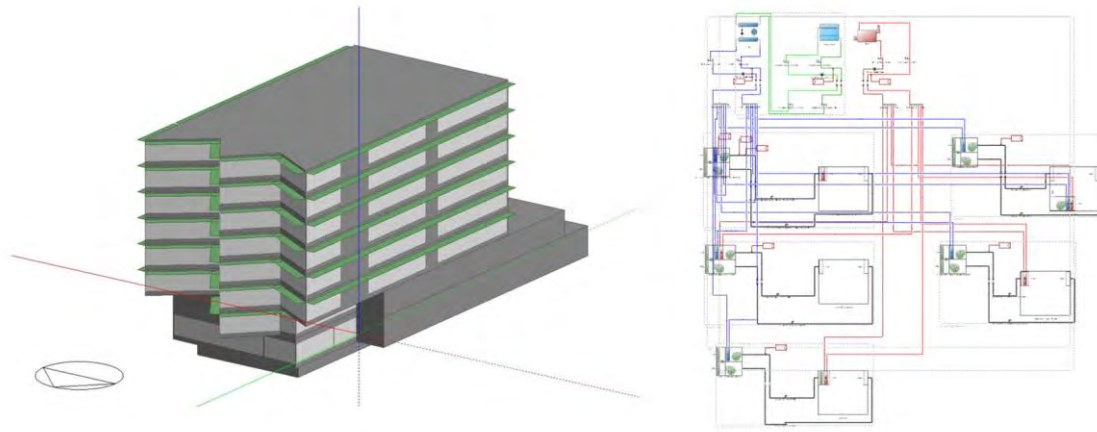


Figure 1. *The CCHR building and 3D DesignBuilder model*

1.2 Building simulation parameters

The CCHR building envelope materials and construction are summarised in Table 1, which are referenced from the BCA2010 Deemed-to-Satisfy requirements because this code was followed at the time of the building construction. The internal load profiles and schedules for lighting, equipment, occupancy, and infiltration are also referenced from the BCA2010, with infiltration rate of 1 ACH, lighting power density of 9W/m², equipment power density of 15W/m², and occupancy density of 10m²/person (Australian Building Codes Board, 2010). The HVAC schedules and temperature set-points are shown in Table 2 based on the CCHR HVAC system design.

Name	Construction (outside to inside layer)	Total U value (W/m ² K)
External wall	Concrete block, air gap, R2.7 insulation, 19mm plasterboard	3.3
Roof and Ceiling	Concrete roof tiles, R3.6 roof insulation, 13mm ceiling board	4.2
Floor	Concrete slab on ground, R1.0 insulation	1.25
Window U-value		1.56
Window SHGC	Aluminum frames	0.28 on East and 0.22 on others

Table 1. *CCHR building envelope physical properties*

System type	Schedule	Heating set-point	Cooling set-point
Single Zone CAV	7:00-18:00 & 24/7	21°C	23°C
Multi Zone CAV (with humidity control)	24/7		20°C, 50% RH
Multi Zone CAV (with local hot water heating coils)	24/7	21°C	24°C
Multi Zone VAV	7:00-18:00	21°C	24.5°C
FCU	7:00-18:00 & 24/7	21°C	24.5°C

Table 2. HVAC system schedules and temperature set-points

Properties	Parameters
Solar Panel Model	LG420N2W-L5
Module Dimensions (L x W x H)	2,024mm x 1,024mm x 40mm (~2m ² active area)
Solar PV area [m ²]	1740 x 30% = 522
Cell Properties (Material/Type)	Monocrystalline/N-type
Total solar PV capacity [kW]	109.6
Electrical Properties (STC*)	
Maximum Power (Pmax) [W]	420
MPP Voltage (Vmpp) [V]	42.1
MPP Current (Impp) [A]	9.98
Open Circuit Voltage (Voc, ±5%) [V]	49.7
Short Circuit Current (Isc, ±5%) [A]	10.63
Module Efficiency [%]	20.3
Temperature Characteristics	
NMOT** [°C]	42±3
Pmax [%/°C]	-0.35
Voc [%/°C]	-0.26
Isc [%/°C]	0.025

*STC (Standard Test Condition): Irradiance 1000 W/m², cell temperature 25°C, AM 1.5

**NMOT (Nominal Module Operating Temperature): Irradiance 800W/m², Ambient temperature 20°C, Wind speed 1 m/s, Spectrum AM 1.5

Table 3. Solar PV parameters

The proposed solar PV system parameters are listed in Table 3. The selected solar PV module is LG's best-selling solar module NeON[®] 2, which is one of the most powerful and versatile modules on the market today¹. The total solar PV area is assumed to be 30 per cent of the total roof area by considering the roof located cooling towers, other equipment and maintenance activities occupation.

1.3 Climate weather files

The current and future climate files used for simulation are sourced from CSIRO (Ren et al., 2021a, 2021b). Climate files using the RCP8.5 pathway are chosen for Brisbane 2030, 2050, 2070, and 2090 future climates due to its nature as 'worst-case' scenario (Foo, 2020).

2. RESULTS AND DISCUSSIONS

2.1 Effects of heating electrification on HVAC performance under current climate

2.1.1 Annual HVAC energy performance

The annual HVAC energy performance of the base case and the heating electrification scenarios are shown in Figure 2. The base case total annual on-site energy use is 4,811GJ, including 814GJ natural gas consumption for gas boiler heating, 80GJ electricity energy use for FCU electric heating, and the rest of 3,879GJ electricity use for other HVAC components. While the annual HVAC energy consumption for the heating electrification alternative (by

¹ SolarDesignTool, LG Solar Panels (PDF).

replacing the natural gas-powered boiler in the base case scenario with a resistive electric powered boiler) is 4,647GJ with 655GJ on-site solar PV electricity generation for the proposed 109.6kW solar system, resulting in a net on-site annual electricity consumption of 3,992GJ only. This leads to about 17 per cent total annual on-site energy savings.

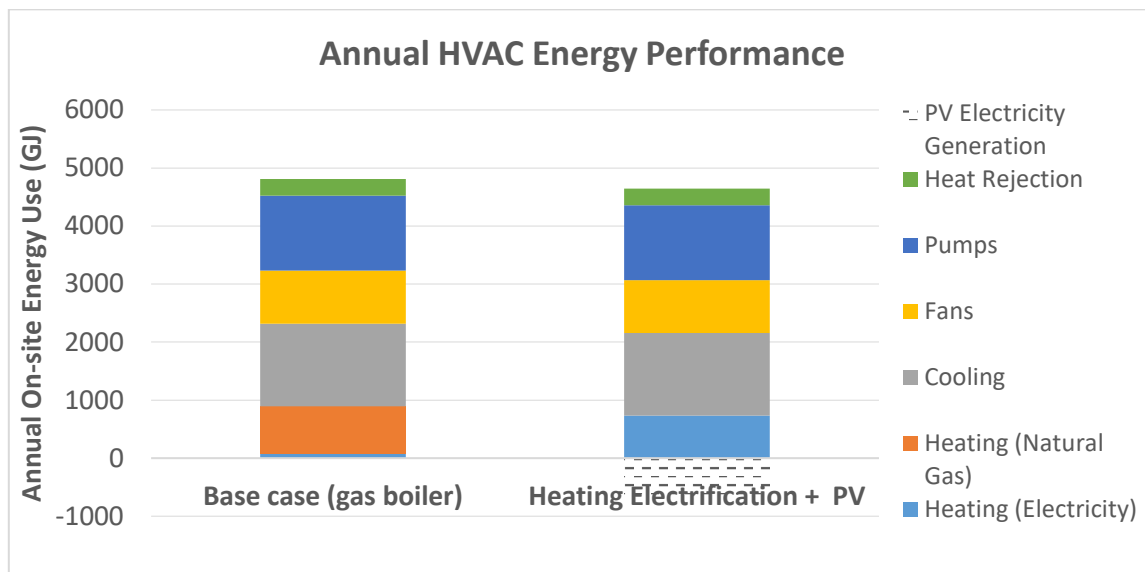


Figure 2. HVAC energy performance of the base case and heating electrification alternative

The heating electrification impacts on cooling, fans and pumps are negligible, while heating demand is significantly reduced from 894GJ (both natural gas and electricity) to 733GJ (electricity only), which results in 18 per cent of the annual total on-site energy reductions for heating. The reduced consumption for heating is mainly due to the higher efficiency of the electric boiler compared to the natural gas powered boiler.

2.1.2 Annual CO₂ emissions

The annual CO₂ emissions calculation is based on the following formula:

$$M_{CO_2} = E_{Gas} \times CO_2factor_{Gas} + E_{Elec} \times CO_2factor_{Elec} \quad (1)$$

where:

M_{CO_2} = annual total on-site CO₂ emissions in kg;

E_{Gas} = annual natural gas consumption in GJ;

E_{Elec} = annual electricity consumption in GJ;

$CO_2factor_{Gas}$ = the CO₂ emission factor for natural gas in kgCO₂-e/GJ;

$CO_2factor_{Elec}$ = the CO₂ emission factor for electricity in kgCO₂-e/kWh.

The CO₂ emission factor for natural gas is assumed to be 51.53kgCO₂-e/GJ referenced from the National Construction Code (Australian Building Codes Board, 2019), and the CO₂ emission factor for electricity is assumed to be 0.78kgCO₂-e/kWh based on 2020 Indirect Scope 2 emissions factors (Department of Industry Science Energy and Resources, 2020).

The annual CO₂ emissions results are illustrated in Figure 3. It indicates that heating electrification with solar PV integration would result in about 4.7 per cent reduction in annual CO₂ emission compared to the base case scenario, which is equivalent to 42,993kg annual CO₂ emissions reduction.

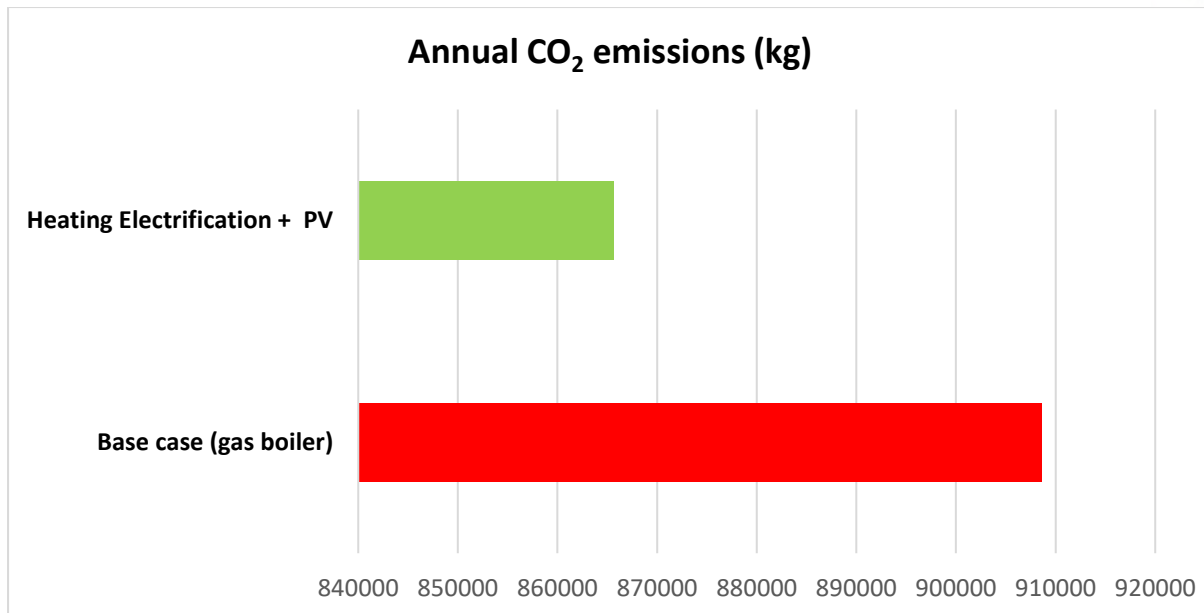


Figure 3. Annual CO₂ emissions

2.1.3 Annual operational energy cost

The annual operational energy cost is calculated using equation (2). In this study, only the general energy charge in annual consumption is considered (i.e. peak demand charges and connection fees are excluded).

$$OC = E_{Gas} \times c_{Gas} + E_{Elec} \times c_{Elec} \quad (2)$$

where:

c_{Gas} = natural gas price in \$/GJ, and assumes 7\$/GJ (Lewis Grey Advisory, 2020);

c_{Elec} = electricity price in \$/kWh, and assumes 0.12\$/kWh (Regional Queensland, 2020).

Figure 4 demonstrates the annual operational energy cost of the heating electrification alternative compared to the base case. It can be seen that under current conditions, heating electrification with solar PV has the potential to achieve 4.2 per cent annual operational energy cost savings. This is equivalent to reductions of about \$5,859 operational energy cost per year.

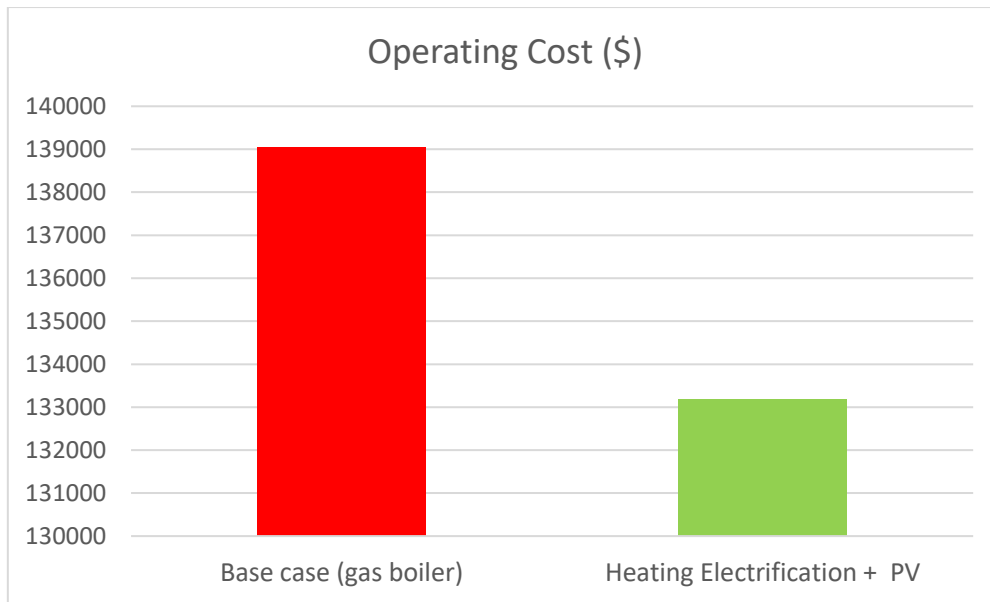


Figure 4. Annual operational energy-cost

2.2 Effects of heating electrification on HVAC performance under future climate

2.2.1 Annual future HVAC energy performance

Figure 5 below shows the impacts of future climates on CCHR’s HVAC energy performance for both of the base case and heating electrification scenarios.

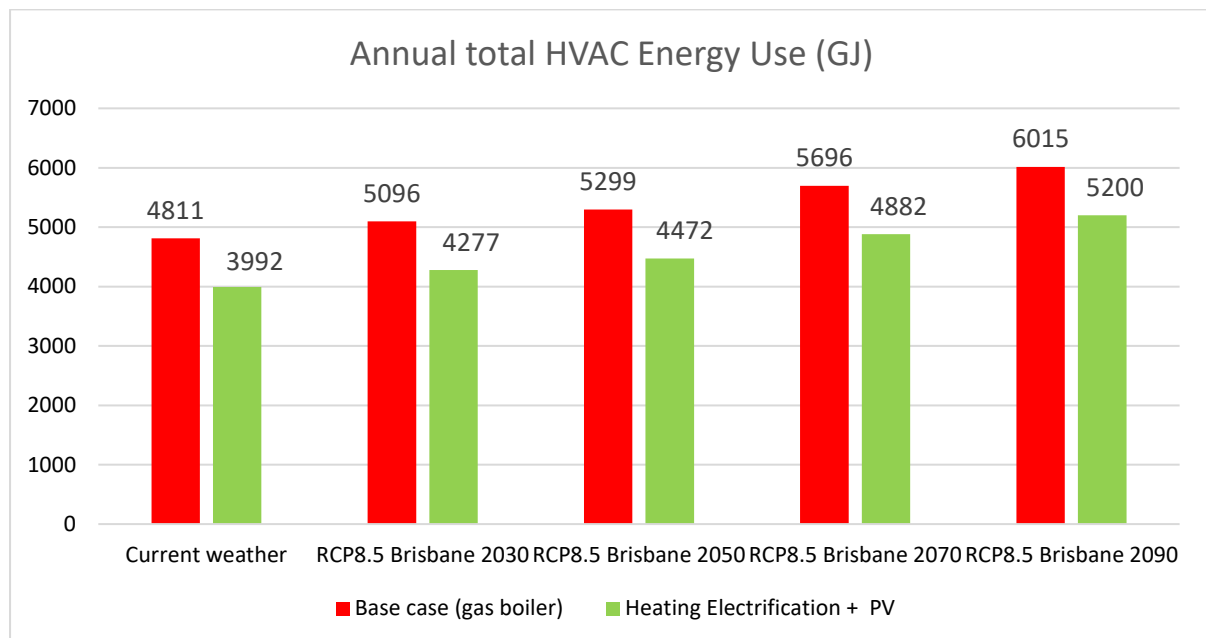


Figure 5. Impacts of heating electrification on HVAC energy performance under future climates

Compared to the current climate conditions, the HVAC energy consumption for the base case natural gas fuelled system would increase by 5.9 per cent in 2030, 10.1 per cent in 2050, 18.4 per cent in 2070, and 25 per cent in 2090. The HVAC energy use for the heating electrification alternative scenario would result in an increase of 7.1 per cent in 2030, 12 per cent in 2050,

22.3 per cent in 2070, and 30.3 per cent in 2090. The increased total HVAC energy use for both scenarios under the future climates is mainly due to the increased ambient temperature, which significantly impacts the cooling energy requirements.

The increase of the HVAC energy use due to climate change seems to be higher in percentage for the heating electrification alternative scenario than the base case scenario. However, this does not mean that heating electrification is not beneficial in terms of energy efficiency for future climates, with the simulations indicating that the heating electrification scenario could achieve 16.1 per cent annual HVAC energy savings in 2030, 15.6 per cent savings in 2050, 14.3 per cent savings in 2070, and 15.7 per cent savings in 2090.

	Heating Energy (GJ)	Current weather	RCP8.5 Brisbane 2030	RCP8.5 Brisbane 2050	RCP8.5 Brisbane 2070	RCP8.5 Brisbane 2090
Base case	Natural gas	814	717	698	651	617
	Electricity	80	75	71	63	56
Heating Electrification + PV	Electricity	733	649	629	585	551
	PV Generation	655	674	686	682	690

Table 4. *Heating energy end use comparison with future climates*

Due to the rising temperatures in future climates, cooling demand is increasing while heating demand is decreasing. Table 4 summarises the heating energy end use and solar PV generation with climate change for both scenarios. It demonstrates that compared with the current climate, by 2090, heating energy demand could be reduced by up to 24.2 per cent and 30 per cent from natural gas and electricity, respectively, and a combined total heating end use reduction of 24.7 per cent for the base case. While for the heating electrification scenario, heating demand from electricity could be reduced up to 24.8 per cent by 2090. Although the percentage of heating demand reductions under future climates are quite similar for both scenarios, the solar PV electricity generation for the heating electrification alternative scenario outweighs the heating electricity consumption after 2030 under current solar PV system design conditions. This proves that zero energy heating is achievable through heating electrification with renewable energy resources to be resilient to future climates.

2.2.2 Annual future CO₂ emissions

Due to the global warming effect and increased HVAC energy demand, the annual CO₂ emissions for both scenarios are increasing with future climates. However, the potential of CO₂ emissions reduction by using the heating electrification alternative is also increasing. Compared to the base case (gas boiler scenario), as shown in Figure 6, heating electrification with solar PV scenario would achieve 59,214kg (6 per cent) annual CO₂ emissions reduction in 2030, 63,993kg (6.19 per cent) annual CO₂ emissions reduction in 2050, 68,927kg (6.11 per cent) annual CO₂ emissions reduction in 2070, and 74,871kg (6.23 per cent) annual CO₂ emissions reduction in 2090. Heating electrification with solar PV integration becomes more environmentally beneficial for building decarbonisation when considering global warming.

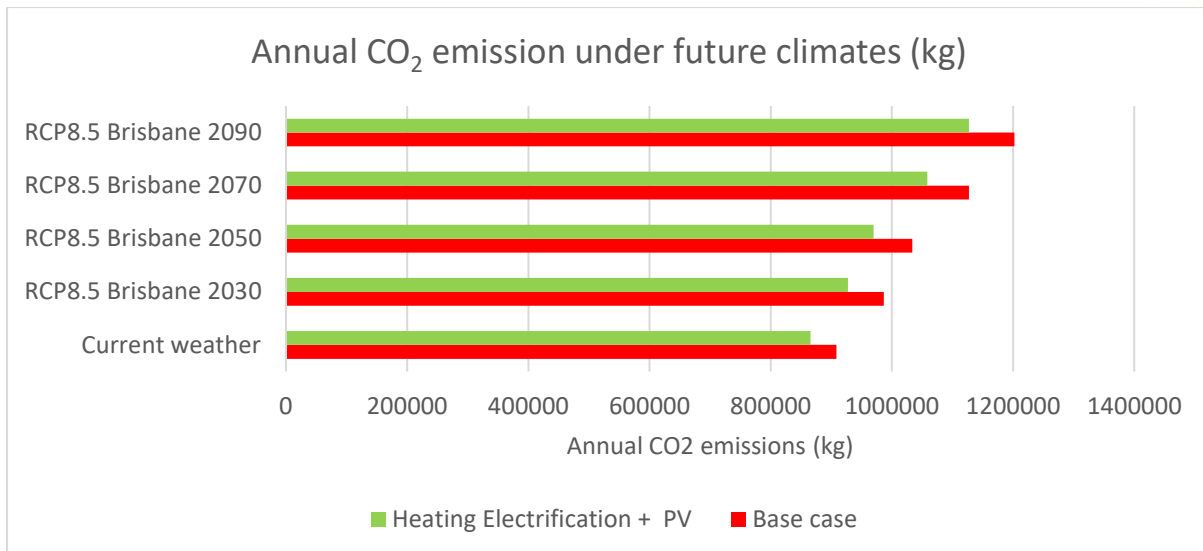


Figure 6. Annual CO₂ emissions under future climates

CONCLUSION

Global warming and climate change would significantly impact the energy efficiency and carbon footprint for commercial buildings and commercial HVAC systems. Heating electrification with renewable energy investment is a low risk, technically feasible, economically attractive, and environmentally friendly solution for large commercial building decarbonisation. This study investigated the impacts of heating electrification with renewable energy investment for a case study building in Brisbane under both current and future climates. Our case study results indicated that heating electrification with solar PV integration has significant potential to reduce energy consumption and CO₂ emissions under both current and future climate conditions.

Simulation results showed that under current climate conditions, by replacing the natural gas boiler with an electric boiler with installed 109.6kW solar PV system, the CCHR building could achieve 819GJ (17 per cent) reductions regarding on-site HVAC energy use and 42,993kg (4.7 per cent) reductions in terms of CO₂ emissions, with \$5,859 (4.2 per cent) operational energy cost savings per year.

Future climates modelling results demonstrated that heating electrification alternative with renewable energy is beneficial to building decarbonisation from both energy and environment perspectives. Despite of the increased total HVAC energy demand due to climate change, future heating energy demand would be reduced by up to about 24 per cent by 2090 and heating electrification with solar PV would have the potential to provide net-zero heating after 2030. In addition, more than 15 per cent of the HVAC energy use and 6 per cent CO₂ emissions could be saved in the future by switching the natural gas fired boiler to heating electrification coupled with solar PV. Economic analysis and peak demand impacts under future climates for heating electrification will be conducted for future work.

ACKNOWLEDGEMENTS

This study is supported by the Innovation Hub for Affordable Heating and Cooling (iHub) project led by the Australian Institute of Refrigeration, Air Conditioning and Heating (AIRAH), and funded by Australian Renewable Energy Agency (ARENA) to facilitate the heating, ventilation, air conditioning and refrigeration (HVAC&R) industry's transition to a low emissions future, stimulate jobs growth, and showcase HVAC&R innovation in buildings.

REFERENCES

- AIRAH. (2015). *i am your optimisation guide - heating, ventilation and air conditioning systems*. Office of Environment and Heritage. www.environment.nsw.gov.au
- Australian Building Codes Board. (2010). BCA2010 Building Code of Australia - Volume One. In. Canberra, ACT: Australian Building Codes Board,.
- Australian Building Codes Board. (2019). NCC 2019 Building Code of Australia - Volume One. In. Canberra, ACT: Australian Building Codes Board,.
- Department of Industry Science Energy and Resources. (2020). *Australia's emissions projections 2020*. Department of Industry Science Energy and Resources.
- DesignBuilder. (2019). *DesignBuilder v6 Simulation Documentation* <https://designbuilder.co.uk/download/documents>
- Eguiarte, O., Garrido-Marijuán, A., de Agustín-Camacho, P., del Portillo, L., & Romero-Amorrortu, A. (2020). Energy, Environmental and Economic Analysis of Air-to-Air Heat Pumps as an Alternative to Heating Electrification in Europe. *Energies*, 13(15). <https://doi.org/10.3390/en13153939>
- Ernst & Young. (2019). *Achieving Low Energy Existing Commercial Buildings in Australia*. Department of Environment and Energy. <https://www.energy.gov.au/government-priorities/buildings/commercial-buildings>
- Foo, G. (2020). *Climate Change - Impact on Building Design and Energy*. COAG Energy Council.
- Harrington, P., Zhang, H., Bloomfield, C., Johnston, D., & Shen, D. (2018). *Achieving Low Energy Commercial Buildings in Australia*. Department of Environment and Energy.
- Lewis Grey Advisory. (2020). *Gas Price Projections for the 2021 GSOO*. Australian Energy Market Operator.
- Liu, A., Ma, Y., & Miller, W. (2020). *Healthcare Living Laboratories: Queensland Children's Hospital - Operation Manual and Baseline Data*. Australian Institute of Refrigeration Air Conditioning and Heating. www.ihub.org.au
- Padovani, F., Sommerfeldt, N., Longobardi, F., & Pearce, J. M. (2021). Decarbonizing rural residential buildings in cold climates: A techno-economic analysis of heating electrification. *Energy and Buildings*, 250. <https://doi.org/10.1016/j.enbuild.2021.111284>
- Pease, P., Chhabra, J., & Zolfaghari, Z. (2021). Planning for net zero by 2050, what HVAC system interventions will today's code minimum commercial buildings require? <https://doi.org/https://doi.org/10.48550/arXiv.2111.03899>

- Regional Queensland. (2020). *Final determination: Supplementary review: Regulated retail electricity prices 2020–21*. The Queensland Competition Authority.
- Ren, Z., Tang, Z., & James, M. (2021a). *Predictive weather files for building energy modelling User Guide*. CSIRO.
- Ren, Z., Tang, Z., & James, M. (2021b). *Typical meteorological year weather files for building energy modelling - User Guide* CSIRO.
- Tarroja, B., Chiang, F., AghaKouchak, A., Samuelsen, S., Raghavan, S. V., Wei, M., Sun, K., & Hong, T. (2018). Translating climate change and heating system electrification impacts on building energy use to future greenhouse gas emissions and electric grid capacity requirements in California. *Applied Energy*, 225, 522-534. <https://doi.org/10.1016/j.apenergy.2018.05.003>
- U.S. Department of Energy. (2021). *Decarbonizing HVAC and Water Heating in Commercial Buildings*. U.S. Department of Energy. <https://betterbuildingssolutioncenter.energy.gov/>
- Walker, I. S., Less, B. D., & Casquero-Modrego, N. (2022). Carbon and energy cost impacts of electrification of space heating with heat pumps in the US. *Energy and Buildings*, 259. <https://doi.org/10.1016/j.enbuild.2022.111910>

DISCLAIMER

The information or advice contained in these technical papers is intended for use only by professionals who have had adequate technical training in the field to which the paper relates. At the time of publication, these technical papers have undergone a formal peer-review process.

These documents have been compiled as an aid only, and the information or advice should be verified before it is put to use. The user should also establish the applicability of the information or advice in relation to any specific circumstances. While the information or advice is believed to be correct, no responsibility is taken by AIRAH or IBPSA Australasia for any statements made within.

AIRAH and IBPSA Australasia, its officers, employees and agents, disclaim responsibility for any inaccuracies contained within the documents, including those due to any negligence in the preparation and publication of the said technical papers.

COPYRIGHT

This work is copyright. Apart from any use as permitted under the Copyright Act 1986, no part may be reproduced by any process without prior written permission from either the Australian Institute of Refrigeration, Air Conditioning and Heating (AIRAH) or the International Building Performance Simulation Association (IBPSA) Australasia.

STUDY OF USING A SIMPLIFIED TRANSIENT HEAT TRANSFER MODEL FOR BOREHOLE HEAT EXCHANGERS USING ARTIFICIAL NEURAL NETWORK TO PREDICT VARIOUS OUTPUT PARAMETERS

**MICHAEL KOSTEVSKI
DR. ALAN S. FUNG, PHD
DR. WEY H. LEONG, PHD
DR. ESA D. KERME, PHD**

ABSTRACT

A simplified numerical heat transfer model was used to analyse single and double U-tube borehole heat exchangers (BHE) with various outputs consisting of heat transfer, overall heat transfer per unit borehole length, thermal effectiveness, thermal resistance, and fluid temperature change. Through performing both single and double U-tube BHE analyses, simulation times have shown to be quite long. In developing an artificial neural network (ANN), these simulation times can be reduced to quickly obtain output values, as an ANN model can be used to predict the output parameters without requiring compute-intensive simulations to be run. To run these simulations, eight different input parameters were required. These input parameters are borehole radius, length, grout and soil thermal conductivity, half shank spacing, inlet fluid temperature and flow rate, and ground temperature. Numerous simulations were run varying the eight input parameters, providing corresponding output parameters. The data obtained through running the simulations were used to develop an ANN model. Specified parameters were also needed to create the ANN, such as the number of layers and neurons used. It was found that using 3 layers with 10 neurons each, the ANN would provide optimal results. Through creating an ANN, the five output parameters were tested simultaneously, and it was concluded that both single and double U-tube vertical BHE had both validation and training sets with R values greater than 0.999, meaning the ANN can provide quick results with high accuracy.

INTRODUCTION

In running the simulations to analyse the single and double U-tube BHE's, a simplified numerical method was used. Although providing accurate data for the performance of BHE's, the inputs parameters are required to be manually changed when analysing different scenarios. Attempting to analyse the BHE with different input parameters can be time consuming as after each simulation, the written code will need to be manually changed. The main goal of developing the ANN is to reduce these simulation times and allow for numerous scenarios with the BHE to be analysed quickly. The main benefits of using an ANN based approach is that complex modelling and computations are not required to determine output data [1]. In modern day applications of implementing single and double U-tube BHE, being able to analyse different scenarios can help in determining an optimised design with given parameter constraints. Developed ANN models have been proven to show capability of predicting outputs with low computation times and high accuracy [2]. In many real-world applications, analysing trends with many input parameters is very

difficult. Artificial neural networks can effectively be used to provide preliminary results in simplified models that can better reflect the parameters of the design in early stages with limited information available [3].

1. THEORY

In analysing both single and double U-tube borehole heat exchangers, a simplified transient heat conduction model was numerically simulated through a MATLAB code to generate borehole parameter outputs. The entire length of the BHEs is divided into several control volumes. Each control volume contains two or four fluid nodes in pipes, a grout node, and a borehole-wall node, as well as a series of cylindrical ground control volumes outside of the borehole. The thermal resistance circuits of each BHE control volume and the ground control volumes are shown in Figure 1.

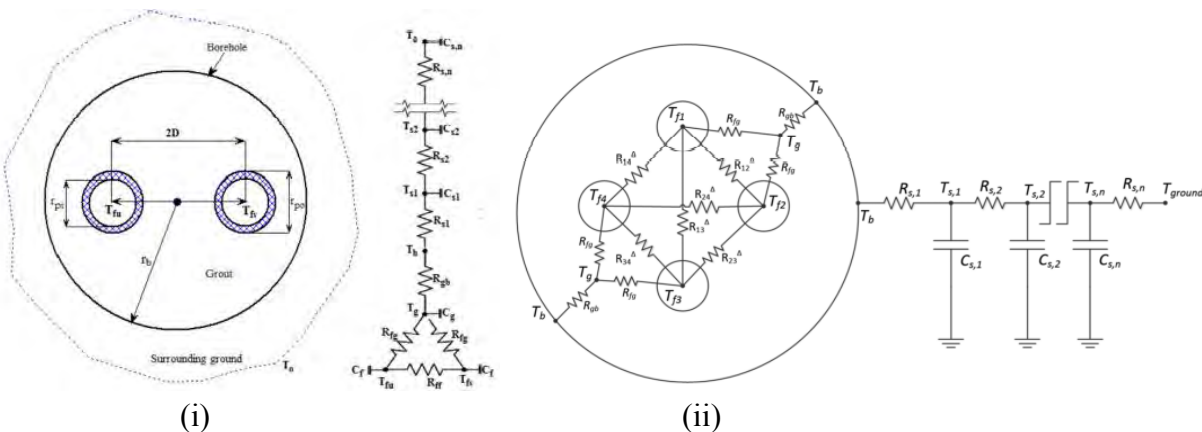


Figure 1. Thermal Resistance Circuit for (i) Single BHE [4] and (ii) Double BHE [5]

An energy balance was applied to the nodes of both the single and double U-tube scenarios which aided in the development of the energy balance equations for all nodes in the BHE control volume and ground control volumes outside the borehole. Based on the thermal resistances in Figure 1, the energy balance equations of all nodes were generated and coupled. The energy balance equations were then solved using the Crank-Nicolson method, which is a fully implicit numerical method, for advancing in time. This method was used for obtaining the algebraic 3 equations to guarantee stability in the numerical model [3X]. The algebraic equations were formulated unto matrix format and then solved for the temperatures of all nodes throughout the BHE at each time step. Then, based on the numerical results, the borehole loading, and thermal effectiveness of the BHE were calculated over a one-month period. The details of the numerical models can be found in [3X] and [4X].

A MATLAB model was used to manually obtain data by running simulations individually, in which this data was then implemented into the ANN. Neural networks mimic the human brain in how information is processed and contain multiple layers with interconnected neurons that are used to solve specific problems [6]. The ANN used to train and model the simulated BHE result data sets is a feedforward network meaning the signals travel only from input to output without loops [7]. This type of network is associated with pattern recognition which is the main goal in

generating the outputs for the BHE's. An ANN model consists of three major components. These components are the artificial neurons, the decision layout, and the learning algorithm [8]. The artificial neurons contain several major components within them. Firstly, weighting factors are used to define relative importance to different components in the data set. These weights are similar to the varying synaptic strengths of biological neurons. A summation function is needed to compare the weighted sum of all the inputs through converting the weighted inputs into input signals. These input signals are then processed through a transfer function to determine a neural output. Values obtained from the transfer function are either scaled or limited to prevent exceeding a specified bound. Once output values are received errors are calculated through comparing the difference between current and desired output values, altering the values respectively. Finally, an adaptation function modifies the weights of the inputs to achieve desired results. To properly generate the ANN model, input parameters, output parameters, number of hidden layers, and number of neurons are all needed. The input parameters consist of all the varying parameters within the MATLAB code which can be seen below in Table 1.

Borehole Radius (m)	0.05, 0.073, 0.10
Borehole Depth (m)	50, 100, 150
Grout Thermal Conductivity (W/m-K)	0.8, 1.1, 1.4
Half Shank Spacing (m)	0.032, 0.042, 0.052
Soil Conductivity (W/m-K)	3.0, 4.0, 5.0
Inlet Fluid Mass Flow Rate (kg/s)	0.15, 0.30, 0.45
Inlet Fluid Temperature(°C)	30, 40, 50
Ground Temperature (°C)	10, 15, 20

Table 1. *Varied Borehole, Soil, and Grout Properties used in manually input simulations*

The values shown in Table 1 were used to generate corresponding outputs used train and develop ANN. As the number of neurons used to generate an ANN increase, the performance of the ANN correspondingly decreases [9]. However, ANN results developed with 5-25 neurons have higher prediction performance compared to other models outside this range [9]. Staying within this range, in developing the ANN it was decided that 10 neurons would be used. In terms of the number of hidden layers used in the ANN, increasing the number of layers generally provides higher reliability for more accurate prediction [10]. Common ANN models generally have two hidden layers, however increasing this should also increase prediction performance. For this reason, it was chosen that while generating the ANN model, three hidden layers would be used. Through generating the ANN used to model single and double U-tube BHE, the five output variables were tested simultaneously. Given that a feedforward ANN is used in this analysis, a schematic outlining the comparison between the inputs, outputs, and hidden layers can be seen in Figure 2.

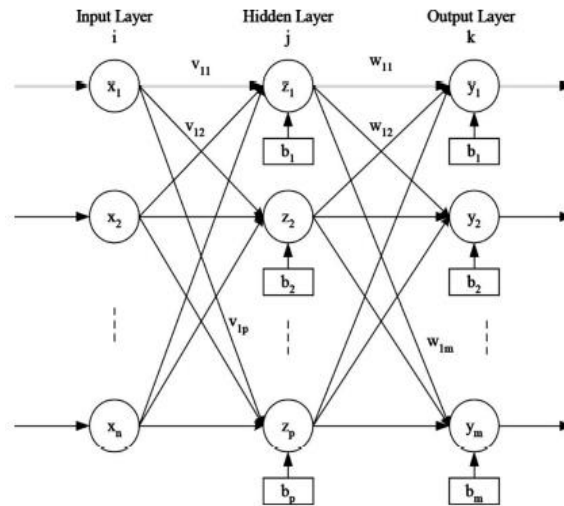


Figure 2. Main Layers comprising ANN model [8]

In Figure 2, comparing that diagram to ANN model developed, there would be eight input parameters, five output parameters (outlined in the Discussion section), and three hidden layers each with 10 neurons. The final major component of the ANN is the learning algorithm. In this scenario, a supervised learning algorithm is used. A supervised learning algorithm uses known input and output parameters and compares them in the neural network. Weighting factors are initially random, but as epochs are completed these values adjust to produce closer matches between the actual and desired outputs. An epoch means that each sample in the training dataset has had an opportunity to update the internal model parameters. The main purpose of the supervised learning algorithm is to minimise errors to be able to predict output values through unknown inputs. This directly correlates to the main purpose of this paper as being able to predict output values will greatly reduce time in analysing the BHE's. A simplified diagram of the main function of the ANN is shown in Figure 3.

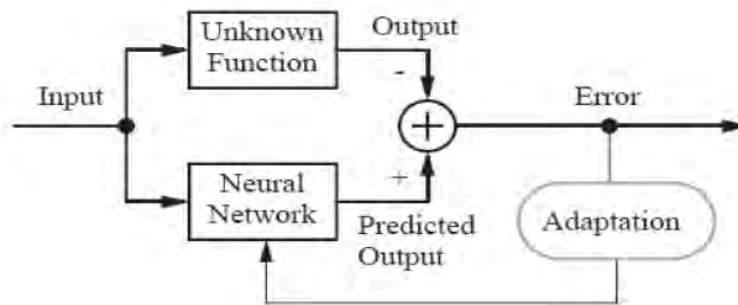


Figure 3. Simplified Schematic of ANN process [7]

Figure 3 visually outlines how few of the major components of the ANN work to predict output values.

2. DISCUSSION

The main purpose of this paper is to outline how an effective ANN model can be used to determine both single and double U-tube BHE output parameters. Through running a total of 13,122 simulations with eight input parameters resulting in five output parameters, the ANN can be used to quickly predict output values for inputs within the testing data set. This greatly simplifies the design process as the overall BHE system can be quickly analysed based on variable input parameters. The variable input parameters come from running individual simulations which were then used to model the ANN. An ANN would be able to provide faster results when determining output variables within the training dataset. When initially obtaining the data required to model the ANN, a simplified numerical method simulation was used. In running these simulations for both single and double U-tube borehole heat exchangers, eight input parameters were varied. These input parameters as well as the values they were varied by are shown in Table 1. The output value obtained through testing these simulations were as follows:

- Overall Heat Transfer (Watts)
- Borehole Loading or Heat Transfer Per Unit Length (Watt/meter)
- Borehole Effectiveness
- Overall Borehole Thermal Resistance (Kelvin/Watt)
- Fluid Temperature Difference (°C).

All these output parameters were tested simultaneously in the ANN model. In doing this, the model was trained analysing so assess how all the outputs are affected with similar inputs. Through running testing simulations and obtaining all of the required data, the validation performance was obtained for both single and double U-tube BHE seen in Figure 4.

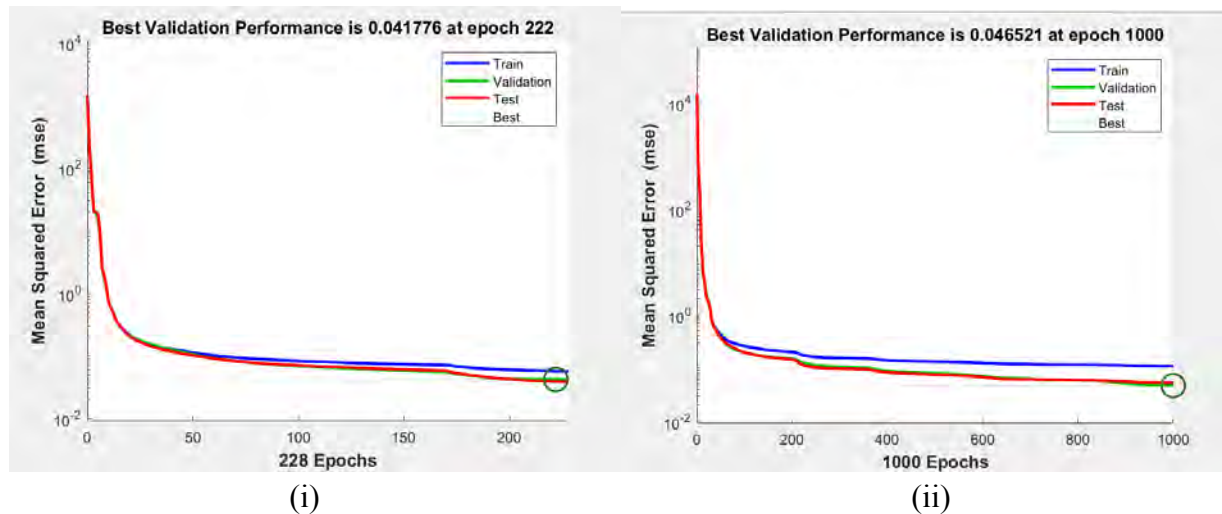


Figure 4. *Validation Performance Testing for (i) Single U-tube BHE and (ii) Double U-tube BHE*

Figures 4(i) and 4(ii) show the validation performance of the single and double U-tube borehole heat exchangers when implemented into the developed MATLAB code. The test set which represents the known input parameters can be seen to be very similar to the validation set. Each epoch tested defines the number of times the ANN will work through the entire training set. As

seen in Figure 4(i), through roughly all 240 epochs in the single U-tube BHE, the neural network training almost directly correlates to the validation and testing sets. Similarly, with Figure 4(ii), 1000 epochs were used to validate the testing for the double U-tube BHE. In both training sets, 70 per cent of the simulation data was used for training, 15% of the data was used for validation, and 15 per cent of the data was used for testing. The post processing of all these tests is applied on a network for validation results, which are used to describe, analyse, and improve the final performance.

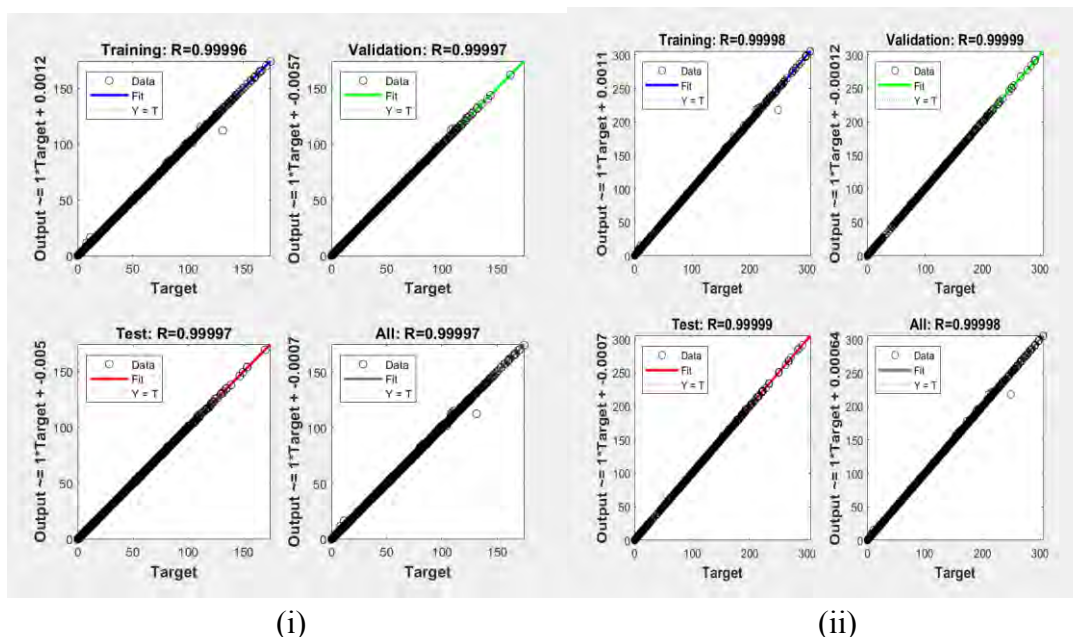


Figure 5. (i) Single BHE Regression Data (ii) Double BHE Regression Data

Figures 5(i) and 5(ii) show the regression statistics between ANN prediction and actual data for both single and double U-tube BHE. Through all these tests, there is minimal variation between the test sets. This shows that the ANN model would be effective in predicting data within the minimum and maximum boundaries tested with the input parameters. Shown in Figures 5(i) and 5(ii), the regression values greater than 0.999 outlining the validity of the tests. Using the previously inputted parameters to train the set, the ANN was able to create a model that can provide output parameters when using the variable input parameters within the training set. The regression data also outlines how the ANN model was not overtrained, meaning the model recognised an underlying trend. The obtained data from the ANN shows that a proper model was simulated for both the single and double U-tube BHE. Given that the ANN model is validated, the output parameters of the overall system can be determined for any set of input parameters, not just the ones tested. This means that the ANN model can predict BHE performance, such as predicting the overall heat transfer, heat transfer rate per unit length, effectiveness, thermal resistance, and fluid temperature difference. Through analysing the various output parameters, the most important are the heat transfer and effectiveness of the BHE. These two output parameters were implemented individually to generate their own specified ANN models. The regression values of these models can be seen in Figures 7 and 8.

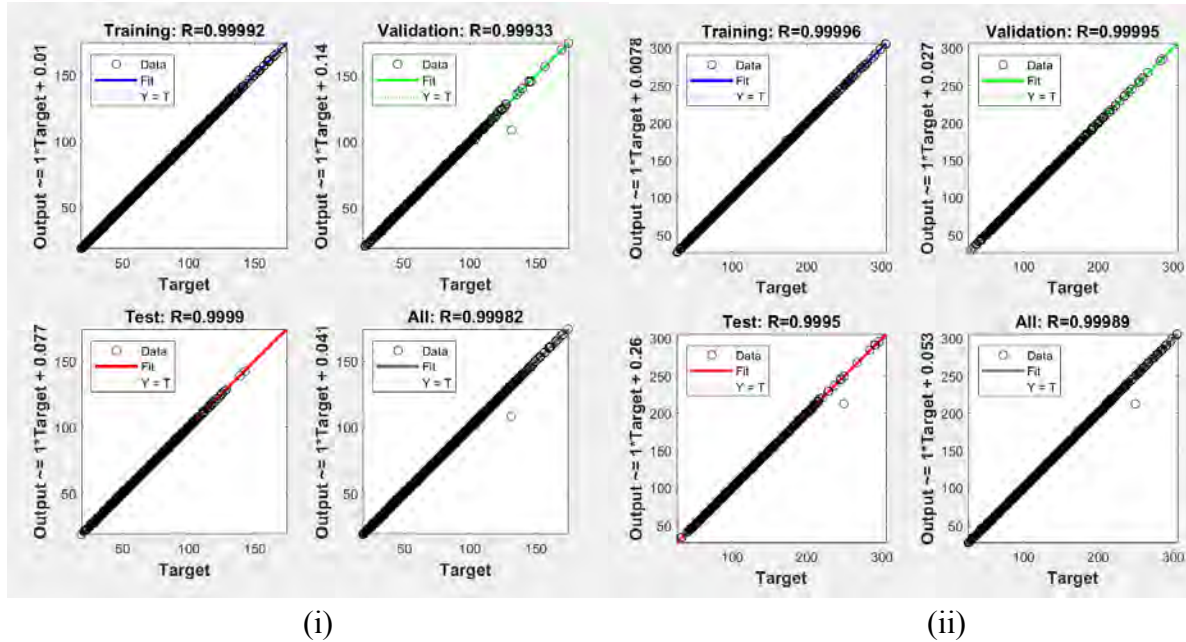


Figure 6. Overall Heat Transfer Regression Data for (i) Single U-tube BHE (ii) Double U-tube BHE

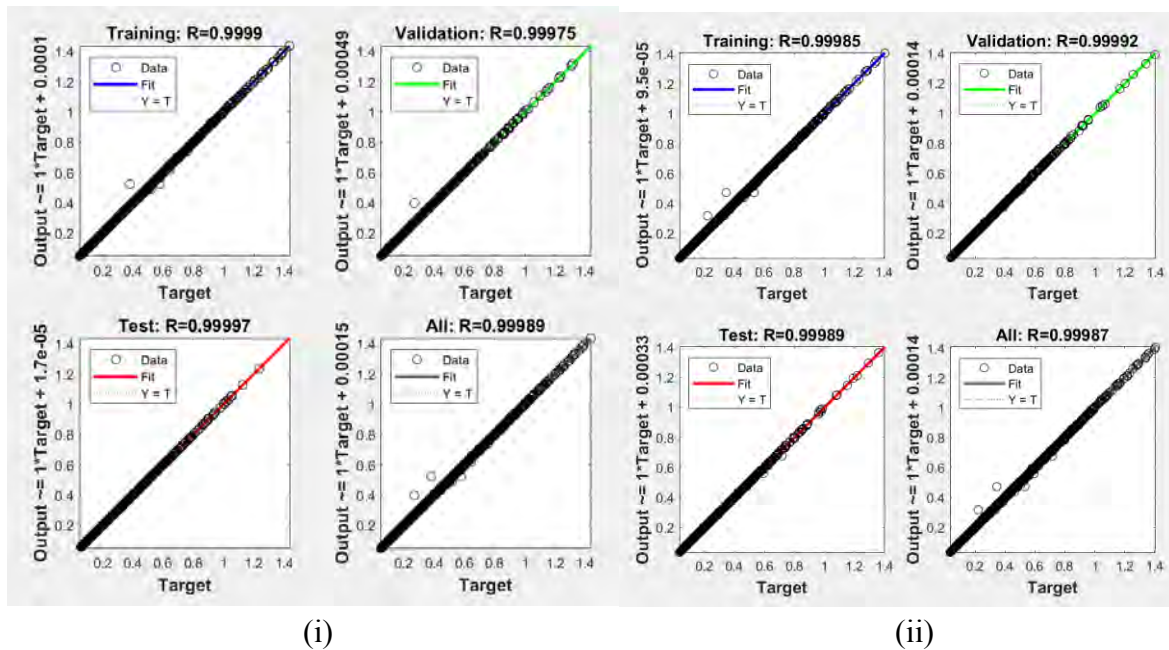


Figure 7. Effectiveness Regression Data for (i) Single U-tube BHE (ii) Double U-tube BHE

Figures 6 and 7 both outline high regression values, indicating that both heat transfer and effectiveness of the single and double U-tube BHE can be predicted. Being able to predict these parameters, alongside the other previously mentioned outputs will allow for quick analysis of BHE designs. The accuracy of the data allows for a model to be generated which can test various input parameters outside the tested values in Table 1. As stated previously, this would greatly reduce the

time required for determining the output parameters of the system and would aid in achieving a set of specific values for the output of the single or double BHE. Through using the simulated results to generate an ANN, the properties of the BHE can be easily determined.

CONCLUSION

After running a combined total of 13,122 simulations for single and double U-tube BHE, the artificial neural network was able to train itself for both single and double BHE's using all the given data. Through analysing the graphs, the data input into the code was able to be used to create different output data to be used. Since the regression values were very similar to the tested line in Figure 4, the neural network can be used to determine any reasonable output through any different input that was not already used to train the data. The use of artificial neural networks can help to determine various parameters through using known input parameters. This can help the design and optimisation of numerous borehole properties, including soil property, grout property, and other input parameters, from which the trained neural network can output reliable performance data.

ACKNOWLEDGEMENTS

The authors would like to thank the Ryerson FEAS Dean's Research Fund-Undergraduate Experience (DRF_URE) and Department of Mechanical and Industrial Engineering Undergraduate Student Research Assistant fund, and the Natural Sciences and Engineering Research Council (NSERC) of Canada Discovery grant for their financial support for this research.

REFERENCES

- [1] M. Ding, L. Wang, and R. Bi, “An ann-based approach for forecasting the power output of Photovoltaic System,” *Procedia Environmental Sciences*, vol. 11, pp. 1308–1315, 2011.
- [2] M. Saqib, M. I. Ansari, and P. Agarwal, “Effectiveness of ANN for seismic behaviour prediction considering geometric configuration effect in concrete gravity dams,” *Perspectives in Science*, vol. 8, pp. 432–434, 2016.
- [3] D. Ruff, K. Cant, T. Christiaanse, R. Evins, “Analysis of Feature Importance in Modeling Ground Source Heat Pump Systems Using Broad Parametric Analysis, Load Characterization and Artificial Neural Networks”, *Energy Cities Group*, Victoria, British Columbia, pp. 1-8
- [4] E. D. Kerme and A. S. Fung, “Heat transfer simulation, analysis and Performance Study of single U-tube borehole heat exchanger,” *Renewable Energy*, vol. 145, pp. 1430–1448, 2020.
- [5] E. Dube Kerme and A. S. Fung, “Transient heat transfer simulation, analysis and thermal performance study of double U-tube borehole heat exchanger based on numerical heat transfer model,” *Applied Thermal Engineering*, vol. 173, p. 115189, 2020.
- [6] “Neural networks - what are they and why do they matter?” *SAS*. [Online]. Available: https://www.sas.com/en_ca/insights/analytics/neural-networks.html. [Accessed: 12-Jan-2022].
- [7] O. Awodele, O. Jegede, “Neural Network and Its Application in Engineering”, *Science and IT Conference*, Ilishan-Remo, Nigeria, 2009, pp. 85-91
- [8] M. E. Poulad, D. Naylor, and A. S. Fung, “Prediction of local heat transfer in a vertical cavity using artificial neural networks,” *Journal of Heat Transfer*, vol. 132, no. 12, 2010.
- [9] A. B. Çolak, “A novel comparative investigation of the effect of the number of neurons on the predictive performance of the Artificial Neural Network: An experimental study on the thermal conductivity of ZRO 2 nanofluid,” *International Journal of Energy Research*, vol. 45, no. 13, pp. 18944–18956, 2021.
- [10] J. N. Ogunbo, O. A. Alagbe, M. I. Oladapo, and C. Shin, “N-hidden layer artificial neural network architecture computer code: Geophysical Application Example,” *Heliyon*, vol. 6, no. 6, 2020.

DISCLAIMER

The information or advice contained in these technical papers is intended for use only by professionals who have had adequate technical training in the field to which the paper relates. At the time of publication, these technical papers have undergone a formal peer-review process.

These documents have been compiled as an aid only, and the information or advice should be verified before it is put to use. The user should also establish the applicability of the information or advice in relation to any specific circumstances. While the information or advice is believed to be correct, no responsibility is taken by AIRAH or IBPSA Australasia for any statements made within.

AIRAH and IBPSA Australasia, its officers, employees and agents, disclaim responsibility for any inaccuracies contained within the documents, including those due to any negligence in the preparation and publication of the said technical papers.

COPYRIGHT

This work is copyright. Apart from any use as permitted under the Copyright Act 1986, no part may be reproduced by any process without prior written permission from either the Australian Institute of Refrigeration, Air Conditioning and Heating (AIRAH) or the International Building Performance Simulation Association (IBPSA) Australasia.

GAP ANALYSIS: PUSHING NABERS RATINGS THROUGH ENERGY SIMULATION

MANASA MARASANI (B. MECH ENG, M. ARCH SCI)

Environmental Engineer

Atelier Ten

Level 1, 79 Myrtle Street, Chippendale NSW 2008

manasa.marasani@atelierten.com

ABOUT THE AUTHOR

As an Environmental Designer, Manasa is experienced in Building physics and Energy modelling. Her practice includes design for thermal comfort, environmentally sustainable and healthy buildings. Manasa has previously worked in detailed HVAC design and coordination, having experience in commercial, educational, and residential facilities.

ABSTRACT

Achieving a NABERS 6 star rating is increasingly hard as it requires cutting in half the carbon emissions of a NABERS 5.5 star building, which itself is already an efficient building. The paper presents the potential of a typical 10 storey office in Sydney to push the NABERS ratings from 5.5 star to 6 star by targeting energy efficiency measures of the HVAC system design and equipment selection. Detailed energy modelling in IES-VE software was carried out to estimate the performance uplift derived from the mechanical system design changes and efficiency measures. This analysis showed us the key role fan and pump energy play in a building's energy consumption and the important role the economy cycle can play in the reduction of chiller energy in Sydney's climate zone. An early collaboration with the design team to facilitate implementable improvements proved to boost a building's energy rating.

INTRODUCTION

NABERS is a national initiative by the NSW Department of Planning, Industry and Environment on behalf of the federal, state and territory governments of Australia. It stands for National Australian Built Environment Rating System (NABERS) and is a national rating system that measures the environmental performance of Australian buildings and tenancies (*NABERS, 2022*). Put simply, NABERS measures the energy efficiency, water usage, waste management and indoor environment quality of a building or tenancy and its impact on the environment.

With the widespread recognition of climate change and its effects, and the push to reduce carbon emissions, most commercial buildings with sustainability goals target at least a 5 star NABERS rating. The majority of the ratings gravitate towards the base building energy rating of a commercial building that quantifies energy consumption of all possible end uses of a commercial building that is provided by the building owner to the tenant.

HVAC systems in commercial buildings use roughly 50 per cent of the total base building energy demand (this includes fan, pump and heat rejection energy) while the other ~50 per cent is taken up by other end uses like vertical transportation, domestic hot water, miscellaneous lighting and ventilation etc (DPIE, 2021). Since the amount of energy consumption by these other end uses depends heavily on the building design and use requirements, this paper concentrates on how the HVAC energy demand can be reduced through free running and equipment efficiency measures to push the building towards a better NABERS energy rating.

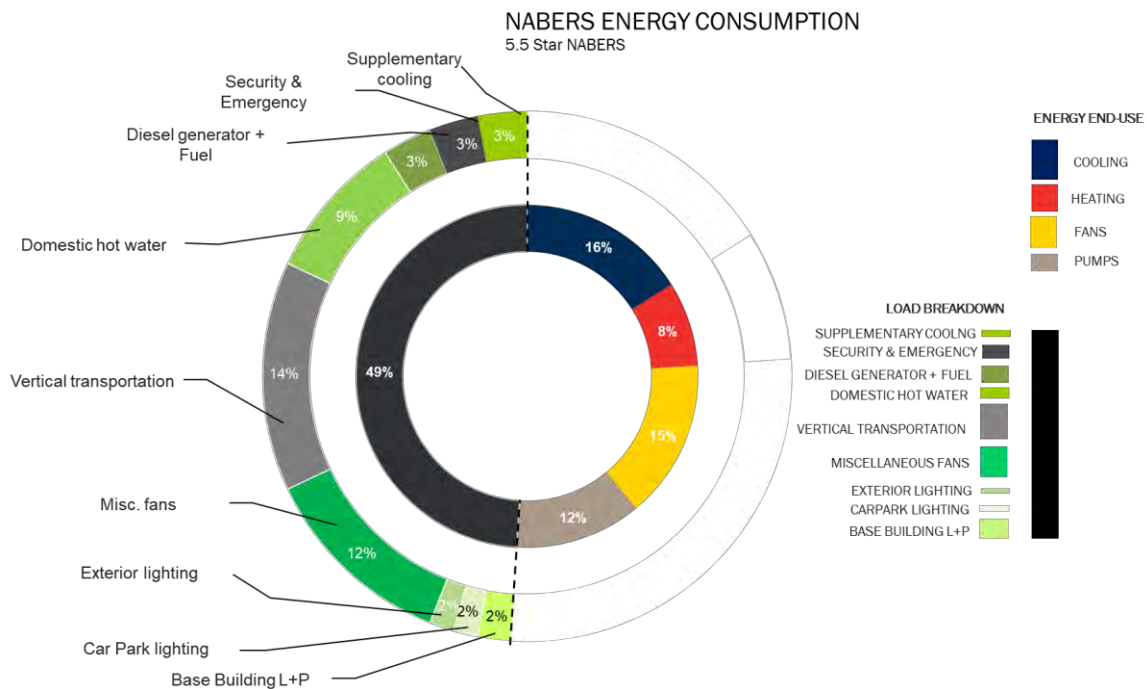


Figure 01: Typical breakdown of energy by end use, in a commercial building (Author)

1. DETERMINATION OF HVAC EFFICIENCIES

Considering, A gap analysis was conducted on a typical office building in the Sydney CBD to see what a combination of mechanical and miscellaneous system efficiencies, plus onsite solar photovoltaics system could do to push the expected energy rating of the project. The analysed building has a total of 10 floors with a net lettable area of 14,528m². It is designed to have floor by floor Air Handling Units (AHU's) with Variable Air Volume (VAV's) boxes to the central zones and Dedicated Outdoor Air System (DOAS) Fan Coil Units (FCU's) for the perimeter zones. Envelope construction details are designed to pass the NCC 2019 Section J requirements (performance solution), with R-2m².K/W external walls, R-3m².K/W, R-0.48m².K/W spandrel, and commercial windows with a system U value of 3.1W/m².K and Solar Heat Gain Coefficient (SHGC) of 0.25.

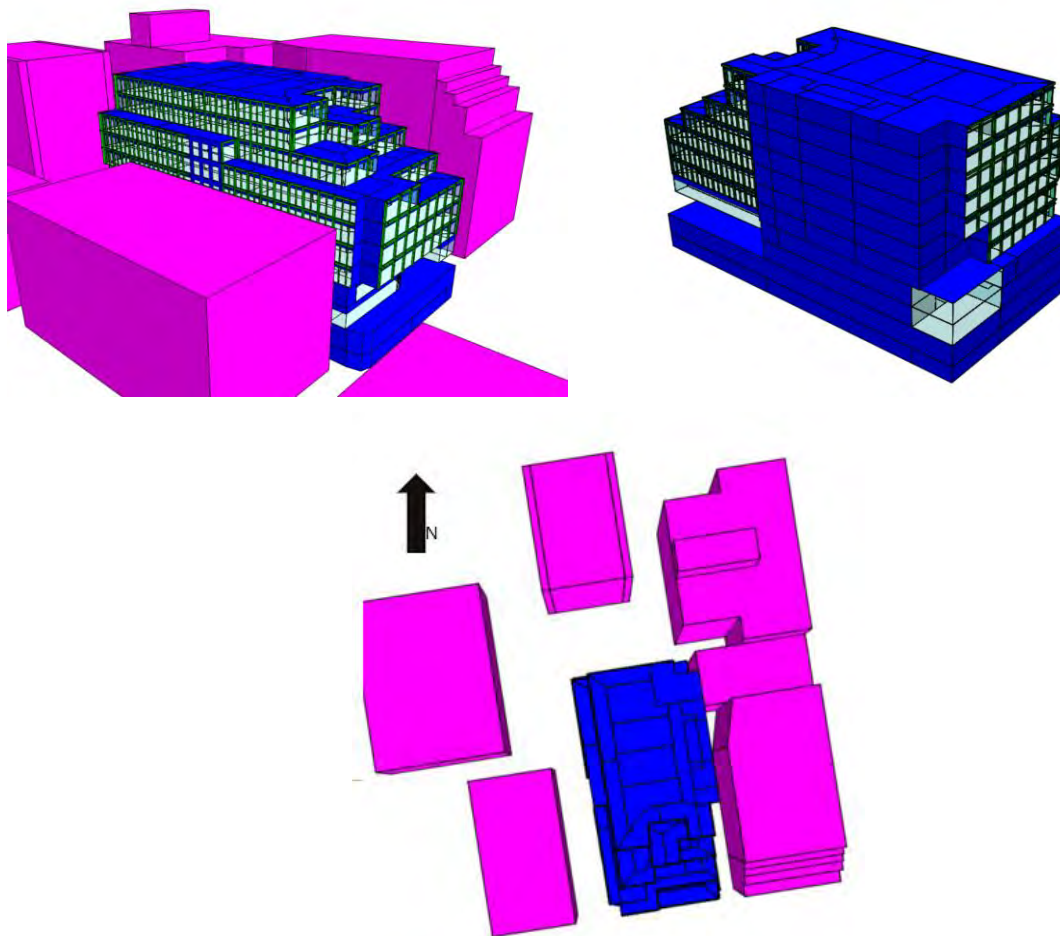


Figure 02: *Snapshots of the building taken from IES-VE 2019 software (Author)*

1.1 Methodology

The project requires a total $14 \text{ kgCO}_2/\text{m}^2$ to reach the 6 star NABERS target.

An extensive list of potential Energy Efficiency Measures (EEMs) (As seen in Table 01) was created by analysing the existing HVAC technology available and the technical specifications of systems in the market that are designed at high Coefficient of Performance factors. The ones listed were specifically chosen as they usually can be implemented in most office buildings and were hence analysed for their effectiveness.

These recommended measures, when incorporated with onsite PV, can help close the gap to achieve a 6 star NABERS rating. The various EEMs identified can be seen in Figure 03.

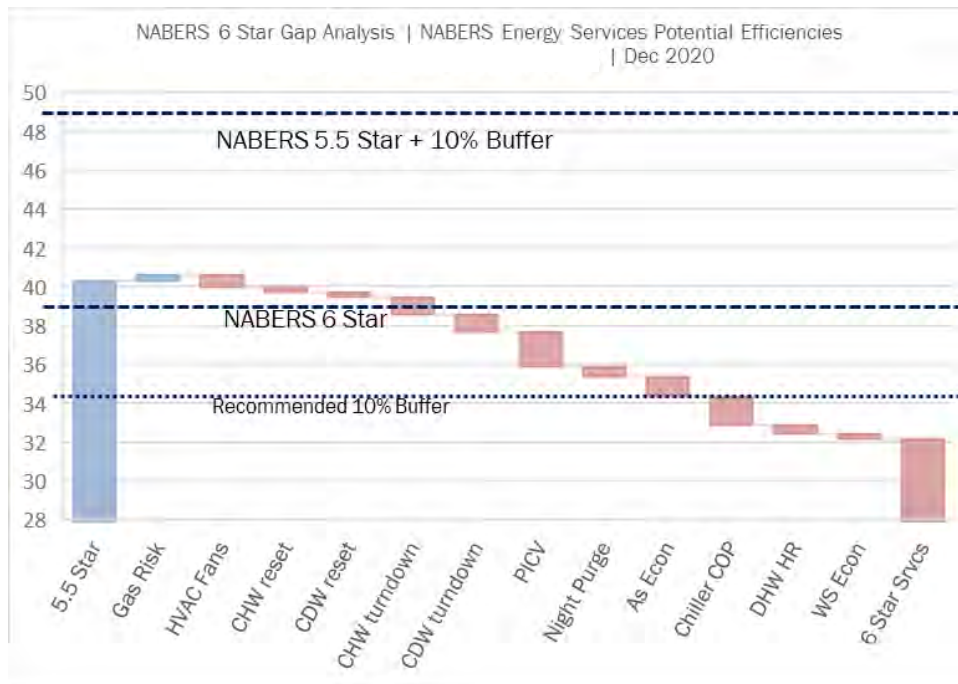


Figure 03: Identified probable Energy Efficiency Measures

Legend	Efficiency Measure
5.5 Star	5.5 Star baseline kgCO2/m2/annum
Gas Risk	Gas carbon coefficients and changes in 2021
HVAC Fans	Push fan efficiency to 64%
Pressure independent Control Valves (PICV)	Use of PICV - drop Cp to 250
CHW reset	Chilled water temperature re-set
CDW reset	CDW temperature re-set
CHW turndown	Push CHW turn-down from 40% to 33%
CDW turndown	Push CDW turn-down from 70% to 50%
Night purge	Night purge ventilation
AS Econ	Airside Economy Cycle
WS Econ	Water side economiser
Chiller COP	Chiller efficiency with oversized coils
DHW HR	Heat recovery for DHW at EOTs (chillers or outflow)
6 Star Services	6 Star performance achieved via services efficiencies kgCO2/m2/annum

Table 01. Description of EEMs

1.1.1 Recommended EEM's

This list of EEMs was workshopped with the project team (technical and suppliers) through workshops and iterative energy simulation. The measures that were not suitable due to technical constraints were ruled out and streamlined to arrive at the advice as seen in Figure 04 below.

For example, a waterside economiser could not be implemented as calculations showed that Sydney's climate has less than 12 days a year when the economiser would be operational (i.e., when the chilled water flow could bypass the chiller). Similarly, there were site spatial constraints which ruled out domestic hot water heat recovery and increased chiller sizes.

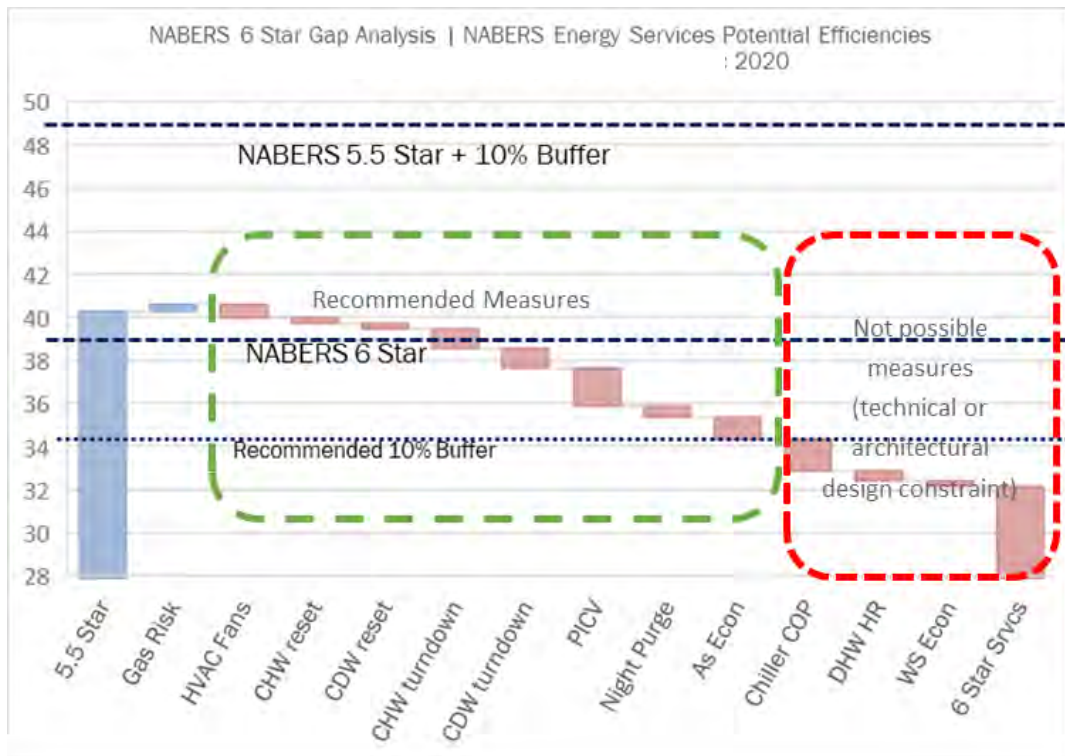





Figure 04. Energy Efficiency Measures recommended for the project after workshop (Author)





2. DISCUSSION OF ENERGY EFFICIENCY MEASURES


The extent of investigation into each energy efficiency measure is summarised in the table in this section. This includes the modelled or estimated energy benefit and whether it was recommended for inclusion in the NABERS 6 Star services proposal.



2.1 Content

For better comprehension of the results, the outcomes are discussed in the form of a table as seen below.

Efficiency Measure	Description	Source	Energy benefit	Comments	Recommended / Not possible
Thermally broken facades	Thermally broken façade system. Improve thermal performance (U Value) by 15% from U 3.1 to U 2.64	Façade engineers. comparison of WERS and AFRC precedents.	- 4.62% heating - 0.06% cooling - 0.4 kg CO ₂ /m ² (0.97% CO ₂)	The investment into thermally broken facades would not be justified as the consequent energy reduction is poor in comparison and cannot pay for itself over the building life	
HVAC fan efficiency	Increase HVAC fan efficiency from 60% to 65%	Mech Engineers and supplier provided detailed efficiencies for each fan, with average performance of 64%	- 7800 kWh fan energy - 0.52 kg CO ₂ /m ² (1.26% CO ₂)	Included in design, the manufacturer cut sheets for the chosen fans show an average efficiency of 64%	
CHW turndown	Target lowest chilled water flow turndown without affecting chiller performance . Reduce from 40%.	Mech Eng. and supplier confirmed that chiller can achieve 33% turndown on flow.	- 2,500 kWh pumping energy - 0.21 kg CO ₂ /m ² (0.51% CO ₂)	Not possible with screw chiller selected at tender stage. Alternate chiller with variable Primary Flow being	

CDW turndown	Target lowest condenser water flow turndown without affecting chiller performance . Reduce from 70%.	Mech Eng. and cooling tower manufacturers confirmed that the tower can achieve 50% flow turndown.	- 6,650 kWh pumping energy -1.26 kg CO ₂ /m ² (3.18% CO ₂)	investigated by Mech Eng.	
CHW temperature reset	Temperature reset at part loads to reduce the load on the chiller (9 deg -7 deg temperature reset for chillers)	In discussion with Mech Eng. and the manufacturers (Carrier). A new Variable Primary Flow Chiller system is proposed that encompasses all these measures. Final performance characteristics to be confirmed by mechanical designers.	Estimate - 0.26 kg CO ₂ /m ² (0.63% CO ₂)	Further design required to simulate.	
CDW temperature reset	Temperature reset at part loads to improve energy efficiency of cooling tower		Estimate - 0.22 kg CO ₂ /m ² (0.53% CO ₂)	The interdependency of reduced chiller flow rates, pumping power and temperature flexibility must be assessed by the engineer & manufacturer. (Can be done)	
Pressure Independent Control Valves (PICV)	Install PICV's to reduce pressure drop across the system and reduce pumping energy.		Estimate - 1.77 kg CO ₂ /m ² (4.3% CO ₂)		

Night purge	Allow the AHU's to run overnight (Between 12am and 8am) on 'outside air only' when ambient conditions will pre-condition of the space, reducing start up load.	Mechanical team to confirm technical capability of systems and potential uplift in cost.	Estimate – 5% peak electrical load - 0.52 kg CO ₂ /m ² (1.26% CO ₂)	Building controls engineer to include in control specifications	
Airside Economy Cycle	Return air to be 100% exhausted and 100% outside air circulated when ambient conditions permit.	Risers are not allocated to allow sufficient exhaust, unless through street facing facades.	Estimate - 1.07 kgCO ₂ /m ² (2.6% CO ₂)	Under investigation by Contractor	

Heat recovery for EOT (chillers or outflow)	Heat recovery via a heat exchanger with the wastewater outflow or from condenser water loop to pre-heat potable water before domestic hot water boiler.	Reviewed by Mech Eng. Advised ΔT between CDW and DHW is too low for effective heat exchange. Proposed wastewater heat recovery product is not approved for use in Australia	Estimate - 0.23 kg CO ₂ /m ² (0.56% CO ₂)	Technical constraint	
Waterside economiser	Bypass the chiller with heat exchangers between the CDW and CHW loops to allow the building to reject heat via the cooling tower only when conditions permit.	ESD conducted a weather analysis study finding only 70 hours in the year that the ambient WB temp is suitable for cooling tower to take on the building part load.	Estimate - 0.25 kg CO ₂ /m ² (0.605% CO ₂)	Technical constraint	


Oversizing chiller coils	Propose that the chiller coil frame size be oversized from a 1200kW to a 1600 kW system, improving heat exchange efficiency.	Mech Eng. and manufacturer advised against this as due to low pressure drop across the chiller, reducing performance and causing the chiller to trip in operation.	Estimate - 1.43 kg CO ₂ /m ² (3.5% CO ₂)	Not endorsed by suppliers	
Predicted Total CO₂ savings potential			<i>10.99 kg CO₂/m²</i>		
Revised Total CO₂ savings potential			<i>8.72 kg CO₂/m²</i>		
Total CO₂ savings (Recommended initiatives only)			<i>6.59 kg CO₂/m²</i>		

Table 02. Summary of simulated results

2.1.1 Discussion

The extent of the investigation into each energy efficiency measure is summarised in the table in the previous section. The results include the modelled or estimated energy benefit of each as seen. It is important to note that workshopping the suitable efficiency measures will be unique to each project, as every project comes with different constraints and not all tested EEM's in this paper will be applicable. Hence, the recommended/not possible column is integral to this assessment to ensure the project assessed allows for the measures to be implemented.

We were able to shave off ~7kgCO₂/m² which amounts to ~98 tonnes of prevented CO₂ emissions. And with the installation of 89kWp of PV and offsetting the last 7kg CO₂/m² it is possible to reach the NABERS 6 star + buffer rating for the project.

A major lesson learnt in this process was that once the spatial layout of the project is determined it is difficult or impossible to consider specific EEMs. For example, to include an airside economy cycle would require more riser space or space from the plant room away from exhaust for fresh air intakes, similarly for improving fan efficiency and reducing static pressure, duct runs & sizes need to be planned well ahead. Thus, carrying out such HVAC efficiency studies for the project is most effective when done in the concept stage.

Another lesson was that initiatives sometimes do not work in the real world with the changing economic and technical conditions. For example, it is not common to find projects installing Air Handling Units with internalised heat recovery components in Australia, although it may

be common in Europe. Another example in this particular project: the perimeter zones were designed to have Dedicated Outdoor Air Fan Coil Units (DOAS FCU's), but due to the current economy, procuring steel from China became too expensive, causing the entire perimeter system to be redesigned to a parallel fan assisted variable air volume (VAV) system. This is what is seen in Figure 05 as the incumbent efficiencies are just a part of those explored in the table of EEMs.

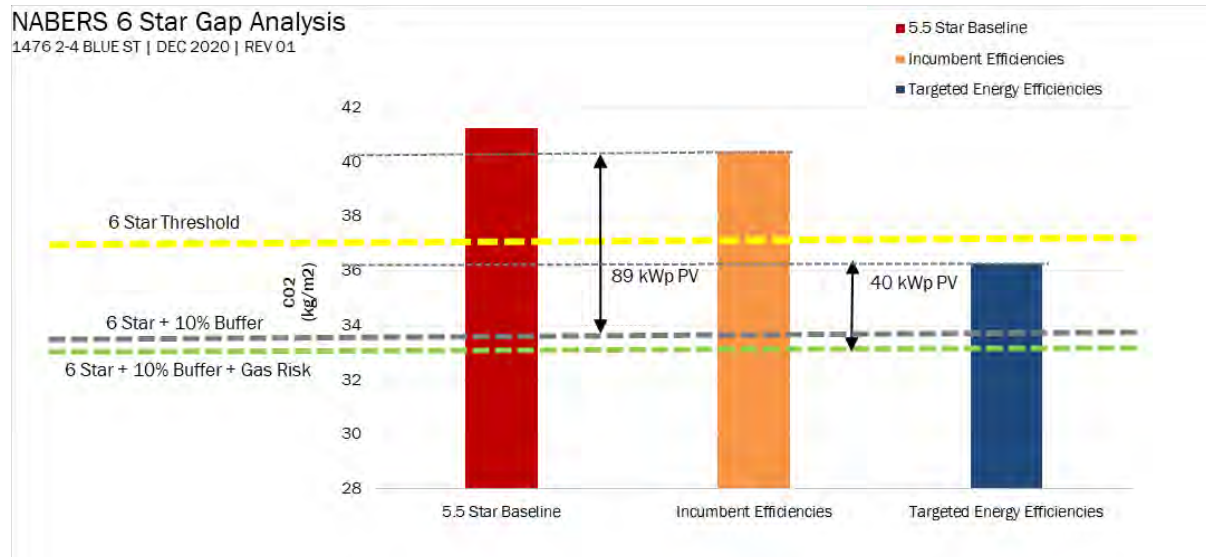


Figure 05: NABERS Gap analysis overview chart (Author)

CONCLUSION

The results of this analysis demonstrated that the highest predicted energy savings come from improved fan efficiency, decreased duct static pressures, installing variable flow valves, and implementing CHW/HHW turndowns as these reduce fan and pump energy. Enabling the design to accommodate maximum airside economy, especially in Sydney's climatic conditions, proved to be very effective, along with oversizing the chillers to perform at higher part load efficiencies.

It is extremely important to workshop and discuss EEMs and their design integration potential with the project team early to determine the feasibility for the site in terms of constructability, space constraints, cost restraints, and limits in terms of supplying particular systems.

It is also critical to keep in mind the plausibility of implementation of the suggested measures in real life. This can either come with extensive experience and research or seamless coordination with all members on the project team. But as stated, each project is different, and while the results of this paper may be transferable to similar projects, we have also provided an example methodology for investigating EEM's through simulation, estimation, and close coordination with the design team.

ACKNOWLEDGEMENTS

I would like to acknowledge and thank my manager Priya Gandhi and my team at Atelier Ten Australia for the help in putting together this study. I would also like to acknowledge the mechanical team at Intrax with whom we worked closely for the said project to confirm the possibility of applying the said EEMs.

REFERENCES

2021. Handbook for estimating NABERS ratings. 2nd ed. NSW. (*DPIE, 2021*)
2022. NABERS. [online] Available at: <<https://www.nabers.gov.au/>> [Accessed 9 May 2022]. (*NABERS, 2022*)

DISCLAIMER

The information or advice contained in these technical papers is intended for use only by professionals who have had adequate technical training in the field to which the paper relates. At the time of publication, these technical papers have undergone a formal peer-review process.

These documents have been compiled as an aid only, and the information or advice should be verified before it is put to use. The user should also establish the applicability of the information or advice in relation to any specific circumstances. While the information or advice is believed to be correct, no responsibility is taken by AIRAH or IBPSA Australasia for any statements made within.

AIRAH and IBPSA Australasia, its officers, employees and agents, disclaim responsibility for any inaccuracies contained within the documents, including those due to any negligence in the preparation and publication of the said technical papers.

COPYRIGHT

This work is copyright. Apart from any use as permitted under the Copyright Act 1986, no part may be reproduced by any process without prior written permission from either the Australian Institute of Refrigeration, Air Conditioning and Heating (AIRAH) or the International Building Performance Simulation Association (IBPSA) Australasia.

THE INCORPORATION OF PRECIPITATION INTO CLIMATE DATA AND ITS IMPACTS ON HYGROTHERMAL SIMULATIONS

FREYA SU

PhD Candidate

School of Architecture and Design

University of Tasmania

Locked Bag 1323

LAUNCESTON TAS 7250

freya.su@utas.edu.au

DR. MARK DEWSBURY, DR. RICHARD BURNHAM, DR. ROGER FAY

School of Architecture and Design

University of Tasmania

Locked Bag 1323

LAUNCESTON TAS 7250

ABOUT THE AUTHOR

Freya Su is a PhD student in Mark Dewsbury's architectural science lab at the University of Tasmania. Freya's PhD investigates the relationship between hygrothermal simulation and climate data. Before beginning her current studies, she worked as a research assistant in Mark's lab and co-authored condensation-related publications. In 2015, Freya founded Snug House Tasmania, conducting airtightness testing and energy efficiency assessments in a multi-disciplinary building design studio.

ABSTRACT

Wind Driven Rain (WDR) is the single most significant environmental factor in hygrothermal analysis. Without the inclusion of precipitation data in climate datasets, hygrothermal simulation programs do not calculate the effects of WDR, producing inadequate and misleading simulation outcomes, often underestimating interstitial moisture. This paper looks into methods for incorporating precipitation into existing climate datasets as well as alternative approach to account for climate variability.

INTRODUCTION

Climate change has driven the global need to reduce anthropogenically generated Green House Gases (GHG) leading to the requirement for building envelopes to provide more energy efficient enclosures for buildings. This has concurrently led to a greater occurrence and awareness of moisture accumulation and mould growth in buildings. Within the suite of contemporary building simulation tools, hygrothermal simulation is used to inform decisions on envelope design. To provide practical results, appropriate data inputs of building materials, and internal and external environments are required.

Although there is a substantial body of work to verify that precipitation is critical in hygrothermal analysis, there is a lack of research that explores how precipitation can be incorporated into climate data and, if it can be used in the selection of climate data. With the advent of climate change, there is growing interest to see how buildings perform in extreme conditions.

WUFI PRO 6 will be used in this technical paper to demonstrate how WDR is handled in simulation and its effects on moisture content in interstitial spaces in external walls.

1. CATALYST: CLIMATE CHANGE

Australia's objective to reduce GHGs led to incremental changes in the National Construction Code (NCC) beginning with the first envelope thermal performance requirements in the 2003 BCA 1996 Amendment 13. Continual enhancements in 2004, 2007 and 2010 to insulation and airtightness requirements to increase energy efficiency has brought about some unfortunate side-effects: condensation and mould growth in new residential buildings (Nath et al. 2020, Dewsbury et al. 2016, Dewsbury and Law 2016, Bulic, Paton-Cole, and Erbas 2019).

It is a shame that energy efficiency and hygrothermal simulations are not regularly undertaken simultaneously. In overlooking the connection, a "dark side" of building energy efficiency (Brambilla and Sangiorgio 2020) is becoming widely recognised from scholarly circles to workers within the construction industry (Dewsbury and MacAlister 2021). The current proliferation of mould growth in buildings is evidence of the failure to consider everyday physics, the interconnectedness of water and temperature; relative humidity is dependent on temperature and pressure.

2. WIND DRIVEN RAIN MODELS

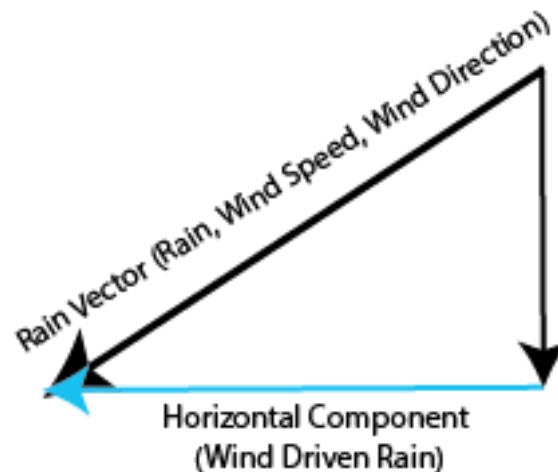


Figure 1. *What is Wind Driven Rain?*

Wind Driven Rain (WDR) or Driving Rain's is horizontal component of rain as it is driven by wind. It's mechanisms and effects on buildings and building performance have been studied comprehensively over the years, in 2004 Blocken and Carmeliet conducted a thorough review of WDR research in building science, detailing experimental, semi-empirical and steady-state numerical methods, they concluded semi-empirical methods would suit a wider user-base given the cost and complexity involved in experimental and numerical methods (Blocken and

Carmeliet 2004). For detailed forensic examinations, Kunzel recommends a weather file of observations collect on the site of the building under investigation (Kunzel and Schmidt 2021).

WUFI uses two semi-empirical methods to calculate the effects of Driving Rain; one developed by the Fraunhofer Institute of Building Physics using coefficients in a 1997 study (Karagiozis, Hadjisophocleous, and Cao 1997) and the other based on ASHRAE 160. Both methods require the climate file to contain Rain Normal (RN), hourly meteorology observations of precipitation in mm. Both require the definition of coefficients as inputs for semi-empirical analysis.

2.1 WUFI Rain Model

The WUFI method relies on two coefficients to estimate driving rain; the facade's exposure and its inclination to the horizontal plane.

$$\text{Rain Load} = R_h \times (R_1 + R_2 \times U) \quad (1)$$

where:

- rh [mm/h] = rainfall intensity on a horizontal surface
 R_1 = inclination coefficient, $R_1 = 0$ for inclination of 90°
 R_2 = exposure coefficient, increases as height increases.
 U [m/s] = wind velocity, hourly average wind speed at 10 m height

	Height (m)	Exposure coefficient R_2 (s/m)
Short	Up to 10m	0.05
Tall, middle section	10-20m	0.1
Tall, upper section	More than 20m	0.2

Table 1. Building height and R_2 exposure coefficient for WUFI WDR model

2.2 ASHRAE 160 Driving Rain Model

ASHRAE 160 offers a more comprehensive model with additional consideration for roof runoff and exposure includes an additional component for site specific conditions and topography.

$$\text{Rain Load} = R_h \times F_E \times F_D \times F_L \times U \times \cos(q) \quad (2)$$

where:

- R_h [mm/h] = rainfall intensity on a horizontal surface
 F_E = rain exposure coefficient
 F_D = rain deposition coefficient (roof runoff)
 F_L [kg s / (m³ mm)] = empirical constant, 0.2
 U [m/s] = wind velocity, hourly average wind speed at 10 m height
 q [°] = angle between wind direction and normal to the wall

	Type of Exposure Category		
	severe	medium	sheltered
Height < 10 m:	1.4	1.0	0.7
> 10 and ≤ 20 m:	1.4	1.2	1.0
> 20 m:	1.5	1.5	1.5

Table 2. Building height, Exposure and F_E exposure coefficient for ASHRAE 160 WDR model

	F_D
Walls below a steep-slope roof	0.35
Walls below a low-slope roof	0.5
Walls subject to rain runoff	1.0

Table 3. Roof type and F_D deposition coefficient for ASHRAE 160 WDR model

3. SIGNIFICANCE OF WIND DRIVEN RAIN

Wind Driven Rain (WDR) is critical in hygrothermal analysis (Koronthalyova and Matiašovsky 2001), without it, the moisture content simulated in walls remain the same throughout the seasons. It has been shown to increase interstitial humidity, hampering the performance of insulation and membranes, decreases evaporation potential, and increases moisture loads (Zhou, Derome, and Carmeliet 2016).

Salonvaara et al. analysed the impact of WDR (Salonvaara and Karagiozis 1998) in hygrothermal analysis. A brick veneer wall in Vancouver, Canada, showed that interstitial moisture increased 10-fold when taking WDR into consideration.

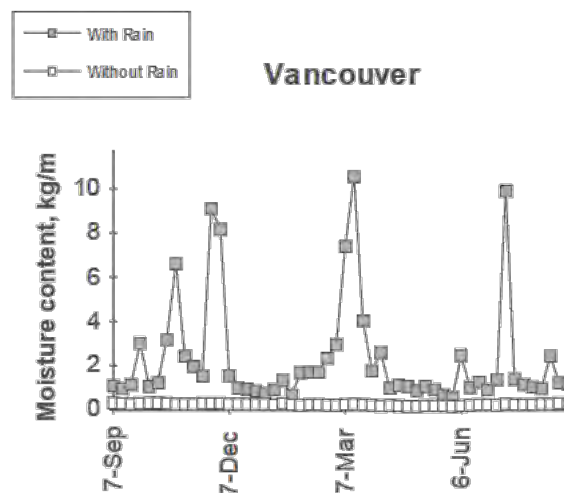


Figure 2. Moisture content of Brick Veneer wall and impact WDR in hygrothermal analysis (Salonvaara and Karagiozis 1998).

3.1 Experiment One

The aim of the Experiment One is confirm Salonvaara’s result with WUFI PRO in Australian conditions. Melbourne airport at Tullamarine (NatHERS CZ60) was chosen for its rich observational data due to its proximity to an international airport, a brick veneer wall was modelled in WUFI PRO 6.

3.1.1 Methodology

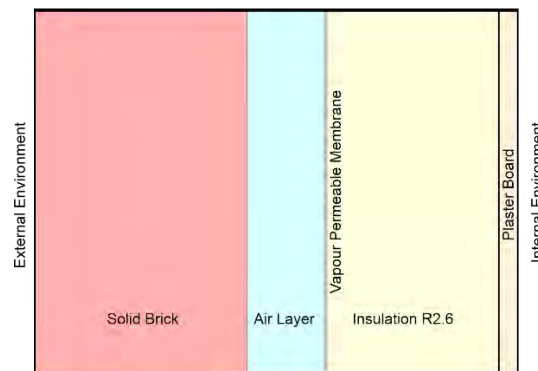


Figure 3. *External brick veneer wall component*

Simulation	Climate dataset	Converted by	Rain status
1	RMY 2005	WUFI Spreadsheet	No rain
2	RMY 2005	AusHygroOne	Rain

Table 4. *Climate files used for Experiment One*

A climate file for NatHERS CZ60 was obtained, it’s native Australian Climate Databank (ACDB) format is not directly compatible with WUFI Pro, therefore, it was prepared using the two methods below for each simulation.

Simulation 1

The climate file for NatHERS CZ60 was converted into the .WAC format with the spreadsheet provided by WUFI (Fraunhofer IBP 2021).

Simulation 2

The climate file for NatHERS CZ60 was run through University of Tasmania software, AusHygroOne (Condensation Project Group 2019). It converts ACDB format and synthesises rain by taking the daily observed precipitation and dividing it by 24 to obtain an hourly precipitation.

Two simulation cases were set up, all inputs are set out in Appendix A and were identical apart from the weather file.

3.1.2 Results

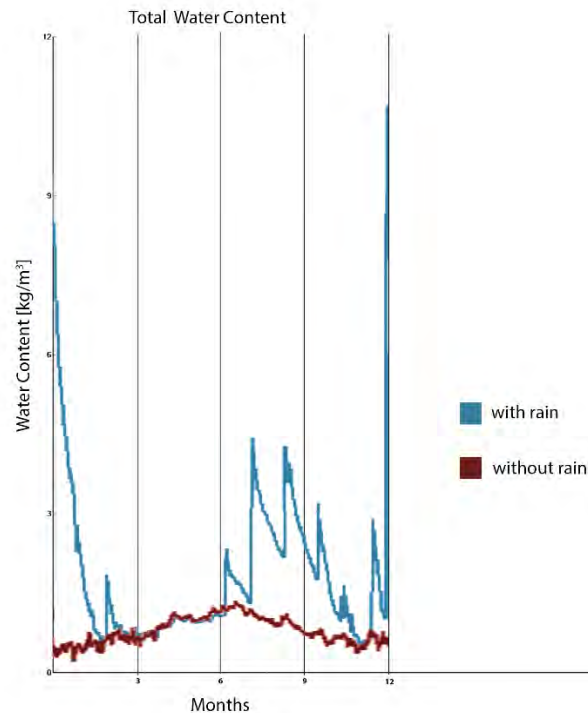


Figure 4. *Moisture content of Brick Veneer wall and impact of the effects WDR.*

A comparison shows a ten-fold increase in December/January in Simulation 2.

3.1.3 Discussion and Conclusion

In hygrothermal simulation, if precipitation is left off climate files, WDR is not considered, and moisture content is grossly underestimated. Precipitation must be included in climate files to if these simulations are to be useful for informed decisions in envelope design.

The experiment confirms the observations for Vancouver apply in Australia in the Southern hemisphere.

4. CLIMATE FILES

Experiment One shows the need to include precipitation into climate data. At first glance, one can simply add a column to existing data, in the same manner as it was done above. However, on examination, some factors emerged that could have an impact on hygrothermal simulation and they need to be considered. As the research progressed, the question of whether climate data was adequate for hygrothermal analysis arose.

4.1 Existing Climate Data is Focused on Solar Radiation

Hourly climate datasets were developed as inputs for simulations of photo-voltaic systems and thus is heavily weighted on solar radiation and did not include precipitation (Hall et al. 1979). The datasets are a concatenation of 12 months of hourly meteorological observations. Each month in the dataset is chosen by comparing that month's cumulative distribution function (CFD) to an average long-term CFD taken over the period of record, essentially a distribution of the averages over time. The Finkelstein-Shafer goodness-to-fit test produces a statistic to

gauge each month's proximity to the long-term CFD. The methodology produces a dataset of months that is the most typical, or the most average.

Each weather element varies in importance when calculating the CFD. In the original weighting schema, solar radiation is considered more important than any other index, coming in at 12/24, producing a thermally-selected climate dataset.

Weather Element	Weighting
Dry Bulb Maximum	1/24
Dry Bulb Minimum	1/24
Dry Bulb Mean	2/24
Dew Point Maximum	1/12
Dew Point Minimum	1/12
Dew Point Mean	2/12
Wind Velocity Max	2/12
Wind Velocity Min	2/12
Global Radiation	12/24

Table 5. *TMY climate dataset weighting 1979 (Hall et al. 1979)*

As the datasets became an input for energy efficiency and hygrothermal simulations, they evolved and some now include a column for precipitation data. Nonetheless, solar radiation remains heavily weighted at 10/20.

Weather Element	Weighting
Dry Bulb Maximum	1/20
Dry Bulb Minimum	1/20
Dry Bulb Mean	2/20
Dew Point Maximum	1/20
Dew Point Minimum	1/20
Dew Point Mean	2/20
Wind Velocity Max	1/20
Wind Velocity Min	1/20
Global Radiation	5/20
Global Radiation	5/20

Table 6. *TMY climate dataset weighting 2008 (Wilcox and Marion 2008).*

The focus on solar radiation raises the question of whether these datasets are suitable for hygrothermal simulation, given that precipitation is so crucial and was not included as a criterion in the file's development.

An alternate weighting table with the addition of precipitation as a weather element could be used to consider it in the formation of climate files to produce a precipitation-selected representative year. Extreme precipitation years could be created by adjusting weather elements.

Weather Element	Weighting
Dry Bulb Maximum	1/20
Dry Bulb Minimum	1/20
Dry Bulb Mean	2/20
Dew Point Maximum	1/20
Dew Point Minimum	1/20
Dew Point Mean	2/20
Wind Velocity Max	5/20
Wind Velocity Min	2/20
Global Radiation	1/20
Global Radiation	1/20
Daily Precipitation	5/20

Table 7. Alternate weighting to include precipitation.

4.2 Climate Datasets are Typical Years

These climate datasets miss the point for hygrothermal simulation as they produce a climate dataset for a year which is the closest to the long-term average CFD. However, hygrothermal simulations are often undertaken to stress test building envelopes to determine how they may fail. Simulations to the point of failure will not be possible with climate data that represents average conditions.

50 years of observational precipitation data obtained from the Bureau of Meteorology for Tullamarine (Melbourne Airport). A basic statistical analysis shows:

Statistic	Value (mm)
Min	310.2
Max	820.8
Average	534.92
Median	548.8

Table 7. Analysis of 50 Years of Precipitation at Tullamarine (Melbourne Airport)

The total rainfall in Tullamarine's RMY climate file totals 469mm per year. Upon comparison to long term observations, this figure is low, coming in at 65.92mm less or 12.32% lower than the average observed over 50 years.

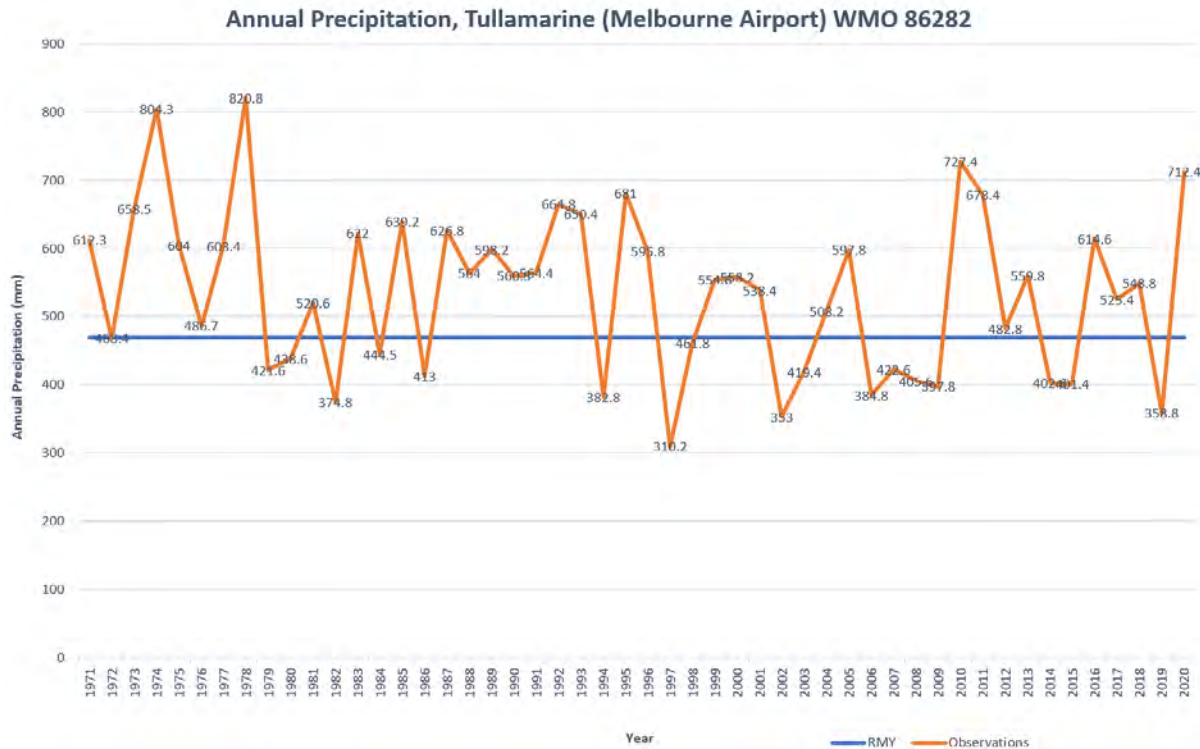


Figure 5. Annual Observed Precipitation vs RMY Precipitation Tullamarine (Melbourne Airport)

The external wall system will perform as expected or better in years with less rainfall than the total for the RMY climate file, and it is therefore, not critical. However, in years when there is more rainfall, the behaviour of water ingress and water vapour in that wall system is unknown and unsimulated; it is assumed to contain higher quantities of water vapour and moisture, potentially causing building damage or failure.

5. CLIMATE VARIABILITY

5.1 Oceanic Influence on Climate

Oceans cover a larger proportion of the earth's surface in the southern hemisphere than in the north, making it more vulnerable to climate diversifiers from the sea. When compared to northern hemisphere climates, humidity and precipitation variations are exaggerated in the south due to the higher proportion of water to land.

The Indian Ocean Dipole (IOD), Southern Annular Mode (SAM) and El Nino-Southern Oscillation (ENSO) are driven by sea surface temperature fluctuations and are significant contributors to climate and rainfall variability in Australia (Ummenhofer 2008).

5.2 Climate Change

Climate change has come back into the picture again. This time as it begins to impact climate variability as we see increased intensity and frequency of storm events.

The higher water-to-land ratio in the southern hemisphere makes it vulnerable to evaporation caused by rising sea surface temperatures and the resulting intense storm events that feed off the increase in water vapour in the atmosphere.

Oceanic patterns and currents have also been disrupted by climate change, resulting in a feedback loop that raises sea surface temperatures even more.

The RMY dataset is made up of weather observations dating back to 1970, and as our climate changes, one wonders if observations from 50 years ago are still relevant for current and future simulations.

CONCLUSION

Precipitation is used to calculate Wind Driven Rain and is a critical input for hygrothermal simulation.

Precipitation is not considered in the current climate data and, by definition, represents a typical or average year, rendering it unfit for hygrothermal modelling. A comparison of meteorological observations and climate data reveals a difference of 12.32 per cent in average annual precipitation, casting doubt on its reliability for precipitation.

In recognition of the shortcomings of the existing climate datasets for hygrothermal simulation, ASHRAE Research Project Report RP-1325 (Salonvaara, Pezoulas, and Karagiozis 2011) investigated several methods for creating a Moisture Reference Year (MRY). It reported the most significant influence on wall performance was orientation, leading to a methodology using weather parameters (including precipitation) experienced in a polar-facing wall, that is north or south depending on your hemispherical location, to calculate a damage function predicting the conditions experienced by materials in that wall. The damage function method can be used to produce an MRY that is either average or severe. The problem with this method is that it still generates a climate file that may not accurately reflect the harshest environment that external walls may encounter.

Climate variability whether caused by the influences of water to land ratios or climate change can be addressed by using a set of recent multi-year meteorological observations.

ASHRAE160 addresses climate data's representative nature by by-passing climate files altogether, instead, it suggests using Moisture Design Weather Data (MDWD) rather than compiling an MRY. They state a MDWD should cover a period of at least ten years and include typical weather element data columns from a climate reference year, as well as rainfall.

There's still a lot of work to do. Comparison simulations of climate and weather inputs in action will assess the impacts on hygrothermal simulation. Although there are some test walls located in the southern hemisphere, the most comprehensive setup is in Holzkirchen, which is located in the north and will not reveal southern climate variability. A similar set up in the south would provide the best empirical confirmation of results.

ACKNOWLEDGEMENTS

Supervisory assistance by Dr. Hartwig Künzel of Fraunhofer Institute for Physics, Holzkirchen, Germany.

Rain and polar-facing conversations with Mr. Trevor Lee and Dr. David Ferrari of Exemplary Energy Partners Pty Ltd.

Thanks also go to Adjunct Professor Michael Lorber, New York University for his expert guidance in statistics.

Freya Su acknowledges the permission of the Commonwealth of Australia to access and use Nationwide House Energy Rating Scheme Climate Files in the preparation of this technical paper.

This research was supported by an Australian Government Research Training Program (RTP) Scholarship.

REFERENCES

ASHRAE. 2016. 'ASHRAE 160-2016 Criteria for Moisture-Control Design Analysis in Buildings'.

Blocken, Bert, and Jan Carmeliet. 2004. 'A Review of Wind-Driven Rain Research in Building Science'. *Journal of Wind Engineering and Industrial Aerodynamics* 92 (13): 1079–1130. <https://doi.org/10.1016/j.jweia.2004.06.003>.

Brambilla, Arianna, and Alberto Sangiorgio. 2020. 'Mould Growth in Energy Efficient Buildings: Causes, Health Implications and Strategies to Mitigate the Risk'. *Renewable and Sustainable Energy Reviews*, no. 132 (July).

Bulic, Tom, Vidal Paton-Cole, and Bircan Erbas. 2019. 'Review of the Effects of Condensation in Low-Rise Residential Buildings'. In *Built to Thrive: Creating Buildings and Cities That Support Individual Well-Being and Community Prosperity*, 321–30. Noosa, Qld: Central Queensland University. https://www.researchgate.net/profile/Arzoo-Shirazi/publication/337811399_A_cost_benefit_analysis_of_retrofitting_public_policies_on_Atlanta_residential_housing/links/5e33c713458515072d710ada/A-cost-benefit-analysis-of-retrofitting-public-policies-on-Atlanta-residential-housing.pdf#page=324.

Condensation Project Group. 2019. *AusHygroOne*. Launceston: University of Tasmania.

Dewsbury, Mark, and Tim Law. 2016. 'Recent Increases in the Occurrence of Condensation and Mould within New Tasmanian Housing'. In *Fifty Years Later: Revisiting the Role of Architectural Science in Design and Practice*, 715–24. Adelaide: The Architectural Science Association (ANZAScA). https://www.researchgate.net/profile/Mark-Dewsbury-2/publication/309571442_Recent_increases_in_the_occurrence_of_condensation_and_mould_within_new_Tasmanian_housing/links/58b60cf5aca27261e5166282/Recent-increases-in-the-occurrence-of-condensation-and-mould-within-new-Tasmanian-housing.pdf.

Dewsbury, Mark, Tim Law, Johann Potgieter, Desmond Fitz-Gerald, Bennet McComish, Thomas Chandler, and Abdel Soudan. 2016. 'Scoping Study of Condensation in Residential Buildings Final Report Scoping Study of Condensation in Residential Buildings: Final Report'. University of Tasmania. https://www.abcb.gov.au/-/media/Files/Resources/Research/Scoping_Study_of_Condensation_in_Residential_Buildings.pdf.

Dewsbury, Mark, and Clarence MacAlister. 2021. 'Condensation and Mould Mitigation within the Construction Industry'. Grant. Master Builders Association of Tasmania.

Fraunhofer IBP. 2021. 'Creating Weather Files'. WUFI. 23 July 2021. <https://wufi.de/en/service/downloads/creating-weather-files/>.

- Hall, I J, R R Prairie, H E Anderson, and E C Boes. 1979. 'Generation of Typical Meteorological Years for 26 SOLMET Stations'. In *ASHRAE Transactions*, 85:507–8. No 2. Detroit MI: ASHRAE.
<https://www.ashrae.org/File%20Library/Technical%20Resources/ASHRAE%20Transactions%20and%20Conferences%20Programs/1979-Detroit-TOC.pdf>.
- Karagiozis, Achilles, George Hadjisophocleous, and Shu Cao. 1997. 'Wind-Driven Rain Distributions on Two Buildings'. *Journal of Wind Engineering and Industrial Aerodynamics* 67–68 (April): 559–72. [https://doi.org/10.1016/S0167-6105\(97\)00100-1](https://doi.org/10.1016/S0167-6105(97)00100-1).
- Koronthalyova, Olga, and Peter Matiašovsky. 2001. 'Driving Rain Course Simulation Based on Daily Data'. *Journal of Thermal Envelope and Building Science* 25 (1): 51–66. <https://doi.org/10.1106/N8XW-R4CU-62TM-4J2H>.
- Kunzel, Hartwig, and Thomas Schmidt. 2021. 'Wufi Pro Calculation of WDR', 14 September 2021.
- Nath, Shruti, Mark Dewsbury, Phillipa Watson, and Heather Lovell. 2020. 'A Bio-Hygrothermal Analysis of Typical Australian Residential Wall Systems'. In *Imaginable Future: Design Thinking, and the Scientific Method*, edited by Ali Ghaffarianhoseini, Amirhosein Ghaffarianhoseini, and Nicola Naismith. Auckland, NZ: The Architectural Science Association (ANZAScA). <https://doi.org/10.13140/RG.2.2.32164.91523>.
- Salonvaara, Mikael, and Achilles N Karagiozis. 1998. 'The Influence of Waterproofing Coating on the Hygrothermal Performance of a Brick Façade Wall System'. STP1314. American Society for Testing and Materials (ASTM). https://www.astm.org/DIGITAL_LIBRARY/STP/PAGES/STP12113S.htm.
- Salonvaara, Mikael, Lambros Pezoulas, and Konstantinos Karagiozis. 2011. 'RP 1325 - Environmental Weather Loads for Hygrothermal Analysis and Design of Buildings'. ASHRAE RP-1325.
- Ummenhofer, Caroline C. 2008. 'Southern Hemisphere Regional Precipitation and Climate Variability: Extremes, Trends, and Predictability'. PhD, Sydney, NSW, Australia: University of New South Wales. http://www.who.edu/cms/css/sb/ummenhofer/publications/Ummenhofer_PhDthesis.pdf.
- Wilcox, S, and W Marion. 2008. 'Users Manual for TMY3 Data Sets'. *Technical Report*, 58.
- Zhou, Xiaohai, Dominique Derome, and Jan Carmeliet. 2016. 'Robust Moisture Reference Year Methodology for Hygrothermal Simulations'. *Building and Environment* 110: 23–35. <https://doi.org/10.1016/j.buildenv.2016.09.021>.

APPENDICES

1.1 Appendix A - Experiment One WUFI PRO settings

Material	Density [kg/m ³]	Porosity [m ³ /m ³]	Spec. Heat Capacity [J/kgK]	Thermal Conductivity [W/mK]	Vapour Diffusion Resistance [-]	Thick-ness [m]
Extruded Brick	1650	0.41	850	0.6	9.5	0.11
Air Layer	1.3	0.999	1000	0.23	0.38	0.04
Vapour Permeable Membrane	130	0.001	2300	2.3	100	0.001
Insulated Timber Frame	32.5	0.95	840	0.032	1	0.09
Plasterboard	850	0.65	850	0.2	8.3	0.01

Table xxxxx. *Experiment One: Assembly Details*

Parameter	Value
Orientation	South
Inclination	90°C
Driving Rain Model	ASHRAE 160

Orientation, Inclination and Driving Rain Model

Parameter	Value
F _E	1.0
F _D	0.5

ASHRAE 160 settings

Parameter	Value
Ext. Heat Resistance [m ² K/W]	0.0588
Ext. Wind-dependent	FALSE
Ext. sd-Value [m]	No coating
Ext. Short-Wave Absorptivity [-]	0.8
Ext. Long-Wave Emmissivity [-]	-
Ext. Reduction Factors	-
Ext. Explicit Rad. Balance	FALSE
Ext. Ground Short-Wave Reflectivity [-]	0.2
Ext. Adhering Fraction Rain	0.7
Int. Heat Resistance [m ² K/W]	0.125
Int. sd-Value [m]	No coating

Surface Transfer Coefficients

Parameter	Value
Initial Moisture	Constant
Initial Relative Humidity [-]	0.8
Initial Temperature	20

Initial Conditions

Layer	Water Content [kg/m ³]
Extruded Brick	9.2
Air Layer	1.88
Vapour Permeable Membrane	0.0
Insulated Timber Frame	0.82
Plasterboard	6.3

Initial Water Content in Layers

Parameter	Value
Start	1/04/2020
End	1/04/2030
Time Steps [h]	1

Calculation Periods

Parameter	Value
Heat Transport Calc.	TRUE
Moisture Transport Calc.	TRUE
Exclusions: Capillary Conduction	FALSE
Excl: Latent Heat Evaporation (LHE)	FALSE
Excl: Temp. Depend. LHE	FALSE
Excl: Latent Heat Fusion (LHF)	FALSE
Excl: Temp. Moist. Depend. of Thermal Conductivity	FALSE
Increase Accuracy	TRUE
Adapted Convergence	TRUE
Adaptive Time Step Control	FALSE
Geometry	Cartesian

Numerics

Simulation	File Name
1	Tullamarine CZ60 WufiSpreadsheet noRAIN.wac
2	Tullamarine CZ60 AusHygroOne withRAIN.wac

Outdoor Climate File

Parameter	Value
AC Type	Air-conditioning
Floating temp. [°C]	2,8
Set point Heating [°C]	21,1
Set point Cooling [°C]	23,9
Number of Bedrooms	3
Jetted Tub	FALSE
User Defined	FALSE
Air-Exchange Rate [1/h]	0.5
Building volume [m ³]	380

ASHRAE 160 Indoor Climate

DISCLAIMER

The information or advice contained in these technical papers is intended for use only by professionals who have had adequate technical training in the field to which the paper relates. At the time of publication, these technical papers have undergone a formal peer-review process.

These documents have been compiled as an aid only, and the information or advice should be verified before it is put to use. The user should also establish the applicability of the information or advice in relation to any specific circumstances. While the information or advice is believed to be correct, no responsibility is taken by AIRAH or IBPSA Australasia for any statements made within.

AIRAH and IBPSA Australasia, its officers, employees and agents, disclaim responsibility for any inaccuracies contained within the documents, including those due to any negligence in the preparation and publication of the said technical papers.

COPYRIGHT

This work is copyright. Apart from any use as permitted under the Copyright Act 1986, no part may be reproduced by any process without prior written permission from either the Australian Institute of Refrigeration, Air Conditioning and Heating (AIRAH) or the International Building Performance Simulation Association (IBPSA) Australasia.

CELLULAR BLINDS EFFECT ON AGED CARE NOW AND IN THE FUTURE

SHERIF ZEDAN (PhD)¹

Research Fellow, School of Architecture and Built Environment
Queensland University of Technology
2 George St, Brisbane CBD, QLD 4000
S2.zedan@qut.edu.au

WENDY MILLER (PhD)²

Associate Professor, School of Architecture and Built Environment
Queensland University of Technology
2 George St, Brisbane CBD, QLD 4000
W2.miller@qut.edu.au

AARON LIU (PhD)³

Research Fellow, School of Architecture and Built Environment
Queensland University of Technology
2 George St, Brisbane CBD, QLD 4000
L50.liu@qut.edu.au

YUNLONG MA (PhD)⁴

Research Associate, School of Architecture and Built Environment
Queensland University of Technology
2 George St, Brisbane CBD, QLD 4000
yunlong.ma@hdr.qut.edu.au

ABOUT THE AUTHORS

- 1- Dr Zedan is a certified energy efficiency assessor, with a PhD in stakeholder management of energy efficient housing. He has a degree in Architectural Engineering, and over 10 years' experience in the construction industry. After finishing his PhD at QUT, Dr Zedan participated in several research projects that cover diverse areas of energy efficiency such as, building passports, indoor air quality, occupants' health and comfort, human behaviour, and social network analysis. He is currently the project manager for one of the iHub living labs, where innovative technologies are implemented, tested, and evaluated.
- 2- Dr Wendy Miller is an Associate Professor, School of Architecture and Built Environment at QUT. Dr Miller has a long history of engagement with industry and government on issues relating to energy and the built environment, and research on socio-technical challenges, such as the emergence of prosumers and the growth in onsite renewable energy generation. She is Living Laboratory Activity Leader for the Innovation Hub for Affordable Heating and Cooling. She engages with the international community through IEA Annex 80 – resilient cooling, and with industry through AIRAH's Resilience Taskforce.
- 3- Dr Liu is a research fellow at QUT's Faculty of Engineering, an Australian Representative on International Energy Agency Annex 82 Energy Flexible Buildings and a registered professional engineer with a PhD in energy investment decisions. He is a Fellow of Higher

Education Academy and previously worked with ABB and A. O. Smith. Currently, Dr Liu is the project manager for one of the ARENA iHub living labs, testing innovative technologies at a major Australian public hospital.

- 4- Dr Ma is a Research Associate in School of Architecture and Built Environment, QUT. He is a specialist in building and HVAC energy simulation. His research interests include: building energy simulation, HVAC, solar cooling, renewable energy, building energy code, and life cycle assessment.

ABSTRACT

Cellular (honeycomb) blinds are a cost effective and feasible method that can reduce heating and cooling energy consumption. However, the energy efficiency potential of the blinds is highly impacted by how they are operated.

This paper investigates the benefits of using cellular (honeycomb) blinds in residential aged care facilities under current and future weather conditions in a subtropical climate. A whole building model was created for an existing residential aged care (RAC) facility. The effect of installing and operating the cellular blinds in the residential rooms of the RAC was evaluated through simulating operational patterns that were devised based on interviews with the residents of the RAC about their daily routine, behaviours, and preferences.

Findings show that blinds can reduce energy consumption by 6 per cent when they are operated in an informed manner, and that they can provide additional 18 per cent energy savings in the year 5050, compared to what they are providing under current weather conditions.

INTRODUCTION

Heat gain or loss through the building envelope can account for 20-50 per cent of air conditioning energy consumption (Fang *et al.*, 2014; Yu *et al.*, 2015). Windows are considered the lowest thermally resistant envelope component, which can account for 50 per cent of the total envelope heat gain (Humaish, 2018). Internal window dressings can be a low cost, easy to implement solution to reduce heat gain through windows in existing buildings, in addition to other benefits such as providing privacy and avoiding glare (Petersen, Cort and Widder, 2016). Research by Fitton *et al.* shows that window dressings can contribute to reducing thermal transmittance (U value) by up to 63 per cent for the case of well-fitting shutters. Their research confirms that dressing types can add different thermal resistance values to windows, with honeycomb blinds being one of the highest thermally resisting window dressings, providing 54 per cent reduction in windows' thermal transmittance (Fitton *et al.*, 2017).

Honeycomb (Cellular) blinds (Figure 1) are made of a continuous piece of fabric that can roll up, sideways, or top down/bottom up. The blinds' hexagonal shaped cells can trap air inside, reducing the thermal transmittance through the covered window. The size and number of cells (single, double, or triple), and the way the blinds are fitted can influence the R-value that they add to the window. Adding a layer of metallized Mylar to the air pockets can minimise radiant heat transfer and further improve the resistance of the blinds (Ariosto *et al.*, 2013; Mansouri Birjandi, 2015).



Figure 1: *Single and double cell honeycomb blinds*

Honeycomb blinds can help reduce air conditioning energy consumption, through minimising conductive heat transfer, reducing radiative energy losses, and optimising solar gains. With advanced operational scheduling, blinds can contribute to 8.1 per cent reduction in heating energy when compared to no blinds and 6.5 per cent reduction in cooling energy when compared to vinyl blinds (Petersen *et al.*, 2016).

Despite the significant potential of window dressings to reduce energy consumption, this potential is highly impacted by how the blinds are operated. To maximise blinds' potential, they must be operated as a response to external factors such as solar radiation and temperature. This informed operation should achieve passive heating, for instance through opening blinds at daytime to increase the solar heat gain and closing them at night to prevent heat loss, and vice versa for passive cooling (Ascione *et al.*, 2016; Baniassadi and Sailor, 2018).

However, a study by Bickel *et al.* shows that most household users rarely move their window dressing, where 75-84 per cent of window dressings remain at the same position throughout the day (Bickel, Phan-Gruber and Christie, 2013).

Little research has focused on the effect of different operational scenarios of blinds on reducing energy consumption, and how to maximise their benefits while maintaining user preferences and needs such as access to daylight, views, fresh air, etc.

1. METHODOLOGY

The main objective of this paper is to identify how simulation tools can be used to maximise the benefits of using honeycomb blinds in residential buildings. Quantitative and qualitative data is collected through interviews with residents and simulation of an existing Residential Aged Care (RAC) facility. The methodology is divided into two streams.

Stream one aims to simulate the maximum effect of opening/closing the blinds for 100 per cent of the time on reducing energy use, electricity bills, and carbon emissions.

Stream two aims to investigate the actual control/operation of the blinds onsite and simulate its impact on energy consumption to identify the limitations of inefficient operational patterns. Stream 2 is done through two stages:

- 1- In-situ research: include fitting honeycomb blinds into selected rooms and interviewing residents about their operation patterns and behaviours.
- 2- Simulation of rooms fitted with honeycomb blinds to:
 - Compare the energy simulation results of the multiple operation scenarios derived from the in-situ interviews, and passive heating/cooling principles.
 - Investigate the benefits of using honeycomb blinds in future climate.

1.1 Case study

The case study where the blinds were fitted and their effect simulated, is an existing RAC building in subtropical Queensland, Australia. The building comprises 6 levels (basement, ground level, and levels 1-4). 36 residential rooms are located on each of levels 1-4, with two room sizes: standard (26m²) and premium (35m²). Premium rooms are normally located on the corners of the building, and therefore have walls facing two orientations. They also have a sliding glass door that leads to a balcony.

The building was designed to enable mixed-mode ventilation and heating/cooling. Residents therefore can operate louvred windows, window dressings, ceiling fans, and ducted air conditioning. Rooms on the northwest of level 3 (Figure 2) were all fitted with honeycomb blinds and their residents participated in an interview.

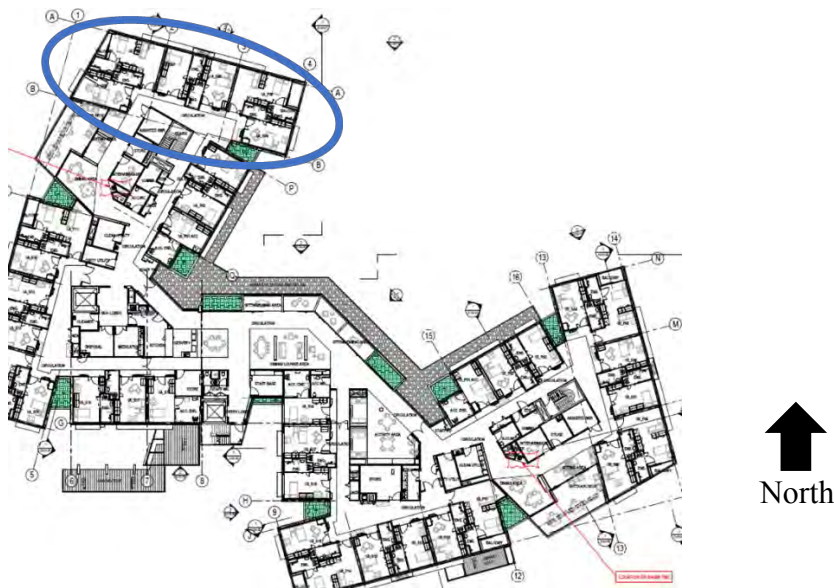


Figure 2: Typical RAC floor – levels 1-4, with ‘rooms fitted with honeycomb blinds’ circled

1.2 Tested honeycomb blinds description

The thermal transmittance of the blinds fitted into the rooms on level 3 are shown in Table 1. All blinds are a light colour and 100 per cent UV Blockage. All window blinds can be operated through remote controls and are opened horizontally. Sliding door blinds can only be operated manually.

Description	Single cell-25mm	Single cell-45mm	Single cell-62mm	Double cell-45mm	Double cell-62mm
Thermal transmittance (U value) of covering layer (W/m ² K)	5.27	4.16	4.16	4.34	3.13
Thermal transmittance (U value) of window with blinds (W/m ² K)	2.62	2.34	2.32	2.35	1.96

Table 1. *Tested honeycomb description*

The U-values in the table were calculated through equation (1) using the heat flux method (HFM) (ISO, 2014; Gaši, Milovanović and Gumbarević, 2019).

$$U = Q / (T_{in} - T_{out}) \quad (1)$$

Where:

T_{in} = inside temperature in Kelvin

T_{out} = outside temperature in Kelvin

Q = the corresponding heat flux through the element measured in W/m² using a heat flux sensor.

Comparing the results of Table 1 to other window dressings shows that the U-value of double cell-62mm is lower than roller blinds by 56 per cent, heavy curtains by 50 per cent, roller blinds with low E by 6 per cent, and higher than well-fitting shutters by 3 per cent (Fitton *et al.*, 2017).

1.3 Building simulation

The effect of blinds on the energy consumption of the existing RAC according to current and future weather, was simulated using Design Builder v7.0 Software, using EnergyPlus simulation engine (Crawley *et al.*, 2001). The model in Figure 3 includes the building envelope materials, insulation, solar absorptance, and a detailed HVAC that resembles the existing plant. The HVAC system comprises a variable air volume (VAV) system serving circulation areas and multiple fan coil units (FCU) serving dedicated resident rooms and common areas. The central chilled water plant is comprised of three air cooled chillers in parallel connection, with two smaller reverse cycle chillers that provide both chilled water and hot water, and one bigger chiller that only provides chilled water. For the VAV air handling unit, cooling and heating is provided by the chilled water and hot water from the central plant, while for the FCUs, cooling is provided by the chilled water from the central plant and heating is provided locally by the electric heating coil in the FCU.

The Australian National Construction Code (Australian Building Codes Board, 2019) guidelines in specification JVC were utilised to set the air conditioning schedule, temperature setpoints, occupancy schedules, and internal load profiles for building class 9c (aged care).

Two scenarios were created to identify the maximum effect of the honeycomb blinds on reducing energy. Scenario 1 simulates the effect of the glass installed in the RAC (low E tinted glazing of U-value=4.2 and SHGC=0.47) on energy consumption, assuming that blinds will be open all the time.

Scenario 2 simulates the energy consumption when the best performing blinds (Double cell - 62mm) in residential rooms are closed all the time. The simulated effect is for a total

specification of U-value of 1.96 and SHGC of 0.01 according to the measured values in Table 1.

Other scenarios were formulated based on interviews with the residents of the rooms fitted with the honeycomb blinds. These scenarios were then compared to identify which scenario is more effective in reducing energy consumption for the building.

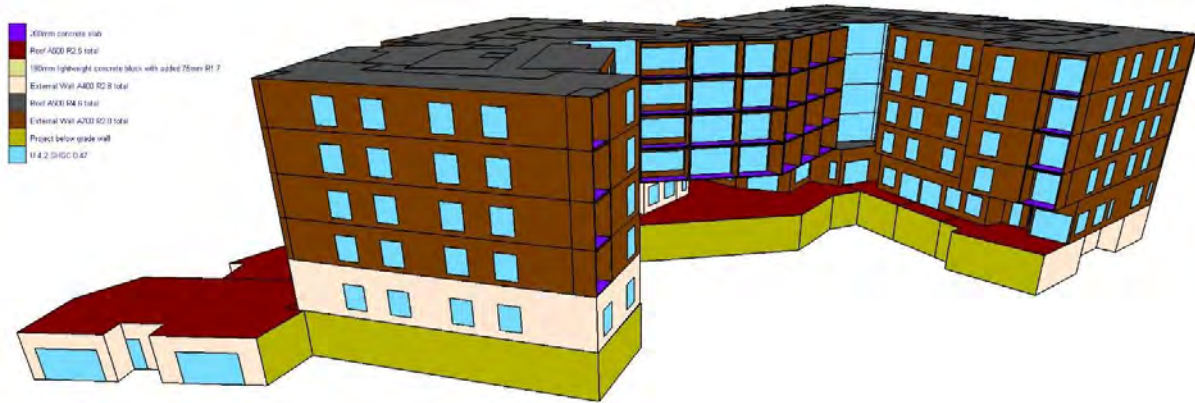


Figure 3. *Building simulation model*

2. RESULTS

2.1 Annual analysis

Scenario 1 (Figure 4) results show heating and cooling account for 38 per cent and cooling only is accounting for 28 per cent of the total energy when blinds are not used.

When comparing scenario 1 to scenario 2 (Table 2), it was found that energy consumption and emissions reduction can reach 4.6 per cent when blinds are used. Cooling energy reduction was the highest (12.5 per cent), which can be explained by the significant reduction in solar heat gain (57.7 per cent) and heat loss (64.3 per cent) because of closing the blinds.

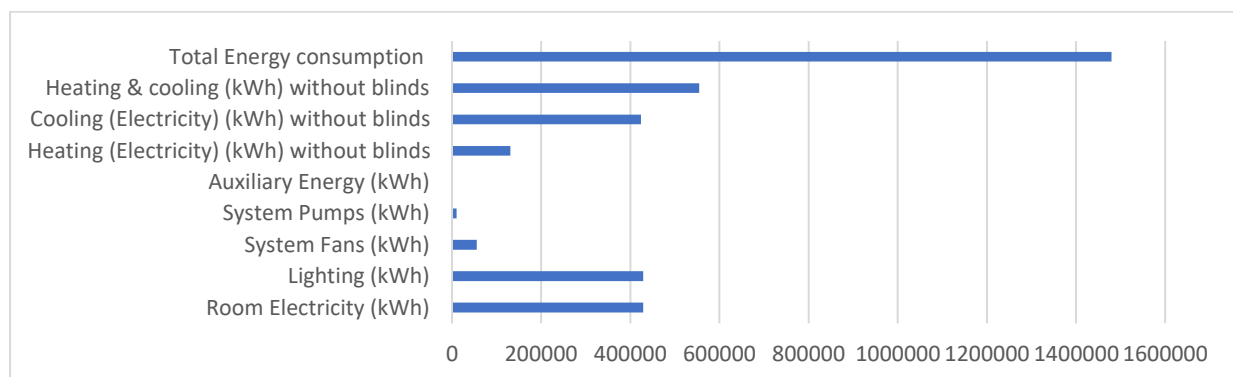


Figure 4. *Energy consumption simulation results with no blinds*

	Without blinds	With blinds	Reduction percentage
Heating (Electricity) (kWh)	130,925	124,903	4.6%
Cooling (Electricity) (kWh)	423,931	371,012	12.5%
Total Energy Consumption (kWh)	1,479,338	1,411,116	4.6%
CO ₂ Emissions (kg) $\times 10^3$	1,363,357	1,300,484	4.6%
Solar Gains through Exterior Windows (kWh)	209,069	88,518	57.7%
Heat Flow through Exterior Windows (kWh)	-23003.7	-64504.61	64.3%

Table 2. The effect of blinds on reducing energy and CO₂ emissions

2.2 Monthly analysis

The average monthly energy consumption (Figure 5) is plotted to compare how closing the blinds affects energy consumption in different seasons. Electricity consumption is higher in summer with a maximum of 163.3MWh without blinds, and 152.5MWh with blinds. The high electricity consumption in summer is predominantly due to cooling loads as evident in . Figure 6. Electricity consumption is lower in winter with a minimum of 95.8MWh without blinds and 94.2MWh with blinds.

The effect of the blinds is more significant in summer, which results in more reduction in summer (January) cooling energy reaching 6.6 per cent compared to the one in winter (July) reaching only 2.8 per cent. The small heating energy reduction in winter shows that opening the blinds does not help reducing heating loads by much. This is due to the nature of climate with mild temperatures during winter. The limited benefit of solar heat gain during winter highlights that closing the blinds the whole time would have a positive impact on reducing heating and cooling energy consumption. Lack of daylight might have, however, a negative impact on the health and wellbeing of occupants (Salonen *et al.*, 2013; Aries, Aarts and van Hoof, 2015). Addressing these negative impacts is outside of the scope of this paper, however, a more accurate representation of how the blinds are operated at the RAC will be discussed at a latter section.

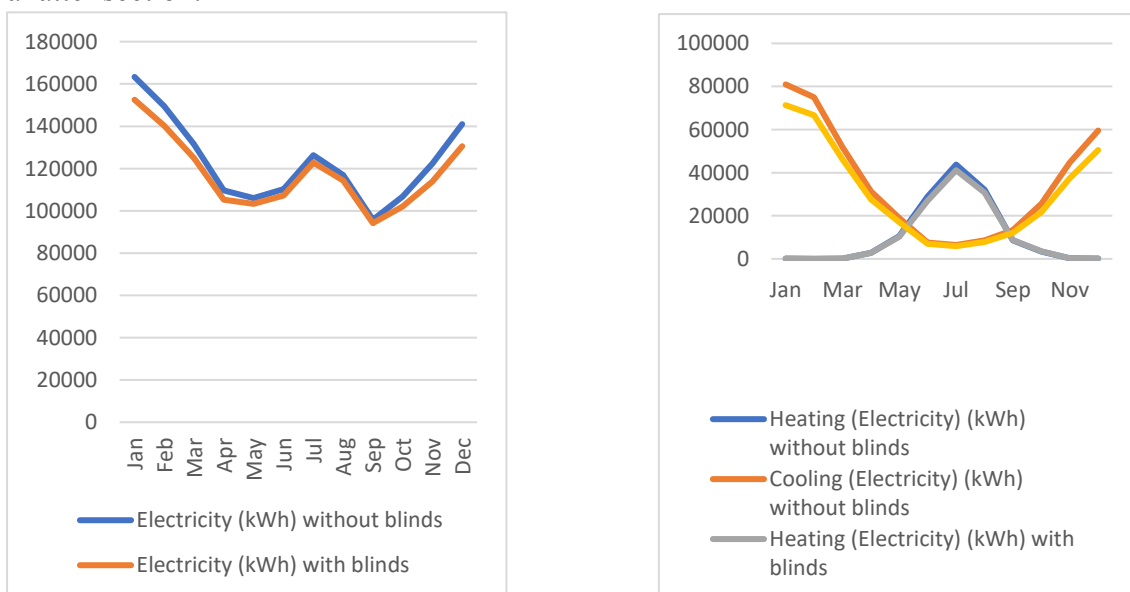


Figure 5 (left): Total energy consumption with and without blinds. Figure 6 (right): Monthly heating and cooling energy with and without blinds

3. USER FEEDBACK AND INSIGHTS

To simulate a more realistic operation of the blinds, the research team conducted interviews with five of the residents of the six rooms with honeycomb blinds. The aim of the interview was to identify operation schedules, and reasons for opening and closing the blinds.

Operation schedules of the 5 rooms are summarised in Table 3.

Question 1: Operation schedule	
Room 1	Open in the morning and closed at night
Room 2	Open in the morning and closed at night
Room 3	Always open
Room 5	Open/close as response to daylight. Open during night-time
Room 6	Rarely closes it (moves chair to avoid the sun)

Table 3. Residents' operation schedule summary

The responses show that most residents operate the blinds for reasons that are not related to thermal comfort or to optimise reliance on air conditioning. They mostly use the blinds for visual comfort or sense of security/privacy. One of the reasons that residents are not utilising blinds for thermal comfort, is the reliance on air conditioning that does not have any cost implications on them. Another reason is the lack of knowledge of residents and staff about how blinds can contribute to reducing energy costs.

4. SIMULATION OF OPERATION SCENARIOS

Following feedback from residents, level 3 of the case study building was simulated with 62mm double cell honeycomb blinds, based on the assumption that the air conditioner is operational 24/7. Simulation was according to six operation scenarios. Three of these scenarios were formulated from users' feedback:

- 1- Blinds always open
- 2- Blinds are closed at night and when solar radiation incident on the window exceeds $120\text{W}/\text{m}^2$
- 3- Blinds are always open during the day and closed at night

Except for scenario 2, none of these scenarios contribute significantly to reducing energy consumption in subtropical climate. Scenario 1 contributes to increasing heating and cooling loads. Scenario 3 is common for reducing heating loads in colder climates. However, as seen in section 2.1 of this paper, the blinds had very little effect on reducing heating loads in this subtropical climate. This scenario was mainly used by residents for security/privacy reasons, rather than thermal comfort or energy efficiency.

Three more scenarios that have the potential to maximise energy reduction were simulated to be compared to the commonly used scenarios in the RAC:

- 4- Blinds are always closed
- 5- Blinds are closed when solar radiation incident on the window exceeds $120\text{W}/\text{m}^2$
- 6- Blinds are closed when outside air temperature is above 24°C .

Simulation results (Figure 7) show that heating and cooling energy consumption can be grouped into three categories of operational scenarios.

- Category one is the conservative that reflects closing blinds the whole time (scenario 4). This scenario is unrealistic when the rooms are occupied, however, it is recommended for rooms that are unoccupied, since it shows the maximum energy reduction when compared to all other scenarios.
- Category two is the informed operation. It covers all operations that reflect direct response to external conditions such as solar radiation and temperature (scenarios 2, 5, and 6).
- Category three is the uninformed operations that do not respond to external conditions (scenarios 1 and 3). These two scenarios show very similar energy consumption results, which indicates that for sub-tropical climate the benefits of closing the blinds at night to prevent heat loss during cold seasons is not significant, and that blinds' benefits are evident mainly in reducing cooling loads during daytime.

Informed operation can help reduce heating and cooling kWh/annum by 6 per cent when compared to uninformed operation. The conservative scenario can reduce it by 9.4 per cent when compared to uninformed scenario.

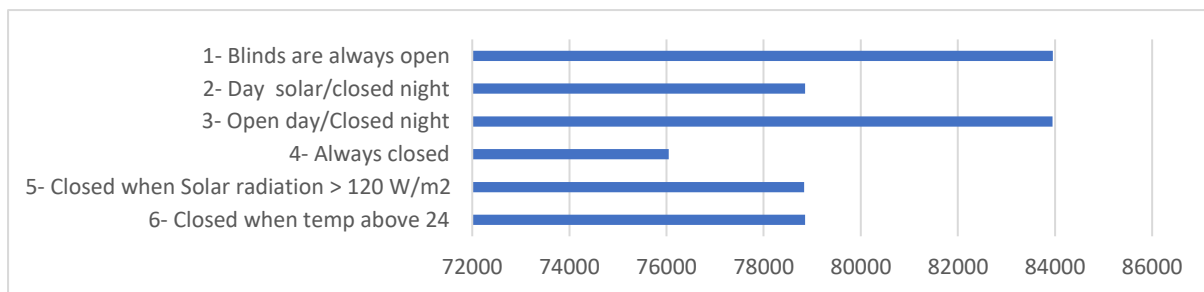


Figure 7. *Effect of different shading scenarios on heating + cooling energy consumption*

Figure 8 shows that the differences between the three categories are predominantly due to energy consumption reduction resulting from closing the blinds are higher in the summer months, whereas reduction in winter months is very low.

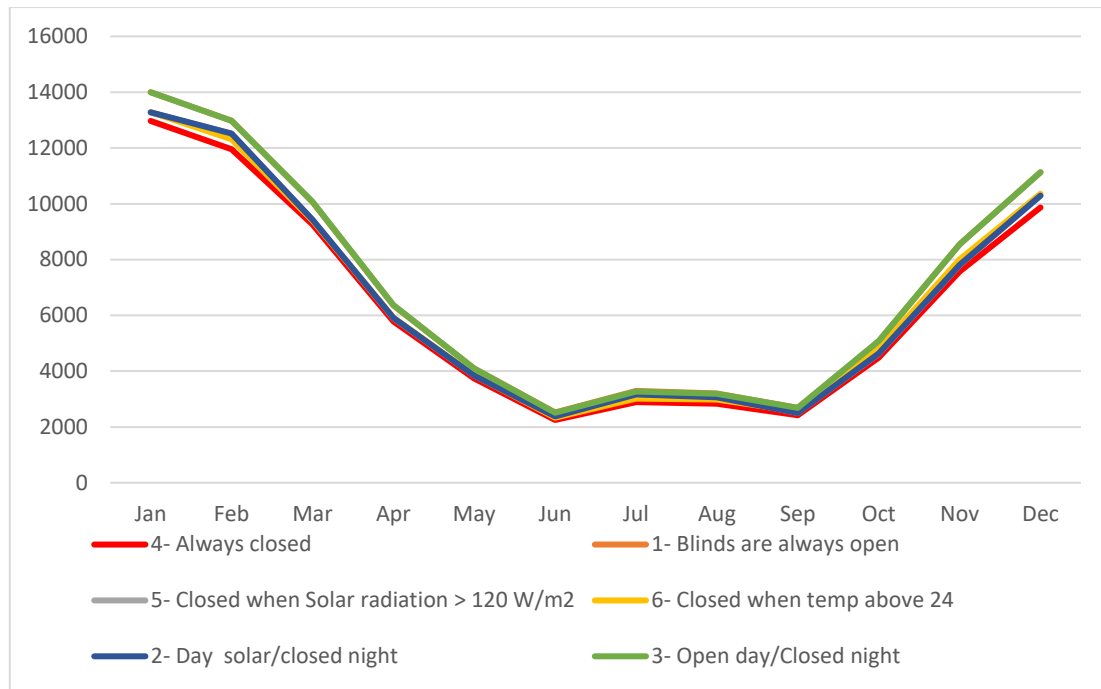


Figure 8. Monthly heating and cooling kWh of different scenarios

5. COST EFFECTIVENESS ANALYSIS

Table 4. Estimated energy and carbon emissions savings Table 4 presents the estimated reduction in carbon emissions and electricity bills cost when the blinds are closed in all residential rooms. The CO₂ emissions reduction is based on the NCC Volume 1, greenhouse gas emission factor of 256kgCO₂-e/GJ (Australian Building Codes Board, 2019). The estimated electricity bill savings per year is \$10,233, with the most significant reductions being in summer months, reaching a maximum of \$1,622 savings in January.

	Estimated Emissions Reduction (kg)x10 ³	Estimated kWh Savings	Estimated Bill Savings \$0.15/kWh
Jan	10	10,813	\$1,622
Feb	9	9,330	\$1,400
Mar	6	6,436	\$965
Apr	4	4,353	\$653
May	3	2,732	\$410
Jun	3	3,014	\$452
Jul	3	3,550	\$533
Aug	2	2,580	\$387
Sep	1	1,603	\$240
Oct	4	4,695	\$704
Nov	8	8,578	\$1,287
Dec	10	10,537	\$1,581
Total	63	68,222	\$10,233
Mean	5	5,685	\$853

Table 4. Estimated energy and carbon emissions savings

Reduction in energy costs per annum can reach 6 per cent when blinds are operated in an informed manner, compared to no blinds. This analysis did not include the cost of installation or maintenance.

6. FUTURE WEATHER SIMULATION

Global climate change is causing rising temperatures, and affecting humidity, precipitation patterns. It is affecting weather extremes such as number of heat waves, droughts, and tropical cyclones (IPCC, 2021). According to CSIRO, Australia's climate is warmer by 1°C since 1910 (Whetton and Chiew, 2021). The changes in climate should impact how buildings and HVAC plants are designed and simulated, as a way to adapt to future conditions.

A future weather file was used to simulate the effect of informed operation on energy consumption under future weather conditions. The file predicts the effect of global warming on weather conditions in the year 2050, assuming that efforts to reduce global warming will remain at their current state. The file was created through hourly interpolation of the nominal 1990 Reference Meteorological Years (RMYS) for the following climatic conditions (Lee, 2011):

- Temperature (°C)
- Relative humidity (%)
- Wind speed (m/s)
- Global solar radiation on the horizontal plane (W/m²).

Level 3 of the RAC was simulated with and without blinds using current and future weather files. Results (Figure 9) show that energy consumption will increase by 22.5 per cent if blinds were not used, and by 22.7 per cent if blinds were used. The effect of using blinds on energy savings is 5858kWh/annum for current weather, compared to 6914kWh/annum for future weather.

This highlights that there will be significant increase in energy consumption to maintain thermal comfort in the future, with blinds providing 1056kWh/annum (18 per cent) additional energy savings in hotter future weather when compared to the savings they are providing currently.

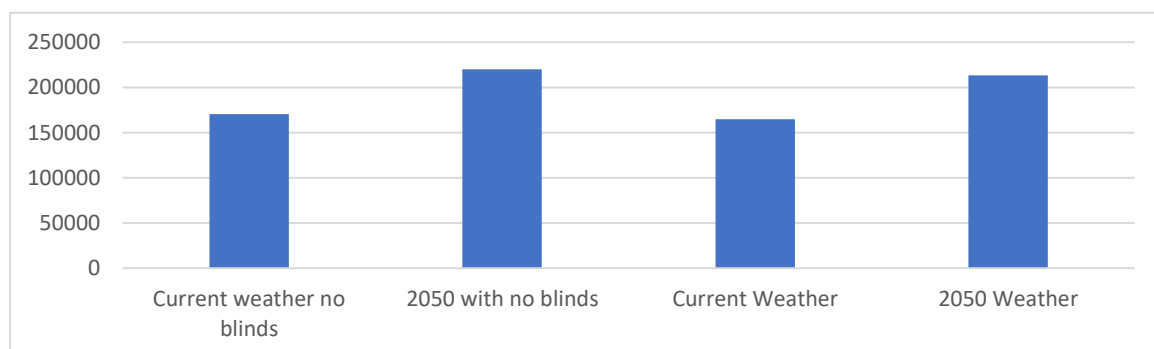


Figure 9. *Energy simulation of blinds in current and future weather*

CONCLUSION

Internal window dressing provides a cost effective and easy method that can be retrofitted in existing buildings to reduce heating and cooling energy consumption. Honeycomb blinds is one of the most effective window dressings in terms of adding insulation layer to windows that can reduce thermal transmittance. The effectiveness of honeycomb blinds is determined by many aspects such as its installation method, number and size of cells, material and colour. However, the effectiveness of the blinds is highly influenced by how they are operated.

This paper investigates the potential of simulation tools as a method to maximise the benefits of honeycomb blinds. An existing residential aged care (RAC) was utilised as a case study, where honeycomb blinds were installed in residential rooms, and the residents of those rooms were interviewed to identify how they normally operate the blinds and what trigger them to open or close it.

An energy model for the RAC was built to simulate:

- a) The effect of opening /closing the blinds for a whole year on energy consumption
- b) The effect of operating the blinds in different scenarios. These scenarios were devised based on findings from interviews with the residents, and compared to scenarios that reflect informed operational patterns that can optimise thermal comfort, visual comfort, and access to daylight without increasing reliance on air conditioning.

Findings show that 38 per cent of energy consumption for the simulated case study when blinds are open is for cooling. This cooling energy can be reduced by 12.5 per cent if blinds were closed the whole time, which can result in around AU\$10,000 savings per year.

User experience and operational patterns interviews show that most residents leave the blinds open most of the time and rarely operate them as a response to external conditions.

Comparing how the blinds were actually operated with informed patterns that respond to solar radiation and/or temperature show that informed operation can reduce energy consumption by 6 per cent.

Simulating the building using future weather files, shows that there will be approximately 23 per cent increase in energy consumption, with blinds providing 18 per cent additional savings to what they are providing under current weather conditions.

According to these findings, residential facilities are encouraged to invest in retrofitting high performance blinds. The simulation results suggest that for subtropical climate, closing the blinds all the time could be the most effective solution in reducing heating and cooling energy. However, applying this solution is difficult and could have negative health implications. Therefore, it is important for facilities managers/users to ensure implementation of informed operational patterns that can optimise occupants' comfort and energy efficiency.

This paper presents the potential of simulation tools in identifying how can blinds be operated in a manner that maximise energy efficiency and reduce ongoing costs. Further research is required to investigate the best methods to implement simulation findings regarding recommended operational patterns.

ACKNOWLEDGEMENTS

The research is part of an Australian Renewable Energy Agency iHub project (www.ihub.org.au) funded by the Australian Government and Industry. The funding bodies did not influence the findings of this paper

The authors sincerely thank Bolton Clarke for facilitating data collection from their facility, and Norman Australia for providing the honeycomb blinds to be tested.

REFERENCES

- Aries, M. B. C., Aarts, M. P. J. and van Hoof, J. (2015) ‘Daylight and health: A review of the evidence and consequences for the built environment’, *Lighting Research & Technology*, 47(1), pp. 6–27.
- Ariosto, T. *et al.* (2013) ‘Evaluation of Residential Window Retrofit Solutions for Energy Efficiency’, The Pennsylvania Housing Research Center.
- Ascione, F. *et al.* (2016) ‘Multi-objective optimization of the renewable energy mix for a building’, *Applied Thermal Engineering*, 101, pp. 612–621.
- Australian Building Codes Board (2019) National Construction Code Series 2019. Canberra, Australia.
- Baniassadi, A. and Sailor, D. J. (2018) ‘Synergies and trade-offs between energy efficiency and resiliency to extreme heat—A case study’, *Building and Environment*, 132, pp. 263–272.
- Bickel, S., Phan-Gruber, E. and Christie, S. (2013) ‘Residential Windows and Window Coverings: A Detailed View of the Installed Base and User Behavior’, Prepared for the US Department of Energy’s Office of Energy Efficiency and Renewable Energy.
- Crawley, D. B. *et al.* (2001) ‘EnergyPlus: creating a new-generation building energy simulation program’, *Energy and buildings*, 33(4), pp. 319–331.
- Fang, Z. *et al.* (2014) ‘The effect of building envelope insulation on cooling energy consumption in summer’, *Energy and Buildings*, 77, pp. 197–205.
- Fitton, R. *et al.* (2017) ‘The thermal performance of window coverings in a whole house test facility with single-glazed sash windows’, *Energy Efficiency*, 10(6), pp. 1419–1431.
- Gaši, M., Milovanović, B. and Gumbarević, S. (2019) ‘Comparison of infrared thermography and heat flux method for dynamic thermal transmittance determination’, *Buildings*, 9(5), p. 132.
- Humaish, H. (2018) ‘Evaluate heat loss through windows by using Guarded Hot Box (GHB)’, in *Journal of Physics: Conference Series*. IOP Publishing, p. 12025.
- IPCC (2021) *Change, Climate Change 2021: The Physical Science Basis*. Contribution of Working Group I to the Sixth Assessment Report of the Intergovernmental Panel on Climate Change. Cambridge, United Kingdom and New York, NY, USA. Available at: https://www.ipcc.ch/report/ar6/wg1/downloads/report/IPCC_AR6_WGI_Full_Report.pdf.
- ISO, B. S. (2014) ‘9869-1: 2014 Thermal insulation, Building elements, In-situ measurement of thermal resistance and thermal transmittance-Part 1: Heat flow meter method’, London: BSI.
- Lee, T. (2011) ‘Changing Climate: ersatz future weather data for lifelong system evaluation’, in *Building Simulation*, pp. 633–640.

Mansouri Birjandi, N. (2015) ‘Convective Heat Transfer from a Recessed Window Covered By a Top Down–Bottom Up Single-Layer Honeycomb Blind’.

Petersen, J., Cort, K. and Widder, S. (2016) ‘Mind the Gap: Summary of Window Residential Retrofit Solutions’.

Petersen, J. M. *et al.* (2016) Evaluation of Cellular Shades in the PNNL Lab Homes. Pacific Northwest National Lab.(PNNL), Richland, WA (United States).

Salonen, H. *et al.* (2013) ‘Physical characteristics of the indoor environment that affect health and wellbeing in healthcare facilities: A review’, *Intelligent Buildings International*, 5(1), pp. 3–25.

Whetton, P. and Chiew, F. (2021) ‘Climate change in the Murray–Darling Basin’, in *Murray-Darling Basin, Australia*. Elsevier, pp. 253–274.

Yu, J. *et al.* (2015) ‘Evaluation on energy and thermal performance for office building envelope in different climate zones of China’, *Energy and Buildings*, 86, pp. 626–639. doi: <https://doi.org/10.1016/j.enbuild.2014.10.057>.

DISCLAIMER

The information or advice contained in these technical papers is intended for use only by professionals who have had adequate technical training in the field to which the paper relates. At the time of publication, these technical papers have undergone a formal peer-review process.

These documents have been compiled as an aid only, and the information or advice should be verified before it is put to use. The user should also establish the applicability of the information or advice in relation to any specific circumstances. While the information or advice is believed to be correct, no responsibility is taken by AIRAH or IBPSA Australasia for any statements made within.

AIRAH and IBPSA Australasia, its officers, employees and agents, disclaim responsibility for any inaccuracies contained within the documents, including those due to any negligence in the preparation and publication of the said technical papers.

COPYRIGHT

This work is copyright. Apart from any use as permitted under the Copyright Act 1986, no part may be reproduced by any process without prior written permission from either the Australian Institute of Refrigeration, Air Conditioning and Heating (AIRAH) or the International Building Performance Simulation Association (IBPSA) Australasia.

DOUBLE SKIN FAÇADE'S ENERGY PERFORMANCE IN A MIXED-MODE OFFICE BUILDING

SOHA MATOUR

School of Architecture and Built Environment, Faculty of Engineering, Queensland
University of Technology, Australia
s.matour@qut.edu.au

KEIVAN BAMDAD MASOULEH

School of Engineering, Design and Built Environment, Western Sydney University,
Australia

NIMA IZADYAR

School of Built Environment, College of Engineering and Science, Victoria University,
Melbourne, VIC, Australia

VERONICA GARCIA-HANSEN

School of Architecture and Built Environment, Faculty of Engineering, Queensland
University of Technology, Australia

ABOUT THE AUTHOR

Soha Matour is an architect working in the building science field. She has obtained experience in designing efficient building façades, natural ventilation and climate resilience buildings. Soha's PhD topic focused on reducing the cooling load of tall buildings by introducing an innovative design for DSF. The project aimed to improve the thermal performance of glazed-façade buildings by utilising wind-induced ventilation and external shading devices.

Soha is currently working as a research assistant at QUT focusing on sustainable design in both buildings' indoor environments and urban scales. She has a growing number of publications in peer-reviewed journals and conferences in the field of ventilation, climate change and energy-efficient buildings.

ABSTRACT

Double Skin Façade has been recognised as an advanced façade technology for improving buildings' thermal performance. However, the integration of DSF with a building in the Mixed-Mode ventilation has not adequately been studied yet. Hence, this study develops a control algorithm based on the adaptive thermal comfort model to control openings operation in the MM building utilising the energy management system module of EnergyPlus. This study reveals the energy-saving potential of DSF compared to Single Skin Facade in two Australian climates. DSF showed an energy saving potential of 10.2 per cent in Brisbane and 9.4 per cent in Melbourne. Additional energy savings of 7.4 per cent and 9.9 per cent were achieved using tinted glass as the external skin compared to clear glass in Brisbane and Melbourne.

INTRODUCTION

The combined application of Natural Ventilation (NV) and mechanical cooling, known as mixed-mode ventilation has widely gained attention in order to create a sustainable, thermally comfortable and healthier indoor environment. In mixed-mode (MM) buildings, mechanical ventilation is used only when natural ventilation alone cannot provide a comfortable indoor condition for occupants. A high rate of occupants' satisfaction with the thermal environment and indoor air quality in a Mixed-Mode (MM) building demonstrates that MM ventilation exceptionally outperforms other ventilation systems (Kim & de Dear, 2021). In addition, the considerable energy-saving potential of a MM system which lies in the range of 20 to 47 per cent (on average for temperate climates) (Bamdad et al., 2022; Ledo Gomis et al., 2021), has introduced this system as an energy-efficient strategy in response to the increasing trend of cooling demand in the building sector.

However, mixed-mode ventilation efficiency depends on both environmental factors such as the Climatic Potential of Natural Ventilation (CPNV) and building characteristics, including windows placement and the building's envelope configuration that can control or encourage environmental factors for effective utilisation of NV in buildings. One of the extensively addressed impediments to deploying NV in dense urban areas tends to be the noise pollution that prevents occupants from opening windows (de la Hoz-Torres et al., 2021; Nicol & Wilson, 2004). Bajraktari et al., 2015; Morshed, 2014). Knowing that facade openings act as both noise entries and NV paths, windows operation for NV increase in a MM building can conflict with the attempt to decrease noise ingress and will be limited by the outdoor noise sources (Barclay et al., 2010; Fusaro et al., 2020; Lam et al., 2021).

Double Skin Facade is an advanced technology that allows a successful implementation of NV and reduces background noise associated with windows opening. DSF generally consists of two glazed skins separated by a cavity space with the possibility of employing openings on both skins. Research shows that the noise protection of a DSF with well-designed openings would be comparable to the sound insulation potential of many common (fully closed, airtight) windows (Kuri & Pérez R, 2022) (Bajraktari et al., 2015). This potential of DSF, along with other advantages of this system, such as solar heat gain reduction, could introduce it as an alternative façade design for MM buildings.

The thermal performance of DSF depends mainly on the climate and meteorological factors, geometrical features of the DSF and material properties (Hazem et al., 2015). Several classifications have been defined for DSFs mainly based on three items: 1- ventilation mode (natural, mechanical or hybrid), 2- DSF configuration and 3- airflow paths through the cavity (Loncour et al., 2004). One of the well-known classifications is based on the configuration of DSFs (Oesterle, 2001): Box windows, Corridor, Shaft box, and Multi-storey. The concept of these types of DSFs is mostly based on using absorbed solar radiation to increase the stack effect and airflow rate in the cavity while controlling the buffer zone for less building heat loss in the cold seasons.

Airflow path classification defines how DSF is connected to the indoor and outdoor environment. Haase et al. (Haase & Amato, 2009) presented five DSF categories based on their airflow path: Supply Air (SA), Exhaust Air (EA), Air Buffer (AB), External Air Curtain (EAC) and Internal Air Curtain (IAC). These predefined DSF types can be grouped as non-interactive and interactive configurations to pay attention to indoor space. Table 1 presents a new interpretation of DSF types based on interactive features of DSF. This classification focuses on the building's NV modes, Cross-Ventilation (CV) and Single-Sided Ventilation (SSV) and heating or cooling strategies implemented through each airflow path in DSFs.

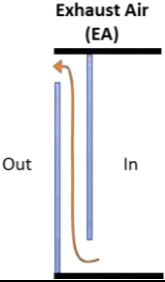
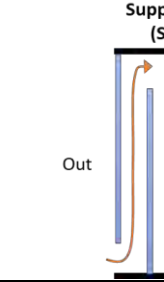
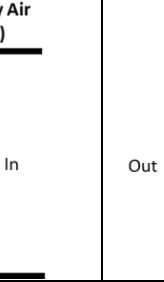
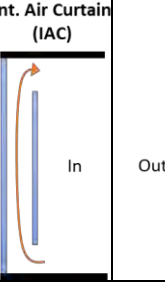
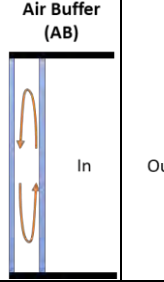
	Interactive configurations (IC)			Non-interactive (N-IC)		
Predefined DSF's airflow path types*						
NV purpose	Cooling	Cooling	Heating	Heating	Heating	Cooling
NV mode	SSV CV	SSV CV	SSV	SSV	-----	----

Table 1. Airflow path in DSF and possible NV modes. *Images are reproduced based on a study by Francesco Pomponi (Pomponi et al., 2016)

Therefore, to increase the year-round energy performance of the DSF in both heating and cooling modes, the openings' control strategies should vary to facilitate different airflow paths in DSF and indoor spaces. In this regard, MM buildings with controllable openings can take advantage of NV in interactive and non-interactive forms as required for occupants' thermal comfort. Based on Table 1, the literature on the energy performance of naturally ventilated DSFs is discussed as follows.

DSF in a mechanically ventilated building (N-IC):

Research shows that the addition of DSF with a shading device to a single skin façade (SSF) can reduce the energy consumption of the building by 17 and 25 per cent in a multi-story DSF with Air buffer (AB) and Interior Air Curtain (IAC) ventilation mode, respectively (Gratia & De Herde, 2007). In some cases, even non-interactive DSF can be integrated into the HVAC system and result in more energy savings. In South Korea, using a DSF in air buffer mode and combined with an HVAC system showed a considerable heating energy reduction of 41 per cent compared to the non-integrated buffer zone (Choi et al., 2012). Another study in Korea proved the applicability of DSF as a suitable retrofit solution saving total energy of 51 per cent and 38 per cent, with and without integrated shading devices, in a 5-storey residential building. In terms of CO₂ emissions, the application of the DSF system was found to be environmental-sustainably feasible in Korea (Kim et al., 2012).

The energy efficiency of a three-story building in the hot climatic condition of Crete, Greece, was improved using a corridor type DSF when a combination of Air buffer (AB) and IAC ventilation mode was applied for winter (9 per cent reduction) and summer (5.5 per cent reduction) seasons, respectively (Papadaki et al., 2014). A further improvement was achieved for the building by adding a shading device either internally or externally. In the hot arid climate of Cairo, the energy performance of a multi-story DSF was compared with SSF featuring reflective glazing and a 40 per cent window to wall ratio (WWR) (Hamza, 2008). Three different glazing materials were tested for DSF external skin, including clear glass and reflective and tinted green glass. While clear glass for outer skin could not compete with SSF in reducing the cooling load, reflective DSF was predicted to decrease annual cooling loads by

approximately 30 per cent. This research highlights the significance of material selection for external glazing of DSF in hot climates.

DSF in a MM building (IC and N-IC)

The energy performance of mixed-mode ventilation becomes more complicated when DSF is in practice. However, controlling both external skin and internal skin openings can provide the opportunity to take advantage of all possible airflow paths based on occupants' thermal comfort and climatic conditions creating a climate-responsive façade that operates DSF more effectively.

A few studies have addressed mixed-mode ventilation in a building equipped with DSF. Zomorodian et al. (Zomorodian & Tahsildoost, 2018) estimated the energy saving of DSF with mixed-mode and single-sided ventilation as about 9–14.8 per cent in the hot and arid climate of Tehran. In South Korea (Joe et al., 2013) studied the effect of a seasonal control strategy for openings of a multi-story DSF in a mixed-mode building. NV was allowed when the cavity temperature was lower than the indoor area. During the heating season, hot air in the cavity was supplied to the HVAC system and used a preheating strategy. By applying this control strategy, 23.8 per cent energy saving was achieved annually. In these studies, attention has been paid to NV under a single-sided ventilation mode. Barbosa et al. (Barbosa et al., 2015) studied DSF performance with cross ventilation in the tropical climate focusing on a free-running building and the thermal comfort of occupants. This study highlights the significant potential of DSF integrated into a mixed-mode building for saving energy. As illustrated in Table 1, two types of airflow path configuration have the potential to be used in both single-sided and cross ventilation modes. Knowing that cross ventilation is far more effective than single-sided ventilation in providing higher air velocity and, consequently, occupants' thermal comfort (Omrani et al., 2017), this ventilation mode is worth studying and applying as a part of mixed-mode ventilation in a building with DSF. Therefore, the current study focuses on a dynamic control strategy of mixed-mode ventilation in an office building with DSF. As a result, different airflow paths will be applied depending on climate suitability, including cross ventilation for cooling purposes.

In contrast with ventilation modes in DSF buildings, the effect of physical parameters of DSF (cavity and openings dimension, shading device and material properties) on the energy and thermal performance of DSF has been widely studied in the literature. Glazing material has been introduced as one of the most significant parameters for energy-saving through DSF application (Preet et al., 2022). However, different material selection has been suggested in the literature for the successful application of DSF; double low-e glazing for both skins (Cetiner & Özkan, 2005), coloured double glazing for both skins (Hamza, 2008) and reflective glass for external skin (Alberto et al., 2017). Single clear glazing as the inner skin and double reflective glazing as the exterior skin in the subtropical climate of Hong Kong showed an annual saving of around 26 per cent in building cooling energy compared to a conventional single skin facade with single absorptive glazing (Chan et al., 2009). Using a CFD simulation of the cavity airflow, low-e glazing for internal skin and clear glass for external skin showed a superior performance to clear glazing for both skins in terms of NV performance in the cavity of a DSF (Tao et al., 2021). Therefore, in DSF studies, there is a lack of agreement on glazing material for a year-round application. This could be due to a strong correlation between DSF thermal performance and climatic factors as well as geometrical parameters. This phenomenon makes it inevitable to determine optimum material selection for DSF glazing considering the building location (Choi et al., 2019).

In this study, in addition to the energy performance comparison between SSF and DSF (both with automated openings), the effect of glazing material properties on the energy performance

of the DSF is evaluated. In order to reflect the significance of climatic conditions on material selection for DSF, two major Australian cities characterised by the specific climatic condition have been approached for this study: Melbourne and Brisbane, representative of Australian temperate (Zone 5) and subtropical (Zone 2) climates, respectively.

1. METHODOLOGY

This study modelled a three-story office building as a case study in Brisbane with a subtropical climate and Melbourne with a temperate climate. This building, recommended by the Australian Building Codes Board (ABCB), is a typical medium-size office building in Australia. This office building has a gross floor area of almost 2000m² and was used as a case study in previous studies (Bamdad Masouleh, 2018; Bamdad Masouleh et al., 2017). However, unlike the earlier studies, an open-plan office (one thermal zone per floor) with more energy-efficient lighting and equipment is assumed. Also, the ideal loads air system is modelled for this building which provides a model for an ideal HVAC system with 100 per cent efficiency (EnergyPlus, 2022). This system is suitable for evaluations of building thermal performance and load calculations. EnergyPlus reports the output of this system under district heating or cooling tabs. The energy use of this system is calculated based on the energy required to condition the required supply air to meet all the load requirements. It should be noted that the energy use of this building may significantly vary if a detailed HVAC system is modelled.

Tables 2 and 3 provide simulation assumptions and specifications of the building. The schedules used for equipment, lighting, occupancy, and HVAC working hours are based on the National Australian Built Environment Rating System (NABERS). A mixed-mode ventilation strategy and a double skin façade (corridor type) were modelled for the building, as shown in Figure 1. The cavity of DSF is simulated with three stacked zones, and EnergyPlus AirFlow Network (AFN) is used to calculate the pressure at each node and airflow through each linkage. At each storey, the upper and lower zones of the cavity are connected to the middle zone via openings that follow the rules stated in Table 5. The connection between air nodes is shown in Figure 1. AFN model is also used to estimate the infiltration rate in the building. Table 4 presents the AFN parameters used in the simulation. To calculate the exterior heat transfer convection coefficient, the MoWiTT model is used (EnergyPlus, 2022; Yazdani & H. Klems, 1993). This model can be used for very smooth and vertical surfaces such as windows in low-rise buildings. The adaptive thermal comfort model based on ASHRAE Standard 55 was used to control windows operation. The adaptive comfort model states that outdoor climate conditions influence occupants' thermal comfort level in the indoor environment, and occupants are able to adapt themselves to thermal environments (ASHRAE & Air-Conditioning Engineers, 2013). According to the adaptive model, the thermal comfort temperature range based on 80% acceptability is calculated as follows:

$$T_{u,j} = (T_{pma} \times 0.31 + 21.3) \quad (1)$$

$$T_{l,j} = (T_{pma} \times 0.31 + 14.3) \quad (2)$$

where T_{pma} is the prevailing mean outdoor air temperature, calculated by the monthly mean dry-bulb air temperature for each Climate Zone (CZ). T_u and T_l is the upper and lower temperature acceptability limits and subscript j refers to calendar months. In order to apply these equations, ASHRAE Standard 55 sets criteria that must be met, such as operable windows, sedentary activities of occupants, and constraints for prevailing mean outdoor air

temperature. Please refer to ASHARE for more details (Ashrae & Air-Conditioning Engineers, 2013).

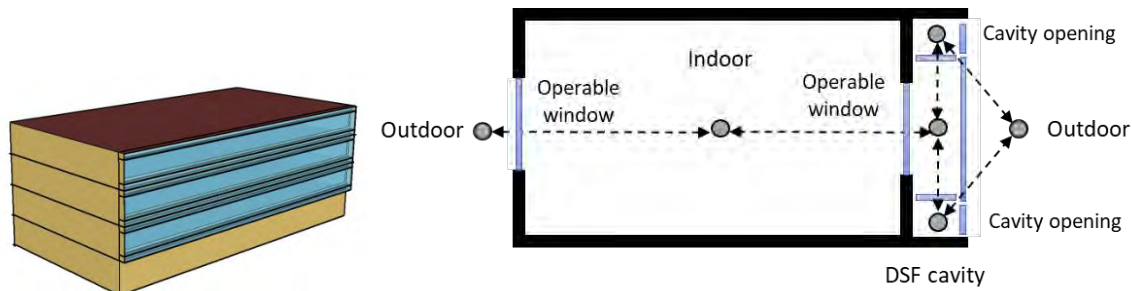


Figure 1. Schematic view of the case study building with corridor type DSF. The DSF cavity is divided into three zones. Dash lines show the connection between air nodes.

Component	Construction materials	U-Value (W/m ² -K)
Roof	Metal deck, air gap, 150 mm heavyweight concrete, roof space, R2.0 batts, 13 mm acoustic tiles	0.27
Wall	200 mm heavyweight concrete R1.5 batts, 10 mm plasterboard	0.54
Window type	Double glazed window (Clear- air-Low-e)	2.4
Window to wall ratio	54% (N), 45% (S)	

Table 2. Building construction details.

Parameters	Values	Parameters	Values
Total floor area (m ²)	2003.85	Lighting load (W/m ²)	5
Geometry (m)	36.5 × 18.3	Occupancy (Person/m ²)	0.1
Number of floors	3	Equipment load (W/m ²)	7.5
Floor to ceiling height (m)	2.7	Temperature setpoint (°C)	21–25
Floor to floor height (m)	3.6	HVAC system	Ideal loads air system

Table 3. Building geometry details and assumptions used for simulation

Simulation Parameters	Description	Value
DSF type / Cavity depth	Corridor Type	70 (cm)
Convective Heat Transfer method (Exterior)	MoWiTT	
Solar Distribution Modelling	Full Interior and Exterior	
Wind Pressure Coefficient Type	Surface Average Calculation	
Vertical openings	Discharge coefficient	0.65
	Air mass flow coefficient when the opening is closed	0.001 (kg/s-m)
Horizontal openings	Discharge coefficient	0.2
	Air mass flow coefficient when opening is closed	0.001 (kg/s-m)

Cracks	Air mass flow coefficient at reference conditions	0.01 (kg/s)
	Air Mass Flow Exponent	0.65

Table 4. *Double skin façade modelling and simulation parameters*

This study developed a control strategy based on outdoor air temperature and adaptive thermal comfort to control cavity openings and rooms' windows. This control strategy aims to i) take advantage of NV whenever the outdoor air conditions are suitable and ii) create an air buffer and trap heat in the cavity to reduce building heating demands by closing the cavity openings when the outdoor air temperature is below a threshold (T_t). The status of cavity openings and windows is shown in Table 5.

	Cavity openings	Room windows
$if (T_o < T_t < T_{l,j})$	closed	closed
$if (T_t < T_o < T_{l,j})$	open	closed
$if (T_{l,j} < T_o < T_{u,j})$	open	open
$if (T_{u,j} < T_o)$	open	closed

Table 5: *Status of cavity openings and windows in DSF building*

In order to find the effect of external skin glass type on DSF thermal performance, three different glass types were simulated in this study. DSF with clear glass (DSF-C), tinted glass (DSF-T) and Low-e glass (DSF-L) as the external skin. The thermal and optical properties of considered glass types in this study are summarised in Table 6.

SSF		THK ^a	Trans ^b	Ri ^c	Re ^d	Em-i ^e	Em-e ^f	SHGC ^g	U-value ^h
	Clear	6	0.77	0.071	0.071	0.84	0.84	0.82	5.8
Air gap	20	---	---	---	---	---	---	---	
Low-e	6	0.6	0.22	0.17	0.10	0.84	0.64	3.4	
DSF external skin	Clear	6	0.77	0.071	0.071	0.84	0.84	0.82	5.8
	Tinted	6	0.48	0.056	0.056	0.84	0.84	0.62	5.8
	Low-e	6	0.6	0.22	0.17	0.10	0.84	0.64	3.4

Table 6: *layers' properties of SSF and DSF's external skin*

^a Thickness, mm. / ^b Solar transmittance of the glazing layer, dimensionless. / ^c Solar reflectance of the glazing layer, interior-facing side. / ^d Solar reflectance of the glazing layer, exterior-facing side. / ^e Infrared (long-wave) emittance of the glazing layer, interior-facing side. / ^f Infrared (long-wave) emittance of the glazing layer, exterior-facing side. / ^g Solar heat gain coefficient. / ^h U-value, (W/m²-K).

2. RESULTS AND DISCUSSION

2.1 Mixed-mode operation and indoor air temperature

Figure 2 compares the outdoor air temperature and indoor air temperature in the base case (SSF) and DSF buildings. Results showed that in the DSF building, indoor air temperature is in close agreement with the base case. As can be seen, indoor air temperature in the DSF building is slightly higher (a few decimal points) than in the SSF building under the NV mode. This phenomenon happened due to marginally higher temperature in the cavity than outdoor. As shown in Figure 2 for Brisbane in January, the MM strategy is used until outdoor temperature reaches the upper acceptability limit of the adaptive thermal comfort model. Then

air-conditioning systems operate until between approximately 10:00am to 2:30pm. After 2:30pm, outdoor temperature drops below the upper limit and MM is used again.

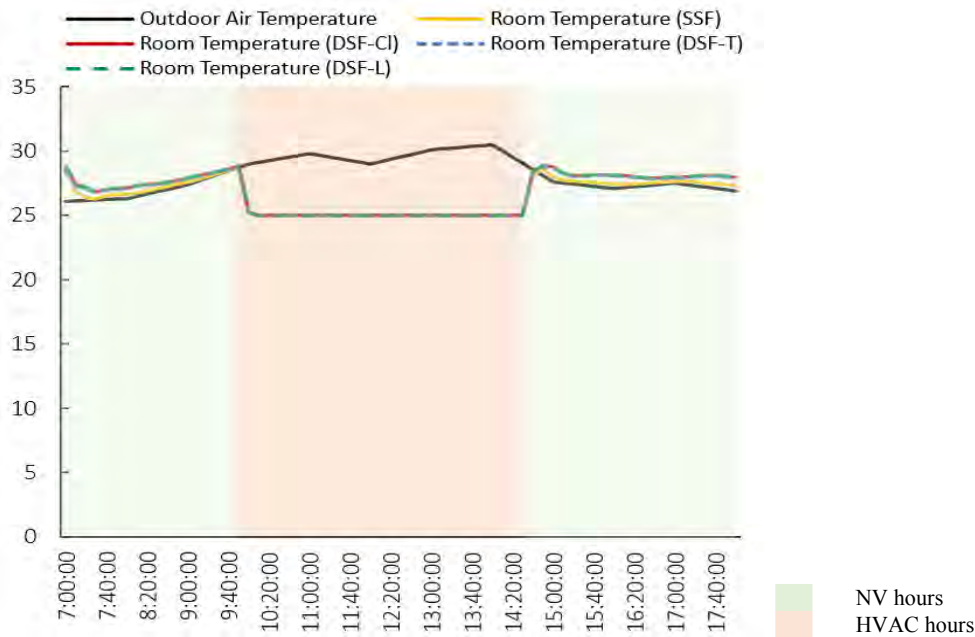
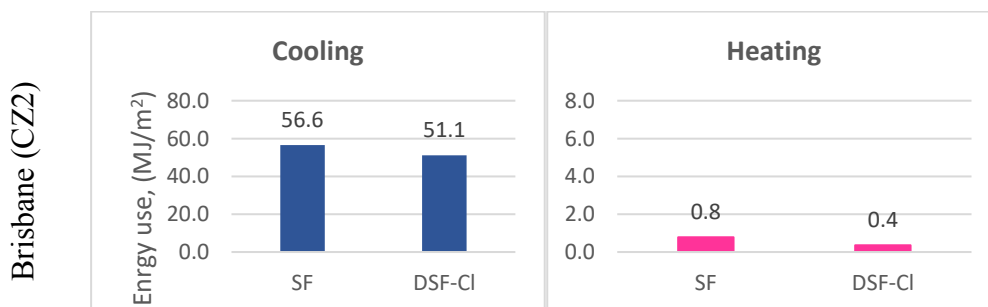


Figure 2. Outdoor air temperature on January 5th and indoor air temperature on the second floor in the base case and DSF buildings

2.2 DSF energy performance

The energy performance of the case study office building was assessed for both SSF and DSF with an external clear glass. The opening control strategy was performed for both buildings to use NV in a mixed-mode ventilation strategy. As shown in Figure 3, a cooling and heating reduction results from DSF implementation in Brisbane and Melbourne. In Brisbane (CZ2), the total site energy use (heating and cooling) was reduced by 10.2 per cent when clear glass was used for DSF’s external skin. This value was about 9.4 per cent for Melbourne (CZ5). This trend highlights the effectiveness of DSF performance for energy saving in two different climates. In Brisbane, almost all of the savings results from cooling reduction by 5.44MJ/m², while in Melbourne, a heating reduction is also a considerable number (2.5MJ/m²) and almost equal to cooling reduction.



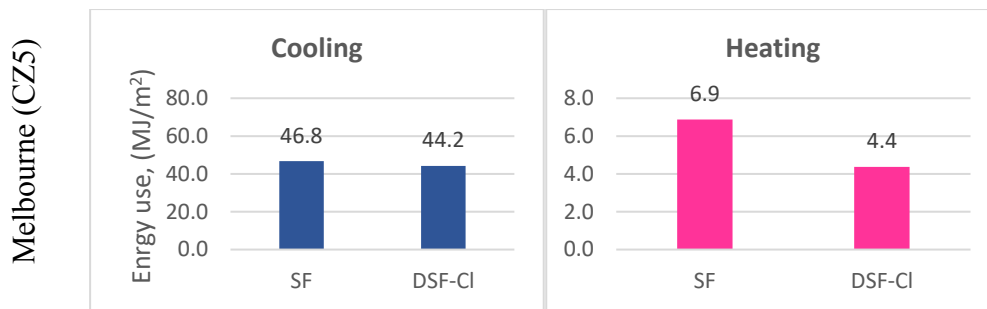


Figure 3 Cooling and heating energy use for SSF and DSF-C in two cities

2.3 Effect of glass selection

In this section, the effect of the external glass properties is discussed. In this regard, DSF with clear glass was considered a base case, and the energy-saving potential of DSF with tinted and low-e glasses was calculated and compared to the base case. Figure 4 shows the cooling, heating and total energy savings resulting from replacing clear with low-e and tinted glasses.

In both cities, the trend of glass material effect on building energy use is the same. However, the magnitude of the impact is different. In Brisbane, using tinted glass for an external layer of the DSF can result in an 8 per cent cooling energy reduction. However, the low SHGC of tinted glass tends to have a reverse effect on the heating load. Knowing that Brisbane is a cooling dominant climate and heating load is a small portion of the building energy use, the total energy saving was not affected significantly by the heating load increase when tinted glass was applied. Therefore 7.4 per cent energy saving can be achieved by using tinted glass instead of clear glass for DSF in Brisbane.

In the temperate climate of Melbourne, the cooling load of the office building still dominates the heating load. However, the negative effect of tinted glass on heating energy use was more notable in the total energy use of the building in comparison with Brisbane. While cooling energy use reduces up to 14 per cent using tinted glass, the total value of building energy-saving tends to be about 10 per cent. Table 7 presents the energy use for all tested façade configurations in both cities. As can be seen, using tinted glass can result in a 17 per cent and 18.4 per cent energy use reduction in Brisbane and Melbourne compared to a thermally efficient SSF in a mixed-mode building.

The energy performance of a DSF building with low-e glass is almost similar to a DSF building with clear glass, even with a lower SHGC. This result can be explained by comparing the U-values of two glass types. The lower U-value of low-e glass can reduce the heat loss through the external glass, and consequently, more heat is trapped in the cavity. This trapped heat can increase the cooling load. This feature of low-e glass is useful for reducing the heating demand of the building. Since, low-e glass slightly reduces heating while increasing cooling demand, the total energy saving is very close to the case with clear glass. Overall, tinted glass with lower SHGC and higher U-value leads to more energy-saving than low-e glass and clear glass in both climates.

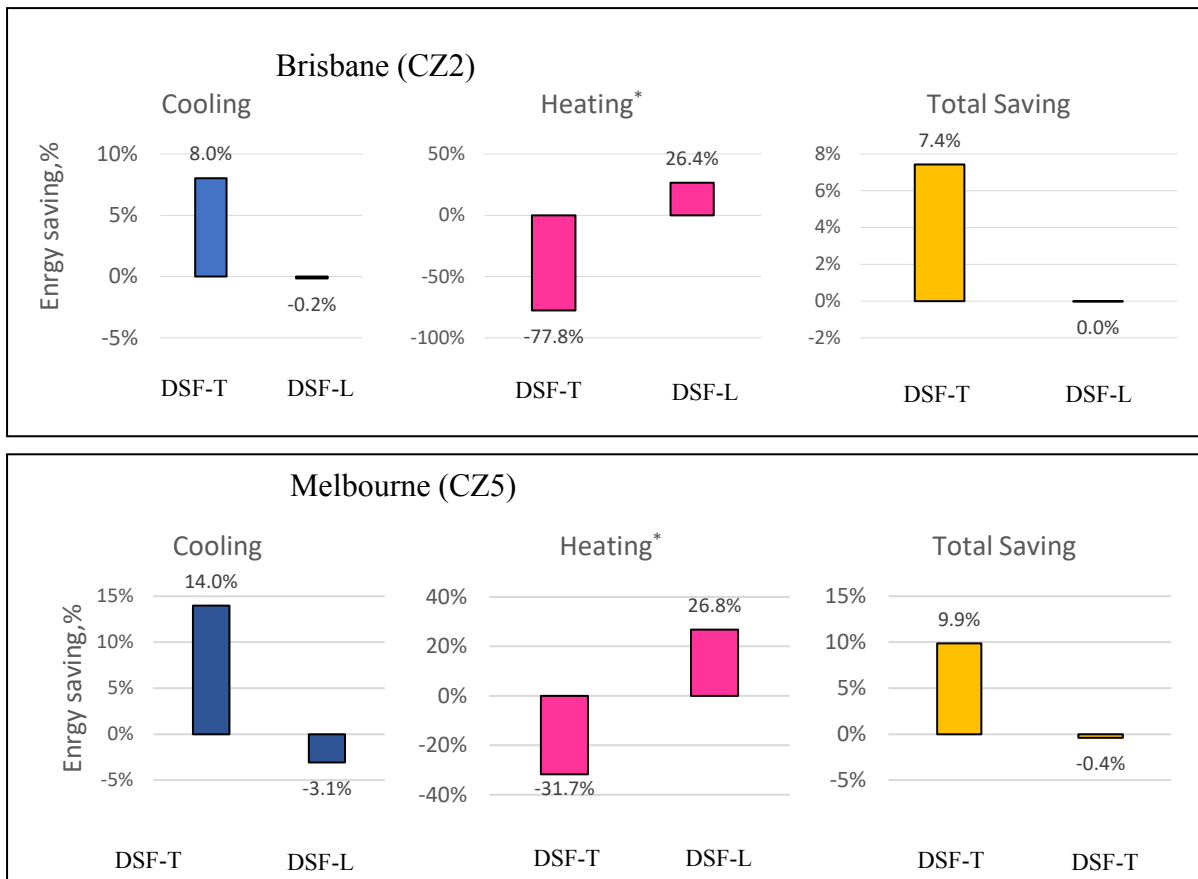


Figure 4. Cooling, heating and total energy saving of tinted and low-e glass compared to clear glass. *Note that the high percentage values are related to very small magnitudes of heating energy

2.5 Effect of temperature setpoint for cavity openings

This section evaluates the effect of the temperature setpoint of cavity openings on building energy consumption. For this purpose, the temperature threshold was changed from 15.5°C to 12°C. Tables 7 and 8 present the energy consumption of the building when the cavity openings' control strategy was set to 15.5°C and 12°C, respectively.

As can be seen, more energy savings were achieved in both cities and all studied glass types by applying a lower temperature for controlling cavity openings. This effect is more pronounced in Melbourne for cooling energy use reduction. The lower temperature setpoint leads to a better trade-off between cooling and heating energy demand for this building, particularly during winter. Therefore, more cooling energy-saving results along with a slight increase in the heating energy demand can be achieved. It can also be concluded that the optimum temperature threshold for cavity openings depends on the climate and should be determined for each city separately.

Cavity opening temperature threshold=15.5°C					
City	Building facade	Cooling (MJ/m ²)	Heating (MJ/m ²)	Heating + Cooling (MJ/m ²)	Total Saving
Brisbane	SSF	56.59	0.77	57.36	---
	DSF-C	51.14	0.36	51.50	10%
	DSF-T	47.04	0.64	47.68	17%
	DSF-L	51.23	0.26	51.49	10%
Melbourne	SSF	46.79	6.88	53.68	---
	DSF-C	44.23	4.38	48.61	9.5%
	DSF-T	38.04	5.76	43.81	18.4%
	DSF-L	45.60	3.20	48.80	9.1

Table 7. Building energy use when threshold temperature for cavity openings is set to 15.5°C.

Cavity opening temperature threshold =12°C					
City	Building facade	Cooling (MJ/m ²)	Heating (MJ/m ²)	Heating + Cooling (MJ/m ²)	Total Saving
Brisbane	SSF	56.59	0.77	57.36	---
	DSF-C	50.50	0.46	50.96	11.2%
	DSF-T	46.58	0.81	47.38	17.4%
	DSF-L	50.34	0.26	50.60	11.8%
Melbourne	SSF	46.79	6.88	53.68	---
	DSF-C	41.66	5.26	46.92	12.6%
	DSF-T	36.16	6.91	43.07	19.8%
	DSF-L	41.76	4.35	46.11	14.1%

Table 8: Building energy use when threshold temperature for cavity openings is set to 12°C.

CONCLUSION

This study investigated the energy performance of a building integrated with DSF in a mixed-mode ventilation strategy. A control strategy was developed to control the openings of DSF (cavity openings) and buildings windows. This control strategy allows the use of different airflow paths for NV of DSF and indoor space based on the outdoor temperature and adaptive thermal comfort model, respectively. The energy performance was evaluated for two cities in Australia with different climates: Brisbane and Melbourne. Three different glass types were tested for the DSF external skin, and the energy consumption was compared to SSF. The results of this research are outlined below.

- DSF is an energy-efficient solution for a mixed-mode building that can reduce the energy consumption of buildings in temperate and subtropical climates. The energy saving of DSF with clear glass as an external skin is about 9.5 per cent and 10 in Melbourne and Brisbane, respectively.
- The energy-saving potential of DSF increases by 7.4 per cent and 9.9 per cent in Brisbane and Melbourne by using tinted glass as the external skin compared to the clear glass.
- In our case study, the low-e glass is not very energy efficient for DSF external skin due to its low U-value, which can increase the cooling demand.

- The temperature setpoint for openings in the cavity should be optimised based on building characteristics and climate to improve the energy efficiency of the DSF in a mixed-mode building.
- Since the type of glazing affects indoor daylighting levels and electricity use of artificial lighting with daylighting control systems, future work should consider this factor in the energy assessment of DSF and glazing selection.

REFERENCES

- Alberto, A., Ramos, N. M. M., & Almeida, R. M. S. F. (2017). Parametric study of double-skin facades performance in mild climate countries. *Journal of Building Engineering*, *12*, 87-98. doi:10.1016/j.jobee.2017.05.013
- Ashrae, A. J. A. S. o. H., Refrigerating,, & Air-Conditioning Engineers, I. A. (2013). Standard 55-2013: Thermal environmental conditions for human occupancy.
- Bajraktari, E., Lechleitner, J., & Mahdavi, A. (2015). The Sound Insulation of Double Facades with Openings for Natural Ventilation. *Building Acoustics*, *22*(3-4), 163-176. doi:10.1260/1351-010X.22.3-4.163
- Bamdad, K., Matour, S., Izadyar, N., & Omrani, S. (2022). Impact of climate change on energy saving potentials of natural ventilation and ceiling fans in mixed-mode buildings. *Building and Environment*, *209*, 108662. doi:<https://doi.org/10.1016/j.buildenv.2021.108662>
- Barbosa, S., Ip, K., & Southall, R. (2015). Thermal comfort in naturally ventilated buildings with double skin façade under tropical climate conditions: The influence of key design parameters. *Energy & Buildings*, *109*, 397-406. doi:10.1016/j.enbuild.2015.10.029
- Barclay, M., Kang, J., Sharples, S., Wang, B., & Du, H. (2010). Estimating urban natural ventilation potential by noise mapping and building energy simulation.
- Cetiner, I., & Özkan, E. (2005). An approach for the evaluation of energy and cost efficiency of glass façades. *Energy and Buildings*, *37*(6), 673-684. doi:<https://doi.org/10.1016/j.enbuild.2004.10.007>
- Chan, A. L. S., Chow, T. T., Fong, K. F., & Lin, Z. (2009). Investigation on energy performance of double skin façade in Hong Kong. *Energy and Buildings*, *41*(11), 1135-1142. doi:<https://doi.org/10.1016/j.enbuild.2009.05.012>
- Choi, H., An, Y., Kang, K., Yoon, S., & Kim, T. (2019). Cooling energy performance and thermal characteristics of a naturally ventilated slim double-skin window. *Applied Thermal Engineering*, *160*, 114113. doi:<https://doi.org/10.1016/j.applthermaleng.2019.114113>
- Choi, W., Joe, J., Kwak, Y., & Huh, J.-H. (2012). Operation and control strategies for multi-storey double skin facades during the heating season. *Energy and Buildings*, *49*, 454-465. doi:<https://doi.org/10.1016/j.enbuild.2012.02.047>
- de la Hoz-Torres, M. L., Aguilar, A. J., Ruiz, D. P., & Martínez-Aires, M. D. (2021). Analysis of Impact of Natural Ventilation Strategies in Ventilation Rates and Indoor Environmental Acoustics Using Sensor Measurement Data in Educational Buildings. *Sensors*, *21*(18). doi:10.3390/s21186122
- EnergyPlus. (2022). EnergyPlus™ Version 22.1.0 Documentation, Engineering Reference Retrieved from https://energyplus.net/assets/nrel_custom/pdfs/pdfs_v22.1.0/EngineeringReference.pdf

- Fusaro, G., Yu, X., Kang, J., & Cui, F. (2020). Development of metacage for noise control and natural ventilation in a window system. *Applied Acoustics*, 170, 107510. doi:<https://doi.org/10.1016/j.apacoust.2020.107510>
- Gratia, E., & De Herde, A. (2007). The most efficient position of shading devices in a double-skin facade. *Energy & Buildings*, 39(3), 364-373. doi:10.1016/j.enbuild.2006.09.001
- Haase, M., & Amato, A. (2009). An investigation of the potential for natural ventilation and building orientation to achieve thermal comfort in warm and humid climates. *Solar Energy*, 83(3), 389-399. doi:10.1016/j.solener.2008.08.015
- Hamza, N. (2008). Double versus single skin facades in hot arid areas. *Energy and Buildings*, 40(3), 240-248. doi:<https://doi.org/10.1016/j.enbuild.2007.02.025>
- Hazem, A., Ameghchouche, M., & Bougriou, C. (2015). A numerical analysis of the air ventilation management and assessment of the behavior of double skin facades. *Energy and Buildings*, 102, 225-236. doi:10.1016/j.enbuild.2015.05.057
- Joe, J., Choi, W., Kwon, H., & Huh, J.-H. (2013). Load characteristics and operation strategies of building integrated with multi-story double skin facade. *Energy & Buildings*, 60, 185-198. doi:10.1016/j.enbuild.2013.01.015
- Kim, G., Schaefer, L., & Kim, J. T. (2012). Development of a Double-Skin Façade for Sustainable Renovation of Old Residential Buildings. *Indoor and Built Environment*, 22(1), 180-190. doi:10.1177/1420326X12469533
- Kuri, A. B., & Pérez R, S. J. (2022). Acoustic study and architectural proposals to improve acoustic comfort in a university campus of Mexico City. *Applied Acoustics*, 185, 108416. doi:<https://doi.org/10.1016/j.apacoust.2021.108416>
- Lam, B., Gan, W.-S., Shi, D., Nishimura, M., & Elliott, S. (2021). Ten questions concerning active noise control in the built environment. *Building and Environment*, 200, 107928. doi:<https://doi.org/10.1016/j.buildenv.2021.107928>
- Ledo Gomis, L., Fiorentini, M., & Daly, D. (2021). Potential and practical management of hybrid ventilation in buildings. *Energy and Buildings*, 231, 110597. doi:<https://doi.org/10.1016/j.enbuild.2020.110597>
- Loncour, X., Wouters, P., Flamant, G., & Blasco, M. (2004). *Impact of double ventilated facades in buildings*. Paper presented at the Building for the Future: The 16th CIB World Building Congress.
- Nicol, F., & Wilson, M. (2004). The effect of street dimensions and traffic density on the noise level and natural ventilation potential in urban canyons. *Energy and Buildings*, 36(5), 423-434. doi:<https://doi.org/10.1016/j.enbuild.2004.01.051>
- Oesterle, E. (2001). *Double-skin facades : integrated planning : building physics, construction, aerophysics, air-conditioning, economic viability*:
Munich : London : Preste.
- Omrani, S., Garcia-Hansen, V., Capra, B. R., & Drogemuller, R. (2017). Effect of natural ventilation mode on thermal comfort and ventilation performance: Full-scale measurement. *Energy & Buildings*, 156, 1-16. doi:doi:10.1016/j.enbuild.2017.09.061
- Papadaki, N., Papantoniou, S., & Kolokotsa, D. (2014). A parametric study of the energy performance of double-skin façades in climatic conditions of Crete, Greece. *International Journal of Low-Carbon Technologies*, 9(4), 296-304. doi:10.1093/ijlct/cts078

Pomponi, F., Piroozfar, P. A. E., Southall, R., Ashton, P., & Farr, E. R. P. (2016). Energy performance of Double-Skin Façades in temperate climates: A systematic review and meta-analysis. *Renewable and Sustainable Energy Reviews*, 54, 1525-1536. doi:<https://doi.org/10.1016/j.rser.2015.10.075>

Preet, S., Mathur, J., & Mathur, S. (2022). Influence of geometric design parameters of double skin façade on its thermal and fluid dynamics behavior: A comprehensive review. *Solar Energy*, 236, 249-279. doi:<https://doi.org/10.1016/j.solener.2022.02.055>

Tao, Y., Zhang, H., Huang, D., Fan, C., Tu, J., & Shi, L. (2021). Ventilation performance of a naturally ventilated double skin façade with low-e glazing. *Energy*, 229, 120706. doi:<https://doi.org/10.1016/j.energy.2021.120706>

Yazdaniyan, M., & H. Klems, J. (1993). Measurement of the Exterior Convective Film Coefficient for Windows in Low-Rise Buildings. *ASHRAE Transactions*, 100, Part 1.

Zomorodian, Z. S., & Tahsildoost, M. (2018). Energy and carbon analysis of double skin façades in the hot and dry climate. *Journal of Cleaner Production*, 197, 85-96. doi:10.1016/j.jclepro.2018.06.178

DISCLAIMER

The information or advice contained in these technical papers is intended for use only by professionals who have had adequate technical training in the field to which the paper relates. At the time of publication, these technical papers have undergone a formal peer-review process.

These documents have been compiled as an aid only, and the information or advice should be verified before it is put to use. The user should also establish the applicability of the information or advice in relation to any specific circumstances. While the information or advice is believed to be correct, no responsibility is taken by AIRAH or IBPSA Australasia for any statements made within.

AIRAH and IBPSA Australasia, its officers, employees and agents, disclaim responsibility for any inaccuracies contained within the documents, including those due to any negligence in the preparation and publication of the said technical papers.

COPYRIGHT

This work is copyright. Apart from any use as permitted under the Copyright Act 1986, no part may be reproduced by any process without prior written permission from either the Australian Institute of Refrigeration, Air Conditioning and Heating (AIRAH) or the International Building Performance Simulation Association (IBPSA) Australasia.

ADAPTATION TO PRESENT-DAY AND FUTURE THERMAL STRESS IN A BANGLADESH READY-MADE GARMENT FACTORY

AARON J.E. BACH^{1,2,*}, JEAN P. PALUTIKOF^{1,2,#}, FAHIM TONMOY^{1,3}, MONIR
HOSSAIN⁴, ASHIKUR RAHMAN JOARDER⁴

¹ National Climate Change Adaptation Research Facility, Griffith University, Gold Coast,
Queensland, Australia

² Cities Research Institute, Griffith University, Gold Coast, Queensland, Australia

³ BMT Commercial Australia Pty Ltd, Brisbane, Queensland, Australia

⁴ Department of Architecture, Bangladesh University of Engineering and Technology
(BUET), Dhaka, Bangladesh

* Presenter. Email: a.bach@griffith.edu.au

Corresponding author. Email: j.palutikof@griffith.edu.au

ABOUT THE AUTHOR

Aaron Bach has a MSc and PhD in human physiology from Queensland University of Technology, and is currently a research fellow at Griffith University within the National Climate Change Adaptation Research Facility (NCCARF) and Cities Research Institute (CRI). Current projects centre around the management of heat stress in vulnerable populations. Topics includes human health, performance, safety, thermal comfort, and risk mitigation for athletes, military personnel, the elderly, and physical occupations. Currently, Aaron's primary work is investigating solutions in building design to reduce present-day and future heat stress in ready-made garment factory workers in Bangladesh.

ABSTRACT

In 2016-17, the Bangladesh Ready-Made Garment (RMG) industry generated USD28.14 billion, contributing 80.7% export earnings and 12.36% GDP, and employing 4 million people. Working conditions inside RMG factories are often difficult. Heat stress is a major factor which is expected to worsen in future due to global warming. The paper reports on a project to understand the exact nature of the heat stress risk to factory workers at present and in a future warmer world, and to explore the potential to introduce sustainable cooling strategies which would reduce reliance on greenhouse-gas-intensive energy sources. The project is based on exploration of two RMG factory buildings (one cooled principally by fans and the other by ducted downward-flowing cooled air) in Dhaka. A range of tools were used including climate-controlled chambers, worker interviews, indoor environmental modelling and data collection of internal and external climate variables (e.g. temperature, humidity, wind speed). The project is described and some preliminary results are presented.

INTRODUCTION

The ready-made garment (RMG) industry in Bangladesh is a mainstay of the economy, a strong driver of economic growth and a major contributor to Gross Domestic Product (GDP) and

export earnings. The industry accounts for 84% of exports by value and 12-15% of GDP (Berg et al., 2021; Islam 2021). Prior to COVID, in 2019 it generated USD34.1 billion to the economy and employed around 4 million people (TBS 2022). It is a major employer of women (60% of the work force are estimated to be female) and, as such, it provides financial independence to young women of modest education, which is rare in low- and middle-income countries.

Clearly any threat to the productivity of the industry and the welfare of the workforce will have major implications for the nation as a whole. Working conditions in RMG factories are known to be stressful to the point of threatening workers' health (Steinisch et al., 2013) and a major contributor is excessive heat. Chowdhury et al., (2017) monitored an RMG factory in Dhaka and showed, using wet bulb globe temperature and predicted heat strain, that conditions exceeded comfortable levels from May to August and posed very high risk levels (up to 38 °C) for 25-38% of the time.

These heat-related risks are only likely to increase in the future as a result of global warming. On the basis of 14 impact indicators, Byers et al., (2018) identified Bangladesh as a climate change hotspot. It is estimated that average annual temperatures will increase by around 3.9°C by the end of the century for a high greenhouse gas (GHG) emissions scenario (RCP8.5), and by 2.1°C for a medium GHG emissions scenario (The World Bank Group 2021). These increases will inevitably lead to more frequent and more severe heatwaves (Choi et al., 2021) and the potential for increased heat stress in RMG factories. Im et al., (2017) found that 75% of the population of South Asia is projected to experience maximum wet bulb temperatures (averaged over a 6-hour window) in excess of 31°C by 2100 for a high GHG emissions scenario (RCP8.5), considered dangerous levels for most humans (Pal and Eltahir 2016), compared to 15% in the current climate and 55% under a medium GHG emissions scenario (RCP4.5).

Many RMG factories use some form of cooling to reduce thermal discomfort. Typically, multi-storied factories have exhaust fans on external walls to remove the indoor hot air and replace it with fresh outdoor air entering through inlet windows located in opposite walls. This arrangement may be augmented with ceiling fans and even pedestal fans for local cooling (Hossain et al., 2019). In a future, warmer world and without any other interventions, the requirement for cooling will only be increased. Electricity to power these cooling arrangements will come either from the grid or from a private diesel generator. Around three-quarters of electricity supplied to the grid is derived from natural gas and oil (Islam and Khan 2017). Cooling in RMG factories therefore has a substantial carbon footprint whether powered from the grid or a private generator which is only likely to increase in the future. However, there is the potential at the individual factory level to introduce passive strategies which can act to reduce reliance on carbon-intensive cooling.

In this paper we report on a project to explore how low- to moderate-cost interventions can alleviate impacts of high temperature and humidity on RMG factory workers, and how they can contribute to improved conditions under future climate change while minimising any increase in the factory carbon footprint.

1. THE PROJECT

The project is part of the Wellcome Our Planet Our Health programme. It commenced in November 2019 and will run for three years (it was originally planned to be a 30-month project but an extension of 6 months was granted due to COVID-related delays). The project participants are based at Griffith University (Queensland, Australia), the Bangladesh

University of Engineering and Technology (BUET) in Dhaka and the University of Sydney (New South Wales, Australia).

2. AIMS OF THE PROJECT

The aims of the project are to:

- (i) evaluate the present-day effects of heat stress on factory workers in the Bangladesh RMG industry;
- (ii) examine the mitigating effects of sustainable adaptation options (cross-ventilation, green roofs and white roofs) in comparison to the use of air conditioning and no intervention to reduce workers' heat stress; and
- (iii) explore how climate change is likely to impact on heat stress, and the extent to which adaptation strategies can delay the onset of dangerous conditions.

To achieve these aims, the project uses a mix of modelling and empirical approaches.

The research questions the project set out to address are:

1. What are the present-day characteristics of the internal climate of RMG factories in Bangladesh (with and without air conditioning)?
2. To what extent does the internal climate cause heat stress in factory workers, particularly those engaged in manual activities (e.g., packers and machinists)?
3. How can sustainable strategies such as cross-ventilation, green roofs and white roofs improve the internal climate and so reduce heat stress, without adding to the burden of GHG emissions?
4. What is likely to be the impact of future climate change, in particular changes in temperature and humidity, on the internal environment of RMG factories and the incidence on heat stress?
5. Can the identified sustainable cooling strategies continue to contribute to reducing heat stress under these worsening conditions and, if so, to what extent?

3. COMPONENTS OF THE PROJECT

3.1 The RMG factory

The project is focussed on two RMG factory buildings located in northwest Dhaka (Table 1).

	Factory 1 Storey (F1S)	Factory 3 Storey (F3S)		
	Floor G	Floor G	Floor 1	Floor 2
Build Year	2013	2013		
Total Levels	1	3		
Building Type	Brick, Metal	Brick, Concrete		
Total Floor Plate (m ²)	863	2461	2435	2435
Factory Floor (m ²)	445	1802	2249	1783
Office Floor (m ²)	161	77	37	452
Storage/Other (m ²)	257	582	149	200
Ceiling Height (m)	4.09-5.05	3.95	3.52	3.52
Typical Number Occupants	200	600	1000	450
Mixed-Mode Operation	Evaporative fans	Nil	Evaporative fans	Nil
Mechanical Ventilation	Exhaust fans			
Window Operation	Some operable windows			
Working Hours	0800-2000 (typical)			

Table 1: Factory characteristics

The factory undertakes garment manufacture from cutting through sewing and ironing to packing. The first building has three storeys, employing extractor and ceiling fans on all floors, constructed in 2013 from concrete and brick with steel pillars, and designated here as factory 3-storey (F3S). The second is single storey, constructed of steel and brick, designated factory 1-storey (F1S). It is more modern and uses ducted down discharge evaporative coolers to deliver much pleasanter conditions. We are therefore able to compare and contrast working conditions in the two buildings, essentially using F1S as a control. There are 2050 workers based in F3S, of whom 60% are women.

3.2 Measurement of the internal and external factory climate

We installed a number of devices across the factory site (specifications shown in Table 2, locations in Figure 1):

- a weather station 2m above on the roof of F3S (height 11 m), measuring air temperature, relative humidity, wind speed and direction, and black bulb globe temperature, powered by a solar panel, and supplied by Envirodata, Australia;
- 36 loggers measuring temperature and humidity at 1.7-2.0m heights: 3 loggers in F1S and 33 in F3S (12 on the ground floor, 10 on the first floor and 11 on the second floor); and
- Kestrel 5400 pro instruments measured air temperature, relative humidity, wind speed, and black and wet bulb globe temperature at 1.1m high and adjacent to the participants during the worker surveys (see Section 3.3).

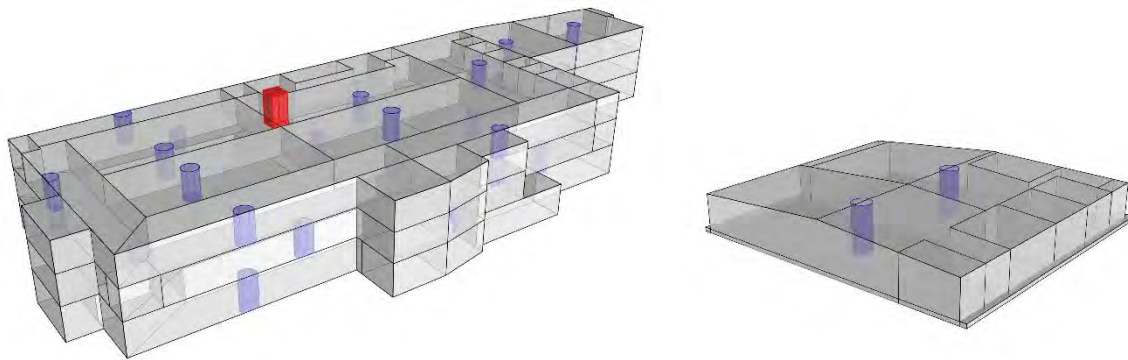


Figure 1: 3D representation of the F3S (left) and F1S (right) with zones and walls, loggers (blue) and weather station (red).

	Make/Model	Sample Rate	Resolution	Accuracy
Outdoor Weather Station (Used for Building Simulation and Thermal Comfort Surveys)				
Dry-bulb Temperature	Envirodata/TA70	<1 sec (averaged 5-60 min)	0.02 °C	± 0.1 °C
Globe Temperature	Envirodata/BG70		0.025 °C	± 0.1 °C
Relative Humidity	Envirodata/RH40		0.1 %	± 2.0 % (10-90%)
Indoor Climate Sensors (Used for Building Simulation)				
Dry-bulb Temperature	Wireless Tag/Pro	30 min	0.02 °C	± 0.4 °C
Relative Humidity		(averaged 60 min)	0.12 %	± 2.0 % (20-80%)
Indoor Climate Sensors (Used for Thermal Comfort Surveys)				
Dry-bulb Temperature	Kestrel/5400	5 sec (averaged 1 min)	0.1 °C	± 0.5 °C
Globe Temperature			0.1 °C	± 1.4 °C
Relative Humidity			0.1 %	± 2.0 % (10-90%)
Air Speed			0.1 m·s ⁻¹	3% of reading

Table 2: Environmental monitoring device specifications

Data were collected for the whole of 2021, yielding a high-quality data set providing spatially intensive monitoring of conditions inside and outside the factory with an hourly time step.

Kestrel devices were also used during the worker surveys (see Sub-heading 4.1) to measure conditions at the workstations of the workers being interviewed at the time of the survey.

3.3 Worker surveys

Three worker surveys were carried out in 2021, during three distinct seasons of the year: cool and dry in January, hot and dry in March and hot and wet/humid in September. The gap between the second and third surveys was necessitated by COVID shutdowns and the need to avoid Ramadan and the two Eid holidays. The survey was carried out three times a day (morning, midday and afternoon) over four days, the goal being to understand the extent to which unpleasantly hot working conditions affected the workers, in what ways, and what mitigation options were open to them. The physical characteristics of survey participants (e.g. weight, height, clothing and primary tasks) were also collected to enable a thermal comfort analysis. An initial survey (Table 3) was constructed based upon consensus recommendations of standards organisations (BS EN ISO 2005, 2012, 2019, ASHRAE 2017), pertinent textbooks (Nicol et al., 2012; Parsons, 2019), and similar field-based studies of thermal comfort (Damiani et al., 2016; Hossain et al., 2019; Indraganti et al., 2015).

Scale		-3	-2	-1	0	1	2	3
Thermal	Sensation	Cold	Cool	Slightly Cool	Neutral	Slightly Warm	Warm	Hot
	Comfort	Very Uncomfortable	Uncomfortable	Slightly Uncomfortable	Indifferent	Slightly Comfortable	Comfortable	Very Comfortable
	Preference	-	Colder	-	No Change	-	Hotter	-
Humidity	Sensation	Very Dry	Dry	Slightly Dry	Neutral	Slightly Humid	Humid	Very Humid
	Comfort	Very Uncomfortable	Uncomfortable	Slightly Uncomfortable	Indifferent	Slightly Comfortable	Comfortable	Very Comfortable
	Preference	-	Drier	-	No Change	-	More Humid	-
Air Speed	Sensation	Very Low	Low	Slightly Low	Neutral	Slightly High	High	Very High
	Comfort	Very Uncomfortable	Uncomfortable	Slightly Uncomfortable	Indifferent	Slightly Comfortable	Comfortable	Very Comfortable
	Preference	-	Less Air Flow	-	No Change	-	More Air Flow	-
Overall	Comfort	Very Uncomfortable	Uncomfortable	Slightly Uncomfortable	Indifferent	Slightly Comfortable	Comfortable	Very Comfortable
	Acceptability	-	-	Unacceptable	-	Acceptable	-	-

Table 3: Subjective rating scales used in the survey questionnaire

Overall, we recruited 67 individuals to the survey, 31 males and 36 females, 22 located in F1S, 45 in F3S (17 on the ground, 10 on the first and 18 on the top floor). Thirty-seven individuals participated in all three surveys (21 men and 16 women). The age range of the participants was 20-56 years, with a mean of 31 years. The mode is 25, indicating the age distribution is right-skewed. Participant jobs ranged across all factory activities, from cutting to packing, with the largest group (11) involved in sewing and ironing. The survey was carried out in Bangla, and open-ended responses were translated. Ten percent of responses from the first and last surveys are being double checked for translation accuracy.

Table 4 provides a snapshot of the mean maximum daily temperature (T_{max}) and mean minimum relative humidity (RH_{min}) of F3S for the three months in which the surveys were administered and the complete measurement period, calculated from the number of days when the factory was operating during those periods. Outdoor data are from the factory roof. Note we show minimum relative humidity because the daily maximum temperature generally occurs in mid-afternoon at a time of low humidity. Table 5 shows the number of days in our dataset in which T_{max} exceeded certain thresholds. These data show the severity of conditions, especially on the top floor.

Preliminary results from the worker surveys indicate that thermal comfort levels are closely related to season, even without partitioning the data by location, task, gender etc. In the winter (January) surveyed workers were largely comfortable with their environment, with 58% desiring no change with respect to temperature (even in this season 38% wished for a cooler environment), and 80% with respect to humidity. On the other hand, in the hot, humid season (September), 78% expressed a desire for colder working conditions, and 69% for less humid conditions.

	Ground floor	First floor	Second floor	Outdoor
January ($n=672$ hours over 28 days)				
T_{\max} ($^{\circ}\text{C}$)	26.7	27.4	30.8	24.5
RH_{\min} (%)	48.0	46.5	46.6	50.3
March ($n= 576$ hours over 24 days)				
T_{\max} ($^{\circ}\text{C}$)	32.5	32.3	36.0	33.3
RH_{\min} (%)	43.1	42.6	38.0	38.8
September ($n= 624$ hours over 26 days)				
T_{\max} ($^{\circ}\text{C}$)	32.7	32.1	34.1	32.6
RH_{\min} (%)	67.5	70.9	63.8	64.3
All of 2021 ($n=7056$ hours over 294 days)				
T_{\max} ($^{\circ}\text{C}$)	31.0	30.8	34.1	30.6
RH_{\min} (%)	57.8	57.5	53.1	55.9

Table 4: Mean maximum daily temperature (T_{\max}) and mean minimum relative humidity (RH_{\min}) for selected months and the complete measurement period, calculated from the number of days when the factory was operating. Data are for F3S, outdoor data are from the factory roof.

	Ground floor	First floor	Second floor	Outdoor
January ($n=28$)				
$>30^{\circ}\text{C}$	0	0	24	23
$>35^{\circ}\text{C}$	0	0	0	0
$>40^{\circ}\text{C}$	0	0	0	0
March ($n=24$)				
$>30^{\circ}\text{C}$	24	24	24	23
$>35^{\circ}\text{C}$	0	0	18	7
$>40^{\circ}\text{C}$	0	0	0	0
September ($n=26$)				
$>30^{\circ}\text{C}$	26	26	26	25
$>35^{\circ}\text{C}$	0	0	9	2
$>40^{\circ}\text{C}$	0	0	0	0
All of 2021 ($n=294$)				
$>30^{\circ}\text{C}$	201	196	278	190
$>35^{\circ}\text{C}$	6	0	110	29
$>40^{\circ}\text{C}$	0	0	6	0

Table 5: Number of days on which the maximum temperature in F3S exceeded certain thresholds

3.4 Modelling the factory environment with EnergyPlus

Two major aims of the project are to, first, explore the use of sustainable passive cooling strategies such as green and white roofs and, second, understand how the factory climate, especially in F3S, will evolve under global warming, and whether these cooling strategies will be effective into this warmer future. To do this, we constructed a model and perturbed it under a range of conditions. The model was created in DesignBuilder (v7.0.0.116) with the underlying simulation calculation run via EnergyPlus (9.4).

As shown by Tables 4 and 5, conditions on the top floor of F3S are substantially worse than on the other two floors. A model of the top floor of F3S was therefore constructed. Using our measurements of the internal and external factory climate for validation, we have shown that this model well simulates the observed internal climate throughout the year.

The F2S top floor model was validated against measured data from zones which factory workers occupy (Figure 2). The final agreement between the calibrated F2S, top floor model and paired measured data (i.e., not including missing data points) are presented in Table 6.

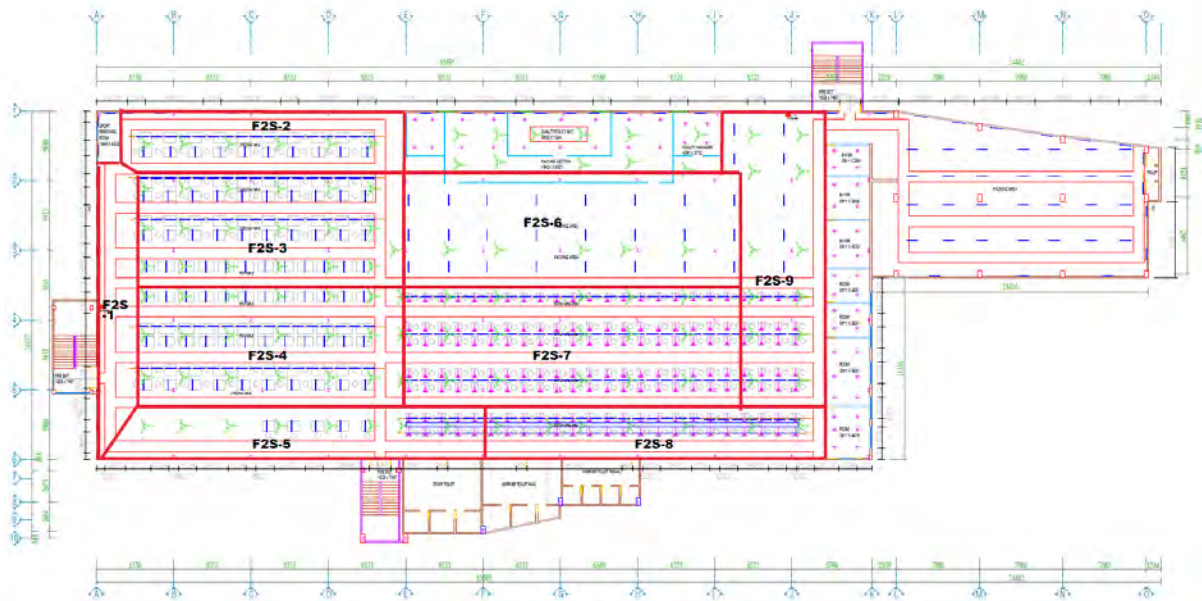


Figure 2: F2S zones with temperature loggers positioned in the middle for validation of the model.

ZONES	2021 HOUR COUNT	% DATA LOSS	NMBE	CV(RMSE)
1	6957	-21	0.71	4.38
2	7486	-15	1.43	4.76
3	7800	-11	0.73	4.65
4	7815	-11	1.33	4.72
5	6908	-21	-0.87	4.38
6	6055	-31	-0.54	4.60
7	6462	-26	0.07	4.18
8	7554	-14	1.45	4.54
9	6706	-23	-0.36	4.41
ALL	63743	-19	0.50	4.53

Table 6: Agreement between the model and measured data of the top floor of F2S. NMBE = normalised mean bias error, CV(RMSE) = coefficient of variation root mean square error. Acceptable NMBE for hourly data = $\pm 10\%$ (ASHRAE, 2014). Acceptable CV(RMSE) for hourly data = $\pm 30\%$ (ASHRAE, 2014).

3.5 Ongoing Work

3.5.1 Future factory modelling

This model is now being forced with various feasible and sustainable cooling strategies: green roof, white roof and shading. Initial simulations suggest these strategies yield additional cooling of 2-3°C indoor air temperature, commensurate with the temperature increases expected due to global warming over the lifetime of the factory (to mid-century).

At the final step, we will use climate model data for future time periods to build typical meteorological years (TMY) (Wilcox and Marion 2008) and use these to explore in detail with EnergyPlus the future internal climate of F3S and the performance of a range of passive cooling strategies.

3.5.2 Climate chamber experiments

The chamber experiments are underway to deliver information on the physiological impact of heat stress on factory workers and the effect of our selected cooling strategies, the goal being to identify the optimum strategy.

Despite delays due to COVID (see Heading 4), the experimental design for the climate chamber experiments has been finalised: tasks have been designed to mimic those of factory workers such as sewing and ironing, and forty individuals have been recruited who replicate the demographic characteristics of the factory survey participants. While wearing sensors to measure body temperatures, heart rate etc., they will undertake their designated tasks in the climate chamber under a range of conditions.

4. INTEGRATING THE PROJECT COMPONENTS

We have described the individual components of the project: measurement of the factory climate, worker surveys, EnergyPlus modelling and climate chamber experiments. Figure 3 demonstrates how these components come together to address the aims outlined in Section 2.

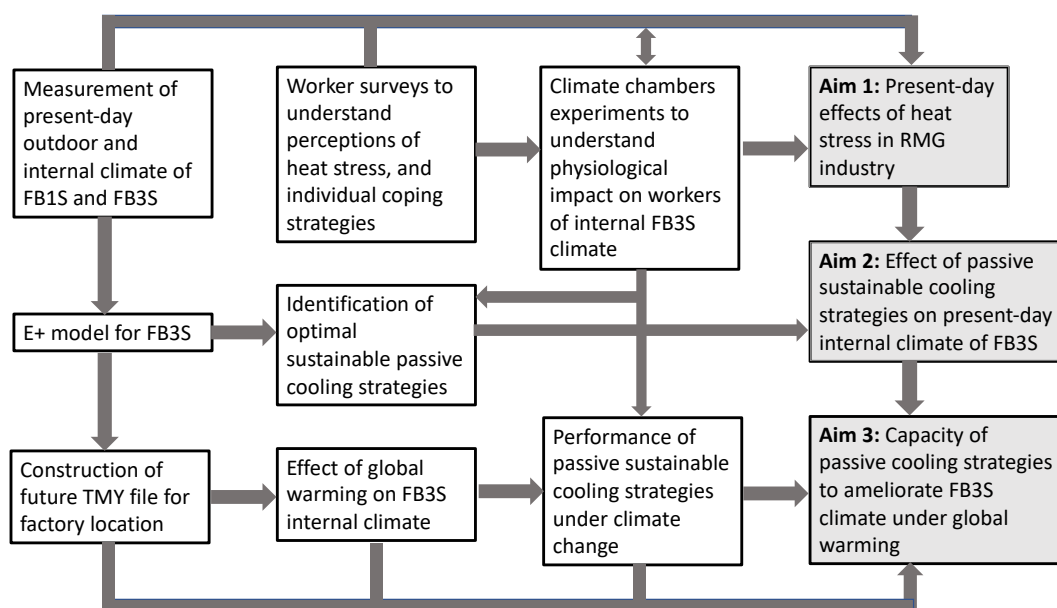


Figure 3: *Workflow and interlinkages of project components (E+ = EnergyPlus)*

5. IMPACT OF COVID ON THE PROJECT

There were both negative and positive impacts on the project from the COVID pandemic. The greatest negative impacts were at the University of Sydney, which is responsible for the climate-controlled chamber experiments. The university campus closed for the last six months of 2021 as part of the New South Wales COVID-related lockdown, so denying access to the climate chamber and substantially delaying the work.

Originally it was planned that Griffith University researchers would travel to Bangladesh to install the instrumentation and contribute to the worker surveys. This proved to be impossible, and instead we had to identify and place contracts with local experts to undertake the work together with BUET. This led to some unanticipated benefits. First, we have greatly reduced the carbon footprint of the project by not undertaking planned flights. Second, we have built relationships with local institutions which we expect to be able to capitalise on in the future through, for example, joint research projects.

6. DISCUSSION AND CONCLUSIONS

This paper outlines a comprehensive assessment of heat stress among factory workers in Bangladesh, the performance of passive low-carbon cooling strategies, and how these strategies will perform in future under global warming.

For the selected two factory buildings in Dhaka, we have demonstrated through a spatially intensive measurement program the severity of conditions, particularly in summer, with temperatures exceeding 30°C on a daily basis. As shown by worker surveys, these conditions lead to substantial thermal discomfort.

We have successfully constructed an EnergyPlus model of the upper floor of F3S where conditions are most severe and are using this to explore the performance of passive cooling strategies (i.e., green, white, shaded roofs) now and in the future under climate change. Preliminary results suggest these strategies can reduce indoor air temperatures in the hottest areas of the factory by 2-3°C, commensurate with the temperature increases expected due to global warming over the lifetime of the factory (to mid-century). This suggests that using these passive strategies could stabilise thermal condition within RMG factories under global warming, without necessarily increasing the carbon footprint of their cooling requirement.

ACKNOWLEDGEMENTS

This project was funded by Wellcome under the Our Planet Our Health programme.

REFERENCES

- ASHRAE. (2014). ANSI/ASHRAE Guideline 14-2014 - Measurement of energy, demand, and water savings. *American Society of Heating, Refrigerating and Air Conditioning Engineers*.
- ASHRAE. (2017). ANSI/ASHRAE Standard 55-2017 - Thermal environmental conditions for human occupancy. *American Society of Heating, Refrigerating and Air Conditioning Engineers*.
- Berg, A., Chhaparia, H., Hedrich, S. and Magnus, K.H. (2021). What's next for Bangladesh's garment industry, after a decade of growth? McKinsey and Company. <https://www.mckinsey.com/industries/retail/our-insights/whats-next-for-bangladeshs-garment-industry-after-a-decade-of-growth> accessed 6 February 2022.
- BS EN ISO. (2005). 7730:2005—Ergonomics of the thermal environment—Analytical determination and interpretation of thermal comfort using calculation of the PMV and PPD indices and local thermal comfort criteria. International Organization for Standardization: Geneva, Switzerland.
- BS EN ISO. (2012). 28802:2012—Ergonomics of the physical environment—Assessment of environments by means of an environmental survey involving physical measurements of the environment and subjective responses of people. International Organization for Standardization: Geneva, Switzerland.
- BS EN ISO. (2019). 10551:2019—Ergonomics of the physical environment—Subjective judgement scales for assessing physical environments. International Organization for Standardization: Geneva, Switzerland.
- ASHRAE. (2017). ANSI/ASHRAE Standard 55-2017—Thermal environmental conditions for human occupancy. *American Society of Heating, Refrigerating and Air Conditioning Engineers*, 145.
- Byers, E., Gidden, M., Leclere, D. et al.,(2018) Global exposure and vulnerability to multi-sector development and climate change hotspots. *Environmental Research Letters* 13: 055012. <https://doi.org/10.1088/1748-9326/aabf45>
- Choi, Y.W., Campbell, D.J., Aldridge, J.C. et al.,(2021) Near-term regional climate change over Bangladesh. *Climate Dynamics* 57: 3055-3073. <https://doi.org/10.1007/s00382-021-05856-z>
- Chowdhury, S., Hamada, Y. and Ahmed, K.S. (2017) Prediction and comparison of monthly indoor heat stress (WBGT and PHS) for RMG production spaces in Dhaka, Bangladesh. *Sustainable Cities and Society* 29:41-57. <https://doi.org/10.1016/j.scs.2016.11.012>.
- Damiati, S. A., Zaki, S. A., Rijal, H. B., and Wonorahardjo, S. (2016). Field study on adaptive thermal comfort in office buildings in Malaysia, Indonesia, Singapore, and Japan during hot and humid season. *Building and Environment*, 109, 208–223. <https://doi.org/10.1016/j.buildenv.2016.09.024>
- Hossain, M. M., Wilson, R., Lau, B., & Ford, B. (2019). Thermal comfort guidelines for production spaces within multi-storey garment factories located in Bangladesh. *Building and Environment*, 157, 319–345. <https://doi.org/10.1016/j.buildenv.2019.04.048>

Hossain, M.M., Wilson, R., Lau, B. and Ford, B. (2019) Thermal comfort guidelines for production spaces within multi-storey garment factories located in Bangladesh. *Building and Environment* 157:319-345. <https://doi.org/10.1016/j.buildenv.2019.04.048>

Im, E.S., Pal, J.S. and Eltahir, E.A.B. (2017) Deadly heat waves projected in the densely populated agricultural regions of South Asia. *Science Advances* 3:e1603322. <https://doi.org/10.1126/sciadv.1603322>

Indraganti, M., Ooka, R., & Rijal, H. B. (2015). Thermal comfort in offices in India: Behavioral adaptation and the effect of age and gender. *Energy and Buildings*, 103, 284–295. <https://doi.org/10.1016/j.enbuild.2015.05.042>

Islam, M.S. (2021) Ready-made garments exports earning and its contribution to economic growth in Bangladesh. *GeoJournal* 86:1301–1309. <https://doi.org/10.1007/s10708-019-10131-0>

Islam, S. and Khan, M.Z.R. (2017) A review of energy sector of Bangladesh. *Energy Procedia* 110:611–618. Available online at www.sciencedirect.com accessed 8 February 2022

Nicol, F., Humphreys, M., & Roaf, S. (2012). *Adaptive thermal comfort: Principles and practice*. Routledge.

Pal, J.S. and Eltahir E.A.B. (2016) Future temperature in southwest Asia projected to exceed a threshold for human adaptability. *Nature Climate Change* 6:197–200. <https://doi.org/10.1038/NCLIMATE2833>

Parsons, K. (2019). *Human Thermal Comfort*. CRC Press.

Steinisch, M., Yusuf, R., Li, J. et al.,(2013) Work stress: its components and its association with self-reported health outcomes in a garment factory in Bangladesh – findings from a cross-sectional study. *Health and Place* 24:123-130. <https://doi.org/10.1016/j.healthplace.2013.09.004>

TBS (2022) Why 300,000 new RMG jobs mask a grave reality about employment growth in the sector. *The Business Standard*, Dhaka. <https://www.tbsnews.net/features/panorama/why-300000-new-rmg-jobs-mask-grave-reality-about-employment-growth-sector-312124> accessed 8 February 2022

The World Bank Group (2021) *Climate Risk Country Profile: Bangladesh*. https://climateknowledgeportal.worldbank.org/sites/default/files/country-profiles/15502-WB_Bangladesh%20Country%20Profile-WEB.pdf accessed 7 February 2022

Wilcox, S. and Marion, W. (2008) *Users Manual for TMY3*. Technical Report NREL/TP-581-43156 Revised May 2008. National Renewable Energy Laboratory, Golden, CO.

DISCLAIMER

The information or advice contained in these technical papers is intended for use only by professionals who have had adequate technical training in the field to which the paper relates. At the time of publication, these technical papers have undergone a formal peer-review process.

These documents have been compiled as an aid only, and the information or advice should be verified before it is put to use. The user should also establish the applicability of the information or advice in relation to any specific circumstances. While the information or advice is believed to be correct, no responsibility is taken by AIRAH or IBPSA Australasia for any statements made within.

AIRAH and IBPSA Australasia, its officers, employees and agents, disclaim responsibility for any inaccuracies contained within the documents, including those due to any negligence in the preparation and publication of the said technical papers.

COPYRIGHT

This work is copyright. Apart from any use as permitted under the Copyright Act 1986, no part may be reproduced by any process without prior written permission from either the Australian Institute of Refrigeration, Air Conditioning and Heating (AIRAH) or the International Building Performance Simulation Association (IBPSA) Australasia.

OPTIMISATION OF A BUILDING INTEGRATED PHOTOVOLTAIC FAÇADE FOR CONCEPTUAL DESIGN SUPPORT

MISS SAMARASINGHALAGE THARUSHI IMALKA

BSc (Hons) Engineering

tharushi.11@cse.mrt.ac.lk

DR W.M. PABASARA U. WIJERATNE

PhD, BSc (Hons) FM, MRICS

pabasara.wijeratne@rmit.edu.au

ASSOCIATE PROFESSOR REBECCA YANG

PhD, MSc, BSc (Hons)

rebecca.yang@rmit.edu.au

PROFESSOR RON WAKEFIELD

PhD, MSc, BE (Hon 1)

ron.wakefield@rmit.edu.au

Solar Energy Application Lab, School of Property Construction and Project
Management RMIT University, Australia

ABSTRACT

Building integrated photovoltaic (BIPV) applications into building envelopes contribute to a sustainable building envelop design. However, designing a BIPV envelope is a very complicated process. A comprehensive approach at the conceptual design stage is needed to explore how to use different BIPV modules to increase the performance of a BIPV system. This paper investigates an optimisation approach to generate feasible BIPV design solutions to support decision making in conceptual design stage of a cladding building envelop in Australia. The study used Autodesk Revit to develop building 3D model and perform solar analysis. Non dominated sorting genetic algorithm (NSGA-II) was used to generate optimised BIPV façade solutions. The results show BIPV optimal cladding envelop designs range between 75° – 80° tilt angles with different BIPV product types. Designs can be selected based on the financial and environmental requirements of the user. The optimised results suggested the energy and economic performances of BIPV facades varies on BIPV module, tilt angle, orientation and window-wall-ratio. The outcome of this study can assist building designers to select suitable BIPV façade design in the conceptual design stage.

INTRODUCTION

As buildings are a major carbon emitter and an energy consumer, sustainable buildings have yielded increasing attention from stakeholders of the building construction industry [1]. Photovoltaic (PV) systems utilised on buildings can be classified into two main categories: Building Attached Photovoltaics (BAPV) and Building Integrated Photovoltaics (BIPV) [2]. BAPVs are attached on top of the building surfaces and have no direct impact on the building structure's functions [3]. Contrarily, BIPVs are specified as PV modules that can be integrated into the surfaces of the building (roof or facade) replacing conventional building materials [4]. As per the IEA-PVPS task 15 report [5], 'Building-integrated photovoltaic modules are considered to be building components installed as part of the building envelope, such as glazing, curtain wall and roof, which are simultaneously photovoltaic electricity generators. Hence, it can be derived that, building functionality and the energy system is influenced by BIPVs. Acting as a boundary separating indoor and outdoor environments, the building envelope controls the performance and determines the quality of a building. The building envelope consists of various components such as walls, fenestration, roof, foundation and thermal insulation.

BIPV modules integrated into building envelopes can be used in different application types such as roofs [6], facades [7] and external shading devices [8]. For BIPV envelopes to play these multi-functional roles in different applications, numerous factors should be taken into account, such as shading, irradiance, thermal conductivity, visual light transmittance, other PV module properties, orientation and installation angle [9]. The complexity of the BIPV systems is higher than that of conventional PV systems as BIPV systems consist of modules oriented in various directions and the shading effects are often more distinct [10]. Design and integrations of BIPVs often involve non-uniform irradiance conditions, partial shading effects and complex building geometries. Consequently, this may lead to high energy losses if not consider properly [10]. Conceptual stage design decisions play a crucial role in determining cost performance and life cycle environmental impact of buildings [11]. Further, undertaking an integrative approach from the conceptual stage of design and merging PV requirements, remains one of the most crucial barriers in BIPV integration and still, BIPV should be integrated into the first design concept along with the formation of the building structure, building skin and energy concept [12]. Consequently, a design approach that includes consideration of PVs only in the later stages is the first reason for the failure of a BIPV system [12].

At present, with the advancement of building performance simulation tools and technologies, it is possible to predict and assess the performance of BIPV systems at the conceptual stage. Although simulation tools integrated with optimisation algorithms has become a common practice at the planning stages of the construction industry, optimisation is not much discussed in BIPV façade design. However, the set of parameters that impact a building's performance is considerably large and, in most cases, different parameters induce opposing influences. Therefore, a large number of simulation cases are required to run to achieve an optimal BIPV design solution. This is an expensive and time-consuming process [13, 14]. Furthermore, another pivotal aspect in sustainable BIPV design is its' conflicting and multiple objectives – the simultaneous maximisation of energy and minimisation of cost for example. A possible approach to dealing with the above issues is through utilising multi-objective optimisation

Australasian Building Simulation 2022 Conference, Brisbane, July 20-21

models [1]. Besides, there are a set of limitations of the BIPV design that should be considered carefully while following an optimisation procedure. For instance, due to determinants such as aesthetics [15] and structural factors, building orientation or shape may only have a certain set of values. Moreover, the particular information of design variables fluctuates case-by-case and may be dependent on the varying requirements imposed by the building design professionals [1]. Additionally, constraints such as construction budget and life cycle cost budget may impact the generation of optimal values for sustainable building design [16]. When it comes to BIPV systems, photovoltaic (PV) modules becomes true construction elements structurally working as building exterior such as roof, façade or skylight [17]. Thus, BIPV is part of the building envelope and therefore, BIPV design should comply with building envelope design requirements as well.

Until recently, most of the related studies concentrated on the evaluation of the potential of BIPV the technology of BIPV structure, BIPV installation methods [9, 18], development of PV cell materials, PV layout optimisation [10] and BIPV system improvements [19] and not much studies focused on optimising building envelope design to integrate BIPVs and thereupon achieve optimum energy production. Moreover, using building envelope design optimisation to directly guide the design has not yet been fully realised due to the high complexity in the parameterisation of decision variables, the integration of different simulation and optimisation tools, screening the results, etc. Hence, conducting a systematic and adequate building envelope design optimisation process is becoming an emerging and crucial topic for researchers in the construction area.

Therefore, the aim of the present research is to investigate alternative designs for a BIPV façade by optimising life cycle energy (LCE) and life cycle cost (LCC) simultaneously considering multiple BIPV products and a set of building envelope features to support BIPV envelope design at the conceptual stage.

The following sections first discusses the methodology and the framework used for the optimisation of a BIPV façade for conceptual design support and then investigate the optimal results generated for a commercial building in Australia.

1. RESEARCH METHOD

This study follows the optimisation framework presented in [20] as shown in figure 1. The framework utilises tilt angle, PV placement, Window-to-Wall Ratio (WWR) and BIPV product type as design variables to optimise LCC and LCE simultaneously considering Payback less than BIPV product life span and positive NPV as constraints. Thus, generated optimised alternative designs have non-dominated LCC and LCE. Furthermore, the designs satisfy the constraints and includes optimal values of the design variables accordingly.

1.1 Data Inputs

Initially Revit software is used to determine the irradiation conditions on each surface of the building. Surface tilt angle, PV placement, BIPV product type and Window-to-Wall Ratio (WWR) were selected as the design variable set for the current optimisation process. Maximise

LCE and minimise LCC are selected as the multiple objectives. Payback period and the net present value (NPV) are selected as the constraints on optimal results set.

1.2 Process

The multi-objective optimisation process proposed in [20] which used NSGA-II as the core optimisation algorithm is selected as the main process used in this investigation.

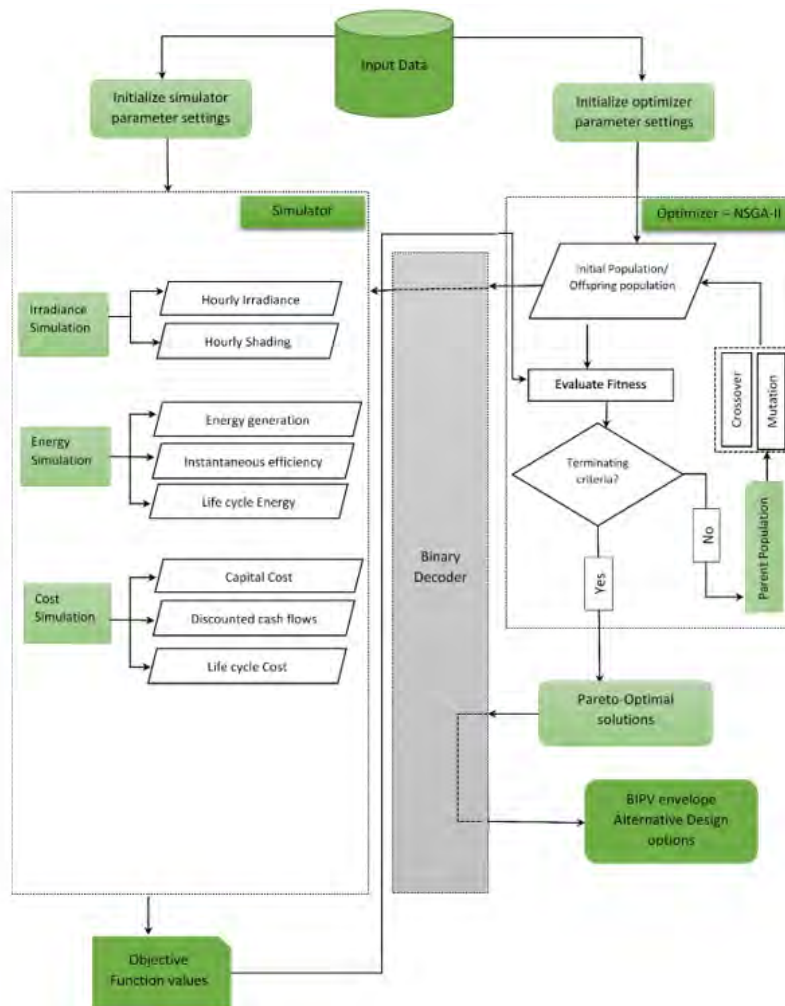


Figure 1. Adopted optimisation framework

Source: Samarasinghalage et al. pp.6 [20]

1.2 Output of the optimisation process

The output of the current optimisation process will include optimal values for the tilt angle, WWR, BIPV product type and the PV placement along with other features such as LCC, LCE, payback period and NPV value.

2. CASE STUDY DEMONSTRATION

2.1 Case study configuration setting

A car park building which is a commercial building in Bendigo, Australia was selected for the optimisation process. Figure 1 displays the sun path diagram generated for the building model using Revit. Figure 2 shows the irradiance levels for each façade in the building model. According to the figure, northeast and southeast facades shows higher irradiance levels than North west and south west facades. Therefore, only the high irradiance facades will be selected for the optimisation process.

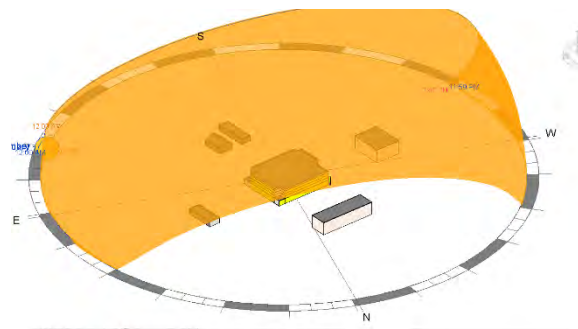


Figure 2. Sun path diagram developed using Revit

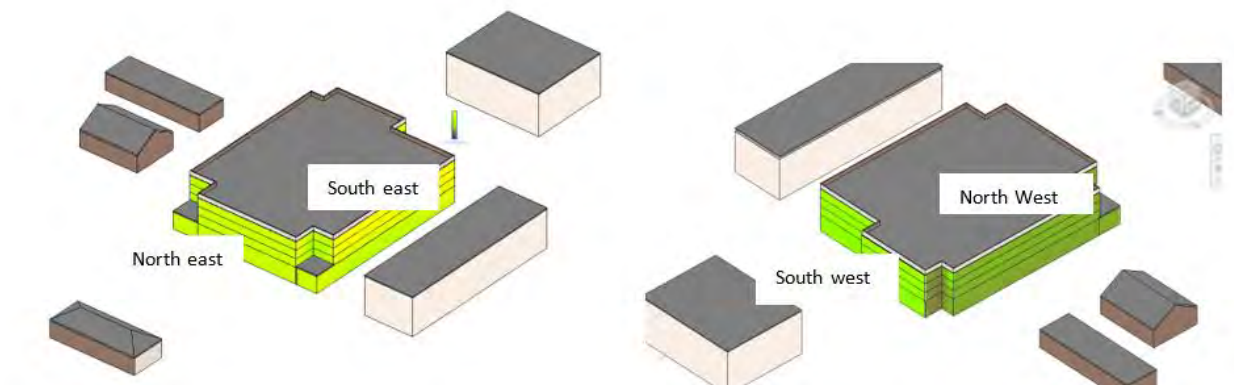


Figure 3. Irradiance simulation using Revit

Building parameter	Value
Building Longitude	144.85 degrees
Building Latitude	-37.67 degrees
South East façade original tilt	90 degrees
North East façade original tilt	90 degrees
South East façade length	51565mm
South East façade width	9800mm
North East façade length	34460mm
North East façade width	9800mm
South East façade azimuth	135 degrees
North East façade azimuth	45 degrees

Table 1. *Building model details*

Design variable	Values
BIPV products	16 products
WWR	0.3, 0.4, 0.5, 0.6
PV placement	YES/NO
Façade Tilt angle	75, 80, 85, 90 degrees
Objective function	Aim
LCC	Minimisation
LCE	Maximisation
Constraints	Values
NPV	> 0
Payback period	< PV life span

Table 2. *Parameters of the optimisation process*

Parameter	Value
Population Size	40
Number of Offspring	40
Number of Generations	100

Table 3. *NSGA-II configurations*

2.2 Results and discussion

Figure 4 displays the LCC and LCE values of the initial population and the optimised results of the optimisation process. This indicated that last population outperforms the initial population that is randomly generated. Two constraints, NPV and payback period were imposed on the generated results and therefore few pareto-optimal results that satisfy the two constraints are outputted.

Table 3 lists the parameter configuration of the NSGA-II algorithm and according to the configuration setting, 4000 BIPV designs are simulated and optimised from the framework. The time required to perform the optimisation for the selected scenario was around 3 hours with the majority of the time being spent on irradiance simulation. This is way better than the time required to do the optimisation manually. For instance, if we calculate the LCC and LCE values using a simulation software and select the optimal design manually, 16,384 cases (BIPV products * northeast tilt * southeast tilt * northeast PV placement * southeast PV placement * northeast WWR* southeast WWR) needs to be compared, which is time consuming. Table 4 illustrates the optimal design variable values (tilt angle, WWR, PV placement) of the generated alternative BIPV designs in grey background, along with other calculated properties such as capital cost, total PV area, LCC and LCE. All the optimal results avoid placing BIPV modules in southeast façade of the building and almost all the results suggest optimal tilt of 75 degrees. Payback years of the given results vary between 12-16 years, and it can be predicted that better payback periods are achievable in more irradiance scenarios. Further, the results with high WWR tend to have lower payback periods. Also, results show positive NPV and therefore, the optimisation results indicate that positive life cycle cost benefit is achievable for BIPV design scenarios.

The results show that by using NSGA-II algorithm BIPV façade design can be optimised to obtain maximum energy and minimum cost simultaneously with a variety of BIPV product types. Decision makers can utilise the optimal solutions for further decision making such as screening the solutions by setting a threshold for the design objective such as limit on LCC or a target on LCE. Moreover, final solution has different BIPV product types, and the designers could select any design based on their preferred product property such as colour, transparency or texture.

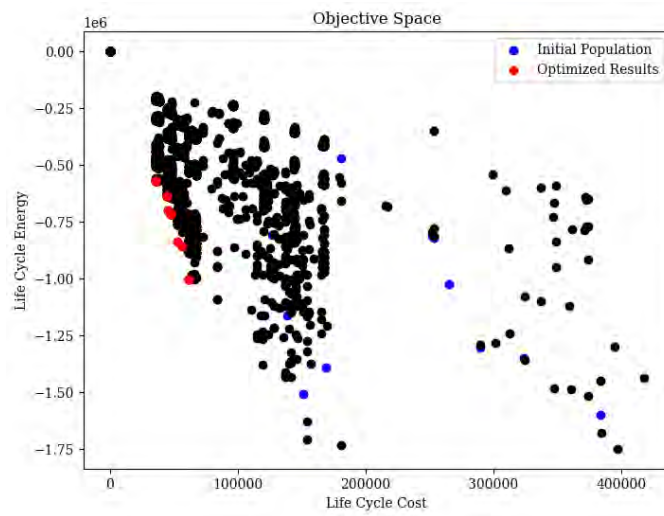


Figure 4. *Optimal results on the pareto front*

	South East façade tilt (degrees)	South East façade PV placement	South East façade WWR	South East façade No of PVs	North East façade tilt (degrees)	North East façade PV placement	North East façade WWR	North East façade No of PVs	PV Type	PV Colour	PV Life Span	LCC (AUD)	LCE (kW)	Payback Period (years)	NPV	Capital Cost (AUD)	LCOE	Total PV area (m ²)	Life cycle saving (AUD)	System Size	AUD/kW	AUD/Sqm
ALT 1	90	No	NA	0	75	1	0.3	313	501	grey	25	53107.2791	1003426	14.8818	13674.35	44170.61	0.061513	225.36	66781.63	16.276	2713.849	196.0002
ALT 2	90	No	NA	0	75	1	0.6	179	401	blue	25	30371.25668	573844	12.7018	11566.85	25260.51	0.061513	128.88	41938.11	9.308	2713.849	196.0002
ALT 3	90	No	NA	0	75	1	0.5	224	204	black/blue/custom	25	39945.44621	718107	14.4691	10766.17	32551.72	0.065771	161.28	50711.61	16.352	1990.687	201.8336
ALT 4	90	No	NA	0	80	1	0.4	268	201	black	25	45472.04484	839572	14.646	12252.49	37820.2	0.062948	192.96	57724.53	13.936	2713.849	196.0002
ALT 5	90	No	NA	0	75	1	0.3	313	505	blue	25	53107.2791	1003426	14.8818	13674.35	44170.61	0.061513	225.36	66781.63	16.276	2713.849	196.0002
ALT 6	90	No	NA	0	75	1	0.6	179	512	bronze	25	30371.25668	573844	12.7018	11566.85	25260.51	0.061513	128.88	41938.11	9.308	2713.849	196.0002
ALT 7	90	No	NA	0	75	1	0.6	179	914	silver	25	30371.25668	573844	12.7018	11566.85	25260.51	0.061513	128.88	41938.11	9.308	2713.849	196.0002
ALT 8	90	No	NA	0	75	1	0.5	224	507	orange	25	39945.44621	718107	14.4691	10766.17	32551.72	0.065771	161.28	50711.61	16.352	1990.687	201.8336
ALT 9	90	No	NA	0	75	1	0.4	268	510	gold	25	47791.86633	859163	15.3065	10965.3	38945.8	0.065771	192.96	58757.17	19.564	1990.687	201.8335
ALT 10	90	No	NA	0	75	1	0.5	224	913	silver	25	39945.44621	718107	14.4691	10766.17	32551.72	0.065771	161.28	50711.61	16.352	1990.687	201.8336

Table 4. Optimal alternative BIPV designs

CONCLUSION

Multi-objective optimisation is an impressive way to support BIPV façade design and it is rarely used in early building design. Even though there are number of optimisation models for sustainable building design, very few of those utilise those in BIPV façade design. The case study demonstration indicates that the utilised NSGA-II based optimisation framework could be a useful tool for designers at the conceptual design phase of a BIPV façade. In addition, optimisation process provides an insight to the design space as well as trade off patterns between multiple design objectives. Consequently, it provides support at the conceptual level to determine the best tilt angle, placement areas, WWR and BIPV product type to achieve maximum LCE and minimum LCE for a façade. It is noteworthy that, for the BIPV application in practise they should consider certainty of cost, safety issues and impact from neighbourhood.

ACKNOWLEDGEMENTS

This study is supported by the ‘BIPV Enabler’ research project funded by the Commercialisation of R&D Funding Initiative Pilot at the Australia Renewable Energy Agency, and the EOF scheme at RMIT University. It is also supported by the industry partners in this research project. The authors appreciate the comments and suggestions of reviewers.

REFERENCES

- [1] M. H. Wu, T. S. Ng, and M. R. Skitmore, "Sustainable building envelope design by considering energy cost and occupant satisfaction," *Energy for sustainable development*, vol. 31, pp. 118-129, 2016.
- [2] S. A. Al-Janahi, O. Ellabban, and S. G. Al-Ghamdi, "Optimal configuration for building integrated photovoltaics system to Mitigate the partial shading on complex geometric roofs," in *2019 2nd International Conference on Smart Grid and Renewable Energy (SGRE)*, 2019: IEEE, pp. 1-6.
- [3] J. Bloem, C. Lodi, J. Cipriano, and D. Chemisana, "An outdoor test reference environment for double skin applications of building integrated photovoltaic systems," *Energy and Buildings*, vol. 50, pp. 63-73, 2012.
- [4] A. Henemann, "BIPV: Built-in solar energy," *Renewable Energy Focus*, vol. 9, no. 6, pp. 14-19, 2008.
- [5] IEA-PVPS, "International definitions of “BIPV”," May, 2018 2018.
- [6] Y. Fan and X. Xia, "A multi-objective optimization model for energy-efficiency building envelope retrofitting plan with rooftop PV system installation and maintenance," *Applied energy*, vol. 189, pp. 327-335, 2017.
- [7] S.-K. Lau et al., "Optimization and evaluation of naturally ventilated BIPV facade design," *Energy Procedia*, vol. 150, pp. 87-93, 2018.

Australasian Building Simulation 2022 Conference, Brisbane, July 20-21

- [8] S.-H. Yoo and E.-T. Lee, "Efficiency characteristic of building integrated photovoltaics as a shading device," *Building and Environment*, vol. 37, no. 6, pp. 615-623, 2002.
- [9] C. Peng, Y. Huang, and Z. Wu, "Building-integrated photovoltaics (BIPV) in architectural design in China," *Energy and buildings*, vol. 43, no. 12, pp. 3592-3598, 2011.
- [10] L. Walker, J. Hofer, and A. Schlueter, "High-resolution, parametric BIPV and electrical systems modeling and design," *Applied Energy*, vol. 238, pp. 164-179, 2019.
- [11] J. P. Basbagill, F. L. Flager, and M. Lepech, "A multi-objective feedback approach for evaluating sequential conceptual building design decisions," *Automation in Construction*, vol. 45, pp. 136-150, 2014.
- [12] P. Bonomo, F. Frontini, P. De Berardinis, and I. Donsante, "BIPV: building envelope solutions in a multi-criteria approach. A method for assessing life-cycle costs in the early design phase," *Advances in building energy research*, vol. 11, no. 1, pp. 104-129, 2017.
- [13] O. T. Karaguzel, R. Zhang, and K. P. Lam, "Coupling of whole-building energy simulation and multi-dimensional numerical optimization for minimizing the life cycle costs of office buildings," in *Building simulation*, 2014, vol. 7, no. 2: Springer, pp. 111-121.
- [14] J.-T. Jin and J.-W. Jeong, "Optimization of a free-form building shape to minimize external thermal load using genetic algorithm," *Energy and Buildings*, vol. 85, pp. 473-482, 2014.
- [15] D. Hou, G. Liu, Q. Zhang, L. Wang, and R. Dang, "Integrated Building Envelope Design Process Combining Parametric Modelling and Multi-Objective Optimization," *Transactions of Tianjin University*, vol. 23, no. 2, pp. 138-146, 2017.
- [16] S. Liu, X. Meng, and C. Tam, "Building information modeling based building design optimization for sustainability," *Energy and Buildings*, vol. 105, pp. 139-153, 2015.
- [17] M. Pagliaro, R. Ciriminna, and G. Palmisano, "BIPV: merging the photovoltaic with the construction industry," *Progress in photovoltaics: Research and applications*, vol. 18, no. 1, pp. 61-72, 2010.
- [18] G. Gan, "Effect of air gap on the performance of building-integrated photovoltaics," *Energy*, vol. 34, no. 7, pp. 913-921, 2009.
- [19] T. Hwang, S. Kang, and J. T. Kim, "Optimization of the building integrated photovoltaic system in office buildings—Focus on the orientation, inclined angle and installed area," *Energy and Buildings*, vol. 46, pp. 92-104, 2012.
- [20] T. I. Samarasinghalage, W. P. U. Wijeratne, R. J. Yang, and R. Wakefield, "A multi-objective optimization framework for building-integrated PV envelope design balancing energy and cost," *Journal of Cleaner Production*, p. 130930, 2022.

DISCLAIMER

The information or advice contained in these technical papers is intended for use only by professionals who have had adequate technical training in the field to which the paper relates. At the time of publication, these technical papers have undergone a formal peer-review process.

These documents have been compiled as an aid only, and the information or advice should be verified before it is put to use. The user should also establish the applicability of the information or advice in relation to any specific circumstances. While the information or advice is believed to be correct, no responsibility is taken by AIRAH or IBPSA Australasia for any statements made within.

AIRAH and IBPSA Australasia, its officers, employees and agents, disclaim responsibility for any inaccuracies contained within the documents, including those due to any negligence in the preparation and publication of the said technical papers.

COPYRIGHT

This work is copyright. Apart from any use as permitted under the Copyright Act 1986, no part may be reproduced by any process without prior written permission from either the Australian Institute of Refrigeration, Air Conditioning and Heating (AIRAH) or the International Building Performance Simulation Association (IBPSA) Australasia.

HEAT AND POWER FLOW: MODELLING, SIMULATION, AND EXPERIMENTAL INVESTIGATIONS OF BIPV

DOMINIKA KNERA, DARIUSZ HEIM, ANNA WIEPRZKOWICZ, MICHAŁ KREMPSKI-SMEJDA

Lodz University of Technology, Department of Environmental Engineering
Wolczanska Street 213, 90-924 Lodz, Poland
dominika.knera@p.lodz.pl

ABOUT THE AUTHOR

Dominika Knera graduated in 2012 in Civil Engineering. In 2019, she received a PhD in Environmental Engineering from Lodz University of Technology. She performs research in the areas of daylighting, modelling of solar radiation, heat and mass transfer, energy systems, building performance simulation, and renewable energy integrated with buildings. She has participated in national and international research projects. She has authored or co-authored more than 30 technical and research papers.

ABSTRACT

The main aim of the study is to present the experimental performance of innovative Building Integrated Photovoltaic (BIPV) component. Subsequently, the experimental results were used to verify the computational model in EnergyPlus. The proposed BIPV is designed and constructed as a surface-stuck flexible photovoltaic, easily applicable on any concrete or cement surface of the building wall. The main challenge identified in the proposed solution is the problem of PV due to the high absorption of solar radiation as well as limited heat extraction from the system to the external environment. The electrical energy generation model provides comparable results with experiments; however, the PV temperature simulations show significant differences.

INTRODUCTION

Modern buildings commonly use renewable energy sources to balance energy consumption. Building Integrated Photovoltaic (BIPV) solutions are the most popular. PV panels can be integrated with different components of building envelope, including roof, façade, shading elements or transparent partitions (Biyik et al. 2017). Each BIPV type has individual advantages and limitations. The BIPV facades are mainly constructed as ventilated facades to remove heat from the PV panels by an air-flow through a cavity behind the PV panels. However, the application of ventilated photovoltaic facades is limited by the weight and the necessity to use a sub construction. In this paper, the new BIPV solution using flexible photovoltaics is presented as a potential solution in applications for non-flat building surfaces or when the system weight is a key requirement (Heim et al. 2020). The proposed system (En-ActivETICS) consists of the traditional low thermal conductivity insulation system ETICS (External Thermal Insulation Composite Systems), layer of high heat capacity phase change material (PCM) integrated with mortar matrix and external surface - flexible photovoltaic

panel. In comparison with traditional ventilated BIPV façade, the proposed system is characterised by a lower weight but also fewer possibilities to dissipate heat from PV panels. The main challenge identified in this case is an overheating problem of photovoltaic due to the high absorption of solar radiation and limited heat extraction from the system to the external environment (Knera, Heim, and Krempski-Smejda 2021).

Detailed prediction of the performance of BIPV facades and interaction with entire building energy system require the usage of comprehensive simulations tool. EnergyPlus is one of the most popular dynamic simulation software used for building energy modelling. EnergyPlus is used by engineers and researchers to model energy consumption for heating, cooling, ventilation, lighting, energy production from renewable energy sources, as well as indoor climate conditions (Glasgo, Khan and Azevedo 2020).

The main objective of the presented study is experimental analysis of the proposed En-ActivETICS component under real weather conditions taking into account the temperature of photovoltaic panel and the generated energy. Furthermore, the new BIPV component was introduced in the EnergyPlus simulation program. Finally, the verification of the model was performed by comparison of the experimental and computational results.

1. SMALL – SCALE EXPERIMENT

1.1 BIPV components

The first part of the paper is devoted to the presentation of the measurements of the proposed En-ActivETICS component under real weather conditions. The construction of tested components, experimental set up and results were presented and described in this section.

Small-scale experiments were conducted for the proposed En-ActivETICS component and reference component consisting of a photovoltaic panel mounted on a metal substructure that imitates a highly ventilated façade. Photos of the new developed and reference systems are presented in Figure 1. The construction of the En-ActivETICS component consists of 5 layers:

- flexible photovoltaic panel (CIGS technology) – 2mm,
- mineral adhesive mortar with PCM – 35mm,
- polystyrene thermal insulation (EPS) – 50mm,
- glue – 2mm,
- OSB board – 20mm.

The PV panel used in the experiment in both components, reference and En-ActivETICS, was a thin film CIGS flexible PV panel. The main electrical parameters of the selected panel are presented in the Table 1. The phase change material implemented in the En-ActivETICS was selected based on the comprehensive preliminary study with consideration of different paraffines and their potential to stabilize the PV panel temperature (Heim et al. 2020). The final selection includes three types of Rubitherm materials: RT25HC, RT28HC and RT35HC. Each of them was obtained by a process of granulation (macro-granules) and encapsulation. Subsequently, the encapsulated PCM granules were mixed with the mortar in equal mass proportions.

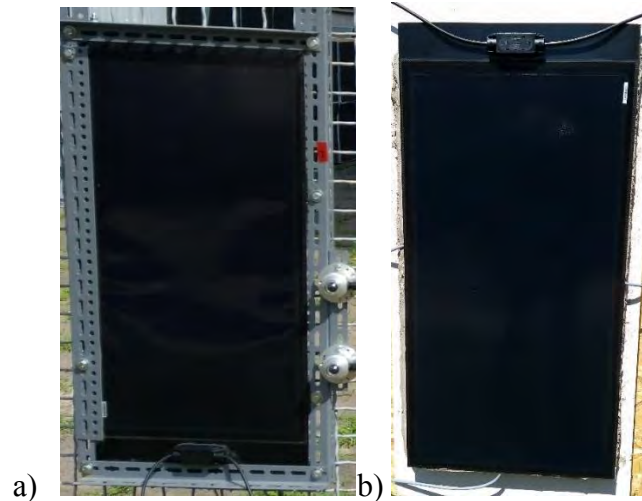


Figure 1. Photo of the experimental a) reference and b) En-ActivETICS component

Parameter		PV panel
Power at maximum power point	P_{mpp} [W]	30
Voltage at maximum power point	V_{mpp} [V]	34
Current at maximum power point	I_{mpp} [A]	0.88
Open circuit voltage	V_{oc} [V]	46
Short circuit current	I_{sc} [A]	0.97
V_{oc} temperature coefficient	γ [$1/^{\circ}C$]	-0.003
I_{sc} temperature coefficient	α [$1/^{\circ}C$]	0.0001
Dimensions	$a \times b \times h$ [mm]	$41 \times 80 \times 2$

Table 1. PV panel electrical characteristics

1.2 Experimental set up

The performance tests of the described components were carried out under real weather conditions. The components were placed in a vertical position with orientation to the south to imitate the BIPV facade. The geographical location of the experiments was Lodz, Poland ($51^{\circ}45'N$ and $19^{\circ}28'E$) classified as the Dfb (cold without dry season with warm summer) climate according to the Köppen-Geiger climate classes (Kottek et al. 2006).

The measurements performed in the framework of experiments include the monitoring of temperature behind the PV panel and electrical parameters of PV panels (voltage, current and power). Furthermore, the continuous measurement of weather data was done in meteorological station located in close distance (including air temperature, global and diffused solar irradiance at horizontal surface, wind velocity and direction, and air humidity).

The temperature behind the PV panels was measured by three PT1000 temperature sensors located in the centre part backside of each PV panel. Electrical parameters were monitored using a Nemo D4-DC network monitor for direct current with a class 1.

The electrical energy generated by photovoltaic panels was used in an off-grid system containing the charge controller, battery, and LED lamps. The MPPT charge controller was used to optimise the current parameters for battery charging and receiver – LED lamps.

The tests were carried out under real weather conditions during two sunny summer days, characterised by high solar radiation. The weather data are presented in Figure 2. The solar

irradiance for both days is comparable with the maximum value of about $850\text{W}/\text{m}^2$. However, significant differences can be observed for air temperature. The air temperature during day 1 is higher with maximum value reaching 28°C , while during day 2 it does not exceed 22°C .

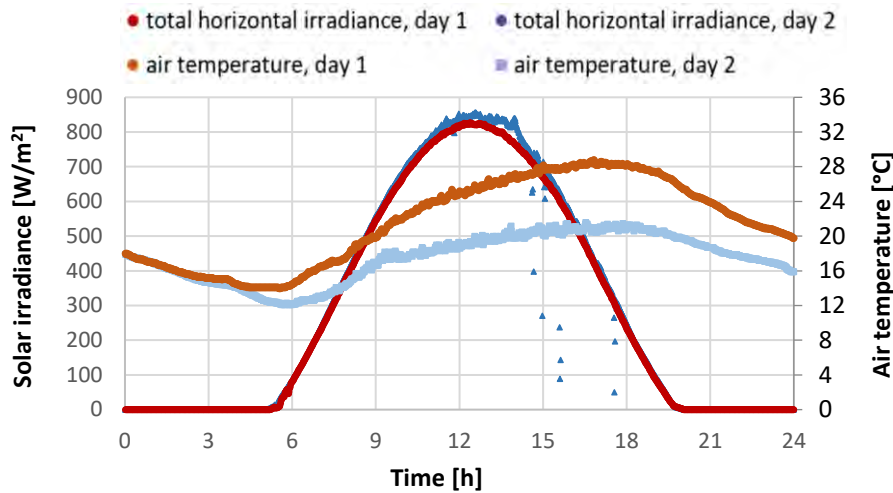
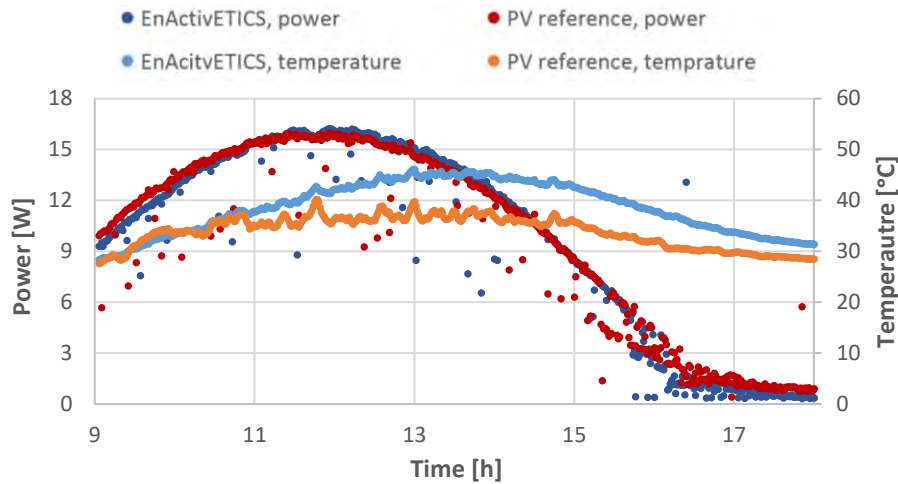


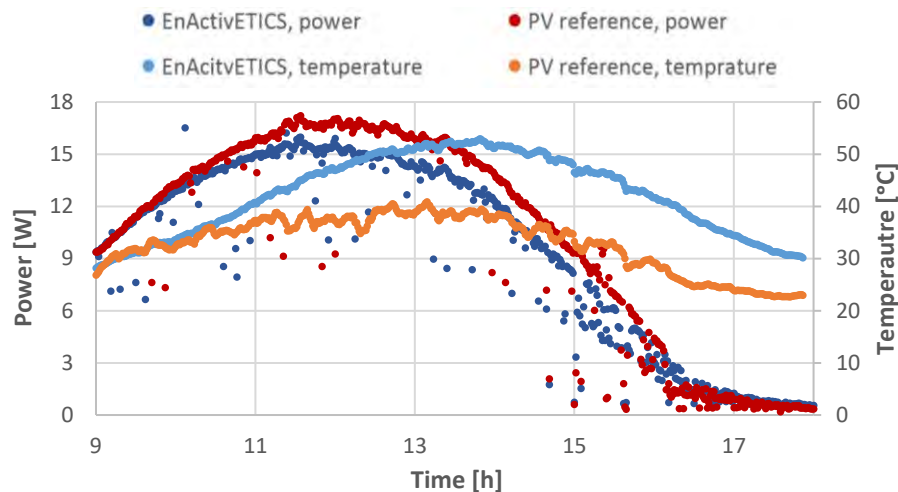
Figure 2. *The weather parameters during experimental days*

1.3 Experimental results

In Figure 3 the measured power and PV temperature for both days of experiments are presented. The differences in surface temperature between the reference and En-ActivETICS components are highest in the afternoon hours because of the limitations in heat dissipation by the En-ActivETICS component construction (the insulation layer). The temperature difference between both components was at a level of 9°C in the first day of measurements and 16°C in the second day of measurements. The highest differences in the power were also visible in second day; however, these variances are lower about 3W . The efficiency for both components is comparable at the level of 8 per cent. The exception is the decrease of efficiency for the EnActivETICS component to 7 per cent in the afternoon hours of day two as a result of high temperature of this component. Small differences in power and efficiency, despite the significant temperature difference, are caused by the electrical characteristics of thin-film photovoltaic panels. Selected PV panels have a low coefficient of power temperature coefficient, which is typical for thin-film photovoltaics.



a)



b)

Figure 3. The measured power and PV surface temperature during a) day 1, b) day 2.

2. COMPUTATIONAL MODEL VERIFICATION

2.2 BIPV model

The second part of the paper contains a description of computational model, simulations, and comparison of the measured and simulated data. The validated and popular EnergyPlus (version 9.6) whole building energy simulation program was used.

In EnergyPlus, the energy generated by photovoltaic panels can be implemented using one of the three models: Simple, Equivalent One-Diode, or Sandia (United States Department of Energy, 2021). In the presented paper, the Equivalent One-Diode, known also as the TRNSYS PV model, was used. The current-voltage characteristics of the PV module are determined based on the equations for an empirical “four-parameter” equivalent circuit model. In this model, the IV characteristics of a PV is dependent on both solar irradiance incident on the PV surface and its temperature.

The temperature of the photovoltaic panel in EnergyPlus can be determined using one of the five methods: Decoupled NOCT Conditions, Decoupled Ulleberg Dynamic, Integrated Surface

Outside Face, Integrated Transpired Collector, Integrated Exterior Vented Cavity (United States Department of Energy 2021). In the study, the integrated surface outside face model of calculating the PV cell was used. In this model, the energy exported from the PV surface as electrical energy becomes a sink in the internal source used for the heat transfer surface calculation. The PCM was modelled using the enthalpy method.

The simulation was carried out for both days of measurements. The new weather data were compiled for calculation considering the data measured by weather station during the measurements. The component constructions were defined according to the description form Section 1.1. The phase change material properties were implemented in the model using tabulated input data of temperature/enthalpy sets. The simulation time step was one minute.

2.3 Simulation results

Figures 4 and 5 present the comparison of the measured and simulation results that include the power generated by both components and the photovoltaic surface temperature.

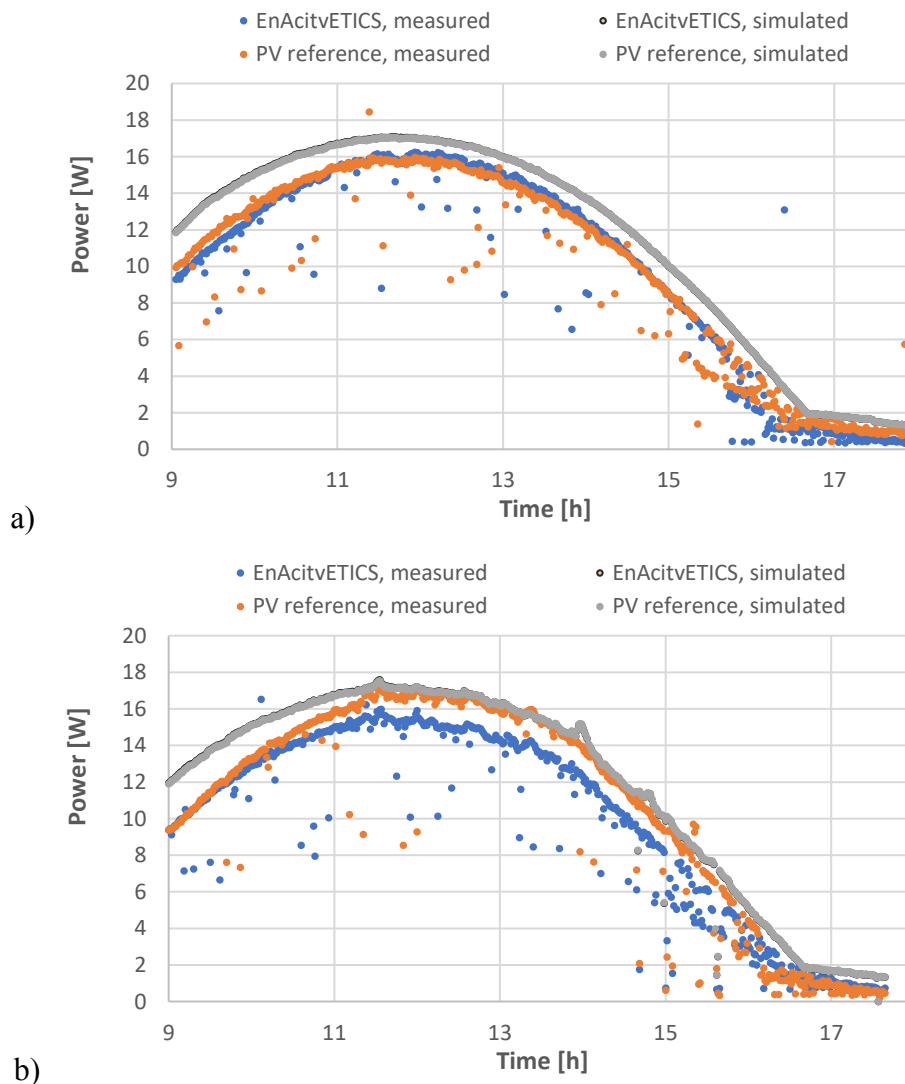


Figure 4. The measured and simulated power of PV panel during a) day 1, b) day 2.

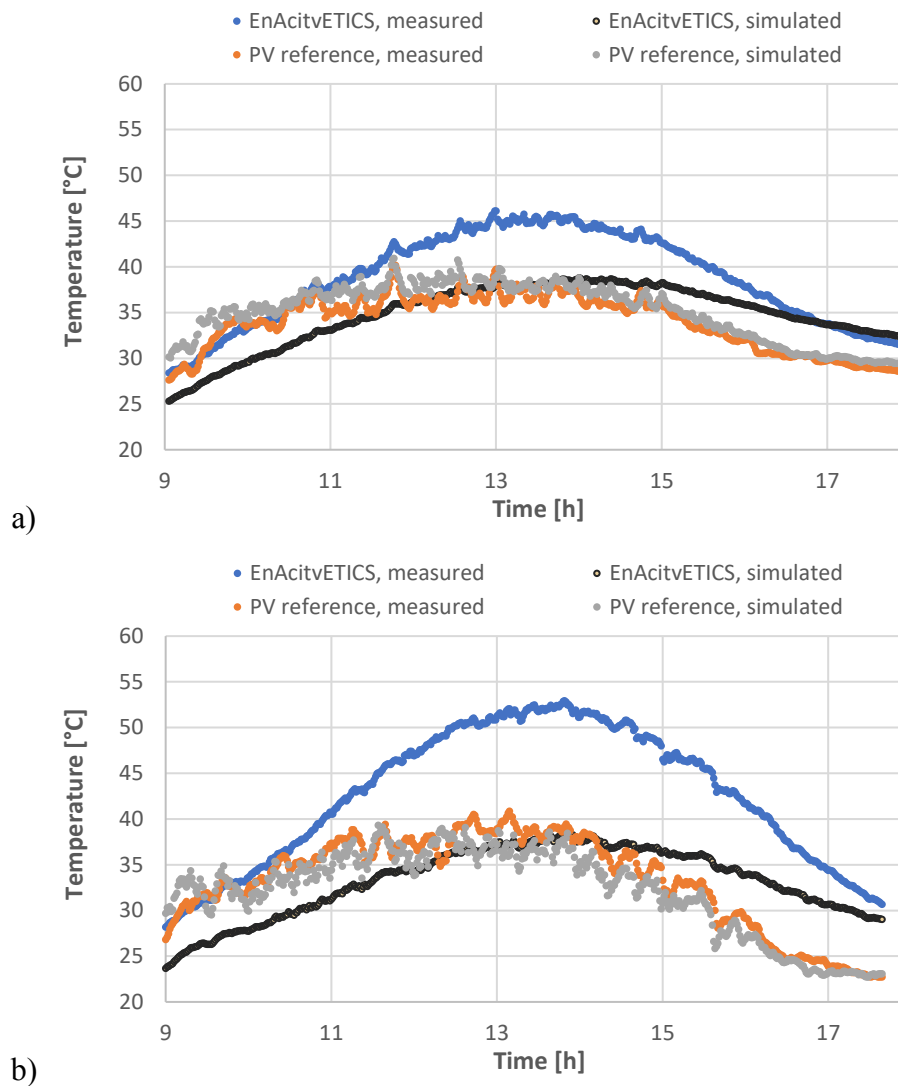


Figure 5. The measured and simulated PV surface temperature during a) day 1, b) day 2.

The obtained results for the power show better adjustment with the measured data than for the temperature results. However, the differences in power results between measured and simulated are about 10-20 per cent for most of the time, only for the afternoon hours of day two, the results for PV reference are comparable. More significant differences between simulated and measured results were observed for temperature, especially for the En-ActivETICS component. The temperatures of both PV panels from simulation are comparable, with maximum differences at the beginning and end of the analysed period. There is no visible increase of temperature in the En-ActivETICS component in the afternoon hours, as it was measured in experiment. The described differences between simulation and measurements were also determined using RMSE and MAE, presented in Table 2. The highest RMSE and MAE are used for the comparison of the PV temperature of En-ActivETICS component.

			MAE	RMSE
Power [W]	EnActivETICS	Day 1	1.67	1.99
		Day 2	2.09	2.43
	PV reference	Day 1	1.59	1.92
		Day 2	1.26	1.85
PV surface temperature [°C]	EnActivETICS	Day 1	4.06	4.62
		Day 2	8.96	9.82
	PV reference	Day 1	1.18	1.43
		Day 2	1.58	1.91

Table 2. Comparison of experimental and simulation results

DISCUSSION AND CONCLUSION

In the presented paper, experimental investigation of the performance of new En-ActivETICS BIPV component was conducted. The construction of the proposed solution had an impact on the limitations in heat dissipation from PV panels, resulting in significantly higher photovoltaic surface temperature during experiments compared to the reference ventilated PV panel. The high temperature of the PV panel influences the decrease of electricity generation and additionally influences the faster degradation or even damage of the PV panel.

The model of the En-ActivETICS component was developed in the EnergyPlus simulation program to verify the possibilities to use computational methods for prediction of BIPV performance. The comparison of the experimental and simulation results shows incompatibility in photovoltaic temperature. The observed difference indicates limitations in the EnergyPlus engine in computational of the thermal interactions between the BIPV systems and the environment with the high accuracy. Similar observations were made by (Peng and Yang 2016, Rodrigues, Carlo and Oliveira Filho 2018, Mun et al. 2020). In the presented paper the preliminary verification of the model for specific weather conditions was presented. However, the obtained results present incompatibility. In the frame of the further part of the research the whole year experimental analysis for different weather conditions (from hot to cold weather) will be conducted. The experimental data from long-term measurements will be used for final model validation.

ACKNOWLEDGEMENTS

This research was supported by the project En-ActivETICS: in a framework of M-ERA.NET by ETAG (grant No. 3-4/MOBERA1719029), NCBiR (grant No. M-ERA.NET2/2018/2/2019) and SAS (grant No. M-ERA.NET 2/2018/786/En-ActivETICS), by the Estonian Centre of Excellence ZEBE (grant TK146), by personal research funding (grant PRG483), and by Finest Twins project (grant No. 856602).

REFERENCES

- Biyik, Emrah, Mustafa Araz, Arif Hepbasli, Mehdi Shahrestani, Runming Yao, Li Shao, Emmanuel Essah, et al. 2017. "A Key Review of Building Integrated Photovoltaic (BIPV) Systems." *Engineering Science and Technology, an International Journal*. Elsevier. doi:10.1016/j.jestch.2017.01.009.
- Glasgo, Brock, Nyla Khan, and Inês Lima Azevedo. 2020. "Simulating a Residential Building Stock to Support Regional Efficiency Policy." *Applied Energy* 261 (March). Elsevier: 114223. doi:10.1016/J.APENERGY.2019.114223.
- Heim, Dariusz, Ivan Chodak, Simo Ilomets, Dominika Knera, Anna Wieprzkowicz, and Targo Kalamees. 2020. "The Integration of Selected Technology to Energy Activated ETICS - Theoretical Approach." In *E3S Web of Conferences*, edited by J. Kurnitski and T. Kalamees, 172:21004. doi:10.1051/e3sconf/202017221004.
- Knera, Dominika, Dariusz Heim, and Michał Krempski-Smejda. 2021. "Initial Validation of the One-Diode Photovoltaic Model for the Flexible Panels." In *Building Simulation 2021 Conference*. Brugge.
- Kottek, Markus, Jürgen Grieser, Christoph Beck, Bruno Rudolf, and Franz Rubel. 2006. "World Map of the Köppen-Geiger Climate Classification Updated." *Meteorologische Zeitschrift* 15 (3). Stuttgart, Germany: Schweizerbart Science Publishers: 259–263. doi:10.1127/0941-2948/2006/0130.
- Mun, Sun Hye, Jeonga Kang, Younghoon Kwak, Young Sun Jeong, Sang Moon Lee, and Jung Ho Huh. 2020. "Limitations of EnergyPlus in Analyzing Energy Performance of Semi-Transparent Photovoltaic Modules." *Case Studies in Thermal Engineering* 22 (December). Elsevier: 100765. doi:10.1016/J.CSITE.2020.100765.
- Peng, Changhai, and Jianqiang Yang. 2016. "The Effect of Photovoltaic Panels on the Rooftop Temperature in the EnergyPlus Simulation Environment." Edited by Ahmad Umar. *International Journal of Photoenergy* 2016. Hindawi Publishing Corporation: 9020567. doi:10.1155/2016/9020567.
- Rodrigues, Thiago, Joyce Carlo, and Delly Oliveira Filho. 2018. "Thermal Modeling of Semi-Transparent Photovoltaics: Impacts on the Cell Efficiency and on the Zone Performance." *PARC Pesquisa Em Arquitetura e Construção* 9: 305–318. doi:10.20396/parc.v9i4.8652785.
- United States Department of Energy. 2021. "EnergyPlus Version 9.6.0 Documentation: Engineering Reference." https://energyplus.net/assets/nrel_custom/pdfs/pdfs_v9.6.0/EngineeringReference.pdf.

DISCLAIMER

The information or advice contained in these technical papers is intended for use only by professionals who have had adequate technical training in the field to which the paper relates. At the time of publication, these technical papers have undergone a formal peer-review process.

These documents have been compiled as an aid only, and the information or advice should be verified before it is put to use. The user should also establish the applicability of the information or advice in relation to any specific circumstances. While the information or advice is believed to be correct, no responsibility is taken by AIRAH or IBPSA Australasia for any statements made within.

AIRAH and IBPSA Australasia, its officers, employees and agents, disclaim responsibility for any inaccuracies contained within the documents, including those due to any negligence in the preparation and publication of the said technical papers.

COPYRIGHT

This work is copyright. Apart from any use as permitted under the Copyright Act 1986, no part may be reproduced by any process without prior written permission from either the Australian Institute of Refrigeration, Air Conditioning and Heating (AIRAH) or the International Building Performance Simulation Association (IBPSA) Australasia.

BUILDING RETROFITS WITH EN-ACTIVETICS – DESIGN IN PRACTICE USING SIMULATION TECHNIQUES

MICHAŁ KREMPSKI-SMEJDA, DOMINIKA KNERA, DARIUSZ HEIM, ANNA WIEPRZKOWICZ

Lodz University of Technology, Department of Environmental Engineering
Wolczanska Street 213, 90-924 Lodz, Poland
michal.krempski-smejda@p.lodz.pl

ABOUT THE AUTHOR

Michał Krempski-Smejda is a chemical engineer and PhD candidate working at the Lodz University of Technology. His research areas are renewable energy sources, heat transfer, intensification, minimisation of heat transfer through partitions, measurements during phase transitions, control and data acquisition systems, and designing experimental installations. In addition, he specialises in drying techniques, in particular low-temperature, freeze, and spray drying techniques.

ABSTRACT

This paper is devoted to an analysis of innovative light wall components developed for retrofitting (En-ActivETICS). The proposed solution integrates the flexible PV panel with ETICS (External Thermal Insulation Composite System) and is thermally stabilised by PCM (Phase Change Material). The main objective of the study is to analyse the proposed system under different climatic conditions (Köppen-Geiger-Photovoltaic classification): tropical, desert, steppe, and temperate. The annual simulations of building equipped with the En-ActivETICS were done using ESP-r software considering the thermal and electrical performance. The highest annual energy was obtained for steppe climatic conditions in consequence of the very high solar irradiance on the BIPV façade simultaneously with the lowest photovoltaic surface temperature.

INTRODUCTION

The requirement of increasing the energy efficiency of buildings impacts the field of development of the building insulation systems. The External Thermal Insulation Composite System (ETICS) is the most popular in countries of temperate, cold, and polar temperature zones. In Europe, more than 50 per cent of the ETICS market is shared between Germany, Poland, Baltic Republics, Czech, Austria, Slovakia, and Switzerland (Ralf, 2015). Moreover, in Central Europe, this technology is the most common in the case of building thermo-renovation. ETICS is mainly based on i) cement products used as adhesives or plasters, ii) glass fibre mesh, iii) insulation products such as expanded polystyrene, extruded polystyrene or mineral wool, and iv) additives (Michalak, 2021). Improving the energy parameters of buildings, the environmental impact of such activities is increasingly taken into account. Towards real decarbonisation of the construction industry, self-sufficiency, and energy independence of individual countries, the building should achieve net zero or even positive

energy balance, which means that renewable energy production on-site should be increased. One of the methods to achieve this goal is the application of photovoltaics, which is clean, durable, and easily applicable by individual market entities. The growing interest in investing in photovoltaic installations is evident in many countries around the world. One of the promising solutions with high application potential is the Building of Integrated Photovoltaic (BIPV) (Kuhn *et al.*, 2021). PV panels can be integrated in a different form from roof to façade construction (Knera, Dellicompagni and Heim, 2021), mainly ventilated facades (Knera and Heim, 2016). The system proposed in this paper, En-ActivETICS, is characterised by a lightweight, flexible photovoltaic technology integrated with the ETICS system. Photovoltaic panels are implemented directly into the system by substitution of cement plaster. The general concept of the system was described by Heim *et al.* (Heim *et al.*, 2020) and finally developed in 2021 by Heim *et al.* (Heim *et al.*, 2021). The graphical representation is shown in Figure 1.

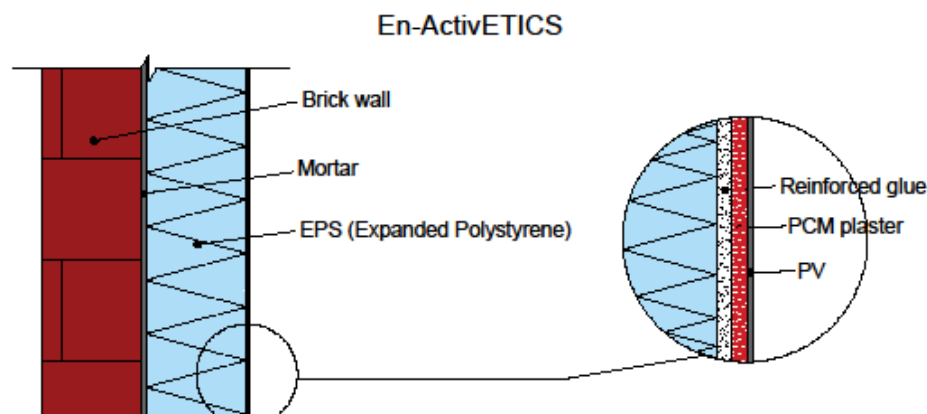


Figure 1. *The cross section through the building wall insulated by ETICS integrated with photovoltaic and refined by a thermal storage layer (En-ActivETICS).*

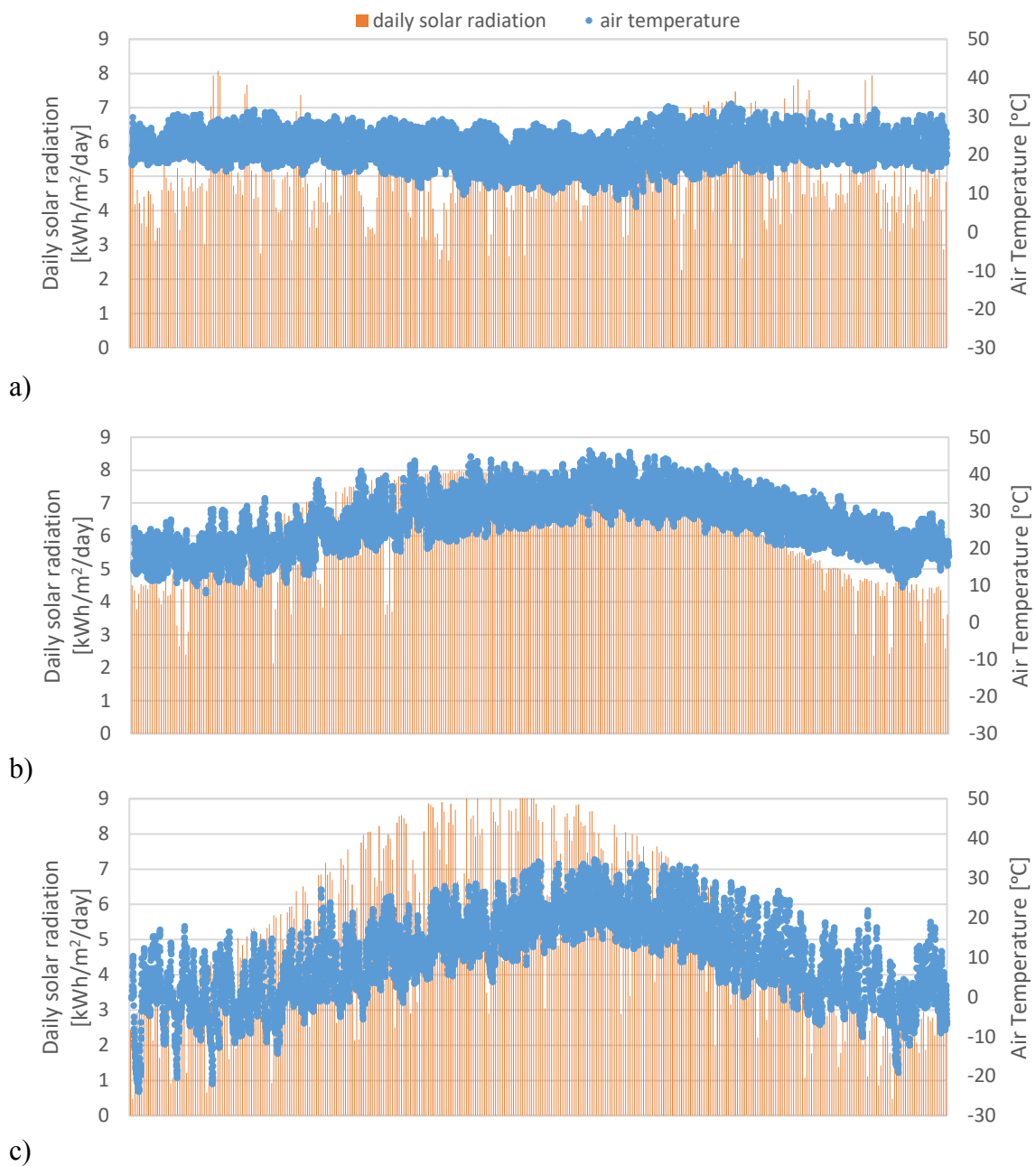
The proposed system consists of polystyrene insulation fixed to the construction wall by adhesives and alternatively mechanical joints. From the outside, polystyrene is reinforced by glass fibre mesh pasted in a cement mortar. An additional layer of render made from phase change material composites (PCM-plaster) forms the outer layer. The finish lining is made of flexible PV adhered to the PCM plaster.

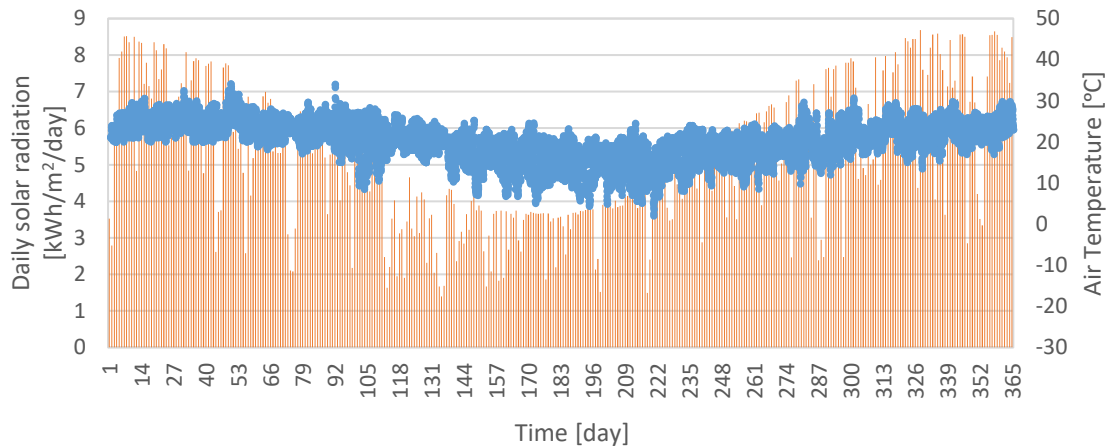
The main objective of the presented paper is to investigate the thermal and electrical performance of the photovoltaic in the proposed system under different climatic conditions. The four considered locations were assigned to different climate zones according to Köppen-Geiger-Photovoltaic classification (Ascencio-Vásquez, Brecl and Topič, 2019): Brasilia (tropical), Abu Dhabi (desert), Denver (steppe), and Brisbane (temperate) (Table 1). On the other hand, according to the Australian standards, Brisbane is considered as a ‘sub-tropical’ climate zone.

The whole year simulation analysis was performed using validated ESP-r software with consideration of coupled model of heat (Heim and Wieprzkowicz, 2016) and power flow (Clarke and Kelly, 2001).

Location	Köppen-Geiger-Photovoltaic climate classification			Geographical location	
	Symbol	Temperature-	Irradiation	Latitude	Longitude
Brasilia	AH	Tropical (A)	High (H)	15.87 S	47.93 W
Abu Dhabi	BK	Desert (B)	Very High (K)	24.43 N	54.65 E
Denver	CH	Steppe (C)	High (H)	39.76 N	104.86 W
Brisbane	DH	Temperate (D)	High (H)	27.38 S	153.10 E

Table 1. Characteristics of selected locations based on the Köppen-Geiger-Photovoltaic classification (Ascencio-Vásquez, Brecl and Topič, 2019)





d)

Figure 2. The daily solar radiation at the horizontal surface and air temperature for a) Brasilia (AH), b) Abu Dhabi (BK), c) Denver (CH) and d) Brisbane (DH)

1. CASE STUDY

1.1 Climate characteristics

The characteristics of annual climate conditions were performed in selected locations considering daily solar radiation at the horizontal surface and air temperature (Figure 2). The entire year weather data was retrieved from the EnergyPlus website (<https://energyplus.net/weather>).

Brasilia and Brisbane are characterised by uniform air temperature throughout the year with changes in the range of 5 to 33°C and average at the level of 20-21°C. The widest range of air temperature was observed for Denver, from -23 to 34°C with an average temperature at the level of 10°C. Abu Dhabi was characterised by the highest temperature from 8 to 46°C and during the year with average value 27°C.

The highest total solar radiation at the horizontal surface was observed for Abu Dhabi (2.26MWh/m²/year). For the remaining locations, this parameter was at the level of 1.9MWh/m²/year. Furthermore, the yearly distribution of solar radiation for Brasilia is quite uniform, while for the remaining cases the significant changes were visible during the year with months characterised by lower and higher solar radiation.

1.2. Simulation model

The performance of the En-ActivETICS component was determined using ESP-r simulation software, a comprehensive modelling tool for building operation analysis including the energy flow or renewable energy sources (Clarke and Kelly, 2001)(Clarke, 2001). Three models of photovoltaic energy are available in ESP-r a simple model with constant PV cell efficiency and two equivalent one-diode models: Kelly's model, and the WATSUN-PV model. In the presented study, the most advanced model considering the impact of cell temperature on the voltage and current of PV panels, WATSUN-PV, was used (Asaee *et al.*, 2017).

The phase change material in ESP-r was modelled by the changeable heat capacity (CHC) using a nonlinear thermal properties subroutine. In the proposed BIPV component, the mixture of three different paraffines was used: RT25HC, RT28HC, and RT35HC where the number

determines the temperature of the phase transition. Each of them was encapsulated in the form of granules and implemented in the mortar matrix in equal mass proportions.

The simulation analysis was performed for a whole year using the weather data for individual locations. The detached building equipped with an En-ActivETICS façade was modelled. The considered BIPV façade (12.06 x 12.40m) consists of 180 flexible monocrystalline photovoltaic panels positioned at the southern elevation (Abu Dhabi, Denver) or northern elevation (Brasilia, Brisbane). The technical parameters of the monocrystalline photovoltaic panels used in the simulation are presented in Table 2. The construction model of the En-ActivETICS component consists of 4 layers mounted on the brick wall (200mm):

- flexible photovoltaic panel (CIGS technology) – 2mm,
- mineral adhesive mortar with PCM – 35mm,
- polystyrene thermal insulation (EPS) – 200mm,
glue – 2mm.

Parameter		PV panel
Power at the maximum power point	P_{mpp} [W]	150.00
Voltage at the maximum power point	V_{mpp} [V]	21.45
Current at the maximum power point	I_{mpp} [A]	6.99
Open circuit voltage	V_{oc} [V]	25.35
Short circuit current	I_{sc} [A]	7.51
Dimensions	a x b x h [m]	1.24 x 0.67 x 0.002

Table 2. PV panel electrical characteristics

2. RESULTS

The highest annual energy and efficiency were obtained for Denver. In the remaining locations, the BIPV façade generates lower energy and performs with lower efficiency. The results for all locations are presented in Table 3. The more detailed consideration of temporal power regarding the solar irradiance incident on the photovoltaic surface is presented in Figure 3. The high correlation between electrical power and solar irradiance is visible in all cases. The lowest solar irradiance incident on the PV surface is observed for Brasilia which impacts directly on the lowest energy production. The highest temporal solar radiation was obtained for Denver (more than $900\text{W}/\text{m}^2$) resulting in the highest electrical power, about $150\text{W}/\text{m}^2$. The solar irradiance distribution for Abu Dhabi and Brisbane are comparable, with a maximum value of over $700\text{W}/\text{m}^2$ causing electrical power about $110\text{W}/\text{m}^2$. The availability of solar irradiance at the photovoltaic surface is caused by the sun position characteristics (annual sun path) for the individual location that impact the absorption possibilities of solar radiation by the vertical surface of the BIPV façade. For the lower geographical latitude (Brasilia), the sun altitude impact on the high angle of incidence of sun rays at the vertical surface.

	Brasilia	Abu Dhabi	Denver	Brisbane
Total electrical energy [kWh/m ² /year]	125.1	151.3	205.7	141.5
Annual efficiency [-]	0.14	0.14	0.15	0.14

Table 3. Annual results for En-ActivETICS façade

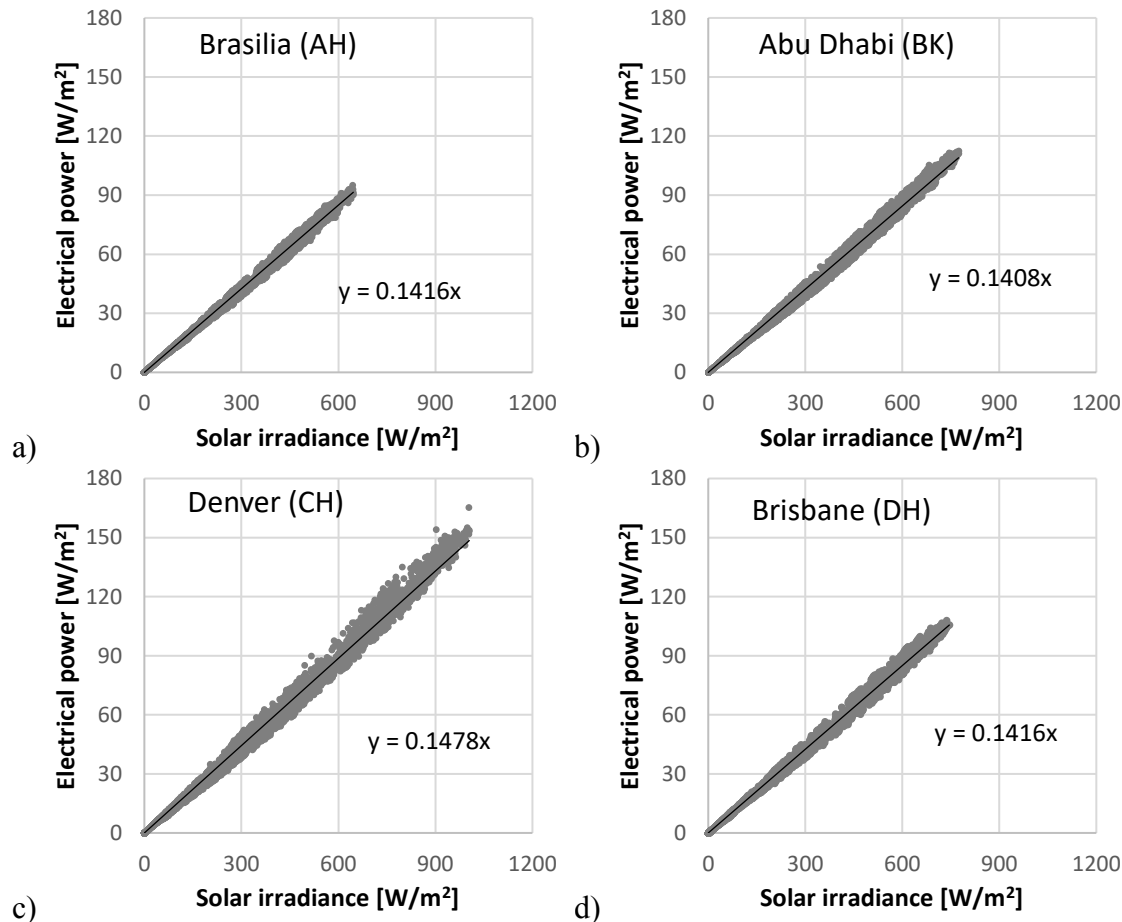


Figure 3. Power generation for a) Brasilia, b) Abu Dhabi, c) Denver, d) Brisbane

Subsequently, the efficiency of the BIPV façade is highly influenced by the photovoltaic temperature. Figure 4 presents the range of the PV surface temperature for the individual location. The temperature lower than 25°C (temperature of the standard test conditions) is considered as correct PV surface temperature when the efficiency is equal to or higher than declared by the producer. The temperature higher than 25°C impact the decrease in efficiency. Furthermore, long-term exposure on the very high temperature (>85°C) results in damage to the photovoltaic panel. The lowest temperature distribution (more than 60 per cent results lower than 25°C) was observed for the façade located in Denver, which can be caused by the air temperature characteristics for this location. The distribution of the PV surface temperature for Brisbane and Brasilia are comparable. The highest temperature was calculated for Abu Dhabi, more than 80 per cent of results are higher than 25°C. Furthermore, more than 420 hours of photovoltaic operation were performed at a temperature higher than 55°C. The long-term performance of BIPV in high temperatures can result in shorter lifetime and the need to replace.

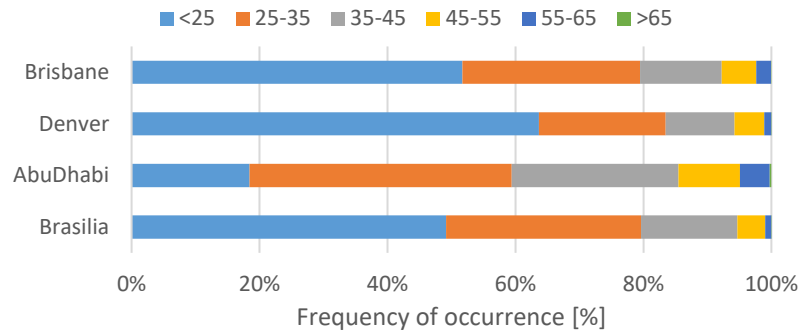


Figure 4. *The PV surface temperature distribution.*

The relations between BIPV efficiency and photovoltaic temperature for the analysed cases were presented in Figure 5. The trend of efficiency decrease with increasing temperature is visible for all cases. The highest temporal efficiency (0.17) was observed for Denver when the PV temperature was about -10°C. For the remaining cases, temperature did not decrease above 0°C and the efficiency did not exceed the level of 0.16.

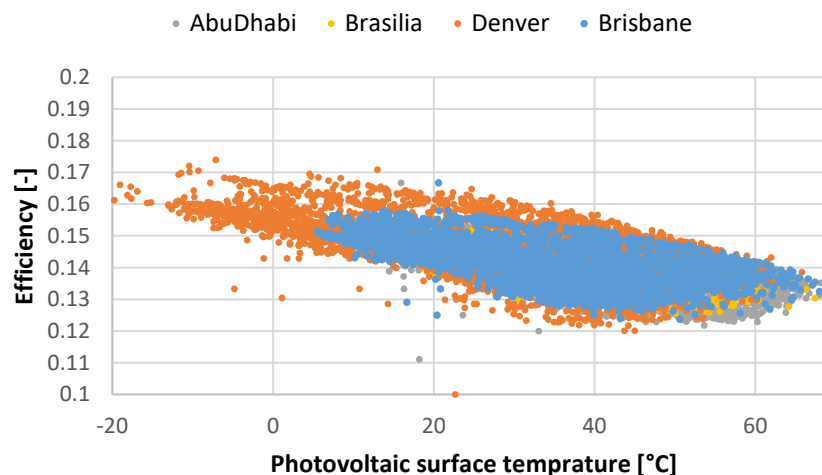


Figure 5. *The effect of temperature on photovoltaic efficiency*

CONCLUSION

The highest annual energy and efficiency was obtained for Denver as a result of the convenient position of the sun, high solar irradiance on the BIPV façade, and the lowest photovoltaic surface temperature. The opposite conditions were observed for Abu Dhabi – the highest PV temperature and the lowest efficiency. The photovoltaic façade located in Brasilia was characterised by the lowest solar irradiance, which resulted in the lowest energy production. The solar conditions of the last considered BIPV facade, located in Brisbane, were similar to a Abu Dhabi case with the maximum solar irradiance over 700W/m². However, the PV surface temperature was lower than that for BIPV in Abu Dhabi, which impacted the higher efficiency. According to simulation results of the thermal and electrical performance of the innovative BIPV façade positioned under different climatic conditions, the application of En-ActivETICS in tropical, steppe and temperate climates with high irradiance allows achieving measurable benefits because of the suitable range of temperature and solar irradiance.

ACKNOWLEDGEMENTS

This research was supported by the project En-ActivETICS: in a framework of M-ERA.NET by ETAG (grant No. 3-4/MOBERA1719029), NCBiR (grant No. M-ERA.NET2/2018/2/2019) and SAS (grant No. M-ERA.NET 2/2018/786/En-ActivETICS), by the Estonian Centre of Excellence ZEBE (grant TK146), by personal research funding (grant PRG483), and by Finest Twins project (grant No. 856602).

REFERENCES

- Asaee, S. R. *et al.* (2017) ‘Techno-economic assessment of photovoltaic (PV) and building integrated photovoltaic/thermal (BIPV/T) system retrofits in the Canadian housing stock’, *Energy and Buildings*, 152, pp. 667–679. doi: <https://doi.org/10.1016/j.enbuild.2017.06.071>.
- Ascencio-Vásquez, J., Brecl, K. and Topič, M. (2019) ‘Methodology of Köppen-Geiger-Photovoltaic climate classification and implications to worldwide mapping of PV system performance’, *Solar Energy*, 191, pp. 672–685. doi: [10.1016/J.SOLENER.2019.08.072](https://doi.org/10.1016/J.SOLENER.2019.08.072).
- Clarke, J. (2001) *Energy Simulation in Building Design*. Butterworth-Heinemann. doi: [10.1016/B978-075065082-3/50000-0](https://doi.org/10.1016/B978-075065082-3/50000-0).
- Clarke, J. A. and Kelly, N. J. (2001) ‘Integrating power flow modelling with building simulation’, *Energy and Buildings*, 33(4), pp. 333–340. doi: [https://doi.org/10.1016/S0378-7788\(00\)00115-8](https://doi.org/10.1016/S0378-7788(00)00115-8).
- Heim, D. *et al.* (2020) ‘The integration of selected technology to energy activated ETICS - Theoretical approach’, in Kurnitski, J. and Kalamees, T. (eds) *E3S Web of Conferences*, p. 21004. doi: [10.1051/e3sconf/202017221004](https://doi.org/10.1051/e3sconf/202017221004).
- Heim, D. *et al.* (2021) ‘Towards improving the durability and overall performance of PV-ETICS by application of a PCM layer’, *Applied Sciences (Switzerland)*, 11(10). doi: [10.3390/app11104667](https://doi.org/10.3390/app11104667).
- Heim, D. and Wieprzkowicz, A. (2016) ‘Positioning of an isothermal heat storage layer in a building wall exposed to the external environment’, *Journal of Building Performance Simulation*, 9(5), pp. 542–554. doi: [10.1080/19401493.2015.1126649](https://doi.org/10.1080/19401493.2015.1126649).
- Knera, D., Dellicompagni, P. R. and Heim, D. (2021) ‘Improvement of BIPV Efficiency by Application of Highly Reflective Surfaces at the Building Envelope’, *Energies*, 14(21), p. 7424. doi: [10.3390/en14217424](https://doi.org/10.3390/en14217424).
- Knera, D. and Heim, D. (2016) ‘Application of a BIPV to cover net energy use of the adjacent office room’, *Management of Environmental Quality: An International Journal*, 27(6), pp. 649–662. doi: [10.1108/MEQ-05-2015-0104](https://doi.org/10.1108/MEQ-05-2015-0104).
- Kuhn, T. E. *et al.* (2021) ‘Review of technological design options for building integrated photovoltaics (BIPV)’, *Energy and Buildings*. Elsevier, p. 110381. doi: [10.1016/j.enbuild.2020.110381](https://doi.org/10.1016/j.enbuild.2020.110381).
- Michalak, J. (2021) ‘External thermal insulation composite systems (ETICS) from industry and academia perspective’, *Sustainability (Switzerland)*, 13(24), p. 13705. doi: [10.3390/su132413705](https://doi.org/10.3390/su132413705).
- Ralf, P. (2015) ‘The European ETICS market - facts & figures’, in. EAE.

DISCLAIMER

The information or advice contained in these technical papers is intended for use only by professionals who have had adequate technical training in the field to which the paper relates. At the time of publication, these technical papers have undergone a formal peer-review process.

These documents have been compiled as an aid only, and the information or advice should be verified before it is put to use. The user should also establish the applicability of the information or advice in relation to any specific circumstances. While the information or advice is believed to be correct, no responsibility is taken by AIRAH or IBPSA Australasia for any statements made within.

AIRAH and IBPSA Australasia, its officers, employees and agents, disclaim responsibility for any inaccuracies contained within the documents, including those due to any negligence in the preparation and publication of the said technical papers.

COPYRIGHT

This work is copyright. Apart from any use as permitted under the Copyright Act 1986, no part may be reproduced by any process without prior written permission from either the Australian Institute of Refrigeration, Air Conditioning and Heating (AIRAH) or the International Building Performance Simulation Association (IBPSA) Australasia.

FEASIBILITY STUDY OF WASTEWATER ENERGY TRANSFER FOR AN EXISTING CAMPUS BUILDING CLUSTER

M. BRANDS¹, DR. A. S. FUNG, M. M. RASHID, AND C. KWIATEK

¹Sustainability Coordinator

Noventa Energy Partners

36 Distillery Lane, Suite 440, Toronto, ON M5A 3C4

mbrands@ryerson.ca

ABOUT THE AUTHOR

Monica is a Master's student whose work focuses on novel heat pumps, building energy efficiency, and wastewater energy transfer. She has studied Aerospace Engineering at Queen Mary, University of London and Mechanical Engineering at Toronto Metropolitan University in Ontario, Canada. She has co-authored three papers on heat pump technology and one on the impact of ventilation on airborne virus transmission and is currently serving as Sustainability Coordinator for Noventa Energy Partners, a renewable energy company in Toronto, Ontario.

ABSTRACT

The HVAC-related energy usage of a group of three existing buildings on a Canadian university campus (the "Cluster") was simulated. Two scenarios were compared: (1) an ambient loop paired with conventional HVAC equipment (boiler plant and cooling tower), and (2) an ambient loop using wastewater energy transfer ("WET"). The study aimed to assess the feasibility of implementing WET as a heating and cooling method for cold-climate institutional buildings, as well as to measure the effects of WET implementation on energy usage, greenhouse gas emissions, and energy costs. It was found that WET implementation provided the Cluster with **significant energy savings** (23.1 per cent reduction in energy usage) **and carbon emissions reductions** (70.2 per cent reduction in GHG emissions). Although the WET system had slightly (8.9 per cent) higher energy costs than the conventional system based on 2019 energy pricing, the gap in energy costs between the two systems narrowed significantly (to 0.3 per cent) under projected 2030 energy pricing. As Canadian carbon prices rise in the coming years, it is likely that the financial viability of WET systems relative to conventional HVAC equipment will continue to increase.

INTRODUCTION

The system investigated in this paper incorporates an **ambient loop system** and **wastewater energy transfer (“WET”)** technology.

In an ambient loop system, a heat transfer medium (often water or a water/glycol mixture) is circulated between/within buildings at ambient or near-ambient temperatures, typically in the 8-25°C or 15-25°C range [1] [2]. End users upgrade the energy from the ambient loop locally via water-to-water heat pumps to produce heating or cooling at-site.

Ambient loops can be implemented within buildings or building complexes, or on a larger scale as part of municipal energy-sharing schemes. When employed in this latter capacity, ambient loops represent an advance on older district heating systems, which have traditionally used a supply temperature of 70°C and a return temperature of 40°C [1]. Advantages of ambient loop systems as compared to traditional district heating and cooling systems (as well as traditional communal heating networks) include: the ability to provide simultaneous heating and cooling; the potential to utilise low-temperature waste heat from various sources (e.g., wastewater, industry, transportation networks, data centres); lowered transmission thermal losses; and a potential reduction in the urban heat island effect [1] [2]. Challenges associated with large-scale ambient loop networks include increased control complexity and difficulties related to seasonal load balancing [3]. Although at least forty (40) district ambient loops currently operate in European cities [4], the technology remains an emerging research area. Increased international interest in decarbonisation will likely attract more attention to the possibilities of ambient loop systems in the coming years.

For installations with on-site renewables or buildings utilising an electrical grid that is not reliant on GHG-intensive energy sources, **wastewater energy transfer (“WET”)** presents a sustainable alternative to conventional space cooling and space and water heating. In the wastewater energy transfer process, wastewater-to-water heat exchangers are paired with heat pumps to produce hot and chilled water streams for space heating and cooling. Because temperatures in urban sewers remain relatively constant year-round, sewers can be used as a heat sink in summer and as a heat source in winter [5] [6].

WET technology is not yet in common use in North America, but it has been studied experimentally and deployed in a number of buildings worldwide. Large-scale WET installations such as the Rechts der Isar Medical Centre in Munich and the Okanagan College Wastewater Heat Recovery System prove that WET can be implemented in urban and rural areas with minimal disruption to wastewater flows and infrastructure [7] [8]. Studies indicate that there is substantial unutilised energy potential in urban sewer sheds. For example, a 2009 study from Vancouver, British Columbia suggested that an area with a population of 100,000 could produce 300,000GJ of recoverable heat per year, enough to heat 3,000-5,000 single-family homes [9]. Further, it is estimated that the potential for recovery of thermal energy from wastewater is much higher than the potential for recovery of chemical energy from wastewater (roughly 90 per cent as compared to 10 per cent), despite the greater scholarly interest which chemical energy in wastewater has traditionally attracted [10]. Wastewater-source heat pumps are capable of efficiently exploiting these vast resources, having been found to achieve coefficients of performance (“COPs”) of 1.77 to 10.63 in heating mode and 2.23 to 5.35 in cooling mode [11]. Put differently, wastewater-source heat pumps generally meet the ANSI/ASHRAE minimum standards for water-source heat pumps, which mandate a COP of 4.3 in heating mode and 3.6 in cooling mode [12]

1. CAMPUS BUILDING CLUSTER

The cluster of buildings under consideration consists of the Library (“LIB”), Podium (“POD”), and Jorgenson Hall (“JOR”), three interconnected structures on the Toronto Metropolitan University (formerly Ryerson University) campus in downtown Toronto, Canada. The three buildings share a 1970s brutalist style and its associated thermal characteristics (i.e., relatively poor insulation compared to more recent buildings).

The Library, which opened in 1974, stands ten stories tall [13]. Floors five through ten contain book storage and private and semi-private study spaces. The 2nd, 3rd, and 4th floors house computer labs and additional study areas. The Toronto Metropolitan University Archives are located on the 4th floor. Laboratory and archive areas of the building require special cooling and dehumidification.

The Podium is a five-storey structure connecting the Library in the south with Jorgenson Hall in the north. It contains offices, classrooms, and study spaces. Under normal (non-pandemic) operations, the lower floors also house a cafeteria-style foodservice location, as well as banking, open areas for eating and studying, and student services.

Jorgenson Hall, originally constructed in 1971, is a fourteen-story, 190-foot tower that primarily contains faculty offices and boardrooms. Its design is somewhat unusual, with some rooms having been deliberately designed without windows [14].

2. CAMPUS ENERGY DEMAND MODEL

Energy demand for the LIB-POD-JOR Cluster was modelled in CarrierHAP (“Hourly Analysis Program”). Energy modelling was not within the scope of this project; rather, a pre-existing campus energy model produced by Fung et al. [15] was used to generate seasonal building loads. ASHRAE simulation weather data was used during load modelling.

2.1. System configuration

Heating, cooling, and ventilation in the Library-Podium-Jorgenson Hall cluster are provided by a water-to-air system which includes both variable air volume (“VAV”) and constant air volume (“CAV”) systems. The Library and Podium use VAV systems, while Jorgenson Hall uses a CAV/reheat system.

The LIB-POD-JOR cluster has a conditioned floor area of just over 37,000m² divided into a total of 284 zones. One AHU in the Library (SF-10, 2nd and 3rd floors) and two in the Podium (SF-6, ground and 1st floors; SF-7, 2nd-4th floors) include steam humidification. Simulated per-person ventilation rates range from 18.3-31.2m³/hr.

2.2. Load estimation for Library-Podium-Jorgenson Hall cluster

The LIB-POD-JOR cluster is strongly cooling-dominated due to the large size of the component buildings and the need to compensate for internal heat gains (IHGs) produced by electronic equipment (e.g., computers and lighting). HVAC-related energy demands (cooling, heating, and humidification loads, as well as fan electrical consumption) are shown in Table 1 below.

	LIB		POD		JOR	
	Demand (MWh)	Normalized Demand (kWh/m ²)	Demand (MWh)	Normalized Demand (kWh/m ²)	Demand (MWh)	Normalized Demand (kWh/m ²)
Cooling	1,708	111	1,240	92	1,037	127
Heating	192	12	334	25	405	50
Humidifier	33	2	252	19	0	0
Fans	448	29	339	25	469	57
Total	2,381	154	2,165	161	1,911	234

Table 1. Annual HVAC-related energy demand of the LIB-POD-JOR Cluster

Despite their different floor areas and patterns of space usage, the Library, the Podium, and Jorgenson Hall have a roughly similar annual HVAC energy demand, with the Library being responsible for the largest portion of the Cluster’s demand at 37 per cent (2,381 MWh/year), followed by the Podium at 33 per cent (2,165MWh/year) and Jorgenson Hall at 30 per cent (1,911MWh/year). The Library and Podium have comparable annual HVAC-related energy intensities of 154kWh/m² and 161kWh/m², respectively, while Jorgenson Hall is somewhat more energy-intensive at 234kWh/m².

3. AMBIENT LOOP MODEL

An ambient loop model for the Cluster was developed in Microsoft Excel for two scenarios: (1) ambient loop with conventional heating and heat rejection equipment (boilers and cooling tower), and (2) ambient loop incorporating wastewater energy transfer. For each scenario, system configuration, modelling methodology, and results (including estimated energy, cost, and GHG emissions) are presented.

3.1. Model development

Hourly building loads – including heating, cooling, and humidification loads – were exported from the CarrierHAP model into a comma-separated values (“CSV”) file. Peak loads, simultaneous loads, and no-load hours were determined and quantified. A boiler model and an open-loop cooling tower model were created. XSteam, a MATLAB/Excel plugin, and Psych, a psychrometric plugin, were used to determine the thermodynamic properties of steam/water and moist air, respectively, under given conditions [16] [17]. The boiler and cooling tower models were integrated into a **conventional system model**, with heat pumps being used to upgrade the available heating/cooling. A fixed ambient loop flowrate was assumed.

Next, a sewer energy profile was constructed based on monitored sewer data from various locations in the Greater Toronto Area. The aim of this sewer energy profile was to approximate the flowrate and seasonal/diurnal temperature variation of the sewers near

Toronto Metropolitan University in order to accurately estimate the available wastewater energy for WET. A **WET system model** was constructed based on the projected sewer energy profile.

Finally, energy usage, GHG emissions, and energy costs were compared for the conventional system and WET system. Emissions factors were derived from the Canadian Ministry of the Environment and Climate Change’s NIR (“National Inventory Report”), while energy costs were taken from Toronto Metropolitan (Ryerson) University’s 2021 Carbon Reduction Roadmap [18] [19].

3.2. Conventional system

The conventional system model consists of: (1) a cooling tower model, (2) a boiler model, and (3) a heat pump model, integrated with a fixed-flowrate ambient loop.

An open-circuit cooling tower was modelled as per the schematic in Figure 1 below. Temperature (T , in °C) and specific enthalpy (h , in kJ/kg·K) are given at each state point, along with the relative humidity (RH , unitless) and humidity ratio (ω , unitless) of the incoming and outgoing air. The specific enthalpy of air is denoted h_a (in kJ/kg·K), while the specific enthalpy of saturated liquid water and saturated water vapour are denoted h_f and h_g , respectively (also in kJ/kg·K). Because the flowrate of the ambient loop is constant, warm water entering the tower from the ambient loop (State 1) and cooled water returning to the ambient loop (State 2) share a single flowrate, \dot{m}_w (in kg/s). Likewise, air enters and exits the tower at the same mass flowrate, \dot{m}_a (in kg/s). The tower is assumed to run when there is a net demand for cooling. Analysis was performed using the Excel XSteam plugin to determine water/steam properties and the Excel Psych plugin to determine the properties of moist air.

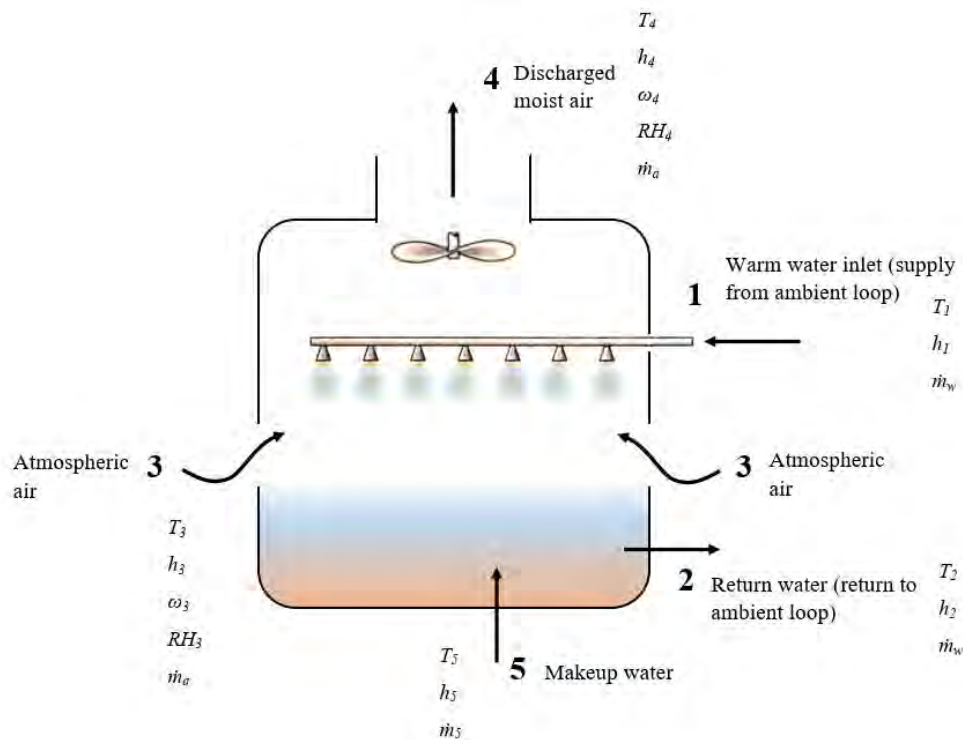


Figure 1. Cooling tower state model schematic (adapted from [20])

Ambient loop flowrate (\dot{m}_w) was set to a constant value of 100kg/s, with makeup water rate and airflow rate determined on an hourly basis as a function of ambient loop flowrate and the properties of supply (State 1) and return (State 2) water in the ambient loop. (The selected ambient loop flowrate is further justified below.)

State points were fixed as follows:

1. **State 1:** The thermodynamic properties of the supply water from the ambient loop are determined by the amount of heat rejected by the heat pumps in the LIB-POD-JOR Cluster. That is, $T_1 = \frac{\dot{Q}_{cool}}{\dot{m}_w C_{p1}} + T_2$ where \dot{Q}_{cool} is the heat rejected by all zones (in kW) and \dot{m}_w and C_{p1} are the ambient loop mass flowrate (in kg/s) and specific heat capacity of the ambient loop (in kJ/kg·K).
2. **State 2:** Water at State 2 is at the *ambient loop temperature*, which, when there is net demand for cooling, is defined as being 5°C above the outdoor wet-bulb temperature. That is $T_2 = T_{AL} = T_{3WB} + 5^\circ C$. When there is no net demand for cooling, ambient loop temperature is constant at 15°C.
3. **State 3:** State 3 is outdoor ambient air. Dry-bulb and wet-bulb temperatures provided by CarrierHAP were used to establish the state.
4. **State 4:** State 4 is moist leaving air. The following assumptions were made to determine the properties of leaving air at State 4:
 - a. Temperature at State 4 was taken as the average of outdoor ambient temperature and supply temperature from the ambient loop. That is, $T_4 = \frac{T_1 + T_{3DB}}{2}$.
 - b. Relative humidity at State 4 was assumed to be 20% higher than outdoor relative humidity, up to a maximum of 100%. That is, $RH_4 = RH_3 + 0.2$.
5. **State 5:** Makeup water, which compensates for evaporation, is also treated as being at the same temperature as the ambient loop temperature.

With these relationships in place, the mass flowrate of air through the cooling tower was found through Equation 1:

$$\dot{m}_a = \frac{\dot{m}_1 (h_{f1} - h_{f2})}{h_{a4} - h_{a3} + \omega_4 h_{g4} - \omega_3 h_{g3} - (\omega_4 - \omega_3) h_{f5}} \quad (1)$$

Note that when the system is in heating mode $h_{f1} = h_{f2}$ and therefore the mass flowrate of air is 0 and the cooling tower is off/bypassed.

Equation 2 below gives the mass flowrate of makeup water in kg/s:

$$\dot{m}_5 = \dot{m}_a (\omega_4 - \omega_3) \quad (2)$$

As with airflow through the cooling tower, the makeup water rate is 0 when cooling is not required.

Boiler efficiency was set to a constant value of 75 per cent following the work of Kwiatek [6]. The boiler and cooling tower models were integrated to create a conventional system

ambient loop model capable of meeting the complete heating, cooling, and humidification demands of the LIB-POD-JOR Cluster.

Once loads were extracted from the CarrierHAP model, heat extracted from and rejected to the ambient loop were defined as follows:

$$\dot{Q}_{cool} = \dot{Q}_{in} \left(1 + \frac{1}{COP_C} \right) \quad (3)$$

Where \dot{Q}_{cool} is heat rejected to the ambient loop (in kW), \dot{Q}_{in} is cooling load (kW), and COP_C is cooling coefficient of performance (unitless).

$$\dot{Q}_{heat} = \dot{Q}_{out} \left(1 - \frac{1}{COP_H} \right) \quad (4)$$

Where \dot{Q}_{heat} is heat extracted from the ambient loop (in kW), \dot{Q}_{out} is heating load (kW), and COP_H is heating coefficient of performance (unitless).

We then define the **net heat rejected** (NHR) as cooling minus heating for a given hour:

$$NHR = \dot{Q}_{cool} - \dot{Q}_{heat} \quad (5)$$

NHR determines how much cooling must be provided by the cooling towers or (if negative) how much heating must be supplied by the boilers. Boiler energy use and chiller fan rate and makeup water rate were set to ensure that NHR was always met.

Heat pump COP in cooling mode (COP_C) was determined based on condenser water temperature ($T_2 = T_{AL}$) from a curve in the work of Kwiatek, and ranged between 5.4 and 6 [6]. Heat pump COP in heating mode (COP_H) was set to 4.2, the high end of the normal range for water-source heat pumps in heating mode as per Natural Resources Canada [21]. Note that this is a simplification, as COP_H would not remain static in actual operation.

We define a further parameter, ΔT_{HP} , representing the temperature difference in degrees Celsius between the indoor setpoint (20°C for heating and 22°C for cooling) and the ambient loop temperature. This difference remains low throughout the year, as the ambient loop temperature is constrained between 8.8°C and 29.9°C due to: (1) a constant ambient loop temperature of 15°C being used during heating season, and (2) the limited variation of outdoor air temperature outside of heating season. In the special case in which $T_{AL} < 22^\circ\text{C}$ – that is, the ambient loop temperature is already below the cooling setpoint – then the system enters free cooling mode. In free cooling mode, a bypass is employed, and the heat pumps are not required to operate.

Ambient loop flowrate was set to 100kg/s of water (via a trial-and-error process) in order to: (1) ensure sufficient available energy, and (2) minimise the temperature difference between supply and return streams of the cooling tower (ΔT_{CT} , in °C). ΔT_{CT} reaches a maximum of 8.72°C in the model, a value which is well within the normal range for a commercial cooling tower.

3.3. WET system

For the WET system, a wetwell – a structure which receives sewage for handling – will be constructed to tap into one of the sewers adjacent to the university campus. Wastewater will be screened for debris, passed through a bank of shell-and-tube wastewater-to-water heat exchangers housed in an Energy Transfer Station (“ETS”), and – once its energy has been extracted – returned to the sewer. The shell side of the heat exchanger will be wastewater, while the tube side will be clean (ambient loop) water. This system configuration will ensure that only clean water circulates on the university side of the heat exchanger. The fluid pressure will also be higher on the tube side of the heat exchanger to ensure that in the event of a rupture clean water enters the wastewater side, and not vice versa, though it should be noted that such an emergency is unlikely.

Although the WET system is capable of meeting the Cluster’s complete heating and cooling needs, a boiler plant and/or cooling tower(s) for may be retained for redundancy depending on local legislation and the preferences of the building operators. Regulations regarding redundancy may differ depending on the exact configuration of the WET system.

3.3.1. Sewer temperature and flowrate estimation

Sewer temperature and flow data were received from Toronto Water for several sites in the Greater Toronto Area. In order to estimate available wastewater energy in a manner consistent with the outdoor air temperatures generated in the CarrierHAP model (and because temperature data was available only for the August-October 2018 period), it was necessary to determine a correlation accounting for the relationship between sewer temperature and: (1) outdoor dry-bulb temperature, and (2) time of day.

Sewer temperature fluctuates seasonally with outdoor air temperature, with average sewer temperatures being higher in summer and lower in winter. Additionally, sewer temperature varies predictably within a 1-2°C window throughout the day; temperatures are lowest around 7AM-8AM and rise steadily towards a high point in the late morning/early afternoon (11AM-2PM). Temperatures then drop steadily until they reach another low point around 5PM-6PM, before climbing towards their highest point around midnight. While there is considerable day-to-day variation in the exact shape of the sewer temperature curve, this general pattern of two peaks and two valleys holds true throughout the year.

The flows from Sewer MH101, Site 005 were used to generate a correlation between wastewater temperature, seasonal outdoor dry-bulb temperature, and time of day according to the following method:

- A fifth-degree polynomial trendline was generated to represent variation in wastewater temperature as a function of time of day (“Correlation A”).
- Mean daily ambient temperature and mean daily wastewater temperature were correlated using a line of best fit (“Correlation B”).
- To capture the effect of seasonal variation, the x^0 value of the fifth-degree polynomial (y-intercept) was replaced with the estimated mean daily wastewater temperature as determined from Correlation B.
- An offset of +0.6°C was applied to reduce error.

RMSE between estimated sewer temperature and recorded sewer temperature under this method (“Correlation C”) was 0.73. The maximum modelled wastewater temperature was 25.6°C, while minimum modelled wastewater temperature was 19.6°C, values consistent

with most urban sewersheds [22] [23]. The coefficients of the line of best fit used are shown in Table 2 below.

x^5	x^4	x^3	x^2	x^1	x^0
9.593×10^{-6}	-0.0005	0.00804	-0.03230	-0.16591	$f(T_{DB})$

Table 2. Sewer temperature correlation coefficients

Where:

$$x_0 = \overline{T_{sewer}} + 0.6 = f(T_{DB}) = [0.1041 \times T_{DB} + 22.634] + 0.6 \quad (6)$$

The estimated temperature profile was paired with a full year of actual flow data from a different monitoring site (103-119) to generate a complete temperature/flowrate profile.

3.3.2. WET system modelling

Maximum available sewer energy (i.e., energy available if the entire sewer flow is utilised) was calculated according to Equation 7 below:

$$\dot{Q}_{sewer} = \dot{m} \times c_p \times \Delta T \quad (7)$$

Where \dot{m} is the mass flowrate of the sewer, c_p is the specific heat capacity of water (wastewater), and ΔT is the inlet-outlet temperature difference across the wastewater side of the heat exchanger, here taken to be 3°C due to municipal safety limits on wastewater temperature.

A 5°C difference between water and wastewater streams was assumed – that is, ambient loop temperature was taken to be 5°C higher than the sewer temperature in the cooling season and 5°C lower than the sewer temperature in the heating season. When these limits were imposed (assuming the same heat pump configuration and efficiencies as in the conventional system), the peak heat rejected to the ambient loop (peak cooling) was 3,647kW, while the peak heat extracted from the ambient loop (peak heating) was 702kW. Meanwhile, the lowest available sewer energy at any point during the year is 5,416kW (occurring in late March). Thus, even if the energy of the sewer is only partially utilised, the WET system will not struggle to meet the peak demands of the LIB-POD-JOR Cluster.

3.3.3. Comparison with conventional system

Marginal energy costs in 2019 and 2030 are shown in Table 3 below. Energy costs are from Toronto Metropolitan (Ryerson) University's 2021 Carbon Reduction Roadmap. Natural gas costs are predicted to rise significantly due to carbon prices gradually increasing throughout the decade, though it should be noted that all energy cost predictions are highly speculative, and that natural gas pricing in particular is volatile and heavily market-reliant.

	2019	2030
Marginal natural gas cost (\$ CAD/kWh)	0.0286	0.0595
Marginal electricity cost (\$ CAD/kWh)	0.1517	0.1566

Table 3. *Energy cost of electricity and natural gas in Ontario, Canada [19]*

GHG emissions factors are shown in Table 4. All emissions factors are from the Canadian Ministry of the Environment and Climate Change’s National Inventory Report. For electricity-related emissions, the average emissions factor (“AEF”) is used; the AEF represents the most basic quantification of carbon emissions, and does not take time-based shifts in the grid’s energy mix (or other complexities of electricity generation) into account.

	Electricity, 2019 AEF (gCO ₂ eq/kWh)	Natural gas (gCO ₂ eq/m ³)
Emissions factor	30	1,899

Table 4. *GHG emissions factors [18]*

Table 5 below shows the annual energy usage, GHG emissions, and energy costs of the conventional and WET-based ambient loop systems. While the WET system provides a significant (70.18 per cent) reduction in GHG emissions and a moderate (23.05 per cent) reduction in HVAC-related energy use, annual energy costs are slightly (8.89 per cent) increased under 2019 energy pricing. However, when 2030 energy pricing is applied, the annual energy costs of the WET system only marginally (0.29 per cent) exceed those of the conventional system. This suggests that rising carbon prices in coming years are likely to make WET a more and more financially viable alternative.

	HVAC-related energy use (MWh)	GHG emissions (tonnes)	Energy cost, 2019 (\$ CAD)	Energy cost, 2030 (\$ CAD)
Conventional	2,988	231	320,361	352,903
WET-based	2,300	69	348,840	353,953
Percentage change	-23.05%	-70.18%	+8.89%	+0.29%

Table 5. *Comparison of conventional and WET-based ambient loop systems (annual values, ambient loop pumping excluded from comparison)*

CONCLUSION

The simulation shows that WET is a feasible solution for the Cluster, providing meaningful reductions in annual energy use and GHG emissions with only a slight (based on 2019 energy pricing) or marginal (based on 2030 energy pricing) increase in annual energy costs. These results suggest that WET may find productive applications within cold-climate institutional

buildings more generally. Future refinements to the Library-Podium-Jorgenson Hall WET model will include: a complete financial analysis including return on investment (“ROI”) calculations, the addition of a detailed ambient loop pumping model, and the development of a hybridised WET-conventional model (i.e., a model in which WET and conventional HVAC equipment are used alternately or simultaneously throughout the year) with optimisations for energy usage, cost, and GHG emissions. It is hoped that the present study will provide a basis for future WET-related research.

ACKNOWLEDGEMENTS

This research was supported by funding from Toronto Metropolitan University, Mitacs Accelerate, and Noventa Energy Partners.

REFERENCES

- [1] London Energy Transformation Initiative, *LETI Climate Emergency Design Guide: How New Buildings Can Meet UK Climate Change Targets*.
- [2] A. Revesz, P. Jones, C. Dunham, G. Davies, C. Marques, R. Matabuena, J. Scott and G. Maidment, “Developing novel 5th generation district energy networks,” *Energy*, vol. 201, 2020.
- [3] S. Buffa, A. Soppelsa, M. Pipiciello, G. Henze and R. Fedrizzi, “Fifth-Generation District Heating and Cooling Substations: Demand Response with Artificial Neural Network-Based Model Predictive Control,” *Energies*, vol. 13, 2020.
- [4] S. Buffa, M. Cozzini, M. D'Antoni, M. Baratieri and R. Fedrizzi, “5th generation district heating and cooling systems: A review of existing cases in Europe,” *Renewable and Sustainable Energy Reviews*, vol. 104, 2019.
- [5] Y. Gu, T. Wang, W. Liu and F. Ma, “Energy-saving Analysis and Heat Transfer Performance of Wastewater Source Heat Pump,” *Applied Mechanics and Materials*, vol. 694, pp. 211-217, 2014.
- [6] C. Kwiatek, *Techno-Economic Feasibility of Wastewater Energy Transfer (WET) Systems for Cold Climates (Master's Thesis)*, Toronto, Ontario, 2020.
- [7] Huber, “Wastewater heat utilisation and reuse of process heat at Munich university hospital "Klinikum rechts der Isar",” [Online]. Available: <https://www.huber.de/huber-report/ablageberichte/energy-from-wastewater/wastewater-heat-utilisation-and-reuse-of-process-heat-at-munich-university-hospital-klinikum-rechts-der-isar.html>. [Accessed 29th April 2022].
- [8] British Columbia Ministry of Community & Rural Development, “Integrated Resource Recovery Case Study: Okanagan College Wastewater Heat Recovery,” [Online]. Available: <https://www.waterbucket.ca/gi/sites/wbcgi/documents/media/270.pdf>. [Accessed 29th April 2022].
- [9] C. Johnston, E. Lindquist, J. Hart and M. Homenuke, “Four steps to recovering heat energy from wastewater,” *British Columbia Water & Waste Association Watermark, Craig Kelman & Associates*, vol. 18, no. 2, pp. 16-18, 2009.
- [10] X. Hao, J. Li, M. C. M. van Loosrecht, H. Jiang and R. Liu, “Energy recovery from wastewater: Heat over organics,” *Water Research*, vol. 161, pp. 74-77, 2019.
- [11] A. Hepbasli, E. Biyik, O. Ekren, H. Gunerhan and M. Araz, “A key review of wastewater source heat pump (WWSHP) systems,” *Energy Conversion and Management*, vol. 88, pp. 700-722, 2014.

- [12] ASHRAE, “Standard 90.1-2019, Energy Standard for Buildings Except Low-Rise Residential Buildings,” 2019. [Online]. Available: https://ashrae.iwrapper.com/ASHRAE_PREVIEW_ONLY_STANDARDS/STD_90.1_2019. [Accessed 29th April 2022].
- [13] M. Lefebvre, “The Library, the City, and Infinite Possibilities: Ryerson University’s Student Learning Centre Project,” 2013. [Online]. Available: <http://library.ifla.org/id/eprint/62/1/081-lefebvre-en.pdf>. [Accessed 15 October 2021].
- [14] Architectural Conservancy Ontario, “Ryerson University; Jorgenson Hall,” [Online]. Available: https://www.acotoronto.ca/show_building.php?BuildingID=1758. [Accessed 15 October 2021].
- [15] A. S. Fung, M. Z. Rahman, H. Taherian, M. M. Selim and M. Hossain, “Energy Audit and Base Case Simulation of Ryerson University Buildings,” *ASHRAE Transactions*, vol. 121, 2015.
- [16] University of Alabama, “Excel Stuff,” [Online]. Available: <https://www.me.ua.edu/me215/f07.woodbury/ExcelStuff.html>.
- [17] UC Davis Western Cooling Efficiency Center, “Psych: An Open Source Psychrometric Plugin for Microsoft Excel by Kevin Brown,” [Online]. Available: <https://wcec.ucdavis.edu/resources/software-resource-applications/>.
- [18] Ministry of Environment and Climate Change Canada, *National Inventory Report 1990-2019: Greenhouse Gas Sources and Sinks in Canada*, 2021.
- [19] Ryerson University Climate and Energy Working Group, *Carbon Reduction Roadmap - Draft Framework*, Toronto, Ontario, 2021.
- [20] M. J. Moran, H. N. Shapiro, D. D. Boettner and M. B. Bailey, *Fundamentals of Engineering Thermodynamics*, 8th ed., Hoboken, NJ: John Wiley & Sons, 2014.
- [21] Natural Resources Canada, “Heating and Cooling With a Heat Pump,” 2022. [Online]. Available: <https://www.nrcan.gc.ca/energy-efficiency/energy-star-canada/about/energy-star-announcements/publications/heating-and-cooling-heat-pump/6817>. [Accessed 2022].
- [22] H. Xiaodi, J. Li, M. C. M. van Loosdrecht, H. Jiang and R. Liu, “Energy recovery from wastewater: Heat over organics,” *Water Research*, vol. 161, pp. 74-77, 2019.
- [23] S. S. Cipolla and M. Maglionico, “Heat recovery from urban wastewater: analysis of the variability of flow rate and temperature in the sewer of Bologna, Italy,” *Energy Procedia*, vol. 45, pp. 288-297, 2014.

DISCLAIMER

The information or advice contained in these technical papers is intended for use only by professionals who have had adequate technical training in the field to which the paper relates. At the time of publication, these technical papers have undergone a formal peer-review process.

These documents have been compiled as an aid only, and the information or advice should be verified before it is put to use. The user should also establish the applicability of the information or advice in relation to any specific circumstances. While the information or advice is believed to be correct, no responsibility is taken by AIRAH or IBPSA Australasia for any statements made within.

AIRAH and IBPSA Australasia, its officers, employees and agents, disclaim responsibility for any inaccuracies contained within the documents, including those due to any negligence in the preparation and publication of the said technical papers.

COPYRIGHT

This work is copyright. Apart from any use as permitted under the Copyright Act 1986, no part may be reproduced by any process without prior written permission from either the Australian Institute of Refrigeration, Air Conditioning and Heating (AIRAH) or the International Building Performance Simulation Association (IBPSA) Australasia.

COMFORT DATA FOR BRISBANE: USING DATA COLLECTED BY LOW-COST MONITORING DEVICES TO IMPROVE PREDICTION ACCURACY

TOBIAS KRAMER

School of Architecture & Built Environment
Queensland University of Technology
2 George St, 4000 Brisbane
t.kramer@qut.edu.au

DR VERONICA GARCIA HANSEN

School of Architecture & Built Environment
Queensland University of Technology
2 George St, 4000 Brisbane
v.garciahansen@qut.edu.au

ABOUT THE AUTHORS

Tobias Kramer is an ESD engineer and PhD candidate from the Human-Building-Interaction (HBI4Climate) Group at QUT, Brisbane. He uses emerging technologies like AI and Data Science to explore the interactions between thermal comfort and climate change. Associate Professor Veronica Garcia-Hansen is a well-known expert on daylighting interested in human-centred approaches to building design. She leads the HBI4Climate group.

ABSTRACT

This paper presents preliminary findings from a thermal comfort field study using low-cost monitoring equipment in Brisbane, Australia. The study involves the collection of occupant feedback and indoor climate data from five different air-conditioned office buildings. Analysing the collected data, it was found that the PMV model partially overestimates thermal sensations indicated by participants. The field study methodology based on low-cost equipment was found to be reliable and user-convenient and can facilitate the collection of more thermal comfort data. This will open new ways to comfort modelling by integrating emerging technologies like AI and Data Science into comfort prediction workflows.

INTRODUCTION

The consequences of climate change call for the reduction of carbon emissions through energy savings and climate resilience in the building sector. A significant amount of energy in the building sector is used for achieving thermal comfort in buildings. Space cooling alone currently accounts for almost 20 per cent of the electricity used in buildings globally and is expected to triple by 2050 (IEA, 2018). Therefore, a better understanding of thermal comfort modelling and prediction is essential in improving buildings' efficiency and future thermal performance (Rupp et al., 2015). The thermal design of many new buildings today is based on comfort predictions by the PMV model that, since its introduction 40 years ago (Fanger, 1972), has made optimal use of then available means of technology. The PMV model is still the

standard for air conditioned buildings, and despite the well-known advantages of this approach, its relatively low accuracy levels have been discussed recently, e.g. by Cheung et al. (2019). Fortunately, the emergence and ever-increasing availability and accessibility of technologies like Artificial Intelligence (AI) and Data Science open new ways to further develop comfort modelling methods and improve prediction accuracy in the building design process. Results from previous work (Kramer et al., 2021) have shown that the use of AI and the availability of thermal comfort data in more richness and variety can be the basis for a more advanced approach to comfort modelling and prediction. However, these promising, new approaches to comfort modelling generally depend on the availability of rich datasets of thermal comfort data. Unfortunately, the essential but rather expensive monitoring equipment for thermal comfort field studies impedes the collection of more valuable data and, in a way, acts as a significant barrier for improving modelling accuracy and expanding knowledge on thermal comfort in the field (Heinzerling et al., 2013).

To this end, this paper addresses selected preliminary findings from an ongoing thermal comfort field study in Brisbane, Australia, involving cost-efficient, user-friendly, and open-source monitoring devices that have been developed by the authors (Kramer et al., 2022). The device development and field study are part of a research project that aims to leverage the potential of emerging technologies like Data Science and Artificial Intelligence to improve the accuracy and scope of thermal comfort modelling in a changing climate. However, these new technologies significantly rely on representative occupant feedback data, which, despite extraordinary efforts like the ASHRAE Global Thermal Comfort Database II (Földvary Licina et al., 2018), does not exist for all locations worldwide.

1. METHODOLOGY

The ongoing field study involves the collection of occupant comfort feedback and indoor climate data in multiple air-conditioned office buildings in Brisbane. The following section is divided into three parts focusing on monitoring equipment, survey, and data analysis.

1.1.1 Monitoring equipment

A low-cost device named *climateBOX* (Figure 1) is used to monitor indoor climate conditions. The development, functionality and calibration of these devices are addressed in (Kramer et al., 2022).

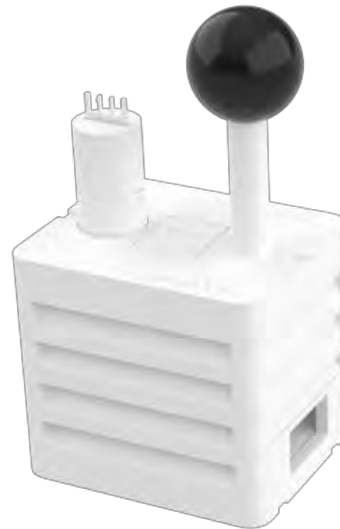


Figure 1. Rendering of *climateBOX* monitoring device.

The construction instructions will be made open source so that other researchers can easily rebuild the devices to support the further growth of openly accessible thermal comfort databases. The relatively compact *climateBOX* design with a size of 80*100*100mm³ allows for a decentralised field study approach where a dozen monitoring devices were distributed within the investigated space and placed near each participant. This approach promises more representative and occupant-centred readings for the measured variables of air temperature, relative humidity, globe temperature, and air velocity.

1.1.2 Survey

For five consecutive days between October and December 2021, participants were provided with their own *climateBOX* to record occupant-focused indoor climate data. Simultaneously the participants were asked to do up to three comfort questionnaires per day to give feedback on climatic conditions. The questionnaire contains common questions about thermal comfort like thermal sensation (7-point scale ranging from 'Cold' to 'Hot'), preference (e.g. 'Warmer', 'No change'), and acceptability ('Yes'/'No'). The questionnaire design is based on suggestions provided in ASHRAE Standard 55 (ASHRAE, 2017) and similar studies like (Kim et al., 2019). It is designed to be as convenient and user-friendly as possible, not interrupting existing working routines and encouraging participants to take the survey multiple times per week. Participants were office workers in five different air-conditioned office buildings in Brisbane. They were invited to register for the field study in an invitation email sent by building managers. In the first phase of the project, 48 office workers in total registered to participate in the field study.

1.1.3 Data analysis

This paper focuses on selected findings from the first phase of the field study and experiences with the *climateBOX* in a long-term monitoring setting. More results and a detailed analysis of the whole study will be published after the data collection has finished.

The analysis is presented in two sections: first, general insights from the field study and data collection, such as the *climateBOX* performance and participant engagement, is addressed. Then the physical data (e.g., air temperature) and self-reported data (e.g., thermal sensation) are analysed using descriptive statistical analysis. After looking into study statistics like data

about the participant response time and rate, the general functionality of the monitoring devices over the study period is addressed. This is followed by an analysis of the actual data collected so far. Starting with the demographical distribution of the recorded data samples, the investigation continues to present findings on standard comfort-related variables like thermal sensation, preference, and acceptability. Then the focus shifts to comparing the actual recorded participants' thermal sensation with the comfort predictions based on the PMV model, which are calculated using the recorded climate variables. Here, the created parameter of 'PMV-TSV discrepancy' similar to Li et al. (2020) is analysed and correlated to other recorded variables. The analysis ends with comparing the collected to previously recorded data from similar buildings in other Australian locations to set the findings into a geographical context.

2. RESULTS

2.1.1 Field study implementation and participant engagement

Regarding the *climateBOX* performance, 98.1 per cent of the recordings made by the devices were found complete and usable for analysis. The minimal amount of faulty or missing readings was mainly caused by human error when participants unintentionally interrupted the power supply of the boxes, e.g., by mistakenly pulling out the power plug while working at their desk. Additionally, minimal issues with the Wi-Fi connection to the data cloud server have been observed. But due to local backup storage on an SD card, a possible loss of data has been avoided. The code for wireless data transmission has been further developed since and transmission problems have been solved. The *climateBOX* devices worked as expected, and regular checks of the devices conducted at the beginning of the study became unnecessary after the first week.

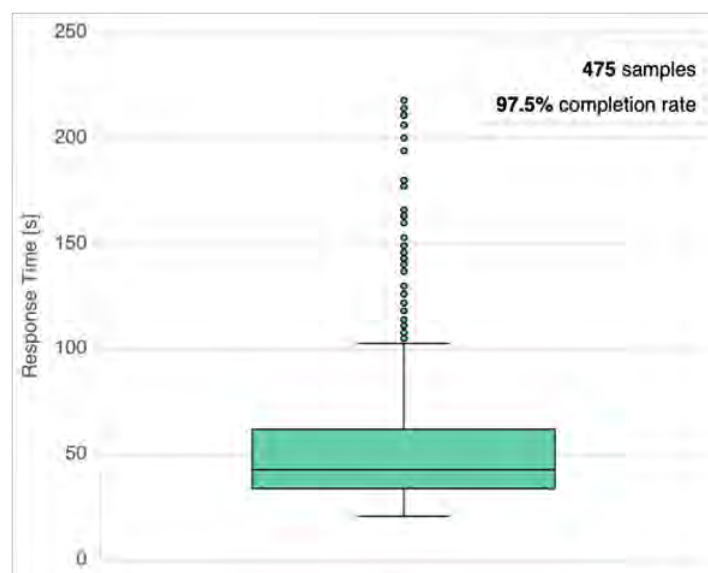


Figure 2. Survey response time.

The boxplot in Figure 2 shows the survey response time distribution for all 475 data samples, corresponding to the total number of fully answered questionnaires. With a median response time of 45 seconds and 75% of the questionnaires answered within a 1-minute time frame, the targeted survey response time of 1.5 minutes at the maximum was met in most cases. In

addition, 97.5 per cent of started surveys were fully completed, and none of the registered participants dropped out during the study. Figure 3 indicates a median number of 10 answered questionnaires per registered participant, where 75 per cent contributed at least seven survey responses distributed over five days.

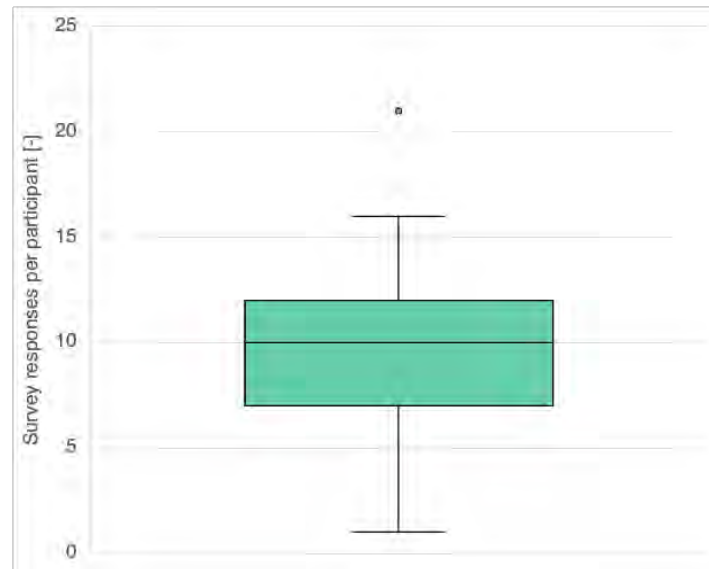


Figure 3. *Survey response rate.*

2.1.2 Demographics

An analysis of the demographic data uncovered a skewed distribution for both demographic variables collected. The breakdown of contributions in age group and gender in Figure 4 highlights a clear majority of votes coming from participants aged between 25 and 34 and female participants, respectively.

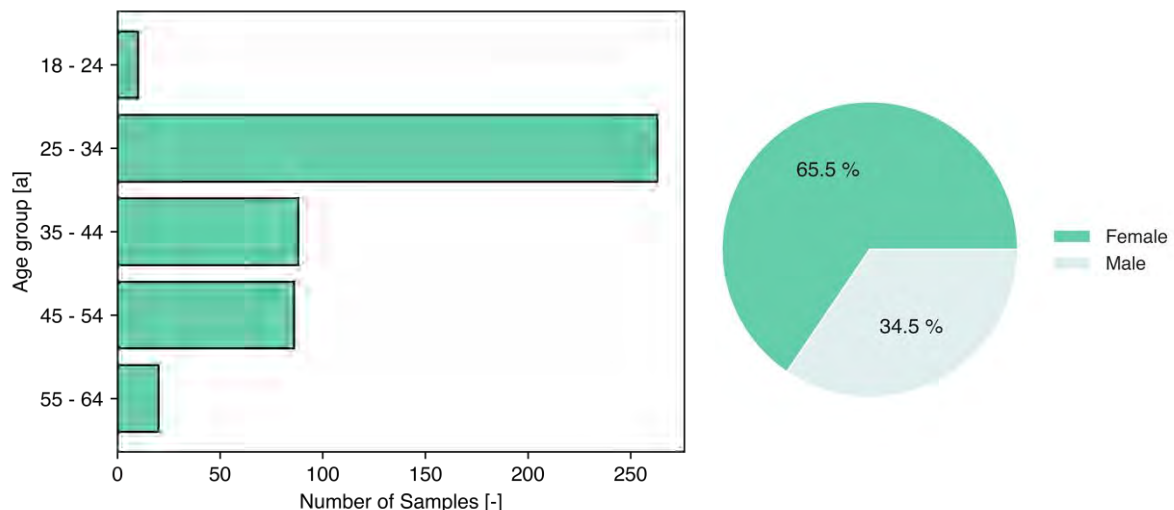


Figure 4. *Participant demographics.*

2.1.3 Thermal sensation, preference and acceptability

Figure 5 shows the results of the thermal sensation vote (TSV), 'Neutral' was the most common response with 39 per cent, followed by "Slightly cool" with 26 per cent and "Slightly warm" (14%). Considering the 7-point ASHRAE Thermal Comfort scale, where comfort is assumed for a neutrality range of $-1 \geq PMV \geq 1$, participants perceived the thermal conditions as comfortable for around 80 per cent of the time. In addition, the histogram demonstrates a slight tendency to the colder end of the comfort spectrum, with almost 43 per cent of survey responses indicating at least a subtle level of discomfort due to cool thermal conditions. Figure 6 presents the thermal preference distribution between the votes. Around 65 per cent of survey responses indicated a preference for no change of thermal conditions at the time of survey submission. While 19 per cent of participants prefer warmer conditions. Concerning the acceptability of the indoor climate conditions, the graph in Figure 7 shows that in over 90 per cent of their survey responses, participants considered their thermal environment acceptable.

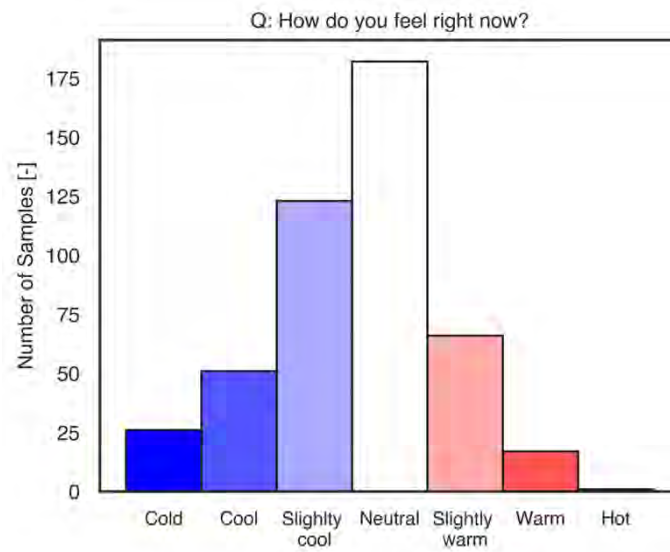


Figure 5. *Thermal sensation.*

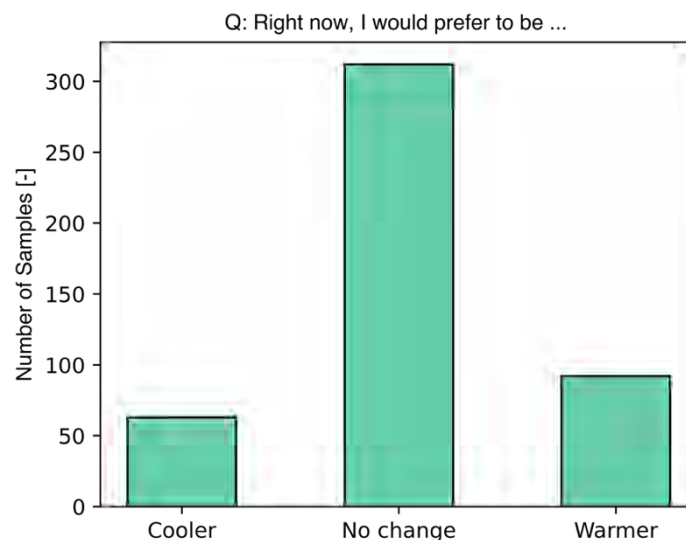


Figure 6. *Thermal preference.*

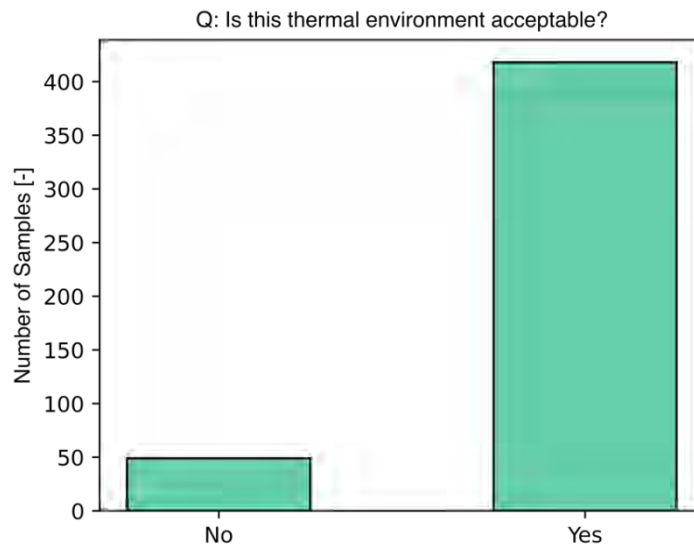


Figure 7. *Thermal acceptability.*

2.1.4 PMV – TSV discrepancy

Figures 8 and 9 show data on the PMV-TSV discrepancy in a histogram and heatmap, respectively. The observations that can be made are twofold. First, in only 37 per cent of the cases, the predicted PMV matched the actual thermal sensation vote given by the participant. Second, the displayed data indicates a tendency by the PMV model to overestimate the mean comfort vote, which can be assumed from the high number of PMV-TSV difference values in the positive range and more considerable differences above the main classification heatmap diagonal.

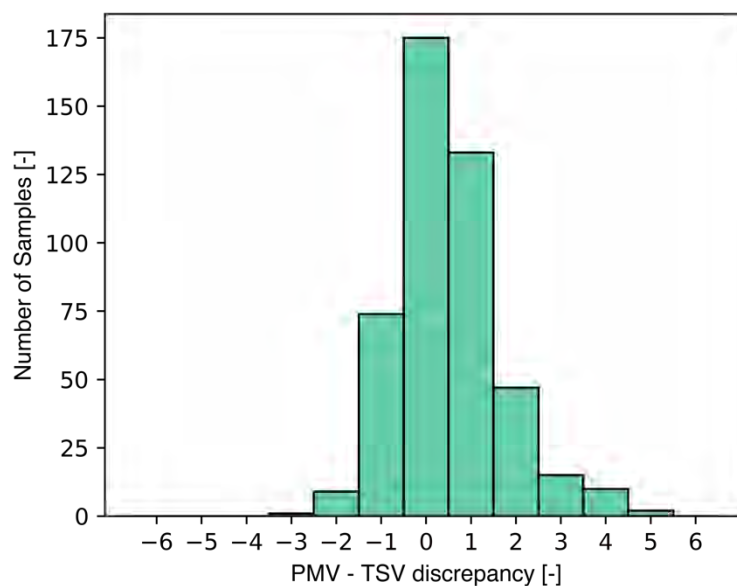


Figure 8. Discrepancy between PMV and participants thermal sensation vote (TSV).

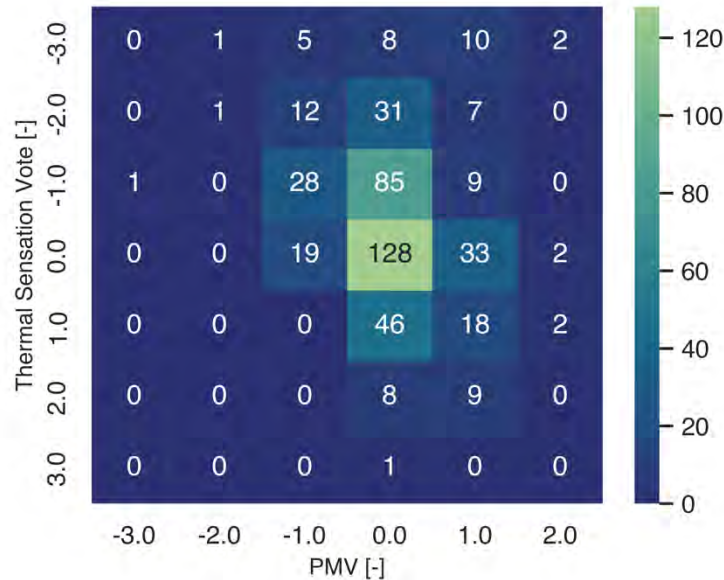


Figure 9. Classification heatmap comparing PMV predictions based on monitoring data compared to actual thermal sensation votes (Legend on the right-hand side represents number of predictions made for each category/value combination).

Figure 10 shows the relationship between the found PMV-TSV discrepancy and the predictions made by the PMV model, binned into the three distinct categories of 'Cool' ($PMV < -1$), 'Neutral' ($-1 \leq PMV \leq +1$) and 'Warm' ($PMV > +1$). Here, PMV predictions differ significantly more from the actual thermal sensation votes when the PMV itself is higher than 1. This again indicates overestimated comfort levels predicted by the PMV, particularly when warmth-induced discomfort above neutral levels is predicted.

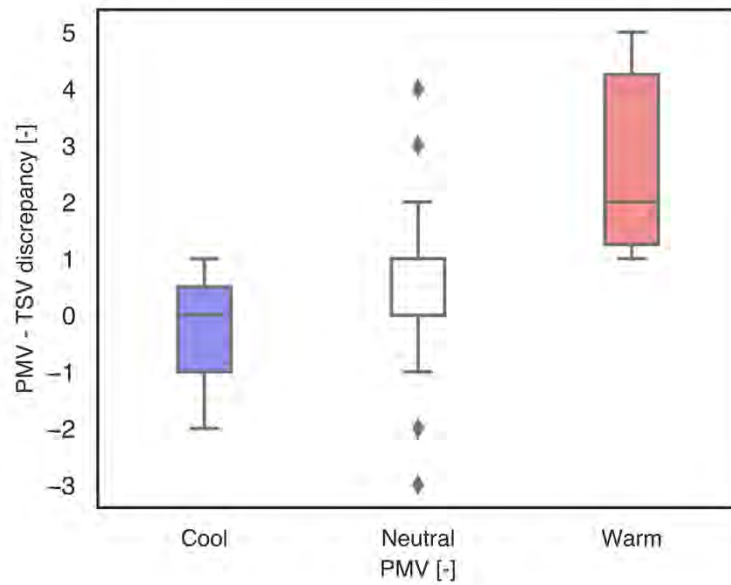


Figure 10. Relationship between PMV predictions and PMV - TSV discrepancy.

2.1.5 Geographical context

Figure 11 compares the collected thermal sensations to similar ASHRAE Global Thermal Comfort Database II (Földvary Licina et al., 2018) data for air-conditioned buildings in Brisbane and other Australian locations. Only data points within a fixed air temperature range of 23/24°C were considered. The TSV distribution of the recorded data mostly resembles the existing data for Brisbane and only shows a slight tendency towards more 'Slightly cool' (-1) votes. In addition, although limited to the same temperature range and building type, the boxplots for Sydney, Melbourne and Kalgoorlie, all locations in more temperate climates, indicate tendencies in the opposite direction and votes between 'Neutral' (0) and 'Slightly warm' (1).

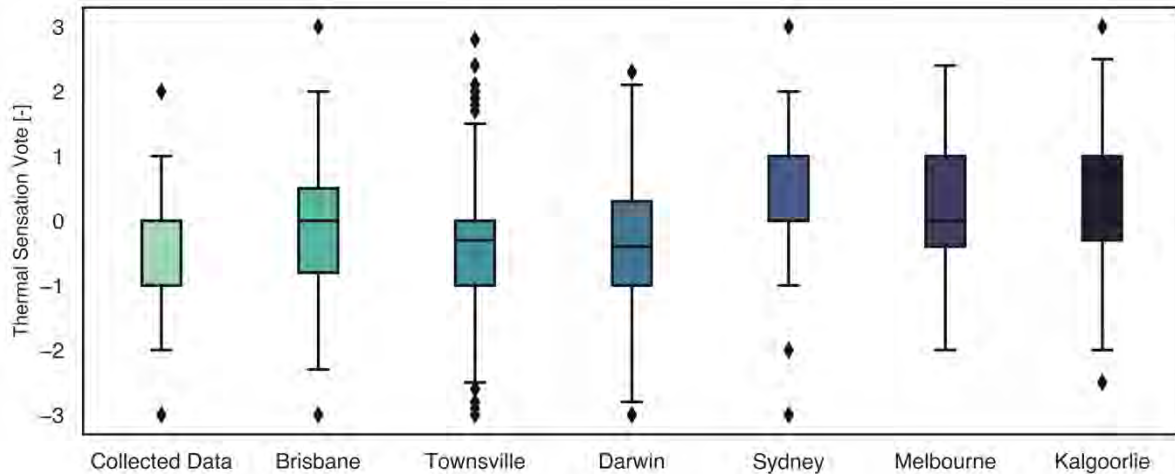


Figure 11. Comparison of collected data to data from other Australian locations and operative temperature range of 23/24°C.

DISCUSSION

First, the relatively short response times and a high response rate in addition to a high level of completion suggests that the objective of avoiding inconvenience for participants is met and that a target of around ten submitted questionnaires per week is realistic. Considering that a significant number of participants partially worked from home and could not participate for an entire week, the response rate can be expected to rise a little when post-Covid more people return to the office. The clearly non-uniform demographical distribution of the collected data samples will probably be more balanced for the final dataset, as current registrations for the second half of the field study contain a higher proportion of male participants and participants from different ages groups.

Regarding the participants' feedback on thermal comfort, the data on thermal preference and acceptability suggests a general satisfaction with the indoor climate conditions. However, the tendency of thermal sensations leaning towards the cooler side of the comfort spectrum, as shown in Figure 5, indicates partial discomfort due to cold conditions. Here it needs to be considered that most study participants have been female so far and an influence of e.g., lower metabolic rates or different clothing routines cannot be excluded at this stage. However, findings made by other researchers like Wang et al. (2020) suggest that temperature-based comfort ranges of female participants might be slightly narrower. In addition, taken together Figures 5 – 7 show that if participants felt discomfort this was mainly caused by cold conditions and consistently lead to a preference for warmer conditions. Yet, Figure 7 indicates that conditions are still acceptable most of the time. This suggests that the slight discomfort perceived still is in the acceptable range. Alternatively, occupants might have got used to prevalent conditions and have developed adaptive strategies like bringing additional clothing to cope with the slight discomfort perceived. Figures 8 -10 highlight inaccuracies of the PMV model and the prediction of a wrong comfort level for almost two-thirds of the data samples, which is similar to observations made by Cheung et al. (2019). The increased inaccuracy and overestimation of comfort levels on the warmer end of the comfort spectrum suggest that office workers in the investigated buildings tend to perceive conditions 'Neutral' at higher temperatures than predicted by the PMV model. This, in turn, emphasises the potential for

higher cooling set-points and lower cooling loads. The apparent differences of the TSV distribution for the collected data in comparison to data from air-conditioned buildings in other Australian locations suggest an influence of the location on the thermal sensation vote. This parameter can be broken down into other factors like outdoor temperature, clothing behaviour, thermal history etc. Due to little variety in outdoor temperatures during the study so far, the influence of the outdoor climate could not be investigated further yet.

The preliminary findings from this field study highlight partial inaccuracies of the PMV model. In the future, these could be improved by collecting more occupant feedback and indoor climate data to further explore the potential of evidence-based comfort prediction models as a viable alternative to conventional approaches. Previous work (Kramer et al., 2021) highlights the potential influence of more simple input parameters, e.g. location/outdoor climate, that can be easily integrated into new comfort modelling practices based on evidence from growing databases of international comfort data. To extend these databases and make comfort models more specific, the availability of low-cost and open-source monitoring equipment is critical.

CONCLUSION

The paper presents preliminary findings from a field study involving low-cost comfort monitoring equipment in Brisbane, Australia. The results show that such devices are a reliable alternative to expensive conventional comfort monitoring equipment. The survey approach selected for this study is user-friendly, which promises a high turnover in collected data samples. In addition, it was found that, even though endorsed for air-conditioned buildings, the PMV model in many cases overestimated the thermal sensation of study participants. Comparing the collected data to similar samples from other Australian locations suggests the influence of additional comfort parameters, which are not considered in the PMV model, such as the geographical location (e.g. outdoor climate). These can be an essential input parameter for an alternative, evidence-based comfort-modelling approach using AI and publicly available datasets. By using data science and Machine Learning algorithms, patterns found in the data can be used for thermal comfort predictions that are embedded in parametric simulation workflows. This allows to perform evidence-based sensitivity analyses and comfort-related performance evaluations of future buildings.

The monitoring method used in this study that focuses on the use of low-cost environmental sensors in a decentralised, cloud-based monitoring system allows to contribute to these AI-based models and extend existing datasets by collecting valuable thermal comfort data at an optimised cost-benefit ratio. This provides an alternative way to conventional comfort field studies, which usually rely on the availability of relatively expensive monitoring equipment. Furthermore, the simplified access to increasingly important comfort data enhances comfort modelling in general and leads to further improvements in building energy efficiency and occupant comfort. Looking ahead, the integration of these 'advanced' comfort models into conventional simulation workflows can provide endless possibilities, like directly linking comfort modelling with future climate datasets to allow climate-resilience proofing of future building designs.

The authors hope that developing the inexpensive and user-friendly devices and open-source distribution of instructional resources for replication will facilitate the collection of more affluent and diverse thermal comfort data in Australia and beyond.

ACKNOWLEDGEMENTS

The authors would like to thank the Building 4.0 CRC for financially supporting the research.

REFERENCES

- ASHRAE. (2017). *ANSI/ASHRAE Standard 55-2017: Thermal Environmental Conditions for Human Occupancy*. American Society of Heating, Refrigerating and Air-Conditioning Engineers.
- Cheung, T., Schiavon, S., Parkinson, T., Li, P., & Brager, G. (2019). Analysis of the accuracy on PMV – PPD model using the ASHRAE Global Thermal Comfort Database II [Article]. *Building and Environment*, 153, 205-217. <https://doi.org/10.1016/j.buildenv.2019.01.055>
- Fanger, P. O. (1972). *Thermal comfort: analysis and applications in environmental engineering*. McGraw-Hill.
- Földváry Ličina, V., Cheung, T., Zhang, H., de Dear, R., Parkinson, T., Arens, E., Chun, C., Schiavon, S., Luo, M., Brager, G., Li, P., Kaam, S., Adebamowo, M. A., Andamon, M. M., Babich, F., Bouden, C., Bukovianska, H., Candido, C., Cao, B., . . . Zhou, X. (2018). Development of the ASHRAE Global Thermal Comfort Database II [Article]. *Building and Environment*, 142, 502-512. <https://doi.org/10.1016/j.buildenv.2018.06.022>
- Heinzerling, D., Schiavon, S., Webster, T., & Arens, E. (2013). Indoor environmental quality assessment models: A literature review and a proposed weighting and classification scheme [Review]. *Building and Environment*, 70, 210-222. <https://doi.org/10.1016/j.buildenv.2013.08.027>
- IEA. (2018). *The Future of Cooling*. <https://www.iea.org/reports/tracking-buildings-2021>
- Kim, J., Tartarini, F., Parkinson, T., Cooper, P., & de Dear, R. (2019). Thermal comfort in a mixed-mode building: Are occupants more adaptive? [Article]. *Energy and Buildings*, 203, Article 109436. <https://doi.org/10.1016/j.enbuild.2019.109436>
- Kramer, T., Garcia-Hansen, V., Omrani, S., Nik, V. M., & Chen, D. (2021). A Machine Learning approach to enhance indoor thermal comfort in a changing climate. J. Phys.: Conf. Ser, Lausanne, Switzerland.
- Kramer, T., Garcia-Hansen, V., Omrani, S., Nik, V. M., & Chen, D. (2022). climateBOX: a low-cost, open-source monitoring device for occupant comfort in buildings. *Ready for submission*.
- Li, Y., Rezgui, Y., Guerriero, A., Zhang, X., Han, M., Kubicki, S., & Yan, D. (2020). Development of an adaptation table to enhance the accuracy of the predicted mean vote model [Article]. *Building and Environment*, 168, Article 106504. <https://doi.org/10.1016/j.buildenv.2019.106504>
- Rupp, R. F., Vásquez, N. G., & Lamberts, R. (2015). A review of human thermal comfort in the built environment [Review]. *Energy and Buildings*, 105, 178-205, Article 6041. <https://doi.org/10.1016/j.enbuild.2015.07.047>
- Wang, Z., Zhang, H., He, Y., Luo, M., Li, Z., Hong, T., & Lin, B. (2020). Revisiting individual and group differences in thermal comfort based on ASHRAE database. *Energy and Buildings*, 219, Article 110017. <https://doi.org/10.1016/j.enbuild.2020.110017>

DISCLAIMER

The information or advice contained in these technical papers is intended for use only by professionals who have had adequate technical training in the field to which the paper relates. At the time of publication, these technical papers have undergone a formal peer-review process.

These documents have been compiled as an aid only, and the information or advice should be verified before it is put to use. The user should also establish the applicability of the information or advice in relation to any specific circumstances. While the information or advice is believed to be correct, no responsibility is taken by AIRAH or IBPSA Australasia for any statements made within.

AIRAH and IBPSA Australasia, its officers, employees and agents, disclaim responsibility for any inaccuracies contained within the documents, including those due to any negligence in the preparation and publication of the said technical papers.

COPYRIGHT

This work is copyright. Apart from any use as permitted under the Copyright Act 1986, no part may be reproduced by any process without prior written permission from either the Australian Institute of Refrigeration, Air Conditioning and Heating (AIRAH) or the International Building Performance Simulation Association (IBPSA) Australasia.

SENSITIVITY ANALYSIS OF PASSIVE DESIGN STRATEGIES FOR OFFICE BUILDINGS IN THE TROPICS

ARINDA P. RACHMAN, S.T., MSc

Doctoral student

Engineering Physics Graduate Program, Faculty of Industrial Technology, Institut Teknologi Bandung

Jl. Ganesha 10, Labtek VI, Bandung, 40132, Indonesia

arinda.p.rachman@gmail.com

CHALILA ICHWANIA, S.T.

Master student

Engineering Physics Graduate Program, Faculty of Industrial Technology, Institut Teknologi Bandung

Jl. Ganesha 10, Labtek VI, Bandung, 40132, Indonesia

chalila.ichwania@gmail.com

DR. RIZKI A. MANGKUTO, S.T., M.T.

Lecturer and Researcher

Building Physics Research Group, Faculty of Industrial Technology, Institut Teknologi Bandung

Jl. Ganesha 10, Labtek VI, Bandung, 40132, Indonesia

armanto@tf.itb.ac.id

DR. ENG MOCHAMAD DONNY KOERNIAWAN, S.T., M.T.

Lecturer and Researcher

Building Technology Research Group, School of Architecture, Planning, and Policy Development, Institut Teknologi Bandung

Jl. Ganesha 10, Labtek IX-A, Bandung, 40132, Indonesia

donny@ar.itb.ac.id

ABOUT THE AUTHORS

Arinda P. Rachman is currently a doctoral student in Engineering Physics at Institut Teknologi Bandung. She received a bachelor's degree in Engineering Physics from Institut Teknologi Bandung and a master's degree in Architecture, Building, and Planning specialising in Building Physics and Service from TU Eindhoven. Her current field of interest is passive design strategies, robust design strategies for high-performance buildings in the tropics, and climate change.

Chalila Ichwania is currently a master student in Engineering Physics at Institut Teknologi Bandung. She finished her undergraduate study at Telkom University, majoring in Engineering Physics. Her area of interest is building physics, focusing on implementing passive design for high-performance buildings in tropical climates.

Rizki A. Mangkuto is a lecturer and a researcher in the Building Physics Research Group, Department of Engineering Physics, Faculty of Industrial Technology, Institut Teknologi Bandung, Indonesia. His current research is Lighting Engineering and Building Performance

Simulation related to electric lighting, daylighting, energy simulation, and building design optimisation.

Mochamad Donny Koerniawan is a lecturer and a researcher in the Building Technology Research Group, Department of Architecture, School of Architecture, Planning, and Policy Development, Institut Teknologi Bandung, Indonesia. His current research is Building Performance related to thermal comfort, and Urban Performance related to livability and sustainability. He is running some research projects collaborating with several universities in Japan and the US.

ABSTRACT

An optimal passive design strategy to improve building performance can be achieved by optimising the design parameters that have a great sensitivity to the building performance parameters. A sensitivity analysis is therefore conducted to understand the behavior and the sensitivity of each passive design strategy to the building performance. In this study, a sensitivity analysis of several passive design strategies was carried out on a hypothetical office building for tropical climate conditions considering that there are limited references that explore the sensitivity analysis for commercial buildings in the tropics. The tested passive measures include wall, roof, and window U-value; window solar heat gain coefficient (SHGC) and visual transmittance; window-to-wall ratio (WWR); infiltration; building orientation; overhang depth; and window height. Based on 480 samples generated using LHS (Latin-Hypercube Sampling) method, the results of sensitivity analysis using the SRC method show that WWR is the parameter that has the highest influence on cooling demand, cooling degree hour (CDH), percentage of comfort hours (PCH), and $ASE_{1000,250}$. In addition, the transmittance of the glass is a passive design parameter that has the highest influence on $sDA_{300,50\%}$ and daylight factor (DF).

1. INTRODUCTION

Passive design strategies are believed to play an essential role in improving building performance by utilising the external climate to minimise building energy needs and emissions without compromising occupant comfort and productivity (Rabani *et al.*, 2021). To implement optimum passive design strategies, the first step is to understand the sensitivity of the passive design parameters to the performance metric. Thus, the optimisation process can be simplified by focusing on the key design parameters that significantly influence the observed performance metric (Li *et al.*, 2018). The key design parameters can be obtained by performing sensitivity analysis on design parameters that are commonly assessed and implemented, including the shape and orientation of the building, the thermal and visual properties of the building envelope material, infiltration rate, and ventilation.

Several previous studies were conducted to understand the sensitivity of several passive measures on different building types and climate profiles. Chen *et al.* conducted a study to analyse the most influencing passive measures for a typical residential building in Hong Kong. According to this study, it is reported that window Solar Heat Gain Coefficient (SHGC) and window to floor ratio are the most sensitive parameters to thermal and visual comfort (Chen *et al.*, 2016). Jung *et al.* found that infiltration was the passive measures that most significantly influenced energy demand, environmental impact, and economic performance of a typical multi-storage residential building in South Korea (Jung *et al.*, 2021). A similar finding was also

reported in a study on a detached residential building in Niš, Serbia (Vukadinović *et al.*, 2021). Based on the results of this study, it was concluded that WWR was the key design parameter for cooling demand while glazing type is the key design parameter for thermal comfort.

Although sensitivity analysis on passive design strategies has been widely discussed, most studies are conducted on a building with temperate climate profiles (Köppen climate type C). Since exploration on this topic is rather limited for building in the tropics, especially in Indonesia, this study aims to identify the key design parameters in relation to passive design strategies which matter the most on building performance of a typical office building in Indonesia. The key design parameters that were identified from sensitivity analysis can be further used by building designer to focus design and optimisation on these fewer and most important design parameters. Furthermore, because most previous studies only focus on analysing the sensitivity of design variables based on energy demand, this study also involved thermal comfort and daylight availability as the evaluated performance parameter.

2. METHODS

2.1 Building energy and daylighting model

To understand the sensitivity of the most implemented passive design strategies for office buildings in the tropics, a hypothetical building from BESTEST study is used as a case study to represent an office building in this study. A hypothetical building is chosen since there are limited references and research that explain typical typologies and envelope properties of office buildings in Indonesia. In addition, because the hypothetical building performance data in the BESTEST study have been published and verified by many previous studies, the reported study results can be used for the validation and verification process of the model developed and used in this study. Since most buildings in Indonesia are heavy-weight buildings, BESTEST Case 900, a heavy-weight hypothetical building, was chosen and used as the case study. However, the internal heat gain in BESTEST Case 900 is assumed to be constant throughout the year and it does not represent the conditions that generally occur for office buildings in Indonesia. Therefore, the internal heat gain, operating hour, and temperature set point of the case study building is adjusted based on the Indonesian National Standard (SNI) 6390-2020 for Energy Conservation of Building Air Conditioning Systems (Badan Standardisasi Nasional (BSN), 2020).

Basic information of the base-case building model is provided in Table 1, while the building geometry is illustrated in Figure 1. Six performance metrics were employed in this study to assess the building performance. Cooling demand (E_c) and cooling degree hour (CDH) are the performance metrics which represent the energy performance of the building. To analyse the occupant thermal comfort during operational hour, the adaptive comfort model from ASHRAE 55-2004 standard was used since the case study building is a mixed-mode building. The percentage of comfort hours (PCH) is a metric employed to represent the occupant thermal comfort in this study. Three daylight availability metrics, namely spatial daylight autonomy ($sDA_{300,50\%}$), daylight factor (DF) and annual sun exposure ($ASE_{1000,250}$), are chosen in this study to explain the daylight condition inside the building. $sDA_{300,50\%}$ is defined as the percentage of a work plane that received at least 300 lux for at least 50 per cent of annual occupied hours. Equation (1) is used to calculate $sDA_{300,50\%}$

$$sDA_{300,50\%} = \frac{A_{DA300lx \geq 50\%}}{A_{total}} \times 100\% \quad (1)$$

Where $A_{DA300lx \geq 50\%}$ is the total work plane area that received at least 300 lux for at least 50 per cent of annual occupied hours, while A_{total} is the total area of the work plane (Illuminating Engineering Society (IES), 2020).

Daylight factor (DF), which is mathematically expressed in equation (2), is a static daylight availability metric that shows the ratio of inside luminance over outside luminance.

$$DF = \frac{E_{in}}{E_{ext}} \times 100\% \quad (2)$$

Where E_{in} is the total horizontal indoor luminance at the fixed point and E_{ext} represent the outside luminance under CIE overcast sky (Kubba, 2012). The higher the DF, the more daylight is available in the room.

The last daylight availability metric used in this study is $ASE_{1000,250}$, representing the annual risk of glare caused by direct sunlight during occupied hours. $ASE_{1000,250}$ is calculated using equation (3) as follow:

$$ASE_{1000,250} = \frac{A_{E1000lx \geq 250h}}{A_{total}} \times 100\% \quad (3)$$

Where $A_{E1000lx \geq 250h}$ is the total work plane area that received at least 1000 lux for at least 250 hours annual occupied hours and A_{total} is the total area of the work plane (Illuminating Engineering Society (IES), 2020).

The building geometry was modeled using *Rhinoceros* and *Grasshopper* platforms. This study also employed *Honeybee* (HB), which uses *EnergyPlus* for building energy and thermal comfort analysis, while *HoneybeePlus* (HB[+]) was used for daylight analysis. This study uses two *Radiance* ambient parameters for daylight analysis, shown in Table 2. The default setting was set in HB[+] for $sDA_{300,50\%}$ calculation, while the adjusted setting, which removed all reflections from all interior surfaces, was implemented for $ASE_{1000,250}$ calculation. To model the mixed-mode ventilation, the natural ventilation only operates during operating hours when the outdoor and indoor temperature meets the requirement which described in Table 1. If the outdoor and indoor air temperature is outside the specified boundary, then, the air conditioning system will be activated.

Aspects	Description
Location	Jakarta, Indonesia
Opaque envelope	Roof U-value: 0.33W/m ² K, solar absorptance: 0.6 Ceiling Reflectance: 0.8 Wall U-value: 0.56W/m ² K, solar absorptance: 0.6, reflectance: 0.5 Floors U-value: 1.92W/m ² K, solar absorptance: 0.6, reflectance: 0.2 Overhang Solar absorptance: 0.6, reflectance: 0.3
Windows	U-value: 3.00W/m ² K, SHGC: 0.789, visual transmittance: 0.84
Operating hours	07.00 – 18.00
Internal load	People: 0.057people/m ² , Lighting: 11.8W/m ² , Equipment: 10.3W/m ² , Infiltration: 0.5ach, Ventilation: 2.5L/s-person, 3.0L/s-m ²
Ventilation and air conditioning system	IdealAirSystem in <i>Honeybee</i> with cooling set point temperature at 26.0°C Natural ventilation is activated when outdoor air temperature is between 19.5°C – 25.0°C and indoor air temperature is between 21.5°C – 26.0°C.

Table 1. Basic information of the base-case building model

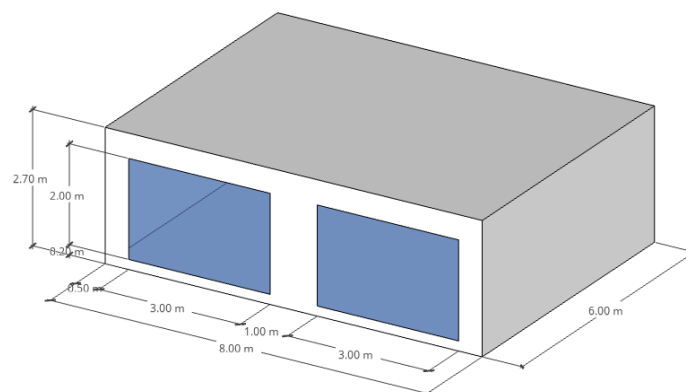


Figure 1. Geometry of the base-case building model

HB[+] default setting	HB[+] adjusted setting
-aa 0.2 -ab 5 -ad 15000 -ar 64 -as 2048 -dc 0.5 -dj 0.5 -dp 256 -ds 0.25 -dr 1 -dt 0.25 -I -lr 6 -lw 6.67e-07 -c 1 -ss 0.7 -st 0.5	-aa 0.0 -ab 0 -ad 512 -ar 16 -as 128 -dc 1.0 -dj 0.0 -dp 64 -ds 0.5 -dr 0 -dt 0.0 -I -lr 4 -lw 0.05 -c 1 -ss 0.7 -st 0.5

Table 2. Radiance parameter for daylight simulation and analysis using HB[+]

2.2 Sensitivity analysis

The variation of passive design strategies for sensitivity analysis is given in Table 3, which also describes the range of values for each input. These variables are assumed to have a uniform probability density function. This study only includes overhang as external shading strategy since it is the most common shading strategy to be implemented in commercial buildings in Indonesia. In addition to its characteristics that can provide a wider view factor, overhang is also considered quite effective in reducing glare and radiation potential since in the tropics the

sun position is mostly located overhead the building (Panghargiyo, 2019). A 480-input data set was generated using *Python pyDOE* library. The Latin-hypercube sampling (LHS) method was chosen due to efficient stratification properties and is generally used for sensitivity analysis using regression method (Tian, 2013). Standardised Regression Coefficient (SRC) is chosen for sensitivity analysis, since it is widely used for sensitivity analysis in building performance and is moderately computationally demanding (Tian, 2013).

However, since SRC can only be employed for uncorrelated input variables (Helton *et al.*, 2006; Tian, 2013), correlation analysis of the input variables sample needs to be done before performing sensitivity analysis. If a strong correlation between variables is founded, only one of the correlated variables is included in the sensitivity analysis so that the analysis process does not give an overestimated value. The Spearman rank correlation was used in this study to know the input variables correlation. The variables that are not significantly correlated are further analysed to find their sensitivity to the observed performance metric.

Variables	Initial	Unit	Lower bound	Upper bound	Resolution
Wall U-value	UWall	W/m ² K	0.31	0.58	0.001
Roof U-value	URoof	W/m ² K	0.15	0.40	0.001
Window U-value	UWin	W/m ² K	0.627	5.914	0.001
Window SHGC	SHGC		0.041	0.861	0.001
Infiltration rate	Infil	ach	0.33	2.02	0.01
Window visual transmission	TVis		0.021	0.899	0.001
Window-to-Wall Ratio	WWR	%	20	80	0.01
Orientation	OR	degree	0	315	45
Overhang depth	OD	m	0.0	1.5	0.01
Window height	HWin	m	1.0	2.0	0.01

Table 3. Parameters used for sensitivity analysis

3. RESULTS AND DISCUSSIONS

3.1 Correlation analysis

The Spearman rank correlation coefficient ($|r_s|$) of the tested input variables is presented in Table 4. The variables are assumed to have a strong correlation as $|r_s|$ closer to 1.00, and a weak correlation is represented with $|r_s|$ 0.00 to 0.39. Since the $|r_s|$ of all input variables are less than 0.39, the tested input variables are insignificantly-monotonic related to each other. Therefore, all the tested variables can be further involved for sensitivity analysis using SRC.

	UWall	URoof	UWin	SHGC	Infil	Tvis	WWR	OR	OD	HWin
UWall	1.00									
URoof	0.07	1.00								
UWin	0.02	0.02	1.00							
SHGC	0.01	0.03	0.03	1.00						
Infil	0.04	0.03	0.11	0.01	1.00					
TVis	0.07	0.02	0.03	0.01	0.04	1.00				
WWR	0.03	0.04	0.02	0.05	0.05	0.03	1.00			
OR	0.02	0.04	0.02	0.06	0.06	0.01	0.01	1.00		
OD	0.06	0.06	0.01	0.06	0.03	0.02	0.02	0.00	1.00	
HWin	0.07	0.01	0.03	0.00	0.06	0.04	0.03	0.02	0.06	1.00

Table 4. Spearman rank correlation coefficient ($|r_s|$) for the tested input variables

3.2 Sensitivity analysis results

The SRC data that was collected from the sensitivity analysis process is shown in Figure 2. As the absolute SRC ($|SRC|$) value is closer to 1, the design variable is assumed to influence the respected performance metric significantly. The sign of the SRC indicates the correlation of the design variables to the observed performance metrics. A positive SRC indicates that the design variable has a positive correlation between building performance, while a negative SRC indicates a negative correlation between design variables and performance metrics.

In terms of energy performance, which is represented by cooling demand (E_c) and CDH, WWR is the design variable with the highest $|SRC|$ followed by overhang depth and infiltration. The same design variables also appear to have high impact on thermal comfort. Based on the $|SRC|$ on the PCH, the results show that WWR is the key design parameter for occupant thermal comfort, followed by overhang depth and infiltration. Both WWR and infiltration positively correlate to cooling demand, CDH, and PCH, while the results show a negative correlation on infiltration to both energy performance metrics. A study by Tong *et al.*, which analysed the impact of several passive design variables on energy demand in a typical apartment building in Singapore, also reported a similar conclusion that WWR has the most significant impact on cooling demand and indoor air temperature (Tong *et al.*, 2021). However, if compared to the findings from other studies on buildings with a Köppen climate type C profile, WWR is not the key design parameter for the energy and thermal comfort performance, although it is one of the sensitive design parameters (Gou *et al.*, 2018; Jin and Overend, 2014).

Considering the daylight availability, window visual transmittance (TVis) is the design variable that has high correlation to $sDA_{300,50\%}$, and daylight factor (DF). However, if the daylight availability is analysed using annual sun exposure ($ASE_{1000,250}$), WWR has a higher correlation than window visual transmittance. Although WWR and visual transmittance plays an important role in determining the daylight availability in the room, the result of this study shows that WWR is a factor that needs to be considered first to prevent potential disturbing glare caused by direct sunlight. In contrast, window visual transmittance is a factor that needs to be considered to increase the daylight sufficiency in a room. This conclusion is in line with the results of a study by Jin and Overend, which also found that WWR and window visual transmittance are the most influencing design variables to daylight availability for an office building in London (Jin and Overend, 2014). Maltais and Gosselin also reported that WWR is the most influential design variable to the annual glaring index (AGI) for an office building in Montreal, Canada (Maltais and Gosselin, 2017). From the results of this study and other

references, window visual transmittance and WWR are the most influencing design factors on daylight availability regardless of the type of building and the type of climate in which the building is located.

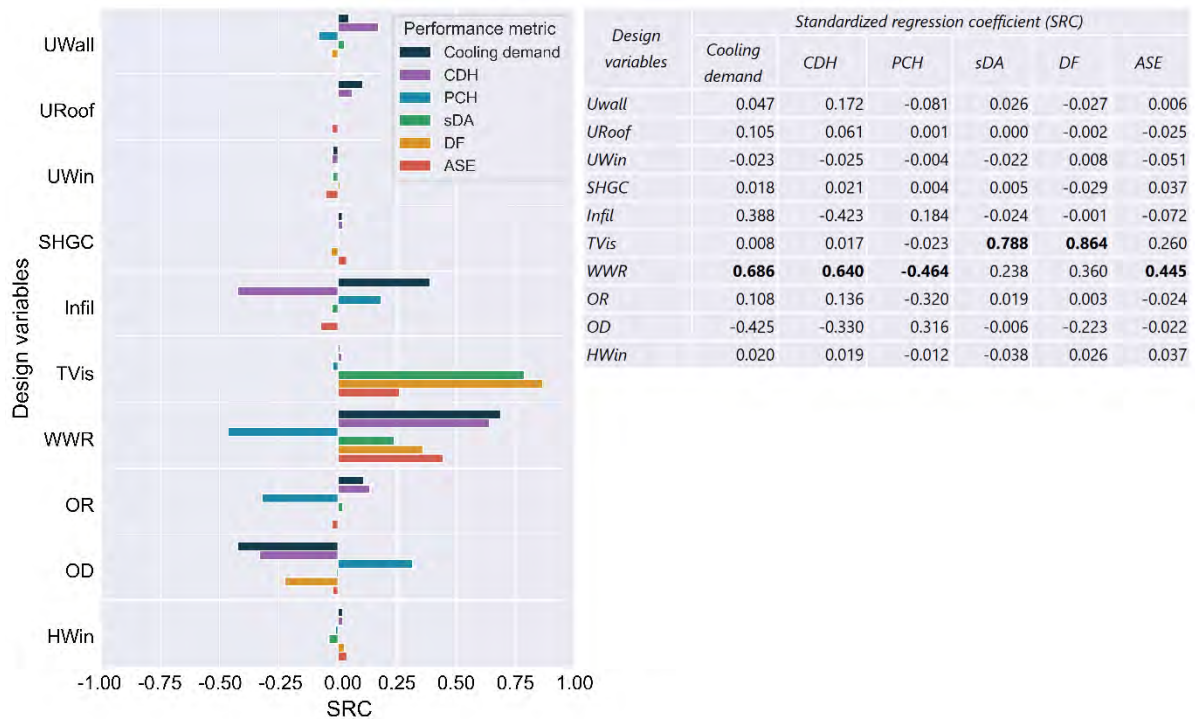


Figure 2. SRC of design variables on the respected performance metric

Figure 3 displays scatterplots of the input data set for the key design parameter against each observed performance metric. These graphs can also be used as an alternative reference for building designers to estimate the range of performance metrics that may be obtained if the design improvements are only implemented on the key design factor. The trend of input-output scatterplot data for the key design parameter to each performance metric is the steepest among other design variables. Comparing all the scatterplots of the observed design variables against each performance metric, the slope of the scatterplot trend is correlated with its $|SRC|$, where the smaller the $|SRC|$ of a design variable, the lower scatterplot gradient trend. Even more, design variables with $|SRC| < 0.5$ rather have a stagnant trend.

Besides, the results in Figure 3 show that the window transmittance coefficient appears to have a non-linear monotonic relation to $sDA_{300,50\%}$. Therefore, it is necessary to conduct sensitivity analysis of the case study using other sensitivity analysis methods, such as the standardised rank regression coefficient (SRRC). This limitation can be considered for future studies.

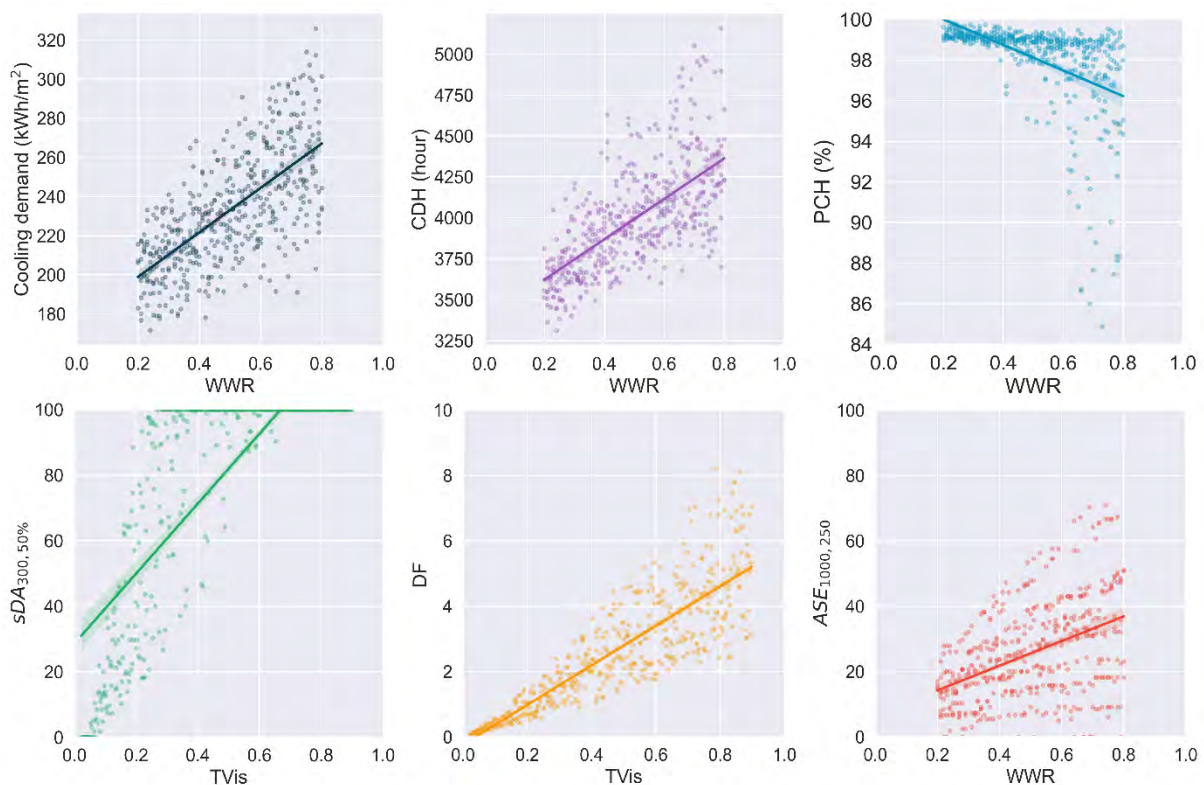


Figure 3. Relationship between key design parameter to the observed performance metrics

4. CONCLUSIONS

This study investigates the key passive design parameters for office buildings in the tropics, particularly in Jakarta, Indonesia. A hypothetical building based on BESTEST Case 900 was used as the case study. A sensitivity analysis using SRC was performed to understand the correlation between the observed passive design variable and the evaluated performance metric. Based on the sensitivity analysis results, WWR is the most influencing passive design variable to energy performance and thermal comfort with SRC 0.686, 0.640, and -0.464 for cooling demand, CDH, and PCH respectively. It also has a significant influence on controlling the amount of direct sunlight in a room that potentially causes disturbing glare. Meanwhile, window visual transmittance is the design parameter that significantly influences daylight availability in the building showed with SRC 0.788 and 0.864 for $sDA_{300,50\%}$ and DF respectively.

ACKNOWLEDGEMENTS

This work is supported by Ganesha Talent Assistantship Research Group (GTA-RG) and the Institute of Research and Community Service of Institut Teknologi Bandung (LPPM ITB) under the Riset Unggulan ITB 2021 Research Scheme.

REFERENCES

- Badan Standardisasi Nasional (BSN). (2020), *SNI 6390-2020 Konservasi Energi Sistem Tata Udara Bangunan Gedung*, Badan Standardisasi Nasional (BSN), Badan Standardisasi Nasional (BSN), Jakarta.
- Chen, X., Yang, H. and Sun, K. (2016), “A holistic passive design approach to optimize indoor environmental quality of a typical residential building in Hong Kong”, *Energy*, Vol. 113, pp. 267–281.
- Gou, S., Nik, V.M., Scartezzini, J.L., Zhao, Q. and Li, Z. (2018), “Passive design optimization of newly-built residential buildings in Shanghai for improving indoor thermal comfort while reducing building energy demand”, *Energy and Buildings*, Vol. 169, pp. 484–506.
- Helton, J.C., Johnson, J.D., Sallaberry, C.J. and Storlie, C.B. (2006), “Survey of sampling-based methods for uncertainty and sensitivity analysis”, *Reliability Engineering and System Safety*, Vol. 91, pp. 1175–1209.
- Illuminating Engineering Society (IES). (2020), “ANSI/IES LS-1-20, Lighting Science: Nomenclature and Definitions for Illuminating Engineering”.
- Jin, Q. and Overend, M. (2014), “Sensitivity of façade performance on early-stage design variables”, *Energy and Buildings*, Vol. 77, pp. 457–466.
- Jung, Y., Heo, Y. and Lee, H. (2021), “Multi-objective optimization of the multi-story residential building with passive design strategy in South Korea”, *Building and Environment*, Vol. 203, p. 108061.
- Kubba, S. (2012), “Chapter 7 - Indoor Environmental Quality”, in Kubba, S. (Ed.), *Handbook of Green Building Design and Construction*, pp. 313–360.
- Li, H., Wang, S. and Cheung, H. (2018), “Sensitivity analysis of design parameters and optimal design for zero/low energy buildings in subtropical regions”, *Applied Energy*, Vol. 228, pp. 1280–1291.
- Maltas, L.G. and Gosselin, L. (2017), “Daylighting ‘energy and comfort’ performance in office buildings: Sensitivity analysis, metamodel and pareto front”, *Journal of Building Engineering*, Vol. 14, pp. 61–72.
- Panghargiyo, M. (2019), “The Effect of Depth Shading Device on Inner Space Illumination in Jakarta”, *International Journal of Engineering, Technology and Natural Sciences*, Vol. 1 No. 1, pp. 23–29.
- Rabani, M., Bayera Madessa, H. and Nord, N. (2021), “Achieving zero-energy building performance with thermal and visual comfort enhancement through optimization of fenestration, envelope, shading device, and energy supply system”, *Sustainable Energy Technologies and Assessments*, Vol. 44, p. 101020.
- Tian, W. (2013), “A review of sensitivity analysis methods in building energy analysis”, *Renewable and Sustainable Energy Reviews*, Vol. 20, pp. 411–419.
- Tong, S., Wen, J., Wong, N.H. and Tan, E. (2021), “Impact of façade design on indoor air temperatures and cooling loads in residential buildings in the tropical climate”, *Energy and Buildings*, Vol. 243, p. 110972.
- Vukadinović, A., Radosavljević, J., Đorđević, A., Protić, M. and Petrović, N. (2021), “Multi-objective optimization of energy performance for a detached residential building with a

sunspace using the NSGA-II genetic algorithm”, *Solar Energy*, Vol. 224, pp. 1426–1444.

DISCLAIMER

The information or advice contained in these technical papers is intended for use only by professionals who have had adequate technical training in the field to which the paper relates. At the time of publication, these technical papers have undergone a formal peer-review process.

These documents have been compiled as an aid only, and the information or advice should be verified before it is put to use. The user should also establish the applicability of the information or advice in relation to any specific circumstances. While the information or advice is believed to be correct, no responsibility is taken by AIRAH or IBPSA Australasia for any statements made within.

AIRAH and IBPSA Australasia, its officers, employees and agents, disclaim responsibility for any inaccuracies contained within the documents, including those due to any negligence in the preparation and publication of the said technical papers.

COPYRIGHT

This work is copyright. Apart from any use as permitted under the Copyright Act 1986, no part may be reproduced by any process without prior written permission from either the Australian Institute of Refrigeration, Air Conditioning and Heating (AIRAH) or the International Building Performance Simulation Association (IBPSA) Australasia.

PREDICTION OF OCCUPANTS PERCEPTION OF NATURAL VENTILATION EFFECTIVENESS

LE LI

Lecturer

Victoria University

70/104 Ballarat Rd, Footscray VIC 3011

le.li@vu.edu.au

NIMA IZADYAR

Lecturer

Victoria University

70/104 Ballarat Rd, Footscray VIC 3011

nima.izadyar@vu.edu.au

TIM LAW

Lecturer

Victoria University

70/104 Ballarat Rd, Footscray VIC 3011

tim.law@vu.edu.au

KEIVAN BAMDAD

Lecturer

Western Sydney University

School of Engineering, Design and Built Environment Western Sydney University

Victoria Rd, Rydalmere NSW 2116

k.bamdad@westernsydney.edu.au

ABOUT THE AUTHOR

Le's research interests cover a wide range of topics, including durability assessment, life-cycle assessment of buildings, the built environment, and construction management.

In the area of durability and life-cycle assessment, Le has been working on deterioration models of construction materials (e.g., steel, concrete, etc.) under different environments from 2014–2018. From 2018–2019 he continued to work on service-life prediction and maintenance plan development for buildings under various loading and deterioration environments. And since 2021, Le has been working on the durability assessment of buildings using artificial intelligence techniques.

Le has used life-cycle assessment in the circular economy for the built environment since 2018. He has also worked on building defect detection (e.g., water leakage detection) using advanced visual technologies since 2022.

Apart from research experiences, Le also has industry experience working as a project coordinator at a construction company. This work has focused on quality management, health and safety management, and defect management.

ABSTRACT

Natural ventilation (NV) is an effective strategy to reduce building energy use and improve the indoor air quality. Prediction of occupants' perception of NV effectiveness can provide insights into better design of NV strategies in buildings. Accordingly, in this paper, firstly, data from influential variables on NV including balcony and room features along with demographic characteristics in 195 number of apartments was collected. Two datasets were then developed to represent apartments with single-sided and double-sided natural ventilation. Finally, a fuzzy neural network (FNN) developed to predict occupants' perception of the NV effectiveness. Results showed that FNN model can predict occupants' perceptions with over 90 per cent accuracy in our case studies.

INTRODUCTION

Climate changes due to greenhouse gas (GHG) emissions cast a significant threat to the public's health. It has become a worldwide concern across multiple disciplines, including architecture and built environment. Buildings consume 40% of the energy consumption and 30 per cent to 40 per cent of greenhouse gas (GHG) emissions worldwide (Izadyar et al. 2020). This consumption is largely due to the operation of heating, ventilation, and air condition (HVAC) systems (Izadyar et al. 2020). Apart from that, the frequent implication of the HVAC system can lead to poor ventilation, sick building syndrome, and respiratory diseases (Hiipakka and Buffington 2000). Therefore, it is necessary to implement a sustainable design as an alternative to the HVAC system. The design conserves building energy and provides a comfortable and healthy indoor environment.

Natural ventilation (NV) is one such design. NV is introducing fresh air into indoor spaces without using any mechanical system (e.g., ceiling fans) (Izadyar et al. 2020). It has its advantages against the HVAC system in reducing cooling/heating energy, maintaining adequate thermal comfort, and achieving acceptable indoor air quality (IAQ). Oropeza-Perez and Østergaard (2014) indicated that an efficient NV could lead to 801 to 1,035 million (USD) cost savings for residential buildings. Barbadilla-Martín et al. (2018) further suggested that building with an efficient NV design can lead to 27.5 per cent and 11.4 per cent energy savings during the cooling and heating period.

Although NV has its advantages compared to HVAC, the uncertainty of NV remains a challenging engineering issue (Barbadilla-Martín et al. 2018). The level of satisfaction of occupants against NV, referring to the occupants' perception of NV effectiveness, can be affected by many factors. They include floor plan, outdoor air quality, window configurations and so on (Izadyar et al. 2020). There are many relevant studies. For example, Van Hooff et al. (2012) quantified occupants' perception changes against floor plans through simulation. Chen et al. (2019) investigated the effect of outdoor air pollutants on occupants' perception and IAQ. Wu et al. (2021) investigated the effect of window type, size and location on the occupants' perception of NV effectiveness.

Despite numerous existing studies, there are still limitations. The balcony is desirable for providing fresh air, and in some states, this private open space (POS) is a mandated planning requirement for apartments. However, the added expense of designing for and installing a balcony still needs to be justified. This provides a basis for this exercise to predict the occupants' perception of NV effectiveness based on the balcony design, especially for buildings located in cooling dominant climates such as tropical and subtropical (Izadyar et al. 2020). In this paper, NV effectiveness is defined as the level of occupants' satisfaction (against cross and single-sided ventilation), and frequency of using mechanical ventilation system in a room

ventilated by the balcony. However, at this point there is no reliable algorithm which can predict the occupants' perception of NV effectiveness as a function of balcony design parameters (Izadyar et al. 2020). For example, Jin et al. (2016) and Omrani et al. (2017) estimated the effect of balcony type, depth, and wind direction on the occupants' perception. However, the perception can also be affected by the interaction among balcony and room features (e.g., floor plan, window configuration, etc.) (Jin et al. (2016). The interaction of a complex suite of parameters have not been considered in current studies.

To address this impact of multiple parameters, machine learning (ML) can be an efficient tool to predict the occupants' perception of NV effectiveness by knowing various influencing factors. The ML approach can properly analyse linear or non-linear relationships of data and is suitable for interpreting physical phenomenon (Wang and Elhag 2008). Therefore, it is suitable for solving complex engineering problems. However, limited studies have used ML to predict occupants' perception by considering the balcony and room features of the apartment. For example, Park et al. (2021) and Hiyama predicted occupants' perception against outdoor temperature, relative humidity, wind speed/direction, and solar radiation using various ML methods (e.g., random forest, support vector machine, etc.). The balcony and room features have not been considered in this study. It is also worth noting that occupants' perceptions can be imprecise and fuzzy. Therefore, the fuzzy neural network (FNN) becomes an effective ML method to predict this perception against its influencing factors.

Following the gaps summarised above, the objective of this paper is to develop an ML algorithm that predicts the occupants' perception of NV effectiveness by knowing the design features (especially the balcony features) of apartments in a sub-tropical climate. It is worth noting that the demographic characteristics of occupants (e.g., age, gender) can also affect the perception. Thus, they are also considered as inputs when developing the algorithm. Eight influencing factors are considered attributions for perception prediction. They are classified and processed with details summarised in section 1. The algorithm is then created based on a fuzzy neural network, with training and validation details summarised in section 2.

1. MACHINE LEARNING FRAMEWORK

The machine learning framework is developed in Figure 1, with details explained in sections 1.1 and 1.2.

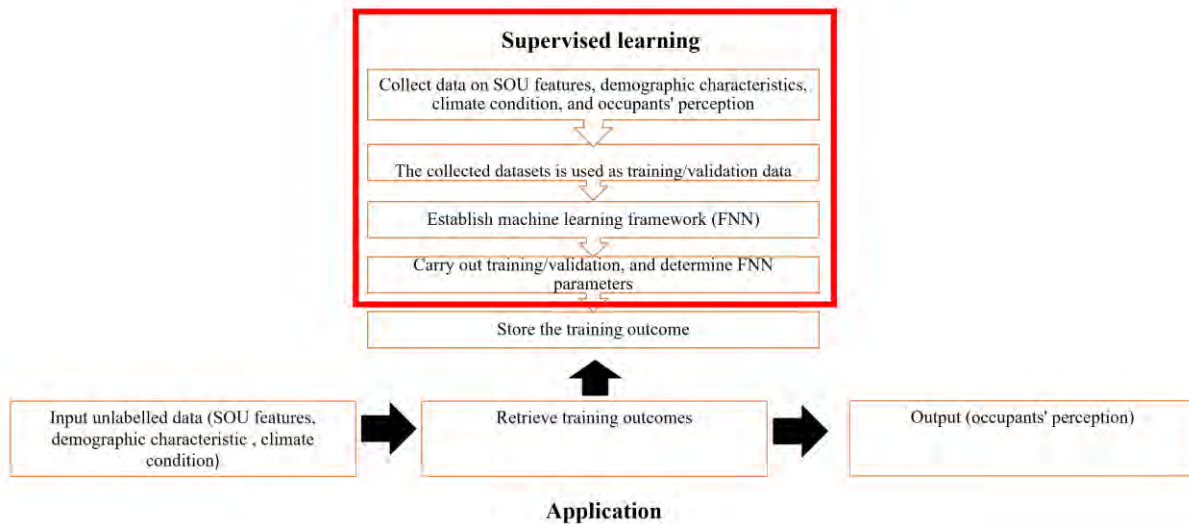


Figure 1. General machine learning framework

1.1 Critical design features affecting occupants' perception

The occupants' perception of NV effectiveness can be treated as a multiplication function of three parameters: balcony features (B_1), demographic features (B_2), and room features (B_3). The three parameters are determined by eight attributes (C_1 to C_8 in Figure 2). The authors' online survey shows that these attributes are dominate in determining occupants' perceptions. The details of the online survey will be published elsewhere. The hierarchy of three parameters and eight critical attributes is shown in Fig. 2. Precisely, balcony type C_1 reflects whether the balcony is open, semi-enclose, or fully enclosed. Balcony to room ratio C_3 is the balcony area to the floor area for each apartment. Windows condition C_6 refers to whether the window is openable for main balconies (balconies for the living room of apartment).

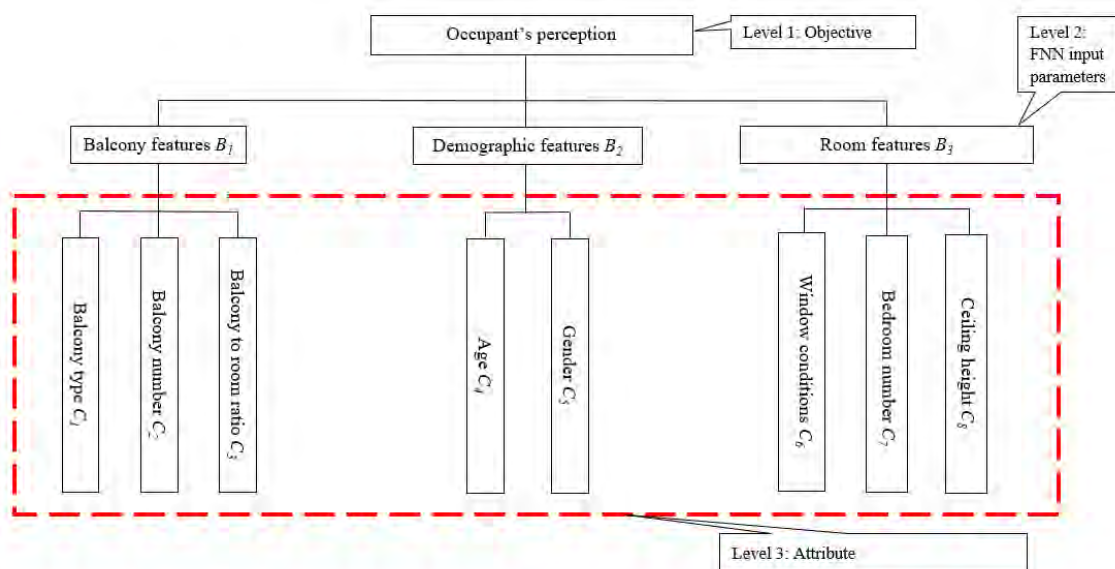


Figure 2. Hierarchy of the identified parameters and attributes

1.2 Proposed occupants' perception assessment

After the hierarchy is established, FNN is established as Figure 3 to assess the occupants' perception. The proposed framework consists of a data processing system and FNN assessment algorithms. Eight attributes (C_1 to C_8) are classified into B_1 to B_3 in the data processing system. The classification is based on the scoring system in the appendix (Tables 2 to 4). B_1 to B_3 are normalised into 0 to 1 range and then served as inputs for FNN. Doherty et al. (2007) summarise the normalisation procedure.

Quantified in Table 5, the outputs include occupants' perception of cross NV effectiveness D_1 , single-sided NV effectiveness D_2 , and HVAC usage frequency D_3 . Apartment has cross NV with openable windows ($B_3 \geq 30$ in Table 4). Otherwise, it has single-sided NV ($B_3 < 30$ in Table 4). Therefore, the setup of the FNN analysis is shown in Figure 3 to differentiate these two NV types based on B_3 . The FNN is calculated through the adaptive neuro-fuzzy inference system (ANFIS) using the MATLAB toolbox (first-order Sugeno fuzzy model). The setup of ANFIS toolbox (i.e., membership function and rules) follows Wang and Elhag (2008) and four ANFISs are established (ANFIS 1 to 4) to determine D_1 , D_2 , and D_3 under different NV types (Figure 3).

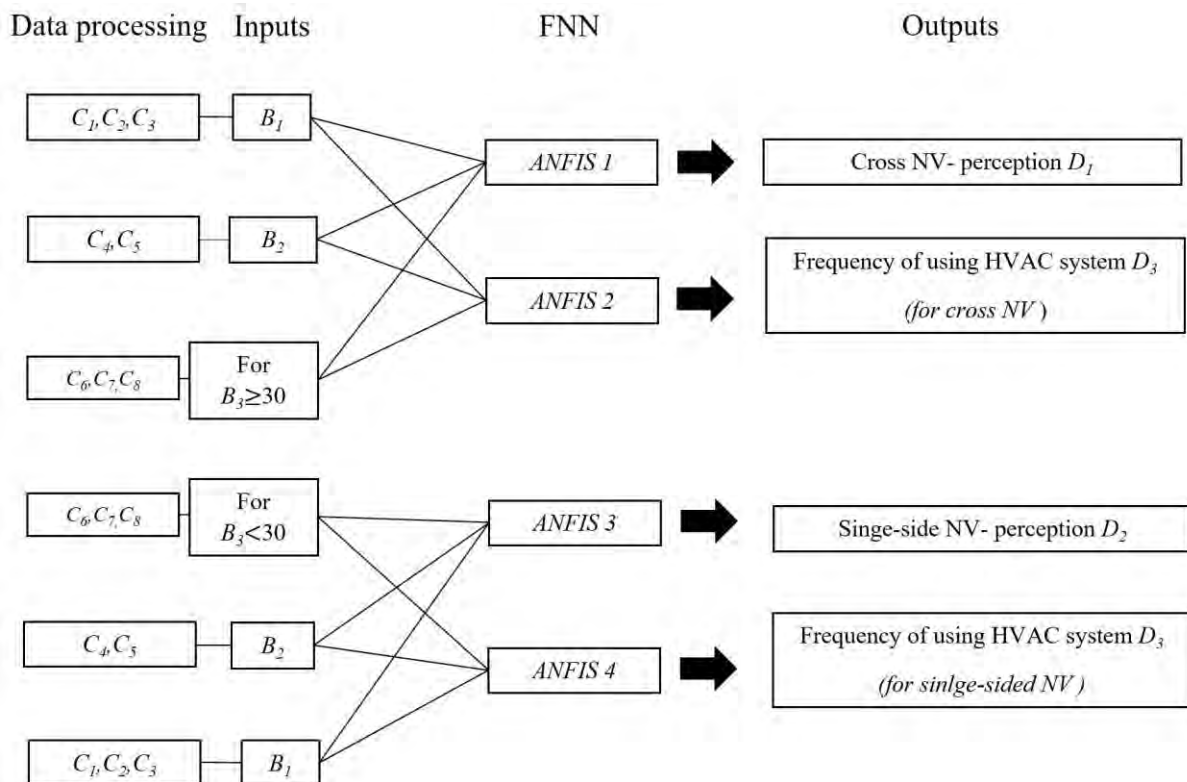


Figure 3. Occupants' perception configuration

2. ML TRAINING AND DISCUSSION

The methodology shown in Figures 1 to 3 is applied to apartments in Brisbane to illustrate its applicability. 195 different data groups are collected through a questionnaire survey. They are split into two datasets based on B_3 : 70 samples for cross NV perception prediction (ANFISs 1 and 2), and 125 samples for single-sided NV perception prediction (ANFISs 3 and 4). The 70 and 125 samples are further split into 50 and 20, and 100 and 25 samples for training and testing

datasets in each case. Figure 4 shows the model structure of the FNN that is built for occupants' perception assessment.

After data normalisation, we choose two generalised bell-shaped membership functions for B_1 , B_2 , and B_3 to build FNN for ANFISs 1 to 4, which leads to 8 if-then rules to be learned in each ANFIS. The training is carried out at 1000 epochs for each ANFIS. The membership functions (shown in Figure 5) and rules are explained in Wang and Elhag (2008).

After training, the testing dataset is input into each ANFIS. Coefficient of determination (R^2) is determined among predicted and actual value from the survey, with results shown in Table 1. It can be seen from Table 1 that R^2 is 0.96, 0.95, 0.91, and 0.94 for ANFIS 1, 2, 3, and 4. This indicates a high correlation between all actual and predicted values. Additionally, root mean squared error (RMSE) between actual and predicted values are also calculated as follows:

$$\text{Root Mean Squared Error (RMSE)} = \left(\frac{1}{n} \sum_{i=1}^n (y_i - \hat{y})^2 \right)^{\frac{1}{2}} \quad (1)$$

where actual value and predicted value are indicated by y_i , and \hat{y} , respectively. n is the several sample points. Specifically, $n = 20$ for ANFISs 1 and 2 and $n = 25$ for ANFISs 3 and 4 in this case. Based on Equation (1), RMSE can be determined as 0.13, 0.63, 0.36 and 0.36 for ANFISs 1 to 4. The RMSE values further indicate that the proposed framework could accurately predict occupants' perceptions.

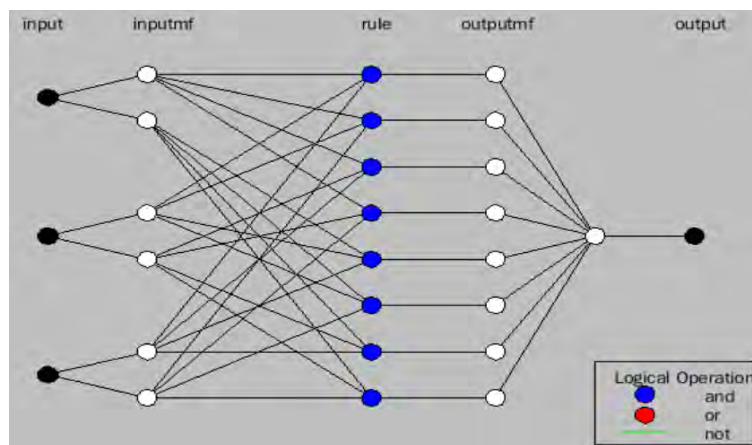


Figure 4. Set up of FNN neural network (ANFIS 1 as the example)

ANFIS	R^2	RMSE
1	0.96	0.13
2	0.95	0.63
3	0.91	0.36
4	0.94	0.36

Table 1. Prediction accuracy of ANFISs 1 to 4

CONCLUSION

This paper aimed to develop a machine learning model that predicts the occupants' perception of NV effectiveness for apartments in a sub-tropical climate (Brisbane). The model used eight variables that affect the occupants' perception, including the balcony type, the number of balconies, balcony to room ratio, age and gender of residents, window condition, bedroom number, and ceiling height of the apartment. Two datasets were created based on survey data collected in Brisbane representing apartments with single sided and cross natural ventilations. FNN neural network was then developed to predict the occupants' perception of NV effectiveness in apartments with two NV configurations: single-sided and cross ventilation. Four adaptive neuro-fuzzy inference systems have been developed (i.e., ANFIS 1 to 4) with the same setups including the neural network structure, initial parameters, functions, and rules. The only differences among these four ANFIS networks lie in the inputs and outputs, and they are trained with different databases. It was found that the FNN neural networks can predict occupants' perception of NV effectiveness (from 0 to 5) and HVAC usage frequency (level 0 to 4) with high accuracy.

REFERENCES

- Barbadilla-Martín, E., Martín, J.G., Lissén, J.M.S., Ramos, J.S. and Domínguez, S.Á (2018). Assessment of thermal comfort and energy savings in a field study on adaptive comfort with application for mixed mode offices. *Energy and Buildings*, 167, 281-289.
- Chen, J., Brager, G.S., Augenbroe, G. and Song, X (2019). Impact of outdoor air quality on the natural ventilation usage of commercial buildings in the US. *Applied energy*, 235, 673-684.
- Doherty, K.A.J., Adams, R.G. and Davey, N (2007). Unsupervised learning with normalised data and non-Euclidean norms. *Applied Soft Computing*, 7(1), 203-210.
- Hiipakka, D.W. and Buffington, J.R (2000). Resolution of sick building syndrome in a high-security facility. *Applied Occupational and Environmental Hygiene*, 15(8), 635-643.
- Hiyama, K., Takeuchi, K., Omodaka, Y. and Srisamranrungruang, T (2022). Operation strategy for engineered natural ventilation using machine learning under sparse data conditions. *Japan Architectural Review*, 5(1), 119-126
- Izadyar, N., Miller, W., Rismanchi, B. and Garcia-Hansen, V (2020). Impacts of façade openings' geometry on natural ventilation and occupants' perception: a review. *Building and Environment*, 170, 106613.
- Jin, R., Hang, J., Liu, S., Wei, J., Liu, Y., Xie, J. and Sandberg, M (2016). Numerical investigation of wind-driven natural ventilation performance in a multi-storey hospital by coupling indoor and outdoor airflow. *Indoor and Built Environment*, 25(8), 1226-1247.
- Oropeza-Perez, I. and Østergaard, P.A (2014). Energy saving potential of utilizing natural ventilation under warm conditions—A case study of Mexico. *Applied energy*, 130, 20-32.
- Omrani, S., Garcia-Hansen, V., Capra, B.R. and Drogemuller, R (2017). On the effect of provision of balconies on natural ventilation and thermal comfort in high-rise residential buildings. *Building and Environment*, 123, 504-516.
- Park, H. and Park, D.Y (2021). Comparative analysis on predictability of natural ventilation rate based on machine learning algorithms. *Building and Environment*, 195, p.107744.
- Van Hooff, T. and Blocken, B (2012). Full-scale measurements of indoor environmental conditions and natural ventilation in a large semi-enclosed stadium: possibilities and
- Australasian Building Simulation 2022 Conference, Brisbane, July 20-21*

limitations for CFD validation. *Journal of Wind Engineering and Industrial Aerodynamics*, 104, 330-341.

Wu, Y., Gao, N., Niu, J., Zang, J. and Cao, Q (2021). Numerical study on natural ventilation of the wind tower: Effects of combining with different window configurations in a low-rise house. *Building and Environment*, 188, p.107450.

Wang, Y.M. and Elhag, T.M (2008). An adaptive neuro-fuzzy inference system for bridge risk assessment. *Expert systems with applications*, 34(4), 3099-3106.

APPENDIX

C₁	C₂	C₃	B₁
Open	>3	>30%	90
		20-30%	85
		<20%	80
	1-2	>30%	75
		20-30%	70
		<20%	65
Semi-enclosed	>3	>30%	60
		20-30%	55
		<20%	50
	1-2	>30%	45
		20-30%	40
		<20%	35
Enclosed	>3	>30%	30
		20-30%	25
		<20%	20
	1-2	>30%	15
		20-30%	10
		<20%	5
No balcony			0

Table 2. *Determination of balcony score*

C₄	C₅	B₂
Senior-aged adults (>45)	Male	30
	Female	25
Middle-aged adults (25-45)	Male	20
	Female	15
Young Adults (<25)	Male	5
	Female	0

Table 3. *Determination of occupants score*

Windows condition (Main balcony) C ₆	Bedroom number C ₇	Ceiling height C ₈	Other building design features B ₃
Openable	≤ 2	>2.7	55
		2.4 – 2.7	50
		<2.4	45
	> 2	>2.7	40
		2.4 – 2.7	35
		<2.4	30
No openable	≤ 2	>2.7	25
		2.4 – 2.7	20
		<2.4	15
	> 2	>2.7	10
		2.4 – 2.7	5
		<2.4	0

Table 4. Determination of other building design features

Item	Level	Value
D₁	Cannot define	0
	Ineffective	1
	Ineffective-neural	2
	Neural	3
	Neural-effective	4
	Effective	5
D₂	Cannot define	0
	Ineffective	1
	Ineffective-neural	2
	Neural	3
	Neural-effective	4
	Effective	5
D₃	Cannot define	0
	Rarely	1
	Sometimes	2
	Ofen	3
	Always	4

Table 5. Determination of output value

DISCLAIMER

The information or advice contained in these technical papers is intended for use only by professionals who have had adequate technical training in the field to which the paper relates. At the time of publication, these technical papers have undergone a formal peer-review process.

These documents have been compiled as an aid only, and the information or advice should be verified before it is put to use. The user should also establish the applicability of the information or advice in relation to any specific circumstances. While the information or advice is believed to be correct, no responsibility is taken by AIRAH or IBPSA Australasia for any statements made within.

AIRAH and IBPSA Australasia, its officers, employees and agents, disclaim responsibility for any inaccuracies contained within the documents, including those due to any negligence in the preparation and publication of the said technical papers.

COPYRIGHT

This work is copyright. Apart from any use as permitted under the Copyright Act 1986, no part may be reproduced by any process without prior written permission from either the Australian Institute of Refrigeration, Air Conditioning and Heating (AIRAH) or the International Building Performance Simulation Association (IBPSA) Australasia.

OPTIMISATION OF ECONOMY CYCLE OPERATION AND SUPPLY AIR TEMPERATURE CONTROL FOR VAV SYSTEMS

DR PAUL BANNISTER FIBPSA FIEAUST LAIRAH

Director of Innovation
DeltaQ Pty Ltd
paul.bannister@dqcs.com.au

HONGSEN ZHANG

Director
Enerefficiency Pty Ltd
hongsen.zhang@enerefficiency.com

ALISHA GARG

Intern
DeltaQ Pty Ltd

ABOUT THE AUTHOR

Dr Paul Bannister is one of Australia's leading experts in energy efficiency in buildings. He was the primary author or significant contributor to all the NABERS Energy and Water tools, and in 2017–18 led the significant update of energy-efficiency provisions for Volume 1 of the 2019 National Construction Code. He was awarded AIRAH's James Harrison Medal in 2021 for his outstanding contribution to the field of air conditioning

ABSTRACT

A range of supply air temperature control strategies for a VAV-serviced office building is tested via simulation across three major temperate Australian climate zones. This is used to determine the extent to which the modulation of supply air temperature control affects the effectiveness of economy cycle operation on an annual basis. The results show some worthwhile improvements in economy cycle savings but limited ability to assess *a priori* whether a given approach will work well. On this basis, at least while fixed annual controls are retained, it is concluded that the primary challenge for economy cycle optimisation is to avoid a poor outcome rather than finding the perfect optimised control.

1. INTRODUCTION

Large commercial buildings in temperate Australia commonly use variable air volume (VAV) air conditioning systems. This preference is also common in the US but is not universal; the UK and Europe, for instance, strongly prefer fan coil systems. From an energy efficiency perspective, one of the key benefits of any system that uses air as its primary form of heat transport is that it can use an economy cycle. Economy cycle is a process whereby outside air provides “free cooling” in the right conditions. This is achieved by increasing the outside air

supply from the statutory minimum (in Australia, 7.5-10 l/s per person, equating to typically around 1 l/s per m² in a typical office) to full airflow (typically between 2.5-5 l/s per m² for centre zones and 4-7 l/s per m² for perimeter zones in a typical office), while rejecting the equivalent volume of relief air from the building.

The benefits of economy cycle control have been calculated via simulation to be in the region of 8-10 per cent of total HVAC energy use in temperate Australia [Bannister and Zhang, 2014]; correlative studies of empirical performance indicated that the presence of economy cycle correlates with a 0.6-star improvement in NABERS base building ratings [Bannister et al 2009]¹. A further benefit, especially salient in the post-COVID era, is the significant increase in ventilation rate that occurs while the economy cycle is in operation.

Bannister and Zhang (2014) also demonstrated that the savings associated with economy cycle can be significantly eroded by control configurations that unnecessarily limit the times at which the control can operate². Furthermore, given the mechanical ability of an economy cycle to flood the building with outside air when it is not beneficial, the presence of an economy cycle is not without risk to building performance.

Previous work by the authors has focussed firstly on economy cycle enablement criteria [Bannister and Zhang 2014] and latterly on supply air temperature control [Bannister and Zhang, 2015]. In this paper, the question of supply air temperature control is examined further, with particular emphasis on the benefits of decoupling the economy cycle and cooling coil for supply air temperature control.

1.1 Purpose of this paper

This paper aims to test supply air temperature control strategies to optimise the energy savings achieved via economy cycle operation, for variable air volume systems.

The analysis is based on simple reset controls for supply air temperature as used in industry.

In the analysis presented below, the conditions of economy cycle enablement are considered to be resolved and are not examined further.

2. ECONOMY CYCLE CONTROLS

In general, the HVAC industry lacks conventions concerning the detail of HVAC control, resulting in a divergence of practices. In Australia, anecdotally, this situation appears to have improved somewhat over the past decade due to the impact of NABERS, which has led to some refinement and convergence in control practices in parts of the office sector at least. Nonetheless, this remains largely undocumented.

The common structure of most economy cycle controls is:

1. Economy cycle is enabled when outside conditions are suitable. Typically, the economy cycle is enabled when the outside air is cooler than the return air temperature, with additional considerations for humidity either in the form of a dewpoint lockout or outside air/return air enthalpy comparison to ensure that excessive latent loads are not brought into the building. A dry bulb temperature

¹ It is important to recognize that this result indicates that *system types with economy cycles* perform better than those without; the 0.6 stars improvement is not necessarily due to the presence of an economy cycle alone.

² Typically through lockouts based on outdoor temperature and humidity

lockout is often added as a failsafe against the accidental operation of economy cycle in grossly unsuitable conditions.

2. The economy cycle operates to achieve the supply air setpoint as a first stage of cooling ahead of the cooling coil. This is normally achieved by using a PI/PID loop for the supply air temperature loop in which the first stage of control operates the economy cycle from 0-100 per cent, and the second stage opens the chilled water valve 0-100 per cent. This ensures that the economy cycle is fully utilised before the chilled water is used.

External references for economy cycle control are relatively rare:

- AIRAH (2011) published guideline control sequences. The supply air temperature control used a reset schedule that reduces the supply air temperatures from 23°C to 12°C (or system minimum) as the control zone temperature ranges from 21°C to 24°C.
- ASHRAE Guideline 36 (2018) presents a supply air temperature control that combines a supply air temperature reset from 18°C to system minimum as the outdoor air temperature varies from 16°C to 21°C. It also incorporates a test and respond control to vary the supply air temperature between this reset and the minimum to meet control zone cooling requirements. The guideline notes that tuning of these variables is required on a case-by-case basis.

The situation is further complicated by the limitations of simulation packages in representing supply air temperature control (without going into more complex programming modes). For the two most used packages in Australia:

- IES<VE>2021 can undertake supply air temperature control based on resets that provide a fixed relationship between supply air temperature and other variables. This enables it to provide a good representation of many common simple controls.
- Energy Plus³ provides a control method (Setpoint Manager: Warmest) that calculates the supply air temperature that meets the maximum loads on the system at maximum zone flow.

Notably, neither of these packages can fully represent the control from ASHRAE Guideline 36. Furthermore, the Energy Plus algorithms are based on the knowledge of the zone loads, which is data unavailable to a real control system. As a result, the Setpoint Manager: Warmest configuration can only be approximated in real building controls.

2.1 The theoretical case for decoupling

When considering the question of supply temperature control for VAV systems, it is necessary to consider the competing factors at play, as summarised in Table 1.

In chiller-only operation (i.e. cooling without economy cycle), the high sensitivity of fan energy to flow leads to the general industry position that low flow/low-temperature operation is preferable. However, in economy operation, the situation is more complex, as there is a decision point that relates to when it is more efficient to use the chiller to reduce the supply air temperature and maintain the current air supply volume than to increase the air volume at fixed supply air temperature.

³ Observation based on available documentation at <https://bigladdersoftware.com/epx/docs/8-7/engineering-reference/setpoint-managers.html>. Other control methods are available but are not applicable to the problem investigated here.

Impact on HVAC energy use			
Energy Use Factor	Lower supply air temperature	Higher supply air temperature	Scale of effect
Fan energy	Lower	Higher	High (fan energy typically x^2 - $x^{2.7}$ with flow)
Reheat energy	Higher (overcooling risk in low load zones)	Lower	High, depending on reheat control and load diversity
Chilled water load	Higher (lower temperature and off-coil velocity leads to increased latent cooling)	Lower	Secondary (basic load is still the same)
Chiller efficiency	Lower (assuming chilled water temperature reset in place)	Higher (assuming chilled water temperature reset in place)	Secondary (2-5% improvement in chiller efficiency per 1°C increase in chilled water temperature)

Table 1. *Competing energy use factors relating to supply air temperature*⁴

This decision point can be characterised simplistically, as follows.

The electrical energy E_{ch} (kW) used by the chiller to produce cooling effect Q (kW) at an efficiency characterised by COP is:

$$E_{ch} = \frac{Q}{COP}$$

Equation 1

For the economy cycle, the energy use E_f (kW) is driven by the fan, i.e.

$$E_f = \alpha \dot{m}^n$$

Equation 2

Where α is a constant, \dot{m} is the mass flow (kg/s), and n is the fan exponent (typically around 2.7). Unfortunately, α is not a readily available figure, so it is helpful to find a way to adjust this equation to relate to design variables. In this context, we can also characterise the fan power as follows:

$$E_{f,d} = \beta \dot{m}_d = \beta \rho \dot{v}_d$$

Equation 3

Where \dot{v}_d is the design volumetric flow of the fan (m^3/s , subscript d designating that this is the design flow) and ρ is the density of air (kg/m^3), and β is a constant of units $kW/(kg/s)$, which is related to the specific fan power or SPF (kW/m^3 , or equivalently $W/(l/s)$) as follows:

⁴ Observations in this table are based on the simulation work conducted for this paper and are intended as general indications to assist in understanding of general system behaviour. Individual systems may have different behaviour.

$$\beta = \frac{SPF}{\rho}$$

Equation 4

Note that for this analysis, the energy fan variables need to be based on the combined supply and return fan energy. This can be readily calculated from design data. We can therefore re-express α in terms of β as follows:

$$E_{f,d} = \alpha(\dot{m}_d)^n = \beta\dot{m}_d \Rightarrow \alpha = \frac{\beta}{(\dot{m}_d)^{n-1}}$$

Equation 5

The cooling energy Q (kW) delivered by the economy cycle (with no chiller cooling) is:

$$Q = \dot{m}\Delta h$$

Equation 6

Where Δh (kJ/kg) is the enthalpy difference between the space and the outside. Thus, the energy use of the system in economy cycle with no chiller operation is:

$$E_f = \alpha(\dot{m})^n = \frac{\beta}{(\dot{m}_d)^{n-1}} \left[\frac{Q}{\Delta h} \right]^n$$

Equation 7

Note that all factors in this equation other than Q are independent of Q .

In seeking the point at which an incremental increase in Q is more efficiently served by the chiller than the increased fan energy associated with remaining in economy cycle we are seeking to identify the situation where:

$$\frac{\partial E_f}{\partial Q} \geq \frac{\partial E_{ch}}{\partial Q}$$

Equation 8

As the right-hand side of the equation is $1/COP$:

$$\frac{\partial E_f}{\partial Q} = \frac{\beta}{(\dot{m}_d)^{n-1}} n \left[\frac{Q}{\Delta h} \right]^{n-1} \frac{1}{\Delta h} \geq \frac{1}{COP}$$

Equation 9

This implies:

$$\frac{\beta}{(\dot{m}_d)^{n-1}} n(\dot{m})^{n-1} \frac{1}{\Delta h} \geq \frac{1}{COP}$$

Equation 10

Which simplifies to:

$$\left(\frac{\dot{m}}{\dot{m}_d} \right)^{n-1} \geq \frac{\Delta h}{n\beta COP}$$

Equation 11

If we assume that the temperature and pressure conditions are not too far departed from the design conditions then the left-hand side of the equation is equal to the flow fraction raised to the $(n-1)^{\text{th}}$ power⁵. So the partial flow % flow at which the chiller becomes a better solution than the economy cycle is:

$$\text{part flow} \geq \sqrt[n-1]{\frac{\Delta h}{n\beta\text{COP}}}$$

Equation 12

In practice, this means that there is a percentage flow for a given AHU above which it is no longer economical to increase airflow. This flow limit:

- increases when Δh is large, i.e. the outside air is much cooler than the inside air; and conversely
- decreases as Δh decreases, i.e. the outside air temperature approaches the indoor air temperature.

Equipment efficiency also plays a predictable role: a more efficient chiller or a less efficient fan system will reduce the part flow limit.

In practice, the part flow figure turns out to only be below 100% at relatively low values of Δh , as shown in Figure 1.

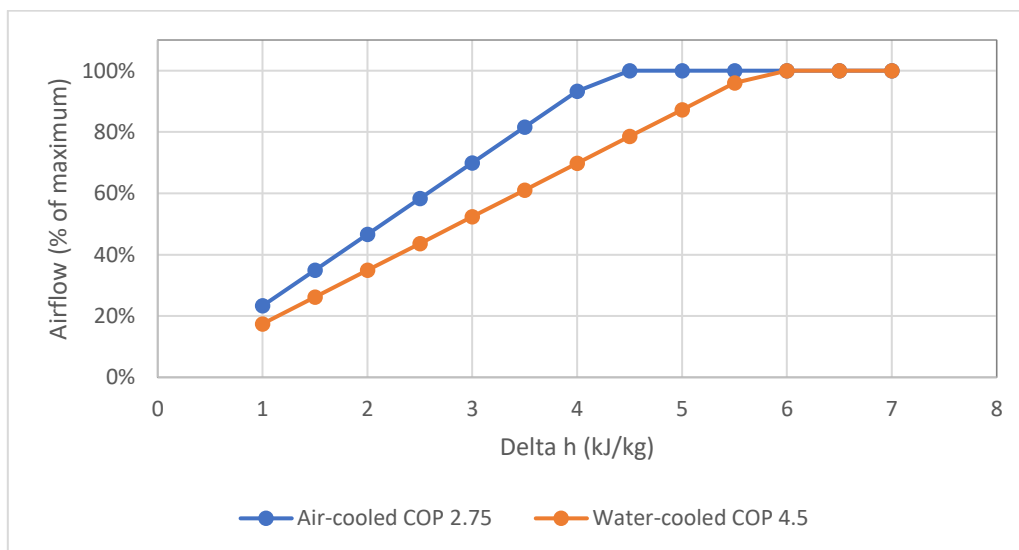


Figure 1. Values of the critical part flow value above which the chiller becomes more efficient than increased economy cycle usage. For this graph β has been set to 1.6 and $n=2.7$

The implication from this is that it is preferable to maintain full economy cycle operation – with no chiller operation, right down to the region of a Δh of 4-6kJ/kg, which is typically around 2-3°C difference between return air and outside air.

This simplistic analysis does not consider the issues associated with latent cooling. Still, it does provide *a priori* indication that a high temperature, high flow configuration is potentially

⁵ The impact of this assumption is typically less than 10% of the final part flow figure (i.e. for a part flow of 50% it would be 5%), which is within the bounds of error; the impact is nearly always a reduction in the part flow threshold..

beneficial in economy cycle, in contrast to the use of low temperature, low flow in chiller-only operation. This, in turn, implies that there may be a benefit in decoupling the control of supply air temperature (for both the economy cycle and the chilled water coil, separately) from that of the chilled water coil in non-economy cycle operation. However, it does not indicate the scale of that benefit.

3. SIMULATION ANALYSIS

Simulations for this project were conducted in IES<VE>, using the model as outlined in the Appendix to this paper. IES is accredited under ASHRAE140, BESTEST and EN13791 and ISO52000 and, importantly, is well configured to represent supply air temperature controls using reset schedules in a manner very similar to how they are used in real buildings.

The analysis commenced with an open-ended exploration of the impact of a wide range of supply air temperature schedules and some variants of system configuration on performance, as described in Section 3.1. This was followed by a more specific analysis of candidate supply air temperature resets that appeared to perform best from the exploratory work, as presented in Section 3.2.

3.1 Initial problem exploration

An extensive initial exploration of possible supply air temperature effects was conducted to understand the energy impacts of the key control parameters. This exploration included 18 to 21 scenarios per climate zone of different arrangements of supply air temperature control for the economy cycle and chilled water coil control, focussing mainly on adjusting the centre point of the respective resets. Most scenarios used 0.5°C control zone reset ranges, although a set of 2°C reset range scenarios was also included. All scenarios featured the same VAV configuration with a heating proportional band from 21-21.5°C and a cooling proportional band from 23.5-24°C.

The depth and complexity of the results from this exploration indicate considerable scope for further study and control nuance to be explored, much of which would appear to lie beyond the scope of current industry control practice. For this paper, however, a decision was made to focus on what can be achieved while maintaining simple approaches that reflect current industry practice. In this context, it was found that:

- Different AHUs serving different thermal characteristics typically (but not uniformly) exhibited the same behaviours concerning energy use relative to various setpoint combinations. This indicates that using a generic control sequence for all AHUs is not incompatible with a reasonable efficiency outcome. A notable exception was when the centre zone AHU was reconfigured to have no reheat (i.e. all heating at the AHU) and average temperature control (as appropriate for AHUs without reheat). This is discussed further below.
- The position of the economy cycle reset had little influence on cooling-related energy use. This is important as the authors had previously thought that a lower temperature economy cycle reset would provide a worthwhile precooling benefit by operating the building at a lower overall temperature during the availability of economy cycle cooling. Indeed, it was found that such a benefit does exist but is massively outweighed by the increased use of reheat caused by the lower supply air temperature, even in a well-zoned building with limited load diversity. It would be

expected that this problem would be exacerbated in a real building with significant diversity in occupancy.

- The use of average rather than high select control⁶ reduced the optimum temperature range for the economy cycle reset. This is unsurprising as the average temperature will tend to be lower than the high select temperature.
- There was a mild energy benefit obtained from operating the cooling coil reset in economy cycle operation so as to prefer higher air volumes and higher supply air temperatures, as suggested by the analysis in Section 2. This is due to the fan energy penalty being less than the chiller energy penalty in meeting the higher loads. For the test building, this corresponded to the cooling coil reset operating between 23.5-24°C, which is the same temperature range as the zone-level VAV cooling proportional band.
- In periods when economy cycle was not available, it was found preferable to engage the cooling coil at a lower temperature to maintain a low temperature/low flow configuration. For the test building, this generally led to a cooling coil reset in the range 23-23.5, which implies minimum temperature operation being achieved before the high-select zone reaches its cooling proportional band.
- Different climates resulted in different optimum control configurations, although a small set of control configurations tended to perform close to optimally across all three climates.

Based on these findings, the control configurations shown in Table 2 were selected to represent the best outcomes. These configurations are constrained to fixed reset schedules that are (largely) constant between air handlers and are unchanged throughout the year.

⁶ Average control uses the average zone temperature to drive the supply air temperature reset, and is a strategy generally better suited to systems where VAV terminals have no reheat, such as centre zone AHUs. Hi-select control uses the warmest zone for the AHU to drive the supply air temperature, and is generally used for AHUs where the VAV terminals have reheat available.

Model	Control Strategy	Economy Cycle Reset Range (°C)	Cooling Coil Reset Range (°C) (Econ ON)	Cooling Coil Reset Range (°C) (Econ OFF)
SC01	Base case	21.5 to 23.5	21.5 to 23.5	21.5 to 23.5
SC02	Base case no economy cycle	N/A	21.5 to 23.5	21.5 to 23.5
SC03	Improved simple reset ⁷	22 to 24	22 to 24	22 to 24
SC04	Decoupled economy cycle controls	22.5 to 23	23 to 23.5	23 to 23.5
SC05	Fully decoupled controls	22.5 to 23	23.5 to 24	23 to 23.5
SC06	Centre Zone AHU adjusted controls	22 to 22.5	23.5 to 24	23 to 23.5
	Fully decoupled controls (all other AHUs)	22.5 to 23	23.5 to 24	23 to 23.5

Table 2. Control strategies used. Economy cycle reset range is the range of control zone temperatures over which the economy cycle airflow modulates from 0% to 100%. The cooling coil reset range is the control zone temperatures over which the chilled water coils are modulated from 0% to 100% of capacity

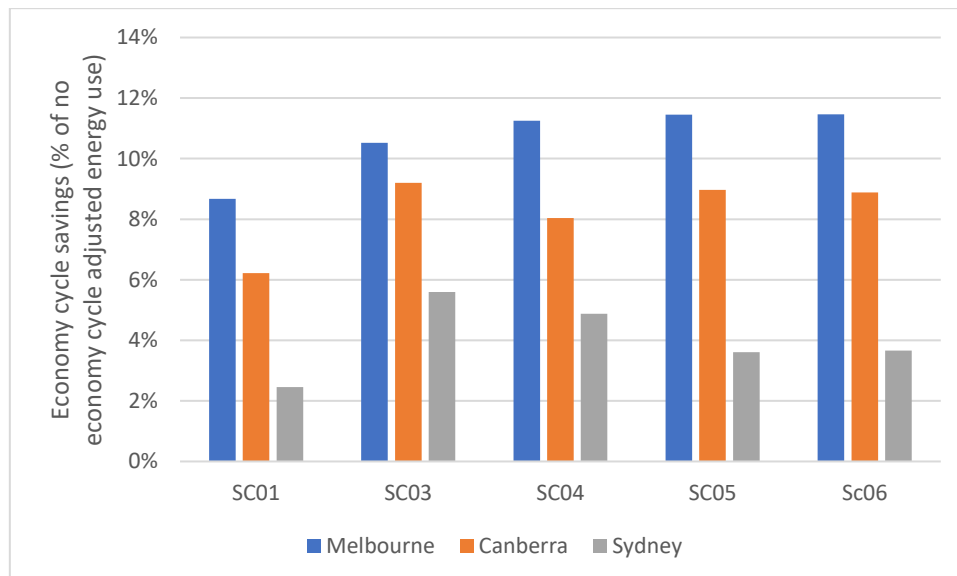


Figure 2. Achieved economy cycle savings (relative to SC02). Energy figures are adjusted by multiplying the gas use by 0.25 to generically approximate emissions intensity differences

3.2 Scenario Analysis

Results for the scenarios in Table 2 are summarised in Figure 2 for the three cities modelled (Sydney, Melbourne and Canberra, representing NCC climate zones 5, 6 and 7, respectively). For presentation, the energy results from the simulations have been modified by multiplying

⁷ This is the simple reset scenario from Bannister and Zhang (2014) found to have the best overall performance.

the boiler gas energy by 0.25. This provides a generic adjustment that represents the difference between gas emissions and electricity emissions without introducing the complication of state-by-state differences⁸.

Two key results are evident in Figure 2:

- Optimum scenarios are different from climate to climate.
- The decoupled control approaches (SC04-06) offer marginal improvements in economy cycle performance in Melbourne and Canberra but perform poorer than the enhanced simple approach in SC03 and underperform the simple scenario in Sydney.

This indicates that as a minimum, a degree of customisation of supply air setpoint control is required on a city-by-city basis. This would also imply that customisation needs to occur on an individual building basis.

Using Melbourne results as an example, it is possible to see how the chiller and fan energy modulate between scenarios, as shown in Figure 3.

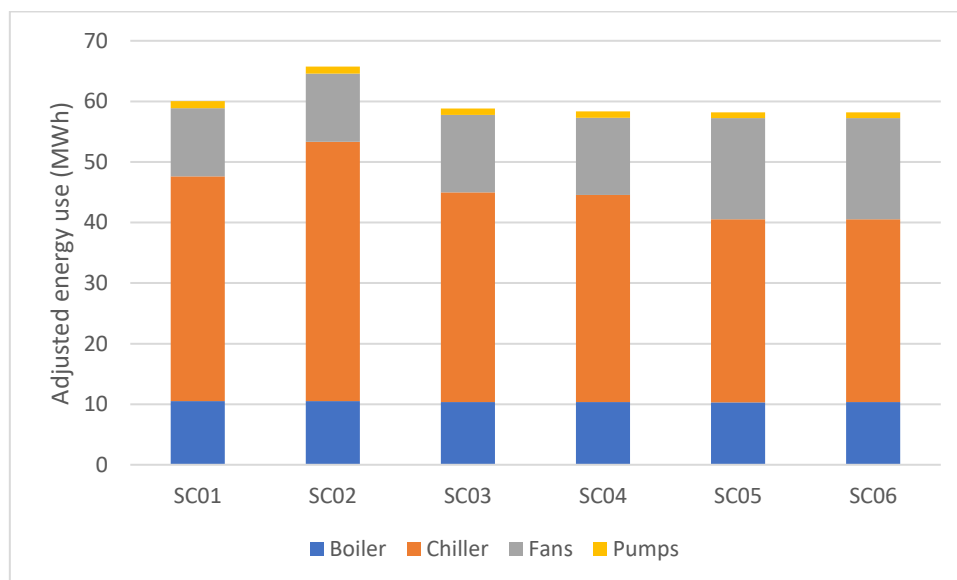


Figure 3. Annual energy end-use breakdowns. Energy figures are adjusted by multiplying the gas use by 0.25 to generically approximate emissions intensity differences

⁸ Modulation of this multiplier, and adjustment of chiller energy to reflect the expected higher efficiency of a water-cooled chiller, gives different results in terms of optimum scenarios and achieved efficiencies, but differs little in terms of the generic findings discussed in this paper.

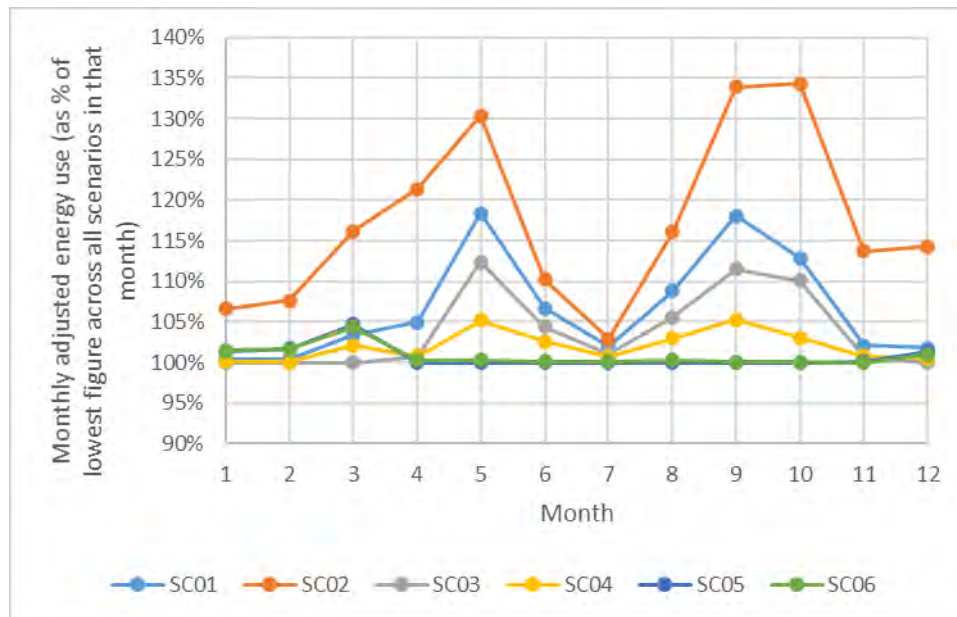


Figure 4. Comparison of scenarios on a monthly basis relative to the lowest achieved energy use in each month (for Melbourne)

Similarly, using Melbourne as an example, the monthly energy use can be compared between scenarios, as shown in Figure 4. It can be seen from the figure that different scenarios perform better in different months, suggesting that there is some potential for further optimisation using adjustments relating to outdoor conditions. However, the associated benefits are relatively small; for Melbourne, Canberra and Sydney respectively, the sum of the lowest monthly adjusted energy use figures was 1.1 per cent, 1.4 per cent and 0.005 per cent lower than the lowest energy scenario.

4. DISCUSSION

The simulation results indicate that while there is a significant difference between a poor economy cycle control and improved control, the various combinations of more complex controls only offer limited improvements. In particular, the decoupled scenarios do not provide improvements relative to well-selected simple coupled control of SC03. This suggests that the additional complexity of a decoupled control may not be merited.

However, the more challenging finding from the results is that it is not necessarily easy to determine which control configuration will result in a poor or improved outcome without a detailed study. As various exploratory simulations were conducted for this paper, minor differences in HVAC configuration and larger scale adjustments like the use of water-cooled rather than air-cooled chillers appear to change optimum scenarios. As a result, the major conclusion from this study is that the determination of the ideal supply air temperature control for a project is problematic and far from self-evident. This may present a risk for projects, especially if the simulation package cannot readily represent realistic controls. A further consequence of this finding is that the specific optimisations presented in this paper should not be considered generalisable.

Using a simple fixed annual control configuration, or even one changed on a seasonal monthly basis, may be constraining optimisation factors. In essence, the limited differentiation in the results presented may indicate the common failings of all the tested scenarios (the use of the

same control irrespective of AHU or the dynamic operating conditions) rather than physical performance limits. While the exploratory simulations conducted for this study hinted at opportunities for further optimisation, they also showed that the problem was highly complex and in need of extensive further work before any useful result could be achieved. It remains unclear whether such further optimisation would yield significant further performance improvements.

Given the results to date, it may be that the main benefit of a more complex and dynamic control approach may not lie in the fine optimisation of performance; but rather the creation of a more robust method to identify an acceptable optimisation customised to the individual circumstances of a given building.

5. CONCLUSION

This paper has explored the impact of supply air temperature control on the effectiveness of economy cycle operation. While theoretical analysis suggests that there may be benefits to decoupling the control of the cooling coil during economy cycle from its control at other times, the simulation studies presented do not show an advantage relative to a well-selected simpler, coupled control that is reflective of current practice. However, the results also highlight the successful selection of such a control is non-trivial and dependent on the details of an individual building's design.

It is concluded that the selection of an industry-standard supply air temperature reset that delivers efficient outcomes for a given building is difficult. Indeed, for current simple control approaches, it would appear that a sufficient goal would be to avoid a poor outcome rather than attain an ideal outcome. Achievement of reliably optimised benefits from economy cycle controls across diverse buildings may justify more complex and dynamic control approaches than the simple fixed controls used in this study and current industry practice.

ACKNOWLEDGEMENTS

The support of DeltaQ Pty Ltd and Enerefficiency Pty Ltd in funding this work (in-kind) is gratefully acknowledged.

REFERENCES

- AIRAH, 2011 *DA28 Building Management and Control Systems Application Manual*. Control sequences are documented in Appendix B.
- ASHRAE 2018 *ASHRAE Guideline 36-2018 High Performance sequences of Operation for HVAC Systems*
- Bannister, P, Salmon, S, Quinn, R, 2009. "What Really Makes Buildings Efficient: Results from the Low Energy High Rise Project" AIRAH Preloved Buildings Conference, Melbourne, 2009.
- Bannister, P, Zhang, H, 2014. "What simulation can tell us about building tuning" Ecolibrium December 2014

Bannister, P, Zhang, H, 2015. “Optimisation of Supply Air Temperature Controls for VAV Systems in Temperate Australia”, Building Simulation 2015, Hyderabad, India, 2015

APPENDIX 1

A typical Australian office building was modelled as the base case for this study. The simulation follows NCC2019 Section Deem-to-Satisfy provisions and NABERS Commitment Agreements Handbook for Estimating NABERS Ratings Version 2.0 – September 2021.

Appendix 1.1 Basic building characteristics

The base model has these characteristics:

- 8 storey building with underground carpark
- 50% WWR
- NCC2019 Section J compliant building envelop
- 25m by 25m floorplate, 4 perimeter and 1 centre zone per floor, the total area is 5,000m²
- Floor to ceiling height 2.7m, Plenum height 0.9m
- HVAC: VAV system with by central plant

Diagrams of the building as shown in Figure 5 and Figure 6:

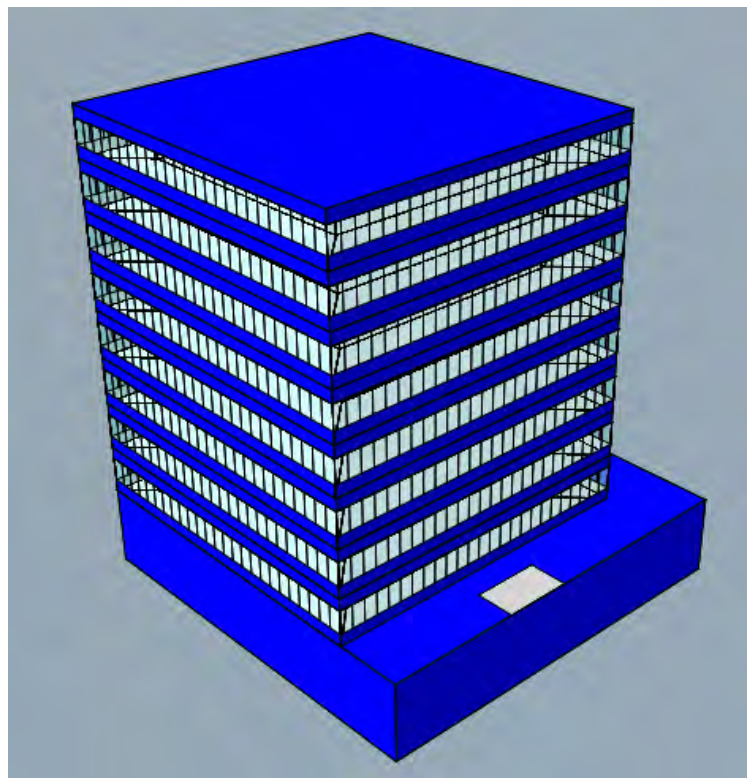


Figure 5 Modelling geometry

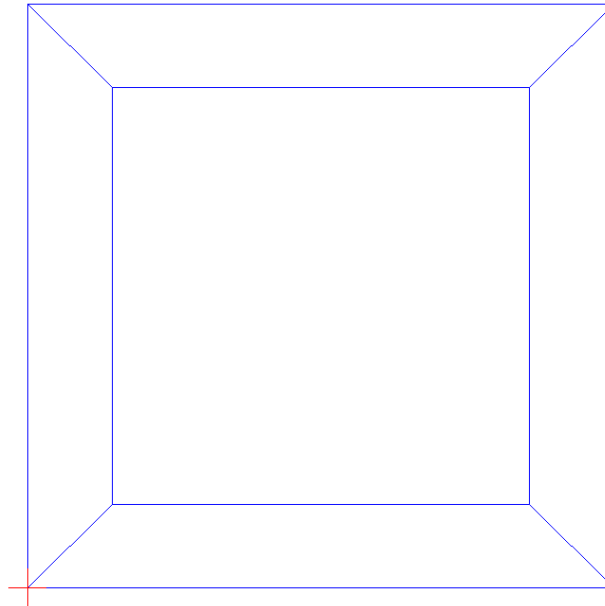


Figure 6. *Floor plant with HVAC zoning*

The total NLA is 5,000 m².

Appendix 1.2 Weather files

TMY weather files appropriate to the region was used in the simulation. TMY weather files were developed by Department of Industry, Science, Energy and Resources and CSIRO for building energy simulation. The building was modelled in Sydney, Melbourne and Canberra.

Appendix 1.3 Modelling software

Modelling was executed in IES<VE> which was developed by Integrated Environmental Solutions Limited and has passed ASHRAE 140, BES TEST and CIBSE TM33 accreditation. The program has been widely used in Australia and has widespread international acceptance.

Appendix 1.4 Building construction

Double glazing with the characteristics shown in Table 3 was used in the simulation.

Material (From outside to inside)	U-Value (W/m²·K)	SHGC
6mm tinted low-E glazing 12mm air cavity 6mm clear glazing	2.4	0.26

Table 3. *Glazing construction*

The opaque construction was modelled to achieve NCC2019 Section J compliant building envelop R-Value:

Construction description	Material (From outside to inside)	Total R-Value (m²·K/W)
External wall	5mm cladding 50mm cavity 20mm insulation 13mm plasterboard	1.0
Roof (Sydney)	200mm concrete 50mm cavity 124mm insulation 13mm plasterboard	3.7
Roof (Melbourne)	200mm concrete 50mm cavity 104mm insulation 13mm plasterboard	3.2
Roof (Canberra)	200mm concrete 50mm cavity 124mm insulation 13mm plasterboard	3.7
Ceiling	13mm plasterboard	0.4
Internal floor	8mm carpet 200mm concrete	0.6
Floor above the carpark	8mm carpet 200mm concrete 58mm insulation	2.0

Table 4. *Opaque construction*

Appendix 1.5 Internal loads

The internal loads were modelled as follows:

- Occupancy: 10m² per person. Sensible heat gain of 75W/person and latent heat gain of 55W/person
- Equipment: 11W/m²
- Lighting: 4.5W/m² distributed equally between office space and ceiling plenum

The operation schedules for occupancy, equipment and lighting were set as per NABERS default schedules.

Appendix 1.6 Infiltration

Infiltration for the main building was modelled as 0.7 ACH throughout all zones when there is no mechanically supplied outdoor air; and 0.35 ACH at all other times. Infiltration for underground carpark is modelled as 2 ACH for 24/7.

Appendix 1.7 HVAC

HVAC system was modelled as follows:

- **Zone temperature control.** The zone temperature control was to 22.5°C with a dead band from 21.5°C to 23.5°C and 0.5°C proportional band. The VAV box minimum turndown was set to 30 per cent for perimeter zones and 50 per cent for centre zones.
- **AHU configuration.** Separate AHUs were provided for each facade and for the centre zone.
 - AHU supply air fans were modelled as having an efficiency of 70 per cent, motor efficiency of 90 per cent and an $x^{2.7}$ turndown (representing variable pressure control). AHU return air fans were modelled as having an efficiency of 70 per cent, motor efficiency of 90 per cent and an x^2 turndown (representing fixed pressure control).
 - Perimeter AHUs only have cooling coils. The heating was supplied to perimeter zones via hot water terminal reheats.
 - Centre AHU has both cooling and heating coils. No terminal reheats were modelled in centre zones.
 - All AHUs were configured with a temperature economy cycle with a dewpoint lockout at 14°C and a dry-bulb lockout at 24°C. The AHU cooling supply air temperature setpoint and economy cycle setpoint were reset from 12°C to 24°C based on high-select zone temperature for perimeter zones and average temperature for centre zones.
 - The centre AHU heating supply air temperature setpoint was reset from 24°C to 30°C base on average zone temperature.
- **Central plant.** The cooling was supplied by two identical air-cooled chillers. The COP and IPLV were modelled as per NCC2019 Section J. The heating was supplied by two identical condensing boilers. The boiler efficiency was modelled as per NCC2019 Section J.

DISCLAIMER

The information or advice contained in these technical papers is intended for use only by professionals who have had adequate technical training in the field to which the paper relates. At the time of publication, these technical papers have undergone a formal peer-review process.

These documents have been compiled as an aid only, and the information or advice should be verified before it is put to use. The user should also establish the applicability of the information or advice in relation to any specific circumstances. While the information or advice is believed to be correct, no responsibility is taken by AIRAH or IBPSA Australasia for any statements made within.

AIRAH and IBPSA Australasia, its officers, employees and agents, disclaim responsibility for any inaccuracies contained within the documents, including those due to any negligence in the preparation and publication of the said technical papers.

COPYRIGHT

This work is copyright. Apart from any use as permitted under the Copyright Act 1986, no part may be reproduced by any process without prior written permission from either the Australian Institute of Refrigeration, Air Conditioning and Heating (AIRAH) or the International Building Performance Simulation Association (IBPSA) Australasia.

INSIGHTS FROM CHANGES TO STRINGENCY IN THE NATIONAL CONSTRUCTION CODE

PC THOMAS
Team Catalyst

GS RAO
Team Catalyst

ABSTRACT

Building design codes are continually changed with increases to the ‘stringency’ of minimum performance requirements. NCC (Australia) Vol 1 deals with non-residential buildings, and there have been some quite significant changes between the ‘Deemed-to-Satisfy’ or DtS requirements for Section-J: Energy Efficiency, between 2010 and 2019. The combined effect of these changes, when viewed through the lens of load calculation (system sizing) and annual energy predictions (simulation), using current and future weather files, provides valuable insights for future building fabric design, HVAC system configuration, and control strategies. A daytime use office building model has been analysed for Sydney (moderate/temperate climate) to review and discuss these insights, which include a change in balance between heating and cooling demand and energy use, and even more importantly, the change in predicted latent and sensible cooling. While the analysis is specific to Sydney, the authors feel that similar outcomes can be expected in coastal Australian locations which bear the brunt of population and development.

INTRODUCTION

The National Construction Code of Australia (NCC), previously the Building Code of Australia (BCA) introduced minimum mandatory energy efficiency requirements in 2005, under Section-J of Volume 1. This volume deals primarily with non-residential buildings, including office buildings (Class 5) which are the subject of this paper. Some of the results discussed here are applicable to other daytime use buildings.

Alternate routes are available to show compliance with the NCC at design stage. These follow the structure of many international building codes. There is a Deemed-to-Satisfy (DtS) set of stringencies that can be used as a compliance recipe, and there are also Verification Methods which are more ‘performance based’. The most popular of these Verification Methods, usually implemented at ‘Development Application’ stage is the *JV3 method or Verification Using a Reference Building*.

In this approach, dynamic energy simulation is used to check that the performance of a ‘Proposed’ design building model, is the same as, or more energy efficient than a ‘Reference’ design building model. The Reference design building model is fitted with minimum DtS requirements, for building elements (walls, windows, roof, floor etc), as well as for lighting and HVAC systems.

The current iteration NCC2019 (ABCB, 2019) of the code requires that the performance of the building envelope provide a minimum level of thermal comfort AND energy efficiency, that is, the minimum thermal comfort performance of the building envelope is independently

determined when the JV3 method is applied. It is useful to understand that major changes to the energy efficiency stringencies were carried out in 2010, 2016 and most recently in 2019. The NCC2019 JV3 clauses that nominates this requirement is reproduced below:

JV3 Verification using a reference building
(a) For a Class 3, 5, 6, 7, 8 or 9 building or common area of a Class 2 building, compliance with JP1 is verified when—
(ii) it is determined that the annual greenhouse gas emissions of the proposed building are not more than the annual greenhouse gas emissions of a reference building when—
(A) the proposed building is modelled with the proposed services; and
(B) the proposed building is modelled with the same services as the reference building; and
(ii) in the proposed building, a thermal comfort level of between a Predicted Mean Vote of -1 to +1 is achieved across not less than 95% of the floor area of all occupied zones for not less than 98% of the annual hours of operation of the building; and
(iii) the building complies with the additional requirements in Specification JVa.
(b) The annual greenhouse gas emissions of the proposed building may be offset by—
(i) renewable energy generated and used on site; and
(ii) another process such as reclaimed energy, used on site.
(c) The calculation method used for (a) and (b) must comply with—
(i) ANSI/ASHRAE Standard 140; and
(ii) Specification JVb

Taken together, clause (a)(i)(B) ensures that the predicted energy efficiency of the Proposed building fabric is no less than that of a Reference building fabric, and clause (ii) ensures that the predicted thermal comfort regime within occupied spaces of the proposed building are within prescribed PMV limits.

The thermal comfort (PMV) test (clause (a)(ii)) was implemented in the 2019 update of JV3, presumably because it was recognised that the use of renewable energy generated and used on-site (as in clause (b)(i)) could lead to very poor building fabric outcomes, unless prevented by this thermal comfort ‘backstop’. This PMV test is the single most significant change in the JV3 method between the NCC 2016 (ASCB, 2016) and 2019 iterations.

The current study will focus on the stringency upgrades to the building fabric (wall glazing) and internal loads (occupancy, lighting and ‘plug’ loads) and their potential impact on predicted heating and cooling loads, and on HVAC design practise in general. It is the authors view, that there are substantial changes to design practise, that are not yet on the radar of HVAC design engineers and ESD professionals. A simple, but representative, building geometry for a daytime use office building is analysed for Sydney (moderate/temperate) climate to demonstrate and discuss these insights.

These insights would be applicable, in a general, to all metropolitan locations in Australia, for example Adelaide, Perth and Brisbane. Each project is different, and the particular combination of glass, thermal mass, shading and insulation could result in significantly different outcomes. However, the selected theoretical geometry is representative of many office tower building configurations. It is however, worth noting that these results are based on predicted outputs from energy simulation results, when an office building is operated as per the schedules

nominated in the NCC Vol 1, and that practical outcomes could be very different if the building was operated differently.

METHOD

A building model similar to the reference building type “A” used for the National Construction Code, Section-J stringency analysis (developed by Team Catalyst for other projects) has been used to test the impact of stringency changes to building fabric and internal load provisions between for Section-J NCC 2016 and NCC 2019. The general arrangement of the building model is described below:

- square floor plate, 30m on all sides
- oriented to cardinal directions
- greenfield site (no shading from adjacent buildings)
- 10 levels (ground plus 9 levels), plus an unconditioned basement floor
- a floor-to-floor height of 4.0m, ceiling at 2.7m
- 2m high vision glazing at 700mm sill height (façade WWR = 50%)
- glazing system performance, mainly window system values for SHGC and U-values, are set based on NCC version requirements
- light weight external wall, R-value based on code requirements
- 200mm concrete roof construction insulated (R-value) to code requirements
- internal floors modelled as uninsulated concrete slabs
- 200mm thick concrete ground floor slabs

It is noted that the building fabric for this hypothetical building is capable of high-performance outcomes. This level of specification can allow an office ‘base building’ in Sydney to easily perform to a 5 star NABERS Energy rated building (see www.nabers.com.au), and would even allow performance at 5.5 stars with a carefully designed HVAC system that is correctly commissioned and monitored post construction.

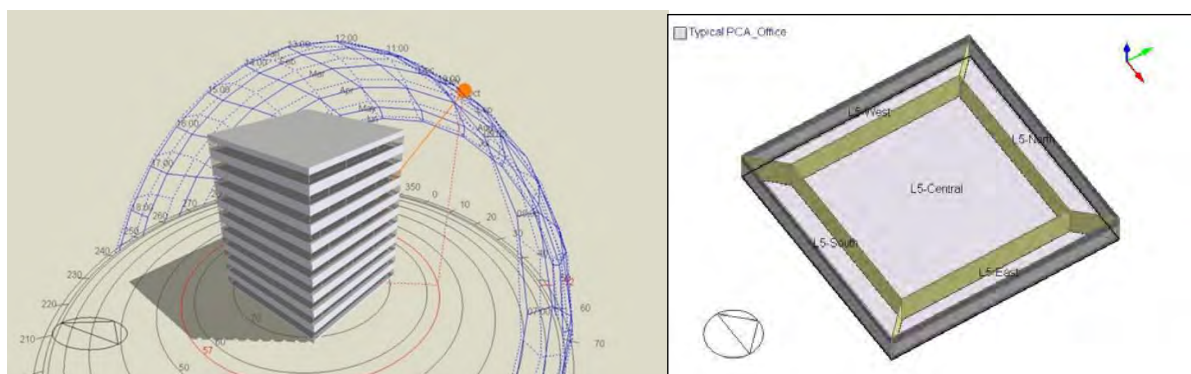


Figure 1: (a) 3D visualisation of the building with superimposition of annual sunpath for Sydney; and (b) Zoning for typical floors; zones are separated by “virtual walls”, i.e., heat transfer boundaries, typically used in HVAC design for open plan offices (amenity/service zones are not modelled)

There have been considerable change to the energy efficiency provisions in Section-J for the NCC2019 upgrade, when compared to NCC2016. To ensure that the study is useful for Australian Engineers, modelling inputs and outputs have been aligned to these newer requirements. Table 1 list the design values (maximums) for internal loads. These values are the maximum design values, and are modified by appropriate hourly schedules for the energy simulation analysis.

There are some differences in the operational profiles (or schedules) for modelling occupancy, lighting, and equipment (plug loads) for NCC2019 and NCC2016, as shown in the tables included in the Appendix. The biggest difference is for occupancy in NCC2019 which assumes that, in operation, the rate of occupancy is limited to 70 per cent of the design value, down from 100 per cent in NCC2016. The tables compare values for weekday (M-F) and weekends (S-S) for each of these internal loads.

Design Internal Load	Occupancy density 1 per 10m ² as per PCA Guide (2012) Standard office occupancy * Occupant heat load of 130 watts per person (55W latent/ 75W sensible) <i>Lighting load: 4.5W/m², (down from 9W/m² in NCC2016) and</i> <i>Equipment load: 11 watts per m² (down from 15 W/m² in NCC2016) **</i> <i>Infiltration: 0.7ACH when no mechanically supplied outside air, and 0.35ACH at all other times (NCC2019); changed from 1.5ACH for the whole building when pressurising plant is not operating, and 1.0ACH for perimeter zones when it is operating</i>
Outside Air Rate	10L/s per person as per AS 1668.2 without filtration for offices
Indoor Temperature	22.5C +/- 1.5C (generally 21C for heating and 24C for cooling)
Design Criteria used to autosize HVAC systems for this study (load calculations are not required for NCC compliance)	0.4% confidence level, ASHRAE monthly design criteria, dry bulb priority (listed in a later section of this report)

* maximum weekday occupancy is modelled at 70% for NCC2019, down from 100% from NCC2016 (see **Error! Reference source not found.**)

** loads in italics are the changes/reductions in modelling inputs required for NCC2019 Vol 1 Section-J JV3

Table 1. Internal loads for DtS Reference building model input for NCC2019 compared to NCC2016

RESULTS

Annual energy simulation studies were carried out on the building described. DesignBuilder V7 was used as a GUI for the EnergyPlus Version 9.4.0 building simulation engine developed and maintained by the USDOE. Graphs in the following section provide a series of comparative results, and the colour selections warrant some explanation. Where the same variable has been compared (hourly cooling or heating predictions), red is used for NCC2016 and blue for NCC2019. Where hourly heating and cooling predictions (for the same version of the NCC) are plotted on the same graph, red is used for heating and blue for cooling. The faded or bold nature of these colours is to ensure values for both series can be seen clearly and compared.

COOLING

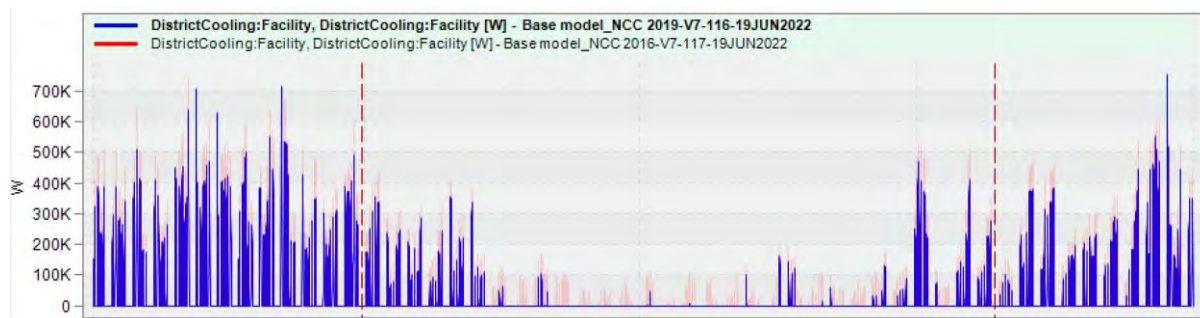


Figure 2. Predicted hourly cooling loads for NCC2016 (faded red) and NCC2019 (bold blue)

Figure 2 compares the predicted hourly cooling load when tested for Reference building models built to 2016 and 2019 NCC Section-J minimum building fabric performance requirements, and operated as per nominated schedules. Reviewing the graph provides the following insights:

The combination of all the changes in NCC2019 (detailed in the previous section) has resulted in generally lower predictions for hourly cooling loads from building fabric and internal loads. Notably, predicted cooling loads have all but disappeared in the winter months for NCC2019 (bold blue), a significant change from the predictions for the NCC2016 (faded red) Reference building model.

Predicted peak cooling loads tell an interesting, and counter intuitive story. An excerpt (from Figure 2) of the hourly cooling load predictions for five weeks, including Feb and the first week of Mar, is shown in Figure 3 below; this excerpt includes the first two predicted cooling peaks (around 700kW) for NCC2019 (bold blue) in Figure 2.

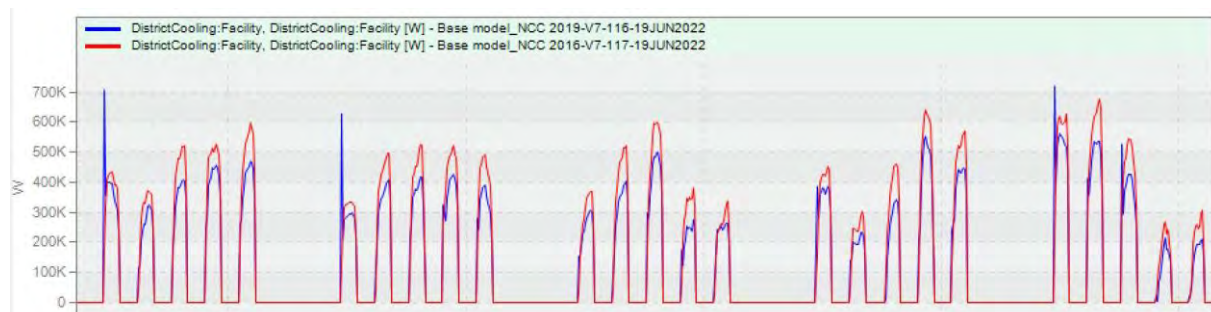


Figure 3 :Predicted hourly cooling loads for Feb and the first week of Mar (using data from the IWECC file used for the simulation analysis); excerpt from Figure 2 above; NCC2016 (red) and NCC2019 (blue)

Figure 3 indicates that, on certain Monday mornings, the predicted cooling peak load spikes for the NCC 2019 building model when the HVAC system is switched on in the morning, but this load rapidly drops away within the first hour or two. These Monday morning peaks are, in fact, higher than the peaks predicted for the NCC 2016 building model outcomes. This atypical behaviour is predicted to only occur a handful of times in the year, during the peak cooling months. The reason for these counter intuitive predictions has not been analysed in detail; it is most likely a combination of higher fabric R-values and lower infiltration rates for NCC2019, which reduce heat loss at night across the weekend. The negative impact on cooling energy due to over insulating building fabric in moderate climates was first discussed in Thomas and Prasad, 1995.

Note that these predicted peak cooling loads are NOT cooling loads calculated for standard design day conditions used to size plant and equipment; rather they are the result of the combination of internal load assumptions that vary as per the NCC nominated operational profiles (or schedules), and the hourly weather data read from the ‘Reference weather file’ used for the energy simulation analysis. Two inferences can be made from the above graph:

- In practise, the atypical Monday morning peaks can be eliminated by starting the HVAC plant and systems an hour earlier in summer months, a commonly used operational strategy. This could increase the real world energy consumption a small amount compared to the predicted value, but the difference can be minimised, for example, by incorporating a ‘purge’ cycle in the BMS programming
- it is clear that there *is* a reduction in the predicted annual energy consumption for cooling, which for this building configuration is 26 per cent.

HEATING

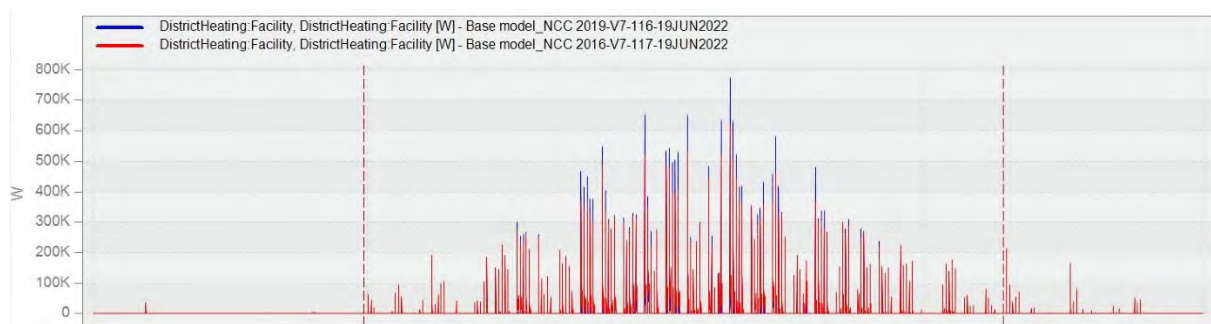


Figure 4. Predicted hourly heating loads for NCC2016 (red) and NCC2019 (blue)

The predicted hourly heating loads for Reference building models for NCC2016 and NCC2019 are shown in Figure 4, and reveal an opposite impact (compared to cooling) due to the change in stringencies. Predicted heating loads from building fabric and internal loads for the NCC2019 model, while they occur at the same times as for NCC2016 model, have increased, *in certain instances by more than a third* (at peak times).

Where real heating loads were previously offset by internal gains in office buildings, sensible heating loads have reduced substantially in modern office buildings due to:

- Reduced solar gain due to use of glazing with lower SHGC, and
- Efficient lighting systems that generate less heat gain in the space, and
- Reduced heat gain in the space from ‘plug’ loads, due to more efficient monitors, laptops, printers, etc

The practical take way for HVAC design engineers from this result is that more care and effort is to be taken for the design, control and operation of heating systems in Sydney (and other moderate location) office buildings. Although energy consumption from heating systems is predicted to increase (as shown in Figure 4) there may be little or no change to specified heating system capacity, since sizing calculations for heating are generally carried out (by many HVAC design engineers) without consideration the impact of internal loads.

HEATING AND COOLING

Reviewing the hourly cooling and heating loads across the year for both Reference case models, NCC2016 and NCC2019, also provides insights for HVAC design practise.

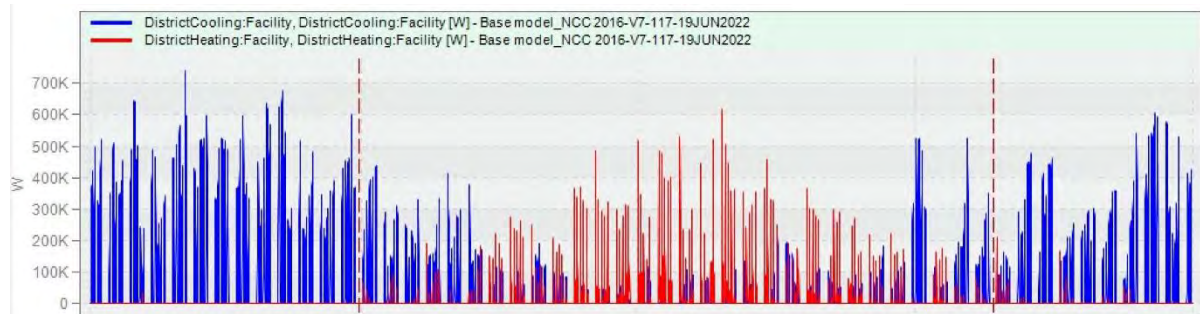


Figure 5. Predicted hourly cooling (blue) and heating (red) loads for the NCC2016 Reference building model from building fabric and internal loads

The graph for NCC2016 (Figure 5) shows predicted peak cooling loads (around 740kW) are larger than predicted peak heating loads (620kW). Winter days have both heating and cooling loads, most often with cooling loads exceeding heating loads during the same day. Detail for the week of 29 July to 03 August for the NCC2016 predictions is shown in (Figure 6), when daytime temperatures are less than 20°C and night temperatures are lower than 10°C. Typically, there is a morning peak for heating, followed by a small but significant cooling load across the day, as can be clearly seen in Figure 6. This result is different to the predictions for NCC2019 (Figure 2) where it is clear that cooling load is predicted to be zero during large parts of winter cold weeks.

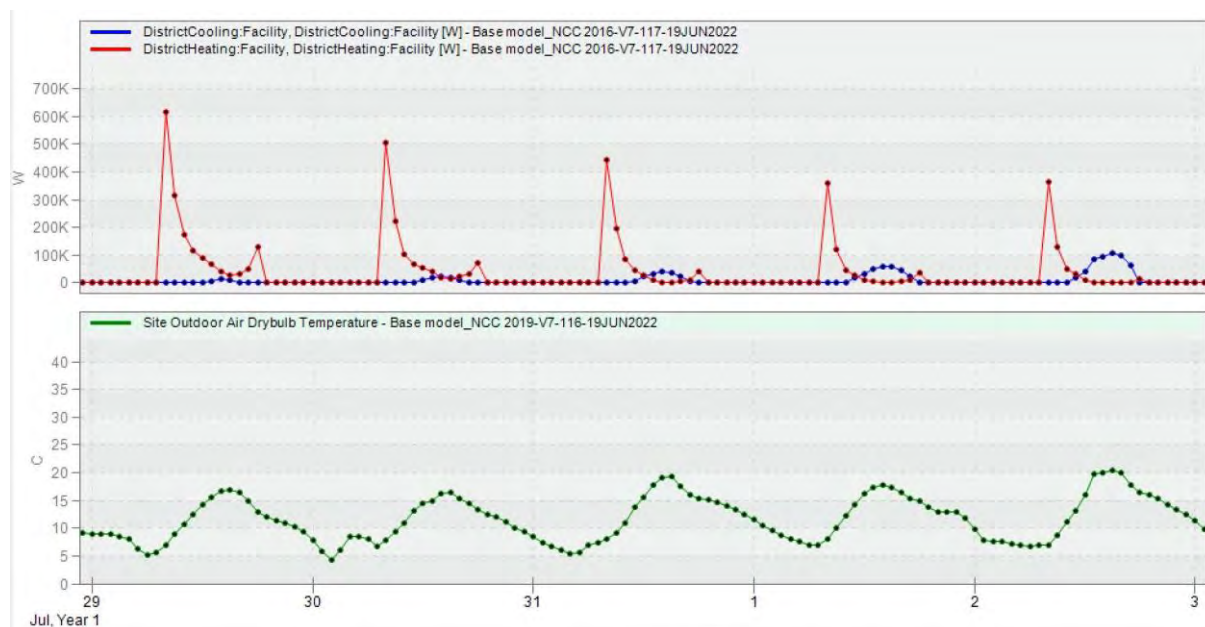


Figure 6. Cooling and heating loads for a winter week (29 July to 03 Aug from weather file) for NCC2016 Reference building model

However, there are significantly different outcomes that can be inferred from reviewing the predicted results for the NCC2019 Reference building model. From Figure 7 it is clear that the predicted hourly thermal demand for heating and cooling loads are *similar* in quantum. In fact,

if the three atypical peak cooling load occurrences on Monday mornings were removed from consideration (as discussed previously) *it is quite possible that the predicted peak heating loads (about 650kW) would be higher than the peak cooling loads (about 550kW)*. This is a significant finding and has implications on HVAC design practise; more works needs to be done to ratify this finding. This change can be attributed to the combination of change to building fabric stringencies, and the drop in internal loads which reflect current practice. These include:

- A 50% reduction in design lighting loads from 9 to 4.5W/m²
- Equipment load reduction from 15W/m² to 11W/m², and
- Peak occupancy loads during weekdays being restricted to 70 per cent of design occupancy for the energy simulation (not for design calculation), and
- Possible reduction in solar heat gain through glazing systems due to increased stringency (depends on building geometry)

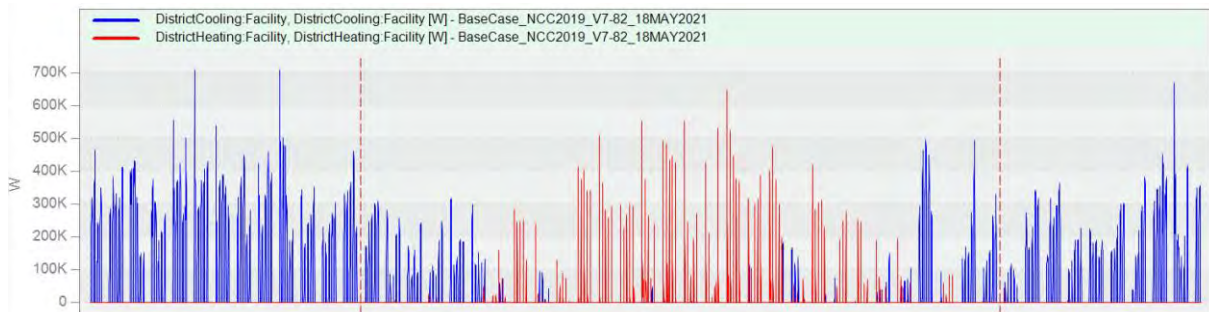
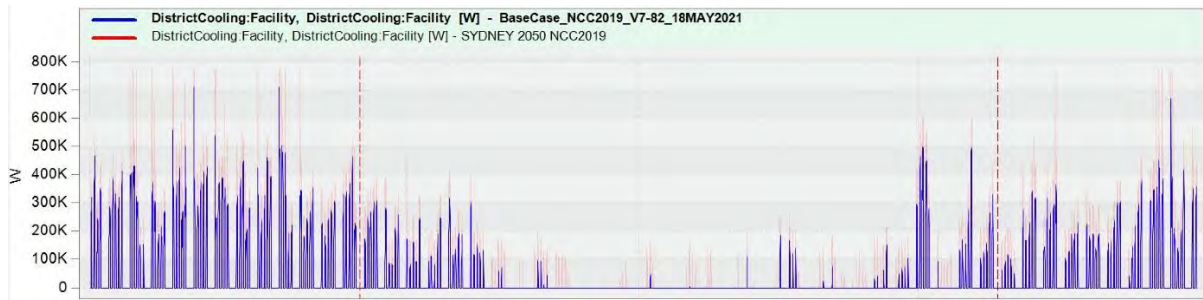


Figure 7. Predicted hourly cooling (blue) and heating (red) loads for the NCC2019 Reference building model from building fabric and internal loads

One of changes to HVAC design practise would be the manner in which design air quantities are selected for AHUs, FCUs or other terminal units. Typically design air quantities for these components are based on sensible cooling loads. The blue lines in Figure 7 are total (sensible + latent) cooling loads; which would suggest that heating loads may now be greater than sensible cooling loads. Therefore, the HVAC design engineer would do well to consider both the heating load (which is purely sensible) and the sensible cooling load, before confirming selection of design (peak) air quantities. This would be particularly important when use of modern, efficient heating technologies like condensing (gas) boilers, or electric reverse cycle heat pumps are considered. These technologies can have smaller loop temperature differential (delta-T) values, and can require higher water flow rates compared to older heating technologies.

FUTURE CLIMATE

The CCWorldWeatherGen software (Belcher et, 2005) from University of Southampton has been used to develop a 2050 future weather file for Sydney. The NCC2019 Reference building model was rerun using this 2050 weather file, and the annual cooling and heating loads were again compared.



- The results are plotted in () and indicate an expected increase in cooling loads across the year, with an increase of predicted operational (not design) cooling peaks by around 9 – 10 per cent. There is an expected reduction in predicted operational (not design) heating peak loads (figure not shown). This reduction is larger in value than the increase in cooling peaks, and is in the order of 18 per cent. The above effects are expected and will not come as a surprise to most engineers. However, there is a further effect that is relevant for HVAC design engineers to be aware of, and that is the change in latent loads, as seen in Table 2. The predicted increase in latent cooling fraction for the case of the NCC2019 Reference building model when tested using the 2050 future weather file may be due to increased moisture in the atmosphere as warmer ambient air can carry much more moisture.

CASE	Annual Cooling Demand (per typical floor)			
	Total kWh	Sensible kWh	Latent kWh	Latent fraction
NCC2019-2050	52,366	41,499	10,867	0.208
NCC2019	31,075	25,693	5,382	0.173

Table 2. *Change in latent loads*

In either case, it is clear that HVAC design engineers need to start paying attention to energy efficient dehumidification. The old adage of ‘let the cooling coil deal with it’ will no longer be sufficient. Latent loads are expected to be particularly difficult to service on days when ambient temperatures maybe just a couple of degrees about the thermostat setting, but relative humidity levels are very high. The summer of 2022 just past is a case in point, when the current La Nina system has resulted in huge amounts of ambient humidity. HVAC systems not designed to explicitly dehumidify outside air would struggle to cope with such loads, and energy use for wasteful reheat would increase overall energy consumption for cooling.

CONCLUSION

This study compares the heating and cooling loads predicted from Reference building models that confirm to building envelope stringencies as required by Section-J (minimum energy efficiency provisions) of NCC2016 and NCC2019. These studies indicate that, HVAC design engineers would benefit from the following considerations:

- Energy consumption for cooling will reduce due to the building fabric and internal loads reductions in NCC2019
- Design of heating systems may require more attention to detail than before, due to a predicted increase in system size and energy consumption. In particular, supply air flow rates will need to be reviewed for both cooling and heating before finalising equipment selections

- HVAC systems will need to respond to more ‘peaky’ building load demands; for example, almost no demand for cooling during winter months
- An inexorable increase in the latent cooling load fraction, requiring HVAC design engineers to focus their attention on efficient dehumidification in their designs

It has been shown (Thomas et al, 2017) that right sizing is the basis for an energy efficient HVAC system design, but energy simulation is required to ensure an energy efficient outcome in operations (that can be tested by an operational NABERS rating). It is hoped that engineers using building energy simulation will be able to use the results discussed in this paper to inform colleagues in their building façade and HVAC design teams to consider these insights in the quest for energy efficient, resilient, low energy use buildings that should primarily deliver occupant comfort.

REFERENCES

Australian Building Codes Board, 2016, National Construction Code, Vol 1 Section-J

Australian Building Codes Board, 2019, National Construction Code, Vol 1 Section-J

Belcher SE, Hacker JN, Powell DS. Constructing design weather data for future climates. Building Services Engineering Research and Technology 2005; 26 (1): 49-61

DesignBuilder V7 online help documentation, <https://designbuilder.co.uk/helpv7.0/>

NABERS or the National Australian Building Environmental Rating Scheme, see www.nabers.com.au

Thomas PC and Prasad DK, Energy Efficient Building Envelopes - An Australian Perspective, Thermal Performance of the Exterior Envelope of Buildings – VI, Clearwater Beach, Florida, USA; ASHRAE, USDOE, ORNL, NRCC DEC1995

Thomas PC, Rao GS, Wong J, Load Calculation and Energy Simulation: The link between design and operation for building design, Proceedings of the 15th IBPSA Conference San Francisco, CA, USA, Aug. 7-9, 2017

USDOE (US Dept of Energy), <https://energyplus.net/> ; EnergyPlus is free, open-source, and cross-platform. The latest version is available at this address. Previous versions are available for download.

APPENDIX

CLASS 5 OCCUPANCY	NCC2019	NCC2016	NCC2019	NCC2016
Time period	2019 M-F	2016 M-F	2019 S-S	2016 S-S
12:00am to 1:00am	0%	0%	0%	0%
1:00am to 2:00am	0%	0%	0%	0%
2:00am to 3:00am	0%	0%	0%	0%
3:00am to 4:00am	0%	0%	0%	0%
4:00am to 5:00am	0%	0%	0%	0%
5:00am to 6:00am	0%	0%	0%	0%
6:00am to 7:00am	0%	0%	0%	0%
7:00am to 8:00am	10%	15%	0%	0%
8:00am to 9:00am	20%	60%	5%	5%
9:00am to 10:00am	70%	100%	5%	5%
10.00 am to 11.00am	70%	100%	5%	5%
11.00 am to 12.00pm	70%	100%	5%	5%
12.00 pm to 1.00pm	70%	100%	5%	5%
1.00 pm to 2.00pm	70%	100%	5%	5%
2.00 pm to 3.00pm	70%	100%	5%	5%
3.00 pm to 4.00pm	70%	100%	5%	5%
4.00 pm to 5.00pm	70%	100%	5%	5%
5.00 pm to 6.00pm	35%	50%	0%	0%
6.00 pm to 7.00pm	10%	15%	0%	0%
7.00 pm to 8.00pm	5%	5%	0%	0%
8.00 pm to 9.00pm	5%	5%	0%	0%
9.00 pm to 10.00pm	0%	0%	0%	0%
10.00 pm to 11.00pm	0%	0%	0%	0%
11.00 pm to 12.00am	0%	0%	0%	0%

Table 3. *Nominated operational schedules for Occupancy compared*

CLASS 5 LIGHTING	NCC2019	NCC2016	NCC2019	NCC2016
Time period	2019 M-F	2016 M-F	2019 S-S	2016 S-S
12:00am to 1:00am	15%	10%	15%	10%
1:00am to 2:00am	15%	10%	15%	10%
2:00am to 3:00am	15%	10%	15%	10%
3:00am to 4:00am	15%	10%	15%	10%
4:00am to 5:00am	15%	10%	15%	10%
5:00am to 6:00am	15%	10%	15%	10%
6:00am to 7:00am	15%	10%	15%	10%
7:00am to 8:00am	40%	40%	15%	10%
8:00am to 9:00am	90%	80%	25%	10%
9:00am to 10:00am	100%	100%	25%	10%
10.00 am to 11.00am	100%	100%	25%	10%
11.00 am to 12.00pm	100%	100%	25%	10%
12.00 pm to 1.00pm	100%	100%	25%	10%
1.00 pm to 2.00pm	100%	100%	25%	10%
2.00 pm to 3.00pm	100%	100%	25%	10%
3.00 pm to 4.00pm	100%	100%	25%	10%
4.00 pm to 5.00pm	100%	100%	25%	10%
5.00 pm to 6.00pm	80%	80%	15%	10%
6.00 pm to 7.00pm	60%	60%	15%	10%
7.00 pm to 8.00pm	60%	40%	15%	10%
8.00 pm to 9.00pm	50%	20%	15%	10%
9.00 pm to 10.00pm	15%	10%	15%	10%
10.00 pm to 11.00pm	15%	10%	15%	10%
11.00 pm to 12.00am	15%	10%	15%	10%

Table 4. *Nominated operational schedules for Lighting compared*

CLASS 5 EQUIPMENT	NCC2019	NCC2016	NCC2019	NCC2016
Time period	2019 M-F	2016 M-F	2019 S-S	2016 S-S
12:00am to 1:00am	25%	10%	25%	10%
1:00am to 2:00am	25%	10%	25%	10%
2:00am to 3:00am	25%	10%	25%	10%
3:00am to 4:00am	25%	10%	25%	10%
4:00am to 5:00am	25%	10%	25%	10%
5:00am to 6:00am	25%	10%	25%	10%
6:00am to 7:00am	25%	10%	25%	10%
7:00am to 8:00am	65%	40%	25%	10%
8:00am to 9:00am	80%	80%	25%	10%
9:00am to 10:00am	100%	100%	25%	10%
10.00 am to 11.00am	100%	100%	25%	10%
11.00 am to 12.00pm	100%	100%	25%	10%
12.00 pm to 1.00pm	100%	100%	25%	10%
1.00 pm to 2.00pm	100%	100%	25%	10%
2.00 pm to 3.00pm	100%	100%	25%	10%
3.00 pm to 4.00pm	100%	100%	25%	10%
4.00 pm to 5.00pm	100%	100%	25%	10%
5.00 pm to 6.00pm	80%	80%	25%	10%
6.00 pm to 7.00pm	65%	60%	25%	10%
7.00 pm to 8.00pm	25%	40%	25%	10%
8.00 pm to 9.00pm	25%	20%	25%	10%
9.00 pm to 10.00pm	25%	10%	25%	10%
10.00 pm to 11.00pm	25%	10%	25%	10%
11.00 pm to 12.00am	25%	10%	25%	10%

Table 5. Nominated operational schedules for Equipment (plug loads) compared

DISCLAIMER

The information or advice contained in these technical papers is intended for use only by professionals who have had adequate technical training in the field to which the paper relates. At the time of publication, these technical papers have undergone a formal peer-review process.

These documents have been compiled as an aid only, and the information or advice should be verified before it is put to use. The user should also establish the applicability of the information or advice in relation to any specific circumstances. While the information or advice is believed to be correct, no responsibility is taken by AIRAH or IBPSA Australasia for any statements made within.

AIRAH and IBPSA Australasia, its officers, employees and agents, disclaim responsibility for any inaccuracies contained within the documents, including those due to any negligence in the preparation and publication of the said technical papers.

COPYRIGHT

This work is copyright. Apart from any use as permitted under the Copyright Act 1986, no part may be reproduced by any process without prior written permission from either the Australian Institute of Refrigeration, Air Conditioning and Heating (AIRAH) or the International Building Performance Simulation Association (IBPSA) Australasia.

THE RIPPLE EFFECT OF SMART ENGINEERING

**AMER NAJJAR MSC, BSC MECH ENG, MIEAUST CPENG NER APEC
ENGINEER INTPE(AUS), RPE(VIC), PMP®, M.AIRAH, M.ASHRAE**

Senior Building Services Engineer
SEED Engineers
Melbourne, VIC – Brisbane, QLD
Amer@seedengineers.com

ABOUT THE AUTHOR

Amer Najjar is a Mechanical Engineer (Building Services) with ~10 years of experience in the building services sector. He has a track record of success leading mechanical and ESD disciplines, building services coordination, project management and on-site construction of complex and multi-disciplinary projects in Australia and overseas.

Amer is the Melbourne office manager for SEED Engineers and is passionate about sustainability, energy and CFD modelling. HVAC experience is complemented with knowledge of other building services disciplines, BMCS and computer modelling.

He holds a MSc in Mechanical Engineering with a specialty in Energy Efficiency and Sustainability in Buildings.

ABSTRACT

It goes without saying, actions have consequences. We often associate this rule with bad actions; however, we can forget that good actions have consequences too, usually really good ones. Building simulation enables us to develop unconventional designs that allow mechanical and natural systems to work together in harmony.

Ever since the dawn of humanity, mankind has been interested in observing and documenting natural behaviour. We have gathered so much information that we are now able to predict what the weather is going to look like tomorrow, or even that the temperature will rise by 1.5°C by 2050 or so. As building services engineers, we try so hard to deviate away from relying on natural systems because we think it is unreliable and unpredictable, while in fact, this is simply untrue.

In this paper, I want to discuss the consequences of unorthodox design decisions in an underground car park ventilation project. The decisions were supported by BOM (Bureau of Meteorology) data analysis and CFD (Computational Fluid Dynamics) modelling, resulting in a ripple effect of direct beneficial impact on the stakeholders, and indirect impacts on the environment at large.

INTRODUCTION

Necessity is the mother of all inventions, or at least that is what we have been taught every time the history behind scientific milestones is being described. One might argue that this is true up to 200 years ago, but ever since the industrial revolution, money has been the fundamental drive to how now mankind addressed technological and industrial advancements. In other words, we want things to be cheaper, yet “adequately” functional. What started as value management exercise, soon developed into a passionate rally to make a point, to prove a concept and tell everyone that it can actually be cheaper but also much better.

The project is a fully automated customer fulfilment centre for one of Australia’s leading FMCG retailer (Fast-Moving Consumer Goods) that is now taking shape in one of NSW’s industrial parks. The facility serves as a major hub for online orders as a highly advanced robotics hive picks and collects goods from all around the facility into small shipping totes, which end up being delivered to the customer’s doorstep.

The facility’s car park has a capacity of almost 600 vehicles, equally distributed over two levels, one of them is on ground and fully exposed, while the other is mostly underground due the steep ground slope. Unsurprisingly, the tender design of the underground car park is a “conventional” mechanically ventilated system following Australian codes and standards’ DTS requirements (Deemed-to-Satisfy), particularly the duct design (AS1668.2, 2012) and minimum acceptable indoor air quality requirements, (NCC, 2019). Soon enough, it was clear to everyone that the project is going over the planned budget, and value management was pivotal to the project moving forward.

At the beginning, the project was addressed solely from a financial perspective, trying to answer one question, how can we make it work, but cost less? That is when it hit me, it has to also be better. As I was reviewing the architectural layouts and site plans, I noticed that the facility is open to surrounding environment and not blocked by large infrastructures, more interestingly, BOM data showed that valley is susceptible to windy conditions almost all year round, with wind speeds reaching 20~30km/h. The mean/dominant wind in Horsley Park is South-East 16.6km/h (4.6m/s) wind, according to BOM data extracted from the Horsley Park Equestrian Centre AWS located at Latitude: 33.85° S and Longitude: 150.86° E, which has been recording weather statistics since 1997. Cheaper but better was right there in front of me, I have to introduce wind into this semi underground car park.

Open-mindedness; even though many projects are driven by reducing the budgets and costs, it can be challenging to obtain a “buy-in” from stakeholders on risky and unusual ideas. Fear of noncompliance is legitimate, but often taints calculated risks. This project was fortunate enough to be surrounded by a group of supportive and open-minded stakeholders, namely the architect, whose support and “buy-in” were pivotal in making this concept work.

A series of façade architectural and structural modifications were the key to allow wind into the underground car park from the lower sloped ground side, which was the South-East facing façade. Once, wind path was established, CFD simulations took place to prove the concept, then it was time to find the sweet spot where mechanical and natural systems can work together in harmony. Due to the long span of the car park, it was clear that “dead spots” with higher concentration CO (Carbon Monoxide) were present in some locations as wind was not reaching into the deeper depth of the underground car park, especially when wind is not coming from the South-East. Four reverse-direction fans were strategically located within the far end of the underground car park to “assist” wind clear any higher concentrations of CO of concern. The direction reversibility was pivotal to interact with multiple wind directions.

1. DESIGN AND CALCULATIONS

The car park in this case study is classified as “Commercial” being associated with a commercial facility. It is unmanned and depends on self-parking, with vehicle types unspecified. Mechanical ventilation is the obvious choice as the underground car park is basically enclosed between the ground slope and the façade.

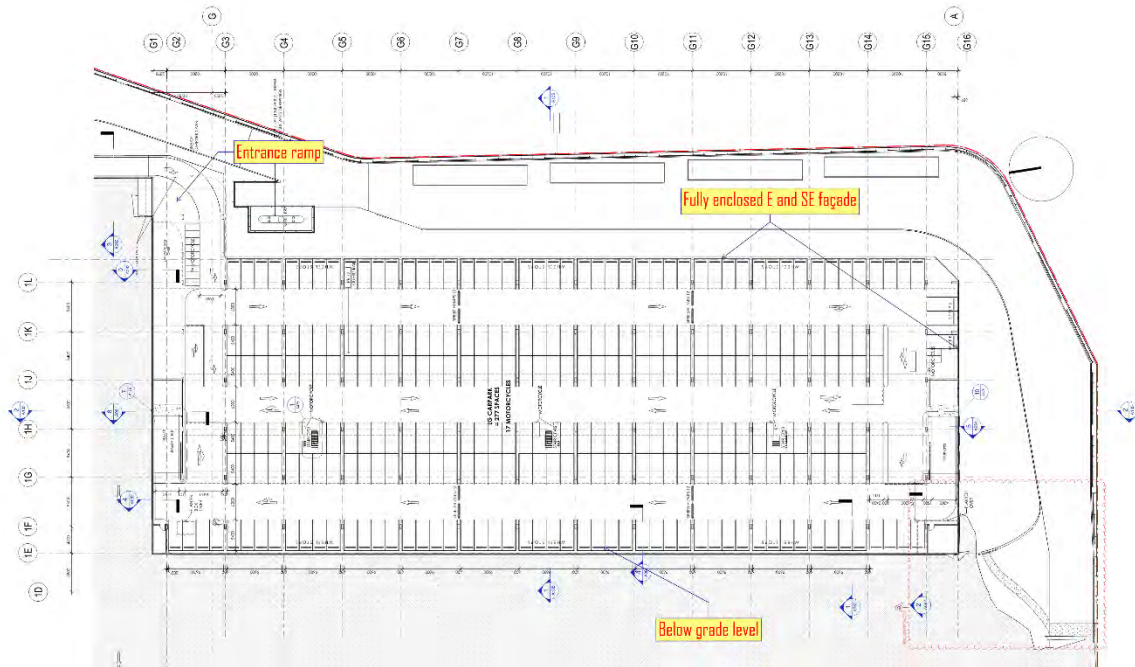


Figure 1. *Underground car park layout*

1.1 DTS design requirements

In line with the DTS requirement of the (NCC, 2019) and (AS1668.2, 2012), CO generation and exhaust air flow rates are calculated as described in the Detailed Procedure Section 4.4.4 of (AS1668.2, 2012).

- Parking usage factor = 0.5 - Commercial
- Vehicle type factor = 1.0 - No special vehicle
- Staff exposure factor = 1.0 - Self-parking
- Staff Usage factor = 1.0 - Self-parking

The CO generation rate and the minimum exhaust air flow required were calculated to be 0.0019872kg/s and 37,230L/s, respectively. Calculation details are summarised in Table 1.

Complying with the DTS requirements mean that a series of exhaust air fans are required to extract more than 37m³ of air out of the car park at its peak operation. This was initially nominated through four fans (10m³/s) each, in addition to 100s of meters of duct work to cover the full length of the car park (AS1668.2, 2012). Additionally, a series of make-up air fans were required to ensure “clean” air is provided into the car park at a rate of approximately 80 per cent of the exhaust air, i.e., ~30m³.

Item	-	#	UoM	Remarks
Carpark area	A	7480	m ²	
No of cars in this zone	n1	292	No	
No of cars other zones with exit path in this zone	n2	0	No	
Driving distance cars in this zone	d1	200	m	
Driving distance cars in other zones with exit path in this zone.	d2	0	m	
Parking usage factor	P	0.5	-	Table 4.1
Vehicle type factor	T	1.0	-	Table 4.2
Staff exposure factor	E	1.0	-	Table 4.3
Staff Usage Factor	F	1.0	-	Table 4.3
CO Generation Rate	CO	0.0019872	kg/s	Appendix J (AS1668.2, 2012)
AIR Generation Rate	AIR	0.3954572	kg/s	Mass Fraction of Car Exhaust
C Formula	=	$Px(100xn1+n1xd1+n2xd2)$		
Contaminant Generation Rate	C	43800	-	Clause 4.4.4.1

Table 1 *Underground car park details and ventilation calculations (AS1668.2, 2012)*

(a) 0.85 C x E x T	37,230	L/s
(b) 2000 x F x T	2,000	L/s
(c) 3.0 x A	22,440	L/s
Required exhaust rate	37,230	L/s
Exhaust Rate	5.98	L/s/m ²
Supply Air Rate @ 80% (75% minimum)	29,784	L/s

Table 2. *Exhaust and supply air calculations (AS1668.2, 2012)*

1.2 Design development of assisted natural ventilation system

The two deciding factors in the façade changes were mainly driven by nature, the first being the ground slope, and the second is the dominant wind direction in Horsley Park.

The ground had lower levels in the East and South sides of the building, hence the opportunity to turn the supporting wall/façade into a source of wind (clear air). A summary of the major climate statistics has been recorded for Horsley Park NSW for the last 30 years is available for the public at the Bureau of Meteorology's website (BoM, 2021). Wind records show that mean wind speed throughout the year at 3pm is 16.6km/h (4.6m/s). The dominant wind directions are East and South-East throughout the year. This, coincidentally, aligned perfectly with the ground slope direction.

A number of façade openings were nominated, which were inspired by early-stage proof-of-concept CFD models. Both the architect and structural engineer were open to the idea of change and were very supportive in making the necessary changes. These façade openings paved the way to introducing wind into the partly underground car park, however, the new design still fails to comply with the natural ventilation requirements (AS1668.4, 2012).

The alternative path of compliance was performance solution, by simply meeting the intent of the code, without meeting the letter of the code. This is permitted by the Australian codes and

standards, (AS1668.2, 2012); “*Any other arrangement may be used, provided it is demonstrated to limit the CO concentration, between 750mm and 1800mm above the floor, less than—*

- (a) *60ppm 1 h maximum average;*
- (b) *100ppm 30 minute maximum average; and*
- (c) *30ppm (TWA) 8h.”*

The early-stage CFD models demonstrated a clear problem, dead spots where CO concentration levels were above the maximum levels allowed by the Australian Standards. A number CFD models were run to understand the behaviour of the car park at different wind scenarios;

- East wind shown the best results due to the large façade opening being on the long side of the car park,
- West wind led to negatively pressurising the car park resulting in low CO concentration levels,
- North and South winds struggled to meet compliance due to the long travel distance within the car park.

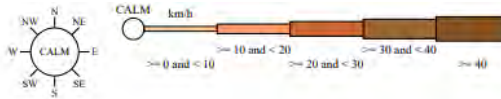
Dead spots mainly clustered around the centre of the car park; it was obvious that the natural ventilation model requires a method to push air further into the car park then out of it. First, a series of jet fans were suggested for this task, however, this could solve the problem from one direction, hence, jet fans had to be doubled. This was an inconvenience solution for a number of reasons, including electrical infrastructure, fire compliance, and cost. Additionally, this solution did not align well with the design philosophy adopted in this project; “cheaper AND better”.

Instead, truly-reversible in-line fans were nominated, which is a concept called “tidal flow”. This is where the fans are controlled to work with the dominant breeze. This is a common concept used in tunnels and we have viewed the car park as a tunnel.

The fans’ operation is supported by a local weather station, which measures wind direction and wind strength. The wind direction is fed to the BMS controller as a degree angle clockwise from North. With this data, the BMS controller will determine which direction the axial fans shall operate in.

However, fan speed is generated from the CO monoxide reading. When the reading gets to 30ppm, the fans shall commence at 30Hz (approximately 50 per cent airflow). The VSD (Variable Speed Drive) shall ramp the fans in direct proportion to the CO reading so that at 50ppm, the fans are operating at 50Hz (100 per cent airflow). Additionally, smoke detectors were nominated to shut the fans off immediately, should smoke is detected within the car park.

As shown in Figure 2, blue wind directions will have the fans work in concert and blow towards the North. Green wind directions will have the fans work in concert and blow towards the South. The remaining directions will have the fans work to blow towards the nearest ramp (i.e. they will blow in opposite directions).



3 pm
8218 Total Observations

Calm 3%

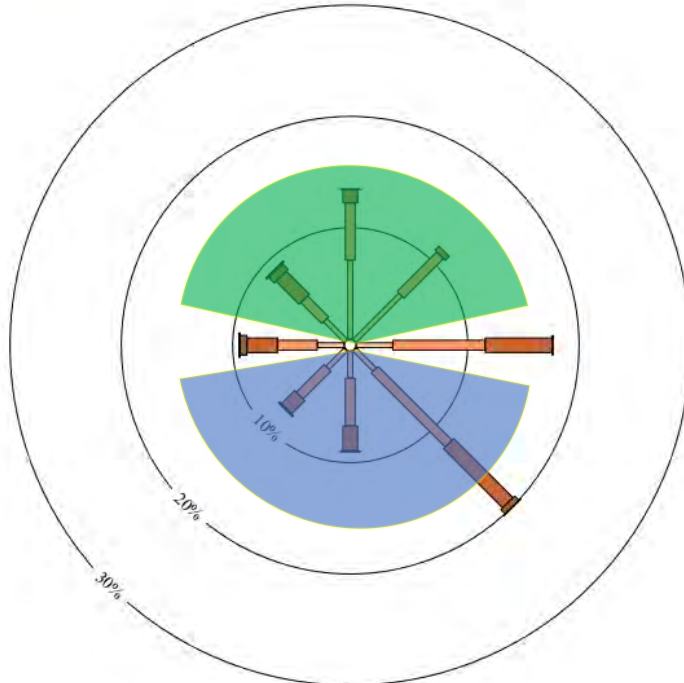


Figure 2 BOM wind rose and fans control strategy, blue directions blow air North, while green blow wind South (BoM, 2021)

2. CFD MODELLING AND RESULTS

2.1 Basis of modelling

The car park was modelled using one of the leading CFD programs to simulate a full hour of peak vehicle use with assisted natural ventilation. The model demonstrated compliance for the relative exposure criterion. The CO generation rate used in the model was derived from formulae obtained from the Australian Standards (AS1668.2, 2012) and applied conservatively throughout.

The simulation was run for the theoretical busiest hour as required by the standard and the average rise in carbon monoxide levels recorded was below 51ppm. As the model never recorded an average reading above 25ppm, the model achieves compliance with both the 1-hour criterion and the 8-hour criterion with a considerable safety margin.

The CO introduced into the model is calculated from the equations given in the Australian Standards (AS1668.2, 2012). It has been assumed that the exhaust gases from the vehicle are at 260°C and made up of only air and carbon monoxide. The percentage of CO in the exhaust gases has been estimated to be 0.5% of the total exhaust volume. The remainder of the exhaust volume has been modelled as heated air. This heated volume of air is intended to give a more

accurate representation of the exhaust gas movement. The exhaust gas is introduced along the floor plate.

A number of safety factors have also been considered to ensure the car park will not exceed the maximum allowable CO concentration levels, even in peak operations;

- The simulation was run with an initial CO concentration rate of 33.5ppm,
- Wind was modelled as a breeze at 0.5m/s, this was a very conservative assumption considering that the mean wind speed in Horsley Park is 4.6m/s,
- The car park was modelled at full occupancy, assuming all vehicles are sitting idle with engines on, which introduces the highest CO generation rate of internal combustion engines.

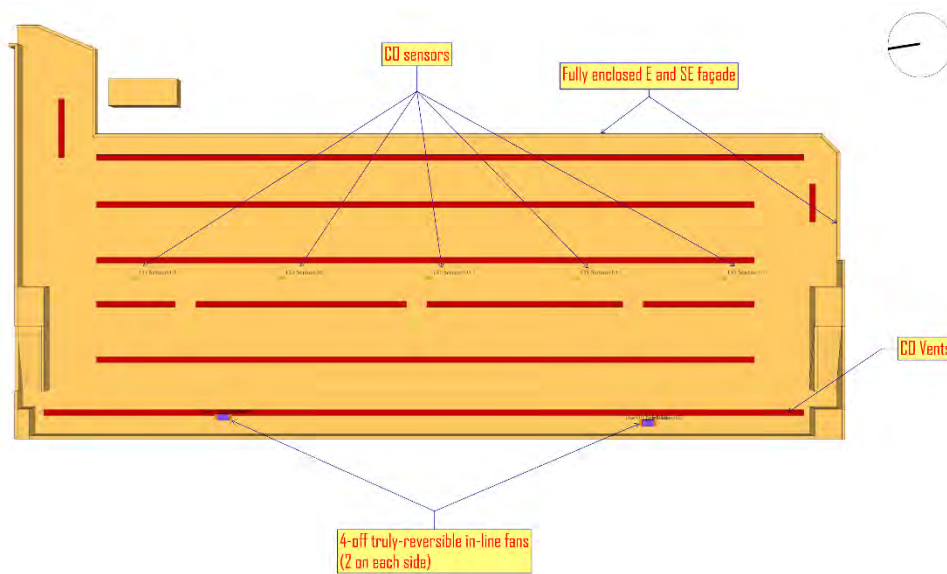


Figure 3. Car park model showing geometry features

2.2 CFD modelling results

The car park was modelling using one of the leading CFD programs to simulate a full hour of peak vehicle use with assisted natural ventilation. The model demonstrated compliance for the relative exposure criterion. The CO generation rate used in the model was derived from formulae obtained from the Australian Standards (AS1668.2, 2012) and applied conservatively throughout.

The Australian Standards (AS1668.2, 2012) outline the basis for the CO generation rate equation used in the design requirements in Clause 4.4.4. The formula aims for a one hour average CO concentration of 60ppm assuming the ambient level of CO is 9ppm (i.e. 51 ppm rise). The car park CFD model measures the rise in CO, and it has 0ppm ambient CO. Therefore, the maximum allowable average in these results is 51 ppm (1 hr criterion). Output slices show the volume fraction of CO in ppm were positioned at 750mm and 1800mm above floor level, Figures 4 and 5.

The output slice results show that the CO levels never exceed 51 ppm in any location in the car park. CO levels build from 0 seconds until it peaks and reaches a quasi-steady state. This

demonstrates that at the theoretical peak car park usage the proposed natural ventilation handles the CO output.

The simulation has been repeated using multiple wind scenarios to ensure the car park will maintain acceptable CO concentration levels all year round.

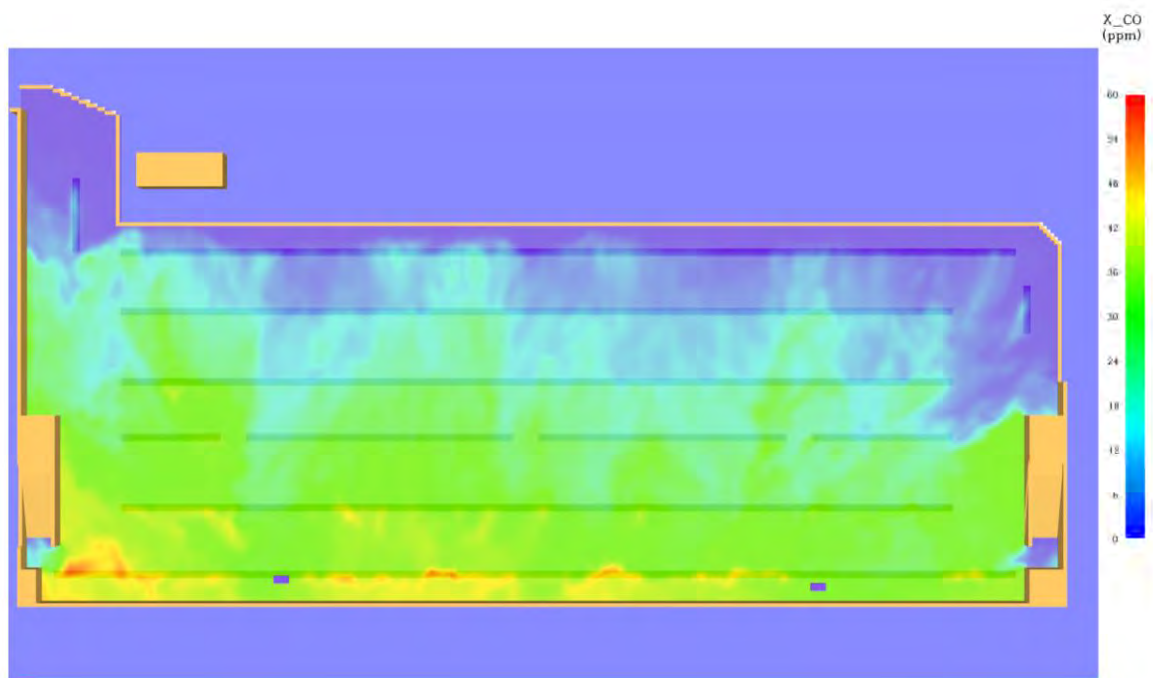


Figure 4. *CO Output slice file in ppm for the underground car park as a prediction for CO at 0.75m above floor level at 1 hours*

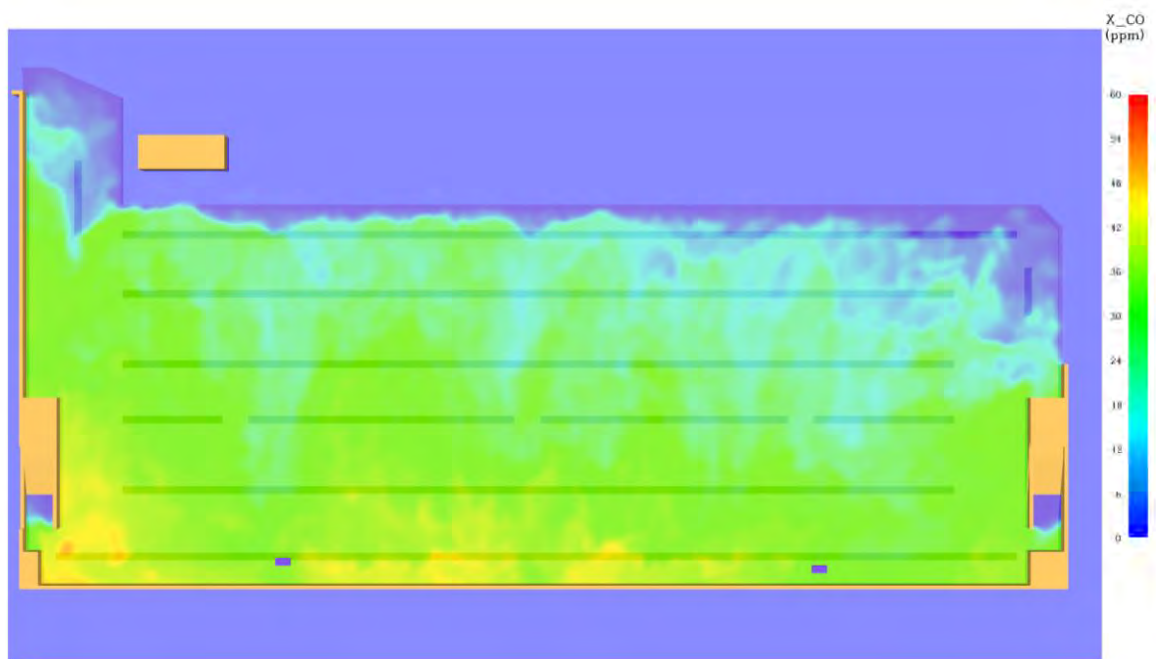


Figure 5. *CO Output slice file in ppm for the underground car park as a prediction for CO at 1.80m above floor level at 1 hours*

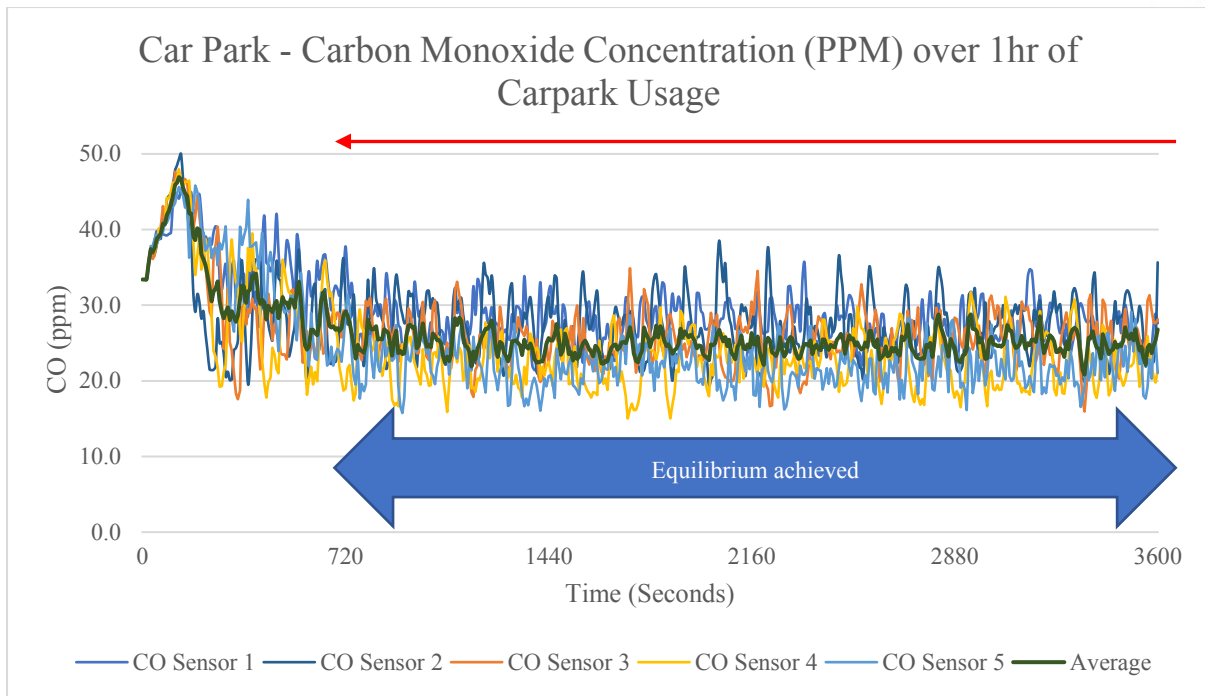


Figure 6. The plot of worst-case 1-hour in the underground car park over 5 sensor locations, Red Line shows compliance criteria for the 8-hour criteria. Equilibrium is established at 16 minutes into the simulation

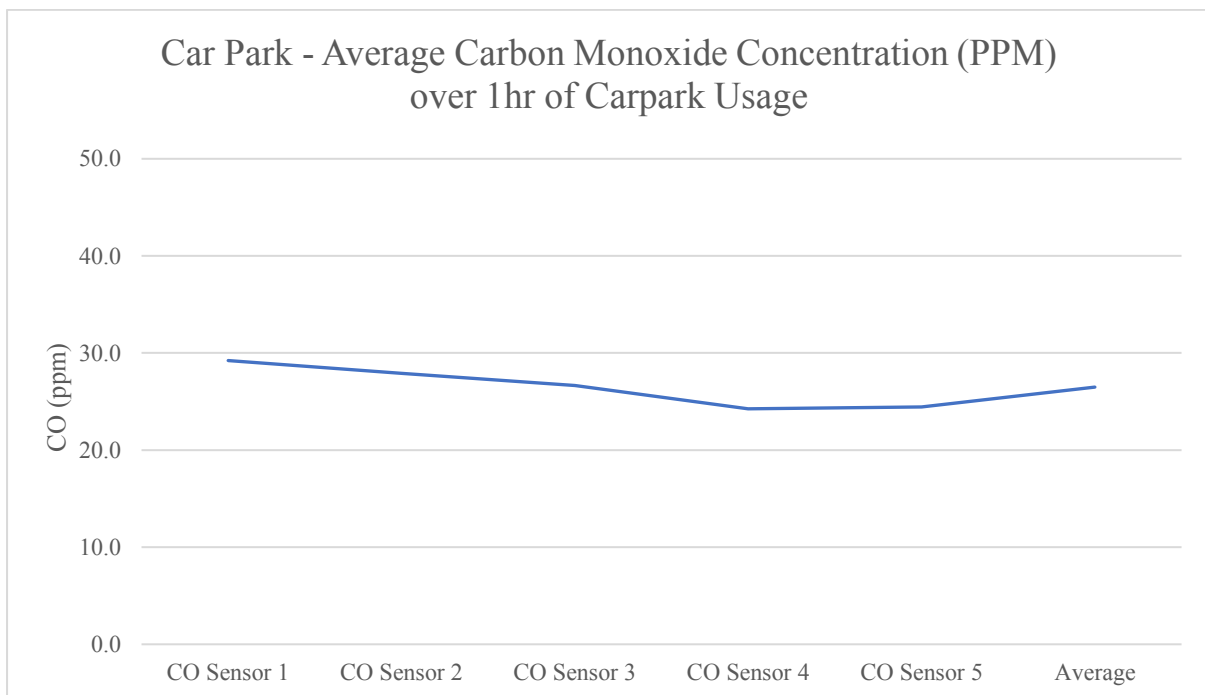


Figure 7. Worst-Case 1 Hour Averages for the underground car park over 5 sensor locations

3. THE AFTERMATH

In hindsight, this project managed to achieve a number of important milestones; the first being the financial savings and cost reduction, the second being the environmental impact. In other words, the carbon footprint of everything that did not need to be manufactured or delivered in the first place.

3.1 The finance

As mentioned earlier, the value management exercise was prompted by tight budget, reducing the overall project budget was pivotal for the project's success. The DTS design included;

- 4-off exhaust air fans, 10,000L/s each
- 3-off make up air fans, 10,000L/s each
- 7-off VSDs
- 400~450 linear meters of ductwork (varying dimensions)

According to the project estimators, this could have had a price tag of approximately \$200,000, excluding the associated electrical works, which were estimated at some point to be around the \$50,000.

Compared to the new design which simply consisted of;

- 4-off reversible fans
- 4-off VSDs
- Local weather station

The contractor confirmed that the cost of the proposed design did not cross the \$40,000 mark, distributed evenly between the equipment and installation (including associated electrical works).

In total, the new design assisted in reducing the project budget by approximately \$200,000, that was well beyond the \$100,000 target set from day 1 by the client.

3.2 The carbon footprint

For every decision we make, there is an impact on the environment. The carbon footprint of the DTS design was not a small one, ductwork manufacturing, fabrication, and transportation require huge amounts of energy.

I mentioned in the beginning that good actions have good consequences, which is very true in this case. It was estimated that the project will require 13~15 tonnes of ductwork, which is made of Galvanised Steel.

The embodied carbon in GI steel is assumed to have two factors; the steel manufacturing, and the galvanisation.

The Galvanisers Association in the UK estimates that the embodied carbon to manufacture and galvanise are 0.919 and 0.215 kgCO₂e per kg of steel (Galvanisers Association, 2021).

Unfortunately, not enough data is available to estimate the carbon footprint of ductwork fabrication and transportation, however, some estimate that the construction industry introduces 50 per cent of its carbon footprint via products, while a whopping 50 per cent is introduced via transportations, installation, operation and decommissioning towards the end-of-life. Table 3 lists the embodied carbon in GI steel manufacturing, while Figure 8 is a summary of the carbon footprint of the construction lifecycle.

Process	Embodied Carbon – kgCO ₂ e/kg Steel
Steel manufacturing (sheets)	0.919
Galvanisation	0.100~0.33

Table 3 Embodied carbon in GI steel manufacturing (Galvanisers Association, 2021)

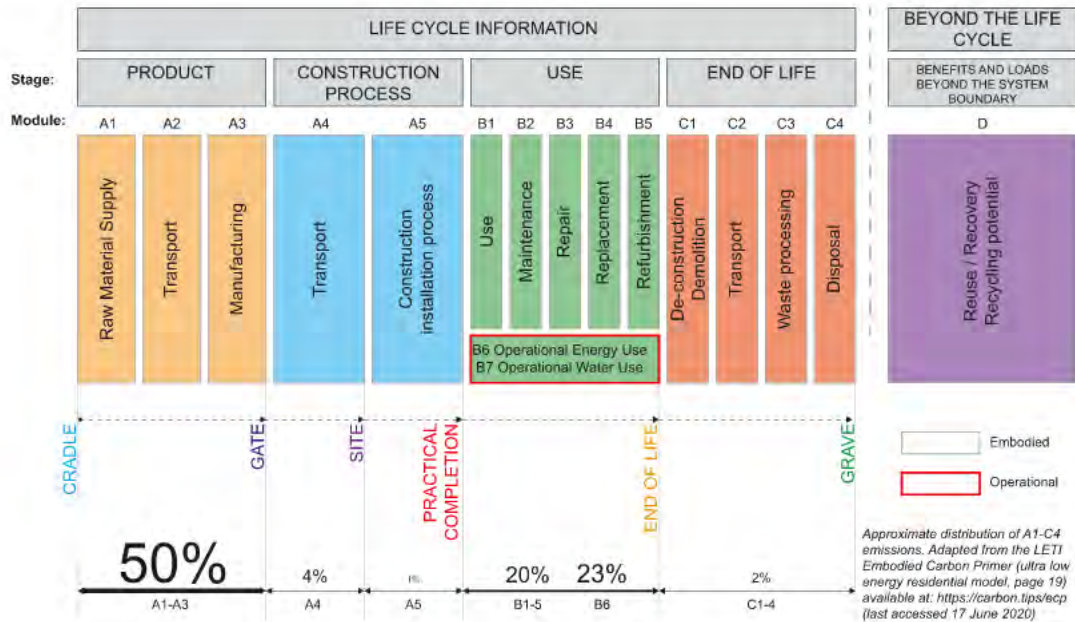


Figure 8. The carbon footprint of the construction lifecycle (The Institution of Structural Engineers, 2020)

With the financial benefits on the side, we estimate that the environmental impact has been reduced by approximately 31,750kgCO₂e, distributed evenly between manufacturing and operation.

This is environmental price tag of everything that did not need to be manufactured, fabricated, transported, maintained or decommissioned in the first place.

CONCLUSION

Ever since the dawn of humanity, mankind has been interested in observing and documenting natural behaviour. We have gathered so much information that we are now able to predict what the weather is going to look like tomorrow, or even that the temperature will rise by 1.5°C by 2050 or so. The predictability of nature is a great tool that, us engineers and architects, should be using more often in our designs.

In this paper, we examine a recent car park case study to demonstrate how CFD simulation allows a designer to exploit the concept of assisted natural ventilation. This led to introducing massive reduction of equipment and material usage compared to the DTS-compliant design, and a reduction in Source-Energy, not only Site-Energy.

The foundation for the new design may simply be open mindedness, but the necessary tools are data analysis and CFD simulation. Ventilation is all about bringing in “clean” air instead of “contaminated” air, and nature does a good job of this easily. Deemed-to-Satisfy (DTS) requirements for natural ventilation cannot always be met for various structural and

architectural reasons, and the Australian standards prefer to address car park ventilation via either mechanical or natural ventilation, not both. Using CFD simulation tactics, this marriage is made possible.

In conclusion, unconventional design strategies, supported by CFD modelling assisted in reducing the project budget by approximately \$200,000, in addition to reducing the carbon footprint of the car park construction by 31,750kgCO₂e.

ACKNOWLEDGEMENTS

The authors would like to acknowledge the work of Rob Lord of SEED Engineers in assisting with the preparation of this paper, as well as the continuous support and encouragement for many years now.

REFERENCES

Australian Building Codes Board (2019). National Construction Code Volume One – Building Code of Australia. SAI Global database.

Standards Australia (2012). The use of ventilation and airconditioning in buildings. Part 2: Mechanical ventilation in buildings, AS 1668.2-2012 (Incorporating Amendment Nos 1 and 2). SAI Global database.

Standards Australia (2012). The use of ventilation and airconditioning in buildings. Part 4: Natural ventilation in buildings, AS 1668.4-2012. SAI Global database.

LETI Embodied Carbon Primer (ultra-low energy residential model, page 19) available at: <https://carbon.tips/ecp> (last accessed 17 June 2020).

ISO 14040 series of environmental standards, the ‘system expansion’ method of life cycle assessment.

John Orr, Orlando Gibbons and Will Arnold, A brief guide to calculating embodied carbon, 2020, <https://www.istructe.org/IStructE/media/Public/TSE-Archive/2020/A-brief-guide-to-calculating-embodied-carbon.pdf>

BoM. (2021). Climate statistics for Australian locations. Retrieved from BOM: http://www.bom.gov.au/climate/averages/tables/cw_067119_All.shtml

Galvanisers Association. (2021). Galvanized steel – embodied carbon. Retrieved from Galvanisers Association UK: <https://www.galvanizing.org.uk/sustainable-construction/galvanizing-is-sustainable/galvanized-steel-embodied-carbon/>

DISCLAIMER

The information or advice contained in these technical papers is intended for use only by professionals who have had adequate technical training in the field to which the paper relates. At the time of publication, these technical papers have undergone a formal peer-review process.

These documents have been compiled as an aid only, and the information or advice should be verified before it is put to use. The user should also establish the applicability of the information or advice in relation to any specific circumstances. While the information or advice is believed

to be correct, no responsibility is taken by AIRAH or IBPSA Australasia for any statements made within.

AIRAH and IBPSA Australasia, its officers, employees and agents, disclaim responsibility for any inaccuracies contained within the documents, including those due to any negligence in the preparation and publication of the said technical papers.

COPYRIGHT

This work is copyright. Apart from any use as permitted under the Copyright Act 1986, no part may be reproduced by any process without prior written permission from either the Australian Institute of Refrigeration, Air Conditioning and Heating (AIRAH) or the International Building Performance Simulation Association (IBPSA) Australasia.

A REAL-WORLD APPLICATION OF MACHINE LEARNING AND OPTIMAL CONTROL SIMULATION FOR CHILLED WATER PLANTS

MICHAEL BERGER

Head of R&D

Conserve It

6/10 Artemis Lane, Melbourne VIC 3000

info@conserveitiot.com

ABOUT THE AUTHOR

As the Head of R&D at Conserve It, Michael leads efforts to research, prototype, and trial machine-learning algorithms for analytics and real-time optimisation of live equipment in the built environment, with applications ranging from innovative chiller plant optimisation and predictive maintenance to advanced controls solutions. Michael graduated with a Master of Engineering in France before gaining experience at a leading research centre and an environmentally sustainable design consultancy in Singapore. Since 2014 he has worked at Conserve It, where he draws on his extensive experience in the fields of energy efficiency, chiller plant optimisation and machine learning.

ABSTRACT

In commercial buildings, the chilled water plant is typically the most energy intensive centralised component, therefore decreasing its energy consumption is key to improving the energy efficiency of buildings and contributing to reducing CO₂ emissions. The complexity of these systems has grown in the past few decades, and today numerous variables that have impact on the overall plant energy usage can be adjusted during operation. This paper proposes an optimal control strategy to select these variables with the objective to minimise energy consumption. The proposed approach relies on developing accurate machine learning models of key equipment within the plant. These models are used to run simulations in real-time to predict the energy consumption of the plant and find the control commands that minimise it holistically. The solution has been deployed in real buildings on embedded computers and has achieved demonstrable energy savings on site without relying on reducing the cooling production of the plant, therefore without compromising on space comfort.

INTRODUCTION

Buildings account for a third of the global energy consumption, and Heating, Ventilation and Air Conditioning (HVAC) systems are responsible for 38 per cent of their energy consumption [5]. Chilled water plants (which include chillers, cooling towers and pumps) are a key component of most HVAC systems [7], and they typically account for up to 49 per cent of the energy use of a building's HVAC system [7]. Due to the proliferation of variable speed drives for chillers, pumps, and cooling towers, the speed of every machine can be adjusted in real-time in most modern plants. This is typically done by an automated management system that controls the speed commands to maintain specific sensor values, like flows or temperatures, commonly known as setpoints in the industry. Given that the plant is an interconnected system,

varying the speed of one machine often impacts the energy usage of other machines in the plant, inducing trade-offs between machines that can be challenging to predict. These interactions will be exposed in more detail further in the paper. Additionally, variation in weather and cooling demand from the building (commonly referred to as cooling load) over both short (hourly) and long (seasonally) timescales affect the performance of some equipment, therefore a fixed control strategy that ignores these factors may not always extract the maximum efficiency from the overall plant. Similarly, degradation of equipment performance over their life span may result in the theoretical optimal control strategy to vary over the years, as some equipment may degrade more than others and their interactions may change.

A real-time model-based optimal controls approach has been developed to tackle these challenges. It has been deployed successfully on site and real-world results are presented in this study. The approach relies on creating a digital twin of the chilled water plant by combining machine learning models of key equipment. The digital twin is then used to run simulations, given the current load and weather conditions, to predict the energy usage of the plant at various setpoints, within the safe operating range of the equipment as documented by the manufacturers, and select the control strategy that results in the lowest energy usage for the overall plant. The digital twin models are updated automatically on a daily basis to capture performance variation of the equipment. The approach aims to maintain the cooling production of the plant, and therefore is not expected to compromise space comfort.

1. MACHINE LEARNING

1.1 Motivations and method

Machine learning allows automated applications to learn the behaviour of systems or processes from historical data in order to predict future outcomes. In the proposed framework, machine learning techniques are used to learn the power usage of each key piece of equipment in the plant given various inputs such as cooling loads, temperatures, or flows. In turn, these machine learning models will be used to predict the overall power usage of the plant in various scenarios, as detailed further in Section 2 below.

The machine learning approach is intended to have the ability to run autonomously and regularly on site and learn in real-time the actual equipment specificities and performance degradation over time without human interaction. As such, constrained least-square multivariate polynomial regression was selected as the machine learning method. This method fits a polynomial equation to a dataset with multiple variables by calibrating the equation's coefficients. It allows for fast computations, thanks to state-of-the-art optimisation algorithms such as Interior Point methods [3]. These methods are effective at finding the best polynomial equation coefficients that minimise the error between the predicted power and the actual power by using the knowledge of derivatives and 2nd order derivatives of the error [3]. The low computational complexity allows the solution to be deployable on low-powered embedded computers on site. Further explanations of the concepts of regression, optimisation algorithms and Interior Point methods can be found in the book *Convex Optimization* by Boyd et al. [3]. The constrained aspect of the method also handles cases where initial data availability is limited by inducing expected behaviours to the model. These expected behaviours of the equipment were gathered by consulting subject matter experts. Such induced behaviours include, for example, that the power usage of a cooling tower is expected to increase when it produces more cooling while all other input variables remain constant.

1.2 Sites for validation

Datasets have been gathered from six different anonymised sites for the purpose of validating the machine learning approach. The first two sites were then used as case studies for the deployment of the whole optimal controls approach, as detailed further in Section 4.

The sites' characteristics are displayed on Table 1.

	Building Type	Location	Climate	Chillers	Cooling Towers
Site A	Hospital	Victoria, Australia	Temperate oceanic	Screw	Evaporative
Site B	Commercial	Hong Kong	Humid subtropical	Screw	Non-evaporative
Site C	Commercial	Western Australia	Subtropical	Centrifugal	Evaporative
Site D	Commercial	Western Australia	Subtropical	Centrifugal	Evaporative
Site E	Commercial	Southeast Asia	Tropical	Centrifugal	Evaporative
Site F	Commercial	USA	Continental	-	Evaporative

Table 1. *Sites used for validation and/or deployment case studies*

1.3 Chillers

Water-cooled chiller power models have been proposed in previous work and in some instances validated with site data [1, 8]. A similar approach is used here, with slight modifications to suit the application of real-time energy usage optimisation. The power usage of a water-cooled chiller is predicted using 2nd order multivariate polynomial regression, which is a version of the regression approach detailed in Section 1.1 using a 2nd order polynomial equation. The input variables to this equation are proposed to be the cooling load (i.e., the amount of cooling produced by the chiller), the leaving chilled water temperature (LCHWT), the entering condenser water temperature (ECWT), and the condenser water (CW) flow, as per Equation 1. Note that the chilled water is the cold water produced by the chiller flowing towards the building, and the condenser water is the water flowing from cooling tower to the condenser of the chiller. Further explanations of these chillers-related terms can be found in the book *Fundamentals of Design and Control of Central Chilled-Water Plants* by Taylor T. S [9].

$$Power_{chiller} = P(Load, T_{ECW}, T_{LCHW}, Flow_{CW}) \quad (1)$$

The modeling approach was validated with various chillers from different anonymised sites in Australia and overseas using recorded operating data on site. As shown on Table 2, the model consistently predicted the power usage with a high degree of accuracy.

	Site A	Site B			Site C	
Chiller n°	2	1	2	3	1	2
MAE (kW)	4.1	2.6	2.8	3.9	11.0	10.6
MAE/Mean	4.6 %	2.4 %	2.4 %	3.4 %	6.5 %	6.4 %
R-squared	0.949	0.990	0.984	0.979	0.949	0.938

Table 2. *Chiller model learning results with site data, Mean Absolute Error (MAE) and R-squared*

This is further illustrated on Figures 1 and 2, displaying the actual recorded power and the predicted power for one chiller with the resulting predicted chiller COP.

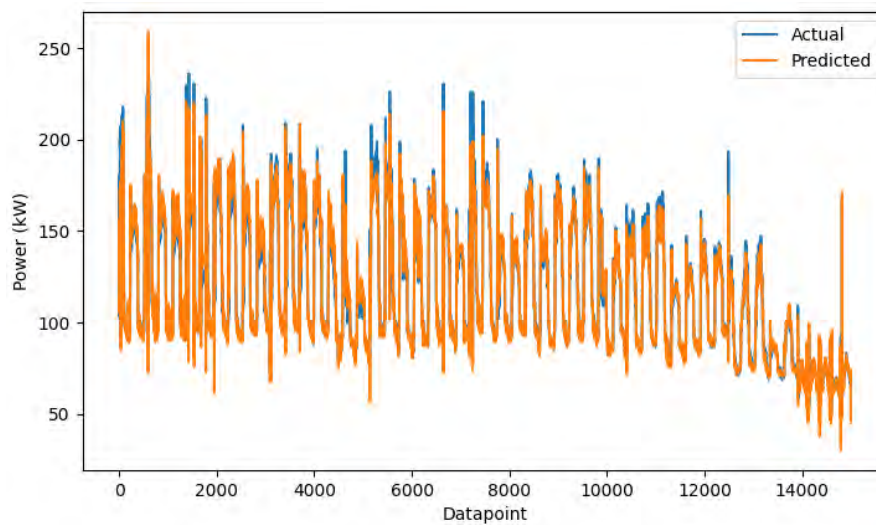


Figure 1. Site B, Chiller 1 predicted power compared to the actual measured power

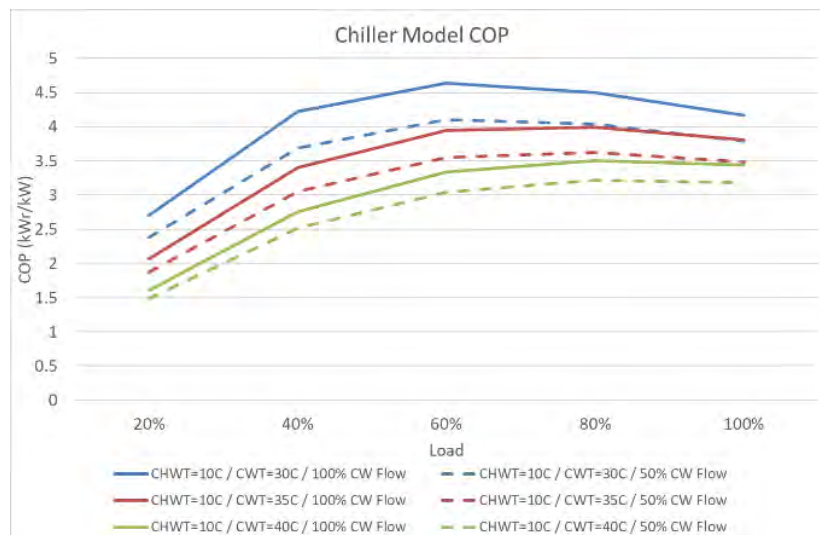


Figure 2. Site B, Chiller 1 predicted COP from chiller model for a range of conditions

1.4 Condenser pumps

The power usage of a CW pump is predicted using Equation 2, a 2nd order multivariate polynomial regression, with the CW flow as the main feature. Refer to Sections 1.1 and 1.3 for further explanations on the concept of regression. In the case of a so-called “headered” pump arrangement, i.e. where the pumps are in manifold to supply all the chillers, the relative number of pumps enabled and chillers enabled was found to be a good additional feature. It captures the variation of pressure differential between the outlet and inlet of the pumps, induced by having more or fewer pumps for the same number of chillers, in absence of differential pressure sensors per pump, which are seldom available.

$$Power_{CW\ pump} = P(Flow_{CW}, Number\ of\ chillers, Number\ of\ pumps) \quad (2)$$

The modeling approach was validated with several pumps from different anonymised sites in Australia and overseas using recorded operating data on site. As shown on Table 3, the model consistently predicted the power usage with a good accuracy.

	Site B	Site C		Site D		Site E
Pump n°	1, 2 & 3 averaged	1	2	1	2	1, 2 & 3 averaged
MAE (kW)	0.7	0.7	0.5	0.6	0.3	0.6
MAE/Mean	4.7 %	2.7 %	2.4 %	4.8 %	3.5 %	2.7 %
R-squared	0.241	0.891	0.986	0.978	0.988	0.971

Table 3. Condenser pump model learning results with site data

Note that at Site B, the pumps were run at a few discrete speed values for most of the learning period, which may explain the relatively low R-squared value. Nevertheless, the low error shows the model performs relatively well even in such case. Note that due to lack of required sensors on Site A, it was not possible to test the condenser pump model learning, hence why it is omitted on Table 3. However, the model did consistently predict the power usage with a good accuracy for a total of 10 pumps at four different sites, so this is not expected to be of significant impact.

This is further illustrated on Figure 3, displaying the actual recorded power and the predicted power for pump n° 1 of Site C.

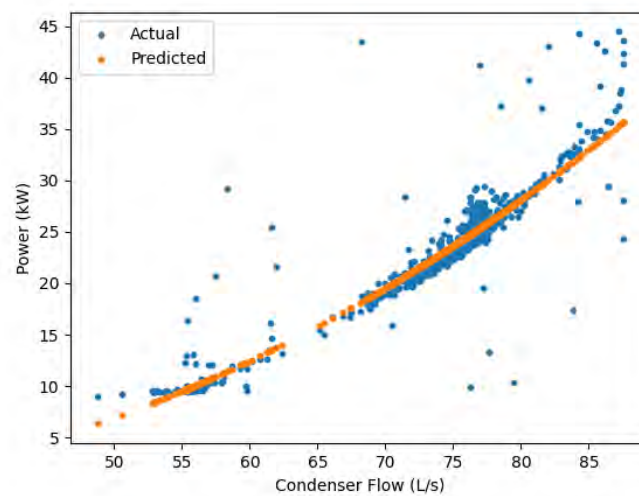


Figure 3. Site C, pump n° 1 predicted power compared to the actual measured power

1.5 Heat rejection equipment

Heat rejection equipment for water-cooled chillers is typically either evaporative cooling towers or non-evaporative so-called “dry-coolers”. Several evaporative cooling tower models have been introduced in the literature [2, 6, 10], but they present characteristics that make them unsuitable for the application. For instance, they are used to predict variables other than the power usage. Still, the proposed variables and type of models have been used as direction to develop the present model, in addition to domain expert knowledge and data analysis from site data. Using Equation 3, the evaporative cooling tower power usage is predicted using 3rd order multivariate polynomial regression, using the heat rejected, wet-bulb outdoor air (OA)

temperature and leaving cooling tower temperature (LCTT). The impact of the CW Flow is expected to be captured by the heat rejected, as it is a function of the CW Flow, and is therefore not included as input variable. Note that the leaving cooling tower temperature (LCTT) can generally be considered equivalent to the ECWT to the chiller, as the water leaving the cooling tower directly flows towards the chillers' condensers.

$$Power_{evaporative-cooler} = P(Heat_{rejected}, T_{LCT}, T_{OA,wetbulb}) \quad (3)$$

In the case of dry-coolers, the dry-bulb outdoor air temperature is substituted, as per Equation 4.

$$Power_{dry-cooler} = P(Heat_{rejected}, T_{LCT}, T_{OA,drybulb}) \quad (4)$$

The modeling approach was validated with numerous cooling towers from different anonymised sites in Australia and abroad using recorded operating data on site. As shown on Table 4, the model consistently predicted the power usage with a good accuracy.

	Site A	Site B	Site C	Site E	Site F
Type	Evap.	Dry	Evap.	Evap.	Evap.
Rated Power (kW)	30	132	12.5	380	5.6
MAE (kW)	1.1	7.9	1.0	10.9	0.2
R-squared	0.829	0.627	0.714	0.919	0.701

Table 4. Cooling towers model learning results with site data

This is further illustrated on Figures 4 and 5, displaying the actual recorded power and the predicted power for a cooling tower with the resulting predicted power over a range of conditions. Note that approach temperature, which is the difference between the leaving cooling tower temperature and the wet-bulb temperature in Kelvin, is used for convenience of visualisation.

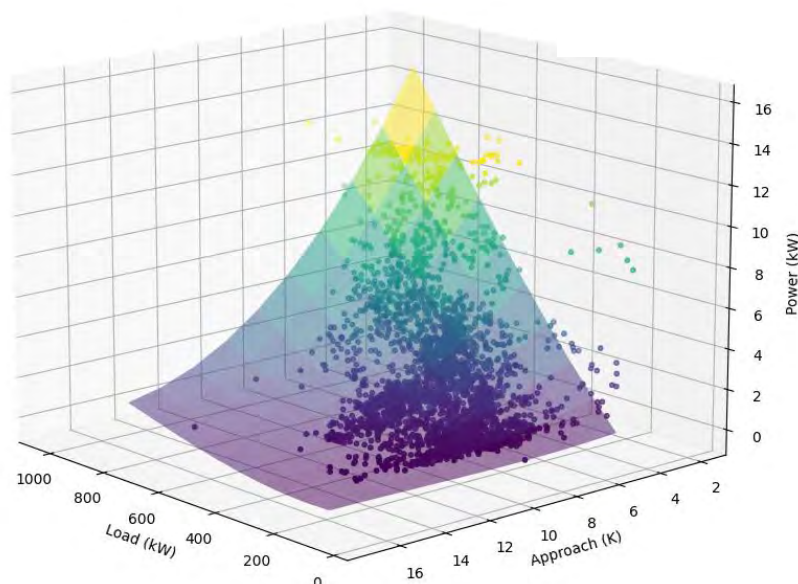


Figure 4. Site C, cooling tower predicted power compared to the actual measured power

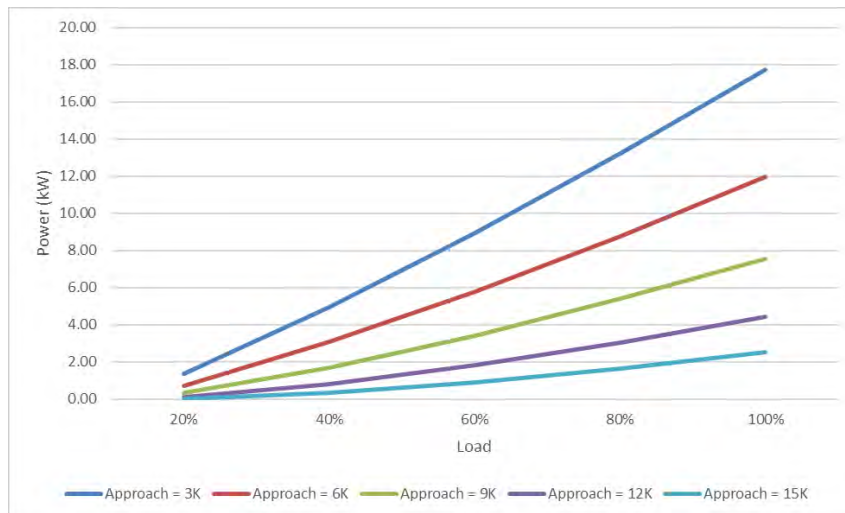


Figure 5. Site C, predicted power from cooling tower model for a range of conditions

2. OPTIMISATION APPROACH

2.1 Formulation

The objective of the optimisation approach is to minimise holistically the power usage of the plant, which can be predicted using the power model of the individual equipment in Equation 5.

$$Power_{plant} = \sum_{i=1}^n P_{chiller,i} + \sum_{j=1}^m P_{cw\ pump,j} + \sum_{k=1}^p P_{coolingtower,k} \quad (5)$$

The decision variables that are being controlled to do so are the leaving cooling towers temperature (LCTT), the CW Flow for each chiller and the cooling load *per* chiller.

The LCTT setpoint value affects not only the speed of the cooling towers, but also the entering condenser water temperature at the chillers, and therefore the power usage of the chillers as well.

The CW Flow setpoint value will affect the speed of the CW pump and also the power usage of the chiller. Lower CW Flow results in higher leaving condenser water temperature (with all other values being equal) and therefore higher discharge pressure in the chiller, which requires the compressor to increase its speed and draw more power.

Finally, the cooling load *per* chiller variable is used to distribute the load between chillers to push them towards their efficiency “sweet-spot”. Note that the overall plant cooling load to be produced is still the same.

There are also a number of key constraints that fall into two categories.

1. To maintain the required level of comfort, which is done by having a constraint to maintain the overall plant cooling load production
2. To maintain the equipment within their safe operating zone

This approach can be formulated as a mathematical optimisation problem, as detailed in Equation 6.

$$\begin{aligned}
 & \text{Minimize } Power_{plant} \\
 & \text{Load}_i, Flow_{CW,i}, T_{LCT} \\
 \text{s. t.: } & \sum_{i=0}^n Load_i = Load_{plant,Target} \\
 & Load_{Min,i} \leq Load_i \leq Load_{Max,i} \\
 & LCTT_{Min} \leq LCTT \leq LCTT_{Max} \\
 & Flow_{CW,Min,i} \leq Flow_{CW,i} \leq Flow_{CW,Max,i}
 \end{aligned} \tag{6}$$

This approach ensures that all the relevant pieces of equipment in the system are considered and accounts for interrelations between the sub-systems. It captures the trade-offs induced by reducing the energy usage of one equipment on the other sub-systems, and it only selects decision variables if they reduce the overall power usage of the plant.

Note that in this proposed approach, the overall cooling production of the chiller plant is not affected. The plant cooling load is still targeted to be the same, as well as the chilled water temperature leaving the plant, the total chilled water flow, and the return chilled water from the building. As such, the output of the optimisation does not affect the comfort in the building, nor the chilled water pumps power usage and fan power usage at the Air Handling Units. Hence why these were ignored in the formulation.

2.2 Solving the optimisation

Simulations can be run to solve the optimisation problem and find the best set of setpoints that minimises the power usage while maintaining the constraints. For every combination of values of chillers' cooling loads, condenser water flows and LCTTs that are within the allowable ranges, the plant power usage can be predicted thanks to the equipment models. This method is suitable for small plants with two chillers or only a sub-set of the decision variables and can be applied for real-time optimisation on embedded hardware. However, for cases with more chillers, the number of combinations to assess increases exponentially and it quickly becomes impractical.

The proposed method for such cases is to use a Sequential Convex Programming Interior-point method for non-linear optimisation (NLP) [11]. This type of optimisation solver leverages the knowledge of derivatives and 2nd order derivatives of the plant power function to converge much faster towards the optimum point without having to assess every possible combination. Further explanation of this optimisation technique can be found in an article by Wächter A. and Biegler L. [11].

3. SIMULATIONS RESULTS

In a first instance, the simulations were run offline to evaluate the methodology and gain insights from the results. As an example, the optimisation of the LCTT setpoint for Site A for a chiller cooling load of 1,200kW and wet-bulb temperature of 18°C is displayed on Figure 6.

In this specific case, it is beneficial to set the LCTT setpoint at a low value. The increase in cooling tower power usage is more than compensated by the decrease in chiller power usage, resulting in overall significant power savings compared to a more standard setpoint of 29°C.

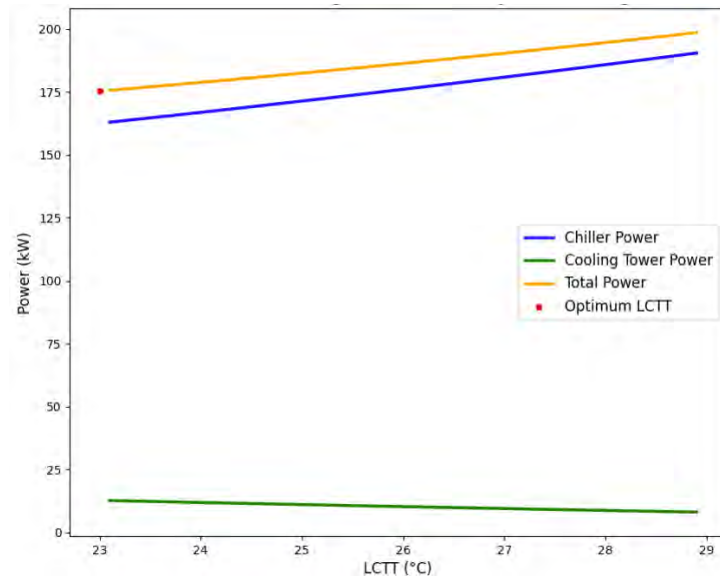


Figure 6. Site A, optimal LCTT showcasing trade-off between chiller and cooling tower power usage

On Site B, the combined impact of the optimal LCTT, CW Flow and chiller loads is displayed on Figure 7 for two chillers enabled simultaneously. Site B is equipped with dry-coolers and the chillers are designed to run at fairly high condenser temperatures. The conditions are at 30°C outdoor air dry-bulb temperature and 10°C Plant LCHWT setpoint, while the simulation is run for plant cooling loads on the whole range of operation. The savings are computed by comparing a case of conventional controls with constant CW Flow at design value, equally distributed cooling load on the chillers and LCTT dynamically reset based on the outdoor air temperature with fixed difference of 5 Kelvin.

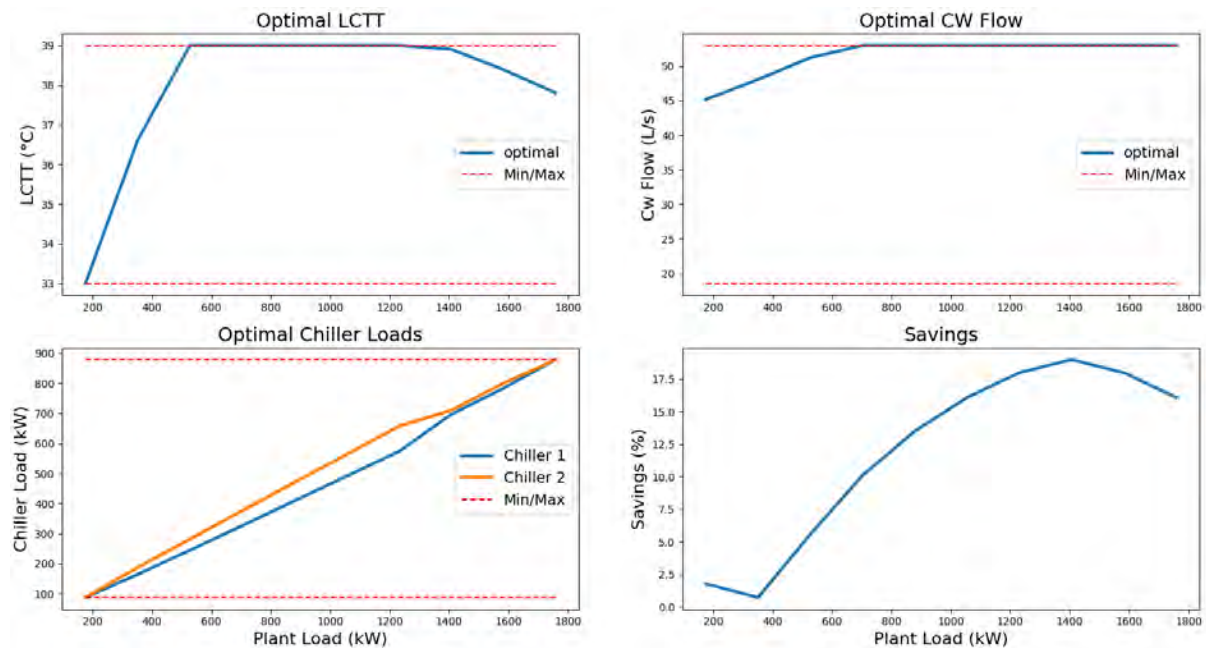


Figure 7. Site B, optimisation results at different plant cooling loads

The optimisation algorithm finds various optimal setpoints at each different plant load, which results in significant energy savings at most plant loads in this scenario, up to 17.5 per cent.

Note that such simulations were carried out on several other sites. It was observed that in most cases, the optimal LCTT was found to be at or near the minimum allowable LCTT. This does contribute to confirm the benefits of the widely used conventional controls strategy that resets the LCTT above the wet-bulb (or dry-bulb for dry-coolers) temperature, which would have been close to optimal in most of these cases. However, it is not the case with Site B on Figure 7, where the optimal LCTT varies significantly at different conditions. This observation highlights the merits of predictive model-driven optimisation for the LCTT as well.

Finally, the combined optimisation of the LCTT setpoint and the CW Flow for Site C for a case of one chiller enabled, a cooling load of 600kW and wet-bulb temperature of 15°C is displayed on Figure 8.

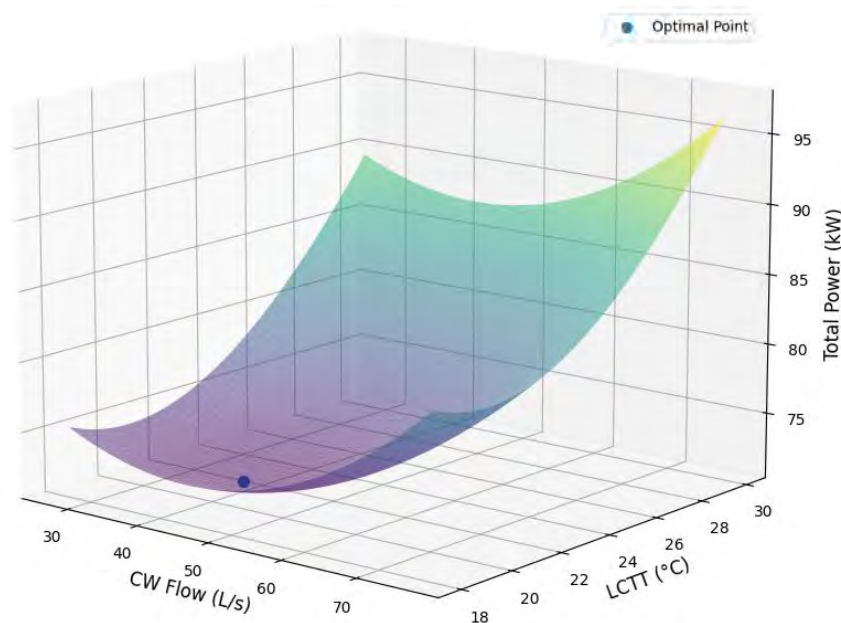


Figure 8. Site C, optimal LCTT and CW Flow showcasing trade-off between chiller, cooling tower and condenser pump power usage

4. IMPLEMENTATION CASE STUDIES

4.1 Site deployments

The approach was implemented on several real sites, while Measurement and Verification (M&V) studies were carried out on Site A and B, following the guiding principles from the International Performance Measurement and Verification Protocol (IPMVP) [4], to assess the actual energy savings achieved while accounting for changes in external conditions.

The machine learning and optimisation software algorithms were implemented within an automation platform on an embedded computer specialised for building automation, with the capability to communicate to other devices in the building using standard protocols such as BACnet or Modbus. The embedded computer is a relatively low-powered device, with a dual core 1.33GHz CPU and 2GB of RAM. For both Site A and Site B, the embedded computer was installed to communicate directly with the pre-existing Building Management System

(BMS) that was already communicating to the chillers, pumps, and cooling towers. It was configured to receive the sensor data points and take over direct control of the equipment through the BMS via a single Ethernet connection on the building secured network. The site deployment process was as straightforward as installing and integrating any other standard building automation device.

The algorithms for the machine learning and optimisation of the CW Flow and chiller loads have been implemented to be flexible to various sites and allow for any configuration in terms of number and sizes of chillers and of pumps and a wide range of types of piping arrangement via a simple User Interface (UI) in a web browser. They can therefore be replicated in other buildings without much more effort than deploying any other standard central plant controller or building automation system.

The algorithms for the machine learning of the Cooling Tower and optimisation of the LCTT were only implemented on a site-by-site basis due to time limitations, but they follow the same principles as the others and are therefore expected to be able to be implemented in a fully configurable UI as well.

4.2 Site operational results

On Site A, only the LCTT optimisation was implemented as a real-time optimisation solution due to site limitations with the other control variables. As such, only the chiller and cooling towers power usage is considered. The baseline case was set with the optimisation limited with a minimum setpoint of 24°C, similar to the previous conventional controls strategy that was maintaining a fixed setpoint of 24°C. A clear improvement of the overall efficiency can be observed on Figure 9 when the minimum allowable setpoint configuration was decreased to 21°C, granting more bandwidth to the optimisation.

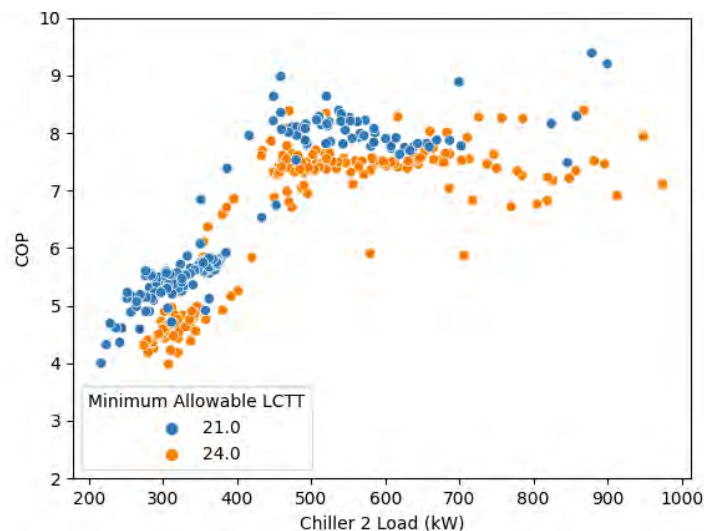


Figure 9. *Instantaneous 5-minutes Plant COP at Site A – limited optimised period compared to optimal controls period, from measured data*

On Site B, the results of the offline simulations at various conditions were used as recommendations to implement dynamic controls logic on site. The predicted M&V baseline, representative of operation before the implementation of the new control logic, is shown on Figure 10. Significant savings can be observed compared to the actual daily energy usage over a 6-month period.

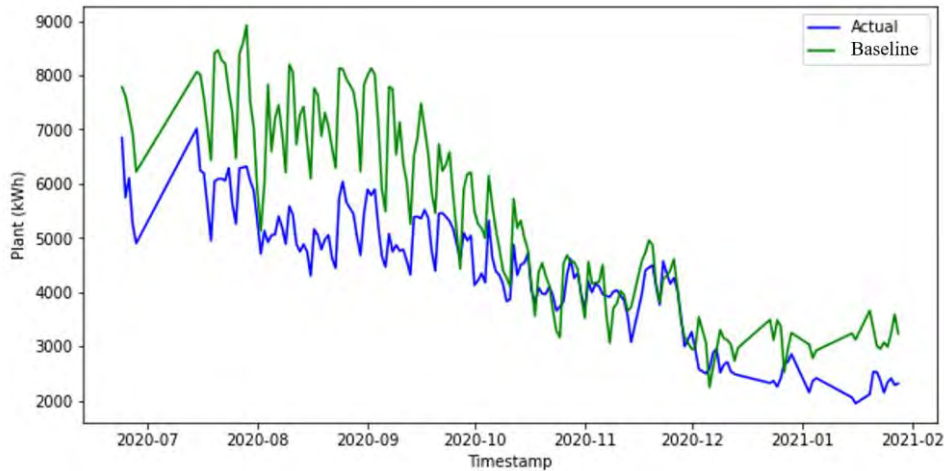


Figure 10. Daily actual energy usage at Site B compared to M&V baseline representative of previous operation and performance

The savings are summarised on Table 5.

Sites	Variables	Duration	Savings kWh	Savings %
Site A	LCTT	1 week	93kWh	9.20 %
Site B	LCTT, CW Flow, and Loads	6 months	174,166kWh	18.75 %

Table 5. Energy savings derived from M&V studies

CONCLUSION

The proposed optimal controls solution to minimise the energy usage of the chilled water plant in real-time without compromising on cooling production and comfort was deployed on several sites and showed significant savings ranging from 9.20 per cent to 18.75 per cent. The approach was designed to require low computational power and be deployable on-premises on an embedded controls board. It is expected to be suitable to be replicated with ease in other buildings, given the high accuracy the machine learning models have shown when validated with data from six sites with various equipment types and different climates, and the straightforward deployment process thanks to the flexible configurability of the algorithms. It would therefore be a key tool to consider in order to reduce other buildings' energy usage and carbon emissions.

ACKNOWLEDGEMENTS

The author would like to acknowledge Shruthi Balaji, Craig Barry, Pravesh Badjoonauth and all the team at Conserve It for their contributions.

REFERENCES

[1] ASHRAE Handbook (2007) Supervisory control strategies and optimization – HVAC Applications – Chapter 41. 2007

- [2] Benton J. B. et al. (2002) An Improved Cooling Tower Algorithm for the CoolTools™ Simulation Model. ASHRAE Transactions 2002 V.108
- [3] Boyd S., Vandenberghe L. (2004) Convex Optimization. Cambridge University Press.
- [4] Efficiency Valuation Organization (2016) Core Concepts – International Performance Measurement and Verification Protocol. EVO 10000.
- [5] González-Torres M. et al. (2022) A review on buildings energy information: Trends, end-uses, fuels and drivers. Energy Reports, Volume 8
- [6] Hirsch J.J. (2014) Building Energy Use and Cost Analysis Program. Volume 2: Dictionary. Lawrence Berkeley National Laboratory.
- [7] HVAC HESS (2013) Factsheet HVAC Energy Breakdown. Department of the Environment and Energy, Australia.
- [8] Hydeman M., Gillespie K. (2002) Tools and Techniques to Calibrate Electric Chiller Component Models. ASHRAE Transactions.
- [9] Taylor T. S. (2018) Fundamentals of Design and Control of Central Chilled-Water Plants. ASHRAE
- [10] Venkatesh P.Y. (2015) Creating a New Model to Predict Cooling Tower Performance and Determining Energy Saving Opportunities through Economizer Operation. Master thesis University of Massachusetts Amherst
- [11] Wächter A., Biegler L. (2006) On the implementation of an interior-point filter line-search algorithm for large-scale nonlinear programming. Mathematical Programming. 106:25-57

DISCLAIMER

The information or advice contained in these technical papers is intended for use only by professionals who have had adequate technical training in the field to which the paper relates. At the time of publication, these technical papers have undergone a formal peer-review process.

These documents have been compiled as an aid only, and the information or advice should be verified before it is put to use. The user should also establish the applicability of the information or advice in relation to any specific circumstances. While the information or advice is believed to be correct, no responsibility is taken by AIRAH or IBPSA Australasia for any statements made within.

AIRAH and IBPSA Australasia, its officers, employees and agents, disclaim responsibility for any inaccuracies contained within the documents, including those due to any negligence in the preparation and publication of the said technical papers.

COPYRIGHT

This work is copyright. Apart from any use as permitted under the Copyright Act 1986, no part may be reproduced by any process without prior written permission from either the Australian Institute of Refrigeration, Air Conditioning and Heating (AIRAH) or the International Building Performance Simulation Association (IBPSA) Australasia.

ENHANCING OF BUILDING SUSTAINABILITY VIA DISARTICULATING OF SENSIBLE AND DEHUMIDIFYING COILS IN HVAC SYSTEMS

ALI REZA HADDADI
HVAC Consultant Engineer
P.E., Tehran, Iran
ar.haddadi@gmail.com

ESMAEIL JALALI LAVASANI
Ph.D. candidate in Energy Conversion
3Nano-SAE Research Center, University of Bucharest, Romania
esmaeil.jalali@3nanosae.org

IOAN STAMATIIN
3Nano-SAE Research Center, University of Bucharest, Romania
istarom@3nanosae.org

ABOUT THE AUTHOR

Ali Reza Haddadi is a HVAC Consultant engineer with professional experience in design of complete mechanical systems including plumbing, heating, air conditioning, fire protection and control systems for commercial, residential, high-rise buildings, industrial and recreational facilities. Ali is skilled in designing of mechanical / HVAC systems for environmentally sustainable buildings and has published several papers in the Iranian HVAC Journals.

Esmail Jalali Lavasani is collaborating and working at the institute 3nanosae research center in the energy field. Collaboration in E.E.B.C (East European Business Center) in the HVAC field. Esmail is an air conditioning equipment designer with experience in the design of hygienic equipment for hospitals and clean rooms.

ABSTRACT

It is common to use a cooling coil with 7.2[°C] supply water temperature for HVAC systems in many buildings, but it is not economical in terms of energy. Cooling coils are used for air cooling with or without accompanying dehumidification. According to ASHRAE, the dry/wet boundary conditions on a cooling coil are where the surface temperature equals the entering air dew point temperature.

However, the typical performance of cooling coils is not desirable for dehumidification purposes because they normally remove both moisture and sensible heat from entering the air. In other words, each cooling coil has got two parts: the first part only reduces dry and wet bulb temperatures without any changes in the humidity ratio (Sensible Process), and the second part consists of decreasing both

temperatures and humidity ratio simultaneously. The more we can reduce the sensible cooling role of cooling coils, the more coils can eliminate the moisture from the air.

This paper proposes a new model to specify dry/wet boundary points on cooling coils by applying the numerical method. It can help us take into hand the coil performance and ensure that the dehumidifying coil's performance is always located in the wet part of the coil. The best solution for this issue would be to use a sensible cooling coil separately because it does not need to be fed by low-temperature chilled water (equal to or lower than the dew point). The first conclusions of this measurement would be the smaller required cooling coil size and decrease in energy usage in the HVAC system.

In this paper, the evaluation of HVAC systems' design of two different commercial buildings is carried out in two scenarios: one, the use of conventional cooling coil, and second, utilizing of sensible cooling and dehumidifying coil separately, and finally, the outcomes were compared. The results indicated that taking advantage of this new approach could prepare the computing infrastructure for sustainability improvement and implementation of energy-efficient solutions in the buildings' HVAC systems.

INTRODUCTION

Coils are one of the most effective parts in saving energy in air conditioning systems. The amount of heat they exchange with the environment can determine the amount of energy consumption. Hence, all of the thermodynamic properties in the coil must be investigated to achieve high performance, such as coil surface temperature, water flow rate, and air and water temperature in the inlet and outlet of the coils. In addition to these parameters, the Boundary Point Temperature (BP) is investigated as an effective parameter on coils performance in this study. Also, its influence on systems efficiency has been studied. Some research about the coil's performance is reviewed in the following.

Vahid Vakiloroyaya [1] has applied the public building in hot climate conditions and suggested utilising a simulation-optimisation technique to predict the best geometry for coils designing. Using computational assessment, Chandra Sekhar [2] demonstrated adaptable cooling coil performance during part loads in the tropics area. The dynamic relationships were obtained between the coil's heat exchange and its essential properties, including inlet air temperature, inlet air humidity, inlet water temperature, airflow rate, and water flow rate in the paper by YeYao [3]. Gartner [4] observed transfer function correlations for various coil properties. Bocanegra [5] designed a model to evaluate the efficiency of a counter flow cooling and dehumidification coil. The whole cooling coil unit dynamics are usually considered a single system, ignoring the essential dynamics of the moving boundary between the wet and dry surface regions. Lebrun et al. [6] used an energy balance to develop a first-order differential equation to characterise the dynamics of a coil with thermal mass. Wang [7] presented a specific method (called the equivalent dry bulb temperature method) to simplify the computation in each zone. Most of the before-mentioned studies were implemented to evaluate the coil performance in terms of various prospects. As a new idea in the present research, the boundary point (BP) characteristics are estimated. This point is used to design the high-performance coil. The BP is the point between the dry and wet parts of the cooling coils. The BP can help the designer investigate the coil performance before coil selection. Also, it gives the ability

to determine the inlet water temperature in the coils based on the project required for sensible cooling, dehumidifying, or both at the same time.

*Component
between
and Coolant*

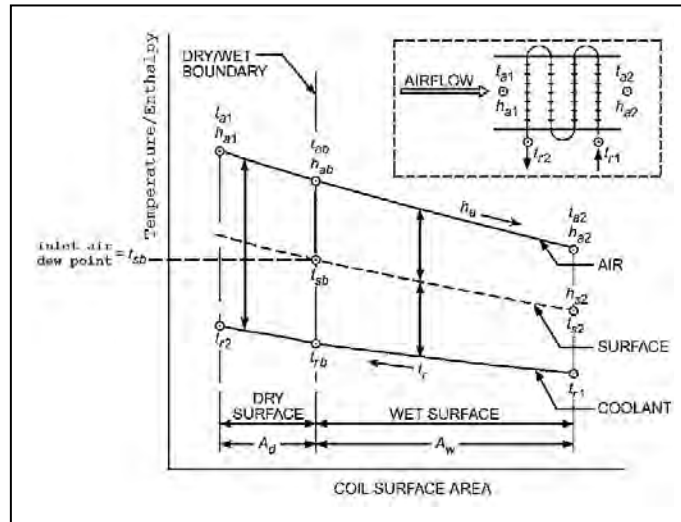


Figure 1- *Two-Driving Force Dehumidifying Air*

1. MATERIALS AND METHODS

1.1 Background

The varieties of parameters such as inlet water temperature, inlet air wet bulb temperature, air, and water flow rate, coil geometry including heat transfer surface area, number of rows, number of fins per inch, coil circuit type, pipe size, pipe thickness, and materials, have a significant effect on the coil performance. In the first step, cooling coils decrease the air temperature and sensible load and then dehumidify the air in the second step. However, in the dehumidification process, the coil reduces humidity and the air temperature again. In other words, the sensible cooling throughout the coil occurs in two stages: the first step, before dehumidification, and the next step, after the beginning of dehumidification. Indeed, in the cooling process in the coil, there is a boundary point that separates the operation of the coil into two distinct parts: the dry part of the coil and the wet part. According to ASHRAE [8]: “The potential or driving force for transferring total heat from the airstream to the tube-side coolant is composed of two components in a series of heat flow:

(a) An air-to-surface air enthalpy difference and (b) a surface-to-coolant temperature difference. Figure 1 is a typical thermal diagram for a coil in which the air and a nonvolatile coolant are arranged in counter-flow. The top and bottom lines in the diagram indicate, respectively, changes across the coil in the airstream enthalpy (h_a) and the coolant temperature (t_r)”.

In Figure 1, the boundary condition of the cooling coil has been drawn (the dashed line). The coil operation in different loads can change this boundary condition. The coil’s performance can be managed by having the thermodynamic characteristics of this “boundary point” (BP). According to

ASHRAE, “The dry/wet boundary conditions are located where the coil surface temperature (t_{sb}) equals the entering air dew-point temperature” [8]. Therefore, the coil is separated into two distinct parts. If the inlet water temperature to the coil is lower than the inlet air dew point, the wet part is called, and if it is higher than that, it is called the dry part. Suppose the inlet air wet-bulb temperature in the BP equals the coil surface temperature at the boundary point. In that case, it means that the wet-bulb temperature must be equivalent to the temperature of the dew point of the air passing through, which is only correct for dots that have been situated on the saturation curve.

So, in this case, the BP has to be on the saturation curve while we know that this point has a distance from the saturation curve in practice. Thus, the wet-bulb temperature of the passing air on the BP cannot be similar to the coil surface temperature at the BP. In addition, the inlet water temperature in the BP cannot be the same as the coil surface temperature due to the thermal resistivity of tubes (R1, R2, and R3) which has been figured in Figure 2.

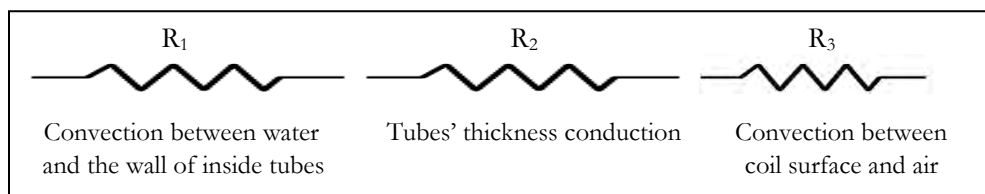


Figure 2. *The thermal resistivity of tubes in the cooling coil*

So, according to the above introduction, the condition of the BP will be:

$$t''_{a1} = t_{sb} , t_{rb} < t_{sb} < t'_{a1} \text{ also:}$$

When ($t_{rb} < t_r < t'_{a1}$), then the coil surface will be dry, and the coil reduces sensible load solely (sensible cooling process).

When ($t_r < t_{rb} < t'_{a1}$), then the coil surface will be wet, and the coil reduces sensible and latent loads simultaneously (dehumidifying process).

In a counter-flow cooling coil, the outlet water from the coil is in contact with the inlet air and vice versa. In other words, at first, the heat transfer is between the outlet water from the cooling coil and inlet air, so the more air goes deep into the coil, the more air becomes cooler in contact with colder water. This ensures a continuous decrement in the air temperature until it leaves the coil. This is why even in the wet part of the coil, the temperature is decreased in addition to dehumidification. Consequently, it is possible to calculate the water and the air temperature in the boundary conditions by calculating the coil surface temperature at the BP. According to ASHRAE, the first condition for computing the coil surface temperature at the BP is to calculate the coil characteristic index from the coil geometry. “Equation 1 shows the basic relationship of the two components of the driving force between air and coolant in terms of three principal thermal resistances. For a given coil, these three resistances of air, metal, and in-tube fluid (R_{aw}, R_{mw} and R_r) are usually known or can be determined for the particular application, which gives a fixed value for C.” [8]. After calculating C from equation 1, the coil surface temperature and enthalpy can be determined using the trial-and-error method from Equation 2 [8].

$$C = \frac{R_{mw} + R_r}{C_p \cdot R_{aw}} \quad (1), \text{ and } C = \frac{t_s - t_r}{h_a - h_s} \quad (2)$$

In addition, “Equation 2 can be used to determine point conditions for the interrelated values of airstream enthalpy (h_a), coolant temperature (t_r), surface temperature (t_s), and enthalpy (h_s) of saturated air corresponding to the surface temperature. When both t_s and h_s are unknown, a trial-and-error solution is necessary; however, this can be solved graphically by a surface temperature chart.” [8]. ASHRAE states that the value of C cannot be calculated without the coil geometry data, including the number of rows, tubes’ size, etc. Hence, without the calculation of C, it is impossible to obtain the coil surface temperature and enthalpy. So, there is no chance of determining the BP consequently. However, in the conventional design method, the coils are selected based on total building load calculations, including the sum of sensible and latent loads. They are not chosen based on the latent and sensible loads separately [8].

1.2 The new approach to specify dry/wet boundary at cooling coils

Unlike the conventional method, this study presents a new solution for the BP estimation before cooling coil selection. Thus, specifying the BP before the coil selection gives the ability to know at what temperature the cooling coil would start to dehumidify. Therefore, it is possible to manage the sensible and latent loads using the two separate coils. This coils’ separation approach gives the designer to handle the energy consumption in the central air conditioning system by knowing the BP characteristic. For this purpose, the psychometric chart is applied to calculate the BP. Point ab in Figure 3 represents the BP (Dry/Wet Boundary). We perform the following steps to find this point using psychometric relations.

1. **Calculating the outlet air temperature from the cooling coil:** The cooling load equations are applied to determine the outlet air temperature from the coil. Since the value of $Q_S, Q_L, Q_T, t_{a1}, h_{a1}$, and the air flow rate are obtained according to the building load calculations, the outlet temperature and enthalpy (t_{a2}, h_{a2}) will be achieved through the psychometric chart.

$$Q_S = 1.23 * \text{Airflow} * \Delta T \quad (3)$$

$$\longrightarrow \Delta T = t_{a1} - t_{a2} = \frac{Q_S}{1.23 * \text{Airflow}} \quad (4)$$

$$\longrightarrow t_{a2} = t_{a1} - \frac{Q_S}{1.23 * \text{Airflow}} \quad (5)$$

$$Q_T = 1.2 * \text{Airflow} * \Delta h \quad (6)$$

$$\longrightarrow \Delta h = h_{a1} - h_{a2} = \frac{Q_T}{1.2 * \text{Airflow}} \quad (7)$$

$$\longrightarrow h_{a2} = h_{a1} - \frac{Q_T}{1.2 * \text{Airflow}} \quad (8)$$

$\longrightarrow (t_{a2}, h_{a2})$ are determined. \longrightarrow Point “a2” is specified.

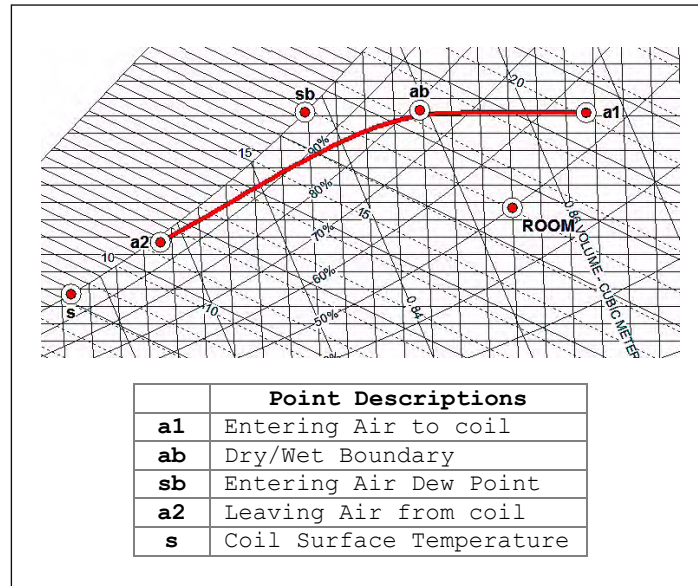


Figure 3. Air Cooling and Dehumidifying Process on Psychrometric Chart

2. **Obtaining the coil's approach temperature and the inlet water temperature to the coil:**

The return water temperature to the chiller unit is attained from different temperatures between the air wet-bulb and the coil's approach temperature [9]. Therefore, to estimate the coil's approach temperature, it is necessary to consider an initial value as the return water temperature to the chiller unit. Correspondingly, the calculations proceed considering the constant coil's approach temperature throughout the coil. Although to prove the latter assumption, some evidence has been demonstrated in the following.

$$t_{r2} = t'_{a1} - t_{app} \quad (9)$$

$$t_{app} = t'_{a1} - t_{r2} = t'_{a2} - t_{r1} \quad (10)$$

With equations 9 and 10, the coil's approach temperature and the inlet water temperature to the coil will be obtained.

3. **Water flow rate calculation:** By specifying the inlet and outlet water temperature, equations 11, 12, and 13 are applied to calculate the water flow rate.

$$q_w = Q_T \quad (11)$$

$$q_w = 4186 * q_0 * (t_{r2} - t_{r1}) \quad (12)$$

$$q_0 = \frac{q_w}{4186 * (t_{r2} - t_{r1})} = \frac{Q_T}{4186 * (t_{r2} - t_{r1})} \quad (13)$$

→ q_0 is specified.

4. **Obtaining the dew point temperature of the cooling coil:** Equation 14 calculates the coil's dew point or the effective coil surface temperature [9].

$$t_s = \left(\frac{t_{r1} + t'_{a2}}{2} \right) \quad (14)$$

5. **Determining the boundary conditions:** After obtaining the effective coil surface temperature (t_s), in the next step, the BP can be calculated. Since the BP belongs to the lines of a1-ab and

ab-s on the psychometric chart (Figure 3), so, this point can be found at the intersection between these two lines. Using the equation of each line, we have:

$$Q_{t1} = Q_{s1} \longrightarrow (h_{a1} - h_{ab}) = 1.025 * (t_{a1} - t_{ab}) \quad (15)$$

$$(h_{ab} - h_{a2}) = \left(\frac{h_{a2} - h_s}{t_{a2} - t_s} \right) * (t_{ab} - t_{a2}) \quad (16)$$

In the above equations, only "t_{ab}" and "h_{ab}" are unknown. So by solving equations 15 and 16 point ab will be specified:

$$(15),(16) \longrightarrow (t_{ab}, h_{ab}) \text{ are determined. } \longrightarrow \text{Point "ab" is specified.}$$

6. **Determining the water temperature at the boundary points:** The next step is to determine the water temperature at the boundary point (t_{rb}). Equations 17, 18, and 19 can be used to attain the water temperature at the boundary point:

$$q_{w1} = 4186 * q_0 * (t_{r2} - t_{rb}) \quad (17)$$

$$q_{w1} = Q_{s1} = 1.23 * \text{Airflow} * (t_{a1} - t_{ab}) \quad (18)$$

$$(17),(18) \longrightarrow t_{rb} = t_{r2} - \frac{Q_{s1}}{4186 * q_0} \quad (19) \longrightarrow t_{rb} \text{ is specified.}$$

Another way to calculate the water temperature at the BP is to apply equation 20:

$$t_{rb} = t'_{ab} - t_{app} \quad (20)$$

2. RESULTS AND DISCUSSION

2.1 Assessment of the introduced method upon the prototype buildings

Two different buildings are studied in distinct climates to evaluate the effectiveness of the proposed method. One is a public building with a passenger terminal application in a humid subtropical region. The other is an arena building in a hot and dry area that both have been placed in Iran. Table 1 shows the summary of the basic information of both buildings.

Building Type	Location in Iran (Altitude)	Area (m ²)	Peak Load Condition DB[°C] / WB	Occupants	Total Cooling Load (kW)	Sensible Load (kW)	SHR	Room Condition DB[°C] / RH (%)	Fresh Air Flow Rate (L/S)	Total Air Flow Rate (L/S)
Passenger Terminal	Hormozgan (Sea Level)	1050	35/27.8	779	456.4	281.1	0.76	24/50 %	3675	15125
Arena	Tehran (1280 m)	1600	40.5/22.2	388	285.6	239.6	0.86	25/45 %	3500	11000

Table 1. The summary of cooling load calculations of the studied buildings

The HVAC systems will be chosen based on the common cooling coil selection for buildings in the first scenario. If the outlet water temperature from the cooling coil is assumed 14[°C] for the

passenger terminal building and 13[°C] for the arena building, table 2 can be extracted following of proposed steps in the new approach:

Building Type	a1	a2	t _{sb}	t _{app}	t _{r1}	t _{r2}	Δt _r	q ₀	t _s h _s	ab	t _{rb}	t _{r2} - t _{rb}
	t _{a1} /t' _{a1} /t'' _{a1} w _{a1} /h _{a1}	t _{a2} /t' _{a2} /t'' _{a2} w _{a2} /h _{a2}								t _{ab} /t' _{ab} h _{ab}		
Passenger Terminal	26.7/20.1/16.9 0.012/57.7	11.6/11.4/11.2 0.083/32.7	16.9	6.1	5.3	14	8.7	12.5	8.3 5 25. 6	20.5/18. 0 50.9	11. 8	2.2
Arena	29.9/18.5/13 0.011/58.2	12.2/11.5/11 0.096/36.6	13	5.5	6	13	7	9.7	8.8 29. 7	15.7/13. 8 43.6	8.3	4.7

Table 2. the results of key parameters' calculations to determine the boundary points for case-study buildings

The following results are obtained according to the boundary conditions:

- In the terminal building, due to the high latent load, the dry part of the coil is less in comparison with the dry part of the coil in the arena building and vice versa.
- The difference in water temperature between the boundary point and the outlet water temperature of the coil (t_{r2} – t_{rb}) in the terminal building is smaller in comparison with the arena building (2.2[°C] to 4.7[°C]). Because in the terminal building, the coil has to start the dehumidification process earlier to provide a high latent load than in the arena building. In other words, in the terminal building, 75% of the coil's surfaces are wet, and only 25% of it belongs to the dry part of the coil.

$$\frac{(11.8-5.3)}{(14-5.3)} * 100 = 74.7\%$$

Nevertheless, in the arena building, where the sensible load is more than the latent load, the dehumidifying process commences later, and about 67% of the coil's surfaces are dry. In comparison, the 33% leftover is dedicated to the coil's wet part.

$$\frac{(13-8.3)}{(13-5.5)} * 100 = 67.1\%$$

- After calculating the boundary conditions, the water temperature can be determined at each point along the cooling and dehumidification process.. To calculate the water temperature (rx) at any point (ax) between the inlet and outlet air, Equation 21 can be used:

$$t_{rx} = t_{r2} - \frac{1.2 * \text{Airflow} * (h_{a1} - h_{ax})}{4186 * q_0} \quad (21)$$

The results of the water temperature estimation at different points in the cooling process for both buildings demonstrate that the obtained water temperature at each point based on the presented equation (Equation 21) maintains an almost constant distance from the corresponding air wet-bulb temperature at that point. Hence, as Figure 4 shows, the constant approach temperature assumption between water and the corresponding air wet-bulb has been correct. Therefore, the simplest solution to calculate the water temperature at each point, especially at the boundary point would be to calculate the difference between the air wet-bulb temperature at that point and the coil approach temperature. However, there is

always a gap between the predicted approach temperature and the actual approach temperature.

- According to ASHRAE [10], dehumidification in coils occurs when the coil surface temperature is lower than the dew point temperature of the entering air. As mentioned earlier, the entering air dew point temperature (t'_{a1}) is equal to the coil surface temperature at the BP. Therefore, dehumidification by the hydronic cooling coil starts when the water temperature (t_r) is lower than the water temperature at the boundary point (t_{rb}); otherwise, the cooling coil cannot dehumidify the air.

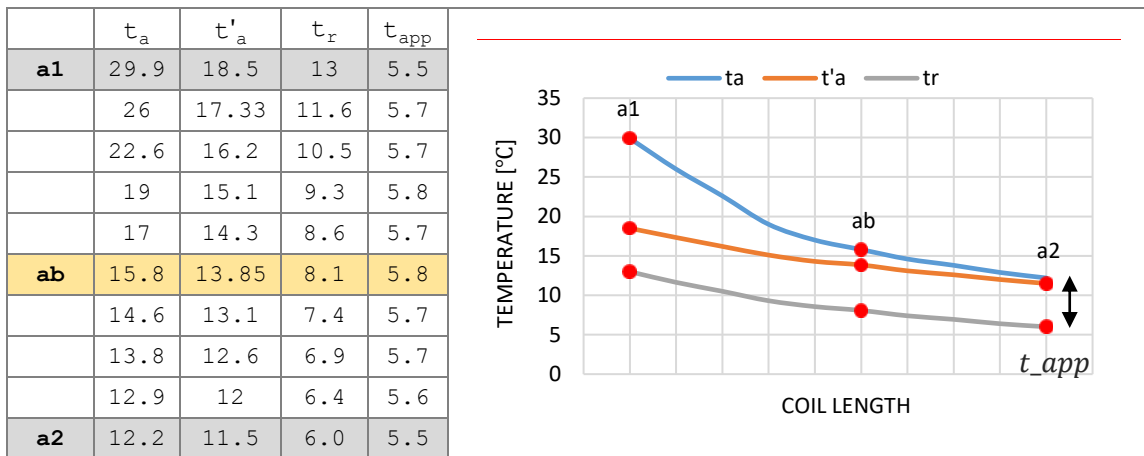


Figure 4 - The difference between the water temperature and the air wet-bulb temperature in the arena building is almost constant throughout the cooling coil

2.2 The impact of “Disarticulating Coils” and “Approach Temperature” on energy-saving

In addition to the water temperature determination, the air temperature is vital in the boundary point. The air temperature at the boundary point can be called either the outlet temperature of the sensible coil or the inlet temperature of the dehumidifying coil (Figure 5). As a practical solution, separating the cooling coil into two sensible and dehumidifying coils can provide more energy-saving opportunities. This separation exactly occurs at the BP. Finding the BP characteristics of the cooling coils in case-study buildings (Table 2), there is the opportunity for each cooling coil to get divided into separate coils: a sensible cooling coil and a dehumidifying coil.

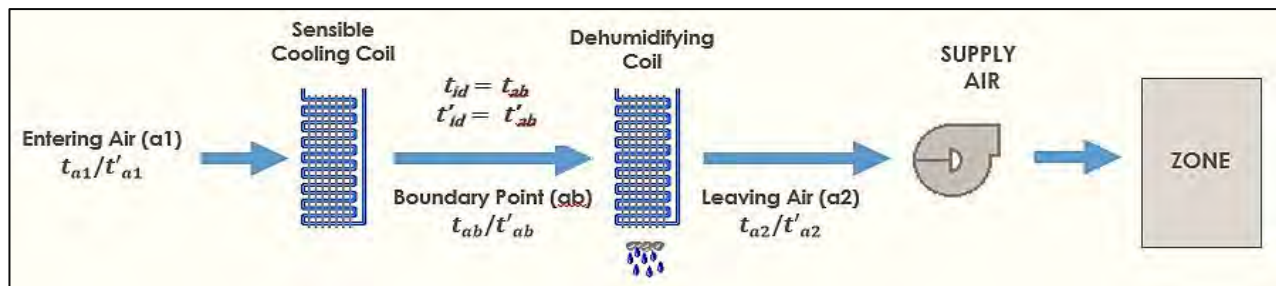


Figure 5. The schematic diagram of disarticulating cooling coils

The effectiveness of this design approach is because of using the air temperature at the boundary point (BP) as the inlet air temperature of the dehumidifying coil. The dehumidifying process begins at the BP, so if the coil's entering air temperature was equal to the air temperature at the BP ($t_{id} = t_{ab}$ and $t'_{id} = t'_{ab}$ in Figure 5), the coil would start to dehumidify the passing air at the first step. Consequently, the coil would allocate more capacity to the latent load. In this case, the air cooling process from the inlet air (t_{a1}) to the BP air temperature (t_{ab}) is achievable using the sensible cooling coil before the dehumidifying coil. So, the sensible and dehumidifying coils' capacities after the coils' separation have presented in Figure 6 based on their obtained BP characteristics for the studied buildings (from Table 2).

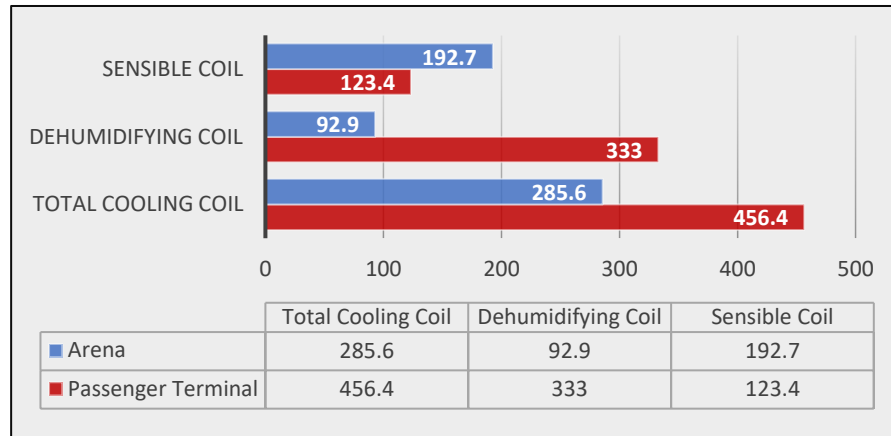


Figure 6. The sensible and dehumidifying coils' loads after estimating of the boundary point for buildings

(Total Cooling Coil Capacity = Sensible Coil Capacity + Dehumidifying Coil Capacity)

The use of a direct expansion system as a dehumidifying coil is one of the energy-saving solutions that arise when the boundary point is identified. Due to the reduction of the approach temperature (the difference between the coil effective surface temperature and the entering air wet-bulb temperature) in DX coils compared to hydronic coils, using DX coil as a dehumidifying coil in cases where the latent load of the building is high such as the terminal building, not only will be more efficient but also can save more energy. Since the refrigerant temperature is constant throughout the DX evaporator, the approach temperature gradually decreases from the beginning of the air entering the coil until the air exits. Specifically, in the terminal building, energy-saving results are evident by separating the cooling coil into two sensible and dehumidifying coils and replacing the hydronic dehumidifying coil using the DX coil. In this case, the air temperature at the BP is considered as the entering air temperature at the DX dehumidifying coil.

Based on the calculations, with the DX evaporator temperature of 9.4 [°C], the dehumidifying load can be provided (333 kW) in the terminal building. In this case, the approach temperature at the end of the DX coil (when the air leaves the coil) is equal to 2 [°C] which has been shown in Figure 7A (11.4-9.4= 2 [°C]). Besides, if the hydronic coil got utilised for dehumidification, a water temperature of 5.3 [°C] would be required to supply the load of the dehumidifying coil, in which case the approach temperature would be 6.1 [°C] (11.4-5.3 = 6.1 [°C]). On the other hand, to supply water 5.3 [°C] in the hydronic coil, the refrigerant must flow at a lower temperature in the chiller evaporator. It depends on the type of chiller evaporator (parallel plates or the shell and tube heat

exchanger) and its design, including the number of tubes, circuit arrangement, etc. If the 4-pass shell and tube evaporator is selected, which has the highest efficiency compared to 1,2, and 3 passes, the approach temperature becomes at least 1.5 [°C] to 3[°C] less than the chiller supply water temperature. So, the evaporator temperature will be equal to 1.5 [°C] to 3.8 [°C] in this case. As a result, the difference between the refrigerant temperature in the chiller evaporator and the air wet-bulb temperature for the hydronic coil (the actual approach temperature) increases by at least 7.6 [°C] which has been shown in Figure 7B (11.4-3.8= 7.6 [°C]). This value is about 3.8 times bigger than the approach temperature when using the DX coil as a dehumidifying coil in this project. The rise of the evaporator temperature from 3.8 [°C] in the chiller evaporator to 9.4 [°C] in the DX coil is a major factor in energy savings in this design due to the lower rate of the approach temperature in the DX systems compared to the hydronic systems.

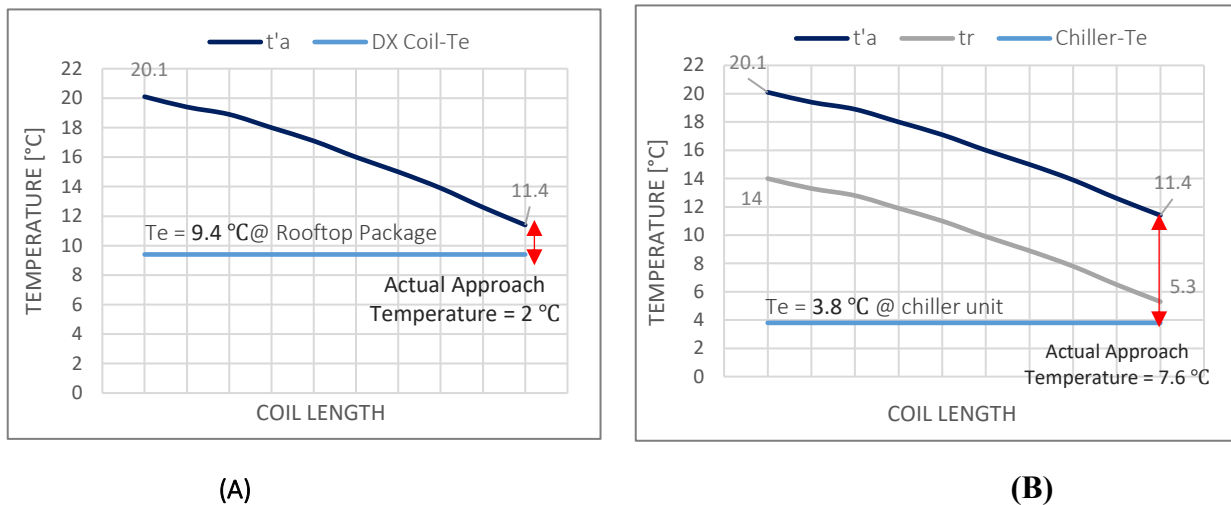


Figure 7. Measurement of the actual approach temperature between the leaving air wet-bulb temperature and the evaporator temperature in two scenarios: A) in a DX system, B) in a hydronic system.

Table 3 shows the amount of power consumption for the terminal building for two different scenarios, one is the use of a rooftop package system (with DX coil) and the other is the use of an air-cooled chiller unit only for the dehumidifying coil without considering the sensible coil in calculations. According to this table, the amount of energy-saving can be calculated:

Energy saving only for the dehumidification process (%) = $(92.2-75)/92.2*100 = 18.6\%$

ROOFTOP PACKAGE UNIT	$t_e=9.4^{\circ}\text{C} / t_c=46^{\circ}\text{C}$ 120 HP Screw Compressor	
	ACT. LOAD (kW)	341
	ACT. POWER (KW)	75
AIR-COOLED CHILLER UNIT	$t_e=3.8^{\circ}\text{C} / t_c=46^{\circ}\text{C}$ 160 HP Screw Compressor	
	CHILLER ACT. LOAD (kW)	349
	CHILLER POWER (KW)	92.2

Table 3. *Electrical consumptions for different HVAC systems for the dehumidifying coil in the terminal building.*

However, if the DX coil is used instead of the hydronic coil as a dehumidifying coil, it is essential to protect compressors against flood back and freeze under part-load conditions such as using the accumulator or increasing the number of circuits. Given the high performance of DX coils in latent load supply, the point is whether using DX coils instead of sensible hydronic coils has the same energy-saving potential as dehumidifying coils or not? To figure out this issue, it is needed to restudy the terminal building. To achieve the air temperature at the boundary point in the terminal building (20 [°C]/18 [°C]), if the DX coil is used instead of the sensible hydronic coil, due to the low approach temperature between the air wet-bulb temperature and the DX evaporator temperature; the DX evaporator temperature is expected to become around 16 [°C] (18 -2=16 [°C]). However, achieving this temperature in the evaporator is out of range and impossible for a refrigeration system. Compressor manufacturers recommend limiting the temperature and pressure at the compressor suction and discharge line to prevent overheating and oil oxidation in the refrigeration system. According to the manufacturers of HVAC systems, the temperature in the discharge shall not exceed 140 [°C] because above this temperature, the oil starts to decompose or oxidize. As the temperature and pressure in the compressor suction line rise, these two parameters will increase in the discharge line, so there are design constraints for these values. In addition, many manufacturers use MOP expansion valves (Maximum Operating Pressure) or OLP controllers (Overload Protector) to prevent overheating in the compressor, which imposes restrictions on temperature or pressure control at the inlet or inside the compressor. These restrictions prevent the temperature of the evaporator and superheat from rising above the allowable value [11],[12].

Therefore, despite the advantages of DX coils, such as high efficiency due to their low approach temperature, replacing them instead hydronic coils as a sensible cooling coil cannot meet the requirements. However, unlike the DX systems, it is allowed to enhance inlet water temperature in hydronic coils because they do not have the DX coils' restrictions. In spaces where the sensible load is significant such as the control rooms or data centers, it is possible to provide the part of sensible load by the higher water temperature than the boundary point (BP). In this situation, it is possible to use cooling towers to provide parts of the sensible load, leading to significant savings in reducing energy consumption. Based on the calculations, the higher the supply water temperature, the more energy-saving opportunities will be available. There will be a high potential for energy-saving if there is a high-temperature difference between the inlet air wet-bulb temperatures and the boundary point (BP). For the arena building, the water temperature at the boundary point is 8.3 [°C]. Since

there is a suitable temperature difference between the inlet air wet-bulb temperature and the air wet-bulb temperature at the BP, selecting a hydronic sensible cooling coil with a high-water supply temperature is appropriate to supply the cooling load between the air inlet (a1) and the air at the BP in this case. Therefore, if the approach temperature is considered 3[°C] in this case (a 6-row coil), the inlet and outlet water temperature at the coil will be equal to:

$$t_{r2} = t'_{a1} - t_{app} = 18.5 - 3 = 15.5 \text{ [}^\circ\text{C]}$$

$$t_{rb} = t'_{ab} - t_{app} = 13.8 - 3 = 10.8 \text{ [}^\circ\text{C]}$$

$$t_{r2} - t_{r1} = 15.5 - 10.8 = 4.7 \text{ [}^\circ\text{C]}$$

We can raise the water temperature by holding the approach temperature constant across the sensible coil as an energy-saving solution. By incrementing the water temperature from 8.3 [°C] to 10.8 [°C], the evaporator temperature will increase as much as 2.5 [°C] in the chiller while the same sensible load is still achievable (192.7 kW). It could reduce energy consumption by up to 16% in the arena building (Table 4).

$$\text{Energy saving only for the sensible coil (\%)} = \frac{56.1 - 47.1}{56.1} * 100 = 16\%$$

State	t_{r2} [°C]	t_{a1} [°C]	t_e [°C]	t_c [°C]	Chiller Evaporator Capacity [kW]	Chiller Power [kW]
1	8.3	13	5.3	51.7	194.9	56.1
2	10.8	15.5	7.8	51.7	194.2	47.1

Table 4. *The effect of increasing inlet water temperature in the sensible coil on energy consumption*

Meanwhile, due to the low share of sensible coil load from the total load (25 per cent) and also the low water temperature difference between the boundary point (BP) and the water temperature at the coil outlet in the terminal building, the sensible coil load can be easily provided by a small chiller unit. However, the energy-saving opportunity in the sensible coil section of the terminal building is less than in buildings with high sensible loads (such as the arena building). In contrast, the energy savings opportunities in the dehumidifying section are much more significant. In both terminal and arena buildings, heat recovery systems such as air-to-air heat exchangers, heat pipes, round-around coils, and enthalpy wheels that directly affect the air temperature; can significantly reduce the coil air inlet temperature and boost efficiency and further reduce energy consumption.

In fact, in the present method, instead of considering a constant water temperature difference of 5 [°C] in the HVAC system design (at chiller units or hydronic cooling coils), the real calculated water temperature difference should be applied to choosing the HVAC equipment. Because in this method, the basis of calculations is the approach temperature, not the constant temperature difference between inlet and outlet water.

CONCLUSION

In this research, a novel technique for calculating the boundary conditions in cooling coils was introduced by dividing them into two parts, dry and wet. Then, a step-by-step estimation method was recommended to calculate all the necessary design parameters at the boundary point. In the next step, the boundary point (BP) was determined in the cooling coil for two sample buildings, one with a high latent load and the other with a high sensible load. After that, energy-saving procedures were discussed in both buildings. Finally, taking advantage of a DX system as a dehumidifying coil and a high-temperature chiller to feed the water of the sensible coil in the studied buildings, the amount of energy-saving was estimated. The outcomes showed that using a DX system as a dehumidifying coil could lead to a decrease in the electrical usage of the HVAC system by as much as 18.6% in the terminal building only for the dehumidification process. On the contrary, by incrementing the water temperature as much as 2.5 [°C] at the inlet of the hydronic sensible coil, the reduction in electrical consumption of the chiller unit became about 16% just for the sensible coil. The results of this research demonstrated capacities of HVAC systems were optimised in the case studies, so it could yield more sustainability in buildings by curbing the dependence of the commercial buildings on electricity usage. In addition, the impact of the approach temperature on developing energy-saving opportunities in air conditioning systems was proved. Due to the focus of this research on introducing a renewed and practical technique to achieve new energy-saving prospects in air conditioning systems, the next step in the future could be on the comparison of different types of systems using this method.

SYMBOLS

Airflow: Air flow rate, [L/s]

C: Coil characteristic, [kg°C/kJ]

h_a : air enthalpy, [kJ/kg]

h_{a1} : Entering air enthalpy, [kJ/kg]

h_{a2} : Leaving air enthalpy, [kJ/kg]

h_{ab} : Air enthalpy at dry/wet boundary, [kJ/kg]

h_{ax} : Air enthalpy at point x of coil, [kJ/kg]

h_s : Enthalpy of saturated air corresponding to the surface temperature, [kJ/kg]

q_0 : Water flow rate, [L/s]

Q_l : Latent heat removed from air between a1 and a2,[kW]

Q_s : Sensible heat removed from air between a1 and a2,[kW]

Q_{s1} : Sensible heat removed from air between a1 and ab,[kW]

Q_T : Total refrigeration load of cooling and dehumidifying coil (between a1 and a2),[kW]

Q_{T1} : Total refrigeration load of cooling and dehumidifying coil (between a1 and ab),[kW]

- q_w : Total cooling load in water-side of cooling coil,[kW]
 q_{w1} : Total cooling load in water-side of sensible coil,[kW]
 q_{w2} : Total cooling load in water-side of dehumidifying coil,[kW]
SHR: ratio of air sensible heat to air total heat, dimensionless
 t_{a1} : Entering air dry-bulb temperature to coil, [°C]
 t'_{a1} : Entering air wet-bulb temperature to coil, [°C]
 t''_{a1} : Entering air dew point temperature to coil, [°C]
 t_{a2} : Leaving air dry-bulb temperature from coil, [°C]
 t'_{a2} : Leaving air wet-bulb temperature from coil, [°C]
 t''_{a2} : Leaving air dew point temperature from coil, [°C]
 t_{ab} : Air dry-bulb temperature at dry/wet boundary, [°C]
 t'_{ab} : Air wet-bulb temperature at dry/wet boundary, [°C]
 t''_{ab} : Air dew point temperature at dry/wet boundary, [°C]
 t_{app} : Approach temperature, [°C]
 t_c : Condenser temperature, [°C]
 t_e : Evaporator temperature, [°C]
 t_{id} : Entering air dry-bulb temperature to the dehumidifying coil, [°C]
 t'_{id} : Entering air wet-bulb temperature to the dehumidifying coil, [°C]
 t_r : Water temperature, [°C]
 t_{r1} : Inlet water temperature to coil, [°C]
 t_{r2} : Outlet water temperature from coil, [°C]
 t_{rb} : Water temperature at dry/wet boundary, [°C]
 t_{rx} : Water temperature at point x of coil, [°C]
 $\Delta t_r = t_{r2} - t_{r1}$, [°C]
 t_s : Coil effective surface temperature, [°C]
 t_{sb} : Coil surface temperature at dry/wet boundary, [°C]
 w_{a1} : Humidity ratio of entering air, $[\frac{kg_w}{kg_a}]$
 w_{a2} : Humidity ratio of leaving air, $[\frac{kg_w}{kg_a}]$

REFERENCES

- 1- Vakiloroya, Vahid. "Design optimization of the cooling coil for HVAC energy saving and comfort enhancement." *Environmental Progress & Sustainable Energy* 32, no. 4 (2013): 1209-1216.
- 2- Sekhar, Chandra, Prashant Anand, Stefano Schiavon, Kwok Wai Tham, David Cheong, and Esmail M. Saber. "Adaptable cooling coil performance during part loads in the tropics—A computational evaluation." *Energy and Buildings* 159 (2018): 148-163.
- 3- Yao, Ye, Zhiwei Lian, and Zhijian Hou. "Thermal analysis of cooling coils based on a dynamic model." *Applied thermal engineering* 24, no. 7 (2004): 1037-1050.
- 4- Gartner, J. R. "Dynamic response relations for a serpentine crossflow heat exchanger with water velocity disturbance." *ASHRAE Trans.* 75 (1969): 53-68.
- 5- Jin, Guang-Yu, Wen-Jian Cai, Yao-Wen Wang, and Ye Yao. "A simple dynamic model of cooling coil unit." *Energy Conversion and Management* 47, no. 15-16 (2006): 2659-2672.
- 6- Lebrun J, Ding X, Eppe JP, Wasacz T. Cooling coil models to be used in transient and/or wet regimes—Theoretical analysis and experimental validation. In: Proceedings of system simulation in buildings, Belgium, 1990.
- 7- Wang, Jianfeng, and Eiji Hihara. "Prediction of air coil performance under partially wet and totally wet cooling conditions using equivalent dry-bulb temperature method." *International Journal of Refrigeration* 26, no. 3 (2003): 293-301.
- 8- ASHRAE Handbook 2020, HVAC Systems and Equipment, Chapter 23- AIR-COOLING AND DEHUMIDIFYING COILS.
- 9- ASHRAE Handbook 2020, HVAC Systems and Equipment, Chapter 13- HYDRONIC HEATING AND COOLING.
- 10- ASHRAE Handbook 2017, Fundamentals, Chapter 1- Psychrometric.
- 11- Copeland Refrigeration Manual Books, Emerson Climate Technologies.
- 12- Copeland Application Engineering Bulletin, AE-1260, Compressor Overheating.

DISCLAIMER

The information or advice contained in these technical papers is intended for use only by professionals who have had adequate technical training in the field to which the paper relates. At the time of publication, these technical papers have undergone a formal peer-review process.

These documents have been compiled as an aid only, and the information or advice should be verified before it is put to use. The user should also establish the applicability of the information or advice in relation to any specific circumstances. While the information or advice is believed to be correct, no responsibility is taken by AIRAH or IBPSA Australasia for any statements made within.

AIRAH and IBPSA Australasia, its officers, employees and agents, disclaim responsibility for any inaccuracies contained within the documents, including those due to any negligence in the preparation and publication of the said technical papers.

COPYRIGHT

This work is copyright. Apart from any use as permitted under the Copyright Act 1986, no part may be reproduced by any process without prior written permission from either the Australian Institute of Refrigeration, Air Conditioning and Heating (AIRAH) or the International Building Performance Simulation Association (IBPSA) Australasia.

PUSHING THE BOUNDARIES OF NET ZERO IN THE AUSTRALIAN OUTBACK

MANASA MARASANI (B.E, M.S)

Environmental Designer, Associate
Atelier Ten

Level 1, 79 Myrtle Street, Chippendale NSW 2008

manasa.marasani@atelierten.com

PRIYA GANDHI (B.S, M.S)

Associate
Atelier Ten

priya.gandhi@atelierten.com

ABOUT THE AUTHORS

As an Environmental Designer, Manasa is experienced in building physics and energy modelling. Her practice includes design for thermal comfort, environmentally sustainable and healthy buildings. Manasa has previously worked in detailed HVAC design and coordination in commercial, educational, and residential facilities.

Priya is driven by the desire to create a built environment that makes a positive impact on the natural environment, believing that good design can solve the climate crisis, one building at a time. Using her building performance modelling and analysis skills, she helps design teams create buildings that are good for people and the planet. Her diverse background in architecture, engineering, research and industry allows her to identify unique, creative and practical solutions to reduce greenhouse gas emissions.

ABSTRACT

For a museum in the remote Australian outback, simulation helped push the boundaries of energy self-sufficiency. Using a hybrid of dynamic thermal simulation and detailed hourly spreadsheet calculations, the analysis identified design and operation strategies to size PV and batteries for various degrees of grid independence. Detailed occupancy patterns, managing internal loads and thermal comfort expectations were particularly influential in the results and therefore critical in optimising PV and battery capacities. In total, six cumulative design cases were developed, illustrating a pathway to reduce energy demand. In addition to the (1) baseline, these cases were: (2) relaxed setpoints, (3) reduced lighting power, (4) reduced AV loads, (5) reduced kitchen water loads, and (6) high performance facilities management. Equipment energy loads and schedules (e.g., on / standby power cycle) were sourced from specific products, where known, and otherwise from the literature (ASHRAE 2013).

INTRODUCTION

The Australian Opal Centre will be a new museum in Lightning Ridge, a remote community in New South Wales, Australia, with a very hot and dry climate. The 3,600m² museum will be built partially underground, with an exposed roof and east façade. The natural ventilation strategy is represented by a significant design feature – a series of malqafs (vertical wind catchers) rising out of the roof to deliver fresh air for ventilation and cooling purposes.

The museum will be built in two stages: stage 1 includes the building enclosure and curator office, stage 2 adds the galleries, auditorium, indoor gardens, and more office spaces. There is no existing grid connection, and the museum intends to be very energy self-sufficient: Stage 1 must be off-grid, while stage 2 may include a grid connection.

The key challenge was to deliver a museum with spaces for sensitive gallery artifacts, human occupancy, and indoor gardens – all within an extreme desert environment with limited energy supply.

The analysis informed key decisions early in design. Therefore, it was critical to include the right level of detail where it mattered, even with an underdeveloped scheme.

METHODS

The analysis started with big picture initiatives and ended with very detailed stress testing of building operations and energy performance through the following steps.

- Initial feasibility testing in IES VE 2018 of big picture design options (thermal labyrinth, ground source heat pump, and natural ventilation potential).
- Stage 1 preliminary energy modelling and renewables sizing, largely through hourly spreadsheet calculations of equipment energy loads, to start understanding off-grid energy requirements.
- Stage 2.1 thermal comfort modelling in IES VE 2018 to inform architectural and mechanical design to ensure critical spaces achieved required conditions for building users and sensitive collections.
- Stage 2.2 energy modelling in IES VE 2018 to predict actual building energy consumption under expected operational conditions, and the resulting PV and battery capacity requirements. This included detailed building occupancy patterns with a 3-hour time-based definition of an occupant. There was also an update to the modelling of ground temperatures, based on site-specific data in the Geotech report.
- Refinement and options testing of Stage 1 and Stage 2.2, including incorporating dynamic energy results into Stage 1 and spreadsheet calculations into Stage 2, with PV and battery capacity sizing and costing occurring with each test.

In total, six cumulative design cases were developed, illustrating a pathway to reduce energy demand. In addition to the (1) baseline, these cases were: (2) relaxed setpoints, (3) reduced lighting power, (4) reduced AV loads, (5) reduced kitchen water loads, and (6) high performance facilities management. Equipment energy loads and schedules (e.g., on / standby power cycle) were sourced from specific products, where known, and otherwise from the literature (ASHRAE 2013).

RESULTS

Code-based occupancy patterns applied flat over the museum space were changed to help save unnecessary oversizing of equipment and subsequent energy demand prediction. Occupancy patterns

were refined to reflect expected actual occupancy with the help of the architects and the client's intended use of the project. As seen in figure 1 & 2 the energy savings achieved with this change is ~14% reduction in cooling energy and 58 per cent reduction in heating energy.

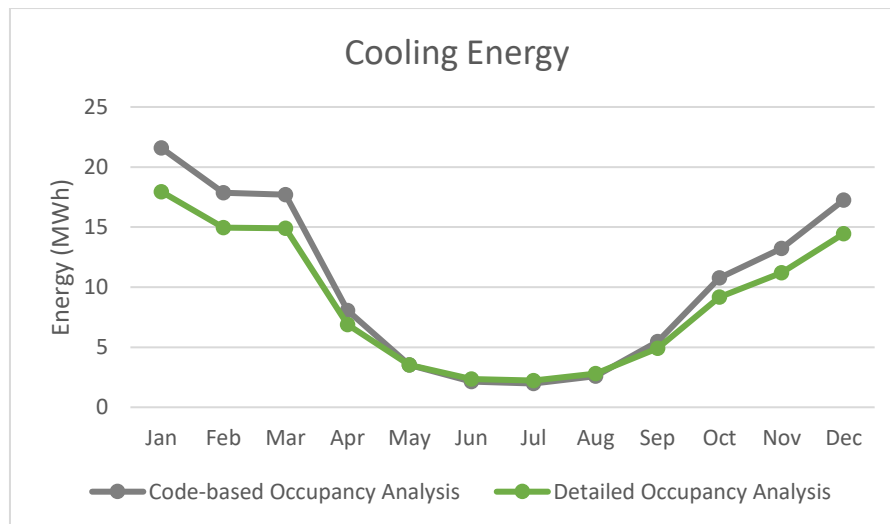


Figure 1. Monthly cooling energy total comparison

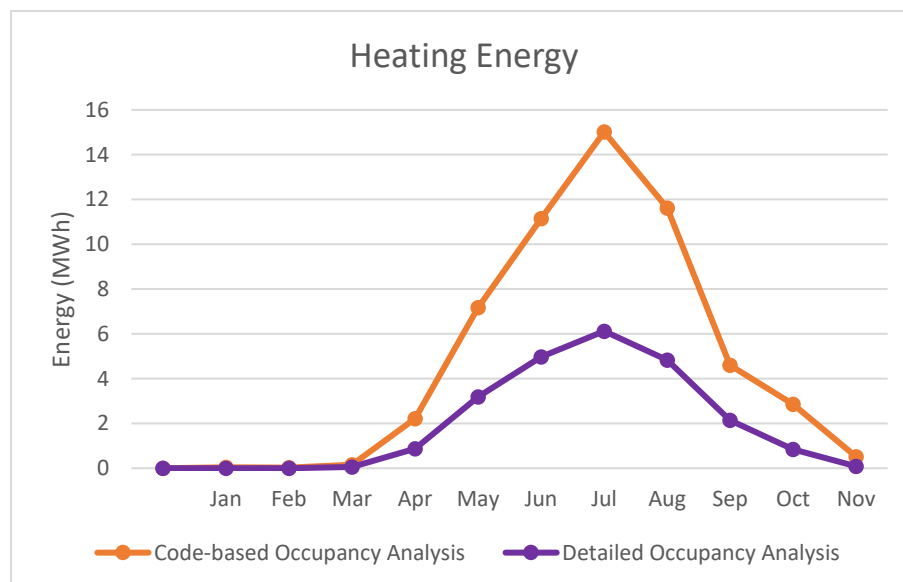


Figure 2. Monthly heating energy total comparison

Figure 3 summarises annual energy demand predicted for each of the six cases. This paper will focus on Cases 5 and 6 due to space limitations.

Case 5 is the cumulative result of all listed measures. Case 6 assumes a 30 per cent reduction in building loads from Case 5 and was used to illustrate how even further reductions (to made during ensuing design phases) could have a significant impact on required PV and battery capacity.

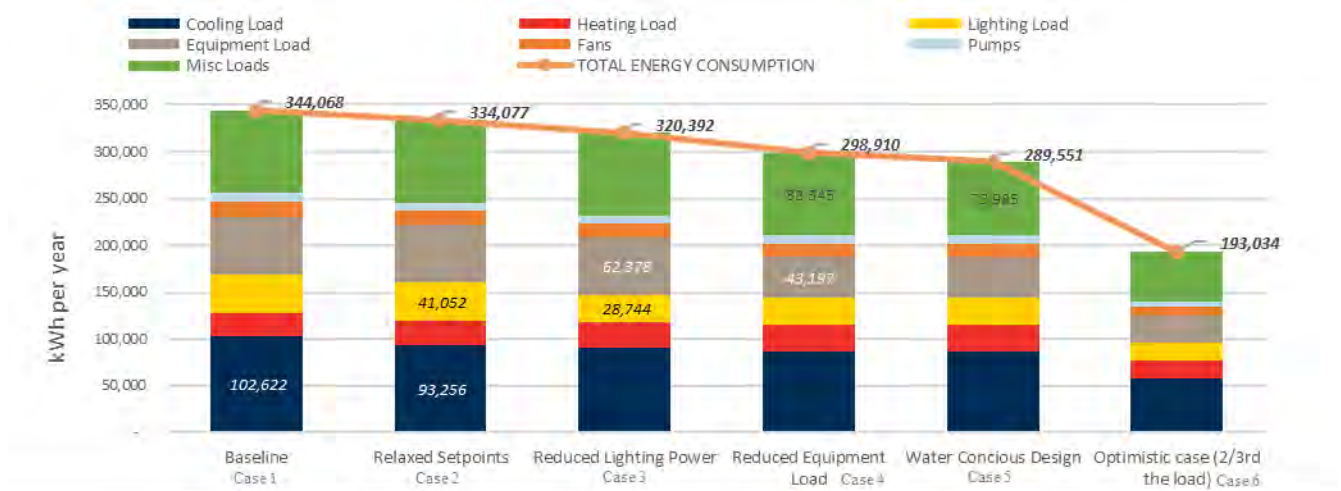


Figure 3. Annual energy demand by end use for each case

The following parameters were especially influential to energy demand: occupancy peaks and patterns (due to higher outside air loads), peak electrical loads, solar loads, and ground temperatures. Figure 4 shows the estimated PV generation and building demand for stage 1 and stage 2, over the course of a year. Stage 2 energy demand is 4-5 times larger than stage 1.

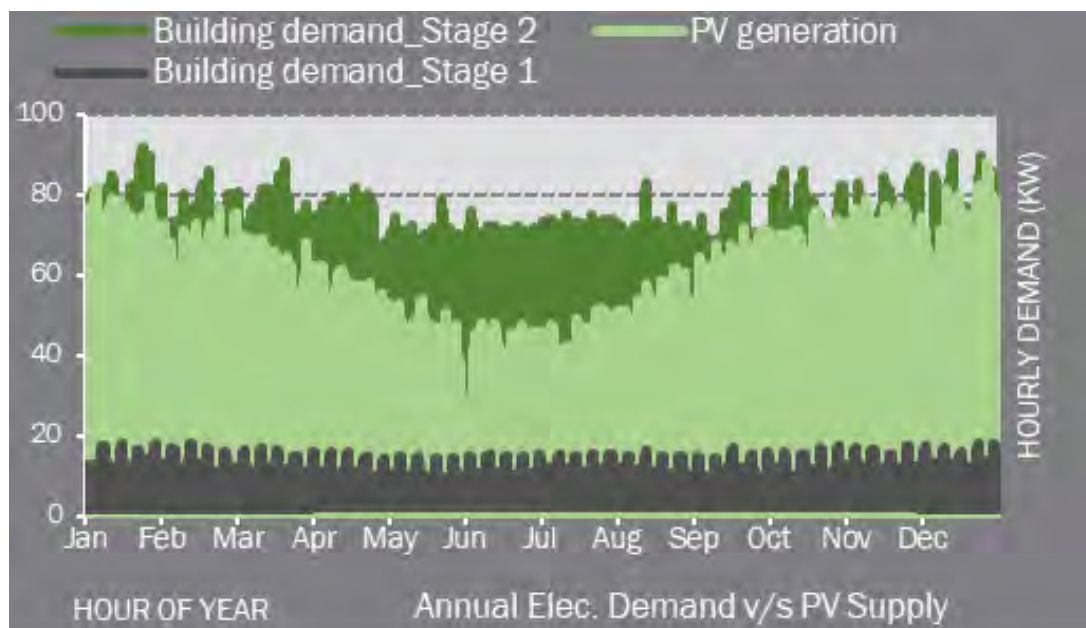


Figure 4. Annual building demand v/s PV Supply: Stage 1&2

Figure 5 charts the relationship between PV array size, battery capacity, and energy undersupply for stage 2. For Case 5, the building requires at least 300kWp PV and 500kWh battery capacity to be effectively off-grid. For Case 6 (30 per cent lower demand than Case 5), the same level of energy independence can be achieved with 33 per cent smaller PV and 40 per cent smaller battery capacity, saving thousands of dollars. This showed that there is a limited return on increasing PV array size, beyond which additional battery capacity does not practically reduce energy undersupply. This analysis draws the line between what is practical and what is possible for the project.

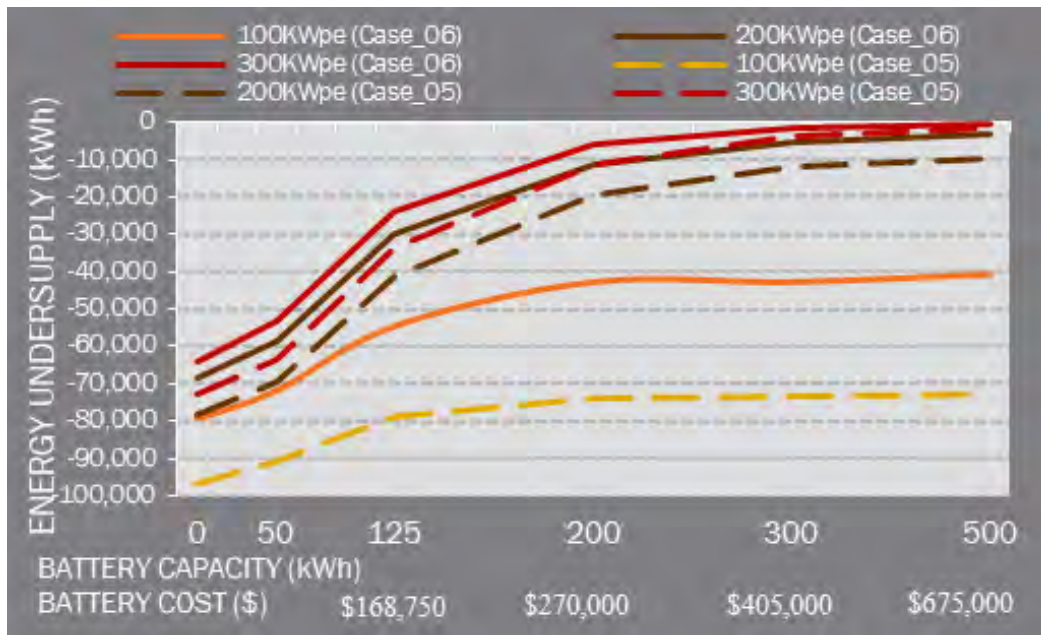


Figure 5. PV Battery required for case 5 and 6

Initial thermal comfort analysis was carried out considering a ground temperature of 20⁰C, based on the average annual dry bulb temperature. This was later proved to be wrong as a site test measured the temperature at 24⁰C. This affected the range of hours within the adaptable comfort range.

We tested comfort conditions with the Passive Cooling system, with new ground temperatures, under two conditions:

1. As designed (malqafs promoting natural ventilation)
2. With added evaporative cooling

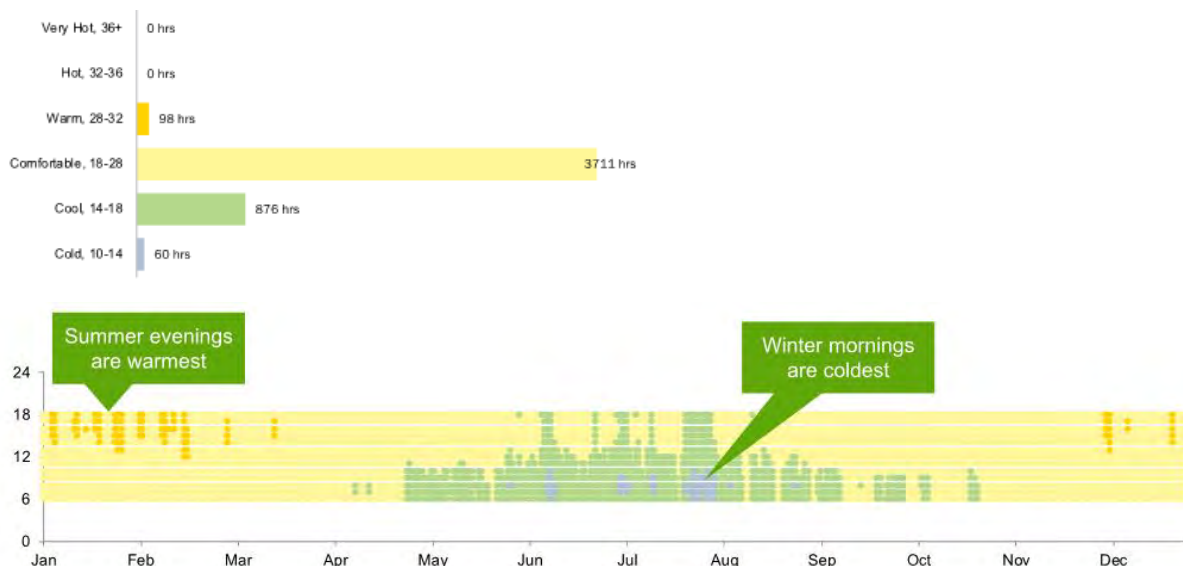


Figure 6. Heatmap of operating hours: Passive cooling system as designed at 20⁰C ground temperature case

Adding evaporative cooling substantially reduces hours above 28°C and adding ceiling fans above front of house spaces like the café, temporary gallery etc, could reduce “feels-like” temperature by another 1-2°C (not modelled) as seen in figure 7 & 8.

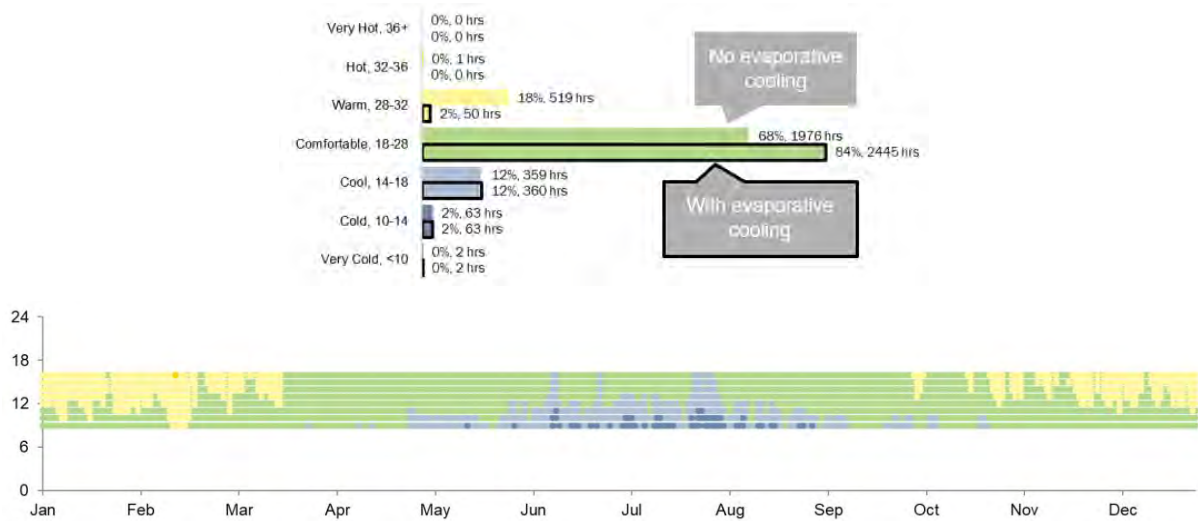


Figure 7. Heatmap of operating hours: Passive cooling system as designed at 24°C ground temperature case



Figure 8. Heatmap of operating hours: Addition of evaporative cooling to the passive cooling system at 24°C ground temperature case

CONCLUSION

There are several key takeaways from this work.

- Accurately modelled detailed occupancy patterns, including understanding the time-based definition of an occupant (i.e. how long an occupant is in the building) was important because outside air volumes were a big driver of space energy consumption.
- Understanding thermal comfort expectations and user behaviour was important. The client has been fully on board with making the museum energy self-sufficient and looked to us to identify limits on electricity loads and thermal comfort expectations to achieve such a result.
- There was a big surprise partway after we did the first round of modelling – the ground temperature turned out to be almost 4 C higher than original assumptions. We learned that due to the high solar loads in Lightning Ridge, the usual rule of thumb (ground temperature equal to average annual dry bulb temperature) did not apply here.
- Increasing the capacity of battery did not reduce energy undersupply. Increasing area of PV meant a decrease in battery capacity but there wasn't sufficient area available. The key to battery and PV sizing for any building is the reduction in building energy consumption by adapting the building to the goals of PV/battery rather than vice-versa

ACKNOWLEDGEMENTS

We would like to thank the Australian Opal Centre and the entire project design team.

REFERENCES

ASHRAE Handbook of Fundamentals (2013), Chapter 18. (Latest version is dated 2021)

DISCLAIMER

The information or advice contained in these technical papers is intended for use only by professionals who have had adequate technical training in the field to which the paper relates. At the time of publication, these technical papers have undergone a formal peer-review process.

These documents have been compiled as an aid only, and the information or advice should be verified before it is put to use. The user should also establish the applicability of the information or advice in relation to any specific circumstances. While the information or advice is believed to be correct, no responsibility is taken by AIRAH or IBPSA Australasia for any statements made within.

AIRAH and IBPSA Australasia, its officers, employees, and agents, disclaim responsibility for any inaccuracies contained within the documents, including those due to any negligence in the preparation and publication of the said technical papers.

COPYRIGHT

This work is copyright. Apart from any use as permitted under the Copyright Act 1986, no part may be reproduced by any process without prior written permission from either the Australian Institute of Refrigeration, Air Conditioning and Heating (AIRAH) or the International Building Performance Simulation Association (IBPSA) Australasia.

CHALLENGES IN COMPUTATIONAL FLUID DYNAMICS (CFD) SIMULATION

KENNETH THOMSON, BENG (MECH), BSC (HMS), RPEQ, M. AIRAH

Fusion HVAC Pty Ltd
281 Montague Road, West End, Qld 4101
ken.thomson@fusionhvac.com

ABOUT THE AUTHOR

Ken Thomson has been working in the construction industry for about 30 years, starting in structural steel detailing and building construction, before moving into mechanical engineering, sustainability, HVAC engineering design and HVAC contracting. He is the AIRAH Associate Director for Queensland, the training officer for AIRAH's NCC Section J training course, and also sits on many panels and committees within the HVAC&R industry. Ken is currently with Fusion HVAC and provides CFD analysis, energy modelling, engineering, and other technical work for the development of Fusion's products and services.

ABSTRACT

Using Computational Fluid Dynamics software (CFD) has become commonplace in the assessment of HVAC systems for determining thermal comfort and Predicted Mean Vote in buildings. CFD is a very powerful tool, but also presents many challenges for validation of HVAC system performance.

This paper is a combination of literature research and practical application of CFD modelling of HVAC solutions for large volume spaces. Using actual project based CFD the thermal comfort assessment, PMV and airflow results of a large volume space are investigated, and representation of results discussed. Ensuring the validity of the results and being able to correlate real world measured outcomes to the CFD simulation should be part of the complete process for validation of a HVAC solution.

INTRODUCTION

This technical paper will look at the fundamentals of Computational Fluid Dynamics (CFD), the use of different software and the application to Large Volume Spaces in the Heating, ventilation, and Air Conditioning (HVAC) industry. The major focus of this paper is on the application of CFD to the determination of the thermal comfort and Predicted Mean Vote (PMV) for determining the performance of the HVAC solution proposed for a large volume space.

CFD is based on the mathematical principles of numerical methods. The use of numerical methods in problem solving is not a new concept and has been around for centuries. It is only with the advent of computers and the rapid increase in computing power and capabilities that

we can use numerical methods to solve the very complex problems associated with understanding fluid dynamics.

1 INTRODUCTION TO CFD

It is important to understand many foundation principles when using CFD, as there are many ways for the results of a CFD simulation to contain errors. Kemal Gungor noted “There is anecdotal evidence that not all of the simulations are performed to the same standards/guidelines/detail/accuracy level.” (Gungor, 2015) Kemal makes note of the 7 main sources of errors and uncertainty as outlined in European Research Community on Flow, Turbulence and Combustion, ERCOFTAC, Best Practice Guidelines. Being able to identify errors and uncertainty and make the appropriate adjustments in the CFD inputs and design of the CFD geometry and mesh are important skills of any good practitioner. In a study paper by (Stern, et al., 2006) a group of fluid dynamics CFD specialists proposed a curriculum for the use of simulation technics in the education of people in the use of CFD, they noted “the lack of trained users is a major obstacle to greater use of CFD”. Searching online, a lot of Australian Universities provide introductory courses in CFD at undergraduate level, but most students are required to continue onto a master’s at least, more often a PHD to get a more detailed understanding of the application of CFD.

To ensure a practitioner has the right skills they must have a decent understanding of the fundamental mathematics and physics behind the application of CFD. Anderson highlights this as the author of Chapter 2 of the textbook ‘Governing Equations of Fluid Dynamics’.

“The cornerstone of computational fluid dynamics is the fundamental governing equations of fluid dynamics—the continuity, momentum and energy equations.

These equations speak physics. They are the mathematical statements of three fundamental physical principles upon which all fluid dynamics is based:

- 1) mass is conserved.
- 2) $F = ma$ (Newton’s second law).
- 3) energy is conserved.”

(Anderson, Jr, 2009)

The use of numerical methods to solve these equations in real world applications is what has developed into the modern field of Computations Fluid Dynamics. Numerical analysis is the study of algorithms that use numerical approximation for the problems of mathematical analysis. Computational fluid dynamics (CFD) is a branch of fluid mechanics that uses numerical analysis and data structures to analyse and solve problems that involve fluid flows. Therefore, the study of fluid dynamics using numerical methods is the study of the above 3 fundamental physical principles via a set of equations that represent the fluid within the boundary conditions defining the problem being studied.

The list of topics compiled below are required understanding for any CFD enthusiast to get started with CFD. (Anderson, Jr, 2009) (Hess & Smith, 1967) (Brezinski & Wuytack, 2012) (Kawaguti, 1953) (Wikipedia, 2022) (Milne-Thomson, 1973)

Fluid Mechanics

- 1) Understand concepts such as density, pressure, and viscosity
- 2) Non-dimensional numbers (Reynolds number, Peclet number and so on...)
- 3) Shear stress, strain

- 4) Fundamental governing equations in fluid mechanics
- 5) Ability to perform dimensional analysis with ease
- 6) Understanding of a control volume

Engineering Mathematics

- 1) Linear algebra – Gauss elimination, Rank of a matrix, Eigen Values, and Vectors
- 2) Vector calculus – Understanding the importance of normals and the calculation to compute them. Gradient and Divergence operators.
- 3) Ordinary Differential Equations (ODEs)
- 4) Partial Differential Equations (PDEs)

Numerical analysis

- 1) Understanding the concept of discretization
- 2) Understanding Eulerian and Lagrangian methods for observing fluid flow

Being able to use the CFD software packages that are now readily available without the understanding of the mathematical and physical fundamentals, and without an understanding of the expected results, and without experience with real fluid flows may result in the exact issues highlighted by (Gungor, 2015). It is therefore important to look at the history of CFD the physics and mathematics involved in the development of CFD and to gain real world experience in fluid properties and fluid dynamics to be able to complete a detailed review of the sources of errors.

1.1 Brief timeline of Computational Fluid Dynamics

- 1) Until 1910: For over 2000 years numerical solutions had been used, then up to 1910 these improvements on mathematical models and numerical methods resulted in the use of these methods to find solutions for fluid dynamics related problems. (Brezinski & Wuytack, 2012)
- 2) 1910 – 1940: Integration of models and methods to generate numerical solutions based on hand calculations. Lewis Fry Richardson did hand calculations for predicting weather in 1910. (Hunt, 1997).
- 3) 1930s methods were first developed to solve the linearized potential equations. Two-dimensional (2D) methods, using conformal transformations of the flow about a cylinder to the flow about an airfoil. (Milne-Thomson, 1973)
- 4) 1940 – 1950: Transition to computer-based calculations with early computers (ENIAC) (Freiberger & Swaine, 2022). Solution for flow around a cylinder by Kawaguti with a mechanical desk calculator in 1953 (Kawaguti, 1953).
- 5) 1950 – 1960: Initial study using computers to model fluid flow based on the Navier-Stokes equations by Los Alamos National Lab, US. Evaluation of vorticity – stream function method. First implementation for 2D, transient, incompressible flow in the world (Johnson N. L., 1996).
- 6) 1960 – 1970: Early scientific papers “Calculation of potential flow about arbitrary bodies” was published about computational analysis of 3D bodies by Hess and Smith in 1967 (Hess & Smith, 1967). Generation of commercial codes. Contribution of various methods such as k- ϵ turbulence model, Arbitrary Lagrangian-Eulerian, SIMPLE algorithm which are all still broadly used (Johnson N. L., 1996).
- 7) 1970 – 1980: In 1973 an estimated 100 to 200 computers run codes generated by Boeing, NASA and some have unveiled and started to use several yields such as

submarines, surface ships, automobiles, helicopters, and aircrafts. (Johnson, Tinoco, & Jong Yu, 2005)

- 8) 1980 – 1990: Improvement of accurate solutions of transonic flows in the three-dimensional case by Jameson et. al. Commercial codes have started to implement through both academia and industry (Jameson, Schmidt, & Turkel, June 1981).
- 9) 1990 – Present: Thorough developments in Informatics: worldwide usage of CFD virtually in every sector. (Johnson, Tinoco, & Jong Yu, 2005)

1.2 Numerical solutions

“The main goal of computational fluid dynamics (CFD) is to translate the mathematical description of the physics of fluids into a set of instructions that can be executed by a computer to reproduce the fluid's motion.” (Sommavilla, 2022) The complex nature of the movement of Fluids, and the interaction of the fluid particles within the man-made and natural environment means there are many assumptions and simplifications to allow for the computation of the fluid behaviours. The two (2) methods for development of the numerical solutions are:

- Mesh-based methods, of which four (4) have been developed:
 - Finite Difference Method (FDM)
 - Finite Volume Method (FVM)
 - Finite Element Method (FEM)
 - Lattice Boltzmann Method (LBM)
- Particle-based methods of which one (1) have been developed:
 - Smoothed Particle Hydrodynamics (SPH)

The Navier Stokes Equations (NSE) are used in four (4) of the five (5) methods, the Lattice Boltzmann Method uses the Boltzmann Equation and the Chapman-Enskog expansion to provide equivalent second order discretization of the NSE. The LBM applies for certain conditions as defined by the Chapman-Enskog expansion and hence should be used with care.

Peter Vilhelm Nielsen has been producing research and technical papers in this field since the 1970's. The significant contribution of work from early CFD numerical solutions to current software provides a very good resource for anyone new to this area to gain a much deeper understanding of the CFD methods and limitations. One of Peter's very early papers is still relevant today and shows the fundamentals of Current CFD solutions are based on those same methods as he was studying in the 1970's. “The numerical method is based on computer-solved flow equations, see e.g., (Nielsen, 1973), (Nielsen, 1975), (Nielsen, Restivo, & Whitelaw, 1978), [4], [5] and [6]. Three momentum equations (Navier- Stokes equations) and the equation of continuity describe the flow. The turbulence is described by a transport equation for turbulent kinetic energy and an equation for dissipation of turbulent kinetic energy. Launder et al. [7] has developed this two-equation turbulence model to its present form.”

1.1.1 Reynolds number and turbulent or laminar flow

“The velocity characteristics of ventilated rooms are important in that they help to control the comfort and wellbeing of individuals.” (Nielsen, Restivo, & Whitelaw, The Velocity Characteristics of Ventilated Rooms, 1978) Hence this is one important aspect of any CFD solution where the numerical estimations can play an important role in determining how closely the CFD will reflect the real situation.

The flow of air over a surface, such as the goods stored on racking, or against a wall will be either laminar or turbulent. The Coanda effect plays a large part in the airflow into and around racking systems when the localised airflows near the racking are above velocities of 0.4m/s.

Airflows above 0.4m/s will likely result in turbulent flows; this is important if the airflow off a supply air diffuser is this velocity or greater.

The flow of air around the racking or other obstructions within a warehouse should be evident in the CFD simulations based on the known effect of boundary layers and Reynolds number associated with the flow patterns. As an example, 27°C air travelling at 2m/s over the surface of boxes (flat plates) calculates to have the following:

Given Data:

$$\text{Air at } 27^{\circ}\text{C} = 27 + 273 = 300\text{K}$$

$$P = 1 \text{ atm} = 1 \text{ bar} = 101.325\text{kPa}$$

$$U = x \text{ m/s (table below shows some velocities and corresponding Re numbers)}$$

$$\mu = 1.85 \times 10^{-5} \text{ kg/m.s}$$

$$R = 287 \text{ (gas constant)}$$

$$\text{Density } \rho = P/RT \quad (1)$$

$$\text{Reynolds Number } Re = \rho UX / \mu \quad (2)$$

The critical Reynolds numbers for development of turbulent flow is around 500,000. Reynolds numbers near and above this are likely to produce a turbulent flow pattern. Calculating the Reynolds number at $x = 1\text{m}$ along the racking for different airflow velocities is shown.

U m/s	Reynolds number
0.4	25444.96
1	63612.39
2	127224.79
4	254449.57
8	508899.14
10	636123.93

Table 1. Reynolds numbers for flat plate flows at different velocities and 1m along the edge

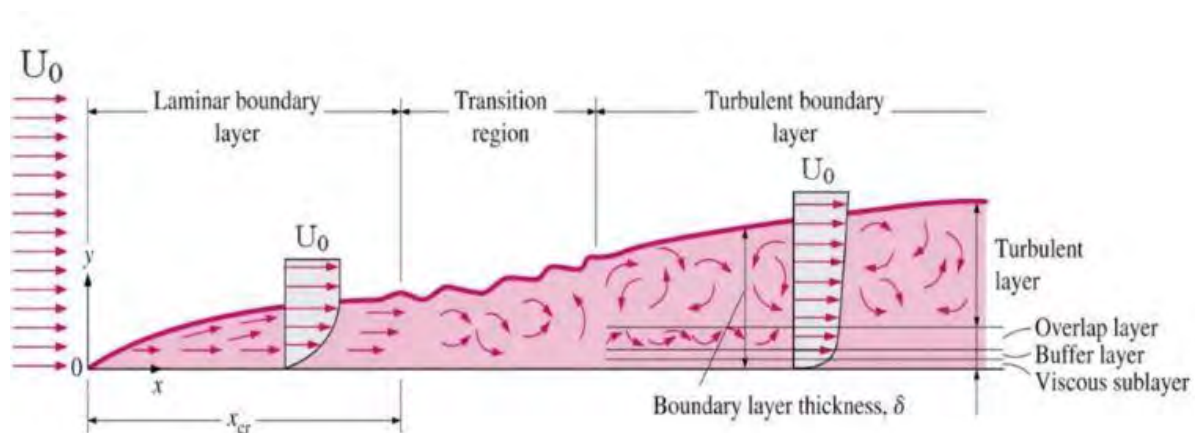


Figure 1. Boundary layer conditions for critical Reynolds numbers of flows along flat plate

In a CFD study with airflow near racking you would expect to see transitions regions and then turbulent flows for any supply air being delivered close the racking at more than 4m/s. typical jet and grille air delivery will have velocities in this region near the top of the racking systems and hence this should be shown in the CFD solution to ensure the solution is accurate.

Air through the racking between boxes and items on racks will have a similar Reynolds number and air flow behaviour to that of flow in a pipe or channel. The critical Reynolds numbers for development of turbulent flow is around 2,500 for this application. For small gaps into and around items on racking you would expect to see turbulent flows above 0.4m/s.

U m/s	Reynolds number
0.4	2544.50
1	6361.24
2	12722.48
4	25444.96
8	50889.91
10	63612.39

Table 2. Reynolds numbers for pipe flows at different velocities for diameter of 0.1m

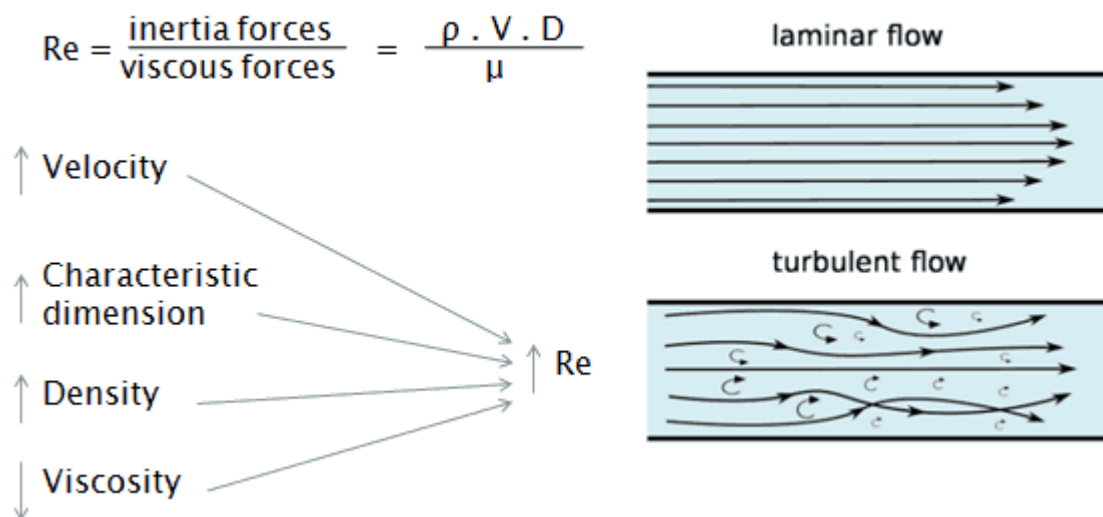


Figure 2. Flow conditions and critical Reynolds number for flow into racking

2 ERRORS IN CFD

Errors in CFD simulation can be overlooked due to the way the information is presented, which is both misleading the client. CFD reports will often contain images to represent the results as that are colourful and easily read, these images can verify the compliance of the proposed solution to the client. Ning Li completes a comparison of three different CFD software packages for the purpose of comparing the results and functionality of each piece of software. Ning Li highlights in his thesis the differences in the software and provides some insight into the comparative ease of use of each. (Li, 2015)

Table 7. Performance of meshing for the three software.

	Meshing		
	ANSYS Mesh	Star – CCM+	IESVE Microflo
Manipulate Difficulty of Interface	Complicate	Intermediate	Simple
Degree of precision	High	Intermediate	Low
Time Spending	Intermediate	Slow	Fast

CFD software can be limited in many ways, each of the limitations can generate a set of errors that must be considered before presenting the results and solutions. For most software there is some level of compromise due to the following:

- 1) Simplification errors - simple flow models or simplified boundary conditions
- 2) Uncertainty errors - possible uncertainties caused by too little computing values per cell and interpolation errors
- 3) Hardware limits - computation time may extend for large models, and lead to terminating solutions that may not have fully resolved
- 4) Human errors – increased costs and consulting time compared to experiments, for more simple applications

2.1 Source of errors in CFD

The sources or errors in CFD have been discussed in many other papers, therefore I will only list the source of errors here. The Ecolibrium article, “Sources or errors for indoor CFD simulations”, (Gungor, 2015) provides detail of each type of error and should be read to understand each source of error.

- 1) Model error and uncertainties: The difference between the actual flow and the mathematical model. Most well publicised errors in this category are the errors from turbulence modelling.
- 2) Discretisation or numerical error: The difference between the exact solution of the mathematical model and numerical solution, with a limited resolution in time and space.
- 3) Iteration or convergence error: Relating to the difference between the exact and iterative solutions of the discretised equations.
- 4) Round-off error: This is caused by the limited number of computer digits available for storage of a given physical value.
- 5) Code errors: Errors due to bugs in the software, unintended programming errors in the implementation of models or compiler errors.
- 6) Application uncertainties: Inaccuracy is also introduced because the application is complex, and precise data needed for the simulation is not always available.
- 7) User errors: Usage errors are due to the application of the code in a less-than-accurate or improper manner. Usage errors may show up as modelling and discretisation errors. Using incorrect parameter values, badly chosen model or boundary conditions are among the typical user errors. Usage errors can exist in the CAD geometry, grid generation, and post-processing software, in addition to the CFD set-up.

For large volume spaces some of the above source of errors become more dominant than others and are also affected by the selection of software used to provide the CFD solution. A list of common CFD packages, both commercial and public domain, can be found on cfd-online (CFD Online, 2022) and TenLinks (Tenlinks, 2022).

3 THERMAL COMFORT AND PMV IN LARGE VOLUME SPACES

The assessment of thermal comfort in large volume spaces needs to be considered in context with the function of the space being assessed. The impetus driving these assessments and the analysis of the HVAC systems in these spaces are 2-fold. The thermal comfort of people working in "big box" retail spaces such as Costco, Bunnings and Ikea, has become important

as retail centres have moved towards this model, Second, such spaces required tightly controlled temperature gradients across their entire racking system so that no product stored there goes outside its temperature requirements, and is then considered damaged due to temperature fluctuations.

Maintaining a controlled temperature in these spaces has many challenges. Typical large volume spaces are over 2,500m² and have ceiling heights in the range of 6-10m, sometimes the spaces can be as high as 15m. Traditional HVAC systems with standard air distribution jets, grilles or slots struggle to deliver the air to the space, and struggle to maintain an even and moving air volume within entire space. Dead spots, stratification, drafts, and temperature fluctuation are typical within these spaces using conventional HVAC design that suit the office spaces with volumes below 4m in height and areas less than 1,500m².

For most energy modelling software packages there is an option to use the in-built thermal comfort tools that assess the building as modelled to achieve the energy predictions or compliance assessment. Most energy modelling software uses what is known as a “stirred tank” model, which assumes an even air temperature and air distribution has occurred in the space. IES-VE for example uses this approach in the energy modelling solution.

“Equation 22 embodies an assumption that the air displaced by the supply air is at the room mean temperature, which is consistent with ApacheSim’s ‘stirred tank’ model of the room air.” (Integrated Environmental Solutions, Copyright © 2011-2021)

For a large volume space with grilles, jets or other high velocity air delivery systems where the air distribution is not uniform and does not meet the “stirred tank” method, the use of the energy modelling software will not give results that represent the thermal comfort achieved within the space, unless it can be demonstrated the supply air patterns are close to a “stirred tank” model.

CFD is often used to demonstrate the effectiveness of a HVC solution. Thermal Comfort and PMV assessments are required in some instances for compliance or validation of a solution and CFD is the only cost-effective way to demonstrate the performance of the HVAC system, and the air distribution patterns. In the instance of large volume space with grilles, jets or other high velocity air delivery systems it is the only method outside of onsite physical testing.

3.1 Example of a large volume space

The typical HVAC solution to a large volume space is to provide a large amount of ducting for distribution of the cold air, and to use radiant heating and fans to move warm air. These solutions do not really require a CFD performance analysis as the distribution of the cold or hot air is managed via systems that direct the air into most areas of the warehouse via localised air delivery. Trying to use a ducted solution for both heating and cooling is difficult as stratification is an issue, and the use of radiant heaters and ceiling fans is more applicable in locations that have very little cooling demand. The drive in the market currently is towards ductless roof mounted HVAC solutions that distribute the air from locations directly underneath each unit and providing air diffusion using outlets local to the unit, without ducts. The location, capacity and air delivery method used for this type of solution must be verified by CFD, laboratory and field testing and measurements during operation to confirm the effectiveness of the overall system in providing efficient cooling to the space.

CFD simulations of large volume spaces attempt to inform the designer of the effectiveness of air delivery systems, and sometimes the effectiveness of ceiling or under roof mounted fans. These simulations are used to provide information to the client about the air movement in the space and the thermal comfort of the occupants, using Predicted Mean Vote (PMV) and Percentage Person Dissatisfied (PPD), as the major to indicators of performance. These CFD

simulations are limited in their accuracy due to limitations in computing power, and limitations in the capabilities of the CFD software.

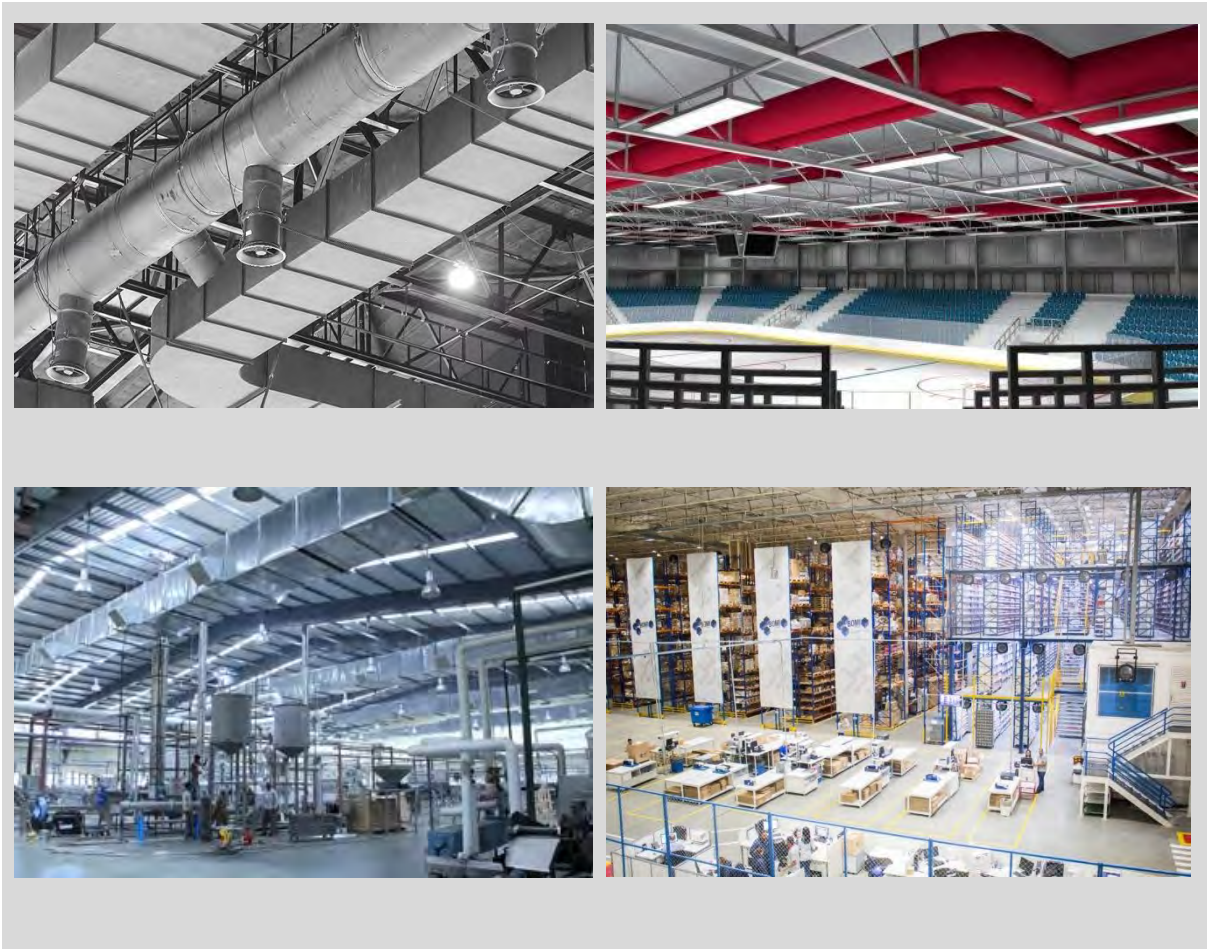


Figure 3. *Examples of Large volume space HVAC solutions*

3.2 Applications of CFD in Large Volume spaces

CFD analysis does not necessarily show the actual performance of HVAC system. Instead it shows the theoretical performance when all boundary conditions are idealised. This can result in a misunderstanding of the true performance of the HVAC system. Large volume spaces have large walls facing different orientations, the CFD analysis may be set with all internal wall temperatures equal around the entire perimeter of the space, depending on the thermal performance of the wall materials this assumption, is sometimes not valid and can provide airflow, temperature and comfort assessments for the space may not represent the performance in the actual space.

Large volume spaces that require temperature control vary significantly and the air delivery effectiveness into these spaces can be highly dependent on the objects in the space and the requirements of the space. A large sports hall typically has a large open space, but also may be used for assemblies, therefore generating a very high occupant load. A warehouse is unlikely to generate a high occupant load, however materials stored, and the way the materials are store can be a major influence on the air movement within the space. Often additional air moving devices are added to a space to increase air movement of the conditioned air. Ceiling or under roof mounted fans and isle fans are used to help direct air down between the racking systems used for storage.

1.1.2 CFD of Ceiling Fans

Most ceiling fans are designed to direct air directly downwards to push the air to the floor level, the size and operational speed of the fan is determined to try and maximise this effect. CFD modelling of ceiling fans can therefore be approximated by a circular or square component that pushes air out the bottom, while bringing in the same amount of air through the top. It is highlighted in many research papers that a comprehensive model of a ceiling fan is not as simple as this. In the paper by (Bala Bhaskara Rao, Bhanuchandra Rao, Siddhartha Yadav, & Sreerama, 2020) a 3 and 4 fin domestic ceiling fan is modelled in a 3 cubic meter representation of a room. Due to the small size of the modelled space Bala points out in discussion the limitations of the CFD results in representing the flow characteristics as air impacts the walls generating additional turbulence. In the paper by (Babich, Cook, Loveday, Rawal, & Shukla, 2017) a larger space is used to test the ceiling fan, and the mesh generated to complete the CFD is approximately 2 (two) million elements. The room size is approximately 40m³, hence the mesh generated is quite dense for such a small space. Even with such a dense mesh the numerical uncertainty of the CFD is reported as 15.80 per cent. The CFD simulations also show high velocities directly below the fan, in a predominantly downwards direction. As per the figure 6 provided in the paper by (Babich, Cook, Loveday, Rawal, & Shukla, 2017).

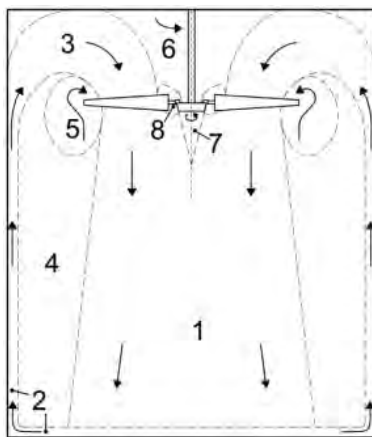


Table 5

Comparison between previous qualitative research and the developed CFD model.

Region	Agreement	Key characteristics
1	Good	Highest higher speed, significant swirling component, divergent flow
2	Good	Very low air speed near walls (moving upward) and ceiling
3	Good	Increasing air speed and development of swirling component
4	Good	Very low air speed and negligible effectiveness of the fan
5	Weak	Local air recirculation underestimated by the CFD model
6	Good	Low air speed, recirculation area
7	Good	Air not driven downwards due to the blockage caused by the motor of the fan
8	Weak	Local air recirculation underestimated by the CFD model

Figure 4. Figure 6 (Babich, Cook, Loveday, Rawal, & Shukla, 2017) “Flow regions identified by (Jain, Upadhyay, Chandra, Saini, & Kale, 2004) with Table 5 the comparison between qualitative research and the developed CFD model of the matching airflow measured locations as numbered”

In large volume spaces it is very important to make sure the modelling of the ceiling fans considers any turbulent flows that may occur due to proximity of racking or other obstacles to free flow for the fans. Also, a large volume space of approximately 80,000m³ is going to require careful mesh generation to capture all the flow patterns around each ceiling fan and nearby racking, walls and buoyancy effects for very tall spaces. Research papers, conference papers and articles by (Liu, Lipczynska, & Schiavon, 2018), (Adeeb, Maqsood, & Mushtaq, 2015), (Babich, Cook, Loveday, Rawal, & Shukla, 2017) and (Lin, 2019) all agree with the above representation of a ceiling fans airflow pattern. The study of ceiling fan performance and CFD simulations have become more frequent recently as the use of ceiling fans is a more sustainable option in comparison to air-conditioning, increasing the interest in understanding the air flow patterns, and the effectiveness of a ceiling fan.

1.1.3 Modelling flows against and through racking

The CFD modelling of a warehouse solution with a racking system for storage of goods is a very complex task. The different air delivery systems that can be used must be modelled in different ways as the effects of velocity and method of air delivery has an impact on how the CFD mesh is generated and the type of numerical solution that is going to provide the best results. It is well known that high velocity air travelling parallel to a surface will induce a Coanda effect and attach the airflow to the surface. Modelling airflows from supply air jets, or other air delivery systems in CFD requires this effect to be accounted for. The higher the velocity of the air the greater the chance of attachment to a surface.

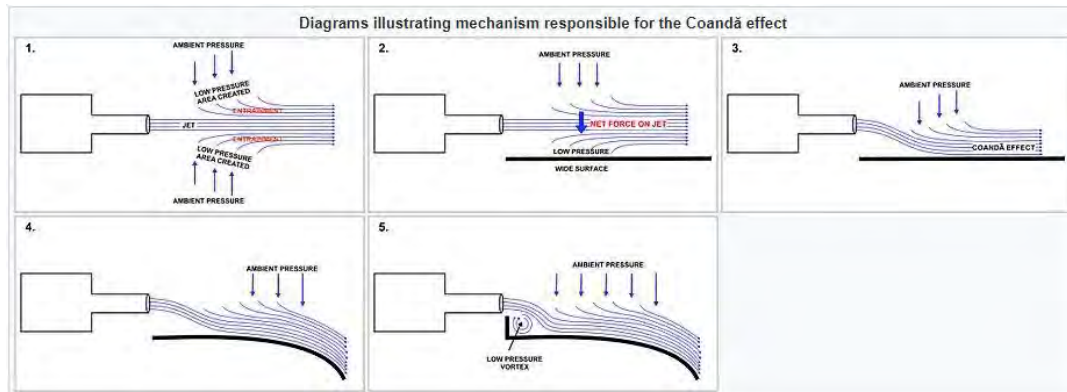


Figure 5. Coanda Effect with jet streams (Wikipedia, 2022)

Knowing the Reynolds number of the air flow and adjusting the CFD mesh to account for the generated Coanda effect is an important part of determining the real flows around the racking. The higher Reynolds numbers associated with jet and grille type air diffusion will result in some Coanda effect, and therefore mesh sizing around racking close to the diffusers must be considered in the CFD solution.

4 RESULTS

The results presented here are from multiple projects that cannot be named due to confidentiality. The results are the typical visual presentations that are provided as validation of the HVAC solution using the CFD analysis completed by a consulting engineering firm or individual. They are from multiple projects and from different CFD software packages.

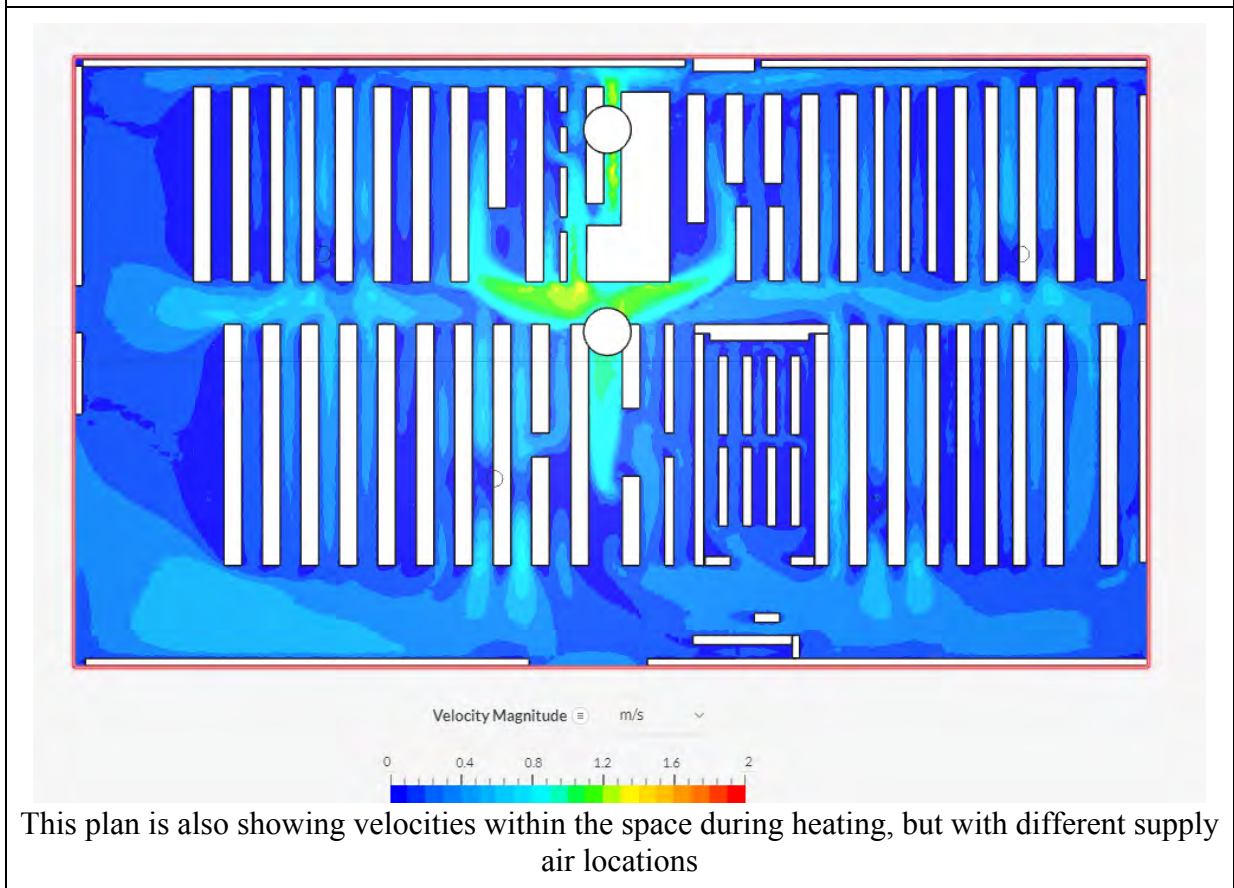
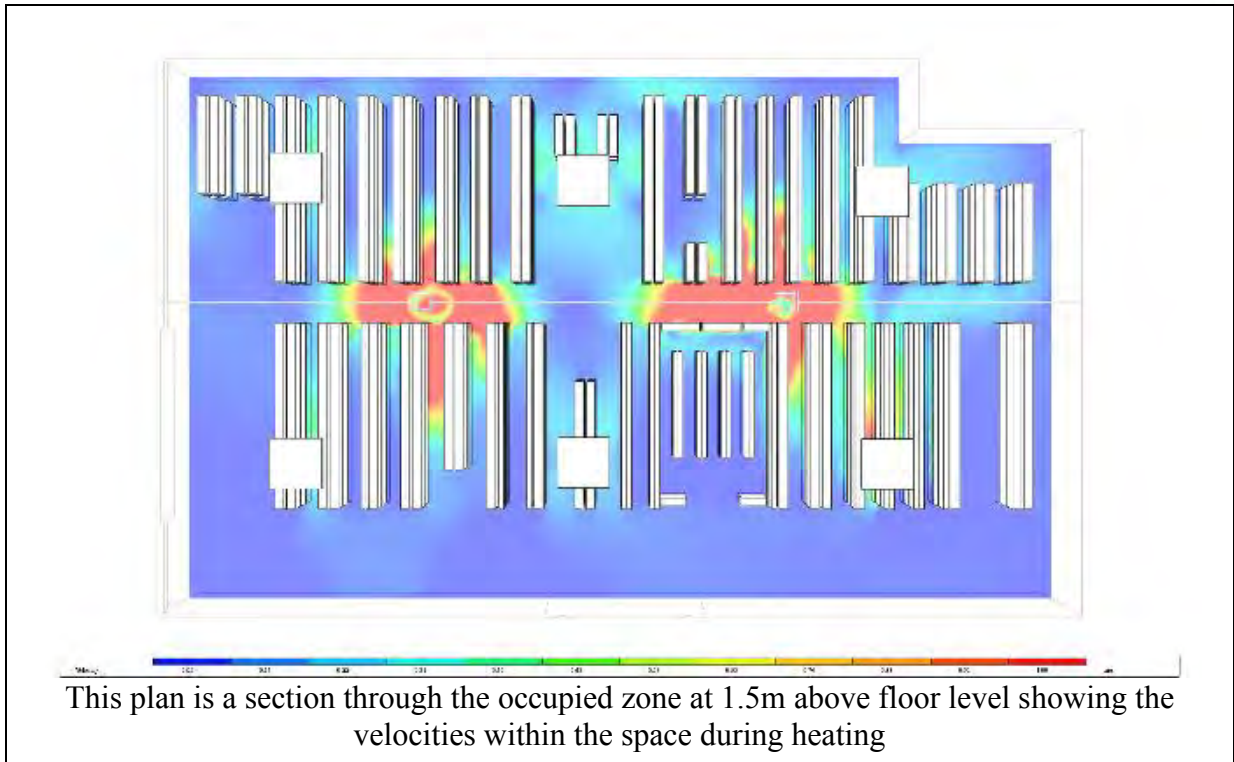


Table 3 *Images and comments of two velocity diagrams from CFD solutions*

The two images above are very similar, there is so much similarity between these results it is not obvious to the reader these are different buildings and the CFD results are from different software packages. This significant level of similarity can result in confusion for the client,

who is not a user of CFD software in being able to determine whether the presented results are actually providing useful detail, or this is just a report provided to ‘tick the box’ in meeting the brief requirement for CFD verification of the solution for their project.

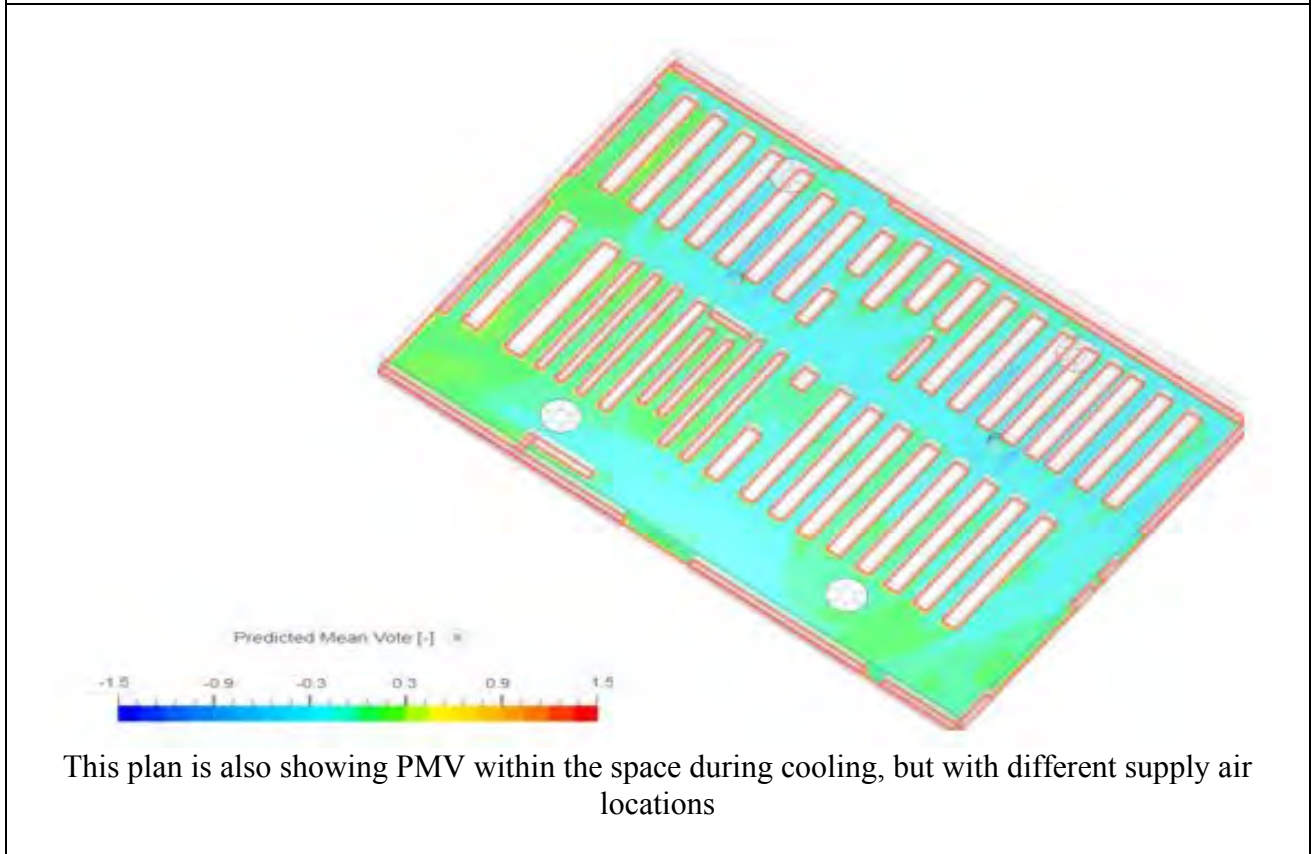


Table 4 Images and comments of 2 PMV diagrams from CFD solutions

Again, each of the above two images are similar, and show results that demonstrate compliance, since these are two completely different buildings modelled in different software packages, the question has to be asked, has the modeller provided results that look similar to another project that is known to receive compliance or have they modelled the building to actually demonstrate the performance of the system? The PMV range in each set of results shows the space at the occupied level is -1 to +1, which is a very good PMV result.

What is clear from the results and images shown and many other images that are produced from different CFD packages is the similarity of the presented outcomes. There is little opportunity for someone reviewing the results to see if the results are truly representative of the actual performance of the system and can be verified against field measurements or onsite testing. Field measurements and onsite testing is not often done and ventilation design where buoyancy effects, large eddy simulation, turbulent intensity values, coupling effects and the lower resolution of the data due to mesh sizing, are all challenges in the generation of the CFD, there needs to be better confirmation of CFD modelling outputs against actual performance measures. (Cao, 2018)

The following images are an example of a solution where the complete set of results and testing has been completed and the CFD generated that match. These results are for a swirl diffuser with a generated set of boundary conditions to represent the swirl diffuser that are then used in the large volume space CFD assessment. Determining the accurate boundary conditions helps in developing the CFD for the much larger area, as it reduces mesh sizing and hence computational load for the large volume space. Matched onsite measurements and Smoke tests confirm the CFD results, providing validation the CFD results for the boundary conditions can be used, and hence providing a high level of confidence in the CFD results that would be obtained from the CFD analysis of the large volume space where these boundary conditions would be applied.

Testing and validation of CFD results is an important step in the process of using CFD. Too often CFD results are relied upon where there has been little or no validation of the CFD results. It must be remembered that CFD is a numerical tool that provides an approximation of real-world applications, and hence has an inherent level of error that needs to be accounted for when producing results. CFD analysis is typically not done in a single run, or single solution and set of results to demonstrate airflow, it often takes multiple runs of the CFD code before results that ‘make sense’ are achieved, and this is especially relevant when assessing large volume spaces where the mesh size and computational capacity are often at the limit.

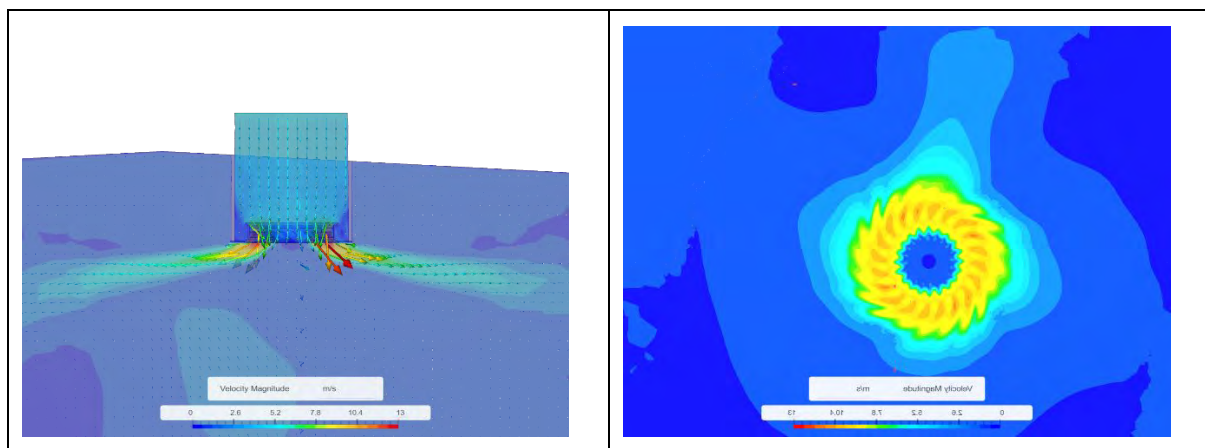




Figure 6. CFD images of Swirl diffuser for generating boundary conditions and matched onsite tests

5 CONCLUSION

CFD is has been used extensively in all areas of engineering with an increased appetite over the past few years from the end user or client. The belief is the CFD results will demonstrate the actual perform of a system with sufficient accuracy that the client can be happy the proposed solution will perform as expected. If we are to use CFD to demonstrate the performance and effectiveness of the air delivery of a proposed system, then there needs to be some way other than the CFD results to demonstrate this. Inherent errors and inaccuracies within a lot of CFD analysis is not always picked up as a deeper understanding of what results should be seen is lacking. The are many reasons why this may not be the case, and this paper highlights quite a few of those. Therefore, it is more important to educate everyone on the use of CFD and provide some simple key indicators that allow everyone to determine if the CFD simulation is providing reliable results that are indicative of the real-world application. Traditionally CFD has been used by experts who are looking at it as way to provide direction for the physical experiments, only recently has CFD started to be used as a validation tool of a proposed design solution.

In large volume spaces it is more important to use the CFD solution to understand the PMV and thermal comfort as this should provide a more accurate presentation of the actual performance within the space. Using PMV and PPD results from the energy modelling software tools is not appropriate due to Coanda effect, boundary conditions, Dead spots, stratification, drafts, and temperature fluctuation. Being able to read and understand the information presented in a typical CFD report is not easy. Images look almost the same from different CFD software, and with different HVAC solutions.

In large volume spaces and in design of ventilation systems in general use of CFD simulation to verify designs is becoming more commonplace. Some software is not capable of providing results, while other software is limited in the application of meshing or boundary condition

inputs. (Li, 2015) Being able to use the right software with the meshing capabilities, boundary condition inputs and then building the correct geometric model with the right number of assumptions can be quite challenging. The presentation of the results in a way that can demonstrate the performance achieved by the system can also be challenging as it difficult for the client who does not have the engineering knowledge and training in understanding the physics and mathematics used in development of the CFD software and hence the limitations of the software in being able to predict the airflow patterns. The high level of similarity in output images of presented information does not provide enough for the client to discern if the CFD results can be trusted.

As the use of CFD becomes more widespread and the costs and time needs are rapidly reducing, with the advent of cloud computing CFD software the development of a set of guidelines and layman level education is needed. Too often the client is left in the situation of blindly trusting the engineer, or CFD modeller as they do not have the knowledge, training or access to simplified detail on how to read and interpret CFD results.

How can you find something that you don't know you need to look for.

ACKNOWLEDGEMENTS

I wish to acknowledge the assistance of my colleagues at Fusion HVAC Australia and in New Zealand. Kevin Harris, Fusion HVAC CEO, Mike Palmer, Sean Badenhorst, Michael Howard, Sam Wissa, and the rest of the team.

REFERENCES

- Adeeb, E., Maqsood, A., & Mushtaq, A. (2015). Effect of Number of Blades on Performance of Ceiling Fans. *MATEC Web of Conferences* (pp. 02002-p1-5). Islamabad: Research Centre for Modeling & Simulation, National University of Sciences & Technology.
- Anderson, Jr, J. D. (2009). Chapter 2 - Governing Equations of Fluid Dynamics. In J. W. (ed), *Computational Fluid Dynamics* (pp. 15-51). Berlin Heidelberg: Springer-Verlag.
- Babich, F., Cook, M., Loveday, D., Rawal, R., & Shukla, Y. (2017). Transient three-dimensional CFD modelling of ceiling fans. *Building and Environment, Vol 3*, 37-49.
- Bala Bhaskara Rao, J., Bhanuchandra Rao, D., Siddhartha Yadav, J., & Sreerama, M. (2020). Simulation of Air Flow Around Ceiling Fan in an Enclosed Space by Using CFD. *INTERNATIONAL JOURNAL OF SCIENTIFIC & TECHNOLOGY RESEARCH Vol 9, Issue 6*, 1061-1064.
- Brezinski, C., & Wuytack, L. (2012). *Numerical analysis: Historical developments in the 20th century*. e-book: Elsevier.
- CFD Online. (2022, March 20). *Wiki/Codes*. Retrieved from CFD Online: <https://www.cfd-online.com/Wiki/Codes>
- Freiberger, P. A., & Swaine, M. R. (2022, January 31). *ENIAC*. Retrieved from Encyclopedia Britannica: <https://www.britannica.com/technology/ENIAC>
- Gungor, K. (2015). Sources of errors for indoor air CFD simulations (Part 1). *Ecolibrium*, 48-53.

- Hess, J. L., & Smith, A. M. (1967). *Calculation of Potential Flow About arbitrary Bodies*. Long Beach, California: Douglas Aircraft Company, Aircraft Division.
- Hunt, J. C. (1997). Lewis Fry Richardson and his contributions to mathematics, meteorology, and models of conflict. *Annual Review of Fluid Mechanics*, pp. Vol 30: xiii-xxxvi. Retrieved from Wikipedia: https://en.wikipedia.org/wiki/Lewis_Fry_Richardson
- Integrated Environmental Solutions. (Copyright © 2011-2021, March 20). *ApacheCalc Methods*. Retrieved from Integrated Environmental Solutions: <https://help.iesve.com/ve2021/>
- Jain, A., Upadhyay, R. R., Chandra, S., Saini, M., & Kale, S. (2004). Experimental investigation of the flow field of a ceiling fan. *ASME 2004 Heat Transfer/Fluids Engineering Summer Conference* (pp. 93-99). Charlotte, NC: American Society of Mechanical Engineers.
- Jameson, A., Schmidt, W., & Turkel, E. (June 1981). Numerical solution of the Euler equations by finite volume methods using Runge Kutta time stepping schemes. *14th Fluid and Plasma Dynamics Conference* (p. 1259). Reston, Virginia: American Institute of Aeronautics and Astronautics.
- Johnson, F. T., Tinoco, E. N., & Jong Yu, N. (2005, December Volume 34, Issue 10). Thirty Years of Development and Application of CFD at Boeing Commercial Airplanes. *Computers & Fluids, AIAA*, pp. 1115-1151.
- Johnson, N. L. (1996). The elgacy and Future of CFD at Los Almos. *1996 Canadian CFD Conference*. Ottawa, Canada: Los Alamos National Laboratory.
- Kawaguti, M. (1953). Numerical Solution of the NS Equations for the Flow around a Circular Cylinder at Reynolds Number 40. *Journal of Physics Society, Japan*, 747-757, Vol 8.
- Li, N. (2015). *Comparison betwene three different CFD software and numerical simulation of an Ambulance Hall*. STOCKHOLM: KTH School of Industrial Engineering and Management.
- Lin, H.-H. (2019, June 18). Improvement of Human Thermal Comfort by Optimizing the Airflow Induced by a Ceiling Fan. *Sustainability*, pp. 11, 3370.
- Liu, S., Lipczynska, A., & Schiavon, S. (2018). *Detailed experimental investigation of air speed field induced by ceiling fans*. Singapore: Berkeley Education Alliance for Research in Singapore Limited.
- Milne-Thomson, L. M. (1973). *Theoretical Aerodynamics. Physics of Fluids A. Vol. 5*. New York: Dover Publications.
- Nielsen, P. V. (1973). Berechnung der Luftbewegung in einem zwangsbelüfteten Raum. *G I - Gesundheits Ingenieur*, 299.
- Nielsen, P. V. (1975). Prediction of air flow and comfort in air conditioned spaces. *ASHRAE Transactions*, Vol. 81, Part II.
- Nielsen, P. V., Restivo, A., & Whitelaw, J. H. (1978). The Velocity Charateristics of Ventilated Rooms. *Journal of Fluids Engineering*, Vol 100, 291-298.
- Sommavilla, S. (2022, April 20). *SMOOTHED PARTICLE HYDRODYNAMICS*. Retrieved from Dive Solutions GmbH: <https://www.dive-solutions.de/>

Stern, F., Xing, T., Yarbrough, D. B., Rothmayer, A., Rajagopalan, G., Prakashotta, S., . . . Moeykens, S. (2006). Hands-On CFD Educational Interface for Engineering Courses and Laboratories. *Journal of Engineering Education*, 95: 63-83.

Tenlinks. (2022, March 20). *Tenlinks.com*. Retrieved from Directory of CAD. CAM and CAE: <http://www.tenlinks.com/>

Wikipedia. (2022, April 02). *Coanda Effect*. Retrieved from Wikimedia Foundation Inc.: https://en.wikipedia.org/wiki/Coanda_effect

DISCLAIMER

The information or advice contained in these technical papers is intended for use only by professionals who have had adequate technical training in the field to which the paper relates. At the time of publication, these technical papers have undergone a formal peer-review process.

These documents have been compiled as an aid only, and the information or advice should be verified before it is put to use. The user should also establish the applicability of the information or advice in relation to any specific circumstances. While the information or advice is believed to be correct, no responsibility is taken by AIRAH or IBPSA Australasia for any statements made within.

AIRAH and IBPSA Australasia, its officers, employees and agents, disclaim responsibility for any inaccuracies contained within the documents, including those due to any negligence in the preparation and publication of the said technical papers.

COPYRIGHT

This work is copyright. Apart from any use as permitted under the Copyright Act 1986, no part may be reproduced by any process without prior written permission from either the Australian Institute of Refrigeration, Air Conditioning and Heating (AIRAH) or the International Building Performance Simulation Association (IBPSA) Australasia.

AUSTRALASIAN BUILDING SIMULATION

PRESENTED BY



International
Building
Performance
Simulation
Association
Australasia

MAJOR SPONSOR



TRADE DISPLAY SPONSOR



INDUSTRY PARTNER

